AIR POLLUTION MODELING AND ITS APPLICATION XV

EDITED BY CARLOS BORREGO AND GUY SCHAYES

Air Pollution Modeling and Its Application XV

Previous Volumes in this Mini-Series

Volumes I–XII were included in the NATO Challenges of Modern Society Series.

AIR POLLUTION MODELING AND ITS APPLICATION I
Edited by C. De Wispelaere

AIR POLLUTION MODELING AND ITS APPLICATION II
Edited by C. De Wispelaere

AIR POLLUTION MODELING AND ITS APPLICATION III
Edited by C. De Wispelaere

AIR POLLUTION MODELING AND ITS APPLICATION IV
Edited by C. De Wispelaere

AIR POLLUTION MODELING AND ITS APPLICATION V
Edited by C. De Wispelaere, Francis A. Schiermeier, and Noor V. Gillani

AIR POLLUTION MODELING AND ITS APPLICATION VI
Edited by Han van Dop

AIR POLLUTION MODELING AND ITS APPLICATION VII
Edited by Han van Dop

AIR POLLUTION MODELING AND ITS APPLICATION VIII
Edited by Han van Dop and Douw G. Steyn

AIR POLLUTION MODELING AND ITS APPLICATION IX
Edited by Han van Dop and George Kallos

AIR POLLUTION MODELING AND ITS APPLICATION X
Edited by Sven-Erik Gryning and Millán M. Millán

AIR POLLUTION MODELING AND ITS APPLICATION XI
Edited by Sven-Erik Gryning and Francis A. Schiermeier

AIR POLLUTION MODELING AND ITS APPLICATION XII
Edited by Sven-Erik Gryning and Nadine Chaumerliac

AIR POLLUTION MODELING AND ITS APPLICATION XIII
Edited by Sven-Erik Gryning and Ekaterina Batchvarova

AIR POLLUTION MODELING AND ITS APPLICATION XIV
Edited by Sven-Erik Gryning and Francis A. Schiermeier

Air Pollution Modeling and Its Application XV

Edited by

Carlos Borrego
University of Aveiro
Aveiro, Portugal

and

Guy Schayes
Catholic University of Louvain
Louvain-la-Neuve, Belgium

KLUWER ACADEMIC PUBLISHERS
NEW YORK, BOSTON, DORDRECHT, LONDON, MOSCOW

eBook ISBN: 0-306-47813-7
Print ISBN: 0-306-47294-5

Created in the United States of America

Visit Kluwer Online at: http://kluweronline.com
and Kluwer's eBookstore at: http://ebooks.kluweronline.com

PREFACE

In 1969 the North Atlantic Treaty Organization (NATO) established the Committee on Challenges of Modern Society (CCMS). The subject of air pollution was from the start, one of the priority problems under study within the framework of various pilot studies undertaken by this committee. The organization of a periodic conference dealing with air pollution modelling and its application has become one of the main activities within the pilot study relating to air pollution. These international conferences were successively organized by the United States (first five); Federal Republic of Germany (five); Belgium (five); The Netherlands (four) and Denmark (five). With this one Portugal takes over the duty.

This volume contains the papers and poster abstracts presented at the 25th NATO/CCMS International Technical Meeting on Air Pollution Modelling and Its Application held in Louvain-la-Neuve, Belgium, during 15-19 October 2001. This ITM was jointly organized by the University of Aveiro, Portugal (Pilot country) and by the Catholic University of Louvain, Belgium (host country).

The ITM was attended by 78 participants representing 26 countries from Western and Eastern Europe, North and South America, Asia, Australia and Africa. The main topics of this ITM were : Role of Atmospheric Models in Air Pollution Policy and Abatement Strategies; Integrated Regional Modelling; Global and Long-Range Transport; Regional Air Pollution and Climate; New Developments; and Model Assessment and Verification.

Invited papers were presented by A. Ebel of Germany (Changing atmospheric environment, changing views); H. ApSimon of Great Britain (Applying risk assessment techniques to air pollution modelling & abatement strategies); and S.E. Gryning of Denmark (Aspects of meteorological pre-processing of fluxes over inhomogeneous terrain).

On behalf of the Scientific Committee and as organizers and editors, we should like to express our gratitude to all participants who made the meeting so successful, resulting in the publication of this book. The efforts of the chairpersons and rapporteurs were especially appreciated. Thanks also to the teams of Aveiro and Louvain-la Neuve that managed all practical matters adequately.

Finally special thanks are due to the sponsoring institutions: NATO/CCMS: Committee on the Challenges of Modern Society; University of Aveiro, Portugal; Catholic University of Louvain, Belgium; FNRS: Fonds National de la Recherche Scientifique, Belgium; EURASAP: European Association for the Sciences of Air Pollution; ICCTI: Institute for International Scientific and Technological Cooperation, Portugal.

NATO/CCMS grants allowed attendance from Central and Eastern Europe. The next conference in this series will be held in 2003 in Istanbul (Turkey).

Guy SCHAYES
Local Conference Organizer
Belgium

Carlos BORREGO
Scientific Committee Chairperson
Portugal

This page intentionally left blank

THE MEMBERS OF THE SCIENTIFIC COMMITTEE FOR THE 25th NATO/CCMS INTERNATIONAL TECHNICAL MEETINGS ON AIR POLLUTION MODELLING AND ITS APPLICATION

Schayes, Belgium
D. Syrakov, Bulgaria
D. Steyn, Canada
S.-E. Gryning, Denmark
N. Chaumerliac, France
E. Renner, Germany
G. Kallos, Greece
D. Anfossi, Italy
P. Builtjes, The Netherlands
T. Iversen, Norway
C. Borrego, Portugal (Chairman)
J.M. Baldasano, Spain
S. Incecik, Turkey
B. Fisher, United Kingdom
F. Schiermeier, USA
Y. Schiffman, USA

This page intentionally left blank

HISTORY OF THE NATO/CCMS AIR POLLUTION PILOT STUDIES

Pilot Study on Air Pollution: International Technical Meetings (ITM) on Air Pollution Modelling and Its Application

Dates of Completed Pilot Studies:

1969 - 1974 Air Pollution Pilot Study (United States)
1975 - 1979 Air Pollution Assessment Methodologies and Modelling (Germany)
1980 - 1984 Air Pollution Control Strategies and Impact Modelling (Germany)

Dates and Locations of Pilot Study Follow-Up Meetings:

Pilot Country – United States (R.A. McCormick, L.E. Niemeyer)

February 1971 – Eindhoven, The Netherlands, First Conference on Low Pollution Power Systems Development
July 1971 – Paris, France, Second Meeting of the Expert Panel on Air Pollution Modelling

All of the following meetings were entitled NATO/CCMS International Technical Meetings (ITM) on Air Pollution Modelling and Its Application

October 1972 – Paris, France - Third ITM
May 1973 – Oberursel, Federal Republic of Germany - Fourth ITM
Jun 1974 – Roskilde, Denmark- Fifth ITM

Pilot Country – Germany (Erich Weber)

September 1975 – Frankfurt, Federal Republic of Germany – Sixth ITM
September 1976 – Airlie House, Virginia, USA – Seventh ITM
September 1977 – Louvain-La-Neuve, Belgium – Eighth ITM
August 1978 – Toronto, Ontario, Canada – Ninth ITM
October 1979 – Rome, Italy – Tenth ITM

Pilot Country – Belgium (C. De Wispelaere)

November 1980 – Amsterdam, The Netherlands – Eleventh ITM

August 1981 – Menlo Park, California, USA – Twelfth ITM
September 1982 – Ile des Embiez, France – Thirteenth ITM
September 1983 – Copenhagen, Denmark – Fourteenth ITM
April 1985 – St. Louis, Missouri, USA – Fifteenth ITM

Pilot Country – The Netherlands (Han van Dop)

April 1987 – Lindau, Federal Republic of Germany – Sixteenth ITM
September 1988 – Cambridge, United Kingdom – Seventeenth ITM
May 1990 – Vancouver, British Columbia, Canada – Eighteenth ITM
September 1991 – lerapetra, Crete, Greece – Nineteenth ITM

Pilot Country – Denmark (Sven-Erik Gryning)

November 1993 – Valencia, Spain - Twentieth ITM
November1995 – Baltimore, Maryland, USA – Twenty-First ITM
June 1997 – Clermont-Ferrand, France – Twenty-Second ITM
September 1998 – Varna, Bulgaria – Twenty-Third ITM
May 2000 – Boulder, Colorado, USA – Twenty-Fourth (Millennium) ITM

Pilot Country – Portugal (Carlos Borrego)

October 2001 – Louvain-la-Neuve, Belgium – Twenty-Fifth ITM

CONTENTS

ROLE OF ATMOSPHERIC MODELS IN AIR POLLUTION POLICY AND ABATEMENT STRATEGIES

INTEGRATED REGIONAL MODELLING

GLOBAL AND LONG-RANGE TRANSPORT

REGIONAL AIR POLLUTION AND CLIMATE

NEW DEVELOPMENTS

MODEL ASSESSMENT AND VERIFICATION

POSTER SESSION

ROLE OF ATMOSPHERIC MODELS IN AIR POLLUTION POLICY AND ABATEMENT STRATEGIES

Chairperson : B. Fisher

Rapporteur : Ph. Thunis

This page intentionally left blank

A POLICY ORIENTED MODEL SYSTEM FOR THE ASSESSMENT OF LONGTERM EFFECTS OF EMISSION REDUCTIONS ON OZONE

Clemens Mensink, Laurent Delobbe and Ann Colles*

1. INTRODUCTION

For the evaluation of ozone abatement measures, modelling tools predicting the long-term effect of emission reductions on ground level ozone are indispensable. In the Flanders region in Belgium such an evaluation is carried out on periodically on a 5-year base[1] with time horizons set at 5 to 10 years ahead. In general, policy makers express in their abatement strategies the combination of economic projections and a set of possible or optional policy measures. Under various sets of constraints, like health effects, social acceptance, costs and economical feasibility, the problem can be reduced to an optimisation problem and as a result the most efficient measures are selected, e.g. by applying multi-criteria analysis[2]. One of the challenges with respect to policy support for ozone abatement is to offer a tool that can provide assessments at low computational cost. In this way a large number of scenarios can be evaluated within a limited time frame.

In terms of its effect, ozone exposure is to be assessed on a long-term base, depending on the evaluation variable that is examined. Moreover the formation and degradation of ozone can cover several days and the transport of ozone and its precursors is not limited to any national border. These considerations should be taken into account by the evaluation instrument as well.

We present a tool that has been designed for the assessment of abatement scenarios. It is applied to calculate the long-term effects of European emission reductions on ozone in Belgium. The model system is based on the results of extensive calculations by two air quality models and uses fast multiple linear regression techniques as proposed and used in the RAINS model[3] for the preparation of the recent Gothenburg protocol and EC national emission ceilings. A first regression model, called OZON94 is based on the results (5 model scenario runs) of the LOTOS model[4] for the summer period of 1994 (1 May – 31 August). OZON94 uses the meteorological conditions of the period May-

* Flemish Institute for Technological Research (Vito), Boeretang 200, B-2400 Mol, Belgium.

Air Pollution Modeling and Its Application XV, Edited by
Borrego and Schayes, Kluwer Academic/Plenum Publishers, New York, 2002

August 1994 and only varies the emissions of the ozone precursors (NO_x and VOC) in 37 European countries. In function of the selected abatement scenario the model calculates various ozone indicators in 15 grid cells covering Belgium. A second regression model is called OZON97. It is based on the results (5 runs) of the EUROS model[5] for the summer period of 1997 (1 May – 30 September) and works in a similar way as OZON94

Various indicators can evaluate the effect of abatement measures on ground level ozone. These indicators are usually based on hourly ozone concentrations that are location dependent. In this study, five different ozone parameters are used to evaluate abatement measures: AOT60, NET60 and ADM as indicators for the protection of human health against ozone exposure, and AOT40_f and AOT40_v as indicators for the effects on forests and on crops and semi-natural vegetation. Their definitions as used in this study are given below:

- AOT60 = Accumulated exposure Over a Threshold of 60 ppb, based on hourly values for the period considered;
- NET60 = Number of days with a maximum 8-hourly value Exceeding a Threshold of 60 ppb for the period considered;
- ADM = Average of the Daily Maximum 8-hourly value for the period considered;
- AOT40_f = Accumulated exposure Over a Threshold of 40 ppb for forests, based on hourly values between 8h and 20h MET from 1 April to 30 September;
- AOT40_v = Accumulated exposure Over a Threshold of 40 ppb for crops and semi-natural vegetation, based on hourly values between 8h and 20h MET from 1 May to 31 July.

Note that, except for the AOT40_v, these definitions are confined to the periods for which meteorological data were available, i.e. between 1 May and 31 August for OZON94 and between 1 May and 30 September for OZON97.

Each of these 5 indicators is used to evaluate a reference situation (1990) and two emission reduction scenario's for 2010. The first one is a business as usual (BAU) scenario in which reduction plans and legislative actions are included, *before* the national emission ceilings provided by the Gothenburg protocol were adopted. This scenario corresponds to the REF scenario belonging to the H1 scenario in the seventh IIASA interim report[6]. A second scenario reflects the national emission ceilings (NEC) as prescribed by the UN/ECE 1999 Gothenburg protocol[7] to abate acidification, eutrophication and ground-level ozone. It sets emission ceilings for 2010 for SO_2, NO_x, VOC and NH_3 as negotiated on the basis of scientific assessment of pollution effects and abatement options.

Section 2 gives an overview of the methodology and the main elements of the model system. It describes briefly how the equations for the regression model have been derived and how the model results set the basis to resolve the coefficients that are used to estimate the long-term ozone effect of the emission scenario's. In section 3 the results for the two scenario's are presented and discussed. In addition a comparison is made between the OZON97 results and the results of the EUROS model, both applied for the emissions prescribed by the NEC scenario. This allows an estimation of the accuracy of the regression model with regard to the scenario calculations for the 5 indicators.

2. METHODOLOGY

The methodology of the model system consists of the following steps:

1. Computation of the hourly ozone concentrations for 15 grid cells covering Belgium for 5 different emission scenarios (base case, -30% NO_x, -30% VOC, -30% (NO_x & VOC) and –50% (NO_x & VOC)) with the LOTOS model for the summer period of 1994 (1 May – 31 August) to obtain the basis for the OZON94 regression model.
2. Computation of the hourly ozone concentrations for 15 grid cells covering Belgium for the same 5 emission scenarios with the EUROS model for the summer period of 1997 (1 May – 30 September) to obtain the basis for the OZON97 regression model.
3. Determination of the regression coefficients for each of the 5 indicators in each of the 15 grid cells by solving a system of 5 equations with 5 unknowns using the ozone calculations performed by LOTOS for OZON94 and by EUROS for OZON97.
4. Computation of the 5 indicators in each of the 15 grid cells by applying the regression model for the 1990 reference case and the BAU and NEC scenario's using the country based NO_x and VOC emission variations as an input.
5. Aggregation of the 15 grid cell values into one value for Belgium by weighted averaging.

In a next section, the successive steps of the methodology are explained. The results from the LOTOS (long-term ozone simulation) model were obtained from Builtjes and Boersen[4]. LOTOS is an Eulerian grid model[8] with a horizontal grid resolution of approximately 60 x 60 km² and 4 vertical layers extending to 2-3 km. The model computations were performed on a grid containing 70 x 70 grid cells covering a domain from 35°N to 70°N and from 10°W to 60°E. Transport phenomena on a regional scale as well as background concentrations on a continental scale are taken into account by the model. The photochemical processes in the model are driven by a slightly modified version of the Carbon Bound IV mechanism[8].

The EUROS (European Smog) model was developed at RIVM in the Netherlands and is also applied for long-term ozone calculations[5]. A detailed description of the EUROS model is given by van Loon[9]. It is also an Eulerian grid model that covers the whole of Europe with a spatial resolution of approximately 60 x 60 km², but a grid refinement procedure allows refinement of the spatial resolution in certain areas of the model domain, for example in areas where strong concentration gradients occur. The (photo)-chemical module is the recent version of the Carbon Bound IV mechanism[10]. It includes 32 chemical species and 87 reactions.

Using the hourly ozone concentrations computed by the LOTOS and the EUROS model, the impact of the emission scenarios on the 5 indicators was calculated by means of a multiple linear regression technique as proposed by Amman et al.[3]:

$$IND_{lj} = k_j + \sum_{i=1}^{M} (a_{ij} VOC_i + b_{ij} NOx_i + c_{ij} NOx_i^2) + \alpha_j \overline{en}_j^2 + \overline{en}_j \sum_{i=1}^{M} d_{ij} VOC_i \quad (1)$$

Where:

IND_{lj} = the calculated values for the indicator 1 (1=1…5) at receptor j
k_j = back ground contribution to the IND_{lj} at receptor j
$a_{ij}VOC_i$ = linear contribution of the VOC emissions from country i to receptor j
$b_{ij}NOx_i$ = linear contribution of the NO_x emissions from country i to receptor j
$c_{ij}NOx_i^2$ = non-linear contribution of the NO_x emissions from country i to receptor j
$\alpha_j en_j^2$ = non-linear contribution of "effective" NO_x emissions (natural sources)
$d_{ij}en_jVOC_i$ = non-linear contribution due to the interactions between NO_x and VOC

The "effective" NO_x emissions are defined as:

$$\overline{en}_j = \sum_{i=1}^{M} E_{ij} NOx_i + \overline{enn}_j \qquad (2)$$

Where:

E_{ij} = a meteorologically dependent variable
enn_j = the "effective" natural NO_x emissions at receptor j

It is assumed that the "effective" natural NO_x emissions for the 15 receptor points in Belgium are negligible, certainly when compared to the anthropogenic contributions. By this assumption equation (2) is reduced to a (non-linear) quadratic NOx_i contribution in (1) which can be attributed to the term $c_{ij}NOx^2$. The last term in equation (1) is replaced by the product of the NO_x and VOC contributions multiplied by the coefficient d_{ij}. This leads to the following expression:

$$IND_{lj} = k_j + \sum_{i=1}^{M} (a_{ij}VOC_i + b_{ij}NOx_i + c_{ij}NOx_i^2 + d_{ij}NOx_iVOC_i) \qquad (3)$$

For 15 receptor points located in Belgium (j=1...15) the coefficients a_{ij}, b_{ij}, c_{ij}, d_{ij} and k_j are determined for the contribution of each emitting country (i=1...37). These contributions are weighted by means of the source-receptor matrices provided by EMEP[11]. The 5 unknown coefficients in expression (3) are resolved by 5 equations related to 5 situations for which the IND and the NO_x and VOC emissions are known (base case and 4 reduction scenarios: -30% NO_x, -30% VOC, -30% (NO_x & VOC) and -50% (NO_x & VOC)). Once the coefficients are calculated they are used to calculate the IND values for 1990 and the BAU and NEC emission scenarios.

An average value for Belgium is obtained by applying weighted averaging. For the AOT60, NET60 and AMD this is based on population density per grid cell. For the AOT40_f the forest density per grid cell is used. For the AOT40_v the cultivated agricultural area per grid cell is used.

3. RESULTS AND DISCUSSION

Figure 1 shows the results of the OZON94 regression model for the 5 indicators (ADM, AOT40_v, AOT40_f, AOT60 and NET60). Results are presented for three cases: 1990, the BAU scenario in 2010 (BAU 2010) and the NEC scenario in 2010 (NEC 2010). For each column in Figure 1, the value of the indicator is divided by the value for the reference situation in 1990. Thus the relative reduction ratios are presented. In a similar way Figure 2 shows the results for OZON97. The results of OZON94 and OZON97 cannot be compared by their absolute values, since different meteorological data and different evaluation periods were used. This should also be borne in mind when comparing the relative reduction ratios. However one can clearly see that both results show the same trend. The average values (ADM) are hardly changing or even show a very slight increase in the case of OZON97. The indicators with a low cut off as threshold value (AOT40) are only slightly decreasing. This means that background concentrations seem to have a tendency to rise in the future. On the other hand, the indicators that reflect the maximum values (e.g. AOT60 and NET60) do decrease significantly for both models. The difference between AOT60 and NET60 seems to indicate that the amount of ozone excess is decreasing faster than the number of days on which the exceedances occur. As a result it can be put forward that the emission reduction efforts seem to be effective to avoid exceedances rather than to reduce background levels.

These trends are more or less confirmed by observations in Flanders between 1989 and 1999[12]. The measured annual average of the daily maximum 8-hourly values (AMD) shows a rising trend with 4% per year since 1991, indicating an increasing background concentration. The measured 5-year sliding average of the AOT40_v shows a very slight decrease (5-10%) over the period 1993-1999. The measured trends for NET60 and AOT60 are less clear. Their values depend strongly on the annual fluctuations in sunshine and temperature. However, one should be careful in comparing these trends. The total emissions in Europe for NO_x and VOC have decreased with 28% and 23% respectively over the period 1989-1999, whereas in the scenario calculations the reduction rates for the NO_x and VOC emissions are 48% and 50% respectively between 1990 and 2010. Since the methodology is expected to be very sensitive to different NO_x/VOC ratios, a very detailed sensitivity study would be needed to confirm the measured trends.

In order to estimate the accuracy of the regression method, in particular of the OZON97 method, the results for the NEC scenario were compared with the results of the EUROS model for the same input data. Figure 3 shows the comparison for the 15 grid locations in Belgium for the AOT40_v. Figure 4 shows the comparison for the AOT60. Table 1 gives the average value of the OZON97 results and the absolute and relative RMS errors for the 5 indicators, when comparing the grid cell values with the EUROS results. It can be seen that the regression method performs well for the ADM, the AOT40_v and the AOT40_f, but is more sensitive with respect to AOT60 and NET60. This is obvious, since in some of the grid cells, the levels of AOT60 are close or just below the threshold value. Notice also that the OZON97 model gives a systematic underestimation of the AOT60 compared to the EUROS results for the NEC scenario.

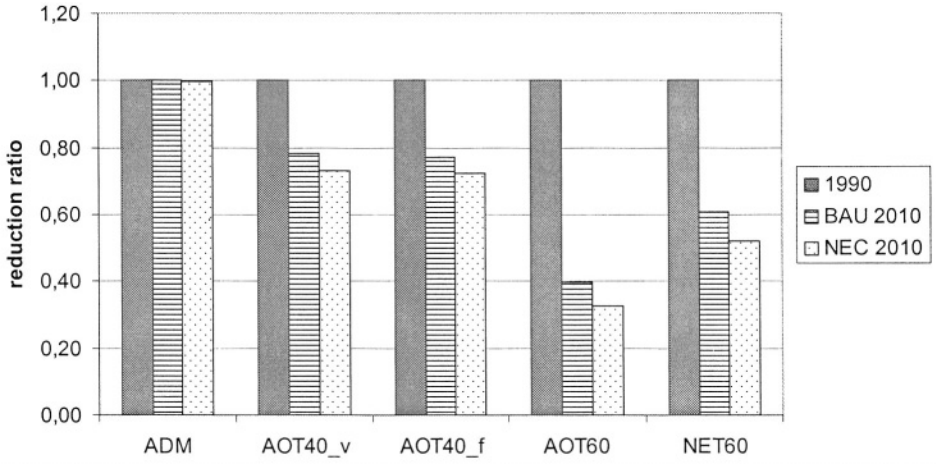

Figure 1. Results for the 5 ozone indicators obtained by OZON94.

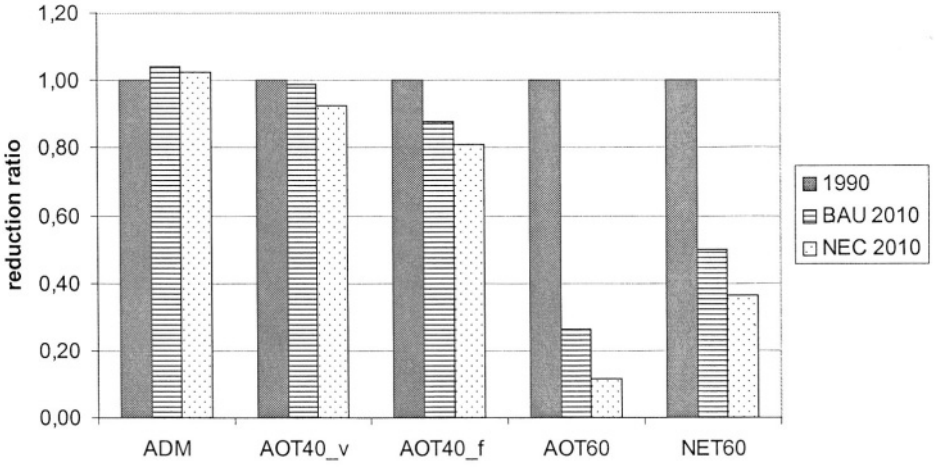

Figure 2. Results for the 5 ozone indicators obtained by OZON97.

Table 1. Calculated average over Belgium by OZON97 and root mean square errors comparing EUROS and OZON97 model results for the 5 indicators

	Average OZON97	RMS	RRMS
ADM (µg/m³)	94.30	0.25	0.3 %
AOT40_v (ppm.h)	5.22	0.11	2.0 %
AOT40_v (ppm.h)	10.01	0.16	1.8 %
AOT60 (ppm.h)	0.38	0.12	57 %
NET60 (days)	11.23	0.92	27 %

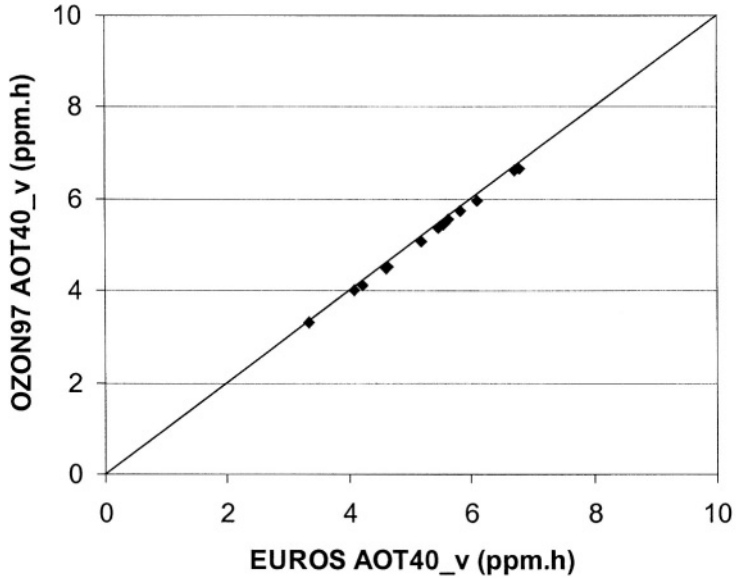

Figure 3. Comparison between EUROS and OZON97 model results for the AOT40_v using emission input data for the NEC scenrio 2010

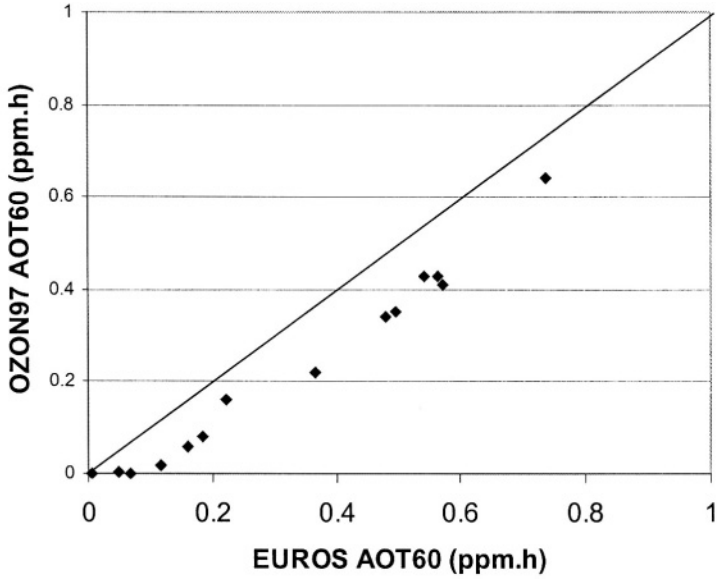

Figure 4. Comparison between EUROS and OZON97 model results for the AOT60 using emission input data for the NEC scenrio 2010

4. CONCLUSIONS

A methodology has been presented for the assessment of long-term effects of emission reductions on ozone concentrations in Belgium at low computational costs. Results for various scenarios show some important trends. The average values (ADM) are hardly changing or show a slight decrease. The indicators with a low cut off as threshold value (AOT40) show a slight decrease. Both trends are confirmed by observations between 1989 and 1999. Indicators representing peak values (e.g. NET60 and AOT60) decrease significantly for the various policy scenarios. From the measurements these trends are not clear, since the annual variation are dominated by the varying meteorological conditions. For the scenario's considered the regression method gives accurate results for the ADM and AOT40 indicators, but less accurate results for the AOT60 and NET60 indicators.

5. REFERENCES

1. VMM (2000) MIRA-S 2000: *Report on the environment and nature in Flanders: scenarios,* Summary, Vlaamse Miliaumaatschappij & Garant, Leuven/Apeldoorn.
2. De Vlieger, I.,Berloznik, R, Duerinck, J. and Mensink, C. (2001) Multidisciplinary study on reducing air pollution from transport. Methodology and emission results, Proceedings of the 7th International Conference on Urban Transport and the Environment for the 21st Century, 14-16 May 2001, Lemnos, Greece, WITpress, Southapmton, pp. 429-440.
3. Amann M., Bertok, I., Cofala J., Gyarfas F., Heyes C., Klimont Z., en Schöpp W. (1999) *Integrated Assessment Modelling for the Protocol to Abate Acidification, Eutrophication and Ground-level Ozone in Europe,* IIASA, Laxenburg.
4. Builtes P.J.H. en Boersen G. (1996) *Model calculations to determine the influence of European emission reductions on ozone concentrations over Belgium,* TNO-report TNO-MEP-R 96/274, Apeldoorn.
5. Matthijsen, J., Delobbe, L., Sauter, F. and de Waal, L. (2001) Changes of surface ozone over Europe upon the Gothenburg protocol abatement of 1990 reference emissions, *Proceedings of the EUROTRAC-2 Symposium 2000,* Computational Mechanics Publications (to appear).
6. Amann, M., Bertok, I., Cofala, J., Gyarfas, F., Heyes, C., Klimont, Z., Makowski, M., Schöpp, W. & Syri, S. (1999) *Cost-effective control of acidification and ground-level ozone, seventh interim report.* IIASA, Laxenburg.
7. UN/ECE (2000) http://www.unece.org/env/lrtap/
8. Builtjes, P.J. H. (1992) *The LOTOS Long Term Ozone Simulation-project,* Summary Report, TNO-report TNO-MW-R 92/240, Apeldoorn
9. Loon M. van (1996) *Numerical methods in smog prediction,* PhD thesis, University of Amsterdam.
10. Adelman Z.A. (1999) A re-evaluation of the Carbon Bond-IV photochemical mechanism, Thesis Msr. Sc., Chapel Hill.
11. EMEP (1998) http://www.emep.int/ozone/webo3sr/
12. Dumont, G. and Mensink, C (2000) Photochemical air pollution, in: M. Van Steertegem et al. (eds.), MIRA-S 2000: Report on the environment and nature in Flanders: scenarios, Vlaamse Miliaumaatschappij & Garant, Leuven/Apeldoorn (in Dutch), pp. 395-409.

DISCUSSION

A. HANSEN

Have the results of the LOTOS and regression models been compared with observational data ?
There appears to be certain degree of faith placed in the regression model results.

C. MENSINK

The results of the LOTOS model for 1994 have been compared with observed values for the northern part of Belgium (Flanders region) as reported in reference 12 in the paper. The following table summarises the results as averaged over the grid cells covering the computational domain and over all monitoring stations in Flanders [12]:

	Modelled	Measured
ADM ($\mu g/m^{3)}$	84	82
AOT60 ($\mu g/m^3$).h	3.550	3.900
NET60 days	25	20
AOT40-v ($\mu g/m^3$).h	15.600	14.400
AOT40-f ($\mu g/m^3$).h	17.000	16.700

The results of the regression models intend to give an indication of the average long-term trends that can be expected for the various ozone parameters as required for policy support in Belgium. For the study of more detailed distributions of ozone in space and time we rather use air quality models (in particular the EUROS model).

B. FISHER

The full ozone model has been fitted by a simple regression model. Applications depend on the coefficients in the regression model, but the spread between results from the two models must also be a factor influencing the application of the regression model ?

C. MENSINK

The regression models OZON94 and OZON97 are applied at each of the 15 grid cells covering Belgium. So each grid location uses its own set of regression coefficients. In this sense the application of the regression models is independent of the grid location. However, the pull air quality models show indeed that there is a considerable variation over the country for most of the ozone parameters (see for example for AOT40-V in Figure 3 in the paper).

This page intentionally left blank

TRANSFORMING DETERMINISTIC AIR QUALITY MODELING RESULTS INTO PROBABILISTIC FORM FOR POLICY-MAKING

S. Trivikrama Rao and Christian Hogrefe*

1. INTRODUCTION

In the United States, the National Ambient Air Quality Standards (NAAQS) for air pollutants such as the 1-hr and 8-hr average ozone and 24-hr average particulate matter concentrations (both $PM_{2.5}$ and PM_{10}) focus on the extreme values of the distribution of observed pollutant concentrations. In regions where the design value has exceeded the NAAQS for ozone, the U.S. Environmental Protection Agency (EPA) mandates the use of a grid-based photochemical model to demonstrate future compliance with the NAAQS with appropriate emissions reductions. However, recent studies have found that the current generation of photochemical models are more capable of simulating average concentrations than the extreme values (Rao et al., 2000; Hogrefe et al., 2001a,b; Biswas and Rao, 2001; Biswas et al., 2001). Thus, it is essential that we address the problem of how to use air quality models in the regulatory framework.

Hogrefe and Rao (2001) proposed a methodology to account for the stochastic nature of the actual observed extreme values (i.e., the design values) in model attainment demonstrations. Rather than thinking of the attainment demonstration process in the pass/fail mode, policy-makers would be able to assess the *probability* that a certain emission control strategy would lead to compliance with the NAAQS with the approach suggested by Hogrefe and Rao (2001). In this paper, we briefly summarize the methodology and key findings described in Hogrefe and Rao (2001). We then perform spectral analysis of both observations and model predictions to investigate the time-scale

* S. Trivikrama Rao and Christian Hogrefe, Department of Earth and Atmospheric Sciences, University at Albany, Albany, New York, 12222, U.S.A.

Air Pollution Modeling and Its Application XV, Edited by
Borrego and Schayes, Kluwer Academic/Plenum Publishers, New York, 2002

specificity of the effect of emission reductions on air quality. We then discuss the need to expand the method described in Hogrefe and Rao (2001) to take this time-scale specificity into account.

2. DATABASE

Hourly surface ozone observations were retrieved from the EPA's AIRS database and the daily maximum 1-hr and 8-hr average ozone concentrations were determined. The analysis domain covers the northestern United States; we analyzed 428 AIRS stations within this doemain. As an illustration for the computation of extreme value statistics, we considered ozone observations during the months May – September for the 1994 – 1996 period, treating 1995 as the base year for the simulation of future emission control scenarios.

For the analysis of the simulated effects of an emission reduction scenario, we used the results from a 3-month modeling study with the RAMS/UAM-V regional scale photochemical modeling system (E. Meyer, personal communication). The base year for the emission inventory reflects emissions for 1995 as described by the U.S. EPA (1998a), and the meteorological fields reflect the conditions in the summer of 1995. The simulation period is June 4 – August 31, 1995. Projected emissions for the 2007 emission control scenario include Clean Air Act Amendment measures and the NO_x SIP call (U.S. EPA, 1998b), which amounts to an average reduction of 16%/21% in NO_x/VOC emissions across all sources and all states (U.S. EPA, 1999a). Further details about this simulation can be found in Hogrefe et al. (2000).

3. METHODS OF ANALYSIS

3.1. Extreme Value Statistics

The design value for the 1-hr ozone concentrations is defined as the 4^{th} highest daily maximum concentration observed over a consecutive three year period. From the statistical perspective, each observation represents an event or a single realization out of an unknown underlying distribution. As described in more detail by Hogrefe and Rao (2001), the exact theory of extreme values can be used to calculate the cumulative distribution function (CDF) for the 4^{th} order statistic (i.e., the design value) based on the information present in the other observations at this site. Although the analytical form of the underlying distribution is generally unknown, the CDF of the tail of most parent distributions can be described by an exponential distribution (Roberts, 1979; Rao et al., 1985; Breiman and Stone, 1985) whose parameters are determined by a fit to the empirical CDF of the tail (Breiman and Stone, 1985). Once the analytical form of the CDF of the tail of the observed distribution has been determined in this manner, the exact theory of extreme values can be applied to estimate the CDF of the 4^{th} order statistic (i.e. the 4^{th} highest observation or design value) (Gumbel, 1958; David, 1981; Rao and Sistla, 1992, Hogrefe and Rao, 2001).

From the statistical perspective, the important difference between the NAAQS for 1-hr and 8-hr ozone concentrations is that for the 8-hr ozone NAAQS, the 4^{th}-highest ozone concentration is determined for each year in the consecutive three-year time period under consideration, and the three values are then averaged to determine the design value. Similarly, the revised NAAQS for the 24-hr concentrations of $PM_{2.5}$ requires calculating the three-year average of the 98^{th} percentile values determined for each individual year. This form of the standard cannot be described analytically by the statistical theory such as the exact theory of extreme values used for the 1-hr ozone NAAQS. Therefore, we apply the bootstrap resampling technique (Efron, 1979; Rao et al., 1985) to estimate probabilities associated with the 8-hr ozone NAAQS. In addition, our approach modifies the bootstrap technique by applying an exponential curve fit to the tail of the CDF for each yearly sample in each bootstrap replication. Further details of this procedure are described in Hogrefe and Rao (2001).

The knowledge of the CDF for the 4^{th} order statistic then enables us to translate the deterministic form of the standard NAAQS into the probabilistic framework. Hogrefe and Rao (2001) discussed the limitations associated with the extreme value analysis.

3.2. Spectral Decomposition

It is well known that pollutant concentrations are influenced by different physical/chemical processes operating on different time scales (Porter et al., 2001). Therefore, to examine the effect of emission reductions on different temporal components, we apply the spectral decomposition technique described by Hogrefe et al. (2000) to time series of hourly summertime ozone concentrations. The moving average filtering technique (see Rao and Zurbenko, 1994) separates the fluctuations present in the time series into fluctuations operating on the intra-day scale (ID, periods less than 11 h), the diurnal scale (DU, periods 11 – 64 h), the synoptic scale (SY, periods 64 h – 21 d), and the baseline scale (BL, periods longer than 21 days). Prior to the analysis, the time series is log-transformed (Hogrefe et al., 2001) to stabilize the variance. Of importance to the analysis in this paper is the fact that the estimated ID, DU, and SY components have a mean value of zero and the BL component contains information about the geometric mean. A more detailed description of the spectral decomposition technique can be found in Rao et al. (1997) and Hogrefe et al. (2000).

4. RESULTS AND DISCUSSION

4.1. Application of Extreme Value Statistics

In this section, we illustrate the estimation of CDF for the present and future ozone design values. As discussed above, the parameters of the exponential tail fit to the empirical CDF of 1-hr daily maximum ozone concentrations have to be estimated in order to construct the CDF of the 4^{th} highest value in the underlying three-year sample, i.e., the 1-hr ozone design value. Figure 1 depicts this CDF of the 1-hr ozone design value at Pittsburgh, PA. The observed design value at this monitor for the period under

consideration (1994 – 1996) was 133 ppb. The information in Figure 1 can be interpreted as follows: The probability that the observed design value at this monitor for the time period under consideration is less than or equal to 124 ppb (i.e. the probability of meeting the NAAQS for 1-hr ozone concentrations) is 10%, or there is a 90% chance of violating the NAAQS. Thus, the deterministic form of the NAAQS can be transformed into the probabilistic framework.

4.2. Using Model Predicted Changes In Attainment Demonstrations

In attainment demonstrations, the model-predicted changes in ozone concentrations resulting from emission reductions have to be combined with the information present in the observations to determine future compliance with the NAAQS. In other words, one attempts to predict how the observed ozone distribution would have looked like had emission controls already been in place. This, in turn, would allow us to apply extreme value statistics as described above to assess the effectiveness of a given emission control scenario in reducing the probability of violating the NAAQS. Obviously, using the model-predicted responses to emissions reductions to scale the observed pollutant concentrations is not a straightforward task and requires certain assumptions. In the following, we will discuss the method stipulated by EPA and suggest possible improvements to this method.

In its recent draft modeling guidance (U.S. EPA, 1999b), EPA stipulated that in order to determine whether the simulated emission reductions would lead to compliance with the NAAQS at a given location, the observed design value would be multiplied (i.e.

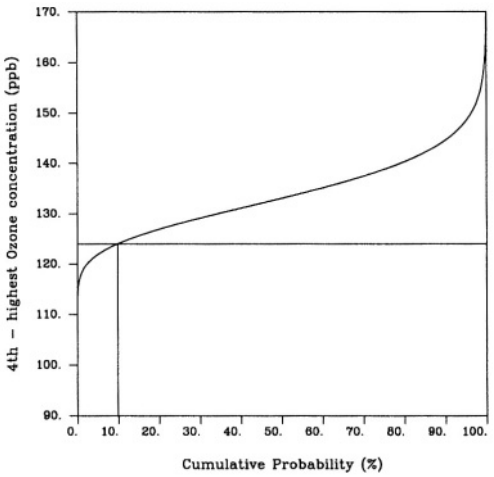

Figure 1: Cumulative distribution function for the fourth-highest 1-hr daily maximum ozone concentration (design value) at Pittsburgh, PA.

scaled) by a site-specific Relative Reduction Factor (RRF). EPA defined the relative reduction factor (RRF) as the ratio of the mean model-predicted daily ozone maxima for the emission control and base cases over all simulated days (U.S. EPA, 1999b). Days with daily maximum 8-hr average ozone concentrations less than 70 ppb would be excluded from the computation of the RRF. The attainment demonstration procedure assumes that the distribution of daily maxima for each site will flatten after controls are implemented (e.g., the difference between the 90th percentile concentration and the median concentration diminishes once controls are in place), but that a day's ranking in the tail of a pre-control distribution is similar to its ranking in the post-control distribution (U.S. EPA, 1999b). The assumption is that lower concentrations which are close to background levels already are unlikely to be greatly affected by control measures (Lefohn, et al., 1998). This assumption is consistent with the above-mentioned practice of excluding days with daily maximum 8-hr average ozone concentrations less than 70 ppb from the computation of the RRF.

However, when focussing only on the effect of emission reductions on the upper tail of the predicted distribution by selecting only high ozone days for calculating the RRF, one does not make use of the entire information about the effect of emission reductions present in the model predictions. Using the spectral decomposition technique detailed in Hogrefe et al. (2000), we calculated the effect of the emission reductions of the 2007 SIP call on the predicted model distributions for the intra-day, diurnal, synoptic, and baseline time scales. For example, controls on the ground-level emissions can be expected to largely affect the diurnal scale while controls on elevated point source would influence largely the synoptic scale forcings.

The standard deviations for the control and base case simulations as well as their ratio for all components along with the means and their difference for the baseline component in both simulations are presented in Table 1. This calculation was performed for AIRS station 420031005 near Pittsburgh, PA. These results illustrate that – by making use of all 2136 hours of model predictions and disseminating them using the spectral decomposition technique – additional information can be gained about the model-predicted effect of emission reductions on ozone air quality. In this case, it is evident that the spread of the distributions changes most significantly for the synoptic and baseline time scales, to a lesser degree for the diurnal component, while no change of the distribution width is predicted for the intra-day component. This suggests that – at least at this location – the simulated emission reduction scenario that focusses on reducing emissions from elevated point sources is likely to reduce the magnitude of high ozone concentrations occurring over extended periods of time (i.e. longer time scales are affected mostly).

While the model prediction of this effect of emission reductions cannot be readily evaluated against observations, analysis of long-year records of ozone concentrations also show that the long-term behavior of ozone is different on different time scales. For example, Chan et al. (1999) found that the magnitude of the observed intra-day fluctuations are nearly invariant in time (i.e., no trend), while changes in the magnitude of fluctuations on other time scales contributed to an overall downward trend in ozone concentrations over Los Angeles. In other words, analyses of observations support the notion that the effect of emission reductions on model predicted ozone concentrations

Table 1: Standard deviations and means of the predicted component distributions for both the base case simulation and the 2007 NO_x SIP call emission control simulation.

	σ_{base}	σ_{cont}	$\sigma_{cont} / \sigma_{base}$	Avg_{base}	Avg_{cont}	$Avg_{base} - Avg_{cont}$
ID	0.02	0.02	1.00	N/A	N/A	N/A
DU	0.23	0.21	0.91	N/A	N/A	N/A
SY	0.21	0.16	0.76	N/A	N/A	N/A
BL	0.11	0.09	0.82	3.77	3.69	0.08

should be analyzed in terms of the predicted changes in the distributions of different temporal components.

To integrate the predicted changes in ozone component distributions into the observed concentrations for attainment demonstration purposes, we propose the following method: spectrally decompose the hourly ozone time series at a given monitor location, then multiply each hourly component time series by the ratio of control case to base case model-predicted standard deviation for the component. Since the baseline component has a non-zero mean, the mean is subtracted before scaling it in this manner and then added back after the scaling. In addition, the model-predicted reduction in the mean baseline values is subtracted from all observed hourly baseline values. The scaled component time series are then added back together; the scaled observed time series is obtained by taking the exponent of this sum so that the daily maxima can be determined in the ppb scale. Subsequently, extreme value statistics can be applied to determine the effect of the simulated emission reductions on the exceedance probability. While this scaling approach is somewhat arbitrary, it takes into account the apparent time-scale-specificity of emission

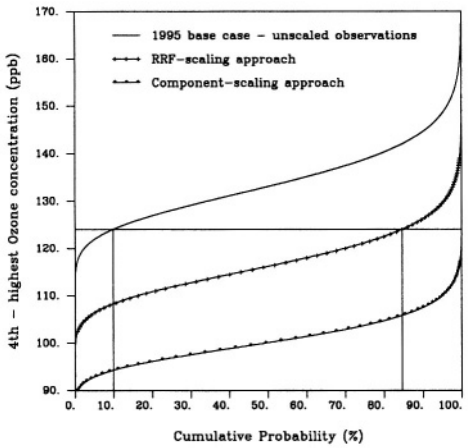

Figure 2: Cumulative distribution function for the fourth-highest 1-hr daily maximum ozone concentration (design value) at Pittsburgh, PA, for both the unscaled observations (i.e., the base case) and the observations scaled with the RRF-approach and component-adjustment approach for the 2007 SIP call.

reductions. Future research should be directed at quantifying the direct effect of the emission control programs that have been implemented on different spectral components of the ozone observations.

To compare the two scaling approaches (i.e., EPA's and the method proposed here), the CDF for the 1-hr design value is re-calculated after all observations are scaled by both the RRF method and the component adjustment method. For the RRF approach, we assume that all observed values in the tail of the observed distribution (which are used to computed the CDF of the design value) are uniformly reduced by the RRF. Figure 2 depicts these design-value CDF's for the Pittsburgh, PA monitor using the 2007 SIP call emission reduction scenario (U.S. EPA, 1998a) relative to the 1995 base case, as described in section 2. From Figure 2, it can be seen that both methods yield different CDF's. At this location, the RRF scaling method predicts that the 2007 NOx SIP call emission reductions would reduce the probability of violating the 1-hr NAAQS from 90% to 15%, while the component adjustment approach predicts that the probability of violating the NAAQS is near 0%. In other words, whereas the EPA-suggested method still shows a 15% probability of violating the NAAQS, the component adjustment method suggests compliance with the ozone NAAQS at this location with emission reductions proposed in the SIP call.

5. SUMMARY

Building upon a recent study by Hogrefe and Rao (2001), we presented an integrated observational-modeling approach to transform the deterministic nature of attainment demonstrations for the NAAQS for 1-hr and 8-hr ozone concentrations into the probabilistic framework. The application of extreme value statistics in estimating the probability of exceeding the NAAQS has been illustrated. The proposed probabilistic framework would enable decision makers to assess their chances of success in meeting the standard when control measures aimed at attaining the NAAQS are implemented. This paper introduced a method to account for the time-scale specificity of the effects of emission reductions when scaling the observations. Extended modeling periods rather than episodic simulations are needed for model evaluation as well as to assess the effect of emission reductions on different time scales.

6. ACKNOWLEDGMENTS

This work is supported by New York State Energy Research and Development Authority under contract No. 6085.

7. REFERENCES

Biswas, J., and S. T. Rao, 2001: Uncertainties in Episodic Ozone Modeling Stemming from Uncertainties in Meteorological Fields; J. Appl. Meteor., 40, 117 – 136.

Biswas, J., S. T. Rao, C. Hogrefe, C. W. Hao, and G. Sistla, 2001: Evaluating the Performance of Regional-Scale Photochemical Modeling Systems: Part III – Ozone Precursor Predictions; Atmos. Environ.; in press

Breiman, L., and C. J. Stone, 1985: Broad Spectrum Estimates and Confidence Intervals for Tail Quantiles; Technical Report No. 46; Department of Statistics, University of California, Berkeley, CA.

Chan, D., S. T. Rao, I. G. Zurbenko, and P. S. Porter, 1999: Linking Changes in Ozone to Changes in Emissions and Meteorology; Proceedings of the Air Pollution '99 Conference, Wessex Institute of Technology, WIT Press, Wessex, U.K., 664 – 675.

David, H. A., 1981: Order Statistics; John Wiley: New York, pp 8 – 22.

Efron, B., 1979: Computers and the Theory of Statistics: Thinking the Unthinkable; SIAM Rev.; 21 (4).

Gumbel, E .J., 1958: Statistics of Extremes; Columbia University Press: New York; pp 75 – 155.

Hogrefe, C., S. T. Rao , I. G. Zurbenko, and P. S. Porter, 2000: Interpreting the Information in Ozone Observations And Model Predictions Relevant to Regulatory Policies in the Eastern United States; Bull. Amer. Meteor. Soc., 81, 2083 - 2106.

Hogrefe, C., S. T. Rao, P. Kasibhatla, G. Kallos, C. J. Tremback, W. Hao, D. Olerud, A. Xiu, J. McHenry, J., and K. Alapaty, 200la: Evaluating the Performance of Regional-Scale Photochemical Modeling Systems: Part I - Meteorological Predictions; Atmos. Environ., 35, 4159 - 4174.

Hogrefe, C., S. T. Rao, P. Kasibhatla, W. Hao, G. Sistla, R. Mathur, and J. McHenry, 2001b: Evaluating the Performance of Regional-Scale Photochemical Modeling Systems: Part II - Ozone Predictions; Atmos. Environ., 4175-4188.

Hogrefe, C., and S. T. Rao, 2001: Demonstrating Attainment of the Air Quality Standards: Integration of Observations and Model Predictions into the Probabilistic Framework; J. Air Waste Manag. Assoc., 51, 1060–1072.

Lefohn, A. S., D. S. Shadwick, and S. D. Ziman, 1998: The Difficult Challenge of Attaining EPA's New Ozone Standard, Environ. Sc. Tech., Pol. Anal., 32, 276a- 282a.

Porter, P. S., S. T. Rao, I. G. Zurbenko, A. M Dunker, and G. T. Wolff, 2001: Ozone Air Quality over North America: Part II – An Analysis of Trend Detection and Attribution Techniques; J. Air Waste Manag. Assoc., 51, 283 – 306.

Rao, S. T., G. Sistla, V. Pagnotti, W. B. Petersen, J. S. Irwin, and D. B. Turner, 1985: Resampling and Extreme Value Statistics in Air Quality Model Performance Evaluation; Atmos. Env., 19, 1503-1518.

Rao, S. T. and G. Sistla, 1992: On the Use of Numerical Models in Ozone Attainment Demonstrations; In Air pollution modeling and its applications IX; Dop, H.v., Kallos, G., Ed.; Plenum Press: New York, NY, 41 - 48.

Rao, S. T., and I. G. Zurbenko: Detecting and Tracking Changes in Ozone Air Quality; J. Air Waste Manag. Assoc., 44, 1089 – 1092.

Rao, S. T., I. G. Zurbenko, R. Neagu, P. S. Porter, J.Y. Ku, and R. F. Henry, 1997: Space and Time Scales in Ambient Ozone Data; Bull. Amer. Meteor. Cos., 78, 2153 – 2166.

Rao, S. T., C. Hogrefe, J. Biswas, H. Mao, I. G. Zurbenko, P. S. Porter, P. Kasibhatla, and D. A. Hansen, 2001: How Should the Photochemical Modeling Systems be used in Guiding Emissions Management Decisions?, Air Pollution Modeling And Its Applications XIV, Gryning, S. E. and F. Schiermeier, Eds., Kluwer Academic / Plenum: New York, 25 – 34.

Roberts, E. M., 1979: Review of Statistics of Extreme Values with Applications to Air Quality Data Part I. Review; J. Air Poll. Cont. Assoc., 29, 632.

U.S. Environmental Protection Agency, 1998a: National Air Pollutant Emission Trends Update, 1970-1997; EPA-454/E-98- 007, U.S. Environmental Protection Agency, Research Triangle Park, NC 27711, 1998. Available online at http://www.epa.gov/ttn/chief/trends/ trends97

U.S. Environmental Protection Agency, 1998b: Finding of Significant Contribution and Rulemaking for Certain States in the Ozone Transport Assessment Group Region for Purposes of Reducing Regional Transport of Ozone; Federal Register, October 27, 1998, Vol. 63, No. 207, pp. 57355-57404. Available online at wais.access.gpo.gov

U.S. Environmental Protection Agency, 1999a: Procedures for Developing Base Year and Future Year Mass and Modeling Inventories for the Tier 2 Final Rulemaking; EPA420-R-99-034, U.S. Environmental Protection Agency, Research Triangle Park, NC 27711. Available online at http://www.epa.gov/orcdizux/regs/ld-hwy/tier-2/frm/tsd/r99034.pdf

U.S. Environmental Protection Agency, 1999b: Draft Report on the Use of Models and Other Analyses in Attainment Demonstrations for the 8-Hour Ozone NAAQS; EPA-44/R-99-0004; United States Environmental Protection Agency, Research Triangle Park, NC 27711.

U.S. Envirionmental Protection Agency, 2000: Regional Modeling Center Homepage. Available online at http://www.epa.gov/ttn/ scram/regmodcenter/t28.htm

DISCUSSION

E. GENIKHOVITCH — Why do you think that the parameters "a" and "b" in the exponential distribution are the same for each of three years ? What is the dispersion of your estimates of the fourth highest value ?

Ch. HOGREFE — To answer the first part of your question, the parameters "a" and "b" are estimated from the total distribution consisting of all 3 years of observations, not for the individual years. When different 3-year periods are considered, the parameters "a" and "b" change, and as a result the calculated CDF of the 4^{th} highest concentration also changes. In other words, the inter-annual variability present in the observations is not accounted for in the methodology. This is due to the definition of the NAAQS which focusses on a single 3-year period for the attainment demonstration process. The dispersion of the estimates of the fourth highest value is introduced by both interannual variability if other 3-year periods are considered, as well as by model-to-model differences in predicted RRF. In our experience, the former is greater than the latter.

B. FISHER — A comment. We cannot change the rules laid down by the US EPA, but this paper shows that the application of the ozone rules is very difficult. Alternative rules could produce equivalent benefits for air quality, but would be easier to assess ?

Ch. HOGREFE — I agree. The present NAAQS rules are very difficult to address with the current air quality modeling tools. The presented approach attempts to bridge this gap, but clearly future efforts are necessary, and a change in the way the NAAQS are defined might lead to a more consistent attainment demonstration process.

This page intentionally left blank

INTEGRATED REGIONAL MODELLING

Chairpersons:	D. Anfossi
	A. Baklanov
	P. Builtjes
Rapporteurs:	J. Brechler
	B. Carissimo
	C. Mensink
	E. Renner

This page intentionally left blank

CHANGING ATMOSPHERIC ENVIRONMENT, CHANGING VIEWS - AND AN AIR QUALITY MODEL'S RESPONSE ON THE REGIONAL SCALE

Adolf Ebel[1]

ABSTRACT

Experiences having resulted from the development and application of a specific air quality modelling system (EURAD) are discussed. Reasons for complex modelling and motivations evolving from a quickly growing field of atmospheric science are presented. It is argued that meteorology and atmospheric chemistry form an integral interdependent system of processes requiring an integral approach to their numerical modelling. A few examples of the application of a regional air pollution model to a broader set of environmental topics including the tropopause region are given. Aerosol simulation, chemical data assimilation and intensification of operational ozone forecast are viewed as important and challenging tasks for air quality modelling in the near future.

1. INTRODUCTION

The aim of this paper is not so much to discuss the development of air quality models than to demonstrate the change of the approach to the tasks and goals of chemical transport simulations by air quality modellers. Of course, there exists an intimate interdependence of intelligent definition of modelling goals and smart model improvement. Yet it may well be debated which really will be the driving force of progress in the field of air pollution modelling in the future: the improvement of the tool, i.e. the model, or the growing skill of controlling the modelling process by the users of the tool, for instance, by putting stronger efforts on the evaluation of numerical simulations. This aspect has clearly and convincingly been emphasized by a critical review of meso-scale air pollution modelling by Russel and Dennis (2000).

[1] Adolf Ebel, EURAD Project, University of Cologne, Institute for Geophysics and Meteorology, and Rhenish Institute for Environmental Research, Aachener Str. 201–209, 50931 Cologne, Germany; eb@eurad.uni-koeln.de

Air Pollution Modeling and Its Application XV, Edited by
Borrego and Schayes, Kluwer Academic/Plenum Publishers, New York, 2002

The study is based on experiences gained with a specific regional air quality model, namely the EURAD system (European Air Pollution Dispersion model: Hass et al., 1993, Ebel et al., 1997) which the author is most familiar with. It is not intended to dwell on the characterization and comparison of different models or modules. There are various publications to which the interested reader may refer (e.g. Russel and Dennis, 2000; Ebel, 2000; Dodge, 2000). Nevertheless, it is hoped that conclusions about changing models and alterations of the modelling process during the last one or two decades also reflect experiences of other modellers with other models and thus can be generalized to a certain degree.

The EURAD modelling project was started when emission of sulfur and acidification were still an issue of highest priority for environmental policy. Therefore, a chemistry transport model focusing on acidic components in the atmosphere was chosen as the core model of the EURAD system. It was the Regional Acid Deposition Model (RADM; Chang et al., 1987, improved chemical mechanism RACM by Stockwell et al., 1990) which was adjusted to European conditions and has gradually been transformed to the so–called EURAD–CTM (EURAD Chemistry Transport Model) and further extended to more comprehensive versions (e.g. CTM2, Hass 1991). Yet due to successful reduction of sulfur emission, a dramatic increase in photo-oxidant levels during summer smog episodes and the public awareness of this change of air quality problems the focus of the model and simulations soon had to move from SO_2 to O_3. A similar modelling strategy as adopted by EURAD for the larger meso–scale was followed by the so–called TADAP project with ADOM (Venkatram et al., 1988) as the core model. There were attempts to organize closer cooperation between these and other regional model activities in the framework of the first European environmental research project EUROTRAC. Unfortunately, their success was rather limited. Yet for the EURAD project strongly involved in EUROTRAC it has to be emphasized that the challenges resulting from this involvement were extremely fruitful for the development of its model system. On the smaller meso–scale an approach similar to that of EURAD was chosen for the KAMM/DRAIS air pollution model system (Nester et al., 1995). The regional modelling initiative in EUROTRAC was successful with initiating and intensifying emission research and modelling for advanced numerical simulations on a European scale (Friedrich, 1997). It also paved the way for cooperative air quality modelling on local and urban scales in the framework of EUROTRAC (Moussiopoulos, 1995).

2. DESIGN OF MODEL AND MODELLING CONCEPT

The EURAD system consists of three models treating chemistry and transport (EURAD-CTM), meteorology (MM5, Grell et al., 1994) and emissions (EURAD Emission Model, EEM; Memmesheimer et al., 1991). It is an Eulerian multilayer gridpoint model system for meso-scale applications. Depending on the problem chemistry and meteorology can be integrated simultaneously or sequentially. The usual mode of application is off-line calculation of chemistry and transport. The horizontal extension depends on the horizontal resolution (Δx) wanted (European scale, Δx

about 50 km; local scale, Δx not less than 1 km). Sequential nesting is possible and now used in most applications. 100 hPa is usually chosen as the upper boundary. It has been extended to 10 hPa for simulations including the tropopause region. More detailed descriptions of the model can be found elsewhere (e.g. Hass et al., 1993; Jakobs et al., 1995). In the context of this paper it is more interesting and adequate to review some basic considerations governing the model design.

The basic philosophy of the design of the EURAD system was that it should be an as complete as possible numerical representation of the environmental system on a regional scale. The EURAD project followed the idea of Earth system analysis (Schellnhuber and Wenzel, 1998) for its atmospheric compartment before this term was coined by modern geoscience. As a consequence one had to go to complexity instead of simplicity. From the scientific view it is clear that the neglect or simplification of processes in the simulation of a non–linear system like the atmospheric environment is always dangerous. From the view of computational science it is obvious that computer and software performance will still considerably grow in the future. Therefore, it would be inexcusable not to aim at an as complete and reliable as possible virtual realization of the atmospheric environmental system through exploitation of fast growing computational power.

The integral view of the atmospheric environment of the EURAD project required to put equal weight on the analysis arid development of the chemical transport and meteorological models. So the aim was not to built new models but to design an interactive dynamical and chemical system with the help of leading experts from both fields. (Looking back there was great excitement in this collaboration. And I want to acknowledge enthusiastically that EURAD considerably gained from friendly help and critical perturbations provided by many colleagues.)

Two decades ago it was not very common (though not completely new) to treat chemical and dynamical simulations with the same weight in the same project. Several CTMs followed the idea that one could treat meteorology simply as an input problem. Yet employing meteorological forecast models to generate this input, it did not last long to recognise that a model with perfect pressure pattern predictions would not necessarily provide good transport parameters. There were (and still are) problems with turbulence, clouds precipitation etc. On the other hand, transport parameterizations and calucations in CTMs, e.g. bounday layer effects, could gain a lot from advanced meteorological schemes. Furthermore, the combination of dynamical, chemical and also emission modelling provided a much higher degree of flexibility for scientific studies and practical applications. Studies of the impact of climate change and geographical conditions (particularly complex terrain) or of different levels of the troposphere up to the lower stratosphere (Ebel et al., 1991) became easier to design. And the range of essential sensitivity studies, for instance, about effects of clouds, fog, aerosols, biogenic emissions or land use changes, could advantageously be expanded. From the view of the integral treament of the atmosphere it was clear from the beginning on that not only global, but also regional modelling had to deal with aerosols, now being a high priority issue of environmental resarch after science has progressed and our views have changed. Yet there was a time when experimental capacities and interests were nearly totally absorbed by

photo–oxidants in regional air quality research such emphasis made it difficult, but not impossible, to find support for the development of modules adequately dealing with particulates in atmospheric and environmental models. Watching weather forecast and its improvement through data assimilation it was easy to conclude at a very early state of air quality modelling that it would also considerably profit from this method in future. The broad (though not yet general) acknowledgement of this concept as a useful feasable improvement of chemical transport simulation needed even more time than the aerosol case.

It is interesting to see that the former disadvantage of long integration times of complex models regarding their practical application to long-term assessment studies or operational air quality forecasts is gradually overcome by increasing computer performance (Jakobs et al., 2001).

The following sections are illustrating the above remarks with selected examples of EURAD system applications. The reader will note that EURAD always was a child of its time but sometimes a little bit special in choosing its playground.

3. EXPLORATION OF PROCESSES

The evaluation of the role of processes controlling the distribution of trace substances in the atmosphere is essential for scientific as well as practical reasons. In both cases they are needed to increase our understanding of cause–effect relationships and to find priorities, i.e. develop strategies, for optimal model development as well as environmental management. Process studies can be carried out in different ways. One of the most efficient methods is sensitivity analysis. Another one which requires larger efforts is process-oriented evaluation. Three examples of analyses concerned with the role of particular processes are addressed in this section.

Firstly, an aspect difficult to deal with but most fascinating for exploring the atmospheric chemistry–transport system is the interaction of processes, particularly with respect to possible non–linearities. Sensitivity studies of the impact of climate change on future air quality are, therefore, an interesting case of model application. For instance, climate trend will cause land type changes (e.g. a possible increase of desertification in Spain) and thus changes of boundary layer behaviour and biogenic emissions. Both will influence atmospheric chemistry. Yet land type changes may also be exptected as a direct consequence of population growth. Furthermore, one can think of scenarios where these direct changes have a larger regional effect on atmospheric composition than those indirectly induced by climate change making the analysis of climate trend effects by only observing air quality trends an impossible task. Models are needed to unravel multiple causes of identical effects.

Another illuminating example is the decisive role which subsidence of ozone containing air from the free troposphere plays for the ozone budget of the atmospheric boundary layer (ABL) during photo-smog episodes (Memmesheimer et al., 1997). It may be as efficient as chemical production regarding the contribution to accumulation of ozone in polluted regions. And chemistry appears to react on such influx becoming less productive with increasing ozone flux convergence. For the first

time this could be shown for a summer smog episode in Central Europe in 1990. The model results also show that vertical transport of ozone through convection during photo-smog episodes into the free troposphere is not very effective since it is counteracted by subsidence. Only at the end of such episodes caused by frontal systems boundary layer ozone can be mixed into upper layers in larger quantities. Of course, substances like SO_2 having no sources at higher levels will experience a significant loss in the ABL due to vertical mixing and advection under the same conditions when the ozone budget is growing through this process.

Atmospheric aerosol offers a third example of possible process interactions. Its complex role for air quemistry and transport is not yet completely understood. Yet regarding air pollution simulations, there have been early suspicions and hints of its relevance though they were ignored or set very low priority for quite a while in European regional air quality research. Implementing a simple mechanism for secondary anorganic aerosol formation in EURAD (Kötz, 1991) it became evident that long-range transport and deposition of nitrogen compounds could more realistically be simulated in several cases (Ackermann et al., 1995). More comprehensive model studies of aerosol formation, transport and effects are needed and going on with the aim to support applied air quality analyses and programmes. In this respect, model development is following practical needs to a great extent.

4. EXPLORATION OF EPISODES AND SEQUENTIAL NESTING

One of the first cases in which the EURAD project became involved was the accident of the nuclear power plant in Chernobyl. Other episodes were focusing on periods and areas which were of special interest to environmental agencies in the framework of assessment studies. The selection of quite a large number of cases was motivated by the involvement in ongoing field experiment or availability of particular atmospheric data for model evaluation. First applications were mainly concerned with the problem of long-range transport of pollutants of different kind in Europe. Small meso–scale aspects were delt with in collaboration with other atmospheric modellers and models (Borrego et al., 1995; Moussiopoulos, 1995; Nester et al., 1995). Yet the recognition of strong coupling of scales, the demand for higher resolution studies motivated by environmental assessment and a growing number of small meso–scale and local field experiments (e.g. TRACT: Fiedler and Borrell, 2000; BERLIOZ: Corsmeier et al., 2001), the need for consistent boundary conditions for urban and local models and the availability of growing computational power finally lead to the installation of a sequential nesting option in EURAD (Jakobs et al., 1995). The increase of information through application of this method is illustrated in Fig. 1 derived from a simulation of a photo-smog episode in August 1993 in Central Europe (Kessler et al., 2001). Using sequential nesting the resolution is increased from 27 km (Central Europe and UK) to 3 km (State of Northrhine-Westfalia). The growth of information about the spatial distribution of pollutants with increasing resolution is obvious. It is also evident from the map of NO_x emissions that the price one has to pay is more detailed input data.

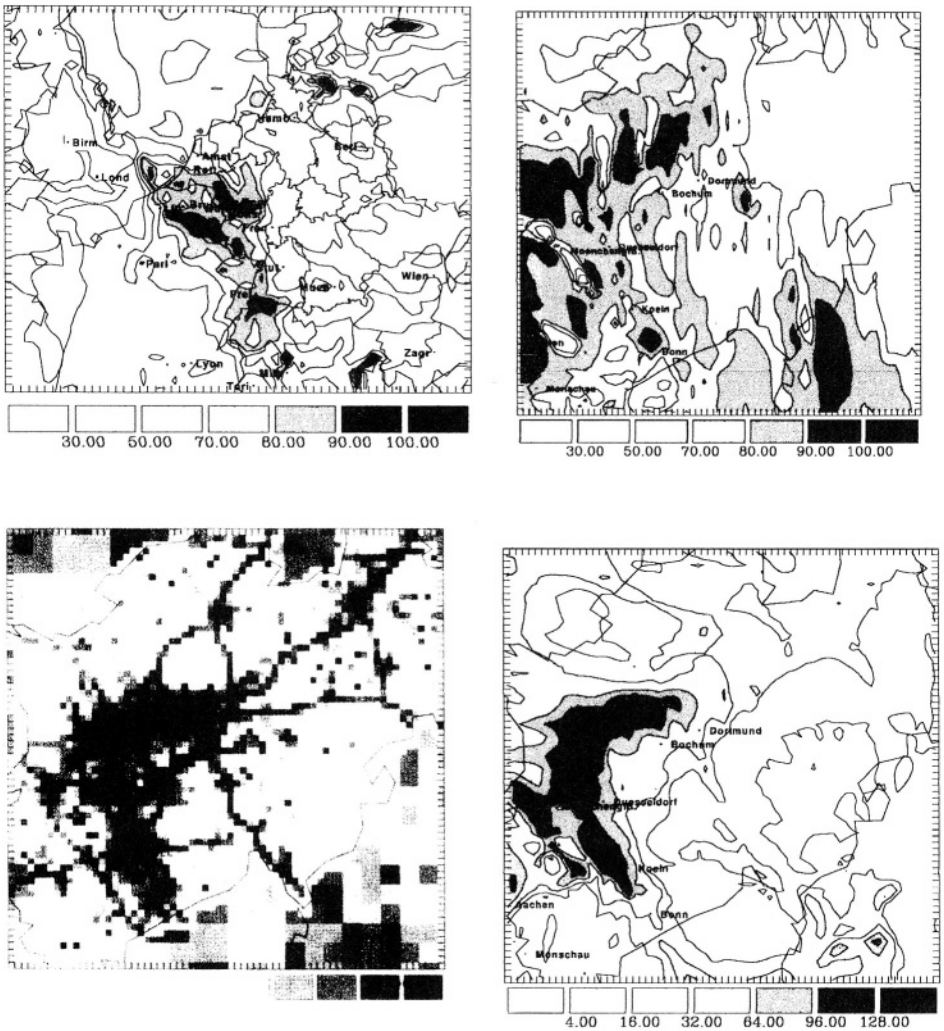

Figure 1: Simulation of a photo-smog episode in summer 1997 using the EURAD system. Upper left panel: Calculated near-surface mixing ratios of ozone (in ppbV), 13 August 1997, 14 UTC, coarse resolution (27 km). Upper right: Same as upper left, for Northrhine-Westfalia with fine resolution (3 km), nested calculation. Lower left: Highly resolved NO_x-emissions (kg/day as NO_2) for the 3 km x 3 km grid. Lower right: Resulting near-surface mixing ratios of NO_x (ppbV) on 13 August 1997, 6 UTC. After Kessler et al., 2001.

This is still a fundamental obstacle to efficient refinement of the simulations. Proceeding to still smaller scales requires explicit calculations of meteorological processes which are parameterized for calculations with coarser resolution. To achieve this EURAD has been expanded by inclusion of a high resolution meteorological driver for local applications (CARLOS system, Brücher et al. 2000, Kessler et al., 2001).

5. EXPLORATION OF ATMOSPHERIC COMPARTMENTS

Feeling committed to an integral view of the atmosphere the application of EURAD has been expanded beyond its main focus, namely the polluted ABL. The modular and multi-layer design of the parent models of EURAD, i.e. RADM and MM5, provided an excellent basis for this aspect of research and application. The conviction was that an advanced tool of computational science like EURAD had to be tried out on less safe grounds where little or no guiding laboratory or field experiments have been available (e.g. near the tropopause) or where the validity of certain model assumptions still had to be tested (e.g. over mountainous terrain). Therefore, the whole system or parts of it were used to look into problems like the Kuwait oil fires during the Gulf war, regional effects of layered and convective clouds in the free troposphere or the behaviour of transport and chemistry in the tropopause region. Two examples are briefly mentioned in this section.

An exciting and quite successful application of the EURAD system was the study of tracer transport over Alpine regions (Seibert et al.). One of the major problems under such extreme conditions is the handling of ABL and free troposphere interactions in the dynamic as well as chemical part of the system. Again, cooperation with experimentalists and data analysts was essential for the generation of sufficiently reliable model results.

The EURAD system provided the first successful meso-scale simulation of a stratospheric intrusion of ozone occuring over Europe (Ebel et al., 1991). The model to handle chemical transport processes in the tropopause region the model was redesigned for the treatment of the upper troposphere and lower stratosphere. RADM2 has been adjusted to the conditions of the tropopause region by inclusion of typical stratospheric gasphase and heterogeneous reactions essential at those heights. The result is CHEST2, a CHEmistry model for the lower Stratosphere and Troposphere, version 2 (Hendricks et al., 1999; 2000). This model version was intensively used in a project on air traffic emissions (Schumann et al., 1997) for the assessment of the regional impact of air traffic on the ozone budget around the tropopause focusing on the Northatlantic flight corridor, also taking into accout the impact of intrusions of stratospheric air into the troposphere. A series of numerical studies was carried out to explore the efficiency of stratosphere–tropsphere exchange at northern middle latitudes and to quantify its contribution to the tropospheric ozone budget in particular (Kowol–Santen et al., 2000; Ebel et al., 1996).

6. EXPLORATION OF VALIDITY, RELIABILITY AND FUTURE: CONCLUDING REMARKS

Expanding the range of application causes a problem of model evaluation. In the case of the EURAD system considerable efforts have been made to find out the validity of simulation results where it was possible. Yet it is obvious that a general confirmation of model validity and, therefore, reliability is difficult to achieve (Ebel et al., 2000). As a consequence, the efforts of model evaluation by comparison with real world data and also model intercomparison still have to be intensified.

Even though the increase of model complexity through addition of new physics and chemistry may cause a problem of general accuracy on short terms this way is necessary to bring CTMs closer to reality. This is clearly evident for the simulation of atmospheric aerosols and their effects, particularly, when its organic fraction is taken into account (Schell et al., 2001).

Future promising directions of model development and application for CTMs in general and EURAD in particular are their perfection with respect to the treatment of aerosols (being a consequence of the changing view of the relevance of particulate matter in the atmosphere), the exploitation of data assimilation methods (Elbern and Schmidt, 2001; being more and more recognised as a feasable and rewarding technique for CTMs, too) and operational air pollution forecasts which are becoming more frequent at present.

7. ACKNOWLEDGEMENTS

The author is greatly indebted to M. Memmesheimer, H.J. Jakobs, H. Elbern, H. Feldmann, G. Piekorz, Ch. Kessler and E. Friese from the Rhenish Institute for Environmental Research at the University of Cologne for kind support of this paper. He gratefully acknowledges fruitful discussions with M. Kerschgens, W. Brücher and H. Kunz. Projects on which this study is based were financially supported by the Ministries of Research of the FRG and the State NRW (BMBF, MWF), the Umweltbundesamt (UBA), Berlin, and the Environmental Agency of NRW (LUA). Data have been provided by the University of Stuttgart (IER), EMEP, UBA and LUA (emissions) and the ECMWF (meteorology) via the German Weather Service (DWD).

8. REFERENCES

Ackermann, I.J., Hass, H., Memmesheimer, M., Ziegenbein, C. , Ebel, A., 1995, The parameterization of the sulfate–nitrate–ammonia aerosol system in the long–range transport model EURAD, *Meteor. Atmos. Phys.* 57, 101–114.

Borrego, C., Coutinho, M., Barros, N., 1995, Intercomparison of two meso–meteorological models applied to the Lisbon region, *Meteor. Atmos. Phys.* 57, 21–29.

Brücher, W., Kessler, Ch., Kerschgens, M., Ebel, A., 2000, Simulation of traffic induced air pollution on regional to local scale, *Atmos. Environm.* 27, 4675–4681.

Chang, J.S., Brost, R.A., Isaksen, I.S.A., Madronich, S., Middleton, P., Stockwell, W.R., Walcek, C.J., 1987, A three–dimensional Eulerian acid deposition model: physical

concepts and formulation, *J. Geophys. Res.* 92, 14681–14700.
Corsmeier, U., Kalthoff, N., Vogel, B., Hammer, M.-U., Fiedler, F., Kottmeier, Ch., Volz-Thomas, A., Konrad, S., Glaser, K., Neininger, B., Lehning, M., Jaeschke, W., Memmesheimer, M., Rappenglück, B., Jakobi, G., 2001, Ozone and PAN formation inside and outside of the Berlin plume – process analysis and numerical process simulation, *J. Atmos. Chem.,* in press.
Dodge, M.C., 2000, Chemical oxidant mechanisms for air quality modelling: critical review, *Atmos. Environm.* 34, 2103–2130.
Ebel, A., 2000, Chemical transfer and transport modelling, in: *Transport and Chemical Transformation of Pollutants in the Troposphere,* P. and P.M. Borrell, eds., Springer, Vol. 1, p. 85–128.
Ebel, A., Hass, H., Jakobs, H.J., Laube, M., Memmesheimer, M., Oberreuter, A., Geiß, H., Kuo, Y.-H., 1991, Simulation of ozone intrusion caused by a tropopause fold and cut–off low, *Atmos. Environm.,* 25A, 2131 – 2144.
Ebel, A., Elbern, H., Hendricks, J., Meyer, R., 1996, Stratosphere–troposphere exchange and its impact on the structure of the lower stratosphere, *J. Geomag. Geoelectr.,* 48, 135–144.
Ebel, A., Elbern, H., Hass, H., Jakobs, H.J., Memmesheimer, M., Laube, M., Oberreuter, A., Piekorz, G., 1997, Simulation of chemical transformation and transport of air pollutants with the model system EURAD, in: *Transport and Chemical Transformation of Pollutants in the Troposphere, P. Borrell et al., eds., Vol. 7: Tropospheric Modelling and Emission Estimation,* A. Ebel, R. Friedrich, H. Rodhe, eds., Springer Verlag, p. 27–45.
Ebel, A., Memmesheimer, M., Jakobs, H.J., Kessler, Ch., Piekorz, G., Feldmann, H., 2000, Reliability and validity of regional air pollution simulations, in: *Air Pollution VIII,* J.W.S. Longhurst, C.A. Brebbia and H. Power, eds., WITpress, Southampton, Boston, p. 12-30.
Elbern, H., Schmidt, H., 2001, Ozone episode analysis by four–dimensional variational chemistry data assimilationr, *J. Geophys. Res.* 106, 3569–3590.
Friedrich, R., 1997, GENEMIS: Assessment, improvement, and temporal and spatial disaggregation of European emission data, in: A. Ebel, R. Friedrich, H. Rodhe, eds., *Tropospheric Modelling and Emission Estimation,* Springer Verlag, Heidelberg, p. 181–214.
Grell, G., Dudhia, J., Staufer, D., 1994, A description of the fifth-generation Penn State/NCAR mesoscale model (MM5), *Technical Note NCAR/TN-398+STR,* National Center of Atmospheric Research, Boulder, Colorado.
Hass, H, 1991, Description of the EURAD Chemistry-Transport-Model Version 2 (CTM2), *Mitteilungen aus dem Institut für Geophysik und Meteorologie der Universitat zu Köln,* Nr. 83.
Hass, H., Ebel, A., Feldmann, H., Jakobs, H.J., Memmesheimer, M., 1993, Evaluation studies with a regional chemical transport model (EURAD) using air quality data from the EMEP monitoring network, *Atmos Environ.* 27A, 867–887.
Hendricks, J., Lippert, E., Petry, H., Ebel, A., 1999, Heteorogeneous reactions on and in sulfate aerosols: implications for the chemistry of the midlatitude tropopause region, *J. Geophys. Res.* 104, D5, 5531–5550.
Hendricks, J., Lippert, E., Petry, H., Ebel, A., 2000, Implications of subsonic aircraft NOx emissions for the chemistry of the lowermost stratosphere: Model studies on the role of bromine, *J. Geophys. Res.* 105, D5, 6745–6759.
Jakobs, H.J., Feldmann, H., Hass, H., Memmesheimer, M., 1995, The use of nested models for air pollution studies: an application of the EURAD model to a SANA episode. *J. Appl. Meteor.* 34, 6, 1301–1319.

Jakobs, H.J., Tilmes, S., Heidegger, A., Nester, K., Smiatek, G., 2001, Short–term ozone forecasting with a network model system during Summer 1999, *J. Atmos. Chem.,* in press.

Kessler, Ch., Brücher, W., Memmesheimer, M., Kerschgens, M., Ebel, A., 2001, Simulation of air pollution with nested models in Northrhine-Westfalia, *Atmos. Environ.* 35 Suppl: S3-S12.

Kötz, A., 1991, Bedeutung der Aerosole für den Ferntransport von Schadstoffen in der Troposphäre, *Mitteilungen aus dem Institut für Geophysik und Meteorologie der Universität zu Köln,* Nr. 81.

Kowol–Santen, J., Elbern, H., Ebel, A., 2000, Estimation of cross–tropopause air mass fluxes at midlatitudes: comparison of different numerical methods and meteorological situations, *Mon. Weather Rev.* 128, 4045–4057.

Memmesheimer, M., Tippke, J., Ebel, A., Hass, H., Jakobs, H.J., Laube, M., 1991, On the use of EMEP emission inventories for European scale air pollution modelling with the EURAD model, in: *EMEP workshop on Photooxidant Modelling for Long-Range Transport in Relation to Abatement Strategies, Berlin, 16.–19. April 1991,* p. 307–324.

Memmesheimer, M., Roemer, M., Ebel, A., 1997, Budget calculations for ozone and its precursors: seasonal and episodic features based on model simulations, *J. Atmos. Chem.* 28, p. 283–317.

Moussiopoulos, N., 1995, The EUMAC Zooming Model, a tool for local-to-regional air quality studies, *Meteor. Atmos. Phys.* 57, 115-134.

Nester, K., Panitz, H.J., Fiedler, F., 1995, Comparison of the DRAIS and EURAD model simulation of air pollution in a mesoscale area, *Meteor. Atmos. Phys.* 57, 135–158.

Russel, A., Dennis, R., 2000, NARSTO critical review of photochemical models and modeling, *Atmos. Environ.* 34, 2283–2324.

Seibert, P., Feldmann, H., Neininger, B., Bäumle, M., Trickl, Th., 2000, South foehn and ozone in the Eastern Alps - case study and climatological aspects, *Atmos. Environ.* 34, 1379–1394.

Schell, B., Ackermann, I.J., Hass, H., Binkowski, F.S., Ebel, A., 2001, Modeling the formation of secondary organic aerosol within a comprehensive air quality model system, *J. Geophys. Res.,* in press.

Schellnhuber, H.J., Wenzel, V., eds., 1998, *Earth System Analysis,* Springer Verlag, Berlin, Heidelberg.

Schumann, U., Chlond, A., Ebel, A., Kärcher, B., Pak, H., Schlager, H., Schmitt, A., Wendling, P. (eds), 1997, *Pollutants from Air Traffic – Results of Atmospheric Research 1992-1997,* Mitteilung 97–04, Deutsches Zentrum für Luft- und Raumfahrt e.V.

Stockwell, W.R., Kirchern, F., Kuhn, M., 1997, A new mechanism for regional atmospheric chemistry modelling, *J. Geophys. Res.* 102, D22, 25847–25879.

Venkatram, A., Karamanchandani, P.K., Misra, P.K., 1988, Testing a comprehensive acid deposition model, *Atmos. Environ.* 22, 737–747.

DISCUSSION

A. HANSEN — As an example of how increasing the complexity of a model can degrade its performance (as measured by point to grid cell comparisons) is the inclusion of clouds. Meteorological models cannot simulate precisely in time and space cloud fields such that actinic fluxes, soil moisture, temperature, etc. are not precisely simulated, although in a statistical sense the model may be performing adequately. How do you deal with this issue ?

A. EBEL — Obviously, the question is touching a rather crucial point of air quality modelling. Various attempts have been made with the aim to improve the model system (EURAD) with respect to performance of cloud and precipitation simulation (exploring, e. g., different parameterizations), but general solutions seem to be far away. It is emphasized that similar problems are encountered in cloud-free photo-oxidant simulations when local changes are controlled by subgrid processes to be parametrized in models. Various methods have been employed to cope with such problems of representativity and uncertainties of estimates of subgrid effects. These are sensitivity studies, model comparisons, adjustment of resolution (nesting) and evaluation studies in cases where suitable data have been available. It has also proven helpful to provide estimates of the range of reliability of simulated data.

T. HALENKA — In context of the models complexity and their “perfection”, could you estimate the impact of uncertainty in emission on the results of the modelling ?

A. EBEL — A large number of studies regarding the role of accuracy of emission estimates for the performance of air quality models can be found in the literature. The results differ in dependence of the scenarios investigated and vary with the chemical species used to evaluate the sensitivity of models to emission uncertainties. For instance, a comprehensive study employing the EURAD model system was recently conducted by B. Wickert (Berechnung anthropogener Emissionen in Deutschland fuer Ozonsimulationen; Modellentwicklung und Sensitivitaetsstudien, Thesis, University of Stuttgart, 2001). The analysis is focusing on ozone formation under conditions of NOx limitation. Such situation is characterized by higher sensitivity to NOx then to NMVOC emission changes. Differences up to 10% were found for spatially averaged ozone

mixing ratios in case of rather strong (and - in special cases - possible) deviations of emissions from a reference scenario.

G. SCHAYES — Data assimilation is important for short term modelling. The improvement degrades rapidly with time. The technique is thus useful for applied models. Is it also important for research models ?

A. EBEL — Formulation of improved initialization fields for chemical transport models is only one aspect of the application of data assimilation methods to air chemistry simulations. The degradation of the initial improvement with time (say, after 24 hours) can be overcome to a certain degree if one succeeds to implement parameters whose future development is known and which exert sufficient control on the simulated chemical species. Using the EURAD system it could be shown that anthropogenic and natural emissions fulfil this condition. Data assimilation is also a promising method to be used for research. In the case of air chemistry it can well be applied to the design of improved and consistent fields of reactive species, to the evaluation of reaction coefficients, to the design of observing systems and the evaluation of models. Refer to H. Elbern and H. Schmidt, 4D-var data assimilation and its numerical implications for case study analysis, accepted for publication in: IMA Series “Mathematics and Its Applications, Reactive Flow and Transport Phenomena”, issue on “Atmospheric Modeling”, Minneapolis, Minnesota, 2002.

DEVELOPMENT OF A REGIONAL MODEL FOR OZONE FORECASTING AND ACIDIC DEPOSITION MAPPING

Al Tang, Neville Reid, P.K. Misra[1]

1. INTRODUCTION

Simulation of atmospheric ozone and acid deposition has been done since the 1980's using comprehensive 3-D models, such as the Acid Deposition and Oxidant Model (ADOM), the Regional Acid Deposition Model (RADM), etc. These models include chemistry modules consisting of large numbers of chemical species and reactions, thus creating large uncertainties and computing overhead in their applications. For operational application of models, however, it is desirable to develop and use models which have reasonable skills in reproducing the observations, and yet do not require large computing overhead.

The Ontario Ministry of Environment has a need for operational application of photo-chemical and acid deposition models to forecast ozone levels in the atmosphere and produce acid deposition maps. Toward that end a model has been developed using the ADOM model, with the chemistry module replaced by the Graham Johnson scheme. This reduces uncertainties and computing time significantly, enabling the model to be run operationally.

The purpose of this paper is to demonstrate how this simplified model can be used, using a first level data assimilation technique to forecast ozone levels and produce acid deposition maps. The premise used in such model application is that a model serves as a better interpolation tool of observations than statistical techniques such as Kriging which

[1] Al Tang, Neville Reid, P.K. Misra, Ministry of Environment, 125 Resources Road, Etobicoke, Ontario, Canada M9P 3V6

Air Pollution Modeling and Its Application XV, Edited by
Borrego and Schayes, Kluwer Academic/Plenum Publishers, New York, 2002

are not based on atmospheric science.

Photochemical smog is produced by the action of sunlight on mixtures of nitrogen oxides and Reactive Organic Compounds (ROC), resulting in accumulation in the air of excessive concentrations of ozone gas. For evaluation of photochemical ozone, the application of air quality models is often limited by the existence of large uncertainties in the input data. Consequently the accuracy of model predications is often less than that required to determine confidently the impact of proposed emissions or to develop ozone strategies. To overcome these difficulties, Johnson (Johnson, G.M., 1984) simplified the chemical process of photochemical ozone formation using a set of generic reactions, which is called the Generic Reaction Set (GRS). He also developed the "Airtrak-Integrated Empirical Rate model (IER) method". This method provides an air quality assessment system which includes a predictive model of smog production that can be executed entirely on the basis of the measured chemical properties of the air. A description of the GRS is given in the following section.

1.1. Generic Reaction Set (GRS)

The GRS equation can be summarized as follows:

1. Radical production (RP) from photo-oxidation of reactive organic compound (ROC)
   $ROC + h\nu \rightarrow RP + ROC \qquad k_1 = 0.0067\, k_3\, f(T)$
   $f(T) = \exp(-1000 \cdot A \cdot (1/T - 1/316))$
   Where hv denotes sun light; T denotes temperature (in Kelvin); f(T) is a temperature function; A is a temperature coefficient determined from smog chamber studies and has value 4.7.
2. Oxidation of nitric oxide by radicals
   $RP + NO \rightarrow NO_2 \qquad k_2 = 3.58 \cdot 10^6 / T$
3. Photolysis of nitrogen dioxide to nitric oxide
   $NO_2 + h\nu \rightarrow NO + O_3$

```
for   0<ZA<47      k3 =  (4.23E-04+(1.09E-04/COS(ZA)))*SWF
for  47<ZA<64      k3 = 5.82E-04*SWF
for  64<ZA<90      k3 =(-0.997E-04+1.2E-03*(1-COS(ZA)))*SWF
for non of above  k3 = 0
 where ZA == ZENITH      SWF = SHORT WAVE FLUX  (W/M**2)
```

4. Nitric oxide-ozone titration reaction
   $NO + O_3 \rightarrow NO_2 \qquad k_4 = 9.24 \cdot 10^5\, T^{-1} \cdot E^{-1450/T}$
5. Radical pools sink through recombination to stable products
   $RP + RP \rightarrow 0.1\, SRP + 0.9\, RP + \alpha H_2O_2 \quad k_5 = 10200$
   $\alpha = \max[0.03, \exp(-0.0261(0.0067 * ROC/(NO+NO_2))]$
6. Sink for nitrogen dioxide to stable nitrates (both gaseous and nongaseous nitrates) and production of nitric acid
   $RP + NO_2 \rightarrow 0.1\, SN + 0.9\, HNO_3 \qquad k_6 = 240$

7. Production of nitric acid
   $ROC + O_3 + NO_2 \rightarrow HNO_3 + RP$ $k_7 = 0.1$
8. Production of sulfate
   $RP + SO_2 = SO_4$ $k_8 = 3$

1.2. Incorporate GRS into ADOM model

Estimating ozone using GRS equations requires the ROC emissions; they were estimated from the emission of individual reactive organic species. To incorporate the GRS into ADOM, it was necessary to: (1) drop the chemical species and their related chemical reactions; (2) edit the model source code accordingly; (3) debug the model; (4) fine tune the chemical reaction coefficients; (5) real time simulation / fine tune the modeling processes.

2. CREATION OF THE VOC EMISSION FILES

There are 18 species in the Area and Point sources emission data file. They are SO2, SO4, NO, NO2, C3H8, ALKA, ETHE, ALKE, TOLU, AROM, HCHO, ALD2, MEK, CRES, NH3, MONO, DUST, ISOP. The VOC species in the about list are not individual species; they represent a combined organic species with similar chemistry. For example, ALKE represents the C3 Alkane and Benzene compound class, which includes Propane, Cyclopropane, and Benzene.

In ADS model, 11 of the VOC species (ETHE, AROM, ISOP, ALKE, HCHO, TOLU, ALKA, ALD2, CRES, C3H8, MEK) were used to estimate the VOC emission using a contribution factor based on those used in TAPM (The air pollution Model) of CSIRO Atomospheric Research (Hurley, 1999). The VOC emission rate (Q_{voc}) from VOC emission sources, which consist of more then one type of VOC species is estimated by the following equation:

$$Q_{voc} = \sum 14 * Q_i * Cn_i * R_i / Mw_i$$

where Q_i is the emission rate of an individual VOC species, R_i is the VOC reactivity, Cn_i and Mw_i are the carbon number and molecular weight of individual VOC, respectively.

3. **WET PHASE REACTION SET**

The reactions related to ROOH were dropped from the original wet chemistry scheme, since it is not modelled. The aqueous and gas/particles species are listed as follows:

AQUEOUS	GAS/PART.
1. HSO3−	1. SO2G
2. H2O2	2. HPXG
3. SO4=	3. H2SO4 = SO4P1
4. NO3−	4. NH4HSO4 = SO4P2
5. NH4+	5. (NH4)2SO4 = S04P3
6. CAT1	6. HNO3G
7. HCO3−	7. NH3G
8. H+	8. NH4NO3 = NNO3P
9. OH−	9. DUST
10. FEMN	10. O3G
11. O3	11. CO2G (CONSTANT)
12. H2OA (CONSTANT)	

The reactions related to the above species are:

```
 1.      1.SO4P1            -->    B1*SO4= +   B3*H+
 2.      1.SO2G             -->    B1*HSO3 +   B1*H+
 3.      1.HSO3 +  1.H+     -->    B2*SO2G
 4.      1.O3G              -->    B1*O3
 5.      1.O3               -->    B2*O3G
 6.      1.HPXG             -->    B1*H2O2
 7.      1.H2O2             -->    B2*HPXG
 8.      1.HNO3             -->    B1*NO3- +   B1*H+
 9.      1.NO3- +  1.H+     -->    B2*HNO3
10.      1.NH3G             -->    B1*NH4+ +   B1*OH-
11.      1.NH4+ +  1.OH-    -->    B2*NH3G
12.      1.DUST             -->    B5*FEMN +   B4*HCO3 + B4*CAT1+
13.      1.CO2G             -->    B1*HCO3 +   B1*H+
14.      1.HCO3 +  1.H+     -->    B2*CO2G
15.      1.H+   +  1.OH-    -->   1.00H2OA
16.      1.H2OA             -->   1.00H+   +  1.00OH-
17.      1.HSO3 +  1.O3     -->   1.00SO4= +  1.00H+
18.      1.HSO3 +  1.H2O2   -->   1.00SO4= +  1.00H+
19.      1.HSO3     (FEMN)  -->   1.00SO4= +  1.00H+
20.      1.SO4P2            -->    B1*SO4= +   B1*H+ + B1*NH4+
21.      1.SO4P3            -->    B1*SO4= + B3*NH4+
22.      1.NNO3P            -->    B1*NO3- + B1*NH4+
```

4. MODEL VALIDATION

Due to the page limitation, no figures will be presented here; they will be presented at the conference. The model was run for six days from 0000GMT August 1, 1988 to 0000GMT August 6, 1988. The input data includes geophysical data, surface meteorological data, vertical meteorological data, area source emission data, point source emission data, and nature emission data. For the first hour, a fixed initial concentration is used for each layer. From the second hour and there after, the previously simulated concentration values were used as input. The model has 33 by 33 grids (127km grid size) and twelve layers over the North America (origin at 95W 26N).

4.1. Ozone

To claim that a model is working, it must prove that it is able to simulate both the temporal and spatial variation of the chemical species. Since this is a preliminary study, long term simulation has not been done. For temporal variation, we will only compare the model output with the hourly observed chemical concentrations in this report. For the spatial variation we will compare the model output with the contour of the observed chemical species. We will also compare the modeled maximum concentration with the observed values.

The hourly data used for validating the Ozone simulation is from the Ozone Transport Assessment Group (OTAG) (downloaded from http: //capita.wustl.edu/otag). A description of this data set will not be given here. This site also provides the Voyager software for data browsing and presentation. By comparing the modelled 24-hour ozone profile with the OTAG data, the following conclusion can be drawn:

- basically, the modelled 24-hour ozone profiles agree with the observed ones,
- the modeled daily maximum ozone concentrations agree well with the observed concentration in rural area,
- for urban areas, the modelled daily maximum ozone concentration is half of the observed,

4.2. Sulfate and Nitrate wet deposition

The data used for validation of wet deposition of sulfate and nitrate is from the Eulerian Model Evaluation and Field Study (June 1, 1988 to May 31, 1990). Due to the non-homogeneous nature of the precipitation event, we know that it is not proper to compare the modelled output for a grid size of 127 km to point measurement. However, a working model should be able to simulate the wet deposition over the period of a precipitation system. Hence, we compare the modelled six-day total wet deposition with the observed data.

By comparing the modelled nitrate wet deposition with the observed data the following conclusion can be drawn:

- modelled nitrate wet depositions agree well with the observed data over the area without heavy point sources,
- observed nitrate deposition is about three to six times the modelled nitrate deposition over the Ohio valley,
- observed nitrate deposition is about two times that of the modelled over the area which is in the downwind direction of the Ohio valley,
- modelled sulfate wet deposition is about 4.6 times higher than the observed over the areas without heavy point sources,
- observed sulfate deposition is about twice that of the modelled over the Ohio valley,
- modelled sulfate deposition is about twice that of the observed over most of the area which is in downwind of the Ohio valley.

5. CONCLUSION

Results of this study indicate that the simple model is sufficient for modelling Ozone concentration and sulfate and nitrate wet deposition. There is systematic bias between the modelled values and observed data, this indicates that it is possible to find adjusting factors applicable to a few regions if we would like to use model as a wet deposition estimation tool. However, further study is needed, for much longer periods, in order to test the validity of using the model to estimate the wet deposition.

6. REFERENCES

G. M. Johnson, A simple model for predicting the ozone concentration of ambient air, *Proceedings of the 8th International Clean Air and Environment Conference,* New Zealand, 1984, Clean Air Society of Australia & New Zealand

P. J. Hurley, The Air Pollution Model (TAPM) Version 1: Technical Description and Examples, CSIRO Atmospheric Research, Private Bag 1, Aspendale, Vic 3195, Australia, 1999

DISCUSSION

A. HANSEN Since the results you showed for urban ozone were over a factor of two different from observations, would you even consider using this simplified model for urban ozone policy analysis studies ?

A. TANG This model has grid sizes of approximately 127 km, hence the model results should be compared with averaged ozone concentrations observed over 127 km by 127 km grids. Since I don't have observed ozone data to calculate grid-cell average concentrations; I presented the point to point comparison. Results of comparisons showed that the modelled results compared well with the ozone concentrations that were observed in rural area, but under predict the observed city ozone concentrations. This is reasonable since grid-cell-average ozone concentrations are expected to be much lower than the observed city ozone concentrations and more closer to the rural observations. The well comparison over rural area indicated that the model performed well as expected and the simplified chemistry set can be used to make the model more efficient (this is one of the purposes of this paper). This is a preliminary study on developing a simplified chemistry model using the existing regional model (ADOM). Further studies will be carried out on one year simulation of acidic deposition and on simulation of ozone concentrations using small grid size.

It is important to apply the modelled results properly; It will be foolish to use a regional model to predict urban ozone concentrations especially when near large cities. I have no intention to use a regional model to predict urban ozone concentration. Sorry for miss-leading someone on my purpose of the model.

This page intentionally left blank

MODELLING OF ATMOSPHERIC RADIOACTIVE AEROSOL DYNAMICS AND DEPOSITION

Alexander Baklanov and Artashes Aloyan*

1. INTRODUCTION

Radionuclides are released into the atmosphere in form of gases or aerosols with a broad range of particle sizes. Even significant for long-range transport particles vary in size in the range of 0.01-60 μm. However, most models of air pollution transport do not consider effects of nuclide particle size and the aerosol transformation.

The physical and chemical form of a nuclide influences its behaviour in the atmosphere and may itself be subject to transformation during atmospheric transport. After the Chernobyl accident there were two distinct components of the release: the first, in nature similar to particles of fuel; and the second, due to volatilisation and condensation of nuclides. The radionuclides might be emitted in various forms, including:

- inert gases, lost from the atmosphere only by decay and producing daughter nuclides;
- reactive species such as elemental I-131 which may interact physically or chemically with other species, e.g., by absorption on the surface of ambient aerosols (SO_4 and other);
- as small nuclei-mode particles (~0.01 μm), which interact with ambient aerosols;
- as attached to coarse fuel particles which sediment out rapidly (e.g., the actinides and more refractory nuclides from Chernobyl).

This paper focuses on an analysis of radionuclide particle sizes in accidental releases, the simulation of the dynamics of atmospheric radioactive aerosols and of different processes, including the nucleation, condensation and coagulation of radionuclides and the removal processes by dry and wet deposition of different-size particles.

*Alexander Baklanov, Danish Meteorological Institute (DMI), Lyngbyvej 100, DK-2100 Copenhagen Denmark. Artashes Aloyan, Institute of Numerical Mathematics (INM) of RAN, Gubkma str. 8, RUS-117930 Moscow Russia

Air Pollution Modeling and Its Application XV, Edited by
Borrego and Schayes, Kluwer Academic/Plenum Publishers, New York, 2002

2. CHARACTERISTICS OF ACCIDENTAL RADIOACTIVE PARTICLES

A nuclear accidental release includes a large number of radioactive isotopes (it can be more than 350). For an analysis of the environment and human health consequences we will focus on simulation of the atmospheric transport, transformation and deposition of the main dose-contributing nuclides. The forms (gases, aerosol particles), size characteristics (distribution of the particle size, the activity median aerodynamic diameter (AMAD) and values of the geometric standard deviation), the half live, reference values of the dry deposition velocity, v_d, for the main dose-contributing nuclides, based mostly on the Chernobyl data from European countries, were analysed by Baklanov & Sørensen (2001) and briefly presented in Table 1.

Table 1. Characteristics of the main dose-contributing nuclides, based on different published data.

Nuclide	Half live, hrs	AMAD, μm	Reference v_d, cm/s**	Geometric standard deviation, σ_g
Cs-137	2.628 e05	0.68	0.05-0.1	1.8-2.5
Cs-134	1.805 e04	0.59	0.12	2-2.5
I-131	1.93 e02	gas/0.48	1.5/0.15	3-4
Te-132	7.82 e01	0.81	0.3	1.5-2.5
I-133	2.08 e01	gas/0.6	1.5/0.15	3-4
Ba-140	3.048 e02	0.45	0.9	
Sr-90	2.549 e05	2.5	2 (?)	2-2.5
Ru-103	9.459 e02	0.65	0.5	1.4-2.5
Pu-238	7.683 e05	4.3	2.0	2
Pu-239	2.111 e08	4.3	2.0	2.1
Sr-89	1.212 e03	2.5	2 (?)	

The particle size is one of the important parameters of the radioactive aerosols. It varies very much from nuclide to nuclide, and each nuclide can have a very broad spectrum of particle sizes. For example, accidental releases from nuclear power plants (NPPs) can have different particle sizes ranging from 0.01 up to 60 μm at distances up to hundreds of kilometres from the source. In general, the atmospheric aerosol particle size distribution has three modes: the nuclei mode (< 0.05 μm), the accumulation mode (0.05-2 μm) and the coarse or mechanically generated mode (> 2 μm). Accidental nuclides can be released as vapour, with subsequent rapid condensation to form aerosol in the nuclei mode. Since nuclei mode aerosol is inherently unstable with respect to growth mechanisms such as coagulation and vapour condensation, there is a tendency for growth, leading to formation of accumulation mode particles (Wagner & Harrison, 1993).

It is natural that the processes of formation and, consequently, the structure, content and other aerosol particle characteristics generated by nuclear accidents differ e.g. from those by nuclear bomb tests. This is due to different physical and chemical conditions of the particle generation, as well as due to differences in the materials of the particles (Crandall et al., 1973; Izrael, 1996). For example, Cs-137 aerosols from Chernobyl measured in European countries had an activity median aerodynamic diameter (AMAD) equal to ~1.1 μm. However, AMAD of Cs-137 from a fuel reprocessing plant was 3 μm (Dorrian, 1997). Besides, the aerosol size distribution may change with the height, time and, correspondingly, with a distance from the release source.

There only limited number of measured particle size distributions exists, so following the recommendations of authors of experimental studies (see an overview by Dorrian

(1997)), we will assume the log-normal distribution of the radionuclide particle size. The AMAD and the geometric standard deviation can be used for calculation of the log-normal distribution of the nuclide particles. Besides, the particle density, ρ_p, is important for the deposition and it can vary for different nuclides, e.g. for Cs-137, ρ_p = 1.88 g/cm^3, but 4.93 g/cm^3 for particles of I-131. Radioactive aerosols differ from other aerosols in that they are capable of charging themselves directly by the emission of charged particles.

3. AEROSOL TRANSFORMATION PROCESSES

In general, the processes of nucleation, condensation and coagulation can play an important role in the formation and transformation of atmospheric radioactive aerosols.

3.1 Nucleation and condensation processes

Some nuclides can transform from a gaseous to particulate form. For example, it is very important for I-131, wich can be released in different forms (molecular, organic and particles). The gaseous form of I-131 usually dominates in releases (more than 90 %). However, the gaseous iodine has a significant tendency to become attached to other particles (usually to SO_4 particles). This is not a one-way process, there is a strong tendency for the effective deposition velocity to decrease with time.

Iodine nuclei mode particles are the product of vapour condensation and gas-to-particle conversion processes. The last transformations happen due to the nucleation processes as well. Nucleation is the formation of a new stable embryonic particle or droplet which is capable of growth by condensation. The nucleation and condensation processes can be simulated by corresponding kinetic equations (e.g. Jacobson, 1999). However, this is very difficult to realise for iodines, because both the homogeneous and heterogeneous (with other existing ambient aerosol particles) nucleations are important, as well as chemical processes. So, as a first approximation, this can be described in the model by a depletion equation (Maryon et al., 1992):

$$\frac{dc}{dt} = \left(\frac{v_{dg}}{h} + \frac{1}{\tau}\right)c + \frac{c_g(0)}{\tau}\exp\left(-\frac{v_{dp}}{h}t\right), \qquad (1)$$

where c and c_g are concentrations of the particle and gas phases, v_{dg} and v_{dp} are the gaseous and particulate deposition velocities, h is the mixing height and τ is a timescale estimated to 47 days from the gaseous/particulate ratio measured after Chernobyl.

However, for main modelling items the prediction time is much shorter (up to 5-7 days), therefore it is possible to simulate the deposition of iodines with the time-independent deposition velocities, but separately for the gaseous and particulate forms. In this case we have to know the I-131 releases for each form. For the gaseous forms of I-131 the reference values for v_{dg} are 1.5 cm/s for the elemental iodine and 0.015 cm/s for the organic bound iodine. For the particle form v_{dp} is correspondent to the dry deposition velocity for SO_4 and equal to ~ 0.15 cm/s.

3.2 Coagulation processes

The aerosol transport is always accompanied with particle growth processes. When the particle concentration is high and the humidity of the atmosphere is sufficiently low, the particle growth by coagulation alone should be accounted for. The Smoluchowski equation describes the coagulation ageing of the particle mass spectrum:

$$\frac{\partial\varphi(g)}{\partial t} = \frac{1}{2}\int_0^g \tilde{K}(g,g_1)\varphi(g-g_1)\varphi(g_1)dg_1 - \varphi(g)\int_0^\infty \tilde{K}(g,g_1)\varphi(g_1)dg_1 + I(g,t), \qquad (2)$$

where g_1 is the integration variable (mass); $\varphi(g)$ is the concentration of particles with masses ranging from g to $g+dg$; $\tilde{K}(x,y)$ is the collision rate of particles of masses x and y; $I(g,t)$ is the formation rate of new particles of mass g. This term is added to the right hand side of the aerosol transport equation.

The problem of the aerosol transformation is solved on the set of non-negative functions. Aerosol particles, emitted in an accidental release, are much smaller or comparable to the mean free path of the molecules in the carrier gas. Then the collision rate $\tilde{K}(x,y)$ has the form (Suck & Brock, 1979): $\tilde{K}(x,y) = A\left(x^{1/3} + y^{1/3}\right)\left(D_x + D_y\right)\beta_{xy}$ where D_x is the diffusion coefficient for a particle of mass x:

$$D_x = \frac{k_B T}{6\pi\eta R_x}\left[1 + Kn_x\left(A + Q\exp\left(-\frac{b_3}{Kn_x}\right)\right)\right], \qquad (3)$$

with k_B being the Boltzmann constant and b_3, A, Q - the empirical constants: A =1.25, Q =0.4, b_3 =1.1. The correction factor β_{xy} is given by Suck & Brock (1979):

$$\beta_{xy} = \left(\frac{R_x + R_y}{R_x + R_y + d_{xy}} + \frac{4\left(D_x + D_y\right)}{\left(V_x^2 + V_y^2\right)^{1/2}\left(R_x + R_y\right)}\right)^{-1} \qquad (4)$$

$$Kn_x = \frac{l_x}{R_x}; \qquad d_{xy} = \left(d_x^2 + d_y^2\right)^{\frac{1}{2}}; \qquad d_x = \frac{1}{6R_x l_x}\left(\left(2R_x + l_x\right)^3 - \left(4R_x^2 + l_x^2\right)^{\frac{3}{2}}\right) - 2R_x;$$

$$l_x = \frac{8D_x}{\pi V_x}; \qquad V_x = \left(\frac{8kT}{\pi x}\right)^{\frac{1}{2}}; \qquad x = \frac{4}{3}\pi R_x^3\rho.$$

Here D_x is the diffusion coefficient of particle i with radius R_x; T is temperature; l_x and V_x denote mean free path and mean particle velocity, respectively; x is particle mass; ρ is particle density; and η denotes the viscosity of the air.

4. DEPOSITION OF AEROSOL PARTICLES

Processes removing radionuclides from the atmosphere, and the interaction of nuclides with the Earth's surface, are very important for modelling of consequences after nuclear accidents and depend on the nuclide particle size and properties.

4.1 Dry deposition

The dry deposition velocity depends on many characteristics of the surface, surface layer and parameters of deposited particles including their size (Slinn, 1977; McManon & Denison, 1979). Therefore, it is reasonable to define the dry deposition velocity as the gravitational settling velocity, v_g, and the inverse of a sum of resistances (Seinfeld, 1986):

$$v_d = \left(r_a + r_b + r_a r_b v_g\right)^{-1} + v_g, \qquad (5)$$

where r_a is the aerodynamic resistance, which describes the turbulent transfer of the contaminant to the near-surface layer, r_b is the resistance to penetration across the atmospheric laminar sublayer (with domination of molecular transport) by convection, diffusion or inertial processes. For deposition of gases the resistance, associated with direct pollutant-surface interaction, r_c, is important as well.

For heavy particles (radius $r_p > 1$ μm), gravitational settling strongly affects the process of deposition to the surface. For particle diameters less than ~ 3.5 μm (for which the airflow around the failing particle can be considered laminar) the gravitational settling velocity v_g, is given by Stokes law (Hinds, 1982) with the Cunningham correction factor for small particles ($r_p < 0.5$ μm).

For larger particles, Stokes law is not valid, and in the turbulent regime we will use an iterative procedure to solve the equation for the terminal settling velocity according to Näslund & Thaning (1991). However, the simulation tests show that the turbulent regime of gravitational settling considerably affects the concentration and deposition fields only for quite large particles ($r_p > 10$-15 μm). Such particles play an important role after accidental radioactive releases for local-scale effects. Thus, the iterative procedure for the terminal settling velocity is more important for local-scale models and does not considerably affect the long-range transport. For several specific problems, like long-range transport of hot particles after a very severe nuclear accident (similar to Chernobyl) or after atmospheric nuclear bomb explosions, the correction of the terminal settling velocity is important.

The aerodynamic resistance r_a depends on meteorological parameters, such as wind speed, atmospheric stability and surface roughness, and can be derived (Wesely, 1989): $r_a = \left(\ln\left(z_s/z_0\right) - \psi_c\right)/\kappa u_*$, where ψ_c is a stability function (Voldner et al., 1986): $\psi_c = -5z/L$ for $z/L > 0$, and $\psi_c = \exp\left[0.598 + 0.390\ln\left(-z/L\right) - 0.09\left(\ln\left(-z/L\right)\right)^2\right]$ for $z/L < 0$. Here L is the Monin-Obuhkov length, z_s - the height of the first reference level, z_0 - the roughness height, κ - von Karman's constant, and u_* - the friction velocity. As it is seen from Eqs. above, the aerodynamic resistance, r_a, in general will be lower during day time and higher during night time.

The surface layer resistance for particles, r_b, can be expressed as a function of the numbers of Schmidt: $Sc = \nu/D$, and Stokes: $St = v_g u_*^2/g\nu$: $r_b = \left(Sc^{-2/3} + 10^{-3/St}\right)^{-1} u_*^{-1}$, where ν is the kinematic viscosity of the air, D - the Brownian diffusivity of particles, $D = k_B TC / 12\pi\mu r_p$, r_p - the particle radius, C - the Cunningham correction factor, T - the temperature, k_B - the Boltzmann constant, and μ - the dynamic viscosity coefficient. Thus, r_b gives an effect of the particle size on the dry deposition intensity due to the Brownian diffusivity: decreasing dry deposition velocity with increasing particle size. For large

particles the gravitational settling gives an increasing dry deposition. Since the dry deposition velocity and surface resistances depend on the type of surface, a classification of the land/sea surface should be used (Baklanov & Sørensen, 2001).

4.2 Wet deposition

Usually the wet deposition is treated in a standard way with a washout coefficient for below-cloud scavenging and a rainout coefficient for in-cloud scavenging (Seinfeld & Pandis, 1998). The scavenging coefficient $\Lambda(r, x_i, t)$ includes the washout and rainout coefficients, but their mechanisms are spatially separated.

The washout coefficient for aerosol particles, as it was shown by many authors (e.g. Hales 1986; Wang & Pruppacher, 1977; Radke et al., 1977; Hicks, 1976), strongly depends on the particle size (the so-called 'Greenfield gap'). According to experimental data (Tschiersch et al., 1995; Radke et al., 1977), the washout coefficient for particles of ~ 0.4 or 1.2 μm size is two orders of magnitude smaller than for particles larger than 4 μm.

Following Baklanov & Sørensen (2001) the washout coefficient, Λ' (sec^{-1}) for aerosol particles can be expressed by two different formulation:

1) as an empirical function of particle radius r (μm) and rainrate q (mm/h):

$$\begin{aligned} &\Lambda'(r,q) = a_0 q^{0.79}, && r < 1.4\ \mu m \\ &\Lambda'(r,q) = (b_0 + b_1 r + b_2 r^2 + b_3 r^3) f(q), && 1.4\ \mu m < r < 10\ \mu m \\ &\Lambda'(r,q) = f(q), && r > 10\ \mu m \end{aligned} \qquad (6)$$

where $f(q) = a_1 q + a_2 q^2$, $a_0 = 8.4 \cdot 10^{-5}$, $a_1 = 2.7 \cdot 10^{-4}$, $a_2 = -3.618 \cdot 10^{-6}$, $b_0 = -0.1483$, $b_1 = 0.3220133$, $b_2 = -3.0062 \cdot 10^{-2}$, and $b_3 = 9.34458 \cdot 10^{-4}$.

2) as an expression including Slinn's formulae for the Brownian capture mechanism, the aerosol capture efficiency due to the impaction of aerosol particles on the rain drop and interception of particles by the rain drop:

$$\Lambda = \frac{q}{2a_m}\left[\frac{4}{Pe}\left(1 + 0.4\,\mathrm{Re}^{1/2}\,Sc^{1/3}\right) + \frac{4r_p}{a_m}\left(\frac{r_p}{a_m} + \frac{(1 + 2\mu_w r_p/\mu_a a_m)}{\left(1 + \mathrm{Re}^{-1/2}\,\mu_w/\mu_a\right)}\right) + \left(\frac{\rho_w}{\rho_a}\right)^{\frac{1}{2}}\left(\frac{St - St_*}{St - St_* + 2/3}\right)^{\frac{3}{2}}\right] \qquad (7)$$

where a_m is the volume-mean raindrop projected radius, St - the Stokes number ($2r_p^2 \rho_p w_r / 9 \mu \rho_a \nu$), St_* - the critical Stokes number $(1.2 + ln(1+Re)/12)/(1+ln(1+Re))$, μ_w and μ_a - the dynamic viscosities of water and air, respectively, and ρ_p, ρ_w and ρ_a - the density of particles, water and air, respectively, Pe - the Peclet number ($a w_r / D$), Sc -the Schmidt number (ν/D), Re - the Reynolds number ($a w_r / \nu$), ν - the kinematic viscosity of the air (μ_a/ρ_a), and D - the Brownian diffusivity of particles.

The process of rainout between the cloud base and top depends on the *convective* or *dynamic* type of precipitation. The rainout coefficient for the *convective* precipitation is more effective/intensive than the washout coefficient and can be estimated according to Maryon et al. (1992) by the following formula $\Lambda'(r,q) = a_0 q^{0.79}$, where $a_0 = 3.36 \cdot 10^{-4}$. Crandall et al. (1973) showed simulations of different mechanism for rainout in which the rainout coefficient is not a strong function of particle size. The rainout coefficient for the

dynamic precipitation is close to being equal to the washout coefficient, and the rainout effect in this case can be also estimated by Eq.(6).

The range of values of Λ for snow is 2 - 10 times lower than the washout coefficient for rain with equivalent precipitation rates. So, we suggest to use the above formulations with other experimental coefficients (Baklanov & Sørensen, 2001).

5. MODELS FOR AEROSOL DYNAMICS STUDIES

5.1 Eulerian model for local- and meso- scale

For the local- and meso- scale simulation of the radioactive aerosol dynamics the Eulerian type atmospheric aerosol transport model of the Russian Institute of Numerical Mathematics was used (Marchuk et al., 1990; Aloyan et al., 1993, 1997). The model in general includes the processes of the nucleation, condensation and coagulation of aerosols. The aerosol model was off-line coupled with a 3D meso-meteorological model for complex terrain (Penenko & Aloyan, 1985; Aloyan & Baklanov, 1985). The numerical algorithm is based on the method of splitting of physical processes. On each small time interval the following scheme consisting of these 3 main steps is used: aerosol transport along trajectories; turbulent diffusion; and coagulation. Full description of the numerical algorithm and general solution technique can be found in (Marchuk et al., 1990; Aloyan et al., 1997). In given simulations the model did not take into account the nucleation and condensation processes.

5.2 Lagrangian model for long-range transport of aerosols

For the regional scale and long-range transport of radioactive aerosols the Danish Emergency Response Model of the Atmosphere (DERMA) (Sørensen, 1998; Sørensen et al., 1998; Baklanov and Sørensen, 2001) was applied. DERMA, a 3-D Lagrangian long-range dispersion model, using a puff diffusion parameterisation (Sørensen, 1998), is developed at the Danish Meteorological Institute for nuclear emergency preparedness purposes. Meteorological fields from the operational DMI-HIRLAM model (Saas et al., 1999) were used. Earlier comparisons of simulations by the DERMA model versus the ETEX experiment gave very good results. Based on analyses from the first experiment, the among 28 models from most European countries, USA, Canada and Japan, DERMA was recognised as very successful (Graziani et al., 1998). For the regional scale it will be shown (see discussions below) that the dry and wet deposition processes become more important than the coagulation processes and the effect of the particle size distribution is extremely important. So, the particle size distribution from the local scale modelling is used as an input for the regional scale model.

6. NUMERICAL SIMULATIONS AND DISCUSSION

Let us to discuss some example simulation study for a hypothetical accident release of Cs-137 from the Kola NPP with respect to the region of Northern Europe.

Local-scale simulation for the Kola Peninsula were done by the Eulerian model (Marchuk et al., 2000). To account for the coagulation process, 20 different aerosol fractions were considered, ranging in the particle radius from 1 to 100 nm in logarithmic scale, and a kinetic block has been incorporated into the radionuclide transport and decay model. Due to a lack of data on the initial size spectrum of emitted nuclei-mode aerosols for the considered hypothetical scenario, the initial size distribution is assumed to be unimodal, with particle radius of 1 nm. Averaged over the grid cell of the source location, the volume concentration peaks at 10^8 cm^{-3}.

Figure 1 illustrates the simulation results and shows the particle size distributions (averaged over the numerical grid cell) at 3 different sites for 80, 240 and 600 minutes after the radionuclide release time at heights of 150 and 400 meters.

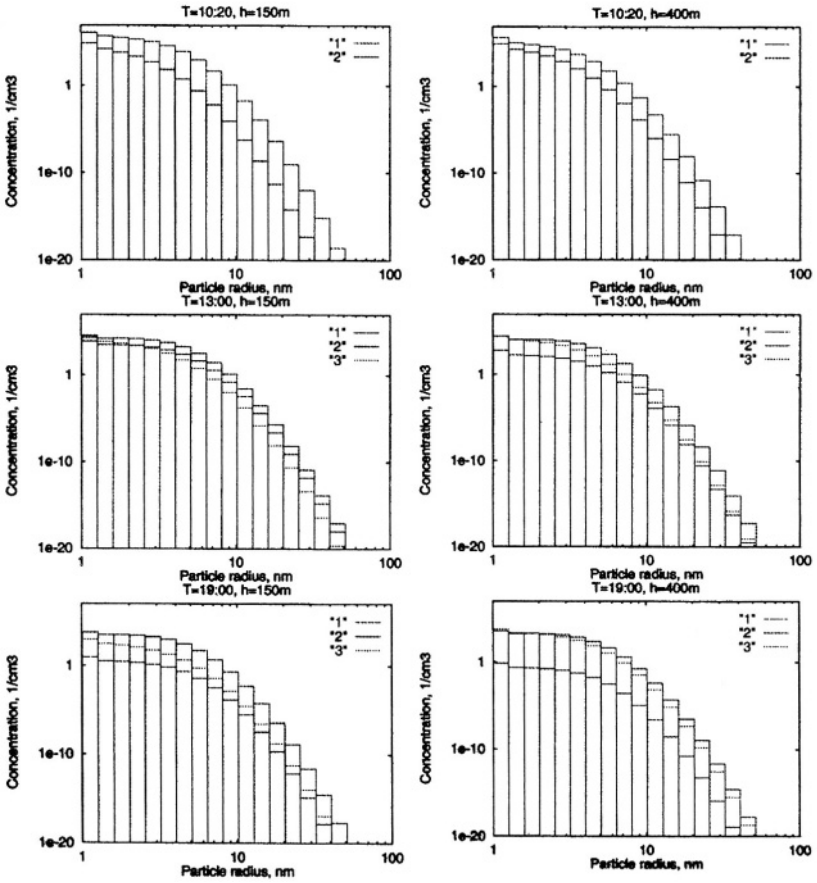

Figure 1. Simulated particle size spectra (in log scale) at heights: 150 m (left) and 400 m (right) for 80, 240 and 600 minutes after the release: 1 – release site, 2 – plume centre, 3 – plume periphery.

Radionuclide particles are mostly concentrated in a narrow area close to the source location. The particle size spectrum is already considerably transformed by coagulation,

especially near the source (point 1), because the coagulation intensity quadratically depends on concentration. At the same time, in the outer region of the radioactive cloud (point 2), the size spectra have no difference at 150 and 400 m heights.

When the emission stops, the radioactive cloud gradually moves in the direction of background flow. One can see that the highest relative share of larger particles is in the area of maximum volume concentration (point 2). It is also noticeable that concentration of larger fractions is higher in the "rear" (Western) part of the cloud than in the "front" (Eastern) one.

One can see that shape of size spectrum in the area of maximum volume concentration (point 2) remains almost similar 4 h and 10 h after the release. The situation is the same at the point 3 in the outer region of the radioactive cloud. It can be concluded that the aerosol concentration has dropped below the level where coagulation intensity is too low, and the size distribution is no longer subjected to shape transformations. Instead, it remains self-similar and lowers with time, as the cloud spreads due to turbulent diffusion. So, it is only in the first few hours after the release, that coagulation kinetics plays an important role in the evolution of radioactive aerosol.

Simulations for the regional scale of Europe were done by the DERMA model, including the effects of the particle size to the deposition processes. The particle size distribution from the local scale modelling was used an input for the regional scale model and was not changed during the long-range transport simulation.

Figure 2 shows simulated washout coefficient, Λ, for different size particle according to the parameterisations (6) and (7). As it is seen, Eqs. (6), (7) have a good correspondence and a better correlation with the measurement data, than other formulations, which do not consider effects of the particle size. One can see the effect of decreasing Λ due to the mechanisms of the impaction of aerosol particles on rain drops and the interception of particles by the rain drops by diminishing the particles from 10 μm down to 1.5 μm, and then increasing Λ for particles less than 1 μm due to the effect of Brownian capture and diffusion mechanism. In Eq. (7), we have included only three of the above-mentioned mechanisms, so, not surprisingly, the curve slightly underestimates Λ in the particle range of 0.5 - 3 μm. For small particles, this can be explained by other

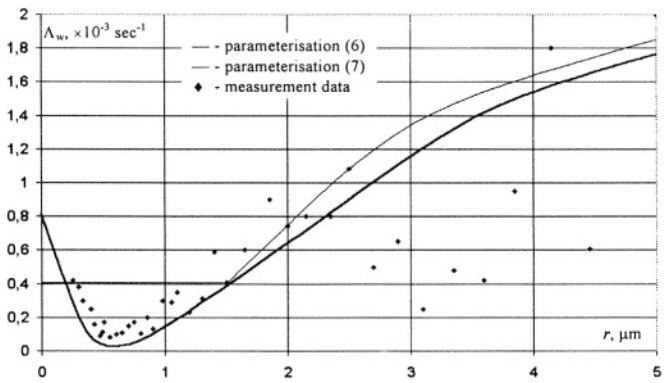

Figure 2. Dependence of the washout coefficient, Λ_w, on the particle radius, r (μm), for q = 10 mm/h, according to the parameterisations: (6) (line) and (7) (bold line) in comparison with the corresponding field measurement data of Tschiersch et al. (1995).

mechanisms such as electrical and thermal attraction, diffusioforesis, and growing of particles due to coagulation and condensation, which gives rise to additional increasing Λ and to a smoother and less gap, which is displayed by the measurement data. Because of this, some overestimation of the Λ parametrisation (6) for particles of 0.6-2 μm in size

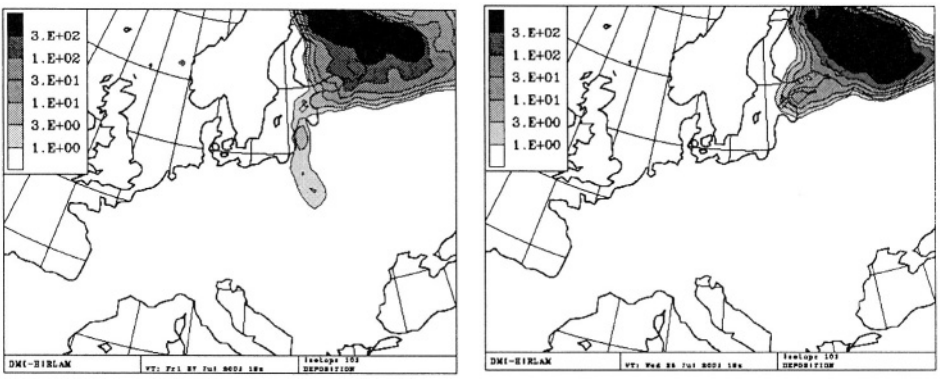

Figure 3 Cumulative deposition pattern of Cs-137 (μBq/m^2) by dry and wet deposition 5 days after the release for two different fractions of the radioactive aerosol: a) 0.5 μm, and b) 6 μm.

can be acceptable.

Figure 3 shows the simulation results of the cumulative deposition pattern of Cs-137 (μBq/m^2) by dry and wet deposition 5 days after the release for two different fractions of the radioactive aerosol: a) 0.5 μm, and b) 6 μm. Effects of size distribution of Cs particles and correspondingly scavenging coefficients to the concentration and deposition fields for the release were compared with other parameterisations. If we consider the radius of Cs particles to be less than 0.5 μm, the ADPIC model parameterisation (Forster, 1992) gives a zero simulated deposition. The formulation (6) gives average values of the wet deposition for such a release 1.8-2.4 times lower than for the similar release of particles with $r > 2$ μm. If e.g. $r = 0.3$-0.7 μm most models of long-range pollution transport, using washout coefficients independent on the particle radius, can show an overestimation of wet deposition by washout about one order of magnitude in comparison with the more sophisticated parameterisation (7).

Preliminary results of numerical simulations of consequences after a severe accident at a nuclear power plant for the European territory and sensitivity analysis of the different processes for the local and regional scales showed that the processes of coagulation are responsible for the transformation of atmospheric aerosols into the released plume during first hours after the accident. They should be included into local scale atmospheric radioactive contamination models. The particle size and density, different for different nuclide releases, are important parameters for the deposition processes, and have to be included into the long-range transport models.

ACKNOWLEDGEMENTS

The authors are very grateful to Prof. Marchuk G.I. for very useful advises, to Drs. Arutyunyan V.O., Louzan P.I. (INM) and Sørensen J.H. (DMI) who took part in the simulations. The study was partly supported by the INTAS-96-1802 project.

REFERENCES

Aloyan, A.E., Arutyunyan, V.O., Lushnikov, A.A., and Zagaynov, V.A., 1997, Transport of coagulating aerosol in the atmosphere. *J. Aerosol. Sci.,* **28**: 67-85.

Aloyan, A.E. and Baklanov, A.A., 1985, Modelling of physical processes in atmosphere over complex topography, In *Numerical Methods for Problems in Atmospheric Physics and Environmental Protection* /ed. by Penenko V.V., Novosibirsk, pp 29-44 (in Russian).

Aloyan, A.E., Lushnikov, A.A., Makarenko, S.V., Marchuk, G.I., and Zagainov, V.A., 1993, Mathematical modelling of the atmospheric aerosol transfer with coagulation taken into account. *Russ. J. Num. Anal. Math. Modelling,* **8**: 17-30.

Baklanov, A. and Sørensen, J.H., 2001, Parameterisation of radionuclide deposition in atmospheric long-range transport modelling. *Physics and Chemistry of the Earth.* 13 pp. (in press)

Crandall, W.K., Molenkamp, C.R., Wiliams, A.L., Fulk, M.M. Lange, R. and Knox, J.B., 1973, *An investigation of scavenging of radioactivity from nuclear debris clouds: research in progress.* Lawrence Livermore National Laboratory, California, USA, Report UCRL-51328.

Dorrian, M.-D., 1997, Particle size distributions of radioactive aerosols in the environment. *Radiation Protection Dosimetry,* **69** (2): 117-132.

Forster, C. S., ed., 1992, *User's guide to the MATHEW/ADPIC models.* UCRL-MA-103581 Rev 1., US LLNL.

Graziani, G., Klug, W., and Mosca, S., 1998, *Real-Time Long-Range Dispersion Model Evaluation of the ETEX first Releas*e (Office for Official Publications of the European Communities, Luxembourg).

Hales, J.M., 1986, The mathematical characterisation of precipitation scavenging. In: *The Handbook of Environmental Chemistry /* O. Hutzinger, editor, Vol. 4, Part A, pp. 149- 217.

Hicks, B.B., 1976, *An evaluation of precipitation scavenging rates of background aerosol.* Argonne Nat. Lab. Radiological and Environmental Res. Division Annual Report.

Hinds, W.C., 1982, *Aerosol Technology.* Wiley, New York. pp. 38-68 & 211-232.

Izrael, Yu.A., 1996, *Nuclear fall-outs after nuclear accidents.* S.-Petersburg, Hydrometeoizdat (in Russian)

Jacobson, M.Z., 1999, *Fundamentals of atmospheric modeling.* Cambridge Univ. Press, 656 p.

Marchuk G.I., Aloyan A.E., Lushnikov A.A., and Zagaynov V.A., 1990, Mathematical modelling of aerosol transport in the atmosphere with regard for coagulation. Prep. DNM. USSR Acad. Sci., #247 (in Russian).

Marchuk, G.I., Aloyan, A.E., Arutyunyan, V.O., Louzan, P.I., 2000, Modelling of the Regional and Global Transport of Radionuclides from the Kola NPP. (ed. R. Bergman) FOA-R-99-01390-861--SE

Maryon, R.H., Smith, F.B., Conwy, B.J. and Goddard, D.M., 1992, The U.K. nuclear accident model. *Progress in nuclear energy.* **26** (2): 85-104.

McManon, T.A. and Denison, P.J., 1979, Empirical atmospheric deposition parameters - a survey. *Atmos. Environ.,* **13**: 571-585.

Näslund, E and Thaning, L., 1991, On the settling velocity in a nonstationary atmosphere. *Aerosol Science and Technology,* **14**: 247-256.

Penenko, V.V. and Aloyan, A.E., 1985, *Models and Methods for Environmental Problems.* Nauka, Moscow.

Radke, L.F., Hindman, E.E. II, Hobbs, V.P., 1977, A case study of rain scavenging of aerosol particles from an industrial plume. Proc. Symp. On Precipitation Scavenging, 1974. *ERDA Symp. Series.* NTIS, pp. 425-436.

Saas, B.H., Nielsen, N.W., Jørgensen, J.U. and Amstrup, B., 1999, *The operational DMI-HIRLAM system.* DMI technical report #99-21.

Seinfeld, J.H. and Pandis, S.N., 1998, *Atmospheric chemistry and physics.* A Wiley-Interscience public. 1326p.

Slinn, W.G.N., 1977, Approximations for the wet and dry removal of particles and gases from the atmosphere. *Water, Air and Soil Pollution,* **7**, 513.

Suck, S.H. and Brock, J.R., 1979, Evolution of atmospheric aerosol particle size distribution via Brownian coagulation: numerical simulation. *J. Aerosol Sci.,* **10**: 581-590.

Sørensen, J.H., 1998, Sensitivity of the DERMA Long-Range Gaussian Dispersion Model to Meteorological Input and Diffusion Parameters. *Atmos. Environ.* **32**: 4195-4206.

Sørensen, J.H., Rasmussen, A., Ellermann, T., and Lyck, E., 1998, Mesoscale influence on long-range transport - Evidence from ETEX modelling and observations, *Atmos. Environ.* **32**: 4207-4217.

Tschiersch, J., Trautner, F. and Frank, G., 1995, Deposition of atmospheric aerosol by rain and fog. In: *EC 'Radiation Protection' Report* # EUR 16604 EN, pp. 3-11.

Voldner, E.C., Barrie, L.A. and Sirois, A., 1986, A literature review of dry deposition of oxides of sulfur and nitrogen with emphasis on long-range transport modeling in North America. *Atmos. Environ.* **20**: 2101-2123.

Wang, P.K. and Pruppacher, H.R., 1977, An experimental determination of efficiency with which aerosol particles are collected by water drops in subsaturated air. *J. Atmos. Sci.,* **34**: 1664-1669.

Warner, S.F. and Harrison, R.M. Editors, 1993, *Radioecology after Chernobyl: Biogeochemical Pathways of Artificial radionuclides.* SCOPE 50. John Wiley & Sons.

Wesely, M.L., 1989, Parametrisation of surface resistances to gaseous dry deposition in regional scale numerical models. *Atm. Environ.* **23** (6): 1293-1304.

DISCUSSION

B. FISHER — The model relies on a description of coagulation. How much is known the mechanism of coagulation of particles and what were the reasons leading to the preferred method of parameterisation? There is a problem of numerical diffusion depending on the number and size of the particle spectra chosen.

A. BAKLANOV — The coagulation mechanism is quite known for aerosol particles, at least due to Brownian and turbulent motions. In this study we used some approximation for a rough assessment of the importance of the coagulation mechanism in the atmospheric aerosol dynamics. For solution of the Smoluchowski equation kernels of coagulation, close to the reality, were chosen. They consider transitions from one collision regime to other (the continuum, free-molecular and transition regimes), depending on the Knudsen number, *Kn.* The coagulation model in a finite-different form possesses the mass conservation property and has a minimal numerical diffusion. So, the chosen coagulation model is one of advanced in the present time. The gravitational coagulation was not considered in the calculations due to small size of considered particles. Of course, we understand that there are many problems in careful simulation of the coagulation processes, it is, actually, the first attempt to include the coagulation mechanism in modelling of atmospheric radioactive aerosol dynamics. As next step we start to consider the electrical forces, which can be important for the coagulation of radionuclide particles, however this effect is not included in this study.

E. GENIKHOVICH — The mixing height, *h,* is a governing parameter in the Maryon equation for depletion. Don't you think that this equation should be used to concentrations averaged over the height rather than to their local values?

A. BAKLANOV — This simple equation is used only in the long-ranger transport model, which accepts the hypotheses of the complete mixing in the boundary layer (see the paper text). So, this equation is used in a right way. For the local scale model, more complex equations for the binary nucleation and further condensation growing of particles are realised, but in the given study they were not considered due to too slow process of the nucleation for Iodine (T ~ 47 days).

This page intentionally left blank

AIR QUALITY STUDY OVER THE ATLANTIC COAST OF IBERIAN PENINSULA

Ana C. Carvalho, Anabela Carvalho, Alexandra Monteiro, Carlos Borrego, Ana I. Miranda, Ivan R. Gelpi, Vicent Pérez-Muñuzuri, Maria R. Méndez, and José A. Souto*

ABSTRACT

The west coast of Iberian Peninsula, surrounded by the Atlantic Ocean, is characterized by complex topography and some favourable synoptical situations, which imply the appearance of mesoscale circulations strongly influencing the transport of pollutants. On the other hand, the regions of Galicia (NW Spain), and the North of Portugal, have important air pollutants sources (power plants, chemical industries, traffic and biogenic emissions), all of them contributing to the air quality along the Atlantic coast and even affecting the centre of the Iberian Peninsula.

In order to achieve the proposed objectives, a hierarchy of models was applied: the results of a global numerical weather prediction model (GCM), namely the AVN (Aviation model from the National Centres for Environmental Prediction of USA) were used as initial and boundary conditions into the regional meteorological model of the Pennsylvania State University/ National Center for Atmospheric Research Mesoscale Meteorology Model (MM5) over an area that includes a large part of the Iberian Peninsula, using its nesting capabilities. To analyse the photochemical production over the fine grid domains an interface between the MM5 and a photochemical model (MARS) was built up, constituting an innovative approach and a first attempt to integrate these two models.

The achieved results must be considered as preliminary, since the application of this particular prognostic numerical system indicates that more refinement on the boundary layer parameterisations as well on the initial and boundary conditions applied to the MARS model is needed, although the systems represents quite well the ozone measured concentrations.

* Ana C. Carvalho, Anabela Carvalho, Alexandra Monteiro, Carlos Borrego, Ana I. Miranda, Department of Environment and Planning, University of Aveiro, 3810-193 Aveiro, Portugal. Ivan R. Gelpi, Vicent Pérez-Muñuzuri, Faculty of Physics, University of Santiago de Compostela, 15706 Santiago de Compostela, Spain. Maria R. Méndez, and José A. Souto, Department of Chemical Engineering, University of Santiago de Compostela, 15706 Santiago de Compostela, Spain.

Air Pollution Modeling and Its Application XV, Edited by
Borrego and Schayes, Kluwer Academic/Plenum Publishers, New York, 2002

1. INTRODUCTION

Studies on atmospheric circulations over the Iberian Peninsula have shown particularities concerning summer dynamics (Millan et al., 1992). Frequently, there is the development of a low thermal pressure area in the centre of the Peninsula, which allows mesoscale processes enhancement such as land-sea breezes. This type of circulations encourages photochemical production of air pollutants leading to smog episodes, which can cause health problems to the population and environmental degradation.

Global numerical weather prediction can provide information about the present and time evolution of the atmospheric situation (wind speed, wind direction, temperature, humidity, etc.). This information is fundamental to estimate the transport, production, dispersion and removal of air pollutants.

Nevertheless, global meteorological models are not suitable for regional studies of transport of pollutants due to their coarse resolution ($1^{o} \approx 100$ km). These models do not simulate properly mesoscale and regional phenomena, but their results may be refined with mesoscale models using dynamical downscaling. In dynamical downscaling, GCM simulations are used to drive regional climate models (RCMs), which simulate mesoscale circulation and physical processes in the land-atmosphere system. The knowledge and characterisation of mesoscale atmospheric flow patterns, as well as, the description, by mathematical models, of dispersion and transformation mechanisms of photo-oxidants are fundamental.

The main purpose of this work is to describe the application of two numerical systems: meteorological model (MM5) (Grell et al., 1995) and the air quality model (MARS) (Moussiopoulos, 1992). These systems simulated the dispersion of pollutants in the atmosphere, during two summer days, in North part of Portugal. It is important to mention that the achieved results should be considered as pilot, because MARS model is very sensible to the initial and lateral conditions of chemical species concentrations as well as to the selected MM5 parameterisations. This represents a considerable field of research in order to better integrate both models.

2. THE APPLIED NUMERICAL SYSTEMS: MM5/MARS

Version 3 of the Pennsylvania State University/ National Center for Atmospheric Research Mesoscale Meteorology Model (MM5V3.4), is a powerful meteorology model that contains comprehensive descriptions of atmospheric motions; pressure, moisture, and temperature fields; momentum, moisture, and heat fluxes; turbulence, cloud formation, precipitation, and atmospheric radiative characteristics.

MM5 is a non-hydrostatic prognostic model with a multiple nesting capability, applying one way or two-way nesting. The most interesting features of MM5V3.4 are related with its different physics parameterisations that can be selected by the user and being capable of running in different computational platforms (Dudhia et al., 2001).

MARS model describes the dispersion and chemical transformation of air pollutants in a three dimensional region (Moussiopoulos, 1992). This model is directed towards the photo-oxidants simulation, from which ozone (O_3) is the major component. It is a fully vectorised model that solves the concentration parabolic equation system for known meteorological variables. KOREM and RADM2 can be used on MARS as chemical

mechanisms. The first one, which has been chosen for the present work, includes 39 chemical reactions with 20 reactive pollutants.

In addition, MARS model needs daily variable chemical species emissions as inputs. These were calculated based on proper approaches depending if the air pollutants are emitted by anthropogenic or biogenic sources.

The MARS model numerically simulates photo-oxidants formation considering the chemical transformation process of pollutants together with its transport in the atmospheric boundary layer (Moussiopoulos et al., 1995). The model solves the parabolic differential concentration transport equation system in terrain-following co-ordinates, with the meteorological variables calculated by MM5, e.g., the mass conservation equations are driven by the momentum equation.

These two models have been applied by a variety of entities and the achieved results are acceptable by the scientific community. MM5 is a wide spread community model with strong user support, that is being tested all over the world (Stockwell et al., 2000; Elbern and Schmidt, 2001). In Iberian Peninsula several institutions are applying MM5 as a real time weather forecast tool (http://meteo.usc.es). On the other hand, MARS is also a well-tested model, in Europe (Baldasano et al., 1993; Moussiopoulos, 1994; San José et al., 1997).

3. METHODOLOGY

The primary work on the numerical system of models MM5/MARS was applied to 15 and 16 June 2000. During the 15^{th} of June the Iberian Peninsula was under the influence of an anticyclone located southern Bretagne, promoting southeastern winds at surface, over the study area. This evolves to a low surface pressure gradient situation in the middle of the afternoon. This kind of meteorological pattern promotes surface O_3 production. The surface pressure charts are similar in both days (http://www.wetterzentrale.de/topkarten/fsavneur.html;http://www.infomet.am.ub.es/arxiu/mapes_fronts/).

Using the MM5 capability of doing multiple nesting, the meteorological model was applied with the one way nesting option and for two nests: (i) a large domain covering the Iberian Peninsula (45 km resolution), (ii) a first nest covering the Atlantic Coast of Iberian Peninsula (15 km resolution), (iii) and a second nest for the North part of Portugal (5 km resolution).

In order to analyse the photochemical production over the fine grid domain, an interface between MM5 and the photochemical model MARS was built up. With this interface all the necessary meteorological parameters to calculate photochemical air pollutants advection, production and removal are fed into the photochemical mesoscale model with the necessary time-step resolution results.

MM5 simulations were initialised from the gridded NCEP/AVN analysis, producing outputs in nested 45 km, 15 km and 5 km grids. The grid sizes are 27 x 31, 31 x 43, and 40 x 40 grid points, respectively. All modelling domains have the same vertical structure with 23 unequally spaced sigma levels. The 5 km grid is governed by the Warm Rain microphysics moisture scheme, no cumulus scheme, and a Blackadar boundary layer.

In order to integrate both models, the meteorological and the photochemical, it was necessary to develop a numerical tool. MARS model runs for the inner domain ($200x200$ km^2 with $5x5$ km^2 resolution) with MM5 outputs and the calculated pollutant emissions

grid. Anthropogenic emissions were calculated applying a disaggregation technique from the national level to the municipal and them to the sub-municipal level. The CORINAIR 95 National Inventory was used to estimate emission data with required spatial and temporal resolution. For this purpose, disaggregation technique based on statistical indicators was applied. As a first step, national emission data are disaggregated to the municipal level using fuel consumption. Then, the data are processed jointly with population statistics in order to obtain sub-municipal resolution. In this work biogenic emissions were not considered.

4. RESULTS AND DISCUSSION

For the present study, ozone measurements were available at three different locations over the study region (see Figure 1): Coimbra, Avanca and Teixugueira. Coimbra is an urban air quality station and, for this reason, maximum ozone concentrations were 86 $\mu g.m^{-3}$ and 88 $\mu g.m^{-3}$, both occurring at noon of the 15th and 16th of June, 2000. On the other hand, Avanca and Teixugueira air quality stations are located near the industrial complex of Estarreja and both present the ozone pick during the afternoon, around 17h and 18h local time, over 160 $\mu g.m^{-3}$ (see Figure 2). The appearance time of these two picks, on both days, indicates that the ozone present in these locations may be due to plume production and advection from urban areas, Oporto and/or Coimbra.

Figure 1. Fine grid domain over the central and north part of Portugal.

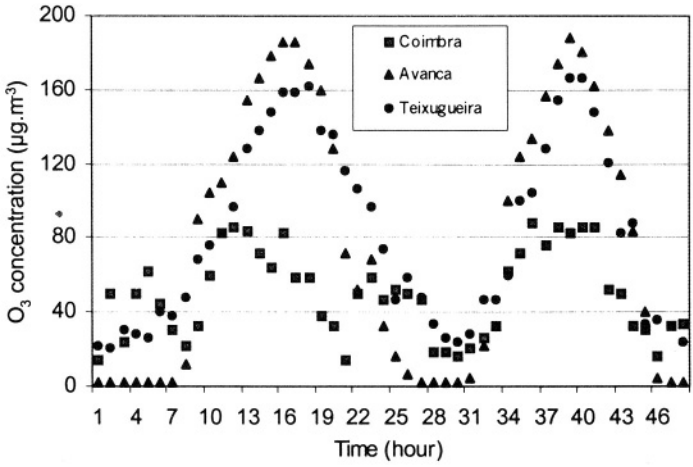

Figure 2. O_3 concentrations measured in three air quality stations located in the study region, for the simulated days (15 and 16 June 2000).

MM5/MARS system shows as results for the two simulated days the same trend as the measured ones, although the picks of ozone are under estimated for Estarreja (the cell containing both Teixugueira and Avanca for the applied resolution of **5 x 5 km^2**). In fact, over Coimbra the daily curve of ozone is quit similar (see Figure 3) to that one presented on Figure 2.

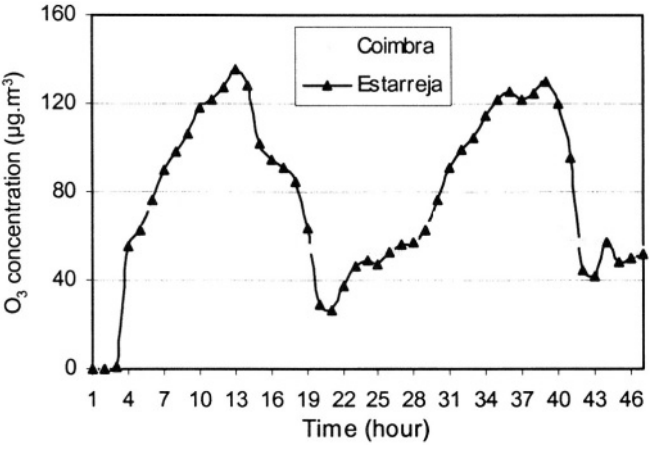

Figure 3. O_3 concentrations estimated over the air quality stations, for the simulated days (15 and 16 June 2000).

Quality indicators reflect the ability of a model to simulate real world phenomena. Applications of such indicators help to understand model limitations and provide a support for model intercomparison. It should be taken in consideration that model evaluation could not be performed on basis of a single quality indicator. A system of quantitative parameters must be identified for each task related to model developing and then, common quality indicators will be established and applied within the project. The performance of the system of models is evaluated through the application of quantitative error analysis introduced by Keyser and Anthes (1977). Consequently, if ϕ_i and ϕ_{iobs} were individual modelled data and observed in the same mesh cell, respectively; ϕ_0 and ϕ_{0obs} the average of ϕ_i and ϕ_{iobs} for some sequence in study, and N the number of observations, then:

$$E = \left\{ \frac{\sum_{i=1}^{N} (\phi_i - \phi_{iobs})^2}{N} \right\}^{1/2} \qquad E_{UB} = \left\{ \frac{\sum_{i=1}^{N} [(\phi_i - \phi_0) - (\phi_{iobs} - \phi_{0obs})]^2}{N} \right\}^{1/2}$$

$$S = \left\{ \frac{\sum_{i=1}^{N} (\phi_i - \phi_0)^2}{N} \right\}^{1/2} \qquad S_{obs} = \left\{ \frac{\sum_{i=1}^{N} (\phi_{iobs} - \phi_{0obs})^2}{N} \right\}^{1/2}$$

The parameter E is the root mean square error (rmse), E_{UB} the rmse after the removal of a certain deviation and S and S_{obs} the standard deviation of the modelled and observed data, respectively. Keyser and Anthes (1977), suggest that rmse decrease significantly after the removal of a constant bias. Further, according to these authors, this deviation corresponds to inaccuracy in specifications of the initial and boundary conditions. It is possible to say that the simulation presents an acceptable behaviour when:

$$S \approx S_{obs}\,,\ E < S_{obs} \text{ and } E_{UB} < S_{obs}\,.$$

Notice that this kind of analysis requires that the standard deviation of the measured data and the simulated data should be approximately equals, to guarantee that the natural variability presented by the measured values is simulated correctly by the numerical model.

Table 1. Quantitative analysis of the system of models performance

	Quality Indicators		
Air quality stations	S/S_{obs}	E/S_{obs}	E_{UB}/S_{obs}
Avanca	0.54	0.71	0.71
Teixugueira	0.77	0.81	0.80
Coimbra	0.75	1.16	1.06

According to Table 1, it can be said that the air quality station over Coimbra presents the worst quality indicators values, may be do to the fact that this station is located near the southern boundary of the fine nested domain. The system of models is not able to

simulate the natural variability of the measured ozone data due to the very low results obtained for the quality indicator S/S_{obs}. The obtained values for E/S_{obs} and E_{UB}/S_{obs}, over Avanca and Teixugueira, reveals that the model produces acceptable results. Once that Teixugueira presents the best data variability one can say that this station can be considered as a more representative air quality station. In order to analyse how measures correlates with simulated data scatter plots were designed. Figure 4 a), b) and c) presents the correlation for the three air quality stations. For Coimbra station the model tends to overestimate the simulated O_3 concentration values for almost of the total simulated period. This tendency is more pronounced during the night time due, probably, to the O_3 consumption by NO_x. For Avanca and Teixugueira stations the system of models does not present good correlations based on scatter analysis. Probably, this could be related to the lack of biogenic emissions as input to the photochemical model. The combined analysis of Figure 4 and Table 1 reveal that the scatter plots should not be seen *per si,* the results quality assurance is easily guaranteed if different kinds of jointly evaluations are executed. Based on the measured data over Teixugueira and Avanca (Figure 2) it is possible to see that the air quality stations location is very important for validation studies on regional scale. Avanca presents O_3 decrease over the night, which does not occur at Teixugueira. This can be related to the fact that Teixugueira is near the coastline and so the remaining O_3 plume from the north part of Portugal is entering with the sea breeze; Avanca is more interior than Teixugueira suffering the direct and local influence of the industrial air pollutants emissions what can explain zero values of O_3 during the night.

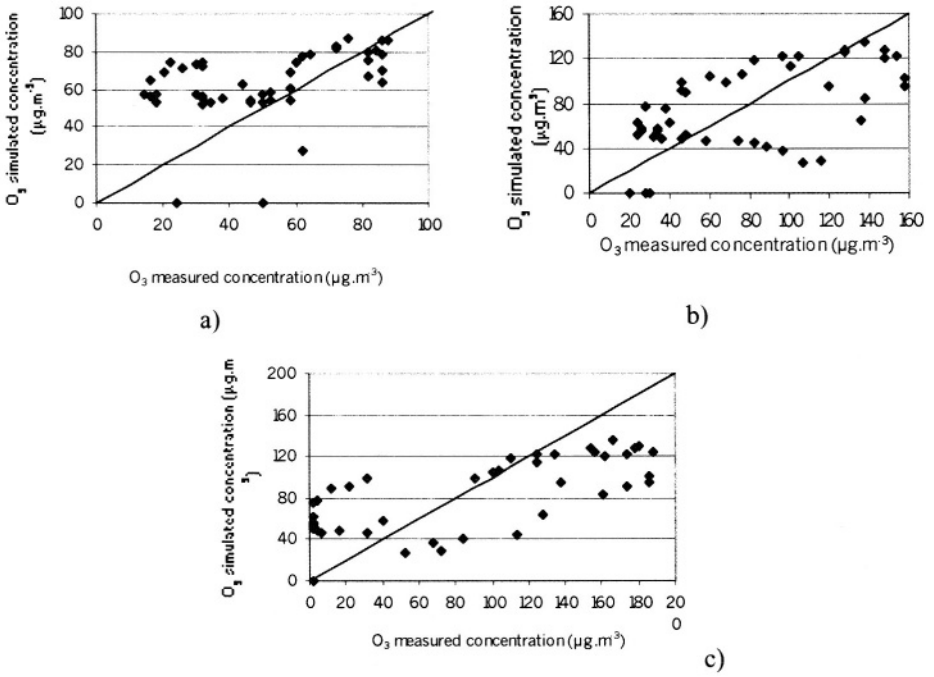

Figure 4. Scatter plots with observed data (x-axis) and modelled data (y-axis) for a) Coimbra, b) Teixugueira and c) Avanca air quality stations.

5. CONCLUSIONS

Although major problems on the integration of these two models did not appeared in this first approach of integration, from this work it can be said that it will be fundamental to validate the meteorological part of the system with the necessary quality indicators. On the other hand, biogenic emissions should be considered and chemical species values on boundary conditions are now under evaluation.

6. ACKNOWLEDGEMENTS

The authors wish to thank the PRAXIS XXI (Foundation for Science and Technology) for the PhD grant of A. C. Carvalho and the European Commission, in the scope of CLIMED project, for the MSc grant of Anabela Carvalho. The authors are also gratefully acknowledged to the Portuguese Environmental Regional Directorate of the Centre for the accessibility to the measured air quality data. Financial support by the Acción Integrada España-Portugal HP1999-0057 is as well grateful acknowledged.

7. REFERENCES

Baldasano, J. M., Costa, M., Cremades, L., Flassak, T., and Wortmann-Vierthaler, M., 1993, Influence of traffic conditions on the air quality of Barcelona during the Olympic Games'92, in: *Air pollution Modelling and Its Application X,* S. Gryning & M.M. Millán, eds., Plenum Press, New York, pp. 643-644.

Dudhia, J., Gill, D., Guo, Y., Manning, K., and Wang, W., 2001, PSU/NCAR Mesoscale Modeling System Tutorial Class Notes and User's Guide: MM5 Modeling System Version 3, Boulder (June 18, 2001); http://www.mmm.ucar.edu/mm5/.

Elbern, H., and Schmidt, H., 2001, Ozone episode analysis by four-dimensional variational chemistry data assimilation. *Journal of Geophysical Research.* **106**.

Grell, G., Dudhia, J., and Stauffer, D., 1995, A Description of Fifth-Generation Penn State/NCAR Mesoscale Model (MM5), NCAR Tech. Note NCAR/TN-398+STR, Boulder, pp. 122.

Keyser, D. and Anthes, R.A., 1977, The applicability of a mixed-layer model of the planetary boundary layer to real-data forecasting. Mon. Weather Rev., Vol. 105, pp. 1351-1371.

Millan, M., Artinano, B., Alonso, L., Castro, M., Fernandez-Patier, R., and Goberna, J., 1992, *Mesometeorological Cycles of Air Pollution in the Iberian Peninsula. Air Pollution Research Report 44,* European Community Commission, Brussels.

Moussiopoulos, N., 1992, MARS (model for the Atmospheric Dispersion of Reactive Species): Technical Reference, Aristotle University, Thessaloniki.

Moussiopoulos, N., 1994, Air pollution modelling in southern Europe, in: *Proceedings of EUROTRAC Symposium 94,* Borrell et al., ed., Academic Publishing, The Hague, pp. 48-55.

Moussiopoulos, N., Sahm, P., and Kessler, C., 1995, Numerical simulation of photochemical smog formation in Athens, Greece: a case study. *Atmospheric Environment,* **29.**

San José, R., Pietro, J.F., Martín, J., Delgado, L., Jimenez, E., and González, R.M., 1997, Integrated environmental monitoring, forecast and warning systems in metropolitan areas (EMMA): Madrid application, in: *1st International Conference on Measurements and Modelling in Environmental Pollution,* R. San José & C.A. Brebbia, Computational Mechanics Publications, Southampton, pp. 313-323.

Stockwell, W., Koracion, D., Klaic, Z. B., and McCord, T. E., 2000, Modeling of ozone, nitrogen oxides and particles in the American northwest, in: *Seventh International Conference on Atmospheric Sciences and Applications to Air Quality and Exhibition,* Taipei, pp. 190.

DISCUSSION

Z. WANG

1) What is the vertical co-ordinate of MARS ? Is it the same as in MM5 or RAMS ? And how much errors do you expect in the transformation between MM5 meteorological output to MARS ?
2) How do you deal with the vertical diffusions coefficients in MARS ? Is it directly from MM5 or calculated by MARS ?

A.I. MIRANDA

1) MARS has terrain following coordinates based on Cartesian coordinate system and vertical resolution with non-equidistant layers. Errors will appear due to the transformation between the Arakawa B grid of MM5 and C grid of MARS.
2) Main feature of MARS is the coupled implicit treatment of vertical diffusion and chemical kinetics.

P. SUPAN

Have you also thought to use another photochemical model than MARS (to improve the results) ?

A.I. MIRANDA

For the study region MARS presents suitable performance using the mesometeorological MEMO model (with 3D results) so, the main problem is related to MM5 model outputs. Outputs improvement should be done firstly on MM5 runs, and this can be achieved through objective analysis.

D.A. STEYN

Your modelling system overestimates ozone concentrations at night. This is probably because it underestimates NO_x scavenging because the meteorological model does not capture surface based radiative temperature inversions due to insufficient vertical grid resolution. Could this be the case ?

A.I. MIRANDA

Although, your guideline is true, in this particular study this is not a justification because NO_x scavenging is not underestimated. The main problem could be related to fixed air quality boundary conditions, namely for O_3 concentration (30 ppb).

F. LEFEBRE Did you perform any sensitivity experiments to the value of the initial concentration ?

A.I. MIRANDA No, we did not.

NUMERICALLY SIMULATED ATMOSPHERIC TRANSBOUNDARY CONTRIBUTION OF LEAD LOADING TO THE GREAT LAKES.

Sreerama M. Daggupaty and Jianmin Ma *

1. INTRODUCTION

Atmospheric deposition of lead (P_b) is one of the significant sources of toxic pollutants entering the Great Lakes. In fact, as much as 90 percent of some toxic loadings to the Great Lakes are believed to be the result of airborne deposition. Because the phenomenon of transport and deposition of airborne toxics is not localized, the problem needs to be evaluated and regulated at least on a regional scale. The purpose of this study is to investigate the contributions of industrial emission sources of lead from parts of Canada and United States to the Great Lakes.

2. NUMERICAL MODEL

A 3-D atmospheric transport model in a regional scale was used to simulate the lead concentrations and depositions over North America following a discrete ordinate (DO) method (Daggupaty and Ma, 1998). The lead emission inventories to the atmosphere were developed for Canadian sources from NPRI (National Pollutant Release Inventory, Environment Canada) data set and for U.S. sources from TRI (Toxic Release Inventory USEPA) data set. These data sets were implemented in the model runs.

Objectively analyzed and predicted meteorological data at 6 hourly data sets from Global Environmental Multi-scale model (GEM) of CMC (Canadian Meteorological Center) and a fine scale boundary layer physics module were utilized to drive the atmospheric transport and deposition model. The model domain covers central and eastern parts of Canada and United States. The model has 10 non-uniformly spaced levels in the vertical, extended from the surface to the height at 3 km. The horizontal grid scale of the model is 35 km with total of 90×90-grid points.

*ARQI, Meteorological service of Canada, 4905 Dufferin Street, Downsview, Ontario, Canada. M3H 5T4
Tel: 416-739-4451, Fax: 416-739-4288; e-mail: sam.daggupaty@ec.gc.ca

Air Pollution Modeling and Its Application XV, Edited by
Borrego and Schayes, Kluwer Academic/Plenum Publishers, New York, 2002

An "effective" dry deposition velocity (Ma and Daggupaty, 2000), which considers the effects of the sub-grid scale surface categories on the heavy metal deposition, was developed and implemented in the model. The wet deposition was computed using the scheme according to Bartnicki et al (1993). The precipitation data used in the computation of wet deposition was from the predicted hourly precipitation rate of CMC's GEM model.

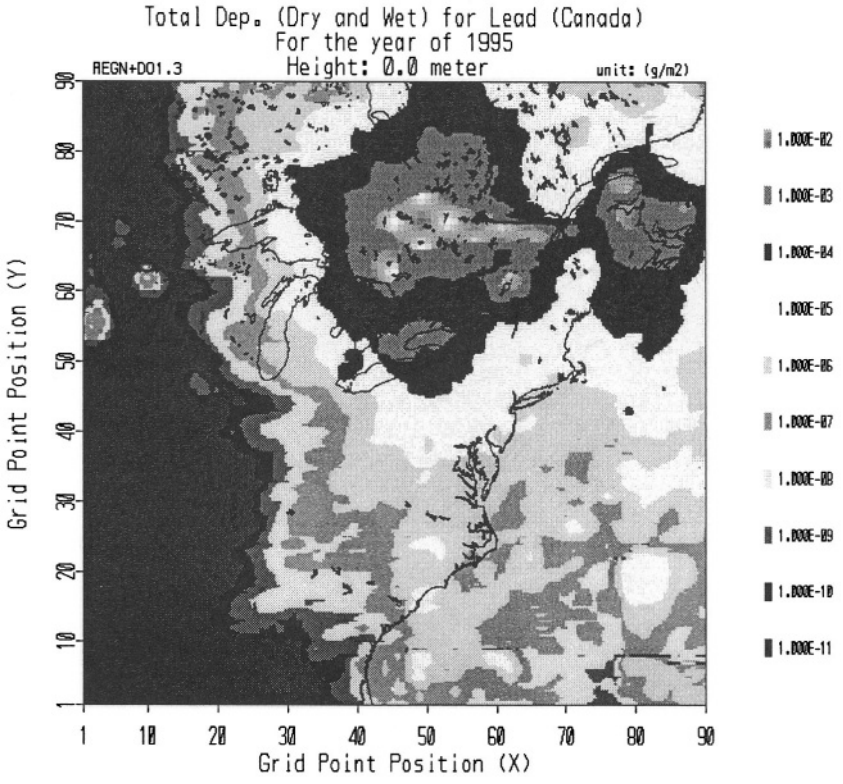

Figure 1. Yearly total deposition in 1995 from Canadian lead emission sources with NPRI data set.

3. RESULTS AND DISCUSSIONS

Figures 1 and 2 display modeled yearly total deposition (dry deposition + wet deposition) in 1995 due to Canadian (NPRI) and US (TRI) emissions respectively. An interesting feature is that there exists a gradient in deposition over the lakes, reflecting the proximity of sources and atmospheric transport. Such sub-lake features are also evident for the modeled air concentration through numerical simulation. This underscores the inadequacy of estimating deposition by assuming a single monitored concentration from

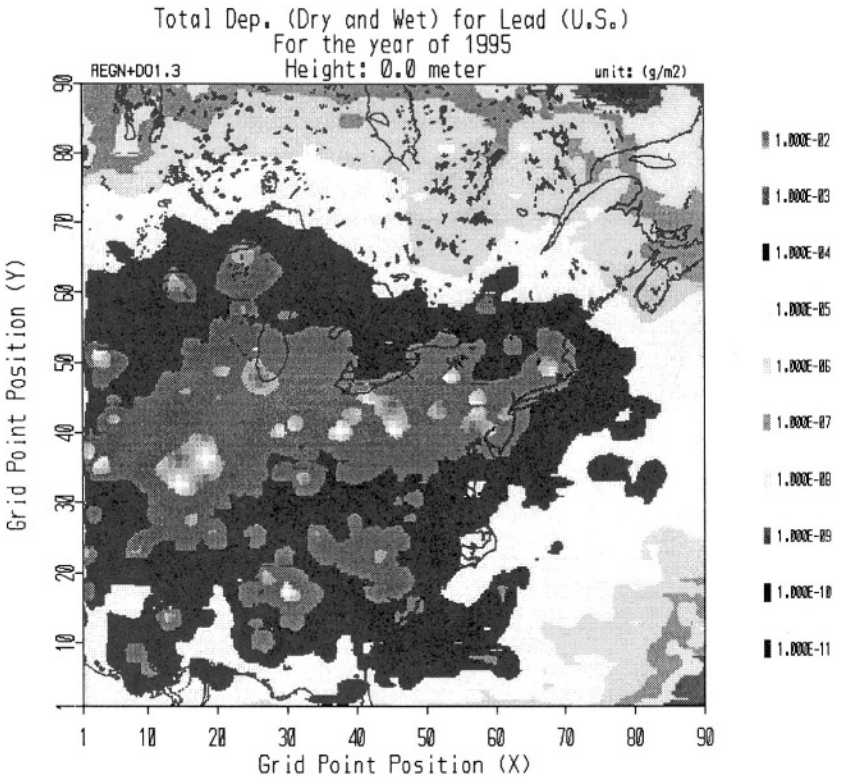

Figure 2. Yearly total deposition in 1995 from U.S.A. lead emission sources with TRI data set.

a land based station nearby the lake as a lake wide representation, for instance in the estimates from IADN (Integrated Atmospheric Deposition Network) data. From Figs. 1 and 2 we can see that the Canadian emissions seem to make little contributions to the lead loading over Lake Michigan and Lake Superior, but form major sources for the lead loading to Lake Huron and Lake Ontario. In contrast, U.S. emissions make major contributions to the lead loading to Lake Michigan, Lake Superior, and Lake Erie. It seems that emissions from both countries have significant effect on the lead loading to Lake Huron.

Tables 1-3 list values of dry, wet, and total depositions to the Great Lakes from 1994-1996. From Tables 1-3, one can identify readily the contributions of different emission sources to the lead loading to each lake. Precipitation data was missing for modellling during 1994; thus model wet deposition estimates and total deposition were not available for the 1994 year.

Table 1. Yearly (dry, wet, and total) deposition to the Great Lakes (kg yr^{-1}) using the emissions from Canada and USA.

Lake	Erie	Ontario	Michigan	Huron	Superior
Year		Dry Deposition			
1994	3565	7006	6036	2945	1813
1995	2131	7751	11722	2860	1424
1996	8328	5197	3812	2337	1137
		Wet Deposition			
1994	N/A	N/A	N/A	N/A	N/A
1995	2561	4093	12275	3341	1200
1996	9005	3171	5750	2398	1960
		Total Deposition			
1994	N/A	N/A	N/A	N/A	N/A
1995	4692	11844	23997	6201	2624
1996	17333	8368	9562	4735	3097

A comparison of Tables 1, 2, and 3 indicates that the U.S sources contribute about 85% of the dry deposition over Lake Erie in 1994, about 87% and 95% in 1995 and 1996 respectively. For the wet deposition, the lead emissions from United States account to about 88% in 1995 and 94% in 1996. This implies that about 87% in 1995 and 95% in 1996 of the total lead loading to Lake Erie are due to the emissions from United States. Similarly, U. S. sources also make the most contributions to lead loading to Lake Michigan, whilst the deposition over Lake Michigan due to the emissions from Canada can be ignored. It is interesting to see that the U.S. sources account to quite large amount of deposition in Lake Superior in 1994 and 1995 compared with Canadian sources. In 1996, however, the depositions over Lake Superior due to the emissions from United States are reduced considerably. However still 50% of the total deposition is due to US sources. Although both United States and Canada have emission sources near the Lake Ontario, it is clear from Tables 2 and 3 that Canadian sources lead to larger amount of depositions over Lake Ontario. In 1995 and 1996, the total depositions are 86% and 84% respectively due to Canadian sources.

Table 2. Yearly (dry, wet, and total) deposition to the Great Lakes (kg yr^{-1}) using the emissions only from USA.

Lake	Erie	Ontario	Michigan	Huron	Superior
Year		Dry Deposition			
1994	3017	599	5942	1203	1581
1995	1846	620	11624	539	1183
1996	7951	499	3768	695	661
		Wet Deposition			
1994	N/A	N/A	N/A	N/A	N/A
1995	2244	1077	12248	1619	1081
1996	8481	825	5549	1412	882
		Total Deposition			
1994	N/A	N/A	N/A	N/A	N/A
1995	4090	1697	23872	2158	2264
1996	16432	1324	9317	2107	1543

Table 3. Yearly (dry, wet, and total) deposition to the Great Lakes (kg yr^{-1}) using the emissions only from Canada.

Lake	Erie	Ontario	Michigan	Huron	Superior
Year		Dry Deposition			
1994	548	6407	94	1742	232
1995	285	7131	98	2321	241
1996	377	4698	44	1642	476
		Wet Deposition			
1994	N/A	N/A	N/A	N/A	N/A
1995	317	3016	27	1722	119
1996	524	2346	201	986	1078
		Total Deposition			
1994	N/A	N/A	N/A	N/A	N/A
1995	602	10147	125	4043	360
1996	901	7044	245	2628	1554

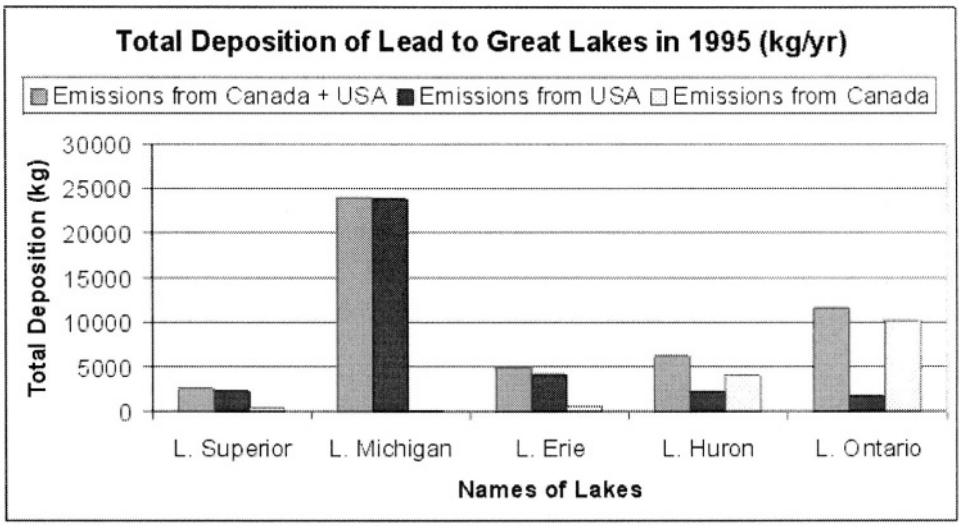

Figure 3. Yearly total deposition in 1995 to the Great Lakes from individual as well as combined lead emission sources from Canadian and USA sources.

Figures 3 and 4 show more vividly contributions from the Canadian and USA sources to the total deposition over lakes. Overall results reveal that among the Great Lakes, Lake Michigan receives the largest lead loading and Lake Superior receives the least amount for total three years of 1994, 1995, and 1996 (Table 1 and Figs. 3 and 4). In most cases the loadings to all lakes have nearly equal contribution of dry and wet deposition (Table 1). It is seen from Table 1 that in 1994 the lead loading due to dry deposition is successively Lake Ontario, Michigan, Erie, Huron, and Superior. In 1995, the total loading is ranked as Lake Michigan, Ontario, Huron, Erie, and Superior. In 1996, however, the order has changed and Lake Erie becomes the largest sink.

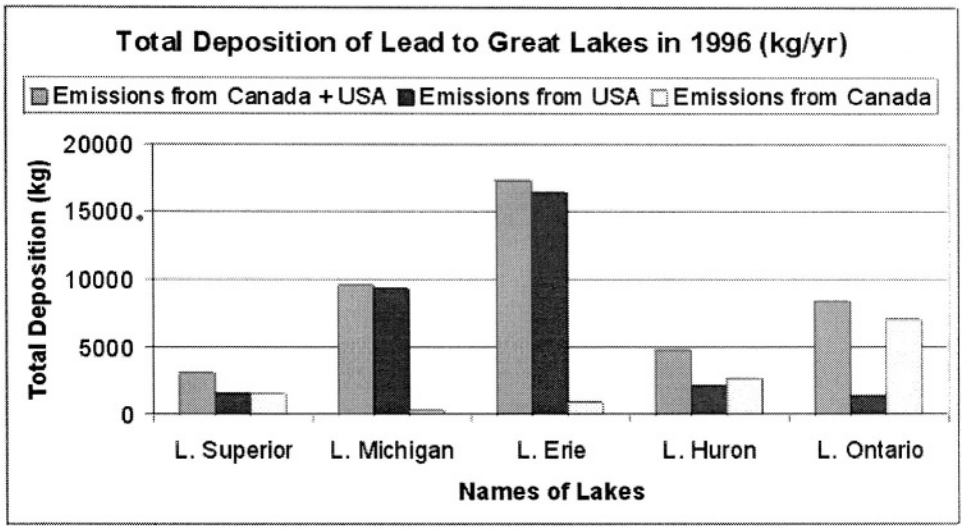

Figure 4. Yearly total deposition in 1996 to the Great Lakes from individual as well as combined lead emission sources from Canadian and USA sources.

Changes of lead loading to the Great Lakes are due, except for the meteorological conditions, to the reductions of emissions from United States in the vicinity of the Great Lakes in 1996. However in this year the U.S. sources still made major contributions of the lead deposition to the Lake Erie, Michigan, and Superior in comparison with the Canadian sources (Fig.4). It is seen (Fig. 4 and Tables 1-3) that the contribution of lead loading to the Lake Erie from U.S sources (TRI) increases drastically in 1996 compared to 1994 and 1995. In general, the modeled total lead loading to Great Lakes is lower than the IADN (Integrated Atmospheric Deposition Network) monitored and estimated data (Hoff et al. 1996). This is mainly due to the model estimated wet depositions are considerably lower than the IADN data. Detailed comparison of depositions to the Great Lakes with IADN data will be reported in a future paper.

In order to demonstrate the model performance, we illustrate in Fig. 5, the comparison of modeled and measured air concentration from IDAN stations at Burnt Island, Egbert, and Pt. Petre in 1995. The comparison was made for sampling days at the monitoring stations with the nearest grid point simulations from the model. Generally at IADN stations once every 12 days the air concentration is monitored for about 24 hours. As shown, the daily averaged predicted surface air concentration is agreeing very well with the measured concentration. Preliminary examination of model predicted dry deposition is lower than that estimated by IADN data. IADN's algorithm of dry deposition uses a constant deposition velocity irrespective of time and surface type. In the case of the model it is a variable function dependent upon the surface characteristics and transient boundary layer dynamic parameters. It is possible that IADN estimated depositions whether dry or wet are not truly representing lake wide loadings. The reason is that IADN estimates are constrained by a single land based monitoring station and hence biased by the conditions at the site.

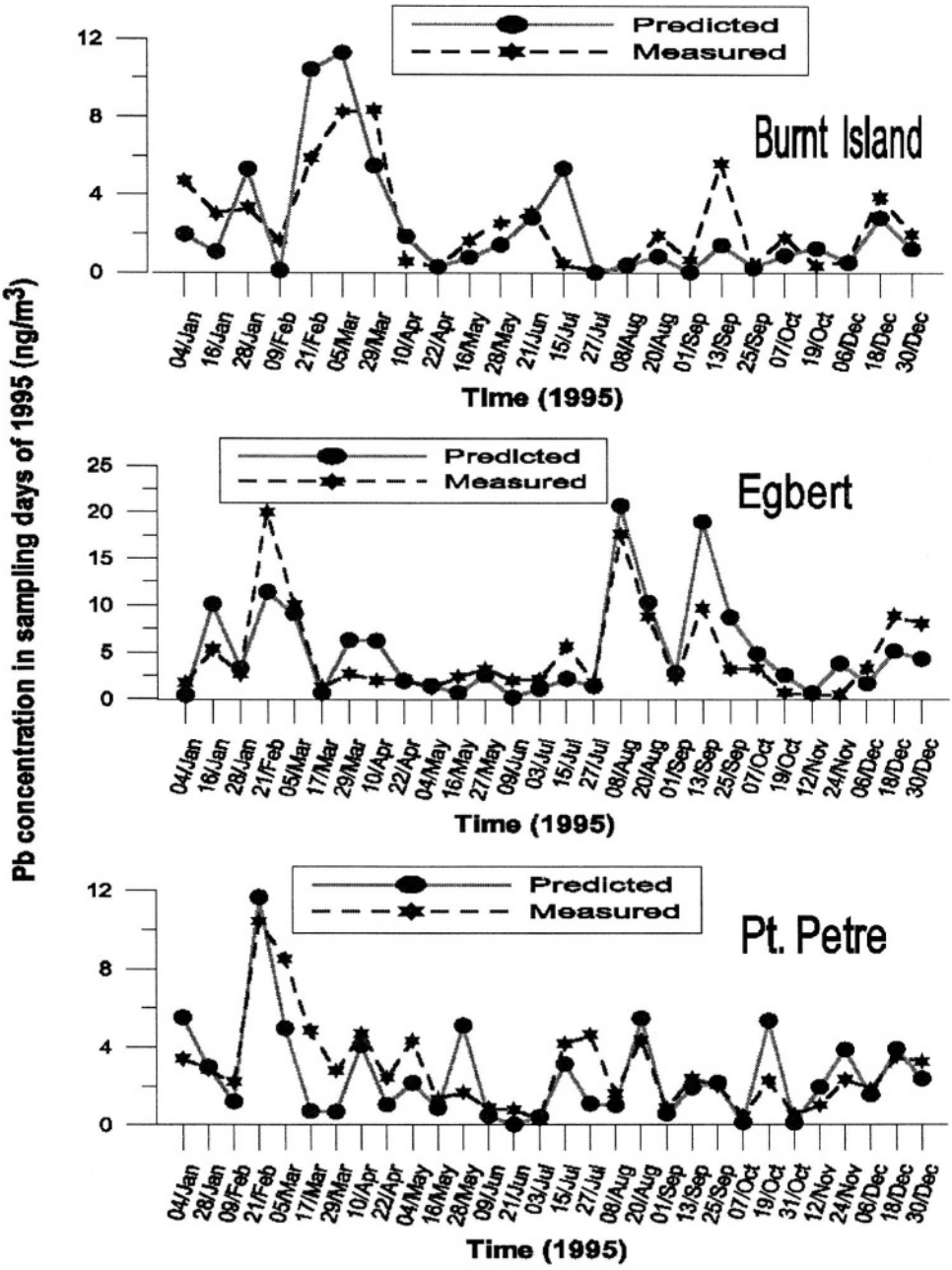

Figure. 5. Modeled and measured concentrations in the sampling days in 1995 at Burnt Island ($45^0$49'42"N, $82^0$56'53"W), Egbert ($44^0$13'57"N, $79^0$46'53"W), and Pt Petre ($43^0$50'34"N, $77^0$09'13"W).

4. CONCLUSIONS

Using a 3-D Eulerian atmospheric transport model, the lead loading to the Great Lakes subject to different emission sources were simulated for 1994, 1995, and 1996. It was found that the lead emissions from sources in the United States made major contributions to the lead loading to the Lakes Erie, Michigan, and Superior, whilst the lead loading to the Lakes Ontario and Huron were determined largely by the emissions from Canada. Overall results reveal that among the Great Lakes, Lake Michigan receives the largest lead loading and Lake Superior receives the least amount for total three years of 1994, 1995, and 1996. In 1994 and 1995, the lead loadings to the Great Lakes did not change dramatically. In 1996, however, we noticed significant changes of the lead loadings in several lakes. Among them the Lake Michigan showed significant reduction and the Lake Erie showed apparent increase. These variations are attributed largely to the changes of the lead emission sources in the United States. Model predicted sub-lake features such as non-uniform air concentration and deposition are noteworthy and such features have strong repercussions in comparison with the estimates of dry and wet deposition from land-based monitored data.

5. ACKNOWLEDGMENTS:

Mr. Philip Cheung's contribution with computer programming and emission data sets is appreciated. Ms. Anita Wong and Mr. Terry Mah are acknowledged for their help with NPRI and TRI data sets. We express our sincere thanks to Ms. Celine Audette, IADN officer of MSC for supplying IADN data. We acknowledge the help of Mr. Vasu Daggupaty with the figures. We appreciate the encouragement and interest of Dr. Keith Puckett.

6. REFERENCES

Bartnicki J, et al, 1993: An Eulerian model for atmospheric transport of heavy metals over Europe. Technique report No. 117, Det Norske Meteorlogiske Institutt.

Hoff R. M., et al., 1996: Atmospheric deposition of toxic chemicals to the Great Lakes: a review of data through 1994. *Atmospheric Environment,* **30,** 3505-3527

Ma J. and S. M. Daggupaty, 2000: Effective dry deposition velocities for gases and particles over heterogeneous terrain. *J. Appl. Meteorol.,* **39,** 1379-1390.

Daggupaty S. M. and J. Ma, 1998: Discrete ordinate/ Pseudospectral simulations of transport of heavy metals over regions of North America. 10th joint conference on the application of air pollution meteorology with the A&WMA. Phoenix, Pre-print volume Amer. Meteor. Soc., January 1998, 410-413.

DISCUSSION

A. HANSEN — Are the Pb sources primarily Pb smelters ? How is the Pb transported ? Primarily as aerosol particles, and, if so, in what size range ?

W. GONG — These questions need to be answered by the authors, i.e. S. Dagguparty and J. Ma.

S. DAGGUPARTY — Yes, the major Pb sources are metal smelting industries, however our data base has some other industrial activities that deal with Pb, but they are minor. It is assumed to be transported as a passive particle. The mean particle size is considered for this study as 0.55um.

This page intentionally left blank

ON THE COUPLING OF AIR-POLLUTION MODEL TO NUMERICAL WEATHER PREDICTION MODEL

Tomas Halenka, Josef Brechler, Jan Bednar*

1. INTRODUCTION

Increasing traffic density gives rise to problems with air pollution that is met mainly in summer months – so called summer photochemical smog. Prague can serve as a typical example of a city where traffic density increased several times that situation a decade ago and as the infrastructure is not prepared for such a rapid changes the problems are quite large. Moreover, as there is no outer ring and also almost all cars passing Prague goes through its center. This situation is improving now, when parts of the city ring is under construction or partly finished but still there are missing very important parts of this important traffic city system. Prague is not only a historical city and capitol of the Czech Republic, it is also a place with a great concentration of industry and other human activity, which leads to problems with air pollution of the above mentioned kind in summer and with nitrogen type of pollution in winter months especially when stagnant condition occurs.

In this contribution we deal with the problem of summer photochemical smog and the episodes of high concentration of it. We are mainly interested in its most important part – tropospheric ozone. Ground ozone concentration is measured in several monitors in Prague, but thanks to the complicated orography of Prague and limited number of monitors it very problematic to obtain information about spatial distribution of this part of summer photochemical smog based on measured data. Another way how to estimate this distribution consists in using appropriate model. This approach supposes to use some meteorological diagnostic or prognostic model (depending on the fact, whether the aim of the activity is a diagnostic field of spatial ozone distribution or its forecast) together with chemical submodel involving the whole cycle of chemical reactions. In the subsequent paragraphs the chemical submodel called SMOG is briefly described together with is prepared link to the meteorological model. A future plans dealing with utilization of more detailed model of higher resolution are also mentioned.

* Tomas Halenka, Josef Brechler, Jan Bednar, Charles University in Prague, Faculty of Math. and Physics, Prague, Czech Republic

Air Pollution Modeling and Its Application XV, Edited by
Borrego and Schayes, Kluwer Academic/Plenum Publishers, New York, 2002

2. CHEMICAL SUBMODEL SMOG

The presented chemical submodel **SMOG** (Bednar *et al.*, 2001) has been developed in the framework of the project "Air Pollution in Prague" at the Department of Meteorology and Environmental Protection, Faculty of Mathematics and Physics, Charles University in Prague in the period 1995-8. It serves as a tool for studying summer photochemical smog episodes. Such episodes can be described as a presence of high ozone concentration produced by photochemical reactions of its precursors, as nitrogen oxides – NO_x and volatile organic compounds – VOC. This high ozone concentration is not caused only with local conditions (local emission) but it is also a consequence of long-range transport. In the model SMOG the attempt was based on the methods that tried to estimate the impact of the local city emission on the level of ozone and it precursors concentrations.

The model has conceptual base in the category of so-called "puff" models. The principle of this type of models consists in hacking of air-pollution plumes into series of puffs. Plume is then supplied by sequence of partly overlapped elements drifted by a wind flow from a source location down the trajectory. That approach allows to reply to rapid changes of meteorological conditions and emissions, however the main advantage of this approach is an ability to involve mixing and mutual chemical reacting parts of plumes proceeded from different sources.

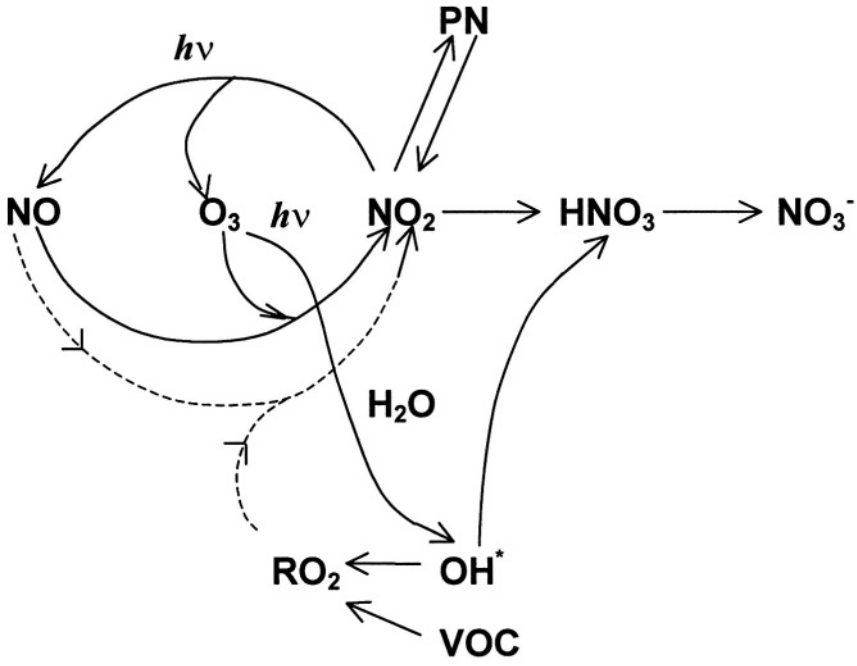

Figure 1. Scheme of chemical reactions involved in the model (RO_2 denotes peroxyradicals, VOC volatile organic compounds).

The model chemical reactions can be characterized with the scheme presented in Fig. 1. Reactions involved can be written in the form of equations described in detailes in Bednar et al. (2001). Usual output of the model involves fields of ground concentration distribution of NO, NO_2 and O_3 in $\mu g\ m^{-3}$. Input data that are necessary for running the submodel SMOG can be divided into three categories. First category can be called as permanent or constant information – this category involves data about orography of the investigated area (model domain). At this moment so called "US NAVY" orography with resolution 10 × 10 geographic minutes has been used. The second and the third category of the data sets consist of emission data and input of meteorological data. Firstly, we will mention emission data in more details as the meteorological data will be discussed in the section where meteorological prognostic model will be mentioned together with performed tests of the link between the meteorological model and chemical submodel.

Chemical submodel SMOG has been used for several studies when the ground distribution of NO, NO_2 and O_3 was computed. Data information on emissions of NO_x and VOC from Prague emission sources and sources from its closest neighbourhood were involved, but there was also information about emission individual (point) sources from the whole area of central Bohemia (approximately to the distances of 70 km from the centre of Prague). The number of involved individual point sources was equal to 177, but the contribution of sources outside of Prague was relatively negligible. Individual point sources creates one group of emission sources and these sources are treated in their real positions with corresponding parameters (building height, emission rate etc.). Model uses also emission data in gridded form. The whole model domain is divided into regular grid mesh of emission squares (in the above mentioned study the squares 5 × 5 km were used) and all the emissions of NO_x and VOC from traffic, area emission sources or small point emission sources located in a given emission square are attributed to the centre of this square. The size of these emission squares is a consequence of a compromise between an attempt to have the most correct emission input and number of puffs that can be treated within one model run as a new puffs is launched from each source each Δt time interval.

Meteorological information consists of data, which are in the first step considered to be homogeneous in model domain, e.g. surface air temperature, cloud cover, solar zenith angle, total amount of O_3 in Dobson units. For wind field vertical changes are taken into account. An example of the results based on homogeneous data in the model domain is presented in Fig. 2.

3. LINK TO METEOROLOGICAL CONDITIONS

If the relatively complicated shape of orography in the Central Bohemia is compared with the used meteorological data (mainly data about wind field – both speed and direction) then it is evident, that a link to some meteorological "pre-processor" that would create more realistic flow field is necessary. At least the flow field could display deformation due to the shape of orography parametrized or modelled in a desired resolution (it means if the model SMOG is used for simulating the impact of the city plume on the surrounding areas, then resolution given with up to now used "US NAVY" orography is sufficient and flow field could be given in the same resolution). But when the submodel

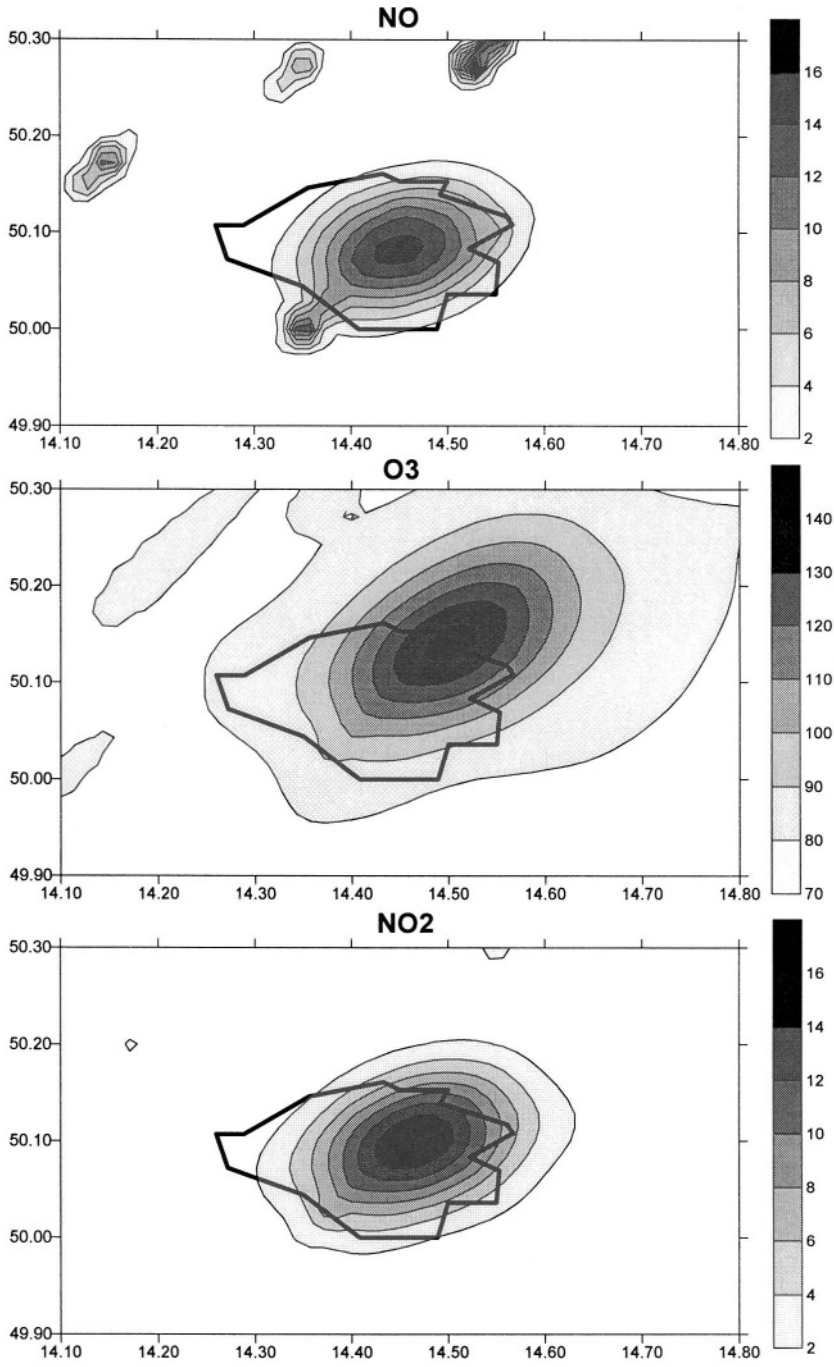

Figure 2. Ground concentration of selected compounds in $\mu g/m^3$ for 11 August 1998, with surface temperature 28°C, wind direction of 220°, wind speed 3 m/s (on 200 m level above terrain) and no cloud cover.

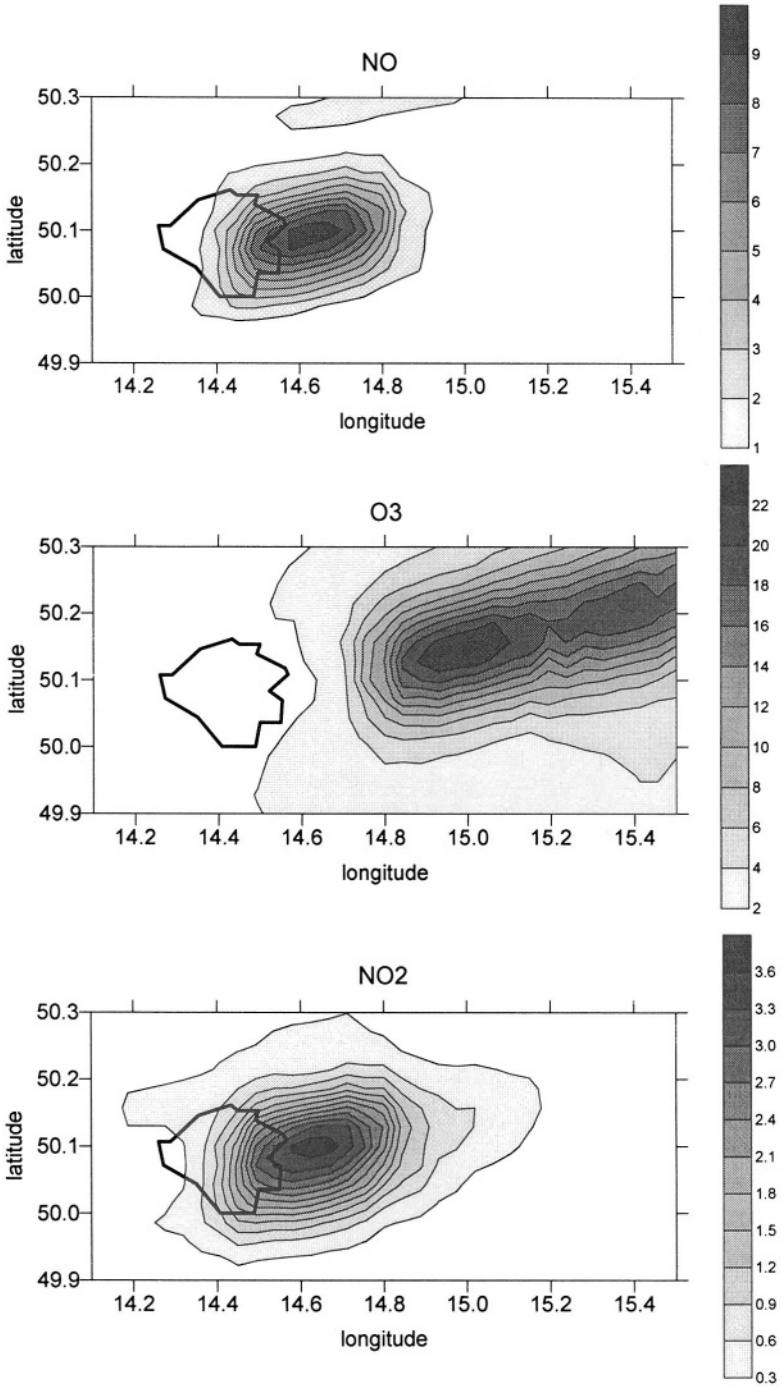

Figure 3. Ground concentration of selected compounds in $\mu g/m^3$ for 10th September 2001, 12 UTC, based on wind field from ETA model.

SMOG should be used simulating the distribution of ozone concentration in Prague and its closest neighbourhood, then some more detailed information about local terrain condition would be necessary together with some more information, e.g. about the structure of build-up area, and some high-resolution model should be used as in this case the local structure of the wind field is consequence of the sum of local conditions acting simultaneously with large scale meteorological situation.

In the first attempt we used the homogeneous fields as we intended to test our coupling routines with meteorological prediction model and the resolution of the model used was comparable with the scale of the area we were interested in concerning the air pollution transport. Further on, the model we are using for our first experiments with real driving of our SMOG model is so-called model ETA (Black, 1988) with resolution of 0.25 degree. The example of the results is presented in Fig. 3, however, this is not typical case of photochemical smog production. Unfortunately mainly the effect of high velocity of wind can be seen there, it should be mentioned that only concentration of produced ozone is displayed although the effect of background concentration is parameterised as well. Moreover, as it is a preliminary study, in this case only trajectories of puffs are driven by wind field from ETA model taking other parameters to be constant and homogeneous in the domain. As the second step we are going to fully couple fields of other parameters like temperature, height of mixing layer, cloudness etc. as well for purposes of regional air pollution transport modelling. Finally, we are taking into account the possibility of experiments with coupling of our chemical submodel to high resolution models MM5 and spectral LAM Aladine.

ACKNOWLEDGMENT

This study was supported in framework of project GACR 205/01/1120 of the Grant Agency of the Czech Republic. The authors wish to express their thanks for the ETA model kindly provided by NCEP.

REFERENCES

Bednar, J., Brechler, J., Halenka, T., and Kopacek, J., 2001, Modelling of summer photochemical smog in the Prague region, *Phys. Chem. Earth (B),* 26, 129-136.

Black, T. L., 1988, The step-mountain eta coordinate regional model: A documentation. National Oceanic and Atmospheric Administration/National Weather Service, p. 47

DISCUSSION

Vl. PENENKO — Do you take into account the feedback relations between the models you use ?

T. HALENKA — No, it is one way nesting, i.e. ETA is used just as a meteorological driver or preprocessor and SMOG as a CTM without any feedback to ETA.

A. HANSEN

1) Because of the large differences in NO_x chemistry between point source plumes and dispersed NO_x sources, do you think use of a pufmodel may be inappropriate for area NO_x sources ?
2) Do puffs originate at regularly gridded points or at point sources, when they exist ?

T. HALENKA

1) Actually, it might be true. However, for more realistic simulation of city plume we have to include area sources as we are not able to simulate each individual stock or chimney. These area sources are taken into account by means of initial spreaded puffs with appropriate values of parameter σ. Comparison of the model simulations with some surface measurements and air-born plume profiling as well has not given us any strong warming concerning this issue till now.
2) Puffs originate at the exact positions of point sources.

This page intentionally left blank

MODELING THE MERCURY CYCLE IN THE MEDITERRANEAN: SIMILARITIES AND DIFFERENCES WITH CONVENTIONAL AIR POLLUTION MODELING

G. Kallos, A. Voudouri, I. Pytharoulis and O. Kakaliagou*

1. INTRODUCTION

Mercury is a toxic metal that is being increasingly recognized as a threat to the health of numerous wildlife species and tens of thousands of people around the world. The anthropogenic sources of mercury in the vicinity of the Mediterranean Sea region include power plants (burning coal and oil), chemical plants (e.g. alkal-cloral plants), waste incinerators, ferrous foundries, non-ferrous metal smelters, refineries, and cement kilns. Additional contributions of mercury come from two mercury-mining sites in Spain and Slovenia, and 3 volcanoes in Italy. The vast majority of the mercury sources in the Mediterranean region are located north of the basin. Hence, they are expected to exert a strong influence on the mercury concentration over the Mediterranean region since the prevailing meteorological conditions favour the transport from north to south. Two main paths of transport have been identified in this region (Kallos et al. 1997a). The one path is from Eastern Europe toward the Middle East and North Africa while the other one is from central and western Mediterranean toward the east. The first path has been found to be the dominant one.

During the MAMCS project two major model developments were performed. These two developments were constructed within two well-known atmospheric models: the Regional Atmospheric Modelling System (RAMS; Pielke et al. 1992) and the SKIRON/Eta (Kallos et al. 1997b and references therein). The use of two atmospheric models allowed the intercomparison of the results and therefore the better development of the mercury modelling system (Kallos et al. 2000). In this development an effort was made to transfer and utilize the modeling techniques applied in conventional air pollution modelling studies. In addition, we developed new methodologies for processes like re-emissions from soil and water bodies and gas to particle conversion (Pirrone and Keeler, 1995). The developed modeling systems have been applied in the Mediterranean Region where the multi-scale atmospheric processes (thermal and mechanical circulations at regional and mesoscale) are considered as important, according to a number of past air pollution studies. Seasonal-type of simulation has been performed for

* G. Kallos, A. Voudouri, I. Pytharoulis and O. Kakaliagou, University of Athens, Department of Applied Physics1 Panepistimioupolis Bldg Phys V, Athens 15784, Greece

Air Pollution Modeling and Its Application XV, Edited by
Borrego and Schayes, Kluwer Academic/Plenum Publishers, New York, 2002

the Mediterranean Sea Region and annual deposition patterns have been estimated. As it was found, the regional-scale pattern, the trade wind systems (from North to South) and the photochemistry are the key factors for controlling the mercury deposition, especially the mercury in particulate form (Hg^P).

2. MODEL SETUP

a. Emissions data (MEI database)

The emission data used in both models were obtained from the Mercury Emission Inventory (MEI) database for the Mediterranean Sea Region and Europe. The MEI database provided information for each point source such as the location of the source, latitude and longitude, stack height, information on the emission type (Hg^0, Hg^{II} and Hg^P) and type of plant. Re-emission involves gaseous evasion of previously deposited mercury in water and soil and is also considered in both models. Fluxes of mercury from soil and water are taken into account.

b. Initial and boundary conditions for Hg^0, Hg^{II} and Hg^P

Horizontally homogeneous initial and boundary conditions are used for the three mercury species. The boundary concentrations of all species are fixed throughout the simulations. Constant initial and lateral boundary concentrations of 1.6 ng/m^3, 80 pg/m^3 and 10 pg/m^3 are used for Hg^0, Hg^{II} and Hg^P respectively, in the lowest 2 km (EPRI, 1996).

c. Wet deposition and dry deposition initialization

Wet deposition of Hg^P, Hg^{II} and Hg^0 adsorbed in rain droplets is activated if there is precipitation. For Hg^P and Hg^{II} the whole concentrations are deposited from that layer where condensation occurs, while for the Hg^0 adsorbed, the concentration that is deposited depends on the amount of water present in the model layers.

The dry deposition scheme proposed by Williams (1982) and modified later by Pirrone et al. (1995) for trace metals and semi-volatile organic pollutants is used to calculate the deposition fluxes over water surfaces. The model of Slinn and Slinn (1981) is used for deposition over soil and vegetation. The deposition velocity for Hg^0 adsorbed in aerosol and for Hg^P is calculated. The value of 0.005 m/s for the deposition velocity of Hg^{II} was used in the final model. This value is in good agreement with Hg^{II} deposition velocities used in previous studies (Pai et al. 1997).

3. RESULTS AND DISCUSSION

It is known that mercury enters the aquatic environment through the deposition processes. For this reason an attempt was made to calculate the accumulated deposition patterns for four different scenarios. Each of the four experimental campaigns was performed in different season of the year. The duration of the model simulations is not large enough, however there is a significant seasonal variability in them. The various

synoptic and deposition patterns in these simulations are considered to be representative of their seasonal values. In the present study the dry and wet deposition patterns of Hg^P, Hg^{II} and Hg^0-adsorbed during the warm (summer and spring) and cold (winter and fall) simulation periods respectively, as well as the prevailing meteorological conditions will be presented and referred as the seasonal patterns.

High pressures and weak anticyclonic circulation characterized the first three days of spring experimental period (1 May - 18 May 1999) over the Mediterranean Sea region. This favored the transport of hot air masses originated in northern Africa. On 4 May a warm core anticyclone installed over the eastern Mediterranean and a low-pressure system covered western Mediterranean. High pressures over western Mediterranean and Africa generated a northwesterly flow. A low-pressure system covered eastern Mediterranean on 8 May. High pressures were extended over the Central and western part of the Mediterranean Sea at the same period. During the last days of the simulation (10 - 18 May) a warm core anticyclone covered the Mediterranean Sea region. Strong southern winds that favored the transport of hot air masses from Africa were also observed.

High pressures dominated over Central and West Mediterranean Region, during the first days of the summer experimental period (17 July - 3 August 1999). During the next two days the high-pressure system extended over the Aegean Sea. Strong northerlies and north-westerlies are predicted over the sea west of Italy on 23 July. These conditions can promote the transfer of mercury from Central Europe towards Central Mediterranean. A trough covered Central Mediterranean and the Balkans on 25 July while it moved towards the Anatolian Plateau on 27 July. Strong northwest winds were predicted over southeastern Mediterranean on 31 July. The combination of the low and high-pressure systems over northern Europe induced strong northeastern winds. During the last two days of the simulation a weak synoptic circulation was observed over the Balkans.

The highest domain-averaged dry depositions of Hg^{II} and Hg^P were observed during summer. The dry deposition patterns of Hg^P and Hg^{II} during the summer integration period (17 July to 3 August) are illustrated (using different deposition scales) in Figures la and Ib. The dry deposition pattern of Hg^P is depended on the pollutant concentration and the deposition velocity. The transport of mercury species is depended on the advective transport by the mean wind and transport by turbulent dispersion. The accumulated (within the 17 days of simulation) amounts of Hg^P that is dry deposited are greater over the sea than over land. The deposition velocity of Hg^P is a weighted average of 15 deposition velocities, corresponding to the 15 size intervals at which particles are distributed. Over regions with high humidity (e.g. over sea surface) greater deposition velocities are observed due to the dependence of the deposition velocity with the size of the particles (the size of the particles is becoming larger in this case). The simulated values of Hg^P dry deposited, reached $180 ng/m^2$ over the water surfaces of South and East Mediterranean Sea region during the summer simulation period. The dry deposition values of Hg^{II} are higher over land than over sea. The simulated values of Hg^{II} dry deposited, reached $700 ng/m^2$ near the sources of the pollutant, as Hg^{II} is fast reacting and deposits quickly (wet and dry).

On the first day of the fall experimental period (21 November - 7 December 1998), a trough was observed over the Central Europe and the Balkans. This trough moved southerly during the next two days, inducing a strong southerly flow over the Mediterranean Sea region. Two low pressures centers existed over the Mediterranean Sea and a weak synoptic circulation prevailed on 27 November. A trough covered Central-

South Mediterranean and the Balkans on 29 November. The first day of December a strong cyclonic circulation over Western Europe and a weak anticyclonic circulation over Eastern Europe was evident. An easterly flow covered Central Europe and the Iberian penninsula. This rather unusual flow observed, covered the main part of Europe. On 3 December a deep trough covered the Iberian while a high-pressure system extended over the Balkans generating a weak anticyclonic circulation. A strong cyclonic circulation was observed over the Mediterranean Sea region during the last days of the simulation.

A deep trough covered Central Europe during the first four days of the winter experimental period (13 February-2 March). A weak flow is also observed over the Balkans. On 17 February northwestern winds were evident over Central Europe and South-Eastern Mediterranean Region. The synoptic conditions prevailing on 19 February, over the North-Eastern Europe and the Balkans induced a northwestern flow over northwestern Europe. A deep trough centered in northeastern Europe covered the Mediterranean Sea region generating a strong westerly flow on 25 February. On 27 February high-pressure systems were spotted over Central Mediterranean and Italy. A weak anti-cyclonic circulation was also evident over the area. The last three days of the simulation high pressures covered northeastern Mediterranean. On the contrary a low-pressure system covered western Mediterranean.

The total domain-averaged seasonal deposition exhibited higher values during the wet season (winter, autumn) than during the dry season (summer, spring) of the year. This is due to the fact that the total deposition is dominated by the wet deposition, which is reasonable to be larger during rainy periods. The seasonal wet depositions of Hg^{II} and Hg^{P} are illustrated in Figures 2a and b and they are in general one order of magnitude larger than the dry deposition ones. The wet deposition pattern of Hg^{II} has several similarities with the wet deposition pattern of Hg^{0}-adsorbed, but the Hg^{II} deposited amounts are four orders of magnitude greater than the Hg^{0}-adsorbed Hg^{II} is also highly soluble so it dominates the wet deposition pattern of gaseous mercury. Wet deposition pattern of Hg^{II} is illustrated in Figure 2a during the cold experimental period. The highest amounts of the pollutant are deposited near the sources. The higher wet deposition amounts of Hg^{P} (Fig. 2b) are predicted, over mountainous areas, as expected due to the higher precipitation usually occurring there. The wet deposition pattern of Hg^{0}-adsorbed is also similar with the Hg^{P} one, as the total amount of precipitation in higher over the Alps, the Greek and East Turkey Mountains.

The "annual" depositions were also calculated using weighted values of the four seasonal runs. The dry and wet "annual" depositions of Hg^{0}-adsorbed, Hg^{II} and Hg^{P} in each simulation are shown in Figure 3. The "annual" deposition of Hg^{0}-adsorbed is generally larger over the land than over the sea (Figs 3a, b). Over the Mediterranean Sea the highest "annual" deposition amounts of Hg^{0}-adsorbed were estimated just off the coast, downstream of the continent. It is reminded that Hg^{0} is deposited only as Hg^{0}-adsorbed. It can be adsorbed either in aerosols when it is dry deposited or in raindrops in wet deposition processes. Thus dry deposition of Hg^{0}-adsorbed is strongly depended on the aerosol concentration and their deposition velocity. The major anthropogenic emissions of aerosol are from sources in Europe. The dry deposition velocity depends on the aerosol characteristics, the type of surface, its roughness and composition, the wind speed, the turbulence and the atmospheric stability. Over Northern Africa where the Saharan dust dominates, large pieces of Hg^{0}-adsorbed settle out of the atmosphere by gravitation after short periods of suspension. Due to these synergetic factors larger

amounts of Hg^0-adsorbed are deposited over land than over the sea. Hg^{II} is deposited rapidly in the vicinity of the sources (Fig. 3c,d), mainly due to its reactivity and solubility. The dry deposition pattern of Hg^P (Fig. 3e) exhibited larger values over the sea, especially

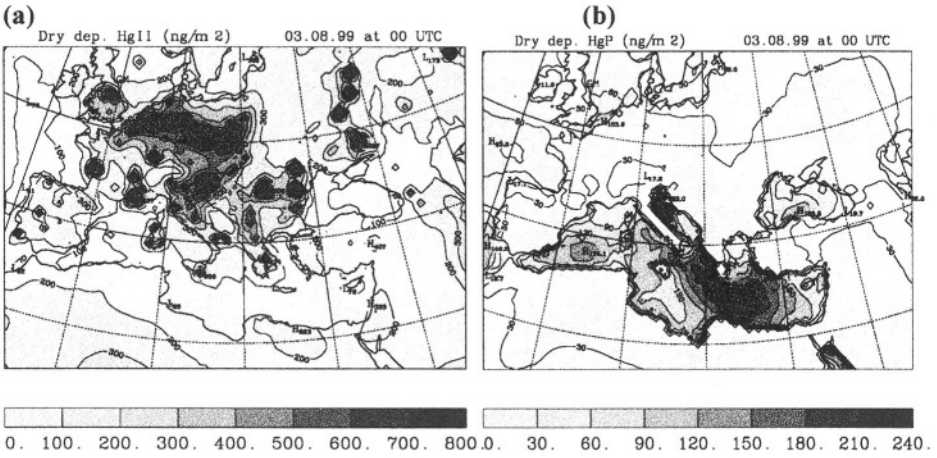

Figure 1. Total dry deposition of (a) Hg^{II} (ng/m^2) and (b) Hg^p (ng/m^2) for the time period 17 July - 3 August 1999. From the SKIRON/Eta model

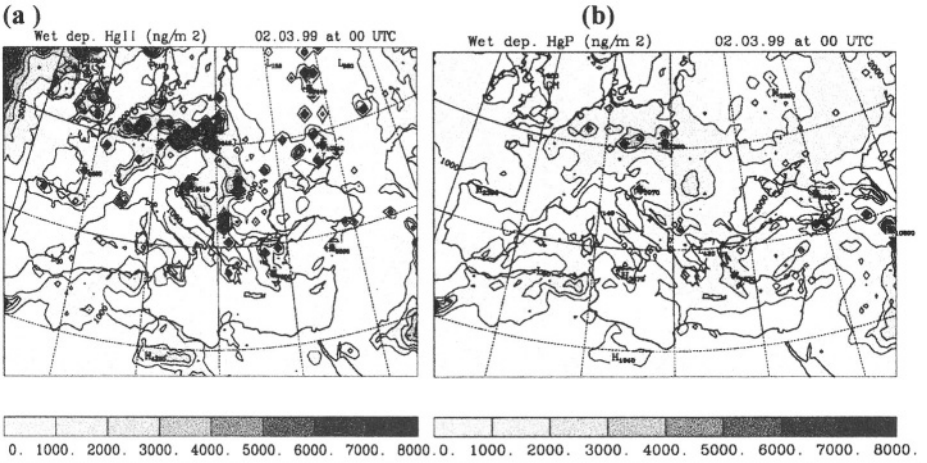

Figure 2. Total wet deposition of (a) Hg^{II} (ng/m^2) and (b) Hg^p (ng/m^2) for the time period 13 February- 2 March 1999. From the SKIRON/Eta model.

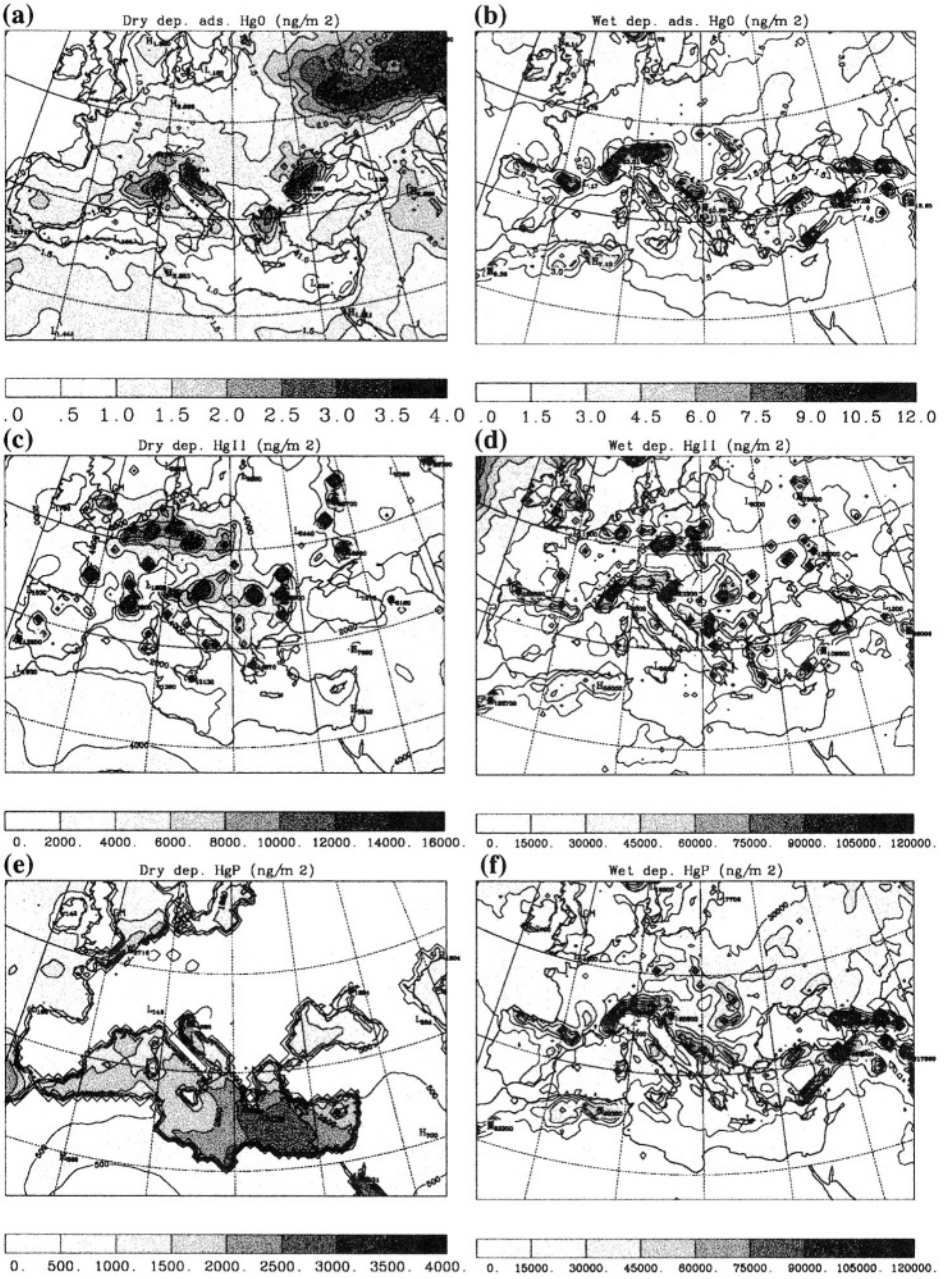

Figure 3. Total annual deposition of Hg species (see text for details of the annual deposition calculation). a) Dry deposition of adsorbed Hg^0 (ng/m^2), b) wet deposition of adsorbed Hg^0 (ng/m^2), c) dry deposition of Hg^{II} (ng/m^2), d) wet deposition of Hg^{II} (ng/m^2), e) dry deposition of Hg^P (ng/m^2), and f) wet deposition of Hg^P (ng/m^2). From the SKIRON/Eta model.

from Europe downstream over the Mediterranean Basin, than over land despite the fact that all anthropogenic sources are located over land. This is due to the dependence of the deposition velocity of Hg^P on the size of the particles. Particle diameter is known to have a great influence on deposition velocities (Sehmel, 1980).

The "annual" wet deposition patterns of the three mercury species are illustrated in Figs. 3b, d, f. The wet deposition patterns follow the rain pattern simulated by the atmospheric model. For example, this can be understood from the fact that the highest wet deposition amounts are estimated in the vicinity of mountainous regions (e.g. Alps, Atlas mountains, Dinaric Alps).

The seasonal and "annual" depositions averaged in the entire model domain are presented in Table 1. The wet depositions of Hg^{II} and Hg^P are in general one order of magnitude larger than the dry deposition ones (Table 1) contradictory to the calculated values of the dry-wet deposition of Hg^0-adsorbed, that are almost the same.

Table 1: The dry and wet depositions of Hg^0-adsorbed, Hg^{II} and Hg^P averaged over the entire model domain.

($ng\ m^{-2}day^{-1}$)	Dry dep. Ads. Hg^0	Wet dep. Ads. Hg^0	Dry dep. Hg^{II}	Wet dep. Hg^{II}	Dry dep. Hg^P	Wet dep. Hg^P	Total "Seasonal" ($ng\ m^{-2}season^{-1}$)
Nov.	$5.163x10^{-3}$	$5.541x10^{-3}$	7.678	66.490	2.024	71.892	13476.6
Feb.	$4.672x10^{-3}$	$6.055x10^{-3}$	7.802	80.176	1.903	78.676	15171.1
May	$4.469x10^{-3}$	$4.094x10^{-3}$	13.268	54.373	2.303	56.905	11670.9
July	$2.430x10^{-3}$	$3.076x10^{-3}$	15.278	34.672	3.115	42.822	8822.0
Total "Annual" ($ng\ m^{-2}\ a^{-1}$)	1.525	1.708	4027.1	21458.5	853.9	22797.8	49140.6 ($ng\ m^{-2}\ a^{-1}$)

In general the deposition patterns show that large amounts of mercury are deposited in the Mediterranean region.

4. CONCLUSIONS

Some of the similarities and differences between conventional air pollution modeling and mercury modeling have been examined in this study. The main differences are detected in the temporal and spatial scales of various physicochemical processes involved in the mercury cycle in the atmosphere. These processes are varying according to mercury species. Hg^0 is considered as long-range transport pollutant, Hg^{II} is fast reacting and deposits quickly (wet and dry) while Hg^p has behaviour similar to the other particulate in the atmosphere. Thus mercury can be considered both long and short-range transport pollutant. The results of this study showed that the Mediterranean Sea region is not only affected by mercury released in its vicinity but also from air masses enriched in mercury from stations in northern and North-eastern Europe. This suggests that local and remote emissions must be taken into account in mercury studies in the Mediterranean.

The deposition patterns of mercury exhibited several similarities with deposition patterns estimated in previous work for other conventional air pollutants. During the summer period, the Mediterranean Sea Region is characterised by anticyclonic

circulations, which are known to be associated with large-scale subsidence and no rain. The amounts of the Hg^{II} and Hg^{p} that is dry deposited during the warm experimental period are higher. The wet deposition patterns during winter showed that the largest amounts of mercury are deposited in Eastern Europe and in the Mediterranean region, especially in its eastern part. The amounts of Hg^{0}-adsorbed that is deposited dry and wet are small compared to the ones of Hg^{II} and Hg^{p}. However the deposition pattern of Hg^{0}-adsorbed is a considerable quantity as it may indicate the aerosol deposition pattern.

The difficulties in measuring the wet and dry deposition of mercury make the deposition patterns estimated by the model very useful. The models are also helpful in estimating the mercury concentration due to the lack of reliable and consistent measuring methods. A well-developed numerical model is also much cheaper than a dense observation network that is required for high-resolution estimations of the concentration and deposition. From this aspect the developed models should be considered as very useful tools for studying the mercury processes and therefore be used by policy makers.

Acknowledgements: This work was supported by the EU-funded projects MAMCS (ENV4-CT97-0593) and ADIOS (EVK3-CT-2000-00035). The authors would like to acknowledge Prof. N. Pirrore and his group, for their cooperation in the model development at the framework of MAMCS project

5. REFERENCES

Electric Power Research Institute technical report TR-107695, 1996: Mercury in the environment-A research update. Final report, EPRI, Palo Alto, CA.

Kallos, G., V., Kotroni, K., Lagouvardos, M., Varinou, M., Uliasz, and A., Papadopoulos 1997a: Transport and Transformation of air pollutants from Europe to East Mediterranean Region (T-TRAPEM). Final Report Athens, Greece, pp.298

Kallos, G., S. Nickovic, A. Papadopoulos, D. Jovic, O. Kakaliagou, N. Misirlis, L. Boukas, N. Mimikou, G. Sakellaridis, J. Papageorgiou, E. Anadranistakis and M. Manousakis 1997b: The Regional weather forecasting system SKIRON. Proceedings of the Symposium on Regional Weather Prediction on Parallel Computer Environments, 15-17 October 1997, Athens, Greece. 109-122.

Kallos, G., V., Kotroni, K., Lagouvardos, A., Papadopoulos, M., Varinou, O., Kakaliagou, M., Luria, M., Peleg, A., Wanger, and M., Uliasz, 1998: Temporal and spatial scales for transport and transformation processes in the eastern mediterranean Proc. of the 22st NATO/CCMS Int. Techn. Meeting on Air Pollution Modelling and Its Application, 2-6 June, Clermont-Ferrand, France.

Kallos G., Kakaliagou O., Voudouri A., Pytharoulis I., Pirrone N., Forlano L., and J. Pachyna, 2000: Modelling of the mercury cycle in the atmosphere. Proceedings, 24th ITM of NATO/CCMS on Air Pollution Modelling and its Application, 15-19 May 2000, Boulder, CO, USA.

Pai, P., Karamchandani, P., and Seigneur, C., 1997: Simulation of the regional atmospheric transport and fate of mercury using a comprehensive Eulerian model. Atm. Env., **31**, 2717-2732

Pielke, R. A., Cotton W. R., Walko R. L., Tremback C. J., Lyons W. A., Grasso L. D., Nicholls M E., Moran M. D., Wesley D. A., Lee T. J., and J. H. Copeland, 1992: A comprehensive meteorological modelling system - RAMS. Meteorol. Atmos. Phys., **49**, 69-91.

Pirrone N., and G. J. Keeler, 1995: Numerical Modelling of Gas-Particle Partitioning of Atmospheric Mercury in Urban Areas. In Proceedings of the *1995 Annual Meeting of the American Association for Aerosol Research (AAAR),* October 9-13, 1995, Pittsburgh, Pennsylvania, U.S.A.

Pirrone N., Keeler G. J., and T. M. Holsen, 1995: Dry Deposition of Trace Elements over Lake Michigan: A Hybrid-Receptor Deposition Modelling Approach. *Environmental Science and Technology,* 29, 2112-2122.

Slinn, S. A., and W.G.N. Slinn., 1981: Modelling of Atmospheric Particulate Deposition to Natural Waters. In: *Atmospheric Pollutants in Natural Waters,* S.J. Eisenreich, Ed., Ann Arbor Science, Ann Arbor, MI. pp. 22-53.

Sehmel G. A., 1980, Particle and gas dry deposition: A Review. Atm. Env., **14**, pp. 983-1011.

Willams, R. M., 1982: A model for the dry deposition of particles to natural water surfaces. Atmos. Environ., 1933-1938.

THE AUSTRALIAN AIR QUALITY FORECASTING SYSTEM: MODELLING OF A SEVERE SMOKE EVENT IN MELBOURNE, AUSTRALIA

Sunhee Lee, Martin Cope, Kevin Tory, Dale Hess, and Yuk L. Ng*

1. INTRODUCTION

The Australian Air Quality Forecasting System (AAQFS) is a joint project between CSIRO Atmospheric Research, CSIRO Energy Technology, the Bureau of Meteorology (BoM), the EPA Victoria and the EPA of New South Wales to develop a high-resolution air quality forecasting system. Currently, numerical air quality forecasts are issued twice daily for two regions: the airshed of Melbourne and Geelong in Victoria (see Figure 1) and the airshed of Sydney in New South Wales. The principal AAQFS role is to issue numerical forecasts to State EPAs in time for guidance and reference against current air quality forecasting procedures.

The AAQFS consists of five tightly coupled components: (a) the Limited Area Prediction System (LAPS, Puri et al., 1998), one of the BoM's operational weather forecasting systems, is used to generate forecasts of the transport fields at 0.05° (~5 km) horizontal grid spacing; (b) a hybrid offline/online emissions inventory module (EIM, Ng et al., 2000), which generates emission flux estimates for 53 chemical species from anthropogenic, biogenic and natural sources on horizontal grids with spacing of 0.01° for urban areas and 0.05° for non-urban areas; (c) a chemical transport model (CTM; Cope et al., 1999), which generates air quality forecasts for 25 pollutants (including PM1; PM2.5; PM10; photochemical oxidants, formaldehyde, butadiene and benzene) on a horizontal grid spacing of 0.01° for the urban areas and 0.05° for the non-urban areas. Forecasts are undertaken using the highly condensed GRS mechanism (Azzi et al., 1992), thus enabling large domains to be simulated within the forecasting window; (d) a validation system in which observed and forecast 1-hour time series of key meteorological variables and air quality species are compared on a daily basis using a range of graphical and statistical tools; (e) a data dissemination and archiving system which consists of an AAQFS web site displaying graphical summaries of the daily

* Sunhee Lee, CSIRO Atmospheric Research, Aspendale VIC Australia, Martin Cope, CSIRO Atmospheric Research and Energy Technology, North Ryde NSW, Kevin Tory and Dale Hess, BMRC Melbourne VIC Australia, Yuk L. Ng, Victoria EPA, Melbourne VIC Australia

Air Pollution Modeling and Its Application XV, Edited by
Borrego and Schayes, Kluwer Academic/Plenum Publishers, New York, 2002

forecasts for use by the EPAs, a PC-based graphical display software for visualising air pollutant species, forecast and observed meteorological variables, and a platform-independent file-archiving system.

On 11-12 January 2001, Melbourne experienced the worst visibility episode since the Ash Wednesday bushfire and the Melbourne Dust Storm in 1983. The episode was caused by thick smoke emitted from bushfires on King Island (some 300 km south of Melbourne) and Winchelsea (100 km south-west of Melbourne). Smoke from the Winchelsea fire arrived immediately behind a cold front in the afternoon of 11 January; smoke from the King Island fire first arrived in the Melbourne area during the evening and continued to cross the region throughout the following day.

This paper describes a study in which the AAQFS was used to simulate the severe smoke event of 11-12 January.

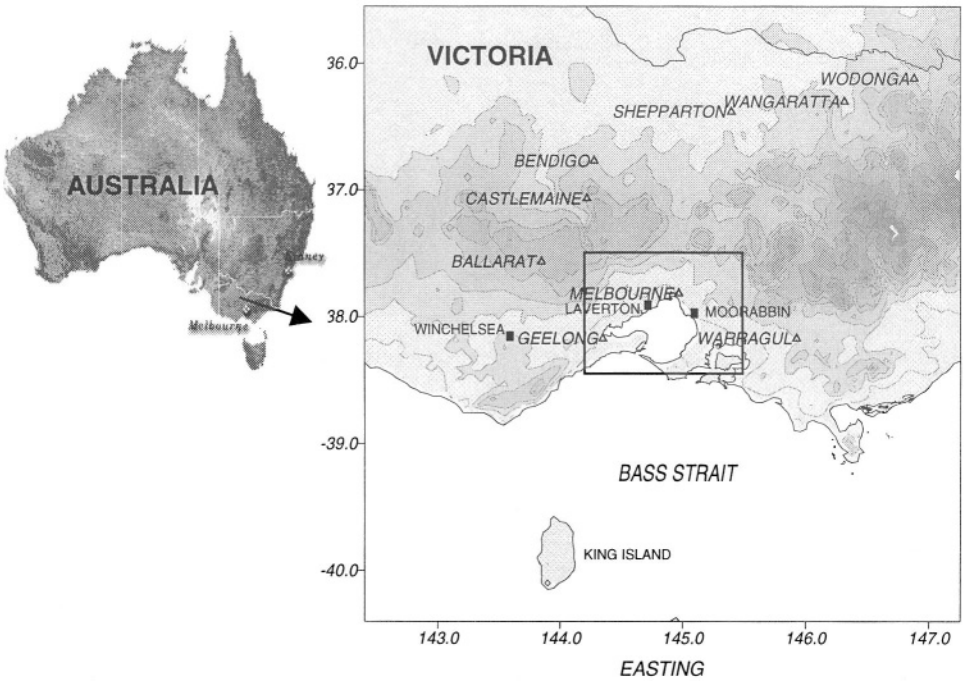

Figure 1. The location of the AAQFS Victorian (0.05° horizontal grid spacing) and Melbourne (0.01° horizontal grid spacing) domains. Note that Winchelsea and King Island are in the Victorian domain.

2. CHARACTERISTICS OF THE KING ISLAND AND WINCHELSEA FIRES

The King Island fire started on 3 January 2001. Over the next 7 days the fire burnt 2000-3000 ha of vegetation; the fire was thought to be under control by 10 January. On 11 January, a strong south-west wind came through and the fire was re-ignited and burnt 4500-5000 ha of tea-tree forest, sage-land and heath-lands. The Winchelsea fire started at 15:55 EDT (Eastern Daylight Saving Time), 11 January and was contained by 18:00

EDT, though smouldering continued for another two days. The area burnt was 320 ha of grass-land.

Figure 2 shows GMS-5 satellite images of smoke from the King Island fire at 7:32 and 12:32 EDT on 10 January and 12:32 and 15:25 EDT on 11 January. During this period the winds shifted from north-easterly to north-westerly, which generated a smoke plume that extended to the south-west and rotated with time to the south-east just prior to the arrival of the frontal wind change. The fire intensified when the winds picked up as the front approached. The south-westerly change advected the plume to the northeast and the most recently emitted smoke began to form a plume directed to the northeast. Smoke from the Winchelsea fire was transported to Melbourne by the cold front and arrived at the same time as the wind changes. The Winchelsea fire was relatively small compared to the King Island fire and the smoke from the fire was not visible in satellite images. The King Island smoke plume was not clearly discernable in the satellite images after 18:30 EDT, because of the presence of clouds.

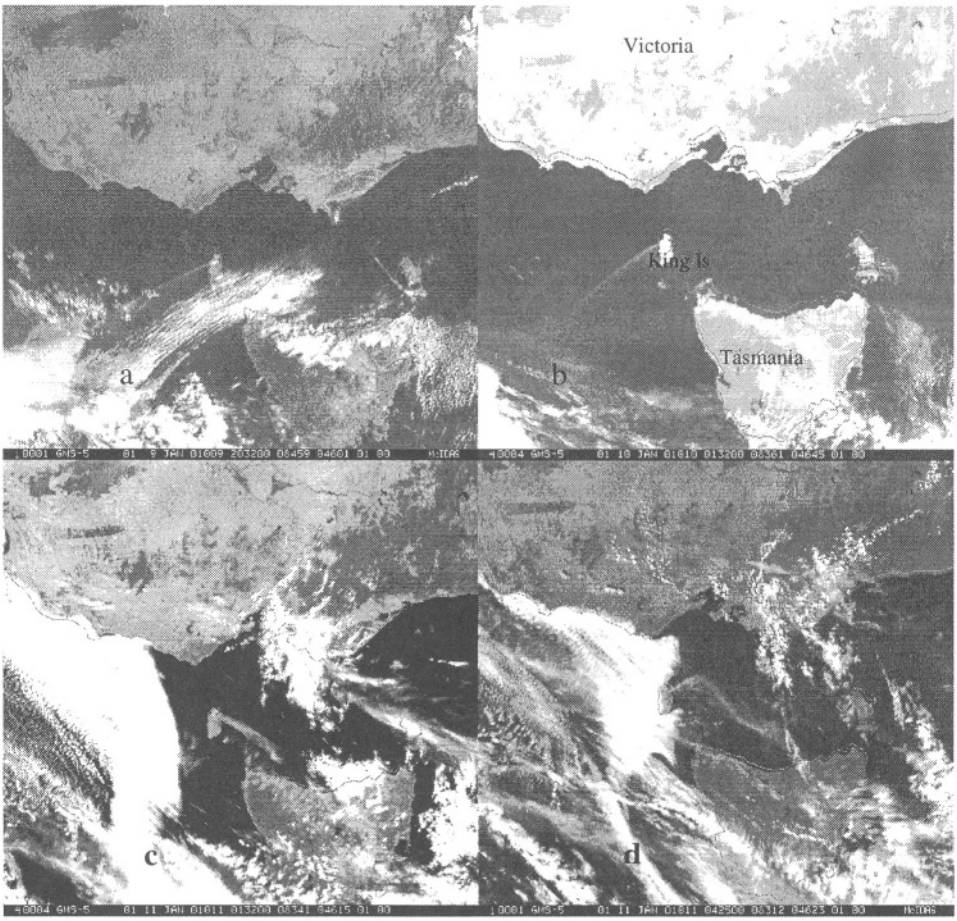

Figure 2. GMS-5 satellite images illustrating the changing direction of the smoke plume from the King Island wildfire. The upper images (a) and (b) are at 7:32 and 12: 32 EDT on 10 January. The lower images (c) and (d) are at 12:32 and 15:25 EDT on 11 January

3. THE AAQFS-LAPS METEOROLOGICAL PREDICTION

A comparison of observed and modelled winds indicated that the cold front was predicted to arrive 1-2 hours earlier than was observed to the southwest and north of Melbourne, while for southeast of Melbourne the timing was close to coincident. Figure 3(a) and 3(b) show time-series of observed and modelled wind temperature and dewpoint temperature at Laverton, west of Melbourne, and at Moorabbin, east of Melbourne, respectively (see Figure 1). The frontal arrival is shown by the drop in temperature, the rise in air moisture (represented by the rise in dewpoint temperature) and the shift in wind direction. This is considered to be a good forecast since the cold front arrival is particularly sensitive to the balance between the weak synoptic northerlies and the development of sea and bay breezes. The latter winds can enhance the frontal structure, and accelerate or stall the larger scale wind change, which further complicates the frontal forecast. In this case the model sea/bay breeze influence differed on either side of the bay.

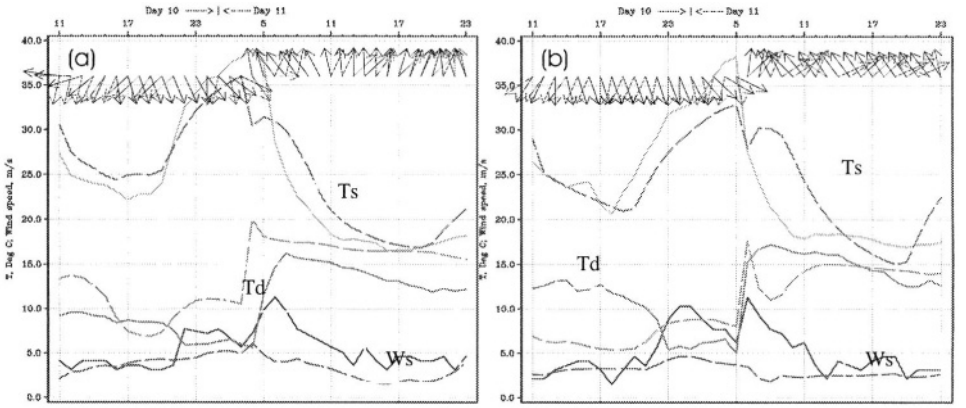

Figure 3. Time series of surface temperature (Ts), dewpoint temperature (Td), and wind speed (Ws) for a period from 1100 UTC (22:00 EDT) 10 January to 2300 UTC 11 January, at (a) Laverton and (b) Moorabbin. The dashed (solid) lines represent LAPS (observed) Td, Ts and Ws, while dark (light) arrows represent LAPS (observed) wind direction.

Figure 4(a) shows the vertical profile of observed temperature and wind structure obtained from data collected by commercial aircraft as they took-off from Melbourne airport. It shows a well-mixed layer extending to 850 hPa after 8:00 EDT 11 January with winds from the north-northwest. After 16:00 EDT, the wind shifted to southerly and the temperature dropped significantly below 950 hPa, as the colder southerly flow arrived behind the front. A very stable layer formed between the lower-level cold air and the remaining warmer air above. This stable layer effectively put a lid on the smoke and helped maintain the high particle concentrations by inhibiting vertical dilution. A similar vertical profile in Figure 4(b) was constructed by interpolating the gridded model data to the flight paths. The timing of the change and depth of the cold air is in very good agreement with the observed profile. The diagnosed PBL height is over-predicted during the day due to slightly cooler temperatures between 800 and 900 hPa. Other differences are largely due to limitations of the model grid resolution.

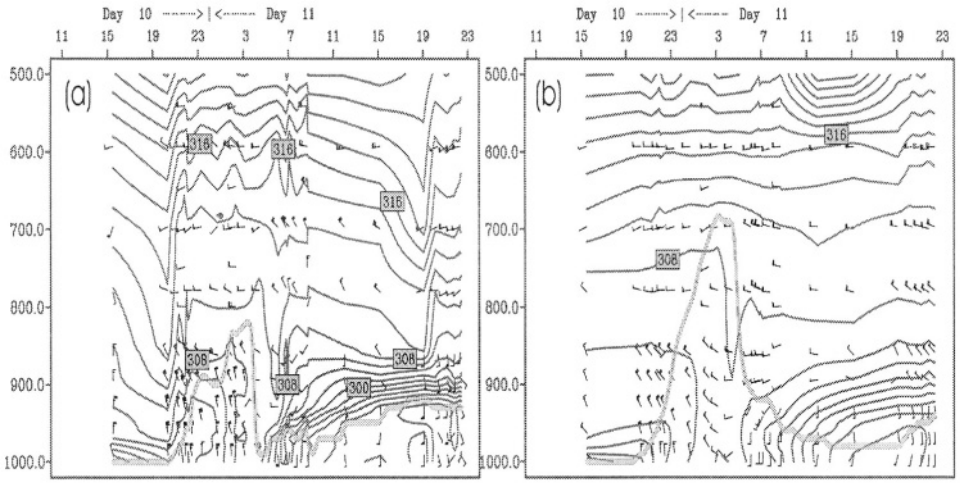

Figure 4. Time-height profiles of potential temperature (contour interval 2 K) and winds (full barb = 10 knots), for the 36 hour period following 1100 UTC 10 January 2001. The thick line marks the approximate position of the top of the mixed layer, determined by the level at which the atmosphere is first 1 K warmer than the 10-m potential temperature. Image (a) was constructed from data collected by commercial aircraft as they took-off from Melbourne airport, and (b) from LAPS data interpolated to the flight paths. The cold front arrival (determined from the wind barbs) occurred near 0600 (17:00 EDT) in (a), and 0500 UTC (16:00 in EDT) in (b).

4. THE AAQFS-CHEMICAL TRANSPORT MODELLING

To investigate the suitability of the AAQFS for forecasting the impact of severe smoke events, a series of hindcasts were carried out. A simple fire emission model was developed to calculate hourly emission of PM10, carbon monoxide, butadiene, reactive organic carbon, and oxides of nitrogen using a constant fuel consumption rate. Emission factors were obtained from studies of USEPA (1995) and SAFARI-92 (Andreae et al., 1997). For the Winchelsea fire, the fire size and fuel loading were assumed to be 320 ha and 5.6 tonnes per ha, respectively. For the King Island fire, the fuel loading was assumed to be 45 tonnes per ha and fire size to be 5000 ha. Table 1 lists the emissions values used in the hindcast. The times stated in hindcast results below are all in EDT.

Table 1. The emissions are in g/s. For the Winchelsea fire, the emission values are for the flaming phase, 16:00 to 18:00 EDT. For smouldering phase after 18:00, emission values are reduced by 2/3.

	PM10	CO	NOy	ROC	BTD
King Island	38887	182028	5200	27563	247
Winchelsea	3733	17474	499	2646	24

4.1. Basecase

A basecase simulation was generated by integrating the AAQFS for a 36-hour period commencing 10:00 11 January. The King Island plume was released uniformly between

the surface and 1000 m, in accordance with visual observations. For the Winchelsea fire, emissions were uniformly placed between the surface and 500 m. Because there is some uncertainty associated with the release heights, a number of sensitivity runs were undertaken to assess the impact on the spatial and temporal distribution of the PM10 plumes (see Section 4.2).

Shown in Figure 5(a) is the ground level PM10 plume as predicted for 12:00 on 11 January. At this time the plume is still within a north-westerly flow. The location of the predicted plume is in good agreement with the observed (see Figure 2c).

Following the passage of the cold front after 17:00, both observed and modelled winds backed from south-westerly to southerly, causing the King Island plume to rotate counter-clockwise. The plume reached the southern edge of Port Phillip Bay at midnight and swept over Melbourne from the southeast at 2:00 12 January (Figure 5b). The eastern edge of the plume had cleared Port Phillip Bay by 6:00 (Figure 5c), and had cleared the eastern metropolitan area by 7:00. However, this region was again affected by smoke between the hours 10:00 to 11:00 inclusive. The simulation suggests that this second impact was caused by fumigation of PM10 from an elevated air mass, in response to convective boundary-layer growth.

Three air quality monitoring stations in eastern Melbourne recorded PM10 measurements during this smoke event. The observed PM10 measurements from these stations showed a similar pattern; three major peaks occurred at 17:00 11 January (60-80 $\mu g\ m^{-3}$), from midnight to 3:00, 12 January (120-140 $\mu g\ m^{-3}$), and 9:00 to 10:00, 12 January (170-220 $\mu g\ m^{-3}$). The initial peak represented the Winchelsea plume and the major peaks were from the King island plume and fumigation. The AAQFS simulation, as described above, agreed well with the observed timing of peak occurrences, however, the observed maximum concentrations of PM10 were under-predicted.

4.2. Sensitivity Studies

In order to investigate sensitivity of plume distribution and timing with respect to release height, two sensitivity runs were carried out.

In the first run, emissions from King Island were allocated with an effective plume height of 1000 m. In the case of Winchelsea, the effective plume height was set to 500m.

The effect of locating all of the plume mass at these heights was seen in both the timing and the magnitude of the PM10 impacts on Melbourne. For example, the smoke plume was now predicted to reach Port Phillip Bay at 2:00 (two hours later than the basecase) and to sweep over Melbourne at 5:00 (three hours later than basecase). On the other hand, the fumigation event occurred two hours earlier (commencing at 9:00 instead of 11:00) and resulted in considerably higher (by up to 100 $\mu g\ m^{-3}$) PM10 concentrations as shown in figure 6(a). Figure 6(b) displays the basecase PM10 concentrations for the Melbourne grid at 11:00 12 January.

In the second sensitivity run, emissions were allocated with an effective plume height of 500 m for King Island and of 250 m for Winchelsea. In this run, the plume reached Port Phillip Bay at 23:00 11 January (one hour earlier than the basecase) and reached Melbourne at 2:00 12 January. It cleared eastern Melbourne then moved slightly back eastward at 9:00 before completely clearing the Melbourne area. This run did not feature strong fumigation.

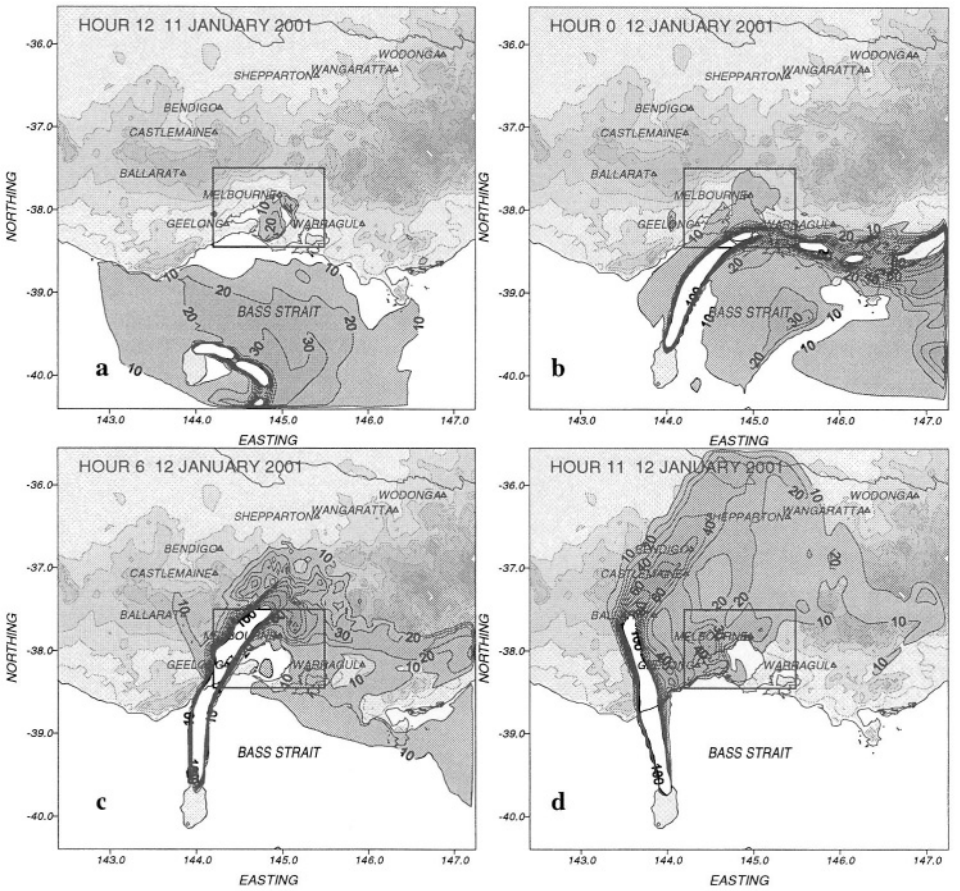

Figure 5. The AAQFS smoke plume from the King Island fire covering period from 12:00 11 January to 11:00 12 January when fumigation started.

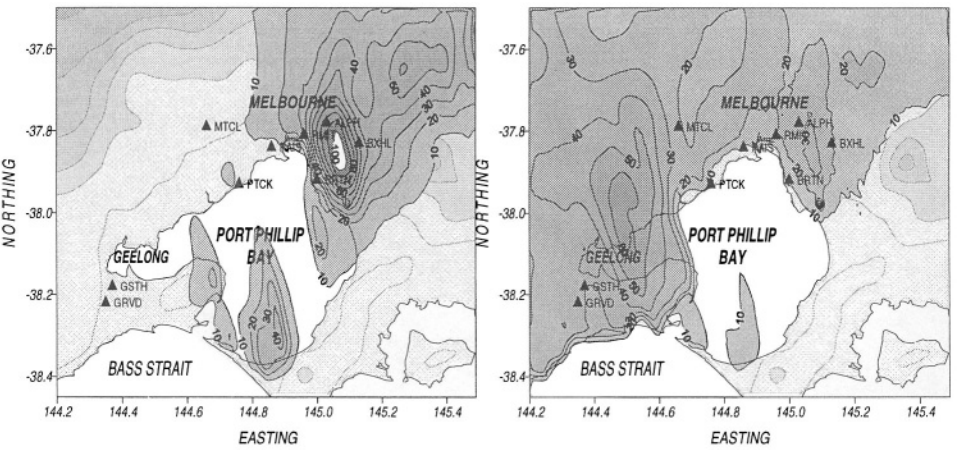

Figure 6. (a) The PM10 concentrations of a sensitivity run with all the emissions at 1000 m height at 11:00 12 January. (b) The same as (a), except for the basecase.

The impact of using different emissions factors and fire size in the simulation was also investigated. The resultant effects on plume distribution and magnitude were insignificant compared to those of using different plume release heights.

The impacts of other air quality species emitted by the wildfires, e.g. NO_2, SO_2, C_6H_6, CH_2O and C_4H_6, were also modelled and found to have a reduced level of influence compared with PM10.

5. SUMMARY

The AAQFS currently issues twice daily 24-36 hour numerical air quality forecast for the Melbourne and Sydney regions for Victoria EPA and NSW EPA in time to provide reference and guidance for air quality forecasting. One of the potential usages of the AAQFS is to provide guidance in the management of prescribed burns and in alerting the public of smoke impacts on air quality.

On 11 January 2000, Melbourne experienced the worst visibility episode since 1983 due to thick smoke from the King Island and Winchelsea bushfires. A series of the AAQFS simulations were carried out to model the severe smoke event and determine the sensitivity to emissions factors, fire size and plume height.

The AAQFS demonstrated that the modelled distribution and transport of smoke plume were qualitatively in good agreement with the observation from the satellite and monitoring stations, with regard to the timing of plume arrival, dissipation, and fumigation. Additional tests showed that the PM10 plume development and magnitude were sensitive to the plume release heights, while they were relatively insensitive to emissions factors and fire size.

6. ACKNOWLEDGMENT

The AAQFS was developed under funding from the Air Pollution in Major Cities Program, sponsored by Environment Australia.

7. REFERENCE

Andreae, A., Atlas, E., Cachier, H., Cofer, W., Harris, G., Helas, G., Koppmann, R., Lacaus, J., and Ward, D., 1977, Trace gas and aerosol emissions from savanna fires, in: *Biomass Burning and Global Change* Vol 1, J. Levine, ed., MIT press, Cambridge, pp. 278-295.

Azzi, M., Johnson, G. J., and Cope, M., 1992. An introduction to the Generic Reaction Set photochemica smog mechanism. Proc. 11th International Clean Air Environment Conf., 5-9 July 1992, Brisbane, Clean Air Society of Australia and New Zealand, 451-462.

Cope, M., Hess, D., Lee, S., Azzi, M., Carras, J., Wong, N., and Young, M., 1999. Development of the Australian Air Quality Forecasting System: Current status. Proc. International Conf. Urban Climatology, 8-12 November 1999, Sydney, 595-600.

Ng, Y. L., Walsh, S. and Wong, N., 2000. Emissions model for the Australian Air Quality Forecasting System. Proc. 15th International Clean Air Environment Conf., Vol. 1, 26-30 November 2000, Sydney, Clean Air Society of Australia and New Zealand, 275-280.

Puri, K., Dietachmayer, G., Mills, G. A., Davidson, N. E., Bowen, R. A., Logan, L. W., 1998. The new BMRC Limited Area Prediction System, LAPS. Aust. Met. Mag., 47, 203-213.

USA EPA, Compilation of air pollutant emission factors, Vol 1, Stationary point and area sources, AP-42, 1995.

DISCUSSION

B.J. ABIODUN

1) Is you meteorology model a hydrostatic or non-hydrostatic model ?
2) Is your dispersion using a Langrangian or a Eulerian model ?

S. LEE

No. LAPS (Limited Area Prediction System) is hydrostatic and Eulerian.

D. STEYN

Australian bushland has plant species not found in North America. How did you find emission factors in the EPA guidelines to match Australian bush ?

S. LEE

For a grass fire, which is the case for the Winchelsea fire, PM10 emission factor was obtained from U.S. EPA fire module manual. For the same reason as the question mentioned, we use PM10 factor for the King Island fire from Andreas (1997) which was obtained from SAFARI-92 experiment in the South Africa. The King Island fire sources are tea-tree forest and heath lands. It is thought to be closer to Savanah vegetation than N. American vegetation.

A.I. MIRANDA

Do you have any information concerning the fire behaviour ? Because, it is possible to estimate forest fires plume rise using the heat release and accordingly to the stability of the atmosphere. There are formulas to do that, specifically developed to forest fires.

S. LEE

Yes, we do use the Briggs formula for neutral and unstable conditions, which has two different formulas depending on the magnitude of heat release. For the stable condition we calculate the plume height from buoyancy flux. The details can be found in the CIT model manual.

A. HANSEN

Do you know why the PM 2.5 fraction of PM 10 for the fumigation episode from 2100-2400 was so much lower than the other smoke episodes ?

S. LEE

The fumigation period was from 9:00 am to 12:00 am. There was no observed PM 2.5 available for the period of 10:00 – 11:00. PM 2.5 curve was drawn from 9:00 to 12:00, which is misleading. At 9:00 and 12:00, the ratio of PM 2.5/PM 10 was 2/3, while other smoke

episodes showed PM ratio of ½ ~ 2/3. All three smoke episodes showed a similar PM 2.5/PM 10 ratio.

A. BAKLANOV — Are there some improvements of the urban layer parameterisations in your NWP model for the city area or you use the same physical parameterisations (like for "rural" areas) but with other values of input parameters in urban zones (z_0, surface flux etc.) ?

S. LEE — In the NWP(LAPS) model we use the same physical parameterisations in the urban and rural areas. We have not yet included a detailed urban boundary-layer parameterisation. The effects of the urban areas are modelled through changes to the input parameters, such as the roughness lengths for momentum, heat and moisture, and leaf-area index. However, we post process these fields over urban areas to force a near-neutral boundary layer (h/L = 1) with h=hmin_urban, where hmin_urban is a representative minimum urban boundary layer height (typically O(100 m)). u* is adjusted accordingly. This scheme is a crude attempt to account for an urban heat island effect.

PRE-PROCESSOR FOR REGIONAL-SCALE FLUXES AND MIXED-LAYER HEIGHT OVER INHOMOGENEOUS TERRAIN

S.-E. Gryning[1] and E. Batchvarova[1,2]

1. INTRODUCTION

The distribution of mixed-layer heights, momentum and sensible heat fluxes are critical factors in the dilution and spread of air pollutants. In dispersion models, the individual horizontal grid cells often enclose regions of pronounced inhomogeneities. The estimation of the regional/aggregated mixed-layer height, momentum and heat fluxes is therefore a central issue for the parameterisation used in those models.

A possible approach to evaluate regional fluxes is through a flux aggregation scheme. Point measurements are combined, in one way or another, to produce regional fluxes. Such methods has received some success for regional heat fluxes, likely because forest edge effects on the heat fluxes (temperature) are rather small as compared to fluxes over forest and grass land - at least for common patch-sizes of agricultural and forested areas typically for Europe. But for regional momentum fluxes it does not work, partly because the regional momentum flux of a patchy landscape of surfaces with different roughness length add up the local momentum fluxes in a highly non-linear way, and partly because the contribution to the regional momentum flux also is composed of effect by isolated trees, houses and sharp edges between forest and grass-land which are not necessarily small. Local momentum and heat fluxes traditionally are determined from mast measurements performed in locally homogeneous terrain, either directly by turbulence measurements, or by applying appropriate profile-flux relationships based on Monin-Obukhov scaling theory on measured profiles of temperature and wind. Such a network of flux measuring stations located over patches of typical and locally homogeneous terrain is inappropriate for the determination of regional surface momentum fluxes and large scale mixing-heights.

[1] Wind Energy Department, Risø National Laboratory, DK-4000 Roskilde, Denmark
[2] National Institute of Meteorology and Hydrology, Academy of Sciences, Bulgaria

Air Pollution Modeling and Its Application XV, Edited by
Borrego and Schayes, Kluwer Academic/Plenum Publishers, New York, 2002

2. METEOROLOGICAL PRE-PROCESSOR

Here is presented a met-processor for regional fluxes of momentum and sensible heat, and mixed-layer height. The method is simplified but reflects some of the basis physical characteristics for meso scale fluxes. The regional momentum flux is determined based on blending height theory, and the regional sensible heat flux as a land use average for the grid cell. These fluxes are used to estimate the mixed-layer height. The information that is needed to apply the met-processor can be obtained from radiosondes, tall mast or acoustic soundings profiles of wind speed, and maps of land use for the area. An estimate for the heat fluxes over the various patches of the area should also be available.

2.1. Regional momentum flux

Near the ground the wind changes over the various surface areas ceaselessly trying to reach balance with the underlying surface. The upward diffusion of information from the surface features reaches a certain height before the flow encounters a new surface type. Because the size of the dominant eddies increases with height, the signature of the individual surface features is blended efficiently at higher levels. Mason (1988) introduced a blending height as the characteristic height where the flow changes from mainly reflecting local surface characteristics, to be independent of its horizontal position and reflecting the influence on the flow of all the various surface scales. Therefore, the horizontal variability and imbalance of the mean flow due to surface variability hardly reaches beyond the blending height. Above the blending height the flow reflects the regional area and is horizontally homogeneous (Mahrt, 1996). Gryning and Batchvarova (1999) discuss the vertical depth of the influence of surface variation by use of other relationships: internal boundary layer growth and footprint analysis. The results are comparable in value to the blending height, but are based on different physical approaches.

The blending height theory in the form applied here is based on a parameterisation of the drag coefficients at the blending height, which is taken as a function of a characteristic horizontal length scale of the land surface variations. Following Mason (1988) and Mahrt (1996 and 1999) a stability-dependent scale value for the blending height can be predicted to be:

$$l_b = 2\left(\frac{\sigma_w}{U}\right)^2 L_s \qquad (1)$$

where σ_w is the standard deviation of the vertical wind speed fluctuations and L_s is the characteristic length scale for the horizontal surface inhomogeneities.

In order to use the method, the length scale, L_s, for the area must be known. It can be estimated from maps of land-cover subjectively or objectively by analysis of the distribution of the surface inhomogeneities. Having an estimate of the length scale, and assuming a value of σ_w / U around 0.1 it is possible to estimate the blending height for the area.

When dealing with inhomogeneous conditions the regional (effective or aggregated) roughness length for momentum can be defined as the parameter that gives the correct surface stress for the area as a whole when used in connection with a wind profile relationship. The blending height can also be considered as the level where the wind-profile becomes independent of the horizontal position and is in equilibrium with the overall surface conditions

$$U(z) = \frac{u_*^{eff}}{\kappa} \left\{ \ln\left(\frac{z}{z_0^{eff}} \right) - \psi_m\left(\frac{z}{L^{eff}} \right) \right\} \qquad z > l_b \tag{2}$$

where κ is the von Karman constant, u_*^{eff} is the effective friction velocity, z_0^{eff} is the effective roughness length for the inhomogeneous area that will yield the correct surface stress from the wind profile and remains to be determined from the surface characteristics, ψ_m is the wind profile stability correction function and L^{eff} is the Monin-Obukhov length incorporating the effective momentum and sensible heat fluxes (Wood and Mason, 1991).

For a homogeneous area the drag coefficient for near neutral conditions, C_{DN} is given by (Stull, 1988)

$$C_{DN} = \frac{\kappa^2}{\ln^2\left(\frac{z}{z_0} \right)} \tag{3}$$

At the blending height the wind speed is nearly horizontally constant. Mason (1988) proposes that the drag coefficient at the blending height for the entire area should be estimated as the drag coefficients for the various sub areas weighted in proportion to their fraction of the area. Therefore

$$\left[\ln\left(\frac{l_b}{z_0^{eff}} \right) \right]^{-2} = \sum_i f_i \left[\ln\left(\frac{l_b}{z_0^i} \right) \right]^{-2} \tag{4}$$

where f_i is the fraction of the total area covered by the *i*th surface having the local momentum roughness length z_0^i. The effective roughness length, z_0^{eff} represents the surface stress that originates from surface roughness and does not include the effect of major obstacles such as topography, isolated buildings, houses and forest edges as discussed by Raupach (1992). Wood and Mason (1991) found that while z_0^{eff} is a function of stability this dependence is small, and for all practical purposes can be neglected.

The effective roughness length for the area can be determined by Eq. (4) from information on land-cover and blending height. To a first approximation the stability dependence on z_0^{eff} in Eq. (4) can be neglected. Knowing z_0^{eff} and l_b, the regional friction velocity, u_*^{eff}, at a given time can be determined from Eq. (2) by use of the wind-speed at

the blending height that is known from i. e. the radiosoundings. Application of the method when the stability correction in Eq. (2) cannot be neglected, require information on the regional heat flux - see the next section.

2.2. Regional heat flux

For the regional heat fluxes, the so-called tile approach is considered. In order to apply this approach, the heat fluxes over the patchy sub-areas most be known as well as the extend of the areas. The applied approach for regional heat flux estimation is a weighted average of the patch estimates of the heat fluxes in relation to the landscape classes:

$$\left(\overline{w'\theta'}\right)_s^{eff} = \sum_{k=1}^{K} \lambda_k \left(\overline{w'\theta'}\right)_s^k \tag{5}$$

$$\lambda_k = \frac{a_k}{A} \tag{6}$$

Here a_k represent a sub-area with heat flux $\left(\overline{w'\theta'}\right)_s^k$. A is the total area. In this process the interaction between the subareas has been neglected. This has in a number of studies been found to be a reasonable assumption for patch sizes of some km or larger, which is typical for most European landscapes. For smaller patch sizes the applicability of the tile method has not yet been investigated.

2.3 Mixed-layer height

The upward diffusion of information on the surface features reaches a certain height before the flow encounters a new surface type. With large scale inhomogeneities or a shallow mixed layer the influence of the individual surface features may extend up to the top of the mixed layer. In this case the time averaged flow at any level within the mixed layer will vary spatially, Mahrt, 1996, and the heat flux estimated by the method presented here will represent local conditions. At smaller scales of the inhomogeneities or a deeper mixed layer the level at which the individual surface features are no longer felt and the time averaged flow properties are spatially invariant is embedded within the mixed layer. In this case a conventional mixed-layer growth model can be applied when the regional values of the parameters are used.

For example the mixed-layer growth model suggested by Batchvarova and Gryning (1991) takes the form for a patchy landscape:

$$\left\{\frac{h^2}{(1+2A)h - 2B\kappa L^{eff}} + \frac{C(u_*^{eff})^2 T}{\gamma g\left[(1+A)h - B\kappa L^{eff}\right]}\right\}\left(\frac{dh}{dt} - w_s\right) = \frac{\left(\overline{w'\theta'}\right)_s^{eff}}{\gamma} \tag{7}$$

where t is time, L^{eff} - the effective Monin-Obukhov length composed of u_*^{eff}, $\left(\overline{w'\theta'}\right)_s^{eff}$ and g/T - the buoyancy parameter, A, B and C are parameterisation constants. Com-

monly accepted values are A =0.2, B =2.5, and C =8. The potential temperature gradient, γ, and the subsidence velocity, w_s, can be extracted from the profile measurements (i.e. radiosoundings).

3. AN APPLICATION

An example of the application of the method will be shown for one of the days during the WINTEX experiment (Gryning et al. 2001), a measuring programme that was carried out in March 1997 at the FMI-Arctic Research Centre (formerly Sodankylä Meteorological Observatory, 67° 22' N, 26° 38' E, 180m) in Finnish Lapland 100 km north of the polar circle. Turbulence measurements at several heights were carried out in a pine forest of trees typically 8 m tall. Here only the measurements at 18 m is used. The measurements included releases of radiosondes every 3 hours. The study region is typical for the sub-arctic Northern Finland with coniferous (37%) and deciduous (12%) forests and large, smooth areas consisting of snow covered mires, peatbogs and shrublands (51%) dominating the landscape. The landscape is strongly heterogeneous in the sense that rough forests (z_0=1.4 m) and the smooth areas (z_0=0.01 m) are interspersed with a typical patch size of a few kilometres. Details on the measurements and site can be found in Batchvarova et al. (2001).

Fig. 1 shows the regional friction velocity (u_*^{eff}) estimates from the radiosoundings. It can be seen that the regional friction velocity is only slightly smaller than the friction velocity measured over the forest, despite the fact that the forest occupy less than half of the area. The regional heat flux is shown on Fig. 2. It is taken as 37% of the heat flux measured over the coniferous forest - assuming that the heat flux over the snow covered open areas and the deciduous forest is negligible. On this day an research aircraft performed measurements, and the regional heat flux over two 30 km long legs near the measuring site are also shown on Fig. 2 - it can be seen that the agreement between regional heat fluxes measured by use of the research aeroplane and estimated from the met-processor is fair. Finally, on Fig 3, the evolution of the mixed layer is shown. The estimated values of the regional friction velocity (taken as 0.9 of the measured friction velocity over the forest), the regional heat flux (taken as 0.37 of the measured heat flux over the forest), and the temperature gradient in the free atmosphere estimated from the radiosoundings (γ=0.003 K/m) were used in Eq. (7). Good agreement was found between the mixed-layer height that can be estimated from the radiosoundings, and predicted by the suggested met-processor.

In conclusion, the forest was found to dominate both the averaged momentum and heat flux, but in very different ways. The area averaged momentum flux is very close to the momentum flux over the forest. It only marginally dependent on the roughness of the smooth open areas, despite the fact that the forest occupies only 49% of the area. The area averaged sensible heat flux is significantly smaller than the sensible heat flux above the forest site, being the main contributor to the sensible heat flux during this part of the year. The regional fluxes of momentum and heat were successfully used to estimate the mixed-layer height.

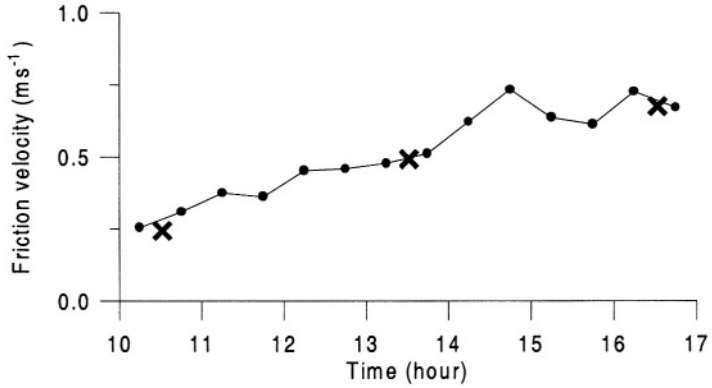

Figure 1. Measured local friction velocities over the forest at the Sodankylä Meteorological Observatory (• connected by full line), and derived regional friction velocities from the blending height method based on radiosoundings(×). Time is given in LST.

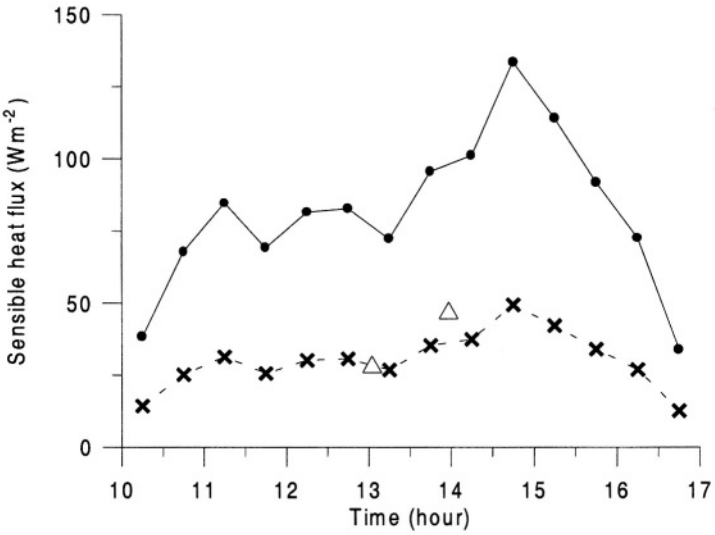

Figure 2 Measured local sensible heat flux over the forest at the Sodankylä Meteorological Observatory (• connected by a full line), and the derived regional sensible heat flux (× connected by a broken line), and the flight-track mean values (Δ). Time is given in LST.

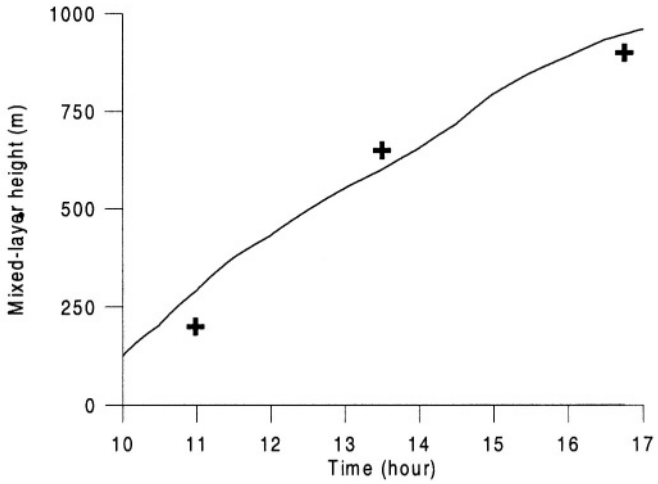

Figure. 3 Simulated mixed-layer height (full line) and derived from radiosoundings (+)

4. ACKNOWLEDGEMENT

We are grateful to Martti Heikinheimo and Markku Kangas from the Finnish Meteorological Institute for the radiosonde data and the aircraft measurements. Rigel Kivi from the Sodankylä Meteorological Observatory is acknowledged for the discussion of the accuracy and resolution of the radiosonde measurements. The hospitality and help of the staff at the Sodankylä Meteorological Observatory and the assistance of John Hansen and Lars Christensen from Risø National Laboratory are acknowledged. The aircraft measurements were performed under the STAAARTE programme funded by the European Commission.

5 REFERENCES

Batchvarova, E. and Gryning, S.-E., 1991, Applied Model for the Growth of the Daytime Mixed Layer, *Boundary-Layer Meteorol.* **56**, 261-274.

Batchvarova, E., Gryning, S.-E. and Hasager, C. B., 2001, Regional fluxes of momentum and sensible heat over a sub-arctic landscape during late winter, *Boundary-Layer Meteorol.* **99** , 489-507

Gryning, S.-E. and Batchvarova, E., 1999, Regional Heat Flux over the NOPEX Area Estimated from the Evolution of the Mixed Layer, *Agric. For. Meteorol.* **98-99**, 159-167.

Gryning, S. E., Batchvarova, E. and De Bruin, H. A. R., 2001, Energy Balance of Sparse Coniferous High-Latitude Forest under Winter Conditions, *Boundary-Layer Meteorol.,* **99**, 465-488

Mahrt, L., 1996, The Bulk Aerodynamic Formulation over Heterogeneous Surfaces, *Boundary-Layer Meteorol.* **78**, 87-119.

Mahrt, L., 1999, Surface Heterogeneity and Vertical Structure of the Boundary Layer, *Boundary-Layer Meteorol.* **96**, 33-62.

Mason, P. J. 1988, The Formation of Areally Averaged Roughness Lengths, *Quart. J. Roy. Meterol. Soc.* **114**, 399-420.

Raupach, M. R., 1992, Drag and Drag Partition on Rough Surfaces, *Boundary-Layer Meteorol.* **60**, 375-395.

Stull, R. B., 1988, *An Introduction to Boundary Layer Meteorology,* Kluwer Academic Publishers, Dordrecth, the Netherlands, 666 pp.

Wood N. and Mason, P., 1991, The Influence of Static Stability on the Effective Roughness Lengths for Momentum and Heat Transfer, *Quart. J. Roy. Meterol. Soc.* **117**, 1025-1056.

DISCUSSION

S. INCECIK

1) What is the reason of the big differences in the first period of modeled and measured mixing layer heights ?
2) What kind of measurement system is used for mixing layer height ?

E. BATCHVAROVA

1) The different performance of the Richardson number methods based on HIRLAM output during the first and the second part of the experimental period is due to the horizontal resolution of the present version (22.5 x 22.5 km) which does not allow to take into account the influence of the island of Bornholm situated 20 km south west of the measuring site. The wind during the first period of the experiment was from south west.
   During the second part of the experiment the wind turned to North with a fetch of 100 km over sea which is well described by the present version of HIRLAM.
2) Slow (boundary-layer) radio soundings were performed to measure the mixed-layer height.

A. HANSEN

There are a large number of techniques for inferring mixing height from observational data from rawinsondes, sodars, radar profilers, lidars, etc. Often they do not agree with one another. What method did you use to determine the mixing height based on the rawinsonde data ?

E. BATCHVAROVA

The mixed-layer height was estimated from radiosonde temperature and humidity profiles. The top of the boundary layer was assigned to the height where the potential temperature starts to increase. The humidity profile was considered simultaneously.

M. KAASIK

Can we expect in winter conditions the prevailing ascending air flow over forest and descending flow over snow surface (in patchy landscape) ?

E. BATCHVAROVA

Yes, this forest-open land circulation can be expected.

A. BAKLANOV I agree with you the slab model is one of the best models for CBL height over inhomogeneous terrain. However, I think, it is not a good way to compare the model with the bulk Ri-method based on so poor resolution NWP data. The island has almost sub-grid scale, so, of course, it is impossible to catch correctly the island effect on mixing height. Do you agree with this ?

E. BATCHVAROVA Yes, thank you for the comment. The idea is to emphasise that output from the HIRLAM model can be used for mixed-layer height estimates based on Richardson number methods only when the upwind area can be considered as homogeneous for several grid steps.
The study on marine boundary layer presented on the talk is not included in the conference manuscript. It is under publication in BLM/2001-2002: Gryning and Batchvarova, “Marine boundary layer height and turbulent fluxes over the Baltic sea; measurements and modelling.”

This page intentionally left blank

VALIDATION OF URBAN AIR-QUALITY MODELLING IN THE EUROPEAN UNION

Peter Suppan[1] and Andreas N. Skouloudis[2]

1. INDRODUCTION

During the AUTOOIL-II Programme of the European Commission (DG-ENV, 1996 and 2001), a large number of air-quality modelling applications were carried out in order to examine the attainment of the new EU Air-Quality standards for NO2, O3, CO, benzene and PM10 in the base year 1995 and forecast the concentrations in 2010. An advanced modelling methodology (Skouloudis and Suppan, 2000) was established incorporating state-of-the-art models and many innovative features (emission source-apportionment, cluster analysis for identifying the representative episodes meeting the objectives of the this programme, two-way nesting, multi-scale simulations down to street-canyon levels, etc). The definition of the modelling domains was linked to the population density, covering 46.7% of the European population living in urban areas at the member states, while at the same time maintaining a consistent platform of comparisons with the AUTOOIL-I programme which was carried out for the base year of 1990. For this a set of ten mega-city domains where defined for which urban air quality modelling applications were carried out (Figure 1). Apart from the objective to meet the new threshold of NO2, also special emphasis was made to examine the consequences for other pollutants simultaneously, for which air quality standards exist (CO, Benzene and PM10). Hence, contrary to the approach from the first AUTOOIL programme, full photochemical simulations were carried out during at least three representative periods.

2. MODEL SETUP

Depending on the topographically complexity of the domain the meteorological modelling was carried out with an incompressible, hydrostatic or a compressible, non-

[1] Fraunhofer Inst. for Atmos. Env. Research, Kreuzeckbahnstr. 19, D-82467 Garmisch-Partenkirchen, Germany
[2] European Commission, Joint Research Centre "Ispra", Environment Institute, T.P. 280, 21020 Ispra, Italy

Air Pollution Modeling and Its Application XV, Edited by
Borrego and Schayes, Kluwer Academic/Plenum Publishers, New York, 2002

hydrostatic model. Both prognostic models have the capability of nesting and four dimensional data assimilation. Detailed information about the meteorological tools can be obtained elsewhere (Arritt, 1985; Systems Application International (1995); Droegemeier et al., 1996; Xue et al., 1995).

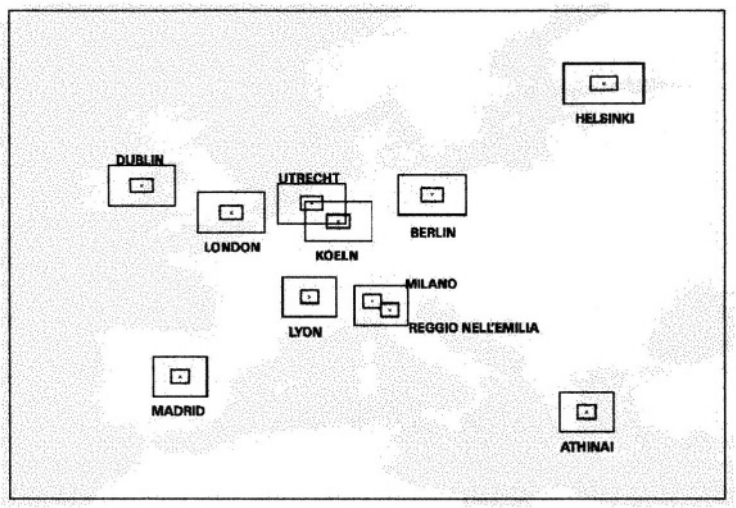

Figure 1. Modelling domains considered in the AUTOOIL-II programme. The ten outer rectangles represent the coarse domains with a resolution of 0.06 x 0.06 decimal degrees.

AQ-IDX	AQ-CODE	CORINAIR	HEIGHT EMIS (m	NAME OF ACTIVITY
1		7	0	Passenger Cars Gasoline+LPG including evaporative emissions
2		7	0	Passenger Cars Diesel
3		7	0	Light Duty Vehicles
4		7	0	Heavy Duty Vehicles
5		7	0	Buses
6		7	0	Two Wheeled Vehicles
7		2	50	Non-Industrial Combustion Plants
8		3	50	Combustion in Manufacturing Industry
9		6	50	Solvent and Other Product use
10		5	50	Extraction and distribution of fossil & other Fuels
11		1	50	Combustion in Energy & Transformation Industries <50MW, gas turbines, stationary engines
12		1	120	Combustion in Energy & Transformation Industries 50-300MW
13		1	Exact or 250	Combustion in Energy & Transformation Industries >300MW
14		4	120	Production Process Industries
15		9	120	Waste Treatment & Disposal
16		8	0	Other mobile sources and machinery
17		10	0	Agriculture
18		11	0	Natural Emissions
19			0-250	
20	TRA_(1+2+3+4+5+6)		0	Total Traffic Sources
21	TAREA_(7+8+9+10+11)		50	Total Area Sources
22	LAREA_(12+13+14+15)		120-250	Total Large Area Sources
23	OSRC_(16+17+18)		0	Other Area Sources

Figure 2. Emission source categories and the grouping according to the height of relevant releases.

Dispersion modelling was carried out with the European version of the urban airshed model (Morris et al. 1990; Hanna et al. 1996). The original of this model is well

documented for three-dimensional photochemical simulations and has been utilised extensively in many US and European domains with two-way nesting in regional and urban scales. In this European set-up, accurate treatment of different emission categories was carried out in order to run different emission scenarios for the estimation of the source attribution to the air quality even for species that are not inert. Special emphasis was put on the treatment to higher-level stationary emissions (industrial, combustion) that were emitted in different altitudes up to 250 m above ground level. The emissions inventories were split into 18 different sources (Figure 2) and air quality calculations were carried out initially in four source categories (traffic, low combustion industry, high combustion industry and natural/biogenic emissions). In case the target concentrations for 2010 were not achieved, the scenario calculations were carried out in the 18 different emission sources.

3. VALIDATION

Although validation comparisons are common in air-quality studies, these are frequently carried out with measurements; these usually are not focused or are not general. Hence, they do not help in increasing the confidence on modelling data, especially if these conveniently examine only one component (e.g. ozone) and ignore evaluations for the precursors or the meteorological data on which the dispersion calculations are based. Even worse some comparisons fail to demonstrate the generalisation aim for which these calculations were carried out.

The purposes of the comparisons carried out in the frame of the AUTOOIL programme are to examine how well the annual average conditions are represented, to examine the time-series simultaneously for two pollutants at the same location. In addition, to examine frequency distribution during the modelled annual-mean period (demonstrate that this is similar to the annual mean distribution); to look into the spatial variability by looking into several monitoring stations and examine at two different sites the wind-speed and wind-direction and compare with the values observed.

3.1 Meteorological Modelling

In the second stage, a validation procedure took place, in which the results of the meteorological model were validated against data from meteorological stations (surface as well as upper air stations), which were not included in the initialisation process. As an example a station in the Athens domain and the Helsinki domain are shown.

Related to the AUTOOIL-II methodology the modelling period in Athens was determined to 23rd to the 27th of September 1995. During this period, the wind-direction was mainly north to northeast with wind speeds over 4 m/s up to 8 m/s. During lower wind speeds, also a sea breeze circulation could be established as to see in Figure 3. Both effects were represented reasonably well by the model.

A performance of the meteorological model is indicated at the domain of Helsinki (Figure 4). The modelling period for the surrogate annual-mean conditions on this domain, were between 11th and 16th of April 1995. Beginning with westerly to northerly winds, the main period was effected with southerly winds from the sea by an increasing wind velocity.

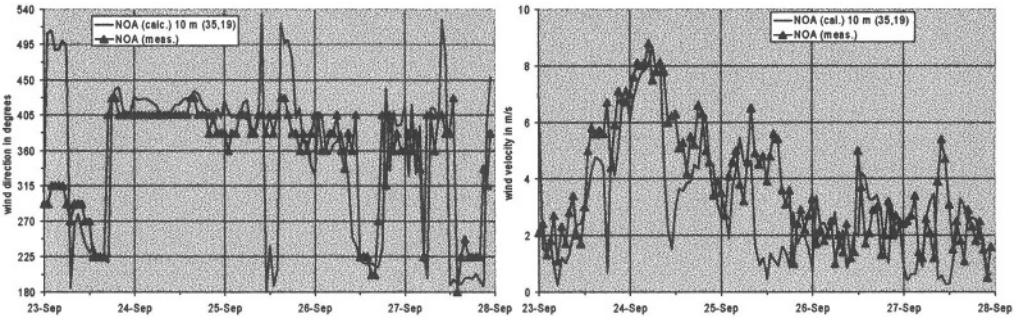

Figure 3. Model calculations (solid line) compared with measured (triangle) wind direction and velocity at the NOA station in Athens for the period 23rd to 27th September 1995.

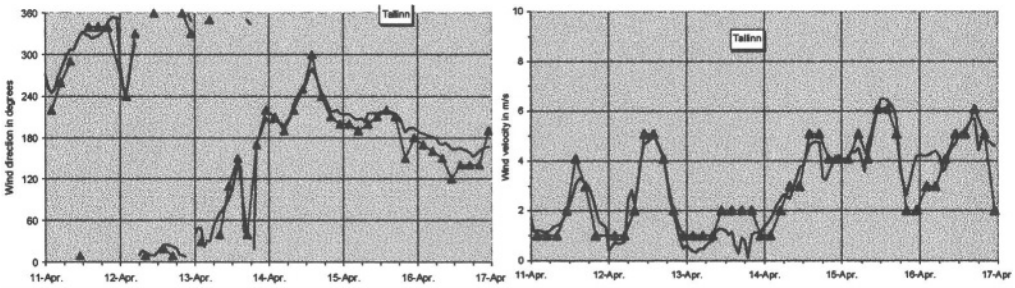

Figure 4. Model calculations (solid line) compared with measured (triangle) wind direction and velocity at the Tallinn station in the domain of Helsinki for the period 11th to 16th April 2001.

3.2 Dispersion Modelling

Due to large number of monitoring sites in each domain and the number of species, the validation of the dispersion model is certainly a complex process. For the interpretation of these data it is necessary to emphasise that the calculated concentrations correspond to averaged values within a three dimensional 'box' of approximately 2 km x 2 km x 10 or 20 m, depending on the depth of the first layer used. On the other hand, fixed monitoring stations provide concentrations for a specific location within that 'box'. In reality, there will be changes in concentrations across the 'box' both horizontally and vertically. Therefore, one would not expect precise agreement. Despite this, the accuracy is obtained by this work better than in simple empirical approaches, which are using arbitrary links between emissions and air-quality concentrations.

It is also worth mentioning that despite the vigorous quality control procedures on many European monitoring networks the existing priorities for representativeness in 1995 were not harmonised. Most monitoring stations depend on the priorities of the network, the position of the measuring inlet was as close as possible to the kerb side, or the station was located within a street canyon etc. For the comparisons shown in Figures *5* and 6, it would be unfavourable to exclude such stations. Hence, data from all available stations were used even if we know that often the conditions are far from optimal for the validations. Even so, the accuracies obtained are within the ±26% lines.

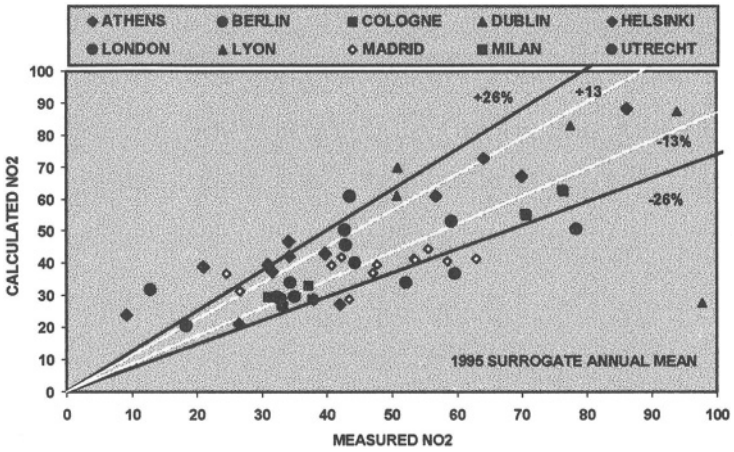

Figure 5. NO2 comparisons for all monitoring stations for which hourly data were provided at the city contact group meetings of the AUTOOIL-II programme.

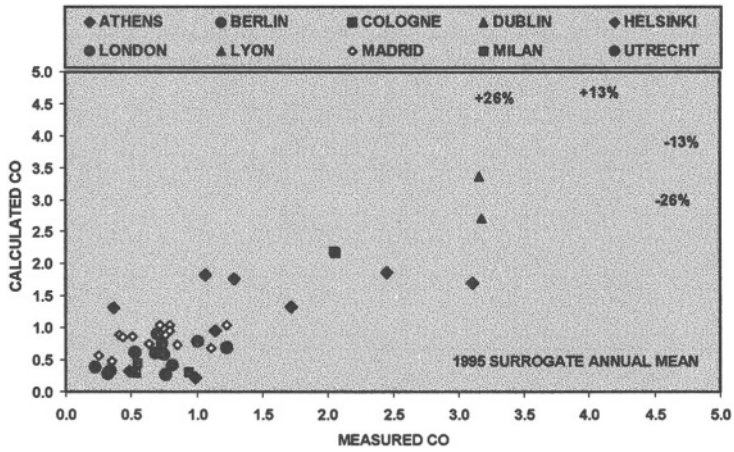

Figure 6. CO comparisons for all monitoring stations for which hourly data were provided at the city contact group meetings of the AUTOOIL-II programme.

In the remaining part of this work is shown a flavour of randomly selected results from comparisons carried out in each city domain during 1995. Comparisons for other pollutants and for other modelled episode periods can be consulted at http://autooil.jrc.cec.eu.int.

In Figure 7 are shown comparisons for the time series for NO2 at two monitoring sites one in Lyon and one in Madrid respectively. Table 1 examines the spatial accuracy of the modelled and measured concentrations simultaneously for NO2, CO and Benzene in London. The period of the quoted data in this table are for the surrogate annual-mean conditions in 1995.

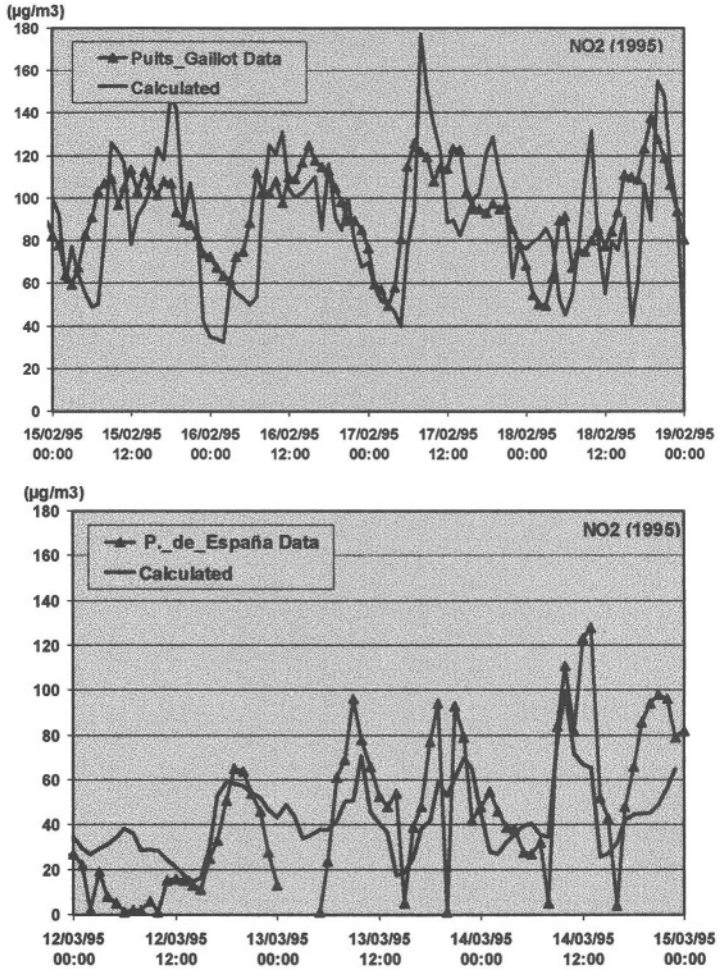

Figure 7. NO2 time series at a site in Lyon (top) and Madrid (bottom) during the surrogate annual-mean period.

Table 1. Spatial comparisons of calculated and measured concentrations in London.

POLLUTANT	Monitoring Site	Measured	Calculated
NO2 (µg/m3)	Bexley	34.4	34.0
	West_London	42.8	50.4
	Bridge_Place	42.9	45.8
	Bloomsbury	59.1	53.3
	Cromwell_Road	78.4	50.8
CO (mg/m3)	Bexley	0.34	0.32
	Bloomsbury	0.70	0.90
	West_London	0.74	0.76
	Bridge_Place	0.64	0.58
	Cromwell_Road	1.01	0.78
Benzene (µg/m3)	Eltham	2.05	1.54

The frequency distributions of the obtained concentrations in Figure 8 show that the middle range of concentrations is accurately represented. This is true not only between measured and modelled results but also for the complete set of annual data. This is in particular correct in most cities both for NO2 as well as for CO.

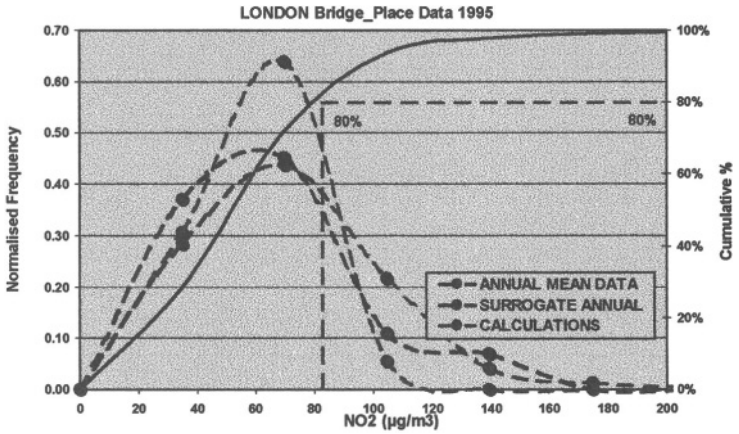

Figure 8. Comparison of NO2 frequency distributions of hourly concentrations with the annual data at Bridge Place in London during the surrogate annual-mean period.

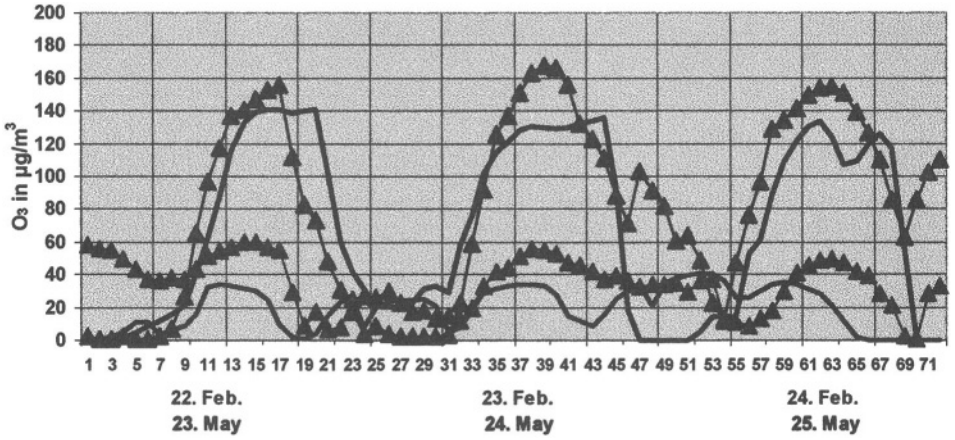

Figure 9. Comparison of calculated and measured O3 (triangles) concentrations (µg/m³) in Berlin-Grunewalt during the 98th-percentile ozone episode (upper set) and during the surrogate annual mean period (lower set).

Good temporal representativeness is achieved not only during the surrogate annual-mean period. Figure 9 shows comparisons of the ozone concentration during the 98%tile episode and during the period representing annual mean conditions. By comparing the results in south and central European cities it was found out that the ozone problem is quite different in the south of Europe. In the latter, high ozone concentrations can be reached even during the surrogate annual mean conditions. This is related with the actual location, the natural background and the regional transfer of pollutants through atmospheric dispersion.

4. CONCLUSIONS

In general, the performance of the advanced methodology followed in the AUTOOIL-II has provided consistent and reliable results for the diurnal variation of pollutant concentrations. Depending on the complexity of the terrain and the meteorological conditions, the results show good agreements on the long time performance (here 3-4 days) as well as on the fluctuations (within hours, e.g. sea breeze circulation). Only in few limited cases the models predicted peak concentrations at different times. In these cases, the diurnal variation of emission were to be blamed which lead to less pronounced effects on local concentrations due to the inaccurate "dilution" of pollutants. Alternatively, the location where these variations were observed might have been subject to localised temporal variations of emissions, which could have not been reflected in the general temporal disaggregation factors used over the whole domain.

The model results on O3 and NO2 show that the nested structure of the modelling domains accurately accounts the urban and regional representation of both pollutants over the modelling domains and therefore this infrastructure provides a broad integrated assessment of the photochemical situation in urban and regional areas.

The extensive comparisons made possible to emphasise that these types of modelling tools are suitable for examining accurately long-range transport processes by inter-relating the coarse and fine grid simulations, for refining the understanding of how strong are the simultaneously occurring effects of dispersion and chemical transformation. It allowed high spatial resolution in "Hot spot areas", accounted correctly for the boundary conditions in each domain and demonstrated that source apportionment depends significantly on horizontal/vertical resolution of the grid cells.

5. REFERENCES

Arritt, R.W., 1985, *Numerical Studies of Thermally and Mechanically Forced Circulations Over Complex Terrain.* Cooperative Institute for Research in the Atmosphere, Colorado State University, Fort Collins, Colorado

DG-ENV, Subgroup-2 of AUTOOIL-1, 1996, "Air-Quality Report of the AUTOOIL-1 Programme", European Commission, Report of DG-XI, Belgium.

DG-ENV, 2001, *The AUTOOIL-II programme: Air-Quality report,* EC DG-ENV, edited at JRC Ispra, Report EUR 19725 EN, version 7.2 and http://europa.eu.int/comm/cnvironment/autooil/index.htm.

Droegemeier, K.K., Xue, M., Sathye, A., Brewster, K., Bassett, G., Zhang, J., Lui, Y., Zou, M., Crook, A., Wong V., Carpenter, R. and Mattocks, C., 1996, *Real-time numerical prediction of storm-scale weather during VORTEX-95. Part I: Goals and methodology.* Pre-prints: 18th Conference on Severe Local Storms, American Meteorological Society, San Francisco, CA, 6-10.

Hanna, R. S., Moore, G.E., and Fernau, M.E., 1996, *Evaluation of Photochemical Grid Models (UAM-IV, UAM-V, and the ROM/UAM-IV Couple) using Data from the Lake Michigan Ozone Study (LMOS).* Atmos. Environ., 30(19):3265-3279.

Morris, R. E., Causley, M.C., Fieber, J.L., Gardner, L., and Myers, T.C., 1990, *Urban Airshed Model Study of Five Cities—Low-Cost Application of the Model to Future-Year SIP Control and Alternative Fuel Strategies for Dallas–Fort Worth, Atlanta, Philadelphia, and St. Louis.* U.S. Environmental Protection Agency (EPA-450/4-90-006F).

Skouloudis, A.N., and Suppan, P., 2000, Methodology for the urban-impact assessment modelling in the frame of the AUTOOIL-II programme, EUR Report No EUR19556 EN, Jan 2000

Systems Applications International, 1995, *SAIMM Version 3.1: User's guide,* October 1995

Xue, M., Droegemeier, K.K., Wong, V., Shapiro, A. and Brewster, K., 1995, *Advanced Regional Prediction System (ARPS)* Version 4.0 User's Guide, 380pp

DISCUSSION

S. RAFAILIDIS Before using the field data for validation, did you "correct" them to account for local effects ? In the urban environment we know there are large gradients present.

P. SUPPAN No, for the validation procedure we have considered only stations which present more than the local effects (e.g. kerb side; street canyons etc.). We know about the local effects and we know that many stations were installed for the purpose of the local air quality and not for the purpose of modelling comparisons.

This page intentionally left blank

DEVELOPMENT AND APPLICATION OF CHEMICAL WEATHER FORECASTING SYSTEM OVER EAST ASIA

Itsushi Uno, Koji Ishihara, Zifa Wang, Gregory R. Carmichael and Marina Baldi *

1. INTRODUCTION

Spring dust episode (Yellow Sand or Kosa) contributes to a number of environmental effects, including visibility impairment, mineral deposition, and enhancement of the pH of precipitation. Origin of yellow sand locates at the inland desert area (such as Gobi and Takla Makan) of Asian continent. It is transported more than several thousand kilometers to Japan due the springtime strong westerly. Transboundary transport of anthropogenic air pollutants is another significant environmental problem in East Asia because of very rapid increase of pollutants emissions due to fast economic growth. Anthropogenic aerosols and natural mineral dusts have a long residence time of more than a week and have a strong radiative forcing. Intercontinental and/or Trans-Pacific pollutant transport becomes also another important environmental issue (e.g., Uno *et al,* 2001b).

ACE-Asia (Asian Pacific Regional Aerosol Characterization Experiment), IGAC core research project, was designed to increase our understanding of how atmospheric aerosol particles affect the Earth's climate system. The intensive observation was carried out during March to May, 2001 participated using aircraft, a research vessel, surface stations and numerical models. Aerosol transport forecast modeling activities played an important role during the ACE-Asia intensive observation period. We developed and operated chemical transport models - RIAM-CFORS (Research Institute for Applied Mechanics, Kyushu University & University of Iowa - Chemical weather FORecast System) in forecast mode and participated in flight planning activities at the operations center of ACE-Asia in Iwakuni, Japan. In this paper we will present an overview of the RIAM-CFORS system and summarize the general aerosol transport pattern and averaged concentration including aerosol optical depth during the March and April, 2001.

* Itsushi UNO, Research Institute for Applied Mechanics/ Kyushu Univ., Kasuga Park 6-1, Kasuga 816-8580, Japan; Zifa Wang, Itsushi UNO, Frontier Research System for Global Change, Yokohama, Japan; Koji ISHIHARA , Japan Science and Technology Corporation, Tokyo, Japan; Gregory R. CARMICHAEL , Center for Global and Regional Environ. Research, University of Iowa, Iowa City, Iowa, U.S.A; Marina BALDI, Institute of Atmospheric Physics (IFA-CNR), Rome, Italy.

Air Pollution Modeling and Its Application XV, Edited by
Borrego and Schayes, Kluwer Academic/Plenum Publishers, New York, 2002

2. OVERVIEW OF CHEMICAL WEATHER FORECASTING SYSTEM (CFORS)

2.1 Overview of CFORS concept

We developed and are applying an operational Chemical weather FORecasting System (RIAM-CFORS) based on 3D on-line regional scale chemical transport model fully coupled with RAMS (Regional Atmospheric Modeling System; Pielke *et al.,* 1992). One of the main purposes of this system is to understand the regional transboundary pollution and to schedule/design the operational field monitoring campaign during the ACE-Asia intensive observations.

This system consists from four important components;

- CFORS ftp manager: accesses to the operational global forecast data set to NCEP (National Center for Environmental Prediction) and Asian forecast data set to Japan Meteorological Agency (JMA) DDB data site.
- RAMS weather forecast for 72 hours based on the NCEP and JMA data set as a lateral boundary condition.
- Chemical Transport Module integrating regional atmosphere and chemical transport (On-line chemical transport model for important chemical tracers).
- CFORS web manager: Post-processing of chemical weather forecast results with 2 & 3-D graphics into the CFORS WWW-page.

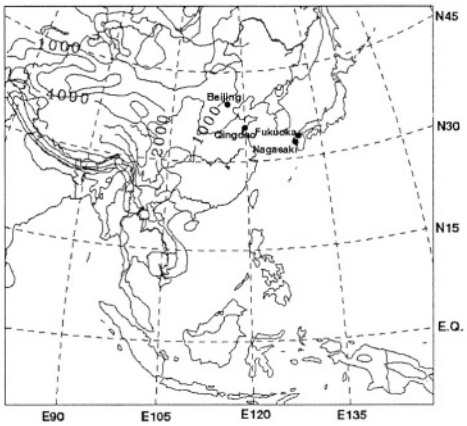

Figure 1 Modeling domain in siumulation. Contours are the topographical elevations of 1000, 2000 and 4000m.

Present RIAM-CFORS system includes the following chemical transport species; Anthropogenic species: SO_2/SO_4, CO, scoot (black carbon and organic carbon), hydrocarbons, NO_x; Natural origin: yellow sand, sea salts, radon, volcanic SO_2, biomass burning pollutants (CO, black carbon and organic carbon). CFORS forecast products consisting of gas and aerosol mass distributions and optical depths for sulfate, black carbon, organic carbon, sea salt, and dust. Figure 1 shows the numerical model domain

which centered at 25N 115E. The horizontal grid consists of 100 by 90 grid points, with a resolution of 80 km. In the vertical, the domain is divided into 23 layers (top level is 20km). These model domain configuration is capable to forecasting the most of important chemical environment in Asia.

RIAM-CFORS tracer model is fully coupled with RAMS, and this is a unique approach because the regional meteorological conditions such as precipitation, cloud microphysics, diurnal cycle of boundary-layer turbulence play significant role in the wet deposition and vertical diffusion of tracers. The on-line tracer model runs with same time step as the RAMS, so that all the on-line meteorological information such as 3-D wind field, boundary-layer turbulence, surface fluxes and precipitation amount is directly used by the tracer model at every time step. Therefore RAMS plays the core part of CFORS to simulate the regional scale 3-D meteorological field. General description of RAMS and its capabilities are given in Pielke *et al.* (1992).

2.2 Meteorological Data set

RIAM-CFORS can be operated both in forecasting and hindcasting modes. During the ACE-Asia operation, RIAM-CFORS was operationally used in forecasting mode and provided regional forecasts of meteorology and gas/aerosol distribution using a limited area transport model coupled with RAMS initialized by NCEP (National Center for Environmental Prediction/ NOAA) and JMA (Japan Meteorological Agency) forecast products from their web page.

After the field campaign, we applied the RIAM-CFORS with the hindcast mode between February 20, 2001 and May 31, 2001 by the updated boundary conditions. In this hindcast (post analysis) study, we used the ECMWF global meteorological data set (6 hour interval with 1 deg resolution), analyzed weekly SST(sea surface temperature) data and observed monthly snowcover information as the boundary condition of RAMS calculation.

2.3 Emission Data set

All the anthropogenic emission inventories (SO_x, NO_x, CO, Black Carbon, Organic Carbon and Hydrocarbons) are taken from the work of Streets (2001). It consisted with the year 2000-based grided annual emission (1 deg resolution). Particulate matter emission from household sector is important to simulate the general background level of $PM_{2.5}$ and PM_{10} aerosol, however because of the lack of such emission data base, we did not include it in the present study.

Natural gas/aerosol sources are assigned by using the information taken from RAMS meteorological field and land use category information.

Identification of natural dust source region is a key issue of dust simulation, but usually detailed source information is difficult to obtain. In this study, natural dust emission area is defined as the area where USGS vegetation type (based on AVHRR data obtained in 1992/93) is assigned as desert or semi-desert. By using this method, most part of Gobi and Takla Makan Desert are indexed as source regions. In the present calculation, Loess Plateau and Nei Mongol's small desert (north west of the Shenyang city) area are also assigned as the dust sources based on TOMS AI (aerosol index) observation. Most of the Himalayan mountain range is also indexed as desert region, but the monthly snow cover data are used to mask the undesirable dust emission from such high mountains.

Dusts are emitted into the atmosphere as a result of high surface winds. One major problem regarding long-range transport of dust is how to calculate emission rate from source into the atmosphere. In this work, simple vertical dust deflatation scheme proposed by Gillette and Passi (1988) is used and 12 dust particles bin (ranged from 0.1 to 20 μm in diameter) are assigned in the model.

Another important aerosol sources in the springtime Asia are biomass burning origin CO and scoot (black carbon BC and organic carbon OC). These emission rate are highly uncertain and changes day by day. In this present calculation, we assigned the monthly averaged CO, BC and OC emission estimates analyzed from AVHRR and World Fire count in the springtime of the year 2000 (Woo and Streets, 2001). This monthly averaged emission are used through out the simulation period. For example, the total biomass burning CO emission intensity exceeded the one from the anthropogenic activity within the modeling domain.

Sea salt also plays an important role for radiative transfer. We simulated sea salt emission and transport process with two bin modes within CFORS framework. Sea salt emission are calculated after Gong *et al.*(1997).

Lighting NO_x is also important as the O_3 precursors and is assigned by the subgrid scale cumulus activity calculated by simplified Kuo cumulus scheme. Lightning NO_x are emitted between cloud base and cloud top as the function of cloud top height when it exists. As the volcano emission gas tracer, estimated SO_2 emission intensity are used at the major active volcanoes within the modeling domain. As the land surface origin air mass tracer, radon emission was assumed by the intercomparion experiments condition specified by Jacob *et al.* (1997).

Chemical reactions are all assumed to be linear reaction. Chemical conversion rate of 1%/hour is assumed from SO_2 to aerosol sulfate formation. Dry and wet deposition processes are treated based on the appropriate reference values and gravitational settling are included into mineral dust and sea salt transport.

2.4 Aerosol optical depth and extinction coefficient

Aerosol optical depths for sulfate, black carbon, organic carbon, sea salt, dust and total value are calculated at 500 nm after Takemura *et al.* (2000). Aerosol extinction coefficient and single scattering albedo (SSA) are also calculated to compare the Lidar observation and satellite remote sensing data.

2.5 RIAM-CFORS daily operational cycle

Chemical weather forecast calculation (in forecasting mode) required huge computer resources. Forecasting work adopts the PC parallel cluster system (Beowulf type 17 nodes Linux cluster; Pentium III 600MHz) to simulate the regional scale 3-D meteorological/ chemical fields. With this hardware configuration, 3 days forecast can be achieved within 4 hours including post analysis.

Figure 2 shows the RIAM-CFORS daily operational cycle. All the meteorological and chemical forecasting calculation (two sets of model calculation based on NCEP and JMA) were conducted in the midnight and then WWW base forecasting information can be ready by the 800 JST.

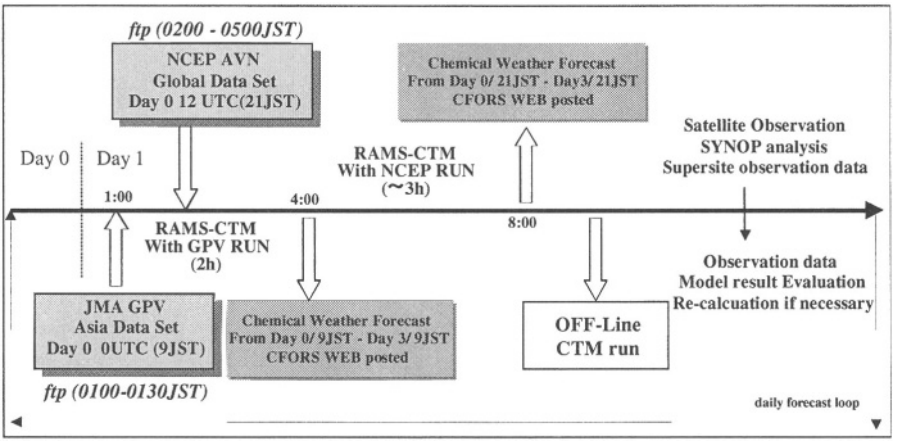

Figure 2 RIAM-CFORS daily operation cycle.

3. RESULTS AND DISCUSSION

Weather pattern is one of the very important factors for the understanding of Asian scale transport of trace gas and aerosols. Previous studies (e.g., Uno *et al.,* 1998; 2001a) pointed out that variations of wind pattern associated with changes of synoptic pressure system play a key role in the transport from Asia mainland to downwind countries in East Asia.

From the middle of November to early March (winter in Japan), strong pressure gradients between Siberia (Continental) High and Okhotsk Low exists in average, which follows the strong winter monsoon in the region. This typical winter monsoon usually lasts a few days, and after this, low pressure system develops and moves from China continent to eastside of Japan as a transition of weather change. Such a transition pattern is usually observed 1 – 2 times per week, and this transition triggers intermittent large scale outbreak of pollutant from Asian continent.

In spring season (typically from middle of March to May in Japan), its weather pattern is mainly characterized by a large scale traveling high/low pressure system, moving slowly eastward over the Japan main island. However, the exact separation by such a weather pattern is difficult. Weather pattern in March and April belongs sometimes in winter mode and/or spring mode. Such a weather pattern alternation is extremely important for large scale dust storm transport and transboundary acidic pollutants outbreak in east Asia in spring.

Figure 3 shows the Air Pollution Index (API) measured for Beijing and Qingdao, China. An air pollution index is derived for each of NO_x, SO_2 and TSP (Total suspended particulates), based on a scale from 0-500 defined by the State Environmental Protection Agency (SEPA) of China. This figure shows the API value of TSP. API (TSP) value of 500 corresponds to the TSP concentration of $1 mg/m^3$. Solid lines in the figure shows the model predicted dust concentration.

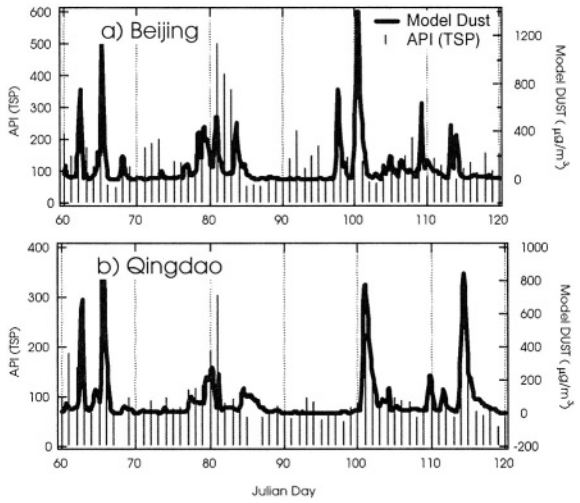

Figure 3 Comparison between API (TSP) and modeled DUST at Beijing and Qingdao, China

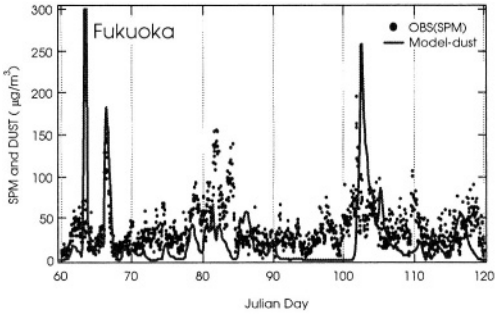

Figure 4 Comparison between SPM concentration and modeled DUST at Fukuoka, Japan

Figure 4 shows the SPM (suspended particle concentration) observed in Fukuoka, Japan and corresponding modeled result.

Figures 3 and 4 clearly showed that modeled results generally underestimate the TSP and SPM concentration because the simulated dust concentration only include mineral fraction of dust. However, it is important to notice that modeled results well simulated the heavy dust episodes (e.g., Julian day of 65-66, 80-82 and 100-102).

Figure 5 shows the time-height cross-section of aerosol concentration simulated over the Nagasaki, Japan. It shows the sulfate, black carbon+organic carbon, mineral dust concentration ($\mu g/m^3$) and aerosol extinction coefficient (m^{-1}) from March 1st to April 30, 2001. In the vertical dimension, it shows from the surface to 6 km level. Several important points are obvious from Figure 5. That is, mainly restricted within BL (boundary layer level).

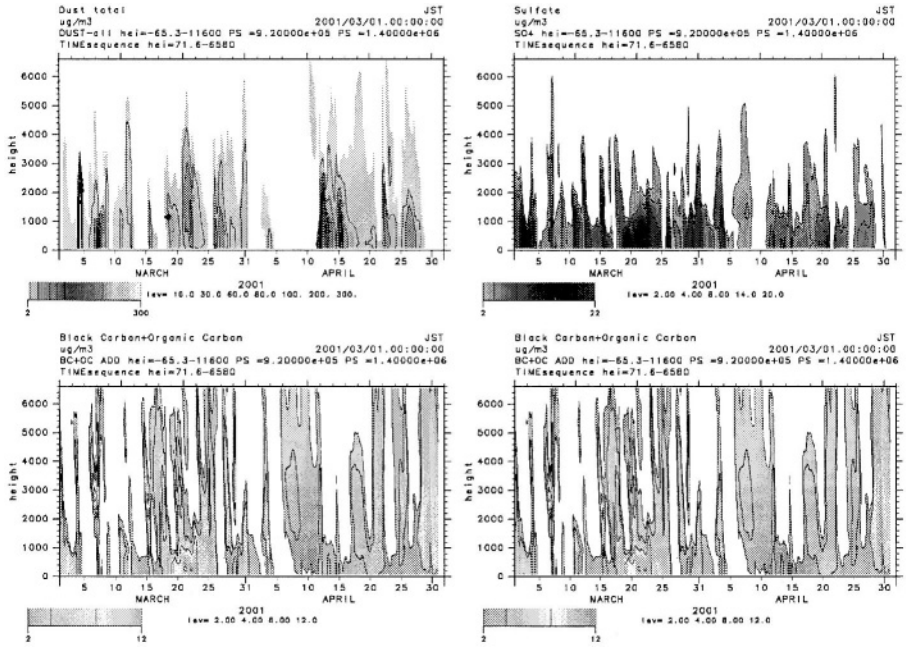

Figure 5 Time-height cross section of (a) dust, (b) sulfate, (c) carbonaceous concentration (black carbon + organic carbon) and (d) aerosol extinction coefficient at Nagasaki. Contour intervals are (a) 10, 30, 60, 80, 100, 200 $\mu g/m^3$ (b) 2, 4, 8, 14, 20 $\mu g/m^3$ (c) 2, 4, 8, 12 $\mu g/m^3$ (d) $4x10^{-5}$, $8x10^{-5}$, $1.2x10^{-4}$, $2x10^{-4}$ (m^{-1}).

- Time variation between mineral dust and sulfate has a strong correlation. Very high concentration is observed intermittently.
- Mineral dust transport height depends on the meteorological condition.
- Carbonaceous concentration (Black Carbon + Organic Carbon) has two layer structures, i.e., transported within BL and above the BL, independently (vertical level from 2000 m to 4000m in the free atmosphere).

Figure 6 shows the horizontal distribution of AOD (aerosol optical depth) from mineral dust and sulfate between March 19 and March 22, 2001. Vector in figure indicates the wind flow at the height of z_*=1500m. This period is chosen because RIAM-CFORS results and surface observation both show the very high concentration of aerosols (Figures 3, 4 and 5). The figure clearly indicated that the sulfate and mineral dust transport to Japan area. It is interesting that the high concentration center of mineral dust and sulfate are separated (e.g., over the mainland China), however, the concentration contour are mixed when it is transported to the Japan Sea and Japan mainland area.

Figure 7 shows the monthly averaged aerosol optical depth (AOD) from mineral dust, sulfate and carbonaceous aerosol and the total AOD from these components + sea salts in April, 2001. This monthly averaged information provides us many interesting phenomena which should be compared with observations. Important information can be summarized as follows;

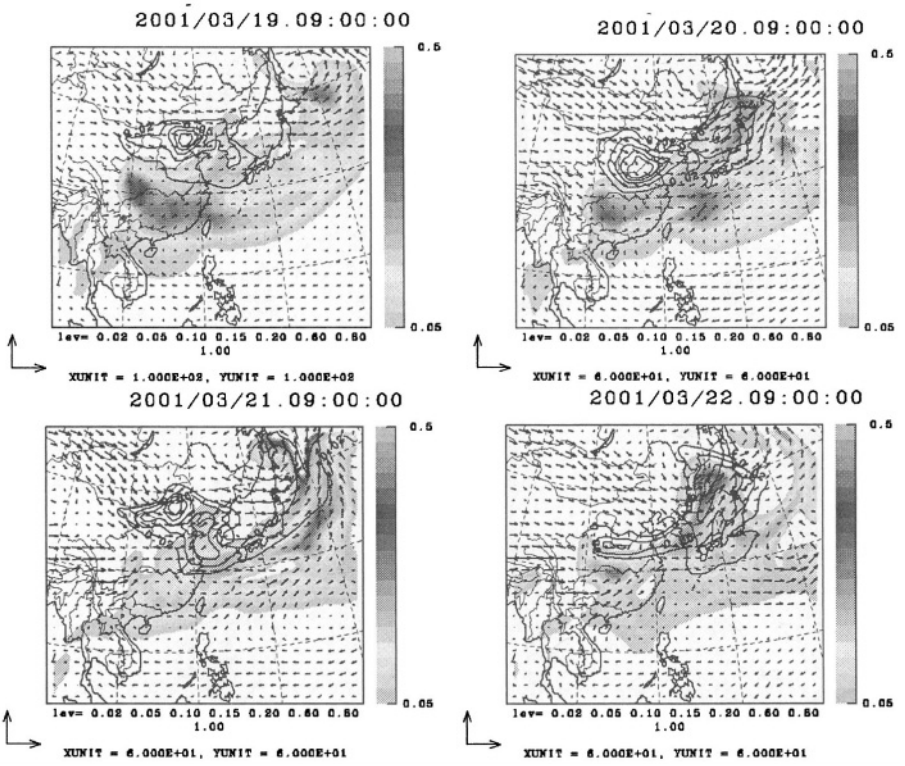

Figure 6 Simulated aerosol optical depth for dust (line) and sulfate (color) with z_*=1500m level wind vectors. (a) March 19, (b) March 20, (c) March 21, (d) March 22 0UTC. Contour interval of dust is 0.02, 0.05, 0.1, 0.15, 0.2 and 0.3

- Mineral dust AOD is centered at the Gobi desert and Inner Mongolia, and the contour lines are moved along the latitude about N 45 °.
- Sulfate AOD is centered in China (especially the central plain area between the Yangtze river and the Huang He (Yellow River) because of their intensive SO_2 emission). Their transport ridge is mainly along the Korea and northern part of Japan (NNE direction).
- Carbonaceous AOD has two peaks. The one in inland Thailand -Laos, the other in southern China. This is because the modeled biomass emission intensity are very high in Thailand and Laos, while the peak in southern China is depending on the simulated relative humidity in the RAMS. Their transport path is from Thailand/Laos - southern coast of China - Okinawa (NNE direction).
- The total AOD field shows the complex structure. The carbonaceous AOD is dominant from the Indochina peninsula - southern China - Okinawa. Its fractional contribution are large along the latitude line of N 30 ° . AOD contribution of sulfate are broadly distributed between N 30 ° and N 45 ° except the mainland China. The contribution of mineral dust is located in mainly northern part of modeling domain.

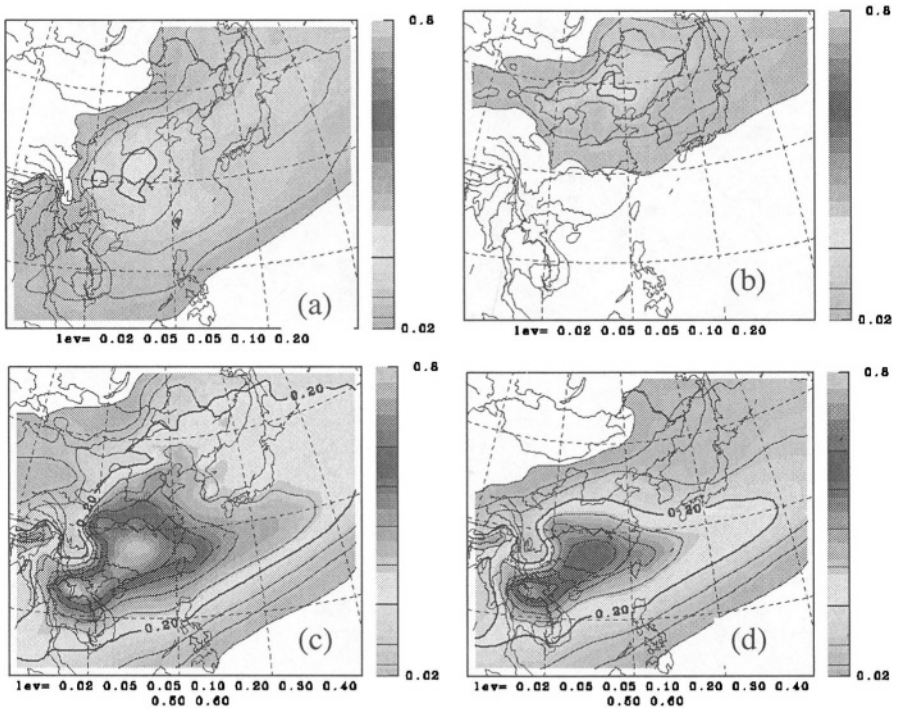

Figure 7 Simulated monthly averaged aerosol optical depth for April 2001, (a) mineral dust, (b) sulfate, (c) carbonaceous, (d) total aerosol optical depth. Contour intervals are 0.02, 0.05, 0.1, 0.15, 0.2, 0.3, 0.4, 0.5 and 0.6.

4. CONCLUDING REMARKS

We developed and operated chemical transport models - RIAM-CFORS in forecast mode and participated ACE-Asia field experiments during March and April 2001. After the field experiment, RIAM-CFORS post analysis was conducted during the time period between March 1 and April 30 2001. Aerosol composition, aerosol optical depth simulation results are summarized. RIAM-CFORS simulation showed that the aerosol optical depth in Asia is controlled by mineral dust, anthropogenic sulfate and carbonaceous aerosol. Each component's AOD peak regions are located at their main emission area. However, during the downwind transporting process, these three major aerosol species are tend to converge over the Japan main island.

Acknowledgements

The authors want to acknowledge Dr. David Streets of Argonne National Laboratory for his co-operation of emission inventory data. This work is partly supported by Research and Development Applying Advanced Computational Science and Technology of Japan Science and Technology Corporation (ACT-JST).

References

Gillette, D. and R., Passi, 1988, Modeling Dust Emission Caused by Wind Erosion, *J. Geophy. Res.,* **93**: 14,233-14,242.

Gong, S.L., L.A., Barrie and J.-P., Blacnchet, 1997, Modeling sea-salt aerosols in the atmosphere 1. Model development, *J. Geophy. Research,* **102** :3805-3818.

Jacob, D.J. *et al.,* 1997, Evaluation and intercomparison of global atmospheric transport models using radon-222 and other short-lived tracers, *J. Geophy. Research,* **102**:5953-5970.

Pielke, R.A., W.R.,Cotton, R.L., Walko, C.J., Tremback, W.A., Lyons, L.D., Grasso, M.E., Nicholls, M.D., Moran, D.A., Wesley, T.J., Lee and J.H., Copeland, 1992, A comprehensive meteorological modeling system -RAMS, *Meteorol. Atmos. Phys.,* **49**: 69-91.

Streets, D, 2001, http://www.cgrer.uiowa.edu/ACESS/ EMISSION_DATA/ED_index.htm.

Takemura, T., H., Okamoto, Y., Maruyama, A., Numaguti, A., Higurashi, and T., Nakajima, 2000, Global three-dimensional simulation of aerosol optical thickness distribution of various origins, *J. Geophy. Research,* **105**:17,853-17,873.

Uno, I, T., Ohara and K., Murano, 1998, Simulated Acidic Aerosol Long-Range Transport and Deposition over East Asia - Role of Synoptic Scale Weather Systems, in *Air Pollution Modeling and its Application* **22,** S.E. Gryning and N. Chaumerliac, Ed., Plenum Pub. Co., pp. 185-193.

Uno , I., S. Emori and M. Baldi, 2001a, Chemical transport model on-line coupled with RAMS for regional chemical climate, in *Air Pollution Modeling and Its Application XIV,* Gryning and Schiermeier, Ed., Kluwer Academinc/Plenum Pub., pp. 75-85.

Uno,I., H., Amano, S., Emori, K., Kinoshita, I., Matsui and N., Sugimoto, 2001b, Trans-Pacific Yellow Sand Transport observed in April 1998: Numerical Simulation, *J. Geophy. Research,* **106**:18,331-18,344.

Woo, J.-H. and D. Streets *et al.,* 2001, http:// www.cgrer. uiowa.edu/people/ woojh21/data_fire_ co_index.html

DISCUSSION

A. HANSEN One calculation you showed indicated that the carbonaceous component dominated the AOD for that episode. Is this dominance the typical case ?

Z. WANG Increased contribution of carbonaceous aerosols to AOD during the experimental period is mainly due to intense biomass burning in the region and considerably lower contribution from mineral dust. Daily variation in biomass burning emissions of BC and OC was estimated using AVHRR and TOMS AI data. For more details, please refer to http://www.cgrer.uiowa.edu

P. BUILTJES Did you compare computed AOD with satellite observed AOD ?

Z. WANG Not yet. But we are planning to compare computed AOD with satellite observed one.

This page intentionally left blank

PHOTO-OXIDATION PROCESSES OVER THE EASTERN MEDITERRANEAN BASIN IN SUMMER

M. Varinou, F. Gofa, G. Kallos, M. O'Connor and G. Tsiligiridis

1. INTRODUCTION

The summertime photochemical activity over the Eastern Mediterranean Basin is examined by applying a multi-scale analysis of the atmospheric circulation. Photo-oxidation is considered to depend on both the distribution of precursor emissions and the atmospheric circulation, from the synoptic scale to the mesoscale. Characteristic spatial and temporal scales of photochemical activity are estimated using atmospheric and air quality numerical modeling in combination with experimental data. Special emphasis is given to the examination of the role of major coastal sources (e.g., urban areas, industrial zones) in the degradation of air quality at remote locations.

Photochemical activity over the Eastern Mediterranean has been examined mainly on the local scale. Extensive studies have focused on the build-up processes leading to photochemical episodes in highly polluted areas, such as urban areas and industrial zones. The most significant efforts concern the metropolitan area of Athens, Greece and the coastal area of Israel (Asimakopoulos et al., 1992; Pilinis et al., 1993; Moussiopoulos et al., 1995;Varinou, 2000). The synoptic circulation over the Eastern Mediterranean basin (as it is described in UKMO, 1962; Varinou, 2000 and references there in) favors transport of air masses from the Western and Central Mediterranean and SE Europe towards the eastern part of the basin, the North African coast and the Middle East (Dayan, 1986; Katsoulis and Whelpdale, 1993). Evidence of long-range transport of air pollutants towards the Middle East was identified by Peleg et al. (1994) and Wagner et al., (2000). Both groups found that the Israeli coastal area was a receptor of secondary pollution. Kallos et al. (1996, 1999) suggested possible transport mechanisms from major coastal sources on the Greek peninsula towards Africa and the Middle East during summer, based on numerical simulations of the atmospheric circulation and dispersion, while Kotroni et al. (1998) studied the Athens plume as it disperses downwind. The areas over the Aegean Sea and the island of Crete were identified as the main transport routes. The regional scale photochemical activity was studied during the T-TRAPEM experimental campaign (Kallos et al., 1997; 1998)

The present study is focused on the investigation of photochemical processes in the greater Aegean area. The behavior of the urban plume of the Greater Athens Area

*F. Gofa, G. Kallos, M. O'Connor , Dept. of Physics, University of Athens, Athens, Greece. G. Tsiligiridis Dept. of Mechanical Engineering, University of Thessaloniki, Thessaloniki, Greece. M. Varinou, Dept. of Physics, University of Athens, Athens, Greece, also, General Secretariat of Civil protection, Ministry of of the interior public administration and decentralization.

Air Pollution Modeling and Its Application XV, Edited by
Borrego and Schayes, Kluwer Academic/Plenum Publishers, New York, 2002

(GAA) is examined as a representative case of coastal urban photochemical pollution. The GAA acts as a large area source of precursors (due to urban and industrial activities) that possibly contributes to the photochemical degradation of air quality in remote areas. The proposed multi-scale (local to regional) analysis is based on numerical simulations with the Regional Atmospheric Modeling System (RAMS) (Pielke et al., 1992), the CAMx (Comprehensive Air quality Model with extensions) air quality model (Environ, 1997) and the Mesoscale Dispersion Modeling System (MDMS) (Uliasz, 1993). The simulations were designed in order to analyze the experimental evidence of regional scale photo-oxidation of urban plumes provided by the airborne measurements performed during the T-TRAPEM project (Kallos, 1997). This work is being continued in the framework of the EU funded projects SUB-AERO and ADIOS.

1.2. Experimental period

The simulation period extended from July 1 to 6, 1995. Experimental data from the T-TRAPEM campaign (Kallos et al., 1997) was available for this period. These data comprise airborne measurements in the marine boundary layer (~1000 ft) over the Central and Southern Aegean Sea and include SO_2 (TEII 43S), NOx, O_3, TSP and Volatile Organic Compounds (VOCs) concentrations. Oxidant measurements over the greater maritime area of the island of Crete were used in order to validate the CAMx model results. The origin of the relatively high ozone (60-70 ppbv) concentration observed from July 3 to 5 in the area of Crete was investigated by applying the MDMS.

The meteorological conditions during the experimental period were characterized by the alternation of typical summer time synoptic circulation types. The general synoptic characteristics were analyzed using: the European Meteorological Bulletin charts (at 0000 and 1200 UTC), the meteorological fields provided by the ECMWF (every 6 hours) and surface-radiosonde data from the National Center of Atmospheric Research of US (every 3 hours). From July 1 to 2 a strengthening of the synoptic flow over the NE Mediterranean occurs as a result of the interaction between the high pressure ridge of the Central Mediterranean and the westward extension of the Anatolian thermal low. The wind speed reaches 12 m/s over the Aegean and 8 m/s over coastal areas. Inland there is a strong modification of the synoptic flow by the local thermal circulations that develop over the complex terrain. During the following days the synoptic flow gradually weakens as the subtropical ridge of the Central Mediterranean extends eastward. Transport of warm air masses from northern Africa is evident in the 700-500 hPa charts and 1000/500 hPa thickness charts. The radiosonde data over Greece (Hellinikon, Athens) show a significant warming of 10°C in the 850-600 hPa layer from July 3 (1200 UTC) to July 4 (1200 UTC) and strong nocturnal thermal inversions on July 4 and 5. The synoptic flow gradually weakens from July 3 to 5 and the wind field is dominated by shallow thermal mesoscale circulation.

2. MODELS AND DATA USED

2.1. Models used

The RAMS model: The Regional Atmospheric Modeling System (RAMS) has been developed at Colorado State University and the ASTER Division of the Mission Research

Corporation (Pielke et al., 1992). RAMS uses the full set of primitive dynamical equations with optional parameterization schemes for turbulent diffusion, solar and terrestrial radiation, sensible and latent heat exchange, multiple soil layers, the kinematic effects of terrain and a vegetation canopy. An important feature of RAMS is its capacity to perform two-way interactive grid nesting, which allows local fine-mesh grids to resolve small atmospheric systems while simultaneously modeling the large-scale environment of the systems on a coarser grid.

The CAMx model: The CAMx model is an Eulerian photochemical model that allows for integrated assessment of gaseous and particulate air pollution over many scales ranging from urban to super-regional (Environ, 1997). The CAMx simulates the emission, dispersion, chemical reactions and removal of pollutants in the lower troposphere by solving the pollutant continuity equation for each chemical species on a system of nested three-dimensional grids. The chemical mechanisms supported by CAMx are based on the Carbon Bond – IV and the SARPC97 mechanisms. The most notable features of CAMx include: two-way interactive grid structure, particulate matter treatment, an advanced photolysis model and detailed cloud impacts on photolysis rates. The required input data include: gridded wind, temperature, vertical diffusivity, pressure, water vapor, cloud cover and rainfall fields, precursor emissions data, air quality data in the form of initial and boundary conditions, land use, surface UV albedo, haze, and ozone column data.

The MDMS model: The MDMS (Uliasz, 1993) includes the Lagrangian Particle Dispersion (LPD) model and the Eulerian Grid Dispersion (EGD) model. The MDMS simulates mesoscale dispersion over complex terrain and calculates influence functions. It is applied on a 3-D domain extended to the meso-α scale. The LPD and EGD models can be used separately or combined as a hybrid Lagrangian - Eulerian system in a source-oriented or a receptor-oriented mode. MDMS uses as input the prognostic meteorological fields calculated by the RAMS model and takes into account turbulence and surface layer parameterizations.

2.2. Models Setup and input data

RAMS model setup: Simulations with the RAMS model were performed for the period from July 1 to 6, 1995. The simulations focused on the analysis of the meteorological conditions over the greater Aegean area. For this purpose a nested-grid configuration was implemented. The model domain was extended to include the greater Mediterranean area with a coarse grid while finer telescopic grids were applied over the area of interest in order to obtain meteorological fields of high resolution. The following grid configuration was used (Figure 1): Grid 1: 160x90 points, 32-km horizontal increment; Grid 2: 130x118 points, 8-km horizontal increment; Grid 3: 64x64 points, 4-km horizontal increment. Concerning vertical structure, the grids were identical: 23 vertical layers in terrain following (σz) with variable vertical resolution. The vertical structure is denser in the lower levels, becoming increasingly sparser towards the top of the domain (at 14 km).

The RAMS model input data: The ECMWF 30" gridded analysis fields were used in order to initialize the model and to nudge the lateral boundary region of the coarser grid. Surface observation data was also used and retrieved from the National Center of Atmospheric Research, US (NCAR). The USGS topography, land-water percentage,

vegetation and soil type gridded data with 30" (~1 km) resolution and the ECMWF sea surface temperature (SST) gridded data with resolution of 1° (~ 100 km) were also used.
CAMx set up and input data: Simulations with the CAMx model were performed for the period from July 1 to 6, 1995. The CAMx simulations focused on the analysis of photo-oxidation over the greater Aegean area. For this purpose a nested-grid configuration was implemented (Figure 1) with two grids. The following grid configuration was used: Grid 1: 143x128 points, 0.226°x0.18° horizontal increment; Grid 2: 227x257 points, 0.045°x0.036° horizontal increment (SW corner at 19.7°E, 32.8°N). The vertical structure was identical for both grids: 7 vertical layers defined in terrain following **(σz)** coordinates. Variable vertical resolution was applied with a denser vertical structure in the lower levels, becoming increasingly sparser towards the top of the domain (at 4km).

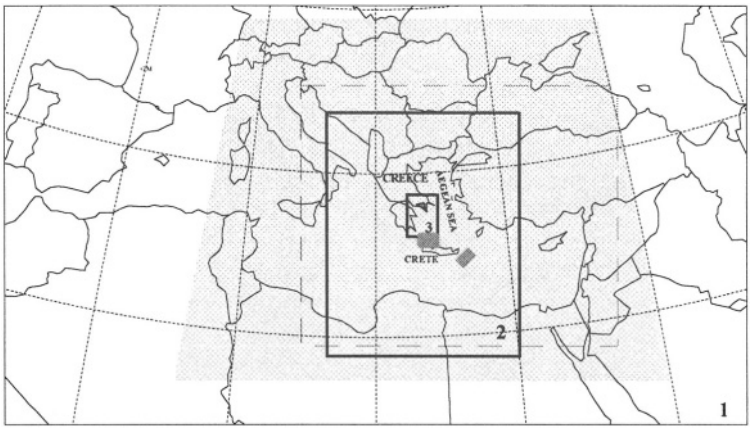

Figure 1. The RAMS model domain and nested grids. The dashed line indicates the area where surface observations are assimilated into the model initialization. The shadowed area indicates the CAMx model domain. The rectangles indicate receptor areas in MDMS simulations. The triangle indicates the GAA.

CAMx input data: The required meteorological datasets were supplied by the RAMS prognostic meteorological fields. The gridded land use data used in RAMS were adjusted accordingly for the CAMx grids. The Total Ozone Column for the area of interest was retrieved from the NASA/Goddard Space Flight Center database and derives from the Meteor3/TOMS dataset. With respect to precursor emissions, the following data sets were adjusted to the CAMx grids and used in the simulations:

1. An anthropogenic surface emissions inventory for Europe was retrieved from EMEP (Co-operative program for monitoring and evaluation of the long range transmission of air pollutants in Europe) for the year 1996. These data are in gridded form with 50x50 km grid increment and include annual surface emission rates (tn/y) of NH_3, NOx, VOCs (Volatile Organic Compounds) and SO_2. The VOC speciation and diurnal emissions profile calculations were based on the factors proposed by Zlatev et. al. (1992).
2. The surface emissions inventory for Greece was provided by Tsiligiridis (1995). This inventory is based on the CORINAIR methodology (CORINAIR, 1992) concerning the types of sources and procedures, the kinds of emitted pollutants and the emission rates. The included air pollutants are: NOx, NMVOCs (Non Methane VOCs) and

CO. The activities contributing to these emissions include: energy import, energy conversions, energy consumption in the industrial, transport, commercial and domestic sectors, etc. The main types of energy included are: carbon, lignite, natural gas, gas, biomass, oil, diesel and various others. The use of solvents in industrial activities was also taken into account. This latter category was analyzed specifically for this study in an 8x8 km grid, while the other types of emissions were analyzed in a 20x20 km grid.

MDMS setup and input data: Simulations with the MDMS model were performed for the experimental periods mentioned above. The MDMS simulations focused on the calculation of influence functions over the greater Aegean area. For this purpose a receptor area with dimensions 10km x 10km x 1km was defined at selected sites indicated by the airborne measurements. The requisite meteorological datasets were supplied by the RAMS prognostic meteorological fields.

3. MODELS RESULTS AND DISCUSSION

The RAMS-CAMx system simulations showed that the GAA plume maintains most of its characteristics over long distances (several hundreds of kilometers) above the Aegean Sea due to poor mixing in the marine boundary layer or in the free atmosphere. Figures 2 and 3 present the calculated ozone concentration in the layer 250-500m above surface on July 3 and 4. During nighttime, the precursor pollutants emitted in the GAA are transported to the south/southeast over the maritime area of the Saronic Gulf, owing to the weak NW land breeze flow. During the day, the northerly regional scale flow over the Aegean transports the plume further to the south. The calculated ozone concentrations at 1200 UTC and 1500 UTC on July 3 (Figure 2) reach approximately 60ppbv over the southern Aegean Sea. As evident in Figures 2a and 2b, the plume reaches Crete on a time scale of about 6h. These values are close to the O_3 concentrations measured during the T_TRAPEM project (presented in Figure 5.2.36b of Kallos et al., 1997), which reach 60–70ppbv. As shown in Figure 2, the RAMS-CAMx results give evidence of regional scale transport from the coastal area of NW Turkey towards the Aegean Sea. The situation changes slightly the following day (July 4) as the northerly flow over the Aegean weakens. The GAA urban plume is transported to the SE of GAA during the night and remains halfway between the GAA and Crete for more than 6h. The model results show concentrations of about 55-60ppbv with a maximum at 65ppbv (see Figure 3). The airborne measurements of O_3 concentrations in this area reach 60-70ppbv (Figure 5.2.36e, Kallos et al., 1997). The GAA plume reaches Crete on a time scale of 12h.

The influence of the GAA urban plume on remote areas was further investigated by calculating influence functions with the MDMS. Moreover, influence function calculations were used in order to identify the source areas of the photochemical pollution measured over the greater maritime area of Crete. Simulations were performed for various receptor areas around Crete. Figures 4 and 5 present the results from the following cases: 1. Influence functions calculated for 88h backward in time, the receptor area (A3) centered at 36.3° N, 23.4° E. Simulation started at 1600 UTC, July 3, 1995. 2. Influence functions calculated for 130h backward in time, the receptor area (A4) centered at 35°N, 26.5°E. Simulation started at 1000 UTC, July 5, 1995.

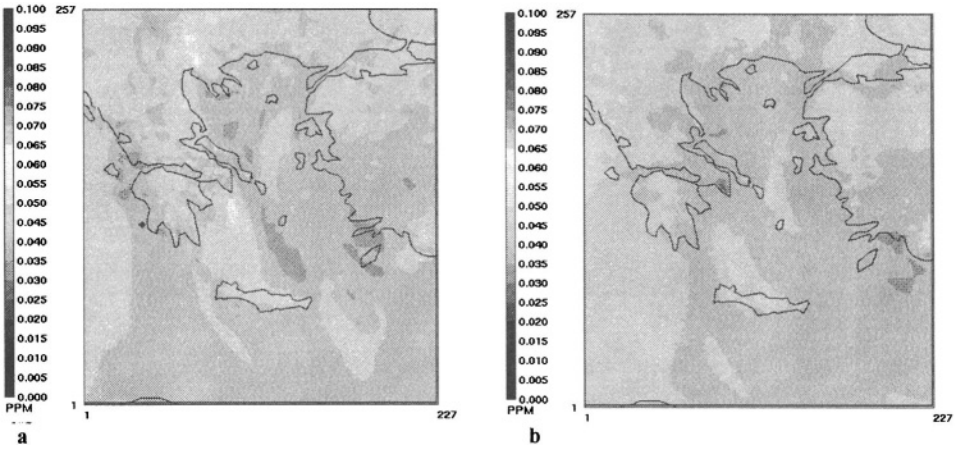

Figure 2. Calculated ozone concentration in grid 2 of CAMx in the atmospheric layer between 250-400m above surface. a) 1200 UTC and b) 1500UTC, July 3, 1995.

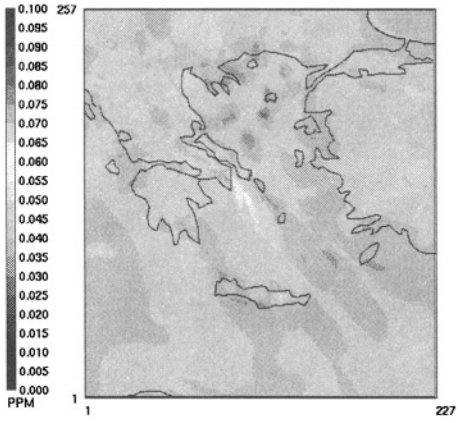

Figure 2. Calculated ozone concentration in grid 2 of CAMx in the atmospheric layer between 250-400m above surface at 1200 UTC, July 4, 1995.

The MDMS simulations confirmed the results of previous studies concerning the identification of the main transport routes in the Eastern Mediterranean (Kallos et al., 1996; 1998; Varinou, 2000). As evident in Figures 4 and 5, the maritime area to the NW of Crete is influenced by remote pollution sources located on the Greek peninsula, over a timescale of 24h. Sources located to the NE of Greece influence this area on timescale of 36h. The same timescale is identified for sources located in SE Italy. As shown by the CAMx model simulations, the GAA plume affects the receptor area after 12h. According to the results from Case 2, the maritime area to the SE of Crete is influenced by pollution sources located in the Southern Greece and Italy. The GAA influence on the receptor area occurs over a timescale of 18h. This result is also evident in the CAMx model simulations.

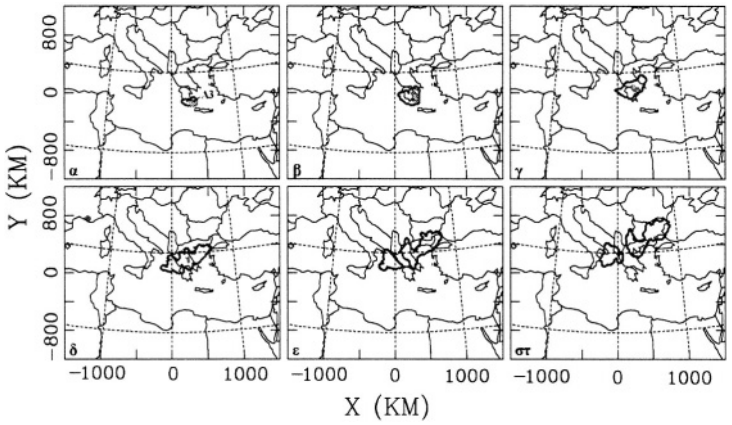

Figure 3. Influence functions calculated for 88h backward in time by the MDMS for a receptor area centered at 36.3^0 N, 23.4^0 E. Simulation started at 1600 UTC, July 3, 1995. Each frame presents 6h of integration. Contour increments: log()=0.01, 5, 10, 20, 30, 50, 100, 150, 200, 250, 500, 1000 sm^{-3}.

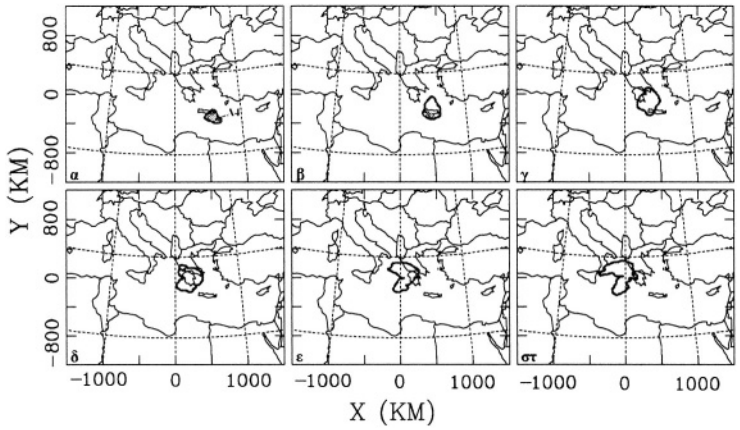

Figure 4. Influence functions calculated for 130h backward in time by the MDMS for a receptor area centered at 35^{0}N, 26.5^{0}E. Simulation started at 1000 UTC, July 5, 1995. Each frame presents 6h of integration. Contour increments: log()=0.01, 5, 10, 20, 30, 50, 100, 150, 200, 250, 500, 1000 sm^{-3}.

4. CONCLUSIONS

In the present study, multi-scale analysis of the atmospheric circulation and photochemical processes was performed in order to investigate the behavior of photochemical plumes emitted from urban coastal areas. The simulations were combined with regional scale marine boundary layer airborne measurements of the atmospheric oxidants. The results showed a strong interaction between local and regional scale fluctuations. The previously identified main routes of transport were confirmed as routes of photochemical fluctuations. The key factor is the marine boundary layer. The plume

maintains its characteristics inside this stable layer and the diurnal fluctuation of NOy in association with precursor VOCs define oxidant concentration at remote areas.

Acknowledgements: This study was supported by the research projects T-TRAPEM (EV*-CT92-0005), SUB-AERO (EVK2-1999-00052) and ADIOS (EVK3-CT-2000- 00035) of the DG-XII of the EU.

REFERENCES

Asimakopoulos, D., D., Deligiorgi, C., Drakopoulos, C., Helmis, K., Kokkori, D., Lalas, D., Sikiotis, and C., Varotsos, 1992: An experimental study of nighttime air-pollutant transport over complex terrain in Athens. Atmospheric Environment, Vol. 26B, 59-71.

CORINAIR Inventory, Default Emission Factors Handbook, Default emission factors from nature, Part 2, 1992.

Dayan, U., 1986: Climatology of back trajectories from Israel based synoptic analysis. J. of Climate and Applied Meteorology, 25, 591 - 595.

Environ, 1997: User's Guide to the comprehensive air quality model with extensions (CAMx). Version 1.10. Report prepared by Environ International Corporation, Novato, CA.

Kallos, G., V., Kotroni, K., Lagouvardos, M., Varinou, and A., Papadopoulos, 1996: Possible mechanisms for long range transport in the eastern Mediterranean. Proc. of the 21st NATO/CCMS Int. Techn. Meeting on Air Pollution Modelling and Its Application, 6-10 November, Baltimore, USA.

Kallos G., K., Lagouvardos, V., Kotroni, A., Papadopoulos, M., Varinou, M., Luria, M., Peleg, A., Wagner, G., Sharf, and G., Tunsel, 1997: "Transport and transformation of air pollutants in the Eastern Mediterranean Area". Final Report prepared for the DG-XII of EC, AVICENNE Initiative. T-TRAPEM Project, ISBN960-8468-07-8.

Kallos, G , V., Kotroni, K., Lagouvardos, A., Papadopoulos, M., Varinou, O., Kakaliagou, M., Luria, M., Peleg, A., Wagner and M., Uliasz, 1998: Temporal and spatial scales for transport and transformation processes in the eastern Mediterranean Proc. of the 22nd NATO/CCMS Int. Techn. Meeting on Air Pollution Modelling and Its Application, 2-6 June, Clermont-Ferrand, France.

Kallos, G., V. Kotroni, K. Lagouvardos, and A. Papadopoulos, 1999: "*On the transport of air pollutants from Europe to North Africa.* Geophysical Research Letters. 25, No 5, 619-622.

Katsoulis, B.D., and D.M., Whelpdale, 1993: A climatological analysis of four-day back trajectories from Aliartos, Greece. Theor. and Appl. Climatol. 47, 93 - 103.

Kotroni, V., G., Kallos, K., Lagouvardos, M., Varinou, and R, Walko, 1998: Numerical simulations of the meteorological and dispersion conditions during an air pollution episode over Athens, Greece. J. of Applied Meteorology, Vol., 38, pp.432-447.

Moussiopoulos, N., P., Sahm, and Ch.S., Kessler, 1995: Numerical simulation of photochemical smog formation in Athens, Greece-a case study. Atmospheric Environment, 29, No 24, pp. 3619-3632.

Peleg M., M., Luria, I., Setter, D., Perner, and P., Russel, 1994: Ozone levels over Central Israel. Isr. J. of Chemistry, 34, 375-386.

Pielke, R.A., W.R, Cotton, R. L., Walko, C. J., Tremback, W. A., Lyons, L.D., Grasso, M. E., Nicholls, M. D., Moran, D. A., Wesley, T. J., Lee, and J. H., Copeland, 1992: A comprehensive meteorological modelling system - RAMS. Meteorology and Atmospheric Physics, 49, 69-91.

Pilinis, C., P., Kassomenos, and G., Kallos, 1993: Modeling of photochemical pollution in Athens, Greece. Application of the RAMS-CALGRID modeling system. Atmospheric Environment. 27B, No 4, 353-370.

Tsiligiridis, G., 1995: Temporal and spatial analysis of energy consumption and the associated emissions of air pollutants during the period 1960-'90 in Greece. PhD thesis, Dept. of Mechanical Engineering, University of Thessaloniki, Thessaloniki, Greece.

Uliasz, M., 1993: The Atmospheric Mesoscale Dispersion Modeling System. J. of Applied Meteorology, 32, pp. 139-149.

UKMO (United Kingdom Meteorological Office), 1962: Weather in the Mediterranean, Vol. I, General Meteorology, 375 pp., H.M. Stationary Office, London, Second Edition.

Varinou, M., 2000: Characteristic spatial and temporal scale of dispersion and photochemical transformations of air pollutants over the NE Mediterranean. PhD thesis, Dept. of Physics, University of Athens, Athens, Greece, pp 300.

Wagner, A., M. Peleg, G. Sharf, Y. Mahrer, U. Dayan, G. Kallos, V. Kotroni, K. Lagouvardos, M. Varinou, A. Papadopoulos, 2000. "*Some observational and Modeling evidence of long-range transport of air pollutants from Europe toward Israeli coast*". J. Geophysical Res., 105, No.D6, 7177-7186.

Zlatev, Z., J., Christensen, and O., Hov, 1992: A Eulerian air pollution model for Europe with non-linear chemistry. J. of Atmospheric Chemistry, Vol.15, pp.1-37.

DISCUSSION

A. EBEL — Has the role of vertical transport of pollutants, particularly ozone, also been studied for the Mediterranean region ?

M. VARINOU — The role of vertical transport of pollutants over the NE Mediterranean has been extensively studied with airborne observations and model simulations. The simulations were performed using RAMS and HYPACT, which is a Lagrangian-type dispersion model. Releases from major coastal urban areas such as the Greater Athens Area were performed for various time periods during the day. The results showed that in the case of weak synoptic flow, dispersion patterns over the Aegean are mainly affected by the release time and the mixing height variability due to the complex land-water distribution. The pollutants released during the night and early in the morning are transported downwards within the marine boundary layer. The modification of the mixing height due to the presence of islands, leads to a considerable intrusion and transport above the marine boundary layer of about 1km. The pollutants released during the day are injected in the free troposphere as soon as they are released. This is attributed to the convergence over rough topography, affecting a layer of 2-4km depth. Vertical mixing between this layer and the surface layer is also evident over the Aegean as a result of convergence over the islands. In the case of strong synoptic flow no significant convergence was found over the land while the pollutants are mainly within a well-mixed layer of about 2km depth.

This page intentionally left blank

NUMERICAL STUDY OF TROPOSPHERIC OZONE IN THE SPRINGTIME IN EAST ASIA

Meigen Zhang, Itsushi Uno, Zifa Wang, and Hajime Akimoto*

1. INTRODUCTION

East Asia is a region of the world with large and rapidly increasing anthropogenic emissions of photochemically active pollutants, such as CO, NO_x ($NO + NO_2$), SO_2, and nonmethane hydrocarbons (NMHCs). Recent research suggests that tropospheric ozone concentrations have increased in the lower troposphere over East Asia in recent decades and that the rate of increase is larger than other areas of the northern mid-latitudes [Akimoto et al., 1994; Oltmans et al., 1998; Lee et al., 1998]. In contrast to Europe, the trend of increasing boundary layer ozone is still continuing in the 1990s in this area, and this is probably due to a trend of increasing emissions of precursors on a regional scale [Lee et al., 1998].

Ozone in the troposphere is supplied by transport from stratosphere, and is produced within the troposphere during the oxidation of hydrocarbons and CO catalyzed by NO_x and HO_x (OH + peroxy radicals). It is removed by photolysis, chemical reactions, and deposition to the surface. Tropospheric ozone has a large variability globally reflecting quite different source/sink strength depending on the geographic location. Most surface ozone measurements in the northern hemisphere show a spring maximum [e.g., Oltmans and Levy, 1994; Pochanart et al., 1999]. Subsidence of O_3 rich air masses from stratosphere by tropopause folding events, which frequently occur in winter-spring over the extratropics, is a possible cause [Oltmans and Levy, 1992; Carmichael et al., 1998]. However, it has also been suggested that the spring maximum is caused by gradual accumulation of ozone and precursors over the winter months when the lifetimes of ozone and precursors are significantly longer than in summer [Penkett et al., 1993; Liu et al., 1987], The role of photochemical production from anthropogenic emissions of precursors and intrusion of stratospheric air with high concentrations of ozone in producing these

* Frontier Research System for Global Change, Yokohama, Kanagawa 236-0001, Japan.

Air Pollution Modeling and Its Application XV, Edited by
Borrego and Schayes, Kluwer Academic/Plenum Publishers, New York, 2002

springtime maxima remain to be quantified [Carmichael et al., 1998].

In this study the transport and chemical production of tropospheric ozone in the early springtime in East Asia are studied by using the Models-3 Community Multi-scale Air Quality (CMAQ) modeling system [Byun and Ching, 1999] with meteorological fields calculated by the Regional Atmospheric Modeling System (RAMS) [Pielke et al., 1992].

2. MODEL DESCRIPTION

The model used in this study contains two parts: a regional chemical transport model - CMAQ and a regional meteorological model - RAMS. CMAQ is designed to be flexible so that different levels of configuration can be achieved. In this study we configured CMAQ with following options: (1) advection with piece-wise parabolic method (PPM); (2) vertical diffusion with K-theory parameterization; (3) Deposition flux as bottom boundary condition for the vertical diffusion; (4) mass conservation adjustment scheme; (5) horizontal diffusion with scale dependent diffusivity; (6) RADM2 chemistry mechanism with the four-product Carter isoprene mechanism; (7) QSSA gas-phase reaction solver; (8) emission injected in the vertical diffusion module; (9) aqueous-phase reactions and convective cloud mixing. For the detailed description of the science algorithms, refer to Byun and Ching (1999).

To provide meteorological data for CMAQ simulations, RAMS was run from February 24 to March 31, 1998. The modeling domain is 6400x5600 km^2 on the rotated polar-stereographic map projection centered at (38°N, 117°E) with 80 km mesh. This region has dramatic variations of topography, land type, and mixtures of industrial/urban centers and agricultural/rural regions. It includes fertile plains of China, the peninsula of Korea, and the islands of Japan. In addition, the interactions between continental and marine influences play a prominent role in determining the effects of pollutant production and transport in this region. There are 23 vertical layers in the σ_z coordinates system unequally spaced from the ground to 20 km, nearly half of the vertical layers are concentrated in the lowest 2 km of the atmosphere in order to resolve the planetary boundary layer. In simulations, the three-dimensional meteorological fields for RAMS input were obtained from European Center for Medium-Range Weather Forecasts (ECMWF) re-analyzed datasets. These datasets are available every six hours.

Emissions of NO_x and carbon monoxide (CO) from fuel combustion and biomass burning were taken from the database prepared in support of the TRACE-P experiment (http://www.cgrer.uiowa.edu/people/woojh21). For anthropogenic emissions, the largest emissions of NO_x occur in China, however, the emission intensity varies significantly from region to region. For example, the highest emission intensities are found around the main industrial and urban centers such as Seoul, Tokyo, and Shanghai. The NO_x emissions from soil were also considered, and were obtained from the Global Emission Inventory Activity (GEIA) [Benkovitz, 1996] 1°x1° monthly global inventory for the month of March. The NO_x sources due to lightning and aircraft were taken from the Emission Database for Global

Atmospheric Research (EDGAR) 1°x1° annual global inventory [Oliver et al., 1996].

Anthropogenic emissions of total non-methane volatile organic compounds (NMVOC) were taken from the above listed website. The ratio of NMVOC specie to total NMVOC is derived form EDGAR. Emissions of isoprene and monoterpene were obtained form GEIA.

Initial and boundary conditions were chosen to reflect East Asian situation. Recent measurements were used whenever possible. To evaluate the impact of the anthropogenic emissions on the distributions of trace species, the initial conditions were chosen at the lower end of their range so as to allow the emissions and chemical reactions to "take them up" to their "actual" values during the 5 day initialization period [Liu et al., 1996; Carmichael et al., 1998].

Stratospheric influence on tropospheric ozone was parameterized by specifying the initial and boundary conditions at the top 3 altitude levels of the model to values proportional to potential vorticity (PV). The proportional coefficient is assumed to be constant. For O_3, 50 ppbv per PV unit was adopted according to the studies by Ebel et al. [1991] and Beekmann et al. [1994], where the PV unit is $10^{-6}\ Km^2 kg^{-1} s^{-1}$.

3. RESULTS AND DISCUSSION

CMAQ was run from February 24 to March 31, 1998, but the model results were discussed for last 31 days. In order to evaluate the model performance, we compare surface ozone and CO monitoring data measured at three remote sites (Okinawa, Oki, and Happo) with model results (cf. Figure 1-2). The Okinawa Islands are located in southern Japan facing the Pacific Ocean to the east and the East China Sea to the west. The Okinawa sampling site (Hedo) at latitude 26°52'N, longitude 128°15'E, 20 m above sea level, is located on the northern tip of the main island where there is little human activity. The Oki Islands are located in the Sea of Japan approximately 100 km north of the main island (Honshu) of Japan. The Oki sampling site (Oki) at latitude 36°17'N, longitude 133°11'E, 90 m above sea level, is located above a coastal cliff at the most northwestern point of the main island in an area of little human activity. The Happo site is situated in a mountainous region in central Japan at latitude, longitude, and altitude of 31°41'N, 137°48'E, and 1840 m above sea level.

Figure 1 shows the time series of hourly averaged surface ozone mixing ratios measured at Okinawa (Figure 1a) and Oki (Figure 1b). Also shown are the results from the model for the lowest model layer, approximately at 50 m above the ground. The figure shows the model reproduces O_3 concentrations reasonably well. For example, the magnitude and the timing of the peak ozone levels and the timing of the low ozone concentrations at both sites are well captured, while the minimum values are overpredicted by ~10 ppbv.

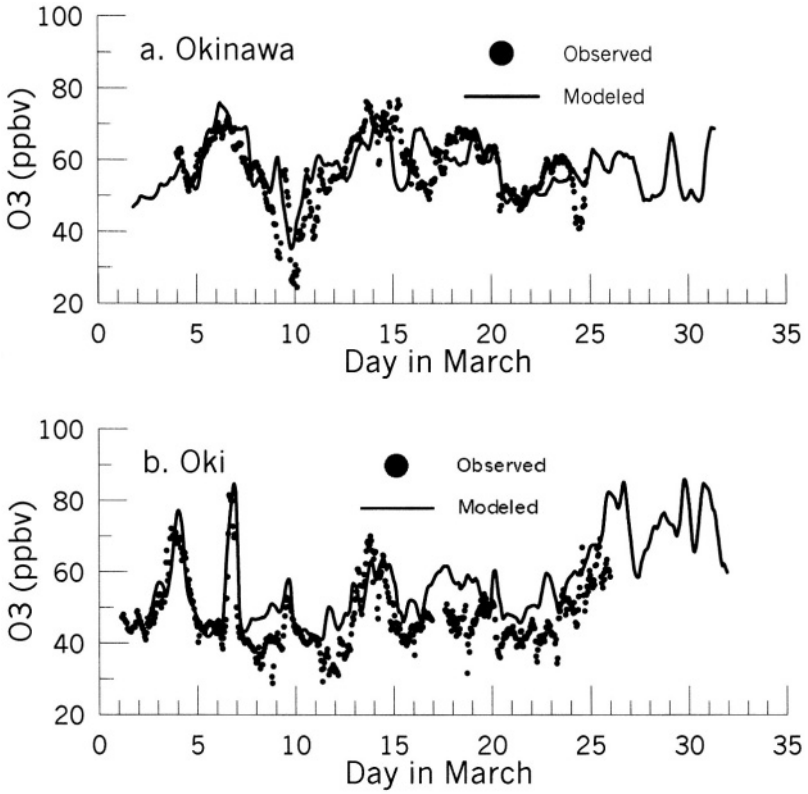

Figure 1. Comparison between predicted hourly average ozone mixing ratios for the lowest model layer (~50 m above ground) and observed ground-level hourly mean ozone concentrations at (a) Okinawa and (b) Oki.

To compare the CO predictions with observations, one important consideration is to account for the effect that its photochemical lifetime has on its distribution [Liu et al., 1996], because a species with a long photochemical lifetime relative to the characteristic time of the transport processes in the model domain is expected to have a more uniform distribution than a short-lived species. CO has the longest photochemical lifetime about 2 months in the troposphere. Its observed mixing ratio rarely got below 80 ppbv. If this value is defined as the initial and boundary conditions, the model is expected to have a background value of about 80 ppbv over areas that are not affected significantly by continental source. Since the model runs for only 1 month, predicted CO values tend to agree well with observations, particularly in areas remote from sources. Of course, the agreement is meaningless and the comparison is ineffective for testing the model performance. Other than increasing the model domain and running the model for a period of time comparable to the lifetime of CO, there is no satisfactory solution to this problem. A partial solution is to avoid the problem by comparing model results only for areas where CO

levels are above the background value. In practice, we can subtract the background concentration of CO from the actual value and compare model results with observations for areas with large residuals only. In the following, we will subtract 50 ppbv from all CO mixing ratios. This value is chosen to be less than 80 ppbv in order to account for the photochemical sink. The series of hourly mean CO mixing ratios from surface observations and model predictions for the lowest model layer are shown in Figure 2. The figure shows that the predicted and measured concentrations are comparable during most of the simulation. The timing of peak CO levels is nearly fully captured at both sites, while maximum values are underpredicted. The underprediction may be caused by inaccurate account of CO emission from biomass burning in Asian continent

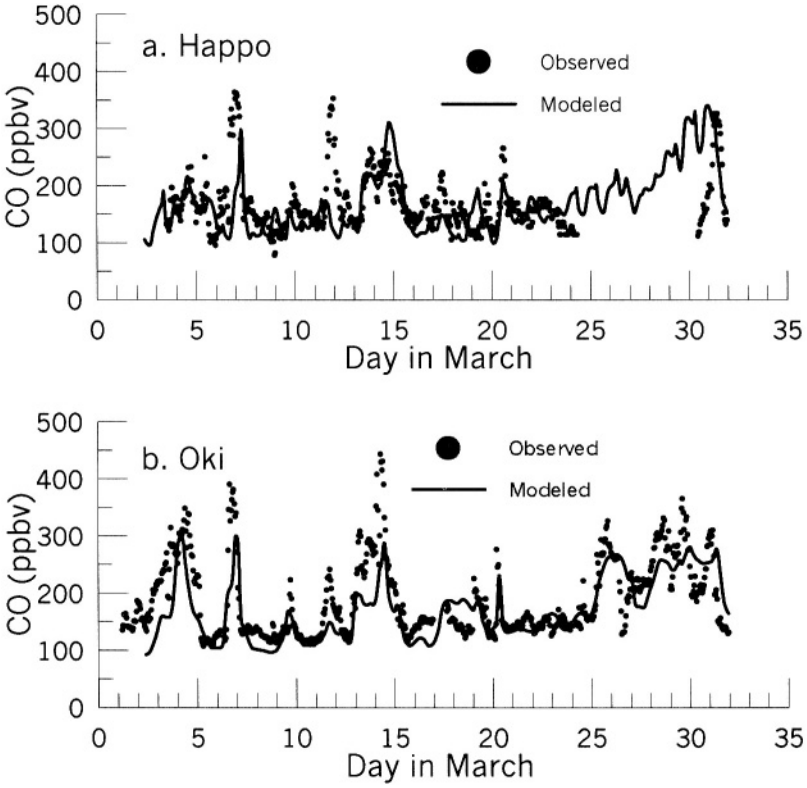

Figure 2. Comparison between predicted hourly average CO mixing ratios for the lowest model layer (~50 m above ground) and observed ground-level hourly mean CO concentrations at (a) Happo and (b) Oki.

CO serves as a good tracer of combustion, correlation between O_3 and CO is often used for evaluating photochemical O_3 production [e.g., Parrish et al., 1993;

Mauzerall et al., 2000]. Checking the observed time series of O_3 in Figure 1 and CO in Figure 2, we can find that at Oki Island high O_3 concentrations were accompanied by high CO concentrations. The positive correlation between O_3 and CO indicates that these high O_3 was a photochemical production from anthropogenic emissions.

In the simulation period, there are some ozonesonde data available at Tateno and Sapporo in Japan. Figure 3 shows mean vertical ozone profiles from ozonesonde and model prediction at Tateno (9 sondings at about 15:00 JST on March 2, 6 9, 13, 16, 19, 23, 26, and 30) and Sapporo (4 sondings at about 15:00 JST on March 2, 18, 25, and 30). The Tateno site is located at latitude, longitude, and altitude of 36°3'N, 140°6'E, and 31 m above sea level, and the Sapporo site – 43°3'N, 141°20'E, and 19 m. From the figure we can see that the predicted O_3 concentrations are in good agreement with ozonesonde data at upper layers, which shows the PV is a good indicator of stratospheric ozone.

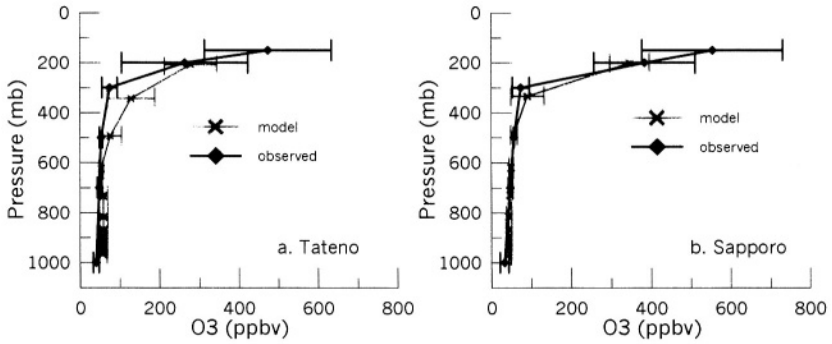

Figure 3. Vertical profiles of ozone mixing ratios from ozonesonde and model results at (a) Tateno and (b) Sapporo, Japan. Horizontal bars indicate one standard deviation.

Comparison of model simulations with near surface observations of O3 and CO, and ozonesonde data indicates that the horizontal and vertical distributions of tropospheric ozone are reasonably well captured in the simulation. Now we try to quantify the contributions from transport versus chemical processes. Figure 4 shows sources and sinks of ozone in an area of $480x480\ km^2$ around Okinawa (remote area) in Japan and Shanghai (source area) in China in March of 1998. In the figure positive values indicate ozone gain, and negative values indicate ozone loss.

From Figure 4 we find that in the surface layer (~100m), the transport processes may play more important roles than photochemical factors in determining ozone concentrations. In Shanghai area photochemical production is low in the surface layer because of titration of excess emission of NO and CO, dry deposition is compensated mainly by horizontal transport and downward transport from above surface layer, where is favorable for ozone production.

In the boundary layer (~1000m), ozone is vertically transported out due to active convection in the springtime, and the supply and loss of boundary layer ozone is

dominated by photochemistry, especially in Shanghai area. In both areas, the photochemical production rate increases with height below 700m.

In the layer below 5000m, ozone is horizontally transported out due to the strong westerlies, and the most important source is downward transport from upper layers, where ozone concentrations are greatly affected by incursion of stratospheric ozone.

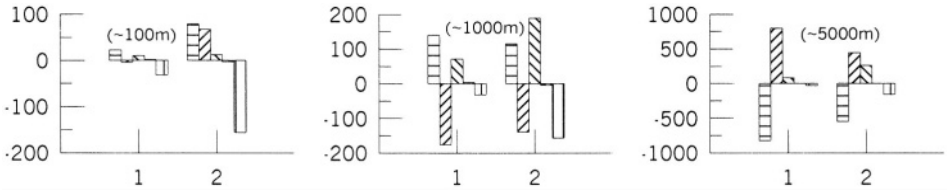

Figure 4. Sources and sinks of ozone (Gg/month) in the layer of 0~100m, 0~1000m and 0~5000m around Okinawa in Japan and Shanghai in China. Group 1 strands for Okinawa and Group 2 for Shanghai, and in each group there are 5 columns representing (from left to right) horizontal transport, vertical transport, photochemical production, vertical mixing associated with convection, and dry deposition, respectively.

4. SUMMARY

A regional three-dimension chemical transport model called the Models-3 Community Multi-scale Air Quality modeling system with meteorological fields from the Regional Atmospheric Modeling System is used to study the transport and photochemical transformation of tropospheric ozone over East Asia for March of 1998. The model calculated mixing ratios of ozone and carbon monoxide were compared with ground level observations in Japan and were found the model reproduces observations very well. In comparison with available ozonesonde data, we found the model calculated ozone concentrations at upper model layers are in good agreement with measurements. Numerical study showed that the model reproduces photochemical ozone production reasonably well and simulates the influence of emissions from the continental boundary layer that was evident in the ground-level observations of ozone and carbon monoxide very well. The ozone budget analysis indicates that the transport processes may play more important roles than photochemical factors in determining surface ozone concentrations, and the supply and loss of boundary layer ozone is dominated by photochemistry.

REFERENCES

Akimoto, H., H. Nakane, and Y. Matsumoto, 1996, The chemistry of oxidant generation: Tropospheric ozone increase in Japan, in the Chemistry of the Atmosphere: Its Impact on Global Change, edited by J. G. Calvet, pp261-273, Blackwell Sci., Cambridge, Mass.

Beekmann, M., G. Ancellet, and M. Megie, 1994, Climatology of tropospheric ozone in southern Europe and its

relation to potential vorticity, J. Geophys. Res., **99**:12,841-12,853.

Benkovitz, C. M., M. T. Schultz, J. Pacyna, L. Tarrason, J. Dignon, E. C. Voldner, P. A. Spiro, J. A. Logan, and T. E. Graedel, 1996, Global gridded inventories of anthropogenic emissions of sulfur and nitrogen, J. Geophys. Res., **101**:29,239-29,253.

Byun, D. W., and J. K. S. Ching, ed., 1999, Science algorithms of the EPA Models-3 community multi-scale air quality (CMAQ) modeling system, NERL, Research Triangle Park, NC.

Carmichael, G. R., I. Uno, M. J. Phadnis, Y. Zhang, and Y. Sunwoo, 1998, Tropospheric ozone production and transport in the springtime in east Asia, J. Geophys. Res., **103**:10,649-10,671.

Ebel, A., H. Hass, H. Jakobs, M. Laube, M. Memmesheimer, and A. Oberreuter, 1991, Simulation of ozone intrusion caused by tropopause fold and cut-off low, Atmos. Environ., **25A**:2131-2144.

Lee, S.-H., H. Akimoto, H. Nakane, S. Kurnosenko, and Y. Kinjo, 1998, Increase of tropospheric ozone at Okinawa, Japan, Geophys. Res. Lett., **25**:1637-1640.

Liu, S. C., M. Trainer, F. C. Fehsenfeld, D. D. Parrish, E. J. Williams, D. W. Fahey, G. Hubler, and P. C. Murphy, 1997, Ozone production in the rural troposphere and the implications for regional and global ozone distributions, J. Geophys. Res., **92**:4191-4207.

Liu, S.C., et al., 1996, Model study of tropospheric trace species distributions during PEM-West A, J. Geophys. Res., **101**:2073-2085.

Mauzerall, D. L., D. Narita, H. Akimoto, L. Horowitz, S. Walters, D. A. Hauglustaine, and G. Brasseur, 2000, Seasonal characteristics of tropospheric ozone production and mixing ratios over East Asia: A global three-dimensional chemical transport model analysis, J. Geophys. Res., **105**:17,895-17,910.

Oliver, J. G. J., A. F. Bouwman, C. W. M. Van der Mass, J. J. M. Berdowski, C. Veldt, J. P. J. Bloos, A. J. H. Visschedijk, P. Y. J. Zandveld, and J. L. Haverlag, 1996, Description of EDGAR Version 2.0: A set of global emission inventories of greenhouse gases and ozone-depleting substances for all anthropogenic and most natural sources on a per country basis and on $1^0 x 1^0$ grid, National Institute of Public Health and the Environment (RIVM) report no. 771060 002 / TNO-MEP report no. R96/119.

Oltmans, S. J., and H. Levy II, 1992, Seasonal cycle of surface ozone over the western North Atlantic, Nature, **358**:392-394.

Oltmans, S. J., and H. Levy II, 1994, Surface ozone measurements from a global network, Atmos. Environ., **28**:9-24.

Oltmans, S. J., et al., 1998, Trends of ozone in the troposphere, Geophys. Res. Lett., **25**:139-142.

Parrish, D. D., J. S. Holloway, M. Trainer, P. C. Murphy, G. L. Forbes, and F. C. Fehsenfeld, 1993, Export of North American ozone pollution to the North Atlantic Ocean, Science, **259**:1436-1439.

Penkett, S., N. Blake, P. Lightman, A. Marsh, P. Anwyl, and G. Butcher, 1993, The seasonal variation of nonmethane hydrocarbons in the free troposphere over the North Atlantic Ocean: Possible envidence for extensive reaction of hydrocarbons with the nitrate radical, J. Geophys. Res., **98**:2865-2885.

Pielke, R. A., W. R. Cotton, R. L. Walko, C. J. Tremback, W. A. Lyons, L. D. Grasso, M. E. Nicholls, M. D. Moran, D. A. Wesley, T. J. Lee and J. H. Copeland, 1992, A comprehensive meteorological modeling system – RAMS, Meteorol. Atmos. Phys., **49**:69-91.

Pochanart, P., J. Hirokawa, Y. Kaji, H. Akimoto, and M. Nakao, 1999, Influence of regional-scale anthropogenic activity in northeast Asia on seasonal variations of surface ozone and its precursors observed at Oki, Japan, J. Geophys. Res., **104**:3621-3631.

DISCUSSION

P. BUILTJES — Do I understand correctly that the Spring time observed ozone maximum is due to production, not to stratospheric intrusions ?

M. ZHANG — Yes. The model simulation shows that subsidences of O_3 rich air from stratosphere can cause high O_3 surface concentration occasionally, but on monthly average the Spring ozone maximum is caused by photochemical production based on O_3 budget analysis.

This page intentionally left blank

TESTING SMOG INDICES USING A COMPREHENSIVE MODEL

Christopher Fung, Hin-Chung Lau, Linda Yu, Kenneth Leung, Alick Chang[1]

1. INTRODUCTION

The term "smog" has been used loosely to refer to air urban pollution in general with the consensus that these pollutants are formed through a transformation process, very often involving photochemistry. For most urban areas, smog encompasses at least three distinct, yet inter-related, pollutants: ozone, NO_2 and suspended particulates. Air quality objectives (AQO) or standards are usually set for each of these pollutants. Despite the separate consideration of these pollutants, attention has traditionally been focused on ozone as an indication of photochemical activities and hence the severity of other photochemical smog species. However, it has been known that ozone and NO_2 concentrations at specific times and locations usually bear an inverse relationship to each other – high ozone is usually accompanied by low NO_2 and vice versa – and that chemical and photochemical activities enhance the production of secondary particulates from gaseous precursors in general. Given that the standards for each of the three smog components are individually health-based and that cumulative or synergistic effects of these pollutants are possible, all the components should be considered together in some fashion. The paper discusses how consolidated smog indices are developed to characterise the three common components of smog as one phenomenon.

Given the location-specific air pollution signature of each urban area and the infancy of our attempt to quantify total smog, local air quality data must be used to understand the behaviour of the developed indices. Two sources of data are potential candidates: measurements from air quality monitoring stations or output from simulation models. The former usually suffers from spatial patchiness and also potentially from a lack of unbroken and consistent historical record to allow us to form a comprehensive picture. On the other hand, a comprehensive air quality model, once validated for a location or region, can be used as a surrogate for measurements and can overcome the problem of spatial and temporal patchiness. In this paper, we will use a comprehensive model code-named PATH[1] for Pollutants in the Atmosphere and their Transport over Hongkong developed from community-based components specifically for the Hong Kong Special

[1] Hong Kong Environmental Protection Department, 33/F Revenue Tower, 5 Gloucester Road, Hong Kong Special Administrative Region, China; e-mail of corresponding author: cfung@epd.gov.hk; Tel: 852-2594-6303; Fax: 852-2827-8040.

Air Pollution Modeling and Its Application XV, Edited by
Borrego and Schayes, Kluwer Academic/Plenum Publishers, New York, 2002

Administrative Region (HK) of China to provide data to analyse the behaviour of the proposed smog indices. This 3-D modeling system puts together MM5, EMS-95 and SAQM in a consistent framework to simulate meteorology, emission and air quality, respectively and is set up on a polar stereographic grid with five nested domains of decreasing grid spacing (by factor of three) centering over HK. The largest domain has horizontal grid spacing of 40.5 km and extends west to the Himalayas, north to central China, east to the central Pacific and south to the Philippines while the 1.5km spacing domain covers all of HK. Simulations on this 1.5km-spacing domain are used for this paper. A two-day smog episode (19-20 August 1996) with generally high concentrations of all smog components is simulated for testing the indices. Though we are using HK's AQO (Table 1) to develop our very preliminary smog indices and will be studying the behaviour of such indices over HK, the work is intended to demonstrate the idea for urban areas in general.

Table 1. HK's Air Quality Objective for O_3, NO_2 and RSP in $\mu g/m^3$

	1-hr	24-hr	Annual
Ozone	240	---	---
NO_2	300	150	80
RSP	---	180	55

2. DEVELOPMENT OF TESTING SMOG INDICES

Three approaches based on different assumptions can be used to characterise smog:

1. An index based on one species concentration normalized by the species' AQO.
2. The maximum of the normalized indices of the smog components as defined above.
3. A single index consolidated by adding the normalized indices as defined in 1 above of each of the three components.

Calculating the indices based on the last two approaches is complicated by the fact that for some smog species, different AQOs are defined based on averaging times. Table 1 shows that HK has a 1-hr objective for O_3 and a 1-hr as well as a daily objective for NO_2. For respirable suspended particulates (RSP), no 1-hr objective has been promulgated, but daily and annual objectives exist. On the other hand, model data are generated hourly and this preliminary study is only limited to using one model-simulated episode spanning two days.

Another set of complications arises from the fact that RSP is defined as all suspended particulates with diameter below $10\mu m$ while the health and visibility effects which are of most concern to the public are most pronounced for fine suspended particulates (FSP) defined as particles having diameter below $2.5\mu m$. It is this fraction of RSP that are the active component of "smog." For HK, RSP has an AQO while FSP does not. It has also been thought that a significant portion of these fine particulates are formed from gas to particulate transformation followed by coagulation and referred to as secondary particulates. On the other hand, the model used in this attempt, though differentiating between FSP and RSP emissions as well as calculating gas to particulate transformation, does not follow the growth of these secondary particulates in size. Given these difficulties, we have opted for the following compromises and assumptions in defining the latter two types of smog index which are all based on the maximum concentrations for the

appropriate averaging times produced by the model during the simulation period:
1. Two individual indices (I) for NO_2 are formed from the 1-hr and daily AQOs through normalizing (i.e. dividing by the AQO values of corresponding averaging time.)
2. The annual AQO for RSP is ignored because it is too long for smog episodes in HK and an hourly AQO for RSP is invented for this study from the daily AQO by applying the same ratio (0.5 for hourly to daily) that is in the Japanese Air Quality Standards[2].
3. To come up with an FSP testing "standard" from RSP, the ratios between the U.S. proposed FSP and RSP standards[3] for one-day and one-year averaging times are averaged and applied to HK's AQO.
4. The modelled concentration for FSP is defined as the sum of primary FSP and all secondary particulates since most secondary particulates are believed to be smaller than $2.5\mu m$ in diameter.
5. The hourly $(I_{max\text{-}hr\text{-}FSP})$ and daily $(I_{max\text{-}day\text{-}FSP})$ FSP component indices are calculated based on 3. and 4. above in the same way as was done for NO_2 in 1 above.
6. Based on the above five individual indices (I), and the three approaches enumerated previously, the following five consolidated indices (CI) are defined:

a. CI_{O3} = maximum hourly normalized ozone concentration $(I_{max\text{-}hr\text{-}O3})$;
b. $CI_{max\text{-}hr} = max\ \{ I_{max\text{-}hr\text{-}O3}, I_{max\text{-}hr\text{-}NO2}, I_{max\text{-}hr\text{-}FSP}\}$
c. $CI_{max\text{-}day} = max\ \{ I_{max\text{-}hr\text{-}O3}, I_{max\text{-}day\text{-}NO2}, I_{max\text{-}day\text{-}FSP}\}$
d. $CI_{sum\text{-}hr} = sum\ \{ I_{max\text{-}hr\text{-}O3}, I_{max\text{-}hr\text{-}NO2}, I_{max\text{-}hr\text{-}FSP}\}$
e. $CI_{sum\text{-}day} = sum\ \{ I_{max\text{-}hr\text{-}O3}, I_{max\text{-}day\text{-}NO2}, I_{max\text{-}day\text{-}FSP}\}$.

It is noted that the indices defined as daily still retains the hourly ozone component and no attempt is made to make it consistent because defining a 24-hr ozone standard or objective is not very meaningful given our understanding of short-term behaviour of ozone. The maximum modeled concentration over the averaging period is used for index value calculation.

3. Testing the Developed Smog Indices for the Base-Case

The modeled data can support the choice of three types of conveniently defined spatial coverage for analysis to form a single view of smog over an area (see Figure 1):
1. At some model grid cells in which air quality monitoring stations are located totaling 15 for our study area;
2. At some heavily populated regions scattered over the study area defined just for the purpose of this preliminary study which number 8 and occupy 55 grid cells with each region composed of between 4 and 11 grid cells;
3. Over the entire land area of HK including the major outlying islands which is represented by a total of 621 grid cells out of a total of 49 x 49 grid cells in the domain currently considered.

Figure 2 shows a plot of the five individual indices (with average and standard deviations as appropriate) calculated for the three coverages. The following features are of note:
1. the average of the indices vary from 35 to 53 showing a 40% difference between the highest and lowest. The average of the indices for the stations cover approximately the same range (37-53) while that of the regions cover a smaller range between 35 and 48.
2. the order of the station and region data for any index can be quite different indicating

that the relative severity of smog is not represented by the stations if the region data, being more representative, are taken to be the standard.

3. the corresponding averages of the indices for stations and regions do not differ by more than 23% while some can be as small as 5% (indices 1 and 2 based on hourly ozone and NO_2) indicating that the model-represented stations, take together, can represent all land area to within this accuracy.

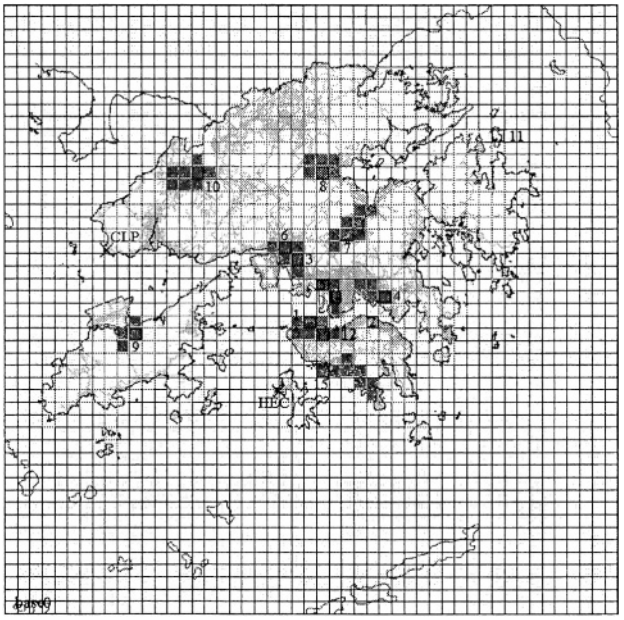

Figure 1. Modelling domain showing grids covering all land area, the regions (highlighted solid squares) and the stations (highlighted open square with number next to or inside them). The road network in HK is also indicated by faint lines. HEC and CLP are power stations.

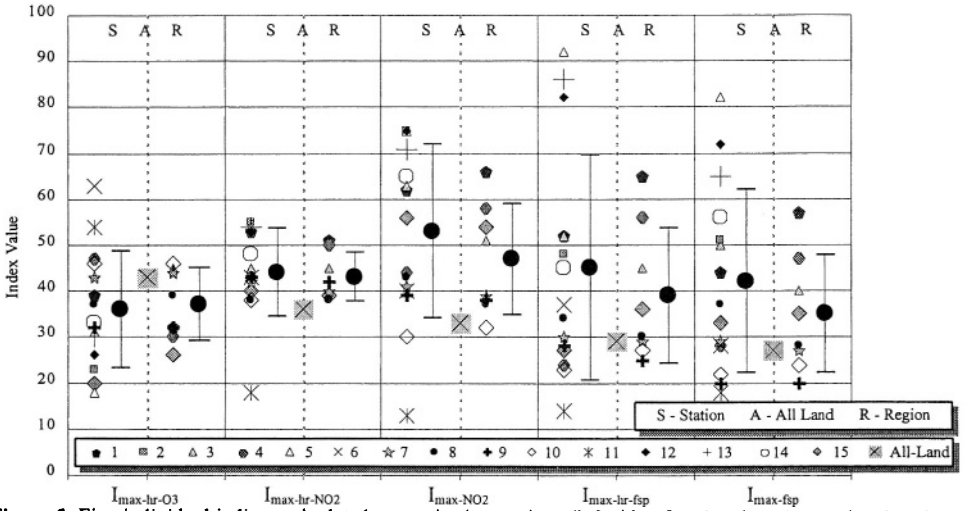

Figure 2. Five individual indices calculated at monitoring stations (left side of each column), populated regions (right side of each column) and all land area of HK (middle of column). The error bars to the left of the data points give the average and standard deviation of the data.

4. both the averages and standard deviations of the indices of the regions are consistently smaller than that for the stations, indicating the averaging effect of considering a wider area in constructing an index and the stability that can result.
5. the value for the all-land index is higher than its "station" and "region" counterparts for O_3 by more than 10%, but lower by a larger percentage for the NO_2 and FSP hourly and daily indices. Though the station and region values for the first index based on O_3 are lower than all their other counterparts based on other species (except for the very last one of maximum daily FSP over the regions), the all-land value for this ozone-based index is the highest among all its counterpart. This is a clear indication of the phenomenon that O_3 is usually strongest away from urban areas where its precursors are emitted while high NO_2 and FSP are more urban phenomena. This reasonable behaviour of the indices also gives them credence. More so, the importance of taking an appropriate spatial average is highlighted.

The consolidated indices based on formulae (1)-(5) above are plotted in Figure 3. The first column of this plot (CI_{O3}) would be the same as that in Figure 2 since the two indices are identical – based solely on maximum hourly ozone concentration. As far as spatial representativeness of these consolidated indices is concerned, points 2 and 4 above for the individual indices also apply here to the consolidated indices. The next two indices, $CI_{max\text{-}hr}$ and $CI_{max\text{-}day}$, show higher values than CI_{O3} due to the "pick-the-winner" approach. What is strikingly different is the magnitude of the last two consolidated indices which are approximately two and a half to three times that of the previous three indices. Yet this is to be expected given that all the component indices shown in Figure 2 are approximately of the same magnitude and it also points out the inadequacy of using any one individual index to represent smog. The values of the first three indices calculated over all-land are the same, indicating that ozone has dominated on this spatial scale. The all-land values for $CI_{sum\text{-}hr}$ and $CI_{sum\text{-}day}$ are lower than their station and region counterparts, indicating dominance on this spatial scale by NO_2 and FSP whose concentrations are generally lower away from populated areas and monitoring stations.

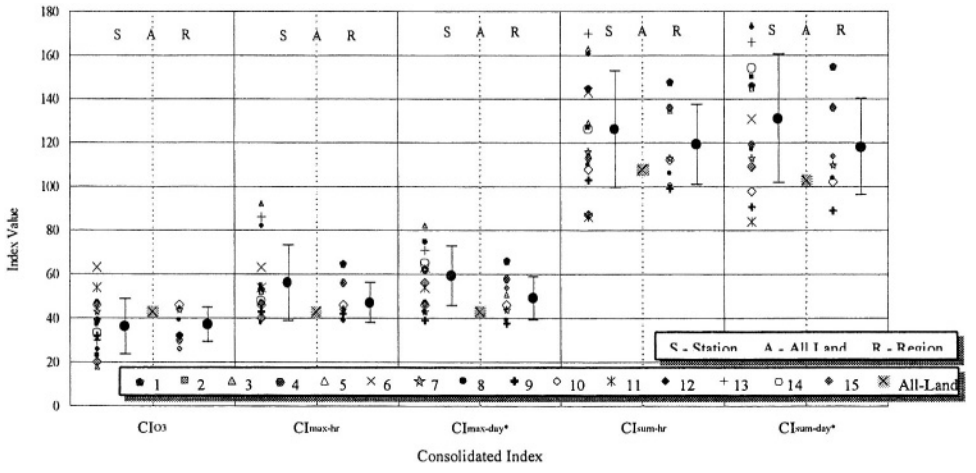

Figure 3. Five consolidated indices calculated at monitoring stations (left side of each column), populated regions (right side of each column) and all land area of HK (middle of column).
* The ozone component index is still hourly

4. TESTING THE DEVELOPED SMOG INDICES FOR EMISSION-CUT SCENARIOS

Since constructing a smog index is ultimately to provide a measure to assess the impacts of policies on human health, it would be instructive to determine how these different definitions of smog index and spatial coverage would respond to emission changes. Halving and total eliminating the following sectors were tested: 1). Power stations; 2). All anthropogenic VOC; 3). All NOx; 4). All motor vehicles; and 5). All anthropogenic emissions.

We start with the individual index ($I_{max\text{-}hr\text{-}O3}$, $I_{max\text{-}hr\text{-}NO2}$, $I_{max\text{-}day\text{-}NO2}$, $I_{max\text{-}hr\text{-}FSP}$, $I_{max\text{-}day\text{-}FSP}$) values for each emission reduction scenario and normalized them by the corresponding base case values. These are plotted in Figure 4. Among the emission cut scenarios, that of NO_x elimination show the largest discrepancies between indices. Judging by the individual indices for ozone averaged over all stations, the ozone problem has worsened by almost 80% while the indices based on NO_2 show as much as 90% improvement in air quality and that for FSP show marginal (~5%) worsening. The NO_2 response to NO_x emission elimination seems to be largely linear to emissions considering the background NO_2 transported from outside of the study area. Since most mitigation scenarios will not achieve total elimination of a species, halving the emission would provide further insight. By halving NO_x, NO_2 has responded quite non-linearly by a mere 20% decrease (between 12 to 30%) while ozone has worsened by 16 to 38% and FSP has increased by 2-3%. Given all these, do we have better air quality if we reduce NO_x emission? For the scenarios with power station, motor vehicle and all emission reduction, FSP has also dropped as expected (very marginally for the case of power station emission), but the same behaviour of opposite trend and consequently the same question of overall change can be raised. For effective ozone mitigation, VOC reduction seems to be the only possibility and in fact the only way not to worsen any component of smog.

To understand how each of the consolidated indices can complement the individual indices, the consolidated index values are normalized and plotted as in Figure 4. Figure 5 shows the following features:

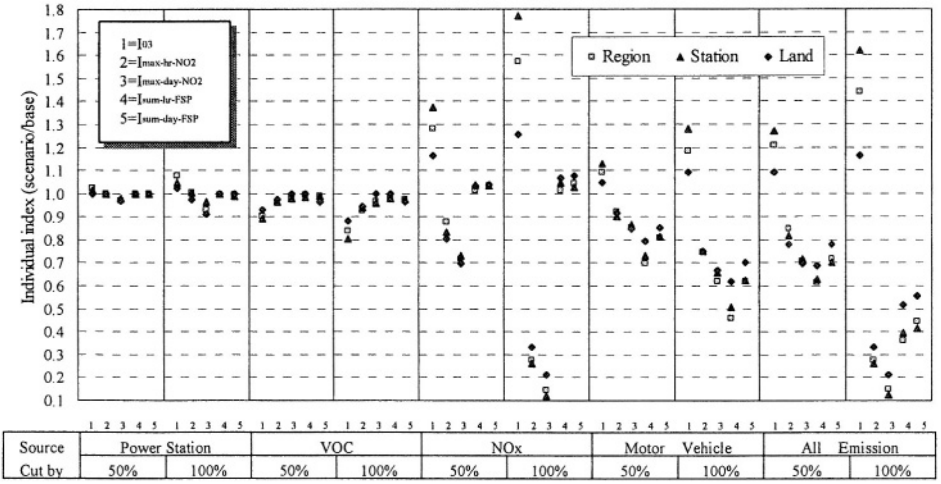

Figure 4. Individual Indices response to emission cut/ elimination scenarios relative to base case.

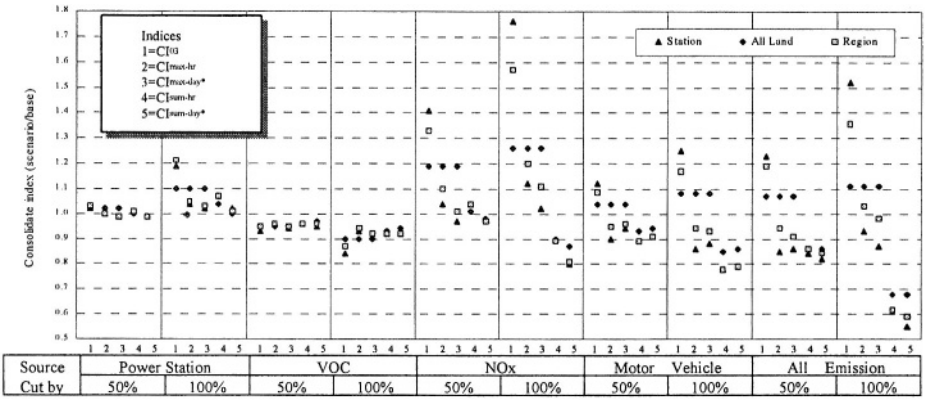

Figure 5. Consolidated Indices response to emissions cut/ elimination scenarios relative to base case.
*The ozone component index is still hourly.

1. From the point of view of where the indices fall with respect to the base case, the scenarios can be classified into three types:

   a). unequivocal improvement, i.e. all consolidated index values are below 1.0; within this category fall only the two VOC scenarios and the one scenario in which all anthropogenic emission in the study area are eliminated. Nevertheless, most of the indices in this group fall within the 0.9 to 1.0 range or very close to 0.9;

   b). unequivocal deterioration, i.e. all consolidated index values are at 1.0 or above; only the case of eliminating all power station emissions belong to this type; though this may be explained by the increase in ozone when the NO_x from power stations is eliminated, it is somewhat unexpected and merits further exploration;

   c.) mixed results, i.e. the consolidated index values are scattered about both sides of the 1.0 line; within this group are the rest of the scenarios though it may be argued that the first case is rather marginal.

2. If it is taken that the order of the arrangement of the consolidated indices represents a general progression from less to more comprehensiveness of our measurement method using indices (summing is more comprehensive than taking maximum than only looking at ozone; daily averaging more comprehensive than hourly averaging), then the slope that best fits the points within each scenario would carry a physical meaning (though a rigorous mathematical calculation of the slopes would not be very meaningful due to the difficulties in quantifying the comprehensiveness of each of the indices) and the scenarios would fall into two categories with:

   a). positive visual slopes indicating that as the measurement index is made more comprehensive, the smog situation is revealed to be worse; only the two VOC cut scenarios fit this category though it must be emphasized that both show net improvements relative to the base case;

   b). negative visual slopes which indicate the opposite of a.) above; all other scenarios would fall under this category and the more negative is the slope the greater is the spread of the index values; contrary to a) above, almost all scenarios show improvement as well as deterioration with respect to the base case depending on which index is used as the measure.

3. The large range of the spread of indices for some scenarios with mixed results (1c above) indicate that the choice of index, like the individual indices, can still give

diametrically opposite results for the same emission reduction / elimination scenarios. For the scenario with NO_x eliminated from the study area, CI_{O3} for stations indicate a 74% increase in smog while $CI_{sum\text{-}hr}$ and $CI_{sum\text{-}day}$ indicate up to a 20% decrease in smog, a 90+ percent difference. The same is true for the scenario when all anthropogenic emissions in the study area are eliminated: CI_{O3} increases by 45%; $CI_{sum\text{-}day}$ decreases by 47%.

4. The all-land values for the indices vary over the smallest range among the three spatial coverages and this is also true of the individual indices in Figure 4. This however does not preclude the observation in 3 above that diametrically opposite conclusions can even be drawn from index values averaged over such a large land area. Large spatial averaging of ozone is no substitute for considering all the components of smog.

5. The all-land values for CI_{O3}, $CI_{max\text{-}hr}$, $CI_{max\text{-}day}$ are identical for all the scenarios considered here indicating that for the day simulated, no amount of emission fiddling can change the fact that ozone dominates if all land area is considered. That does not mean that emission changes cannot bring about significant improvement over all the land area as seen in the large range of index values that exists between scenarios.

6. Relative to the individual indices, these consolidated index values span over a much smaller range with the smallest value for the case of total emission elimination being 0.57 versus the corresponding individual index value of 0.12.

5. SUMMARY AND DISCUSSIONS

The lessons gleaned from the above discussion show that a numerical model is a convenient tool to analyse the behaviour of the experimental indices. From these indices, it is clear that smog in an urban area must be viewed in total to avoid wrong conclusions based on an incomplete consideration. The best indices should be the ones based on a summation of all smog components though a rigorous scientific proof is not yet possible.

We have only used three components and combined them linearly here as a preliminary exploration. Other components and methods of combination can be tried. To more firmly utilize the concept of consolidated smog indices, health based air quality standards with consistent averaging time must be set and the synergistic effects of the components of smog must be explored through health study and built into the combination. Further explorations with other emission scenarios, smog episodes, boundary conditions and in other urban settings can be made to probe the behaviour of the indices further.

Disclaimers

The views expressed in this paper represent only that of the authors.

References

1. ERM-HK (2001) Territory-wide Air Quality Modelling System: Final Report, submitted to the Hong Kong Environmental Protection Department, 132pp.
2. Environmental Quality Standards in Japan – air quality; available on http://www.eic.or.jp/eanet/en/index.html
3. Proposed Air Quality standards for the U.S.; available on http://www.epa.gov/airlinks/airlinks4.html

DISCUSSION

F. LEFEBRE — You showed us that you go down in resolution by an order of three (40.5-13.5 ... 0.5). Can you comment on this ? On which basis did you make your choice ? Did you do sensitivity experiments ? What is most sensitive MM5, CTM, emissions ?

Ch. FUNG — The factor of 3 step down in grid spacing was recommended by the MM5 developer considering the stability of the numerics and the rapidity in getting to the area of interest. This ratio was then applied to SARM + EMS95. We did not do further sensitivity experiments.

G. GENIKHOVICH — When calculating your indices, you were assuming that the toxcitiy of different species at the level of two air quality standards (objectives, for example), is the same. Why do you think so ?

Ch. FUNG — This was based on the common sense assumption and also because we have worked on synergistic effects. We can build in further refinements if information is available.

A. EBEL — What is the accuracy of the NO_x (and other) emission and observational data used for the study ?

Ch. FUNG — We have a fairly good estimate of emissions within the Hong Kong domain, but the further we go away from Hong Kong, the greater the uncertainty. A recent study over the Pearl River Delta which is the region immediately to the north of Hong Kong suggests a factor of 2 difference in the NO_x and VOC estimates. Further out in China/Asia, a preliminary comparison indicates that our estimates based on GEIA/EDGAR differ from that of the Trace-P (David Street, Argonne National Lab.) database by a factor of 2-6 depending on the species. Our first task in model improvement is to narrow down the uncertainties in the emissions. The other observational data, e.g. monitoring, that we use meet international standard.

This page intentionally left blank

AN APPLICATION OF A PHOTOCHEMICAL MODEL FOR URBAN AIRSHED IN ISTANBUL

Umit Anteplioğlu , Sema Topcu, and Selahattin Incecik*

1. INTRODUCTION

Ozone occurs both in the Earth's upper atmosphere and at ground level. Stratospheric ozone shields us from the sun's harmful UV rays. But ground - level ozone is a harmful air pollutant. Surface ozone is formed when NOx emitted by cars, power plants and other industrial sources react chemically in the presence of intense sunlight. High smog levels have been linked to increases in the severity of asthma attacks and other respiratory health problems. When concentrations rise, even from relatively low levels the need for increased medication of asthmatic for especially children and elderly. Otherwise ozone can initiate damage to the lungs as well as damage to trees, crops and materials.

In urban areas of Turkey, there has been a decrease in concentrations of SO_2 and particulates in the 1990s. This is largely due to major changes in the fuel mix used in city centers: domestic coal with high sulfur content has been prohibited for heating and replaced by imported coal. However, as a result of economic growth and despite environmental protection efforts and significant shifts in energy supply emissions of NOx are growing at a very high rate. The transportation by car is growing rapidly in the cities.

According to OECD Report (1999) NOx emissions totaled 844,000 tons in 1997 figures, almost two and half times those recorded in 1980s in Turkey. NOx emissions increases have accelerated since the early 1990s. Mobile sources contribute 43 per cent to total emissions, industrial energy use 19 per cent and power generation 10 per cent. Emissions per capita (13.3 kg) are three times less than the OECD average (39.7 kg). Total NOx emissions have continued to increase. However we do not have emission inventory at national and city level for a range of pollutants, including NOx and VOCs.

Istanbul has experienced a rapid growth in urbanization, industrialization and the number of motor vehicles. The city experienced serious SO_2 and TSP air pollution episodes in between 1980-1995 with economical expanding. Following the banning of poor quality coal burning for domestic and industrial activities in the city, air pollution

* Umit Antepliogu, Division of Meteorology, Kandilli Observatory, Bosphorus University, Kandili Uskudar,Istanbul Turkey, Sema Topcu and Selahattin Incecik, Istanbul Technical University, Department of Meteorology, Maslak Istanbul Turkey 80626.

Air Pollution Modeling and Its Application XV, Edited by
Borrego and Schayes, Kluwer Academic/Plenum Publishers, New York, 2002

levels were reduced to below the national air quality standards. Fuel switching to the natural gas and low sulfur coal usage has been taken a role on this variation in the city. In addition, the number of motor vehicles increased at a very fast rate in the city. As a consequence air quality problems in Istanbul has shifted from conventional air pollution to secondary air pollution in last five years. The history of photochemical air pollution in Istanbul is not long.

In contrast to the increased international concern over ozone, only a very limited analysis of the characteristics of urban ground-level ozone has been conducted in Turkey (Topcu and Incecik, 1999; 2001). In spite of the critical ozone levels have not been yet measured in the city, ozone potential problem is growing with the rapid growing motor vehicles in the city. Although, there has not been yet occurred critical levels, ozone potential problem is growing with the rapid development of transportation in Istanbul.

The goal of this study is to apply and assess the temporal and spatial distribution of photochemical air pollution in Istanbul. The results based on the discussion of July 1999 simulations have been explained by UAM.

2.GENERAL CHARACTERISTICS OF THE ENVIRONMENT IN ISTANBUL

2.1 Population and Climate

Istanbul is located at about 41N and 29E. The city is divided by the Bosphorus as the European and Asian parts. The population of Istanbul currently stands at about 9.2 million and is concentrated along the west and east part of the city.

The climate of Istanbul is governed by the Black Sea and Mediterranean climates. Winter (November to March) is cold and wet. Summer (June to September) is hot and humid. Insolation in the city is strong; average daily values are of order of $21 MJ/m^2$ in summer. In addition, annual average wind speeds in the city are only 3.0 m/s, 8 % calm hours. Prevailing synoptic winds arriving Istanbul are from the north and northeast and southeast in winter, northeast and southeast during the summer months. Daily mean temperature in winter is 6.3°C, and 22.4°C in summer. Average daily values of order of $6400\ W/m^2$ in summer and $1200\ W/m^2$ in winter (Topcu et al, 1995).

2.2 Data and Region

Istanbul has gradually experiencing the highest vehicle densities since 1995. According to the July 1999 figures, a total activity of the vehicles in Istanbul is estimated as an average of 51.3 million km per day for weekdays (Antepliogˇlu, 2000). Vehicle emissions account for a significant fraction of the CO emission. There are about 1.5 million motor vehicles in the city. It is estimated that around 1/3 of the vehicles are in the traffic in a day. There is about 10,000 taxis in the city, driven on the average 100,000 km/year. Besides LPG has been traditionally used since the beginning of 1998 in the taxis. Most of the taxis and some of the cars are running on LPG. Furthermore natural gas usage has been started gradually for domestic purposes in late 1993 in the city from Anatolian side of the city.

Ozone is measured using an analyzer $O_3 41M$ of Environment S.A. based on absorption of UV radiation. The NO_x analyzer is AC31M of Environment S.A. The

measurement system is based on the chemiluminescense effect produced by the oxidation of NO by O_3 molecules. NO_2 is measured by converting it into NO using the

thermal conversion method (GIM, 2000). Furthermore, the hourly data of solar radiation, temperature, wind speed and direction and atmospheric pressure data taken from Goztepe meteorological station.

In Istanbul, the Environmental Protection Section of Greater Istanbul Municipality has monitored ambient ozone levels since February 1998. There are two monitoring stations are located in densely populated urban areas for Asian and European sides respectively. In the year of 2000, the measurements have not been completed for some technical problems. Incecik and Topcu, (1999; 2001) presented the preliminary results on the seasonal variations of ozone and NOx.

To identify which meteorological parameters are strongly associated with the fluctuations of daily maximum ozone concentrations and to perceive the temporal variation patterns of ozone concentrations. We have used a limited period for both explaining and understanding of the ozone formation mechanism and to make simulations both wind field and ozone variation over Istanbul. The available hourly ozone and its precursors data from the months with the potential of the highest photochemical activity, July 1999 case has been selected for simulations by Urban Airshed Model.

3. OVERVIEW OF THE DIURNAL VARIATIONS

The shape of the diurnal pattern in hourly ozone concentrations provides clues as to the formation, scavenging and transport of ozone at a site. As expected that the ozone probably of local origin showed a typical diurnal variation. Besides during daytime ozone concentrations starts increasing gradually after sunrise, attains maximum value during mid-afternoon hours and then decreases. Concentrations in daytime were typically three times as large as it's at nighttime. At nighttime, surface ozone is partly removed by the reaction with nitric oxide and deposition. Due to the complex mechanism of the emissions in urban areas, urban ozone formation has been concerned. Because the ozone data measured during the period of highest NOx including traffic rush hours are somewhat depressed. Ghim et al., (2001) explained the high ozone episodes over Seoul area. Riveros et al.,(1998) made an analysis to estimate the relative contribution of NO_2 and HCs to ozone formation which is the most important air pollutant in Mexico city.

Since no ozone is produced in the absence of sunlight ozone concentrations began to decrease after sunset, reaching minimum in evening after sunset. Due to there is no photo oxidation of precursors, ozone levels are observed to be low during nighttime. As it is expected that the daytime increase in ozone concentration is basically due to photo oxidation of the precursor gases. On the other hand, strong photochemical production and strong convection in the mid-afternoon period caused ozone concentrations to reach peak levels in the late afternoon. The hourly measurements of ozone concentration in the urban area started in the beginning of 1998 in two sites of the city center. Ozone concentrations are greatly influenced by local meteorological and synoptic scale meteorological conditions. A brief overview is given on the maximum concentrations by Topcu and Incecik,(1999). The ozone and NOx data set obtained for 1998-1999 was also discussed by Topcu and Incecik (2001). Maximum ozone concentration at the surface is one of the most desired air pollution indicators. The ozone and NOx concentrations exhibited seasonal variations. NOx concentrations

reached their highest levels in the winter months with typical values from 76 to 194 ug/m3 in both 1998 and 1999 years. The station located in Istanbul Anatolian site experiences concentration > 70 μg/m3 from April to July. Additionally, from the database, exceedences have been determined for thresholds of 70ug/m3. It is found 14 exceedences of 70ug/m3 in total 16 months. Its about 71% of the total exceedences in 1999. According to 60 μg/m3 exceedences (n=40) in total period, the ratio is about 58% in 1999 (Topcu and Incecik, 2001)

As a summary, surface ozone in urban area is generated by reactions of NOx and VOCs in the present of sunlight. It is generated from photolysis of nitrogen oxides in the presence of NMHC and other organics, and is mainly associated with car emissions in urban areas. This production mechanism can be easily understood with the diurnal variation of ozone in urban atmosphere of Istanbul.

4. URBAN AIRSHED MODEL

To make a policy decisions concerning emission controls for urban areas, photochemical models have been used. In this study, we used model simulations of UAM-V which is a three-dimensional photochemical grid model (Anteplioglu, 2001). UAM-V model had never been used before in this area. It was the first time the model was used in this city in connection with ozone studies. This model simulates the physical and chemical processes that affect the concentration of atmospheric pollutants. The UAM-V solves conservation equation for each of approximately 30 chemical species. This equation includes terms representing; advective transport, horizontal and vertical diffusion, emissions, chemical reactions and deposition (SAI, 1996). UAM-V generates three-dimensional gridded fields of each simulated chemical species as hourly output.

In order to better understand the impact of the winds on the surface ozone concentrations, it is necessary to determine the region's airflow, such as sea-breeze circulations. In this study, simulations with the Urban Airshed Model were performed. An application of UAM-V including meteorology, chemistry and emissions based on real ambient conditions is used. However, simulations with the UAM were performed using limited data set in Istanbul. Data from surface meteorological stations and upper air station were obtained from Turkish State Meteorological Service. To compare the wind fields, UAM runs were made. Figures 1 and 2 explain the model simulations on July 11, 1999 for 13:00 and 17:00 LST (Anteplioglu, 2000). The dominant winds in July which is a typical summer month, are northeasterly. The weak local sea-breeze circulations can clearly be seen following the heating hours over Istanbul (Fig. 1). These kind of circulations are disappearing at the late afternoon hours (Fig. 2). The region experiences differential heating and cooling due to the topographical conditions.

4.1. Mobile Emissions

To obtain the realistic emissions in the city it is necessary to know the actual traffic patterns for weekdays and weekend in July 1999. On-road mobile emissions were estimated by using emission factors. Traffic volume, speed and temporal distribution were used for emission inventory modeling. Table 1 gives the estimated total mobile emissions for July 10, 1999. These inventories were used to produce UAM simulations to study the effects of the factors on emissions and the effects of the different emissions on precursor and ozone concentrations.

Table 1. Estimated daily total mobile emissions for July 10, 1999 (tons/day)

NO_X	VOC	CO	SO_X	TSP
31.1	24.1	184.9	6.5	4.4

5. THE RESULTS AND DISCUSSION

Temporal and Spatial variation of surface ozone concentrations predicted by UAM-V are shown in Figs.3 and 4. Higher concentrations of ozone are observed near the southwest coasts of Istanbul. Surface ozone concentrations for 13:00 LST and 17:00 on July 1999 indicate the ozone cumulating at the southwest of the city. However, higher concentrations are usually observed during intense solar radiation times and moved to inland areas following the sea breeze penetration. This result supports the effect of local sea-breeze circulation over the area.

Table 2. Statistical summary of predicted and observed ozone concentrations for Asian side of Istanbul

Days	RMSE (ppb)	σ_{pred} / σ_{obs}	r_{pred} / r_{obs}
10	2.4	0.93	0.93
11	3.6	1.02	0.89
12	3.1	1.17	0.90

Table 2 compares the results of RMSE and the ratios of sigma values of predicted and observed concentrations.

In this study simulated daily patterns by considering weekdays and weekends for July 1999 showed reasonable distribution. The findings support the Wakamatsu et al. (1996;1999)'s results. Wakamatsu (1999) investigated a relationship between emission intensity of NOx, NMHC and O3 concentration covering Tokyo and surrounding areas by using UAM.

As a summary, ozone is formed through non-linear interactions between chemical reactions and atmospheric variables. The resulting increased photochemical precursors have forced environmental policy makers to recognize the potential urban ozone problem. For this purpose we presented the urban ozone levels and hourly simulations by using a three-dimensional Eulerian photochemical simulation model results in the city.

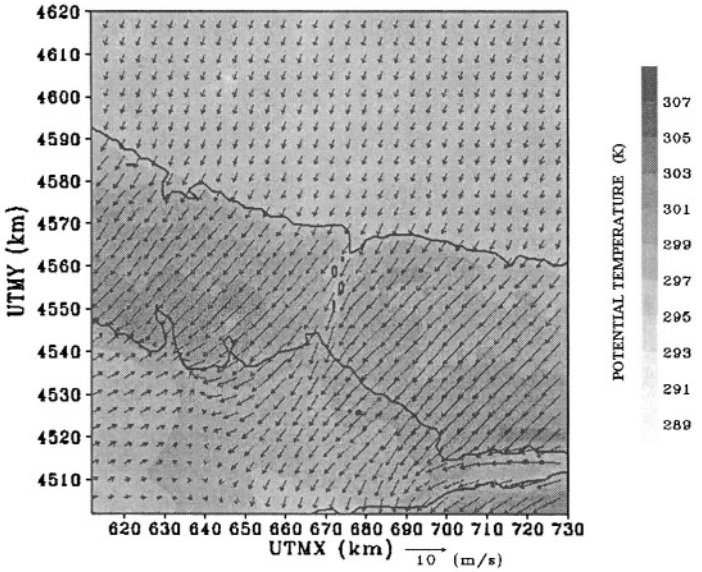

Figure 1 . Wind and potential temperature fields at surface for 13:00 LST on July 11, 1999.

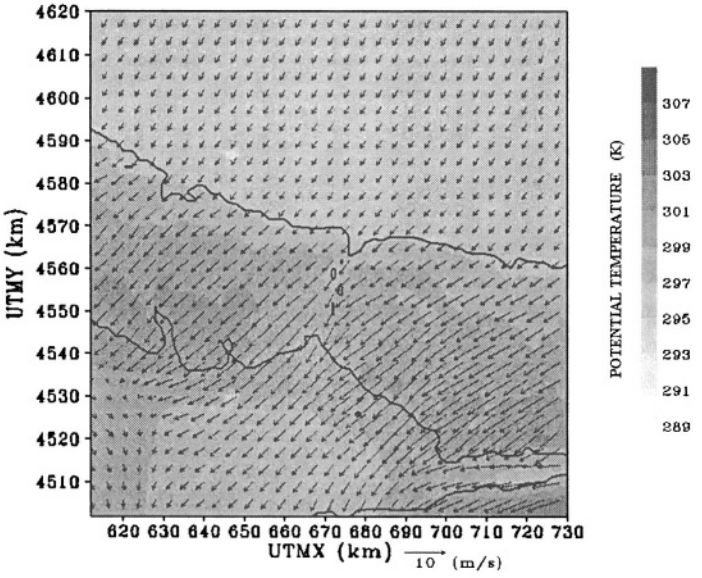

Figure 2. Wind and potential temperature fields at surface for 17:00 LST on July 11, 1999.

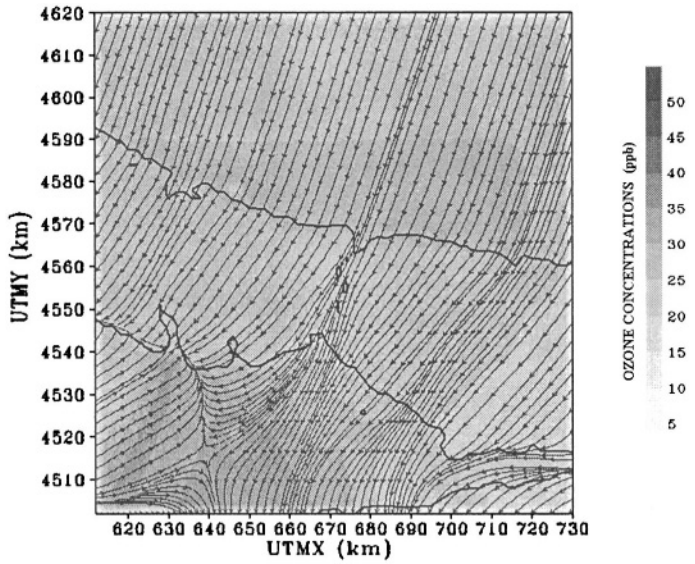

Figure 3. Calculated surface ozone concentration and streamlines for 13:00 LST on July 11, 1999.

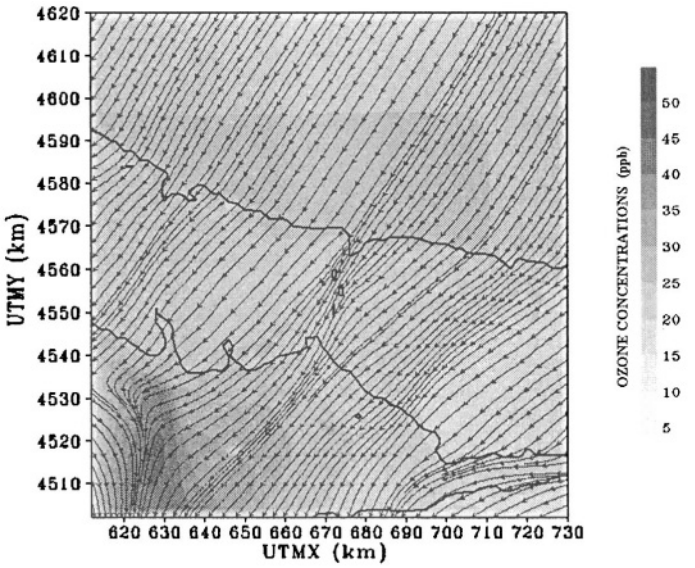

Figure 4. Calculated surface ozone concentration and streamlines for 17:00 LST on July 11, 1999.

5. REFERENCES

Anteplioglu, U., 2000, Istanbul Bolgesinde yüzey ozonun fotokimyasal-dinamik bir modelle incelenmesi (in Turkish), PhD. Thesis, Istanbul Technical University, 147.

Ghim.Y.S., Oh, H.S., Chang, Y.S., 2001, Meteorologically effects on the evalution of high ozone episodes in the Greater Seoul area, *J.Air &Waste Manage. Assoc.* 51,185-202.

GIM , 2000, Greater Istanbul Municipality data archive.

OECD Report, 1999 Turkey,Environmental Peformance Reviews, 186.

Riveros H.G., Arriaga, J.L., Tejede, J., Julian-Sanchez.A., Riveros-Rosas, H., 1998, Ozone and its precursors in the atmosphere of Mexico City. *J.Air &Waste Manage. Assoc.* 48,866-871

SAI, 1996

Topcu, S,Dilmac, S, Aslan Z., 1995, Study of hourly solar radiation data in Istanbul, *Renewable Energy,* 6,171-174.

Topcu, S., Incecik, S., 1999, Istanbul'da sehir ozone seviyelerine ait ilk olcumlerin degerlendirilmesi (in Turkish), National Symposium on Air Pollution and Control, Izmir,279-285.

Topcu, S., Incecik, S., 2001, Surface ozone measurement and meteorological influences in the urban atmosphere of Istanbul, *Int J.of Environment and Pollution (submitted)*

Wakamatsu. S., Ohara, T., Uno, I., 1996, Recent trends in precursor concentrations and oxidant distribution in the Tokyo and Osaka areas. *Atmospheric Environment,* 30, 715-721

Wakamatsu S., Itsushi, U., Toshimasa, O., Kenneth, L.S.,1999, A study of the relationship between photochemical ozone and its precursor emissions of nitrogen oxides and hydrocarbons in Tokyo and surrounding areas. Atmospheric Environment, 33,3097-3108

DISCUSSION

P. BUILTJES Did you make an estimate of the inflow of ozone into the Istanbul area versus the production of ozone by Istanbul emissions ?

S. INCECIK We did not apply a model yet for the inflow of ozone. However we estimate the inflow of ozone from the south parts of the city and south east part of the surrounding areas (Gebre and Kocacli industrial area).

This page intentionally left blank

ONE-WAY NESTING VERSUS TWO-WAY NESTING: DOES IT REALLY MAKE A DIFFERENCE?

Cecilia Soriano, Oriol Jorba and José M. Baldasano*

1. INTRODUCTION

A couple of ITMs ago, an interesting discussion took place in the conference room of the meeting concerning the necessity or not of using one-way or two-way nesting techniques when performing simulations over complex terrain. The contribution leading to that discussion (Soriano et al., 1998) had shown results of a simulation carried out in the Barcelona Geographical Area (BGA) for a typical summertime situation in the region. Simulations had been performed with the model MEMO, and one-way nesting techniques where used (actually, in was more a refined-boundary conditions technique), using three domains at 2, 1 and 0.5 km grid size. The comparison of the measurements with the modeled results for the different resolutions used showed that no significant improvement of the results was produced by using nested domains, from which the authors concluded that the topography resolution used in the outer domain was enough to originate the circulatory patterns in the area.

To improve our knowledge on this important factor in a numerical weather prediction (NWP) model configuration, a simple exercise is proposed in this contribution in order to check if the use of two-way versus one-way nesting techniques does after all produce an improvement of the performance of a mesoscale meteorological model. Comparisons will be shown between simulations conducted with both nesting options for the BGA, a region containing a sea-land interface and complex topography.

The model used for this purpose is MM5 (Dudhia, 1993; Zhang, 1986) one of the few existent mesoscale meteorological models that allows running either with one or two-way nesting. This fact is important since it assures that the Physics of the model will be the same in the two runs. A similar exercise was carried out in Lozej and Bornstein, (1998). On that occasion the simulation was carried out for the San Francisco Bay Area during a winter wave cyclone situation that led to important precipitation in the region. In fact, the authors found weak results in the predicted amount of rainfall for all the nesting cases, which they blamed on the poor quality of the initial condition used.

Besides, in this occasion, in order to check if the influence of choosing one or the other nesting option is more important depending on the meteorological situation, simulation have been performed under two different meteorological situations.

*Laboratory of Environmental Modeling. Department of Engineering Projects, Universitat Politècnica de Catalunya (UPC). Av. Diagonal 647, 08028 Barcelona, SPAIN, baldasano@pe.upc.es.

Air Pollution Modeling and Its Application XV, Edited by
Borrego and Schayes, Kluwer Academic/Plenum Publishers, New York, 2002

2. NESTING TECHNIQUES FOR MESOSCALE MODELING

It is well known the importance of the orographic features in a given region in the establishment of the circulatory patterns of air masses in general and air pollution in particular within its airshed. For a mesoscale model to be capable of reproducing this behavior, it is necessary to introduce a well resolved terrain file, with a resolution such that these orographic features are not smoothed away. The other fact is that the simulation domain has to be large enough to include all the terrain characteristics that are believed to participate in the circulation of air masses, and these can often be far away from the study area. Both conditions would lead to the ideal situation of simulating over a large domain with a very high resolution. However, computational and practical constrains do not allow this approach to be used, since it would require simulation over a large number of cells at small time steps (due to small cell size), and therefore large simulation times and memory requirements.

Nesting techniques are the solution to minimize these problems, increasing spatial resolution only in the domains where small scale phenomena might occur and are relevant for the reproduction of all the forcing mechanisms in the studied area. At the same time, outer domain (or domains) are also included at a coarser resolution, to assure the introduction of larger scale forcings into the inner domain. The interaction between the domains is the big issue at this point, and can be carried out basically through to different techniques: one-way or two-way nesting.

MM5V3 allows the choice of any of these two different types of interaction between the coarser and the inner domains. In the one-way nesting, the model is first run for the outer domain to create an output that is interpolated in time and space to supply the nest as a boundary file, which is run after the coarser domain has finished. For a two-way nesting, both domains are run at the same time and completely interacting. Nest's input from the coarse domain is introduced through its boundary, while feedback to the coarse mesh occurs all over the nest interior, as its values are replaced by combination of fine domain values.

In general, two-way nesting is believed to work better because it allows smaller scale features feedback upscale and influence features in the larger scale. However, detractors of two-way nesting claim that this method somehow "pollutes" results obtained in the outer domain, since they are not longer the solutions of the equations of the system.

3. MODELING SCENARIOS

Two different scenarios have been studied in the BGA in order to see if the chosen nesting option in the model was a more determinant factor under some meteorological situation than under others.

In one of the studied cases, the synoptic situation was predominant, and a synoptic forcing was introduced through important geostrophic winds in the region. In the other case, a meteorological situation with weak synoptic forcing was chosen, so that mesoscale phenomena, induced by the particular topography of the region, would be dominant.

3.1. Modeling Domains

Both runs have been performed over the same simulation domains. Four nested domains were selected, which essentially covered Europe (Domain 1, D1), the Iberian Peninsula (Domain 2, D2), Catalonia (Domain 3, D3) and the BGA (Domain 4, D4). D1 has 90x55 54-km cells. D2 has 115x94 18-km cells. D3 has 76x79 6-km cells. D4 has 61x61 2-km cells. The vertical resolution consisted for all domains of 23 σ-layers, with the lowest one situated at 18-m AGL. The upper boundary was fixed at 100 hPa. Time steps used for the simulations are, respectively, 150, 50,15 and 6 seconds. Initialization and boundary conditions (BC) for the regional model are introduced from reanalysis data from the ECMWF global model. Data were available at a 1-degree resolution (100-km approx. at the working latitude) at the standard pressure levels every 6 hours.

Figure 1 shows the domains and the topography of D3 and D4. The topography in D3 is essentially dominated by the Pyrenees (a mountain range separating Spain and France with mountains of 3000-m height). In the south of the domain, the Ebro Valley will also play an important role in the establishment of the flow patterns. In D4, main features are mountain ranges oriented parallel to the coastline and two river valleys at both sides of the city of Barcelona and running approximately perpendicular to the coast.

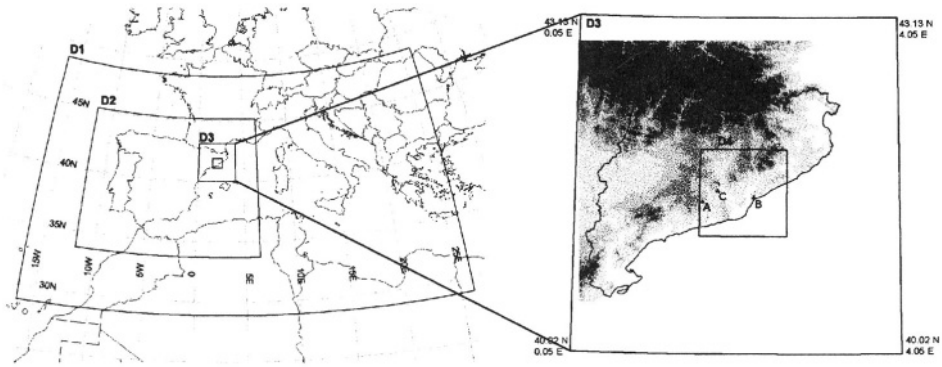

Figure 1. The four simulations domains used in the simulations, and detailed topography of D3 and D4. Letters A,B,C designate surface stations used for validation in sections 4 and 5.

Finally, simulations only for D4, including initial and boundary information from ECMWF, have also been performed. They have been used as control cases to see how well the most inner domain was able to reproduce the circulatory patterns and how different it was from the simulation where information from outer domains is introduced.

3.2. Synoptic Situation: The Western Anticyclonic Advection of May 29, 2000 and the Summertime Barometric Swamp of August 14, 2000

The synoptic situation on May 29, 2000 can be described, using the typical situations described for the Iberian Peninsula as a western anticyclonic advection. A high-pressure area was located over the Atlantic, to the west of the Portugal, advecting westerly winds over most of the Peninsula. The map at 500 hPa also indicated winds from the west (see maps at http://infomet.am.ub.es/arxiu/avn, April 2001). Radiosondes launched in

Barcelona that day confirm the interpretation of the maps (At the web site of the Catalan Meteorological Service, http://www.gencat.es/servmet/radio, April 2001).

Maps corresponding to the 14th of August, 2000 were characterized, both at surface level and in height, by very low baric gradient. This fact, and the strong solar heating, produced the development of mesoscale phenomena. These phenomena in the region are mainly sea-breezes, up-slope and down-slope winds and valley channeled winds. The heating was so intense that a thermal low started to develop in the Peninsula. Again, synoptic maps for the day are available at the Infomet web site mentioned above.

4. THE SYNOPTICALLY-DOMINATED SITUATION OF MAY 29, 2000

4.1. Control Case: 1 Domain Simulation

Figure 2 shows streamlines simulated by the model at 12 UTC on May 29, 2000 in D4. Comparisons with surface stations are also included. No nesting was performed, and data from the ECMWF was used for initialization and middle times BC.

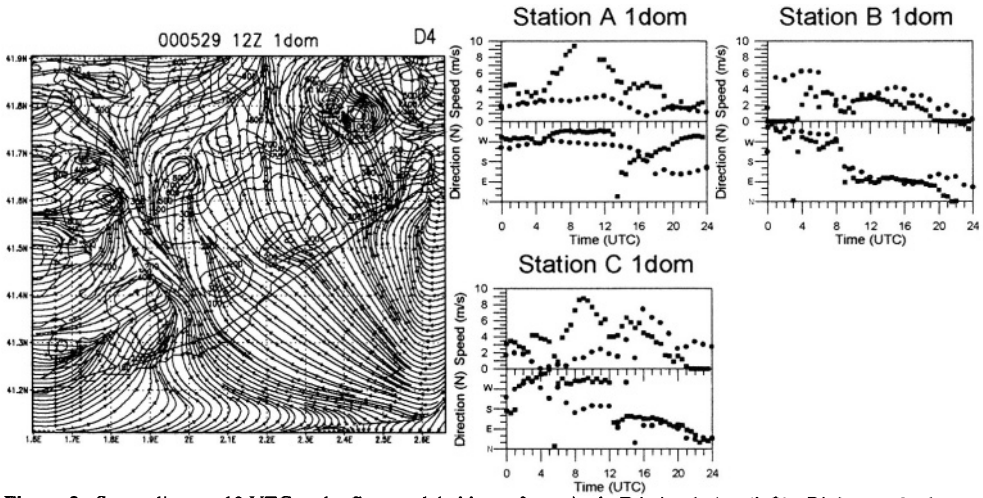

Figure 2. *Streamlines at 12 UTC at the first modeled layer for a single D4 simulation (left). Right panels show comparison of simulated wind speed and direction (circles) vs. measurements (squares). Date is May 29, 2000.*

Results showed that, even when working with a single domain, the topography in D4 had enough resolution to generate the local winds that overwhelmed the synoptic westerly winds, which can only be observed in the left border of the domain.

As far as the comparison with measurements of surface station, note the model's weak performance at station A, where it failed to reproduce the observed high velocity winds, although westerly winds are modeled during most of the day (introduced trough the BC). This station (see Figure1) is located very close to the border of the domain. The model reproduced quite well wind speed and direction at station B, located by the seaside, showing the influence of the sea breeze. Station C showed poor results specially before midday, where the models simulated too low winds. Velocities in the afternoon were more similar to measurements and the agreement in wind directions also improved.

4.2. Nested Simulations

Figure 3 shows streamlines simulated by the model at 12 UTC on May 29, 2000. The different panels show the results over D3 and D4 and when performing one-way or two-way nesting. Note that differences when comparing simulations on D3 with simulation on D4 occur mainly over the region where both domains overlap. The sea-breeze front, identifiable in the one-way simulation by a convergence line, is broken in the two-way simulation. In D4, the sea-breeze front is also very evident and has almost reached the left border of the domain, penetrating further inland when performing one-way nesting.

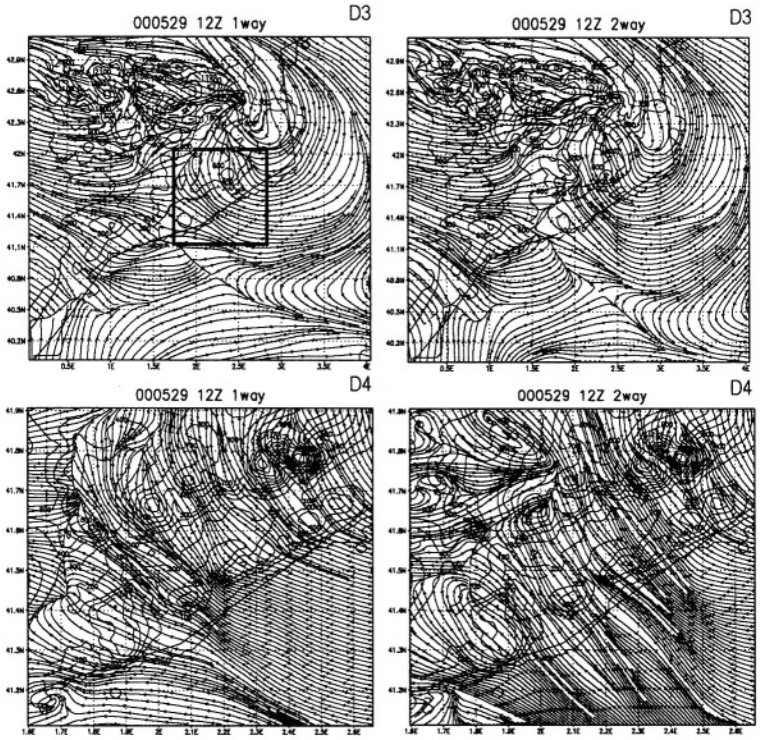

Figure 3. Streamlines at 12 UTC of May 29, 2001, at the first modeled layer for D3 one-way (top-left, with D4 indicated with a square), D3 two-way (top-right), D4 one-way (bottom-left) and D4 two-way (bottom-right).

Evaluation of the model performance for the two cases was carried out by comparison with measurements for the three stations shown in Figure 1 and is included in Figure 4. Comparisons were performed by representing values of measured wind speed and direction with the simulated value in the corresponding cell, both for domains D3 and D4. Nested simulations, when compared with the one-domain simulation shown in Figure 2, were able to generate higher wind speeds in all stations, more in agreement with measurements. However, speeds in station B, located by the sea and with a higher mesoscale influence, showed worst results when using nesting techniques. A slight improvement of the wind direction was also observed, specially in station C during nighttime, for the one-way simulation. Finally, when comparing results for the same nesting techniques at the different resolutions (D3 and D4), more differences between both resolution were present when using two-way nesting techniques.

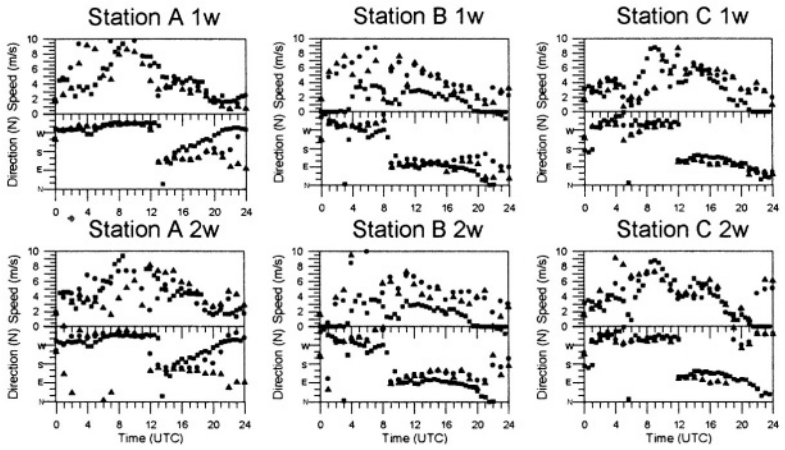

Figure 4. Evaluation of measurements of wind speed and direction at three surface stations (squares) with simulated values in domain D3 (circles) and D4 (triangles). First row corresponds to one-way nesting simulation and second row correspond to two-way nesting simulation. Date is May 29, 2000.

5. THE MESOCALE-DOMINATED SITUATION OF AUGUST 14, 2000

5.1. Control Case: 1 Domain Simulation

Figure 5 shows evaluation and streamlines at 12 UTC for the mesoscale-dominated situation of August 14, 2000 in D4, for the one-domain no-nested simulation.

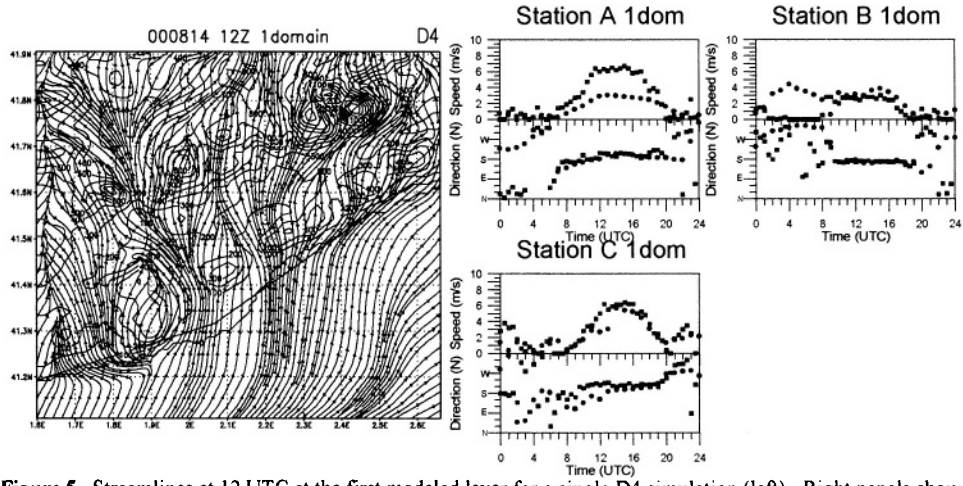

Figure 5. Streamlines at 12 UTC at the first modeled layer for a single D4 simulation (left). Right panels show comparison of simulated wind speed and direction (circles) vs. measurements (squares). August 14, 2000.

Streamlines show a well developed inland sea-breeze flow, which, with the up-valley winds and the up-slope winds produced a general in-shore circulation. Channeling in the river valleys was evident. Note the westerly winds at the left border of the domain, result of the assimilation, in the first rows of cells, of the BC from ECMWF data. Comparison with measurements gave reasonable results, showing that the single-domain configuration was able to generate flows, mainly originated in this scenario by mesoscale phenomena.

5.2. Nested Simulations

Figure 6 shows streamlines simulated by the model at 12 UTC on August 14, 2000. The different panels show the results over D3 and D4 and when performing one-way or two-way nesting. Differences between both simulations were more evident in this case. Note the presence of differences between simulated fields above the sea. If differences are observed over the sea, they should have been originated by larger scale phenomena funneled down to the inner domains. Above the sea, increased resolution does not add further topographical information and therefore no additional forcings are fed back to the coarser domain. As in the previous case, most differences above land were observed on the region where D3 and D4 overlap (overlapping region shown in top-left panel).

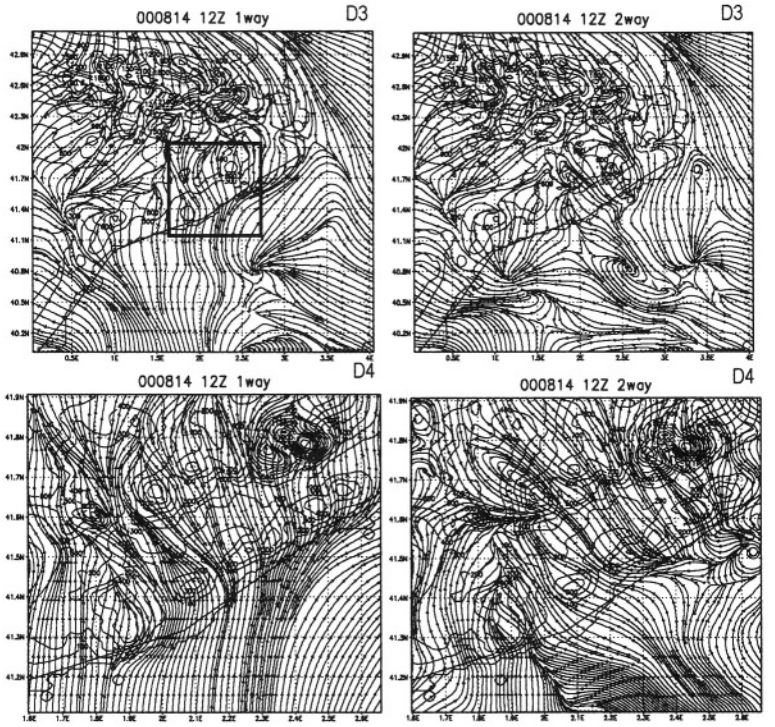

Figure 6. Streamlines at 12 UTC of August 14, 2001, at the first modeled layer for D3 one-way (top-left), D3 two-way (top-right), D4 one-way (bottom-left) and D4 two-way (bottom-right).

Comparison with surface stations are shown in Figure 7. The performance of the model was better than for the synoptically-dominated case, specially for one-way nesting. The model reproduced the daily cycle of the wind, and the timing of the swift from the nighttime to the daytime regime was well captured. Winds during nighttime were very low, which made the prediction of the wind direction difficult. In the one-way simulation, little difference is observed when using a better resolved resolution. Results for D3 and D4 are quite similar. For the two-way simulation, comparisons gave worse results. For station B, located by the sea, this was probably due to differences observed in the simulated fields over the sea when using two-way techniques. Simulated results for station C showed a lot of fluctuation when using two-way nesting, specially on D4.

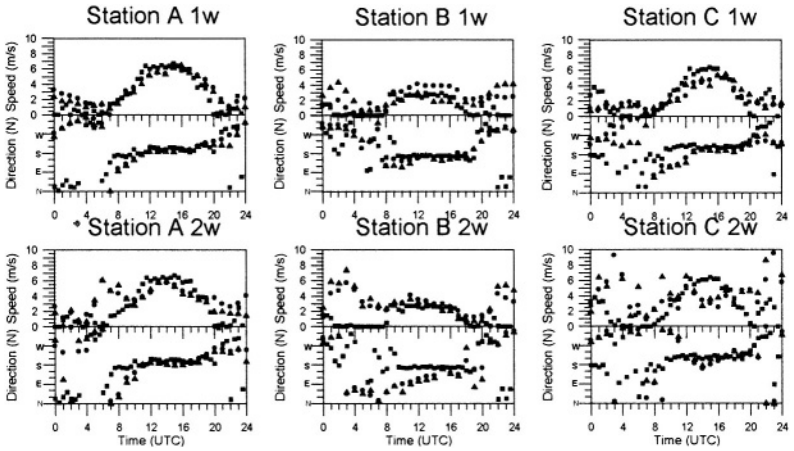

Figure 7. Evaluation with measurements of wind speed and direction at three surface stations (squares) with simulated values in domain D3 (circles) and D4 (triangles). First row corresponds to one-way nesting simulation and second row correspond to two-way nesting simulation. Date is August 14, 2000.

6. CONCLUSIONS

Simulations performed using different nesting techniques have shown that this factor can led to rather different results when applied over a domain with complex orographic features. This differences were more evident on situations under low synoptic forcing. For the mesoscale-dominated case, differences obtained by choosing one or another nesting technique were more important than those produced by using a higher resolution topography, and two-way nesting gave worst results. For the synoptically-dominated case, the two nesting techniques gave more similar results and differences occurred mainly on the overlapping region of the domains. Predicted values at the different resolutions are not as similar as in the other scenario and in general gave higher speeds than observed, indicating that the synoptic component was overestimated by the model.

7. ACKNOWLEDGEMENTS

Authors thank the Spanish Meteorological Institute (INM) for providing ECMWF data and the Catalan Meteorological Service (SMC) for the surface station data. Simulations were run on an HP Exemplar V2500 from CESCA. This work was developed under projects IMMPACTE and CICYT REN2000-1754-C02-01/CLI.

8. REFERENCES

Dudhia, J., 1993, A non-hydrostatic version of the Penn State-NCAR mesoscale model: Validation tests and simulation of an Atlantic cyclone and cold front, *Mon. Wea.. Re*., 121, pp. 1493-1513.

Lozej, C. and Bornstein, R.D., 1999, Comparison of nesting techniques within a meteorological model, in: *Air Pollution VII*, Brebbia, C. A., Jacobsen, M. and Power, H. ,eds., Comp. Mechanics Pub., pp. 1009-1021.

Soriano, C., Baldasano, J.M. and Buttler, W.T. , 1997, On the application of meteorological models and lidar techniques for air quality studies at a regional scale, in: *Air Pollution Modeling and its Application XII*, Gryning, S-E. and Chaumeliac, N., eds., Plenum Press, pp. 591-600.

Zhang, D.-L., H.-R. Chang, N.L. Seaman, T.T. Warner and J.M. Fritsch, 1986, A two-way interactive nesting procedure with variable terrain resolution. *Mon. Wea. Rev.,* 114, 1330-1339

DISCUSSION

G. SCHAYES How can you explain that such a large difference occurs on vertical wind speed in the centre of the domain using 1-way or 2-way nesting ?

J. BALDASANO The centre of domain 3 corresponds with the upper-left corner of domain 4. Instabilities are introduced by the interaction of both domains. In this case, the feedback to the coarser mesh makes the results worse. The lateral boundary placement seems to be an important fact that highly influence the behaviour working with 2-way nesting.

This page intentionally left blank

GLOBAL AND LONG-RANGE TRANSPORT

Chairperson : G. Schayes

Rapporteur : A. Voudouri

This page intentionally left blank

APPLYING RISK ASSESSMENT TECHNIQUES TO AIR POLLUTION MODELLING & ABATEMENT STRATEGIES

Helen M ApSimon, Rachel F Warren and Antonio Mediavilla-Sahagun[1]

1. INTRODUCTION

Atmospheric modelling is widely used to support decision making on environmental matters and pollution abatement. The models used in a regulatory context are often relatively simple, as compared with a range of other more complex models that reflect atmospheric processes in more detail. Model inter-comparisons, validation against measurement, and conventional uncertainty analysis such as sensitivity studies and Monte Carlo analysis, are often used for "quality assurance" of models.

However from the point of view of a decision maker using results obtained from a model, such analysis can cause confusion, and lead to difficulties in justifying or agreeing actions to protect the environment. He/she recognises that the application of models inevitably involves assumptions, simplification and uncertainties, but in regulatory contexts models are often used rather precisely- for example to indicate whether or not a prescribed limit or ceiling is exceeded. The reliability of model estimates, and the robustness of conclusions based on model calculations, are therefore important issues. This paper is therefore written from the point of view of the model user, and suggests a framework for exploring model uncertainty based on risk assessment techniques, and in particular HAZard and OPerability studies (HAZOP), to investigate how uncertainties in modelling might affect decisions based on model results. It will be illustrated by case studies of long-range transport and transboundary air pollution, and urban air quality.

2. HAZARD IDENTIFICATION AND RISK ASSESSMENT

In building an engineering plant to produce a specific product risk assessment is undertaken to examine the safety of the plant and fitness for purpose. The same procedures can be applied to environmental modelling and its reliability with respect to answering the questions posed. We shall therefore examine some techniques commonly applied to the design and specification of industrial plant. Here approaches such as HAZOP are used to identify how hazardous situation might arise, and the potential consequences. A subsequent risk assessment would involve a study of the probability of occurrence of such hazards for those cases where the consequences are significant; and hence to an estimate of potential overall "detriment" due to the plant, and decisions on how the risks should be managed or reduced. In applying similar principles to environmental modelling, instead of the safety issues arising from an industrial plant, we are concerned with the risk that the results derived from the modelling could be misleading to decision makers.

HAZOP techniques

So let us first consider the formal procedures used to pick out potential problems. HAZOP techniques[(1)] provide a systematic method for identifying hazards, treating a composite system component by component. Thus in an industrial plant each pipe, tank, valve

[1] Environmental Measurement, Modelling and Assessment Group, Department of Environmental Science and Technology, Imperial College, Prince Consort Road, London SW7 2BP, United Kingdom.

Air Pollution Modeling and Its Application XV, Edited by
Borrego and Schayes, Kluwer Academic/Plenum Publishers, New York, 2002

etc would be a separate component, for which the first step in HAZOP would be to define the intended function of each one in turn. For example the intended function of a pipe might be to deliver a certain chemical from one tank to another at a specified rate. The next step is to consider deviations from this intended function prompted by a number of guide words such as "NOT", "LESS"/"MORE", "AS WELL AS", "REVERSE", and how such deviations might occur. For example let us suppose that the pipe in our example delivers "LESS" chemical than the specified rate. This could happen because of a failed valve, or a broken pipe, or because the supply tank ran out. The final stage is to consider the consequences of such a deviation, for example an explosion. In many cases deviations identified may lead to no harmful consequences, and hence do not need to be considered further.

3. APPLICATION TO ENVIRONMENTAL MODELLING AND ASSESSMENT

Transferring the same approach to environmental modelling involves an analogous break-down of the modelling process into component parts. The structure of an integrated assessment approach to an air pollution problem is illustrated in figure 1. Thus suppose we are concerned with decisions in how to attain certain improvements by some future date. This may be for example to improve a long-range problem such as acidification, or a shorter range problem such as urban air pollution and attainment of air quality standards. In both cases it is necessary to compile information on how current emissions are likely to evolve without intervention, " a business as usual scenario", and to combine this with atmospheric models to determine predicted exposure patterns. Environmental criteria need to be established as indicators for protection, either as thresholds below which damage is not expected to occur, or corresponding to acceptable levels of risk. The difference between the predicted exposure and the environmental standards is a measure of the "exceedance" that we wish to eliminate. We then need to consider the range of options available that could lead to reduction of this exceedance. Usually this tends to concentrate on emissions, though in the context of urban air quality there may be other effective measures such as pedestrian precincts or low emission zones that separate the emissions and the exposed population. The aim of the assessment is to investigate which options should be implemented in an effective strategy to reduce exceedance, usually with an emphasis on cost-effectiveness. For a systematic evaluation it is necessary to apply HAZOP to each compartment and link in figure 1.

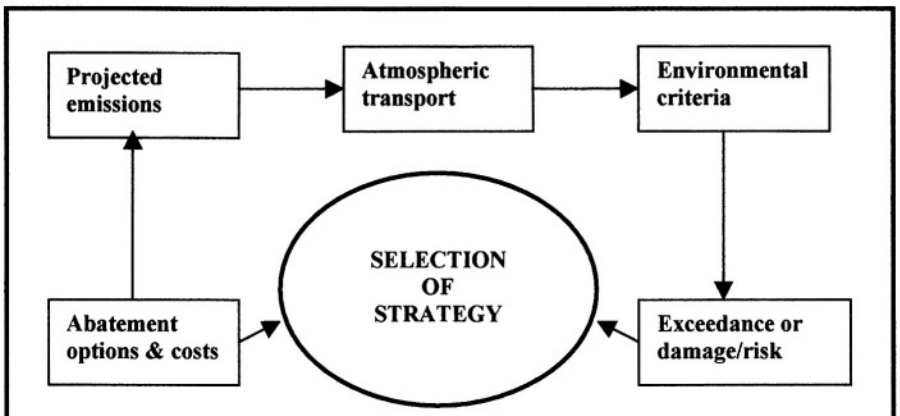

Figure 1: Integrated approach to decisions on abatement strategies

4. CASE STUDY 1: TRANSBOUNDARY AIR POLLUTION

As an illustration we can see how this procedure can be applied in integrated assessment studies of transboundary air pollution in Europe to support development of protocols under the Convention on Long-Range Transboundary Air Pollution, CLRTAP. Using the Abatement Strategies Assessment Model, (ASAM)[2], we have undertaken extensive studies in parallel with work by the International Institute for Applied Systems Analysis, IIASA, with their RAINS model[3], to address uncertainties in assessing effective strategies to combat acidification, eutrophication and excess tropospheric ozone. Here we shall concentrate on deposition and the first two effects, considering air concentrations in the second case study on urban air quality.

Both RAINS and ASAM combine information on emissions from each country in Europe, atmospheric transport and deposition on a continental scale, mapping of "critical loads" as criteria for environmental protection, and data on potential abatement measures and their costs. The aim has been to derive cost effective distribution of emission reductions to be made by the different countries in Europe in order to reduce exceedance of critical loads/levels, defined as limits on exposure below which harmful effects are not expected to occur according to current knowledge. The critical loads are lower in areas of Europe with more sensitive ecosystems., and clearly some countries contribute more to exposure of those areas than others. Targeted strategies[4] were therefore required that placed more emphasis on reducing the more damaging emissions. In this paper we shall explore work undertaken to show that the results obtained from the integrated assessment models provided a robust basis for negotiation of the Gothenburg protocol agreed in December 1999, and prescribing emission ceilings to be met by each European country by 2010 for SO_2, NOx, NH_3 and VOCs.

Before seeing how the HAZOP/risk oriented approach can be applied it is helpful to explain how the ASAM model works, and narrow down the emission scenarios that are of interest. The model structure is consistent with figure 1. The emissions data are provided broken down on a sectoral basis for each country according to a geographical grid spanning Europe, and projected to future situations on the basis of official energy projections, projected agricultural statistics, and technological and other changes in accordance with current legislation. Thus these emissions (the "Current Legislation" scenario) represent the expected emissions in the target year (2010) without further action taken to reduce them. The atmospheric transport is based on the EMEP Lagrangian model which has been used to derive source attribution, calculating the contribution to deposition in each grid cell of the European map area from each country. It is then assumed that changing the emissions by a certain percentage changes the corresponding contribution of that country to the deposition in each grid cell by the same percentage. In other words a linear relationship is assumed.

The criteria for protection of the environment are represented by critical loads, corresponding to annual average levels of deposition which are sustainable in the long term without causing adverse effects. These are defined independently for acidification and eutrophication, and vary geographically and between different types of ecosystem. If deposition is less than the critical load then the corresponding ecosystem is deemed to be "protected"; if it is greater then the ecosystem is at risk, and is "unprotected". " Exceedance" of critical loads is a measure of the excess deposition above the critical loads. In practice it is found that even applying the maximum feasible reductions in emissions regardless of cost, it is not possible to reduce deposition below critical loads everywhere. Hence a lot of discussion has centred on mapping intermediate target loads that close the gap between the current deposition and the critical loads as the ultimate aim[4]. The intermediate aim is then to eliminate exceedance of the target loads.

Information on the abatement measures is summarised in national cost curves for each pollutant in each country. These order the measures available in order of increasing cost per unit emission reduction, and indicate the cumulative cost of achieving increasingly stringent emission reductions in each country.

Optimisation routines in ASAM are then used to derive cost-effective strategies for achieving the prescribed target loads. Using the combined data described above, ASAM cycles through the available abatement options in all the different countries and selects that measure that gives the greatest ratio of improvement (based on overall reduction of exceedance across Europe) to cost. This measure is implemented, and the process repeated., each time adding to the accumulated expenditure. The results can be summarised as a graph- see figure 2, plotting the diminishing area of ecosystems still unprotected in Europe against increasing cost expended on abatement Any point on the graph corresponds to a distribution of emission

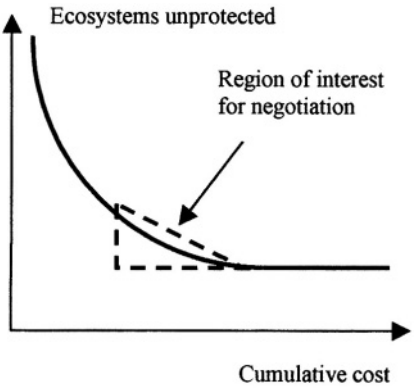

Figure 2: Strategy selection

reductions within the prioritised sequence, and hence to a ceiling on emissions remaining in each country. The steps corresponding to the first steep part of the curve in figure 2 are a definite priority, whereas those on the last part are bringing little improvement for increasing cost. The region of interest for international negotiations is depicted in the triangle.

Inevitably this "integrated assessment modelling" to derive cost effective distribution of effort in reducing across Europe contains many assumptions, simplifications and uncertainties. It is necessary to show that the strategies derived from the models are robust, and to make the assumptions clear and transparent. This involves addressing the whole modelling procedure, but here we shall concentrate on aspects related to the atmospheric modelling and show how the HAZOP techniques may be applied. A broader overview has been described elsewhere[7].

4.1 Atmospheric modelling: source- receptor relationships.

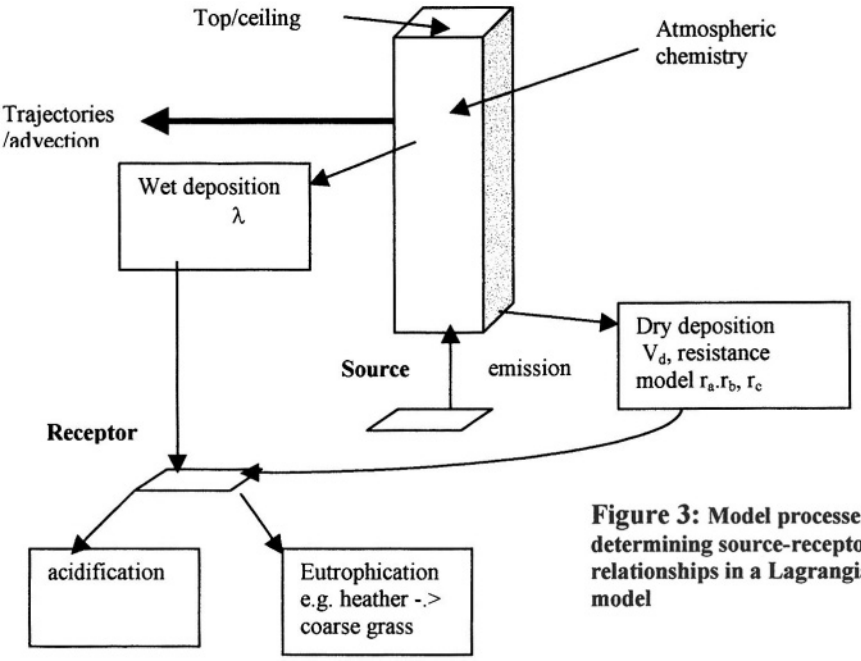

Figure 3: Model processes determining source-receptor relationships in a Lagrangian model

As indicated above the official model used in the integrated assessment work to describe the atmospheric transport and derive source- receptor relationships (or "blame matrices") for sulphur and nitrogen deposition has been the EMEP Lagrangian model[8]. This follows trajectories backwards from each square in the EMEP grid, every 6 hours. A column of air is then simulated moving along each trajectory, picking up emissions of SO_2, NOx, and NH_3 distinguished by the country of origin, with subsequent chemical transformation and dry and wet deposition processes. In this way the deposition at the terminal point of each trajectory can be attributed to sources in the different countries. As compared with a more complex Eulerian model, this simpler Lagrangian model can be run over 10 or more years to average out substantial inter-annual variations in meteorology.

The first step in applying HAZOP techniques is to define the overall purpose of the model within the integrated assessment scheme, and then consider the role of the component parts and links between them. As indicated above the requirement of the atmospheric modelling is that it should not only calculate maps of total deposition, but should also be able to indicate what proportion of deposition at any location comes from each country, or from other sources (e.g. shipping, fluxes from outside Europe). The capability to estimate concentrations and deposition can be checked against monitoring data. This has already been done and reported in EMEP annual reports. The more difficult task is that of the source attribution. Table 1 gives examples of how HAZOP techniques may be applied to review possible causes for deviation in modelling source-receptor relationships.

Model item/guideword	Possible cause of deviation	Consequence	Comments
Emissions "NOT" into air column	Trajectory errors/ large wind gradient eg depressions	Errors in source identification	NB trajec. patterns different years
Advection "MORE"	Wind profiles- higher winds aloft	Shearing of column	Could increase range of transport
Air column: pollutants "NOT" contained	Venting to free troposphere in clouds	Material transported in free troposphere	Could increase range of transport
Winds: vertical, w, "AS WELL AS" u,v horizontal	a) frontal system	Reduces ground conc. Induces wet dep.	Wet dep. displaced?
	b) orographic forcing	Wet dep. enhanced	Enhanced dep. on some sensitive areas
Dry deposition "REVERSED"	Bi-directional fluxes of ammonia	Reduced net dry deposition	Less likely to occur in sensitive areas
Wet deposition e.g. Λ "MORE/LESS"in convective showers	Non-linear cloud chemistry & removal eg NH3-SO2 uptake	Wet dep. more/less, and substantial transfer to free trop.	Changes magnitude of deposition and range of transport

Table 1. Illustration of application of HAZOP techniques to atmospheric transport model

In the overall analysis of the integrated assessment modelling, this process has to be repeated in a similar manner to all the other compartments- the projected emissions, the critical loads and the effectiveness of the abatement measures and their costs. Selected experiments can then be performed to test the robustness of the strategies derived for reducing transboundary air pollution, and the influence of different effects on the emission reduction of

individual countries within these strategies. For example the table above suggests studies a)taking source receptor matrices derived from years with contrasting meteorology to investigate the sensitivity to variable trajectory patterns, and b) altering the range of transport by stretching or contracting the "footprint" of deposition from each source, and c) the sensitivity to increasing or decreasing the deposition. Such studies with ASAM have been reported elsewhere[3,5,6,7]. Traditional methods using Monte Carlo analysis may also be used- for example to introduce random variations in the costs of abatement measures to reflect variations between individual sources. However a full Monte Carlo analysis of an atmospheric model is extremely time consuming compared with the HAZOP approach described above, and achieves little more than indicating the scale of the variance. Also it does not pick out processes that are not included in the model. However complementary modelling studies, for example to examine the implications of cloud venting and removal (e.g. Kayin[9]), and inter-comparison with more complex models can be very informative

As an example of the selected studies identified above here we can consider the implications for the overall integrated assessment modelling if the deposition is greater or less than the base case estimation, and the implications for the overall integrated assessment modelling. This can be combined with uncertainties in the critical loads, since the crucial factor is the exceedance of the critical loads. This is a topic that attracted much criticism of the integrated assessment approach. The reason is that if the IAM models are run to achieve strict attainment of prescribed target loads, the emission reductions required and the associated costs are extremely sensitive to the deposition and critical loads in a few "binding squares" where it is most difficult to achieve the target deposition. A small increase in the estimated deposition or reduction of the critical loads in these squares can imply a very large increase from a moderate to a high cost scenario. However such a revised scenario would be rejected as lying outside the region of interest for negotiation in figure 2. Also if one compares the abatement steps selected across Europe up to a specified level of overall cost in figure 2, these are fairly robust with respect to similar changes in deposition and critical loads. In other words the relative priority of different reduction measures in different countries remains stable, which is important to the negotiator. This also holds when the footprints are stretched to reflect longer-range transport, and when different "damage" functions are used to relate environmental risk to the critical load and magnitude of exceedance. The greatest change tends to be found when using source-receptor matrices from years with different meteorology, emphasizing the need for long-term averaging over 10 years or more to allow for inter-annual variation.

There is however one more fundamental difficulty that emerges when HAZOP is applied to the grid-scale used in linking deposition and critical loads to calculate exceedance, to query the effect of "MORE" spatial resolution. Averaging deposition over large grid cells of ~150 by 150 km does not allow for the considerable variability between different ecosystems and locations within such an area. This is particularly important for reduced nitrogen where the deposition patterns are extremely patchy and influenced by local sources. This can only be resolved by more detailed studies at national or regional level.

In illustrating the HAZOP approach attention has been focused particularly on the atmospheric transport aspects in deriving abatement strategies. Subjecting any model to this type of analysis will bring out many potential sources of error or uncertainty, and the above analysis is not meant to be critical of a well-established and tested model. Even with a far more complex state-of –the-art Eulerian model, such as that now replacing the Lagrangian model at EMEP, many of these limitations and uncertainties are still present. Analysing other parts of the integrated assessment model leads to similar questions and concerns- for example the abatement measures and costs. We can now consider a different case study, and show how similar questions arise concerning the reliability of model results as a basis for decision making.

5. CASE STUDY 2: URBAN AIR QUALITY

We can apply a similar approach to urban air quality, and investigation of different strategies to attain air quality standards – in this case study for PM10, which together with those for NO2, are difficult to achieve. The Urban Scale Integrated Assessment Model, USIAM[10], applies the same approach as ASAM, but in this case we need to use local scale dispersion models e.g. ADMS, and urban canyon models for hotspots. The options for abatement include traffic management and low emission zones as well as technological measures, and these are more difficult to relate to changes in emissions. Again we are concerned with accurate source apportionment for concentrations and exposure in order to examine the effect of different abatement scenarios. In this case we shall illustrate how source apportionment may be queried directly.

The concentration at a polluted location in an urban area is calculated as the contribution from the local street calculated with a street canyon model superimposed on the urban background due the primary PM_{10} emissions from the surrounding city (calculated with ADMS). Since we are interested in traffic control measures and low emission zones over different areas of the city, we also need to differentiate between contributions from different parts of the city- from central London, the surrounding inner London zone, and outer London. We also have a separate contribution from traffic on the surrounding ring road, the M 25 motorway. To this primary PM_{10} contribution we have to add the secondary particulate concentrations, which are deduced from monitoring data.

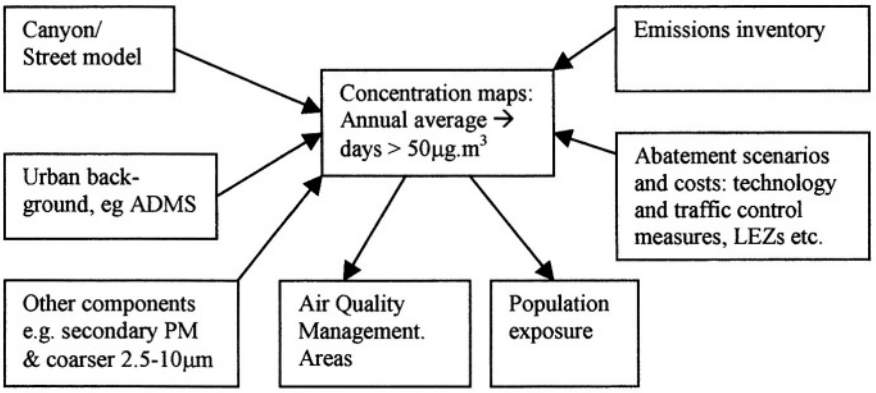

Figure 4: Framework of USIAM model in addressing strategies for urban air quality

The structure of the USIAM model is shown in figure 4. The purpose of the assessment is to consider how different abatement scenarios a) reduce the areas of London with exceedance of air quality standards, and hence classified as Air Quality Management Areas, AQMAs; and b)reduce population exposure. In the risk assessment approach proposed in this paper, HAZOP would need to be applied to each component or sub-model, questioning, for example, the representation of real conditions in the canyon/street model, and the influence of uncertainties about urban boundary layers on modelling of the urban background. This is a similar process to that illustrated above for the long-range modelling.

However in this urban case we will consider instead questions concerning the overall linkage of the sub-models. Here again an overall illustration of source attribution is helpful. Figure 5 gives a break down for a row of 1 x 1 km grid squares from west to east across London. In the column for each grid square the uppermost black portion is the local contribution to annual average concentrations for the busiest road in that grid square. The grey contributions immediately below correspond to the urban background, with the dark grey giving the contribution from outer London, the lighter grey to that from inner London, and the

white due to emissions in central London. Obviously the local street contribution is a very important contribution, and can be further resolved into contributions from different vehicle categories and vintages.

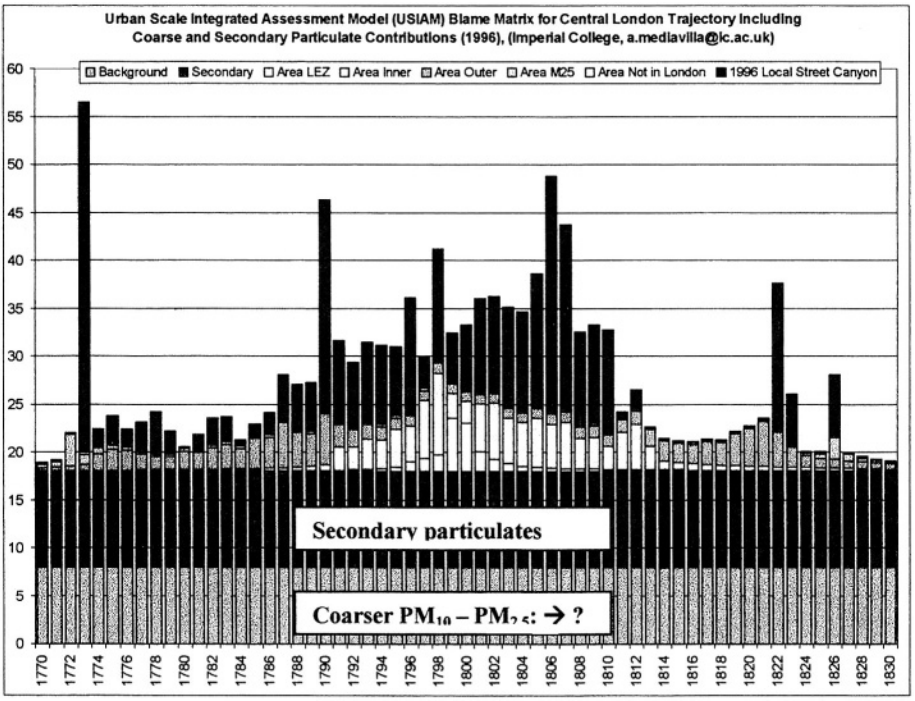

Figure 5: Source apportionment for PM_{10} illustrated for cross section of London

For PM_{10} the HAZOP guide words "AS WELL AS" are particularly significant. Combining the local street and urban background contributions significantly under-predicts observed concentrations. One reason for this is the secondary particulate matter resulting mostly from longer range or regional scale transport. This is likely to be more uniform across a city but requires separate assessment. Supplementary measurements augmenting PM_{10} networks are required to differentiate the SO_4, NO_3 and secondary organic contributions etc., and improvements currently being researched in modelling secondary aerosol concentrations. The constant band right across London immediately below the urban background in Figure 5 gives an indication of the relative importance of this contribution.

Turning to the emissions inventory there is a further question of what other sources contribute to PM_{10} concentrations "AS WELL AS " those considered above. Measurements indicate a significant proportion of PM_{10} is in the coarser range between 10 and 2.5 μm, but this is not consistent with the emissions inventory, which dominated by traffic, is mainly finer particles. There are various suggestions about the possible origins of this coarser component, such as dust from various sources suspended from the roads by traffic, and various studies are in progress to explain it. In figure 5 it is represented as the bottom band beneath the secondary contribution, but it is clearly unlikely to be uniform and this has large implications for whether or not air quality standards can be achieved.[10] Further research is clearly required on this contribution to PM_{10} exposure.

There are further uncertainties in analysing future scenarios and abatement measures where USIAM has been applied to 60 scenarios analysed for London by W.S.Atkins[11]. This is outside the scope of this paper which has emphasized the atmospheric aspects of the assessment, and will be reported elsewhere.

Conclusion

It is hoped that the two case studies considered above have illustrated how HAZOP techniques as part of a formal risk assessment, can be useful as a systematic way of examining model functioning and assumptions when used in assessment of air quality problems. These techniques go beyond the traditional methods such as Monte-Carlo analysis, in addressing what is not covered in the models as well as questioning the representation and parameterisation of what is included. They point towards potential hazards for the decision maker in using the results from a model, and to priority areas for further research. They also provide a framework for linking what are inevitably simplified models in looking at a wide range of possible scenarios in assessing abatement strategies, to a hierarchy of more detailed and sophisticated research concerning the aspects identified. It is suggested that the approach illustrated could usefully provide an appendix to many reports on environmental assessment based on numerical models!

Acknowledgments

The integrated assessment modelling with ASAM used as case study 1 has been supported by the UK Department of Environment, Transport and the Regions. The work of A Mediavilla-Sahagun on development of the USIAM model in case study 2 has been supported by the Mexican Petroleum Institute.

References

1. CIA (1989) *A guide to hazard and operability studies.* Chemical Industries Association

2. ApSimon HM, Warren RF and Wilson JJN. *The Abatement Strategies Assessment Model-ASAM: applications to abatement of sulphur-dioxide emissions across Europe.* Atmospheric Environment 28(1994)p649-663

3. Alcamo J Shaw R and Hordijk L (eds) 1990. *The RAINS model of acidification: Science and Strategies in Europe.* Kluwer Academic Publishers, Dordrecht.

4. Warren R F and ApSimon HM (2000). *Selection of target loads for acidification in emission abatement policy: the use of gap closure approaches.* Water Air and Soil Pollution 121, p229-258.

5. Warren RF and ApSimon HM (1999) *Uncertainties in integrated assessment modelling of abatement strategies: illustrations with the ASAM model.* Environmental Science and Policy vol 2, p439-456

6. Warren Rf and ApSimon HM (2001) *Integrated Assessment modelling of abatement strategies: role of uncertainties.* Air Pollution Modelling and its Applications XIV,p35-43

7. ApSimon HM and Warren RF (2001) *Addressing uncertainty in environmental modelling; a case study of integrated assessment strategies to combat long-range transboundary air pollution.* IUAPPA conference, Korea August 2001.

8. Barret K and Seland O (1995) *European Transboundary Acidifying Air Pollution.* EMEP report 1/95.

9. Kayin S (1993) *Wet deposition in convective storms and effects on transboundary air pollution.* PhD thesis. University of London.

10.Mediavilla-Sahagun A, ApSimon Hm and Warren RF (2001) *Integrated Assessment of Abatement Strategies to Improve Air Quality in London, The USIAM Model.* Urban Air Quality conference, Loutraki, Greece, March 2001.

11. W S Atkins (1999) *An evaluation of transport measures to meet NAQS objectives* .Report to Department of Environment Transport and the Regions.

DISCUSSION

B. FISHER

If one contrasts work undertaken to inform a strategy to control transfrontier pollution with work on urban pollution, the former was associated with extensive testing of models against measurements. The development of strategies for improving urban pollution seem to suffer from insufficient good quality measurements. Would you like to comment ?

H. APSIMON

We have developed integrated assessment modelling along similar lines to analyse strategies to attain air quality standards in London. Here there is quite an extensive monitoring network which we have used as best we can for model comparison, but limited meteorological data-e.g. from Heathrow airport to the west of the city. The difficulty is the small scale spatial variability even round a single street junction, and the representativeness of monitoring points. As far as PM10 is concerned a substantial correction (~30%) has to be made to the TEOM measurements for loss of the volatile fraction, so care is needed in comparing with model results. However there are also large problems in modelling such as the coarse PM10-PM2.5 fraction, for which there is no representation in the emissions inventory. So it is not just the measurements that cause problems in urban assessment, but also the incompleteness of the models and aspects that we do no yet understand. Unfortunately it is not easy convincing our UK research council that fundamental research and data are required !

A. EBEL

The concept of source-receptor estimates using Lagrangian transport modelling appears to work reasonably well for "simpler" species like SO_2. What is the experience with more complicated chemicals, particularly ozone as a secondary pollutant ?

H. APSIMON

The illustration I gave in this paper was concerned with sulphur and nitrogen species, where I mentioned the effects of chemistry on non-linear response of concentrations to emissions. We did not specifically work on ozone in studies for the UN ECE because we were too occupied with concerns about fine particles. The source-receptor relationships for ozone were produced by IIASA, who fitted empirical quadratic expressions to results from the EMEP model to represent the response of excess ozone (accumulated above specific concentration thresholds) to NOx and VOC reductions. A full uncertainty analysis on this would be complex, but needs to include

such factors as trends in background/free troposphere ozone as well as emission abatement scenarios.

P. BUILTJES Can you explain why fixing the total costs is more robust than approaching the problem from the other angle ?

H. APSIMON What seems to be robust is the order of priority of successive abatement steps selected, based on the ratio of their effectiveness in reducing exceedance to their cost. Even quite large changes in for example source- receptor matrices, as for example from years with contrasting meteorology, do not change the order of priority very much; nor changes in the critical loads. Hence if one asks what is the strategy that maximises convergence towards the desired targets or goals for protection up to a fixed level of costs, this strategy also tends to be rather robust. However if one aims at strict attainment of a set of specified target loads for deposition, then usually there are one or two difficult target locations or "binding" grid-cells which are difficult to achieve. A slight tightening of the targets at these locations can have big implications for the extra abatement steps needed to achieve them and their costs. Effectively this is moving onto the flat part of the curve relating ecosystem protection to cost. Thus sometimes it is apparent that a slight relaxation of such targets in binding cells avoids some quite large costs.

This page intentionally left blank

ETEX SIMULATIONS WITH THE DMI-HIRLAM NUMERICAL WEATHER PREDICTION MODEL

Jérôme Chenevez, Alexander Baklanov and Jens H. Sørensen*

1. INTRODUCTION

Eulerian atmospheric long-range dispersion models to predict air pollution episodes are coupled either offline or online with Numerical Weather Prediction (NWP) models. In the perspective of developing such a mesoscale air pollution forecast system, a version of the Danish Meteorological Institute's (DMI) NWP model has been implemented with advection/diffusion of passive tracers, resulting in the model DMI-HIRLAM-TRACER (shortened as TRACER in the following).

The main objective of this work is to simulate the transport of passive tracers in the model using the best possible advection scheme. A very suitable and realistic way to test the advection of a field of passive tracers is supplied by the first European Tracer Experiment (ETEX-1) performed in 1994. This release started on October 23rd 1994 16:00 UTC in Brittany (France) and had a duration of 11 hours and 50 minutes. Its precise location was (2.0083°W, 48.0583°N) at an altitude of 90 m. The total amount of material released was 340 kg of Perfluoro-Methyl-Cyclo-Hexane (PMCH) corresponding to a constant emission rate of 7.95 g/sec. The release was followed during 3 days by a series of measurements of the concentration at specific locations in Europe from which it was possible to observe the plume evolution (Graziani et al., 1998).

2. SIMULATION OF THE ETEX RELEASE

The present numerical simulations start 4 hours before the beginning of the ETEX release by using initial boundary files generated by the European Centre for Medium-Range Weather Forecasts (ECMWF) from October 23rd 1994 12:00 UTC. They were carried out covering more than three days by updating the lateral boundaries every 6

* Jérôme Chenevez, Danish Meteorological Institute (DMI), Lyngbyvej 100, 2100 Copenhagen Ø, Denmark.

Air Pollution Modeling and Its Application XV, Edited by
Borrego and Schayes, Kluwer Academic/Plenum Publishers, New York, 2002

hours (using 6-hour forecasts and new analysis every 12 hours). The numerical simulations were performed with TRACER over a model region covering Europe, in a grid with 92×86 points yielding a horizontal resolution of 0.4° (about 42km × 44km); all experiments were performed using a 31-level resolution in a hybrid vertical coordinate system (Sass et al., 2000).

Indications about the performances of these simulations are given by 1) the geographical position on the surface (more precisely at the lowest model level about 30 m above the ground in the present version of TRACER) of the modelled concentration field at different forecast times after the start of the release, 2) a time-series of averaged concentrations at specific model points corresponding to ETEX measurements sites, and 3) the evolution of total mass in the model compared to the mass emitted at the release location. The two former outcomes can be compared to real measurements and/or results of other models (Graziani et al., 1998; Sørensen et al., 1998, Robertson et al., 1996), while the third allows an evaluation of the stability and the confidence in the scheme used.

Since the conditions of the release are known exactly (location, total mass and rate of release), the main difficulty is to perform such a local release inside an Eulerian grid point model. In the present study, a uniform distribution of the tracer is assumed within the volume of the grid box inside which the release is initiated. The knowledge of this volume makes it possible to calculate the concentration of the passive tracer, in order to compare the simulated tracer field with the observed concentration field.

The model has to solve the following advection-diffusion equation driving the dynamic evolution of the concentration C of a passive tracer field:

$$\frac{\partial C}{\partial t} = -\nabla(\mathbf{v}C) + \nabla(\mathbf{K}\nabla C) + Q \qquad (1)$$

where **v** represents the advecting velocity vector field, **K** is a 3 dimensional eddy diffusivity vector, and Q represents the source term.

From the source term of Eq. (1) one can obtain the value at the next time step $(t+\Delta t)$ of the concentration in the grid box inside which the emission is performed:

$$C^{t+\Delta t} = 2\Delta t\, Q + C^{t-\Delta t}. \qquad (2)$$

That is the concentration of the emitted tracer at the current time step plus the remaining concentration from the previous time step. Hence, during the duration of the emission, the value of the concentration at the point of emission is forced by Eq. (2).

3. TRANSPORT USING DMI-HIRLAM DEFAULT SETUP

Simulations of the ETEX release have first been performed using the default DMI-HIRLAM formulation of Eq. (1) for a scalar. In this formulation, advection is described by the Eulerian central finite-difference scheme in a semi-implicit time scheme where negative values of positive definite quantities are set to zero so as to avoid unrealistic negative concentrations; the consequences of such a resetting procedure will be discussed later. Horizontal diffusion processes, on the one hand, are estimated by an implicit linear 4^{th} order scheme (Källen, 1996), and vertical diffusion, on the other, is computed by a local turbulent kinetic energy scheme known as the CBR method (Cuxart et al., 1999).

Modelled surface concentration at 48 hours after the start of the release is shown on Figure 1 in a zoom inside the model domain. The general shape and position of the plume are rather close to the observations made during the experiment (Graziani et al., 1998), though physical diffusion seems to be too large.

Figure 2 compares measured and modelled one-hour average surface concentrations at the location of Risø (Denmark). The time of the peak is fairly well predicted, but its value is more than twice the observed value, and the shape of the curve is too wide due to diffusion and low grid resolution.

The reason for this too high value is shown on Figure 3, which presents the evolution of the mass of passive tracers relative to the total mass released. The curve obtained with the central difference scheme shows an increase in the amount of passive tracers of more than 1.5 times the total mass emitted, indicating that mass is not conserved during the simulation. Indeed, the mass continues to increase linearly even after the emission phase, thus showing an artificial production of mass in the model.

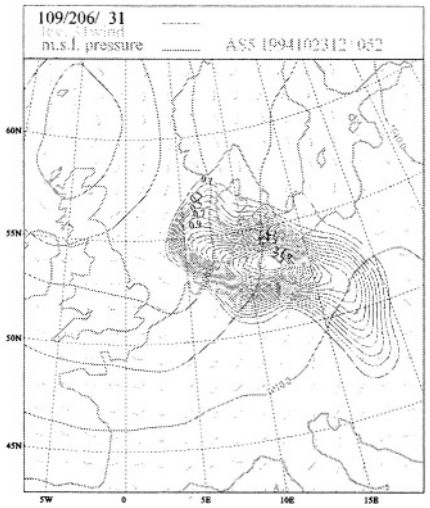

Figure 1. Modelled surface concentration 48 hours after the release beginning (52 hours after the start of the simulation) obtained with the Eulerian central-difference advection scheme.

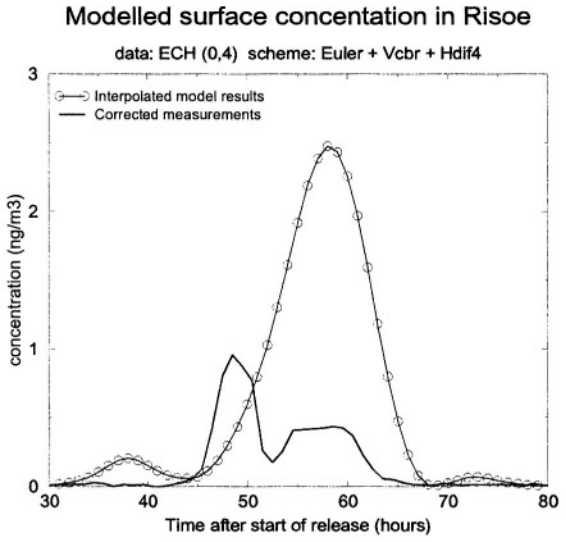

Figure 2. Time variation of one-hour averaged surface concentration at Risø (Denmark). Modelled concentration interpolated at the location of Risø is compared with measurements from which the background concentration has been subtracted.

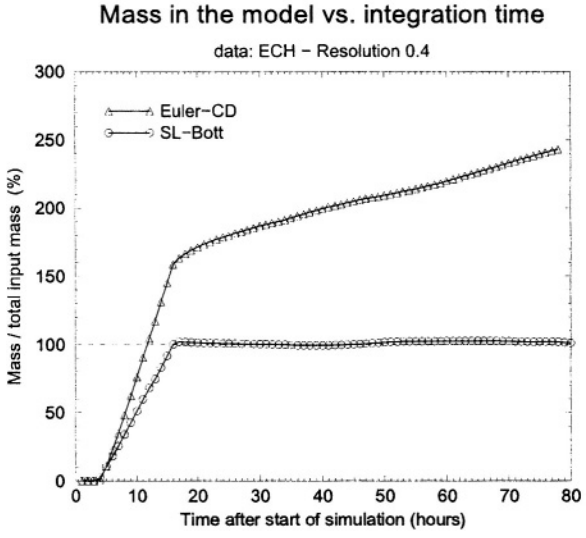

Figure 3. Passive tracer mass evolution during ETEX simulations with two distinct advection schemes (Euler-CD: Eulerian Central Difference scheme; SL-Bott: Bott scheme implemented in the Semi-Lagrangian time integration scheme).

4. SEMI-LAGRANGIAN MODEL WITH THE BOTT ADVECTION SCHEME

4.1 Model

With the aim to improve the mass conservation of the model, a separate numerical scheme for the advection has been implemented in TRACER replacing the default advection scheme for the passive tracer field. The scheme described by Bott (1989a, 1989b) is an Eulerian advection scheme having flux conservation and positive definiteness properties. In the present work the Bott scheme has been combined with the dynamic part of the semi-Lagrangian integration time scheme of the HIRLAM model (Ekman and Källen, 1998). This approach has the advantage to lengthen the integration time steps, and thus significantly reduce the computing time. The constant grid flux form of the Bott scheme is extended to three dimensions by using the time-splitting method in which the one dimension procedure is repeated circularly in each direction. The scheme uses 4^{th} order polynomials in the x and y directions, and a 2^{nd} order polynomial in the z direction so as to save computing time due to the variable vertical grid spacing. To deal with the Eulerian CFL criterion (Courant number ≤ 1) the scheme is run three times inside one dynamic time step, and the Courant number is checked for each direction at each internal time step. Here, no horizontal turbulent diffusion processes have been added (the horizontal part of the 2^{nd} term in the RHS of Eq. (1) is not included).

Though the Bott scheme needs a larger amount of calculations, its combination with the semi-Lagrangian model yields a relatively low computational cost. This procedure needs 41% less computing time than the Eulerian central difference scheme and only 8% longer time than the pure semi-Lagrangian scheme.

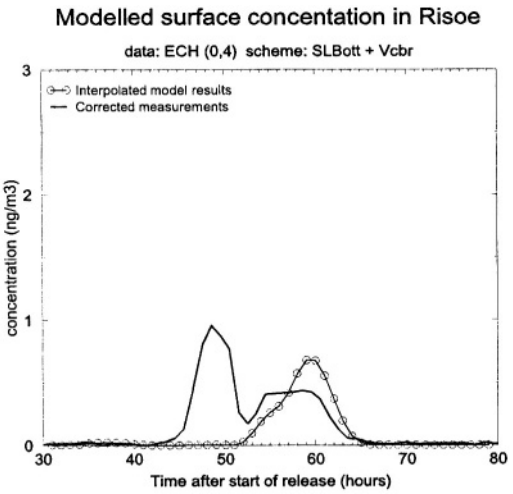

Figure 4. Same as Figure 2, obtained with the Bott advection scheme.

4.2 Results

The Bott scheme has been tested on simulations of the ETEX release as previously. One first result is the variation of the mass shown in Figure 3. Contrasting with the previous simulation, after the end of the emission phase, the mass of passive tracers remains approximately constant during the transport phase. This behaviour confirms the major improvement due to the Bott scheme as regards the mass conservation requirement during advection of passive tracers.

In the same way as Figure 2, Figure 4 shows the modelled surface concentration at Risø obtained by advecting the passive tracer with the Bott scheme. The maximum concentration is much closer to the measurement than previously, but the arrival time of the plume is a bit late. The reason may be found in the meteorological data used here.

The corresponding surface fields obtained every 12 hours are displayed in Figure 5. The respective vignettes show a good agreement with the observed ETEX plume.

5. DISCUSSION AND CONCLUSION

The Eulerian central difference scheme working as default in DMI-HIRLAM has shown reasonably good qualitative results compared with surface concentration measurements (Graziani et al., 1998) and results from other models (Sørensen et al., 1998; Robertson et al., 1996). But this formulation does not respect the mass conservation criterion, since it yields a continuous increase of the mass in the model even after the end of the release. The reason for this increase is that, in the original Eulerian central difference scheme, unrealistic negative values may appear for quantities with sharp gradients, and in order to preserve positive definite quantities, negative values due to non-monotonicity have here been set to zero. Such a behaviour, even if it may not be consequential for simulations of the meteorological fields, is unacceptable for modelling of pollutant transport, where mass conservation is of the highest importance.

On the contrary, the Bott scheme presents mass conservation properties, which have been confirmed here by an almost perfect time evolution of the mass during passive tracer advection in the model. As regards the shape and position of the plume of passive tracers, the surface concentration modelled with the Bott scheme is in better agreement with the observations than for the simulation with the default DMI-HIRLAM model. Nevertheless, the comparison with the measurements showing a double-peak structure at Risø shows some important differences. This can be due to the relatively coarse resolution of the data used here, i.e. initial meteorological fields with 0.4° resolution, which may be not enough to detect such a mesoscale structure (Sørensen et al., 1998).
Apart from the simulations presented in this paper, it has been shown that vertical diffusion has important effects on the results (Chenevez, 2000). To apply vertical diffusion processes to a passive tracer improves the modelled surface concentration field, independently on the advection scheme used, and, as shown here, it does not affect the mass conservation qualities of the Bott scheme. The vertical diffusion scheme (Cuxart et al., 1999) used here is the same as the one used for cloud water in DMI-HIRLAM, and is hence assumed to be mass conserving and thus reliable for transport of scalar quantities

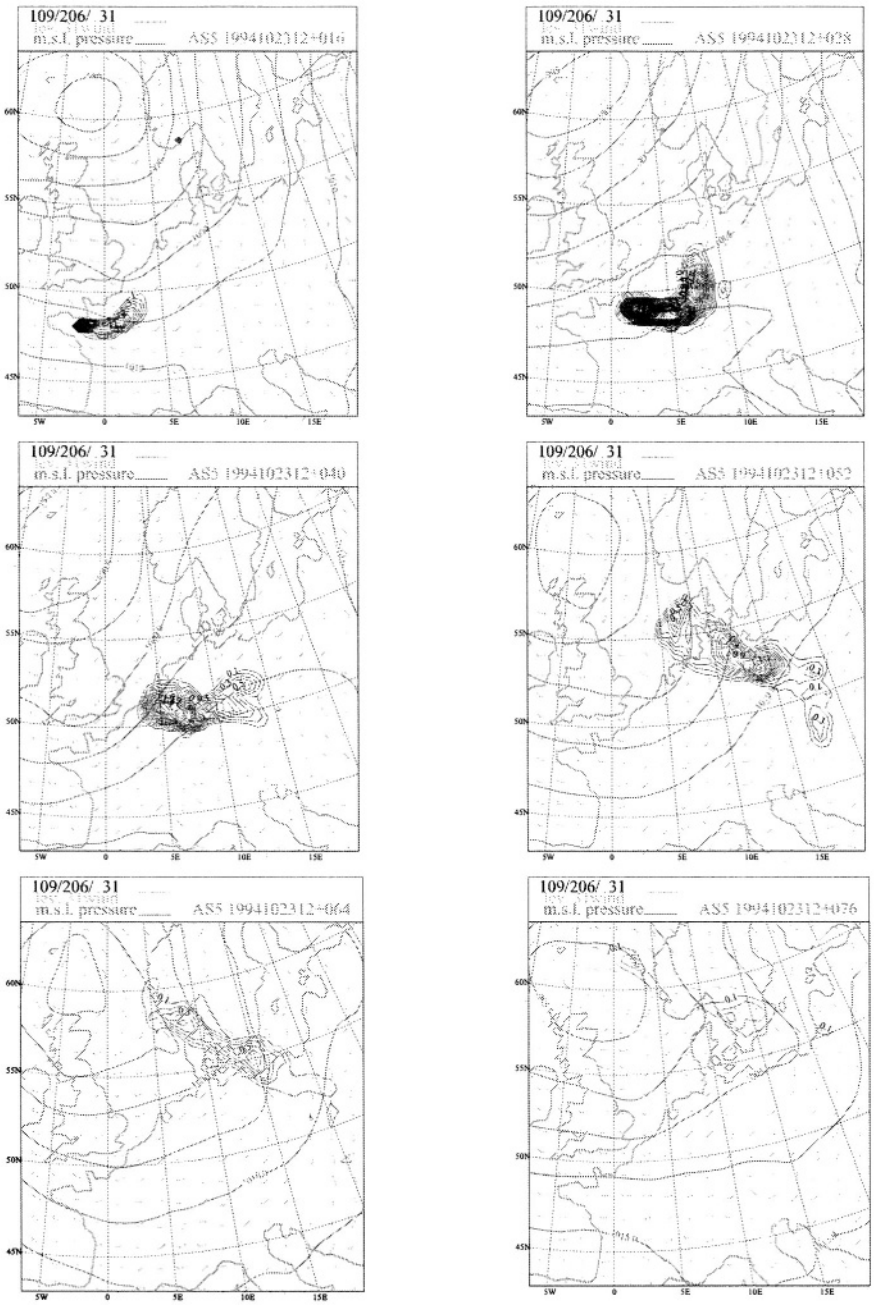

Figure 5. Time evolution of the passive tracers plume every 12 hours after the start of the release.

like chemical constituents and any other pollutants. It has also been shown in the same work that using a 4^{th} order horizontal diffusion scheme (Mc Donald, 1994) together with the Bott scheme corrupts its mass conservation properties. This may be due either to a poor formulation of the horizontal turbulence processes, or to some incompatibilities between the diffusion scheme and the Bott scheme during the splitting step. It is thus preferable at this stage to avoid adding the term of horizontal diffusion in the simulations with the Bott scheme, unless it is formulated in a way that compensates for the numerical diffusion inherent to the Bott scheme.

One of the principal outcomes of this work is that the Bott scheme used inside the semi-Lagrangian model yields only 1.08 longer computation time than the semi-Lagrangian scheme alone, and it is even 1.6 times as faster as the Eulerian central difference scheme. Better results are thus obtained in a shorter time than with the default setting of DMI-HIRLAM.

In conclusion, the present simulation tests have shown that, when including a mass conservative advection scheme together with vertical diffusion processes for the passive tracers, the TRACER model can be used for transport modelling.

ACKNOWLEDGEMENTS

The authors are grateful to Annica Ekman from MISU who have supplied the code of the Bott scheme. Thanks to Leif Laursen, Bennert Machenhauer and Xiang-Yu Huang for their critical reading of the manuscript, and also to Jess U. Jørgensen, Bent Hansen Sass, and Niels Woetmann Nielsen for their helpful advice.

REFERENCES

Bott, A., 1989a, A positive definite advection scheme obtained by non-linear renormalization of the advective fluxes, *Mon. Wea. Rev.* **117**: 1006-1015.

Bott, A., 1989b, Reply, *Mon. Wea. Rev.,* **117**: 2633-2636.

Chenevez, J., 2000, Advection experiments with DMI-HIRLAM-TRACER. *DMI Scientific Report* 00-05; http://www.dmi.dk/f+u/publikation/vidrap/2000/Sr00-05.pdf.

Cuxart, J., Bougeault, P., and Redelsperger, J.-L., 1999, A turbulence scheme allowing for mesoscale and large eddy simulations, *Q. J. R. Meteorol. Soc.* **XXX:** 1-22.

Ekman, A. and Källen. E., 1998, Mass conservation tests with the HIRLAM semi-Lagrangian time integration scheme, *HIRLAM Technical Report* N°39, Dublin, Ireland.

Graziani, G., Klug, W., and Mosca, S., 1998, Real-Time Long-Range Dispersion Model Evaluation of the ETEX first Release, *Office for Official Pub. of the European Communities,* Luxembourg, EUR 17754 EN.

Källen, E., 1996, "HIRLAM documentation manual, System 2.5", SMHI, Norrköping, Sweden.

McDonald A., 1994, The HIRLAM two time level, three dimensional semi-Lagrangian, semi-implicit, limited area, grid point model of the primitive equations, *HIRLAM Technical Report* N°17, Norrköping, Sweden.

Robertson, L., Langner, J., and Engardt, M., 1996, MATCH - Meso-scale Atmospheric Transport and Chemistry modelling system, *SMHI Reports Meteorology and Climatology* N° 70.

Sass, B. H., Nielsen, N. W., Jørgensen, J.U., Amstrup, B., and Kmit, M., 2000, The operational HIRLAM system, *DMI Technical report* 00-26. http://www.dmi.dk/f+u/publikation/tekrap/2000/Tr00-26.pdf.

Sørensen, J.H., Rasmussen, A., Ellermann, T., and Lyck, E., 1998, Mesoscale influence on long-range transport - Evidence from ETEX modelling and observations, *Atmos. Env.***32**: 4207-4217.

DISCUSSION

S.E. GRYNING — The prediction of the time of arrival of the tracer plume is not so well predicted in your simulations as in earlier simulations done at the Danish Meteorological Institute by J.H. SØRENSEN (special ETEX issue on Atmospheric Environment). Do you have any suggestions for an explanation ?

J. CHENEVEZ — We are speaking about two different kinds of models: J. H. Sørensen's model DERMA is based on a Lagrangian transport model, while DMI-HIRLAM is an Eulerian model. However, according to J. H. Sørensen's work, DERMA gave approximately the same results when used with the same model resolution as in the present work, while better results were only obtained with a higher model resolution, showing that a mesoscale structure influenced the tracer plume about one day before arriving to Risø.
Another possible cause of the delay obtained in the modelled peaks may be slide phase errors of the version of the Bott advection scheme employed here, as noticed by Bott himself and corrected in a further version, which we still have to implement.

This page intentionally left blank

IMPACT ASSESSMENT OF GROWING ASIAN MEGACITY EMISSIONS

Sarath K. Guttikunda, James J. Yienger, Narisara Thongboonchoo, Gregory R. Carmichael, Hiram Levy II and David G. Streets*

1. INTRODUCTION

The urban environment is where an increasing share of the world's people live, where most of the energy is consumed, and where the impacts of the pollution are felt the most. While the effects of high pollution levels in Asia are centered in the urban areas, the impacts are not confined to the city boundaries. Polluted air has damaged human health, ecology and environment in a number of urban centers of the developing countries of Asia. Most of the air pollution is emitted by stationary sources like power plants and industrial estates. Pollution from the mobile sources (NO_x, volatile organic carbons (VOC) and particulates) has become a major contributor to increasing human health effects in the urban environments of Asia (OECD, 2000).

Rapid economic growth in Asia over several decades has attracted millions of rural residents to urban areas. Figure 1 presents gridded Asian population for 2000 along with Asian megacities (with population over 10 million) and major urban centers. Asia presently has ~1 billion (~35% of total population) urban dwellers, projected to grow at an average of 4% per year to ~3 billion by 2025 (~55% of the projected total population). Changing standards of living in these centers have fueled increased industrial and transportation sector activities, often associated with unchecked emissions from automobiles, domestic heating, and small-scale industries. Coal (besides bio-fuel (wood, cow dung, and field residue)) being the cheapest and most widely available source of energy, still remains the primary source of energy, and contributes significantly to sulfur

* Sarath Guttikunda, Narisara Thongboonchoo, and Gregory Carmichael (corresponding author, gcarmich@engineering.uiowa.edu), Department of Chemical and Biochemical Engineering, The University of Iowa, Iowa City, IA 52242, USA. James Yienger, Center for Global and Regional Environmental Research, The University of Iowa, Iowa City, IA, USA. Hiram Levy II, Geophysical Fluid Dynamic Laboratories, Princeton University, NJ, USA. David Streets, Argonne National Laboratories, Argonne, IL, USA.

Air Pollution Modeling and Its Application XV, Edited by
Borrego and Schayes, Kluwer Academic/Plenum Publishers, New York, 2002

and particulate concentrations often exceeding the WHO air quality guidelines. Increased use of biofuels, especially in the rural regions of the developing countries, pose severe human health concerns due to increased particulate pollution both indoors and outdoors. Every year, Asian urban centers prone to air pollution incur hundreds of millions of dollars in health and economic damages (OECD, 2000). Presently, the urban air pollution problems in Asia are continuing to increase and air pollutants originating from urban regions are now recognized as increasing sources of regional- and global-scale pollution (Streets et al., 1999).

This study is an effort to understand the nature of growing emissions from the urban centers of Asia, to characterize the impact of these emissions on trace gas species at urban and regional scale. And finally, to evaluate costs and benefits of implementing emission reduction techniques for sulfur, particulates and NO_x for Asian megacities.

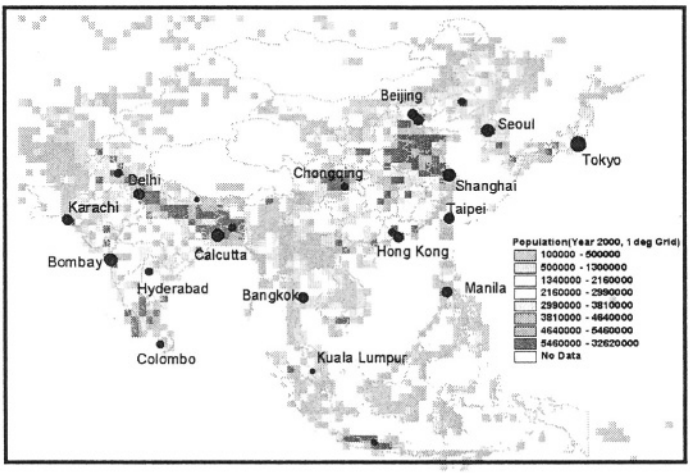

Figure 1. Asian Population in 2000 overlaid with Asian Megacities and urban centers (LandScan 2000[1])

2. MEGACITY EMISSIONS

Emissions of SO_2 and NO_x were estimated through the establishment of emission factors (emissions per unit of energy consumption) by energy source and by sector of energy use, as part of the RAINS-Asia project (Arndt et al., 1997 and van Aardenne et al., 1999). In the case of "business as usual" energy consumption, the projections show an increase of SO_2 and NO_x emissions in the Asian region in 2020 to 2-3 times the levels of 1990 (Foell et al., 1995 and van Aardenne et al., 1999). The fact that the megacities and urban centers in Asia cover less than 1% of the landcover and still produce 10-20% of trace gas emissions signifies their importance.

[1] LandScan 2000, Global Population at 30 Arc Second Grid, developed by Oak Ridge National Laboratory, United States Department of Defense, March 2001.

For 1990, at a 1° x 1° resolution, grid cells containing Karachi, Bombay, Calcutta, Bangkok, Singapore, Jakarta, Manila, Hong Kong, Beijing, Shanghai, Chongqing, Taipei, Seoul and Tokyo each had emissions in excess of 0.1 Tg SO_2 per year (Guttikunda et al., 2001a). Figure 2 presents growth in sulfur emissions for six of the megacities in Asia – Bangkok, Delhi, Jakarta, Seoul, Beijing and Shanghai. Not all the urban centers have had an increase in sulfur emissions in the recent years. Increased pollution awareness campaigns, stringent industrial and power sector pollution control regulations, use of low sulfur coal, implementation of desulfurization techniques and periodic monitoring resulted have in significant reductions of sulfur emissions in some countries. The megacities of East Asia have had a slower increase in emissions from year-to-year for 1990-1997 than any other region, with some cities even showing an average decrease of emissions. The megacities in Japan and Korea have shown an average decrease while the megacities in China had an average annual growth rate of 1.7% in sulfur emissions since 1990.

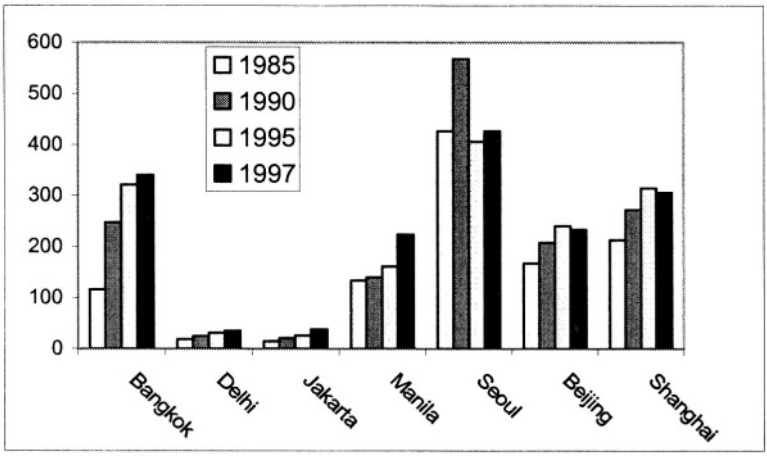

Figure 2. SO_2 Emissions from the Megacities of Asia, ktons/yr

NO_x Emissions has its sources in large industry such as chemical manufacturers, and combustion sources such as power plants burning fossil fuels; automobiles, trucks and buses; and off-road engines such as aircraft, locomotives, construction equipment and gasoline-powered lawn and garden equipment (van Aardenne et al., 1999). In the last decade, NO_x emissions have increased significantly in Asia due to increased mobile sources. Figure 3 presents NO_x emissions for 1990 and projected levels in 2020 for the same six megacities in Asia. In general, emissions are expected to increase 2-3 fold throughout Asia. Besides, NO_x, VOC emissions from industries and automobiles have portrayed an increasing trend, which plays an important role along with NO_x species in enhanced photochemical activity in urban environments. The transportation sector has emerged as a critical source of NO_x, VOC and particulate pollution in the urban centers of Asia. Figure 4 presents percentage contribution from the transportation sector to NO_x emissions in six cities. The contributions varied from as low as 10% for Beijing and Shanghai to as high as 80% for Bangkok and Jakarta in 1990. In 2020, percent

contribution increased atleast 2% for each of the cities and more than tripled for Beijing and Shanghai. In Seoul, it is projected that there will be more stringent controls for NOx and VOC emissions from automobiles by 2020, reducing its contribution.

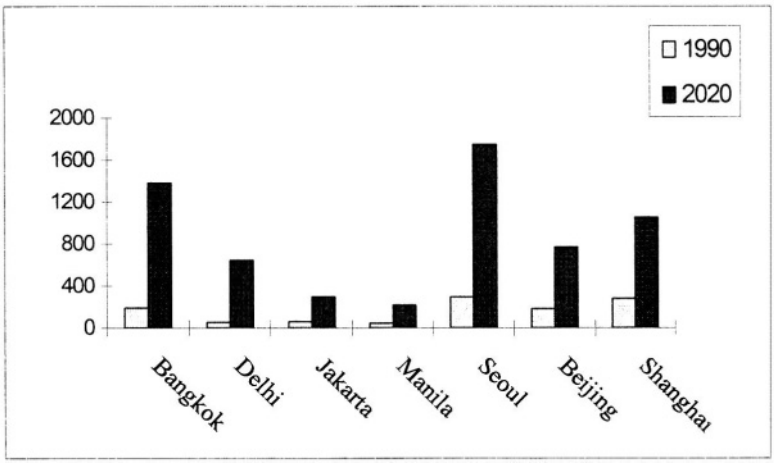

Figure 3. NO_2 Emissions from the Megacities of Asia, ktons/yr

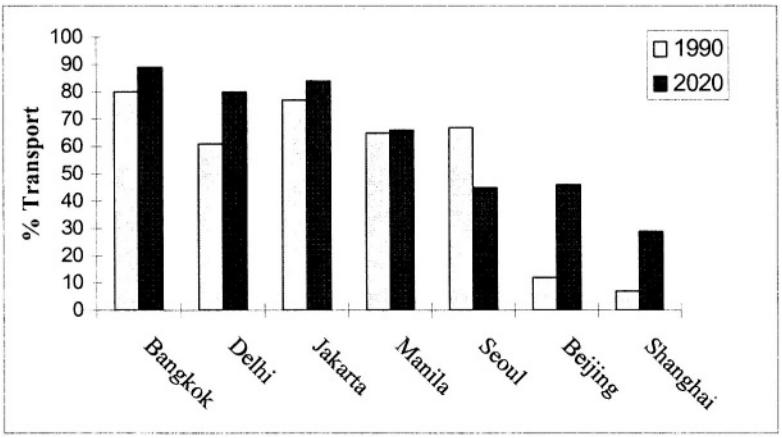

Figure 4. Percentage of NO_2 Emissions coming from the transportation sector in the Megacities of Asia

Though environmental controls are beginning to be implemented in Asian cities, they are insufficient to counteract the growth of emissions (Streets et al., 1999). For a decrease in emission to be realized, the rate of decrease in emissions per unit fuel must exceed the rate of increase in fuel use. However, costs of emission controls are high and the demand for energy is growing, and a balance between economic growth and pollution control is difficult to achieve in developing regions.

3. GCTM SIMULATIONS

The Global Chemistry Transport Model (GCTM) at Geophysical Fluid Dynamics Laboratory (GFDL), Princeton University, was applied to gain an improved understanding of the contribution of growing anthropogenic emissions from the Asian megacities and urban centers on global tropospheric chemistry. In the past, the GCTM was applied to study the nature and frequency of pollution transport from Asia across the Pacific Ocean and impact of Asian fossil fuel combustion on tropospheric chemistry (Yienger et al., 2000). For this study, 27 urban centers, represented in Figure 1 were included, which accounted for 17% of the total NO_x emissions in Asia in contrast to their <1% coverage of landcover. At a global scale, these 27 Asian cities accounted for ~7% of the global anthropogenic NO_x inventory totaling to ~1.54 Tg N/year in 1990. We have conducted simulations for the present and year 2020 emission levels compared to a reference run excluding the Asian megacity and urban center air pollution. Figure 5 presents the percentage contribution due to fossil fuel combustion in Asian urban centers to NO_x and CO levels at 550 mbar and 990mbar respectively. Under present case scenario, average contribution to NO_x levels varied from 4-10% across the Pacific Ocean in the springtime. Contribution to ground level CO concentrations was as high as 10% in the Southeast Asian region.

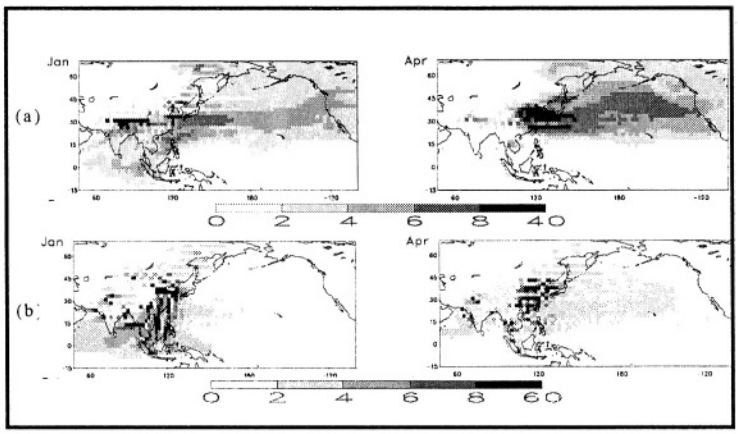

Figure 5. Percentage of contribution to (a) NOx levels at 550mbar (b) CO levels at 990mbar from the Megacities of Asia, present case.

Under a futuristic scenario, the model was run with tripled Asian megacity NO_x emissions and keeping the rest of the fossil fuel emissions constant. An average contribution of ~10% in CO levels is observed from the urban centers signifying the Asian megacity plumes reaching areas away from the source regions. Also, increased photochemical activity due to urban emissions is observed where ozone concentrations of upto 4 ppb were predicted over Indian and Pacific Ocean and Southeast Asia originating from the urban centers. A more detailed animation of GCTM results is available here http://www.cgrer.uiowa.edu/vis5d/index.html

4. INTEGRATED ASSESSMENT OF URBAN AIR QUALITY

Global and Regional scale long-transport models play a critical role in understanding the transport and chemical transformation of trace gas species and particulates. Long range transport models also play a key role in environmental management, in that they link emissions to concentrations, and thus are used to evaluate the impact of emerging energy policies and to analyze the environmental and health effects and the economic benefits of emission abatement options for reducing SO_2, NO_x, VOC and particulate matter emissions. The management of emissions in Asia megacities requires a better understanding on emission sources, distribution and their controls. For this study we developed a conceptual **I**ntegrated **A**ssessment **M**odeling **S**ystem (IAMS), for Asian megacities, which provides a methodology for identifying interactions between environmental drivers (pollutant concentrations and depositions) and endpoints like human health, environmental and structural damage (Guttikunda et al, 2001b).

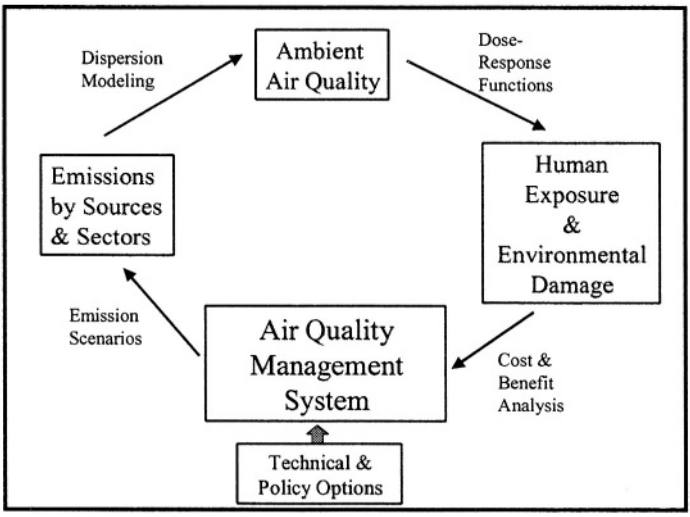

Figure 6. Integrated Assessment of Urban Air Quality

In continuing support of the integrated assessment modeling of air pollution in Asia, which started as part of the RAINS-Asia (**R**egional **A**ir pollution **IN**tegration and **S**imulation – **Asia**) project, the analysis of air quality management studies are extended to include particulates and megacities of Asian developing countries. Figure 6 presents an outline of the modeling system. IAMS has a similar structural framework as RAINS but focuses more on the urban air quality management. Model framework includes a grid-to-grid transfer matrix (generated using lagrangian puff transport model, ATMOS (Arndt, 1997)) for sulfur and particulate concentration and deposition, combined with health and environmental damage assessment and cost-benefit analysis. The framework can be adapted to any urban area of interest enabling a) dispersion modeling of sulfur and particulates b) quantifying costs and benefits of available control strategies c) assessing effects of possible change in energy end-use patterns, technology changes d) assessment

of control options by economic sector e) analysis of pollutant levels in an annual or seasonal time frame. IAMS model was successfully applied to the City of Shanghai China.

Table 1. Summary of Pollution Control Scenarios and Cost-Benefit Analysis for the City of Shanghai, China.

2020 Scenario ==>	C1	C2
% Emission Reduction	Industrial	Power Sector
Sulfur	14	41
NOx	6	13
TSP	9	3
PM10	12	4
PM2.5	13	4

2020 Scenario ==>	C1	C2
Total # of Deaths Avoided	1771	2789
Total # of Chronic Bronchitis Cases Avoided	1106	1740
Total # of Hospital Visits Avoided	60752	95619
Total # of Emergency Hospital Visits Avoided	30603	48166
Total # of Hospital Admissions Avoided	27433	43177
Total Control Costs (US $ in millions)	94	395
Total Benefits Due to Human Impacts Avoided (in millions US $)	106 - 887	168 - 1, 396
Median	265	419
Health Benefit to Scenario Cost Ratio	1.1 - 9.4	0.4 - 3. 5

Two scenarios were evaluated for 2020 for the city of Shanghai, China. Industrial scenario (C1), assumes industrial use of coal is banned in Shanghai City by 2020, of which 75 percent is shut down. And of the remaining 25% coal use is relocated and replaced to the four neighboring counties, the replacement occurs in the future in the form of new industrial boilers erected in existing facilities to increase production capacity in the city and no new plant built, but only boilers. Power Scenario (C2), assumes all new power plants coming online in the period of 2010-2020 are state-of-the-art IGCC, in combination of low-sulfur coal and some limited FGD. For health benefit analysis, dose response functions for mortality and morbidity and willingness to pay statistics were collected from various studies conducted in China and else where. Table 1 presents summary of the control scenarios and cost benefit analysis of the scenarios (Guttikunda et al 2001b and Streets et al, 2001). Cost benefit analysis is conducted for PM_{10} concentrations only with sulfate concentrations from sulfur dispersion modeling added as a surrogate to secondary particulate concentrations.

5. CONCLUSIONS

Urban air pollution in Asia has worsened in the developing countries, a situation driven by population growth, industrialization, and increased vehicle use. With an estimated 3 billion (~55%) urban residents in Asia in 2025 in <5% of the Asia's land cover and human health effects as a primary measure urban environments are the first to react to any of the pollution control regulations. Modeling activities were conducted to understand and characterize the urban air pollution in Asia at local, regional and global scales. GFDL/GCTM simulations under two scenarios were conducted to establish the impact of growing NO_x emissions on regional photochemical activity where contributions of >10% for CO and NO_x at ground level were predicted. Given the growing importance of urban air quality management, we have applied a conceptual integrated assessment modeling system to conduct cost-health benefit analysis for various pollution control options in the city of Shanghai, China. IAMS was applied for PM_{10} ground level concentrations with sulfate concentrations as a surrogate for secondary particulates. In future, we would like to conduct integrated assessment including other secondary components like nitrates, and secondary organic aerosols. Further advancements in modeling activities like nested grid analysis, will help better understand and manage the urban air quality whose influence on regional and global air quality is growing more than ever.

6. REFERENCES

Arndt, R., 1997, *The Role of Sulfur Emissions in Asia's Environmental Change: Analysis on a Regional and Urban Scale,* Ph. D thesis, The University of Iowa, USA.

Arndt, R. L., Carmichael, G. R., Streets, D. G., and Bhatti, N., 1997, Sulfur dioxide emissions and sectorial contributions to sulfur deposition in Asia', *Atmos. Env.,* **31**, 1553.

Foell, W., Green, C., Amann, M., Bhattacharya, S., Carmichael, G., Chadwick, M., Cinderby, S., Haugland, T., Hettelingh, J.-P., Hordijk, L., Kuylenstierna, J., Shah, J., Sherestha, R., Streets, D., Zhao, D., 1995, Energy use, emissions, and air pollution reduction strategies in Asia, *Water, A ir, and Soil Pollut,* **85**, 2277.

Guttikunda, S. K., Thongboonchoo, N., Arndt, R. L., Calori, G., Carmichael, G. R., and Streets, D. G., 2001a, Sulfur deposition in Asia: Seasonal behavior and contributions from various energy sectors, *Water, Air and Soil Pollut,* **131**, 383.

Guttikunda, S. K., Carmichael, G. R., Streets, D. G., and Amann , M., 2001b, An integrated assessment modeling system (IAMS) for sulfur and paniculate air pollution in the megacities of Asia, Technical report submitted to International Institute of Applied Systems Analysis (IIASA), Laxenburg, Austria.

OECD, 2000, *Ancillary Benefits and Costs of Greenhouse Gas Mitigation,* Proceedings of an IPCC Co-sponsored workshop, 27-29 March 2000, in Washington DC, USA.

Streets, D. G., Carmichael, G. R., Amann, M. and Arndt, R. L., 1999, Energy consumption and acid deposition in northeast Asia, *Ambio,* **28**, 135.

Streets, D. G., Guttikunda, S. K., Li, J., Chang, Y-S., Carmichael, and G. R., 2001, Integrated assessment of air quality impacts in Asian cities: SO_2, NO_x, and Particulate Matter in Shanghai., In preparation,

van Aardenne, J. A., Carmichael, G. R., Levy, H., Streets, D. G., and Hordijk, L., 1999, Anthropogenic NO_x emissions in Asia in the period 1990-2020, *Atmos Env,* **33**, 633.

Yienger, J. J., Galanter, M. K., Holloway, T. A., Phadnis, M. J., Guttikunda, S. K., Carmichael, G. R., Moxim, W. J., and Levy, H., II, 2000, The frequency and nature of air pollution transport from Asia to North America, *J of Geophy. Res.,* **105**, 26, 931.

DISCUSSION

A. HANSEN Although your integrated analysis shows promise, I would take issue with the health benefits associated with reductions in particulate sulfate, since epidemiological studies of associations between components of PM10 or PM2.5 and mobility and mortality show no increased risk associated with sulfate.

S. GUTTIKUNDA I agree that mortality and morbidity show less increased association with sulfate concentrations alone, but chemical composition of PM2.5 and PM10 in Asian cities, especially in cities like Shanghai, Seoul have shown that the secondary particulate concentration in the form of sulfate and nitrate is significantly high which in turn prompts us to look into combinedimplications of controlling particulate, Sulfur and NOx emissions.

This page intentionally left blank

TRANSBOUNDARY EXCHANGE OF SULFUR POLLUTION IN THE REGION OF SE EUROPE

Dimiter Syrakov, Maria Prodanova*

1. INTRODUCTION

The Co-operative Programme for Monitoring and Evaluation of the Long-Range Transmission of Air pollutants in Europe (EMEP) was lunched to serve the Convention on Long Range Transboundary Air Pollution. This convention, signed in 1979, is one of the central means for protection of our environment. It establishes a broad framework for co-operative action on reducing the impact of air pollution and sets up a process for negotiating concrete measures to control emissions of air pollutants through legally binding protocols. The main objective of the EMEP programme to is to regularly provide parties under the Convention with qualified scientific information. EMEP have three main tasks: (1) collection of emission data, (2) measurements of air and precipitation quality and (3) modeling of transport and deposition of air pollution. Three main bodies are established for their implementation. The co-ordination and intercallibration of chemical air quality and precipitation measurements are carried out at the Chemical Coordinating Centre (CCC). The storage and distribution of reliable information on emissions is the duty of the Meteorological Synthesizing Centre-West (MSC-W). The MSC-W is also responsible for the modeling assessment of acid and photooxidant pollutants. The modeling development for heavy metals and POPs is responsibility of the Meteorological Synthesizing Centre-East (MSC-E). Initially, all model estimates were performed for a grid with 150-km step covering mainly Europe. Last years the region was enlarged and the resolution was improved to 50 km.

In this paper the EMEP methodology for estimating the exchange of pollution between countries is applied on finer grid for the region of southeastern Europe. A model called EMAP is used to estimate the sulfur deposition over Balkan peninsula for 1995 due to Bulgarian and Greek sources. As only sources over these two countries are handled the

• Dimitar Syrakov, Maria Prodanova, National Institute of Meteorology and Hydrology, Bulgarian Academy of Sciences, Sofia, Bulgaria.

Air Pollution Modeling and Its Application XV, Edited by
Borrego and Schayes, Kluwer Academic/Plenum Publishers, New York, 2002

results can be considered as an estimate of Bulgarian and Greek impact in the acid pollution of the region as well as an estimate of the reciprocal pollution.

SHORT DESCRIPTION OF EMAP MODEL

EMAP (**E**ulerian **M**odel for **A**ir **P**ollution) is a 3D simulation model, which allows describing the dispersion of multiple pollutants (BC-EMEP 1994-1997; Syrakov 1995, 1997b). The processes as horizontal and vertical advection, horizontal and vertical diffusion, dry deposition, wet removal, gravitational settling (aerosol version) and simplest chemical transformation (sulfur version) are accounted for. Within EMAP, the semi-empirical diffusion-advection equations for scalar quantities are treated. The governing equations are solved in terrain-following coordinates. Non-equidistant grid spacing is settled in vertical directions. The numerical solution is based on discretization applied on staggered grids. Conservative properties are fully preserved within the discrete model equations.

Advective terms are treated with a Bott-type scheme called TRAP (Syrakov 1996, 1997a; Syrakov and Galperin 1997b). Displaying the same simulation properties as the Bott scheme (explicit, conservative, positively definite, transportive, limited numerical dispersion) the TRAP scheme occurs to be several times faster. The advective boundary conditions are zero at income flows and "open boundary" - at outcome ones. Turbulent diffusion equations are digitized by means of the simplest schemes - explicit in horizontal and implicit in vertical direction. The bottom boundary condition for the vertical diffusion equation is the dry deposition flux; the top boundary condition is optionally "open boundary" and "hard lid" type. The lateral boundary conditions for diffusion are "open boundary" type. In the surface layer (SL), a parameterization is applied permitting to have the first computational level at the top of SL. It provides a good estimate for the roughness level concentration and accounts also for the action of continuous sources on the earth surface (Syrakov and Yordanov 1997). The simplest decay approach is applied for wet removal, coefficient depending on pollutant properties and on rain intensity. The gravitational settling and the wet removal of pollutants carried by aerosols are described on the base of Galperin's parameterization (Syrakov and Galperin 1997a).

The emissions are provided in mass units per second. For the high sources called Large Point Sources (LPS) {i, j, h, strength} is necessary, for the area sources (ARS) {i, j, strength} is required.

Only 850 hPa U-, V- and θ-fields as well as surface θ-field are necessary as meteorological input, θ being potential temperature. A simple PBL model (Yordanov et al. 1983) is built in EMAP producing U-, V-, W- and K_z-profiles at each grid point. It provides also u_* and SL universal profiles needed by the SL parameterization scheme.

EMAP model was validated in the frame of ETEX-II study: it was ranged 9th among 34 models (Syrakov and Prodanova 1997). It was also validated in EMEP/MSC-E intercalibrations of heavy metal models (Syrakov and Galperin 1997a; Gussev et al. 2000).

3. SULFUR PARAMETERIZATION AND MODEL PARAMETERS

Here, the simplest sulfur model is used. Two airborne species of sulfur are considered - gaseous sulfur dioxide SO_2 and particulate sulfate $SO_4^{=}$. The sources emit SO_2 only. In the air SO_2 is transformed to sulfate with constant transformation rate $\alpha_{tr}=0.01\ h^{-1}$ for winter and $\alpha_{tr}=0.04\ h^{-1}$ for summer. Both species are objects of dry and wet removal. The dry deposition velocity for SO_2 is set to $V_d=0.01$ m/s over land and $V_d=0.03$ m/s over seas. For $SO_4^{=}$ these values are 0.02 and 0.06 m/s, respectively. The wet removal constant is set to $\gamma=0.3\ mm^{-1}$ for SO_2 and $\gamma=0.3\ mm^{-1}$ for $SO_4^{=}$.

4. MODEL DOMAIN AND INPUT FIELDS

The aim of this modeling is to estimate the sulfur pollution in the region of southeastern Europe, taking a territory of 8x9 EMEP's $150x150\ km^2$ grid cells with Bulgaria in the center. Every cell is divided to 36 $25x25\ km^2$ cells. The chosen territory includes entirely Albania (ALB), Bulgaria (BUL), Moldova (MOL) and Marmara sea (MRS), almost all Greece (GRE) - only the most southern islands are out domain, parts of Romania (ROM), Turkey (TUR), Yugoslavia (YUG), Ukraine (UKR), Black (BLS), Adriatic (ADS) and Aegean (AES) seas. In the applied version of EMAP, a 5-layer structure is used. The first four layers have representative levels at 50, 200, 650 and 1450 m with layer boundaries 20-100, 100-375, 375-995, 995-1930 m. The 5th layer accounts parameterically for the free atmosphere. In spite it can contain some mass, the volume of this layer is so big that the concentration tends to be zero, there.

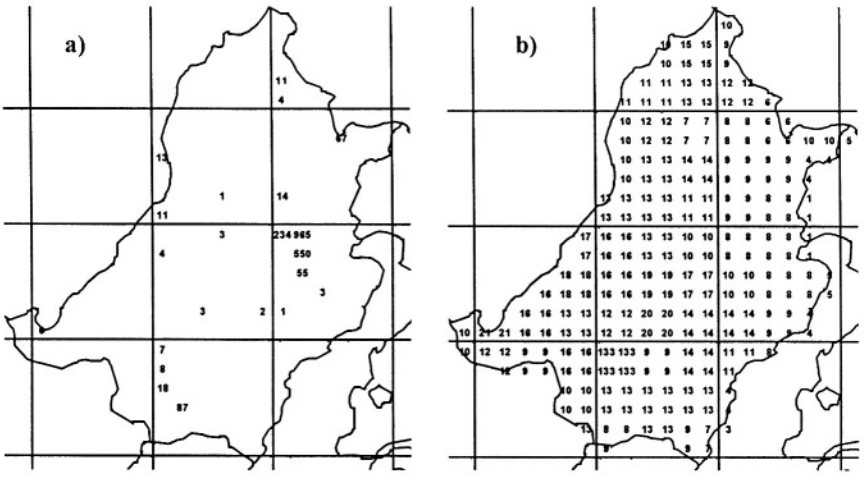

Figure 1. Bulgarian sulfur pollution sources for 1995: a) Large point sources [10 g S/s]; b) Area sources [g S/s]

Two kinds of input are necessary for EMAP performance - emissions (source input) and meteorology.

4.1. Source Input.

The sources are determined through emission inventory based on the CORINAIR methodology. The SO_2 sources of Bulgaria are shown in Fig.1.

They correspond to the official 50x50 km^2 data reported to EMEP/MSC-W by Bulgarian authorities. Additional redistribution of this data is made over the finer grid of 25 km step. The most powerful source in the country is "Maritsa Iztok" - a set of 3 neighboring coal firing thermal power plants. They are so close to each other that occupy three 25 km cells, their total emission rate estimated $SO_4^=$.7.15 kg sulfur per second. The other sources are rather small in comparison with these ones. As all LPS are supplied with high stacks, the emission of these sources is prescribed to be released in layer 2, i.e. between 100 and 375 m. The total amount of sulfur emission of Bulgaria for 1995 is estimated to 748.6 kt S (kilotons); 651.14 kt S due to large point sources and 97.5 kt S - to area sources.

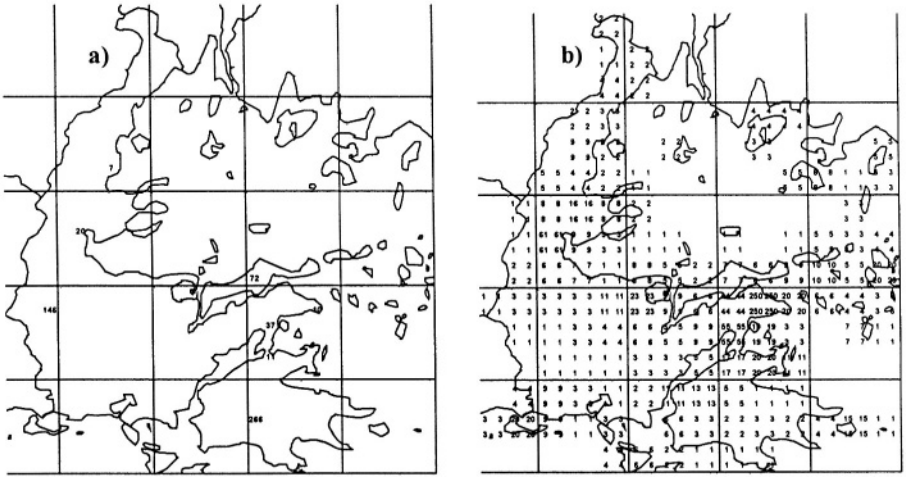

Figure 2. Greek sulfur pollution sources for 1995:a) Large point sources [10g S/s], b) Area sources [g S/s]

The information of Greek sources for 1995 is provided by European Environmental Agency and EMEP/MSC-W as official data in 50 km resolution. Here, only simple dividing of every 50x50 km^2 cell to 4 cells is made, space distribution shown in Fig.2. The total sulfur emission of Greece for 1995 is estimated to 304.7 kt S. The amount released by large point sources is 179.3 kt S and by area sources -125.4 kt S.

As polluters, both countries have almost equal intensity (as order of magnitude), but the structure of sources is very different. 85% of Bulgarian sulfur emission is due to LPS (mainly "Maritsa-Iztok" TPP) while in Greece the emission is divided between the two kinds of sources. Bulgarian release is more than twice the Greek one; the Greek area sources emit more sulfur than Bulgarian ones. All this peculiarities together with the weather character during this particular year determine the way of exchange of sulfur pollution between Bulgaria and Greece.

4.2. Meteorology Input

The meteorology input has time resolution of 6 hours. It consists of sequence of analyzed U_{850}, V_{850}, T_{850} and T_{surf} fields and 6-hour forecast for precipitation. The standard $50x50\ km^2$ output of the "Europa-Model" of Deutscher Wetterdienst, Offenbach, Germany, distributed via the GTS of the WMO is used here.

5. CALCULATION RESULTS

Annual runs with Bulgarian and Greek sources are performed. As the calculations are made month by month, the current concentrations at the end of one month integration is input as initial field for the next month. The initial concentration for the first month of the year is obtained by integration over some final days of previous month or by spin-up procedure using the first days of the current month. The following fields are the final output: annual dry (DD), wet (WD) and total (TD) depositions, mean annual concentration in air (CA) and mean annual concentration in precipitation (CP).

5.1. Comparison with Measurements

Very few measurement data are available as to validate the calculation results. There is not any EMEP station in the region. For some period of time a background station of Bulgarian Ministry of Environment used to operate in the National Astronomic Observatory "Rojen". It is placed on a peak with 1800 m height in the Rhodopy Mountains, situated both in Bulgaria and in Greece. It must be noticed that the observation methodology was not very precise for background purposes, but the results can be used for comparison at least as order of magnitude. Here, the graphical data given in "Status of the environment of Republic of Bulgaria - 1995", Bulletin of the National Center of Environment and Sustainable Development at the Ministry of Environment, page 92. Only mean monthly SO_2 and NO_2 concentrations are presented there. In Fig.3, the measured and calculated monthly and annual SO_2 concentrations are presented together.

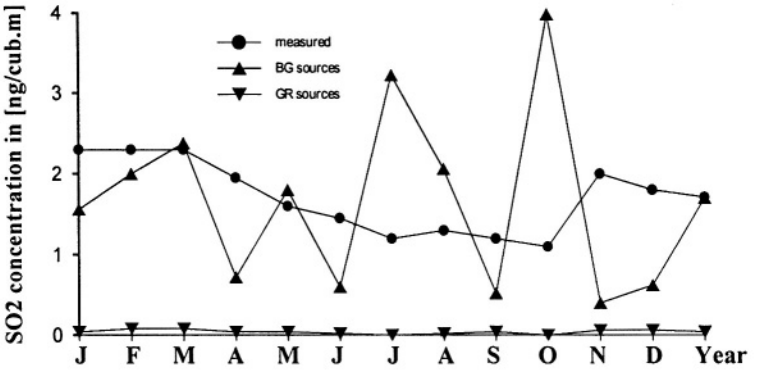

Figure 3. Monthly values of SO_2 concentrations for 1995 at NAO "Rojen" - measured and calculated on the base of Bulgarian and Greek sulfur sources.

It can be noticed from the Figure that the SO_2 concentrations created by Bulgarian sources are much larger than the concentrations created by Greek sources. The mean values in different months vary significantly in comparison with measured values steel remaining in the same order of magnitude. The differences keep less than factor of two. The annual values show remarkable coincidence - 1.71 ng/m^3 from the measurements and 1.74 ng/m^3 from calculations. All these show that the presented results can be considered reliable in some extent.

5.2. Sulfur Pollution Created by Bulgarian Sources

The space distributions of the annual concentration in air and in precipitation due to Bulgarian sulfur sources for 1995 show that the maximums are in the region of the most powerful thermal power plants "Maritsa-Iztok". A secondary maximum is observed over the region of Sofia. The impact of Bulgarian sources in SO_x pollution over Greece is relatively high. Over northern Greece the concentration levels are about one order of magnitude less than the maximums and concentrations over the other part of Greece are 1.5-2 orders less then the maximum.

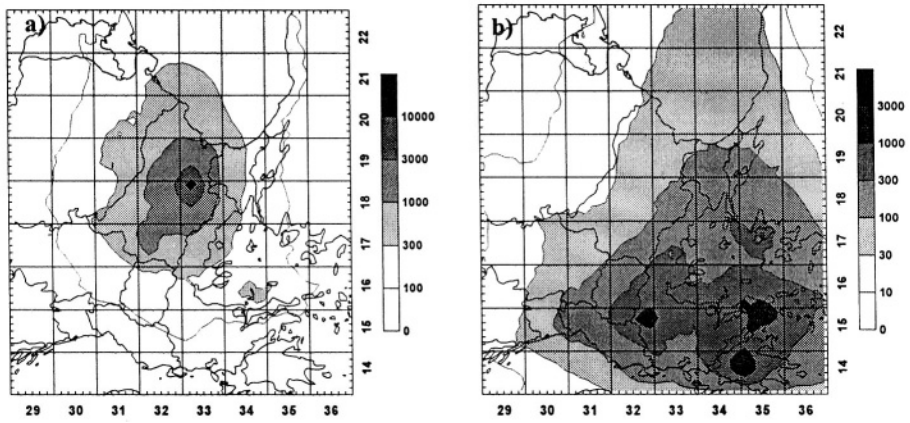

Figure 4. Total annual deposition of sulfur oxides over SE Europe for 1995 in [mg S/m^2]: a) due to Bulgarian sources; b) due to Greek sources

The total deposition of sulfur oxides due to Bulgarian sources is shown in Fig.4a and the distribution of these loads between the different territories, listed in the beginning of part 4, is displayed in Table 1, where the month-by-month variations can be seen, too. The last row and column in the table show the percentage of deposed quantities from the released one. It can be seen that about 27% from the Bulgaria emitted sulfur are deposited over the country itself; other 27% are deposited in the neighborhood; the rest goes out of the model region. Greece receives less than 4% of the produced in Bulgarian pollution, which is estimated to 28.3 kt as sulfur. This quantity is deposed mainly over the Northern Greece and on the neighboring sea regions. As to the annual variation of these loads, a not very expressed maximum can be noticed in the winter with minimum in summer-autumn.

Table 1. Bulgarian impact in sulfur pollution of SE Europe for 1995. Total deposition in [kt]. Bulgarian total emission: 748.631 kt S/year

receiver	Jan	Feb	Mar	Apr	May	Jun	Jul	Aug	Sep	Oct	Nov	Dec	**Year**	%emit
ADS	.6	.0	.4	.0	.2	.0	.1	.1	.0	.4	.0	.2	**2.1**	.3
AES	1.7	3.6	4.1	2.6	.5	.1	1.4	.5	.4	3.9	3.7	1.2	**23.8**	3.2
ALB	.4	.1	.2	.1	.5	.0	.2	.1	.0	.4	.0	.4	**2.4**	.3
BLS	8.7	4.9	3.1	2.6	1.0	1.3	.2	1.4	7.1	1.1	9.8	8.5	**49.8**	6.7
BUL	23.7	12.4	20.5	17.0	13.5	19.3	16.1	16.4	12.3	6.7	18.9	23.8	**200.7**	26.8
GRE	4.0	1.6	3.1	2.2	2.1	.9	3.9	1.6	.6	4.1	2.3	1.9	**28.3**	3.8
MOL	.2	.4	.2	.2	.3	.4	.0	.3	1.1	.0	.4	.2	**3.7**	.5
MRS	.1	.2	.2	.3	.1	.1	.0	.0	.1	.1	.3	.1	**1.8**	.2
ROM	4.8	3.0	4.1	4.1	3.1	6.6	.6	3.0	4.7	.4	3.3	7.9	**45.5**	6.1
TUR	2.2	2.9	2.2	4.0	1.5	1.6	.5	.6	1.8	1.7	3.4	1.8	**24.1**	3.2
UKR	.3	.4	.2	.2	.3	.4	.0	.2	.9	.0	.7	.3	**4.0**	.5
YUG	3.3	.4	1.8	1.1	2.1	.4	2.1	2.5	.4	1.7	.4	4.5	**20.6**	2.8
Total	**50.2**	**30.0**	**40.1**	**34.5**	**25.3**	**31.2**	**25.0**	**26.6**	**29.5**	**20.7**	**43.1**	**50.8**	**406.8**	**54.3**
%emit	6.7	4.0	5.4	4.6	3.4	4.2	3.3	3.6	3.9	2.8	5.8	6.8	**54.3**	

5.3. Sulfur Pollution Created by Greek Sources

The space distributions of the annual sulfur concentrations in air and in precipitation due to Greek sources for 1995 show that there exist two major sources in Greece, namely: the area of Attic in the south and the Greater Thessaloniki and Ptolemais area in the north. There action creates higher then in other areas concentrations and depositions as it can be seen in Fig.4b.

Table 2. Greek impact in sulfur pollution of SE Europe for 1995. Total deposition in [kt]. Greece total emission: 304.672 kt S/year

receiver	Jan	Feb	Mar	Apr	May	Jun	Jul	Aug	Sep	Oct	Nov	Dec	**Year**	%emit
ADS	.9	.1	.7	.5	.4	.1	.3	.4	.4	.4	.3	.9	**5.3**	1.8
AES	5.1	3.4	4.4	2.4	1.5	1.0	1.2	1.5	2.1	2.1	4.5	3.4	**32.7**	10.6
ALB	.6	.2	.3	.4	.6	.2	.6	.5	.5	.2	.3	1.2	**5.5**	1.8
BLS	1.1	1.0	.5	.4	.2	.0	.0	.2	.7	.0	.8	.9	**5.7**	1.8
BUL	.7	.6	.6	.4	.6	.8	.1	.4	.4	.0	.8	.9	**6.2**	2.1
GRE	5.8	2.9	5.2	4.6	3.8	3.1	4.2	4.5	3.9	3.2	5.4	6.7	**53.3**	17.6
MOL	.0	.0	.0	.0	.0	.1	.0	.0	.0	.0	.0	.0	**.2**	.1
MRS	.2	.2	.1	.1	.0	.0	.0	.0	.1	.0	.1	.1	**1.0**	.3
ROM	.1	.2	.2	.1	.2	.4	.0	.2	.2	.0	.2	.3	**2.2**	.8
TUR	1.7	1.3	1.4	.9	.5	.4	.0	.4	.9	.1	1.3	1.1	**10.1**	3.3
UKR	.0	.0	.0	.0	.0	.0	.0	.0	.0	.0	.0	.0	**.2**	.1
YUG	.7	.3	.6	.7	.8	.9	.8	1.1	.7	.1	.7	1.9	**9.3**	3.0
Total	**16.9**	**10.2**	**14.0**	**10.5**	**8.9**	**6.9**	**7.2**	**9.2**	**9.8**	**6.2**	**14.4**	**17.5**	**131.7**	**43.2**
%emit	5.5	3.3	4.6	3.5	2.9	2.3	2.4	3.0	3.2	2.0	4.7	5.7	**43.2**	.0

Table 2 shows the impact of Greek sources to sulfur pollution in the Balkans. More than one half of Greek pollution remains in the country itself. This percent is larger than Bulgarian one due to the prevailing influence of low area sources. Bulgaria receives only 2% of Greek pollution, estimated to 6.2 kt.

6. CONCLUSION

It is shown in the paper that about 4% from the emitted by Bulgaria sulfur oxides are deposited over Greek territory. The deposed quantity is estimated to 28 kt. Only 2% of Greece emitted sulfur compounds are deposited over Bulgaria, quantity estimated to 6.2 kt. It can be seen from the 10-year report of EMEP/MSC-W (Barrett and Berge, 1996) that according to their calculations the exchange of sulfur pollution between both countries is estimated right as order of magnitude, giving in the same time much more details in time and space distribution of deposed quantities. The results of such calculations can be used in decision-making, negotiating and contamination strategies development.

ACKNOWLEDGMENT

This work is done in the frame of the NATO Grant ENVIR.LG 973343.

REFERENCES

BC-EMEP (1994, 1995, 1996, 1997) *Bulgarian contribution to EMEP.* Annual Reports for 1994, 1995, 1996, 1997. NIMH, Sofia, EMEP/MSC-E, Moscow

Gusev, A., Ilyin, I., Peterson, G., van Pul, A., Syrakov, D., 2000, Long-range transport model intercomparison studies. *EMEP/MSC-E Technical Note 2/2000,* Moscow

Barret, K., Berge, E., 1996, Transboundary Air Pollution in Europe. *EMEP/MSC-W report 1/96, Part Two: Numerical Adenddum.* NMI, Oslo, pp. B3-B46

Syrakov, D., 1995, On a PC-oriented Eulerian Multi-Level Model for Long-Term Calculations of the Regional Sulphur Deposition, in: *Gryning S-E, Schiermeier F (eds) Air Pollution Modelling and its Application XI.* NATO/CMS Series, vol 21, Plenum Press, New York London, pp. 645-646.

Syrakov, D., 1996, On the TRAP Advection Scheme - Description, Tests and Applications, in: *Geernaert G, Walloe-Hansen A, Zlatev Z (eds) Regional Modelling of Air Pollution in Europe.* NERI, Copenhagen, pp. 141-152.

Syrakov, D., 1997a, An Effective Advection Scheme for Tracer Transport - Description, Properties and Tests. *Bulgarian Journal of Meteorology and Hydrology* **8**: 14-22

Syrakov, D., 1997b, A PC-Oriented Multi-Level Eulerian Dispersion Model - Model Description, *Bulgarian Journal ofMeteorology and Hydrology* **8**:41-49

Syrakov, D., Galperin, M., 1997a, A Model for Airborne Poli-Dispersive Particle Transport and Deposition, in: *Proceedings of the 22nd NATO/CCMS International Technical Meeting on Air Pollution Modelling and its Application,* June 2-6, 1997, Clermont-Ferrand, France, pp. 111-118.

Syrakov, D., Galperin M (1997b) On a New Bott-Type Advection Scheme and its Further Improvement, in: *Proceedings of the first GLOREAM Workshop,* Hass, H., Ackermann, I., eds. Aachen, Germany, September 1997, Ford Forschungszentrum, pp. 103-109.

Syrakov, D., Prodanova, M., 1998, Bulgarian Emergency Response Models - Validation Against ETEX First Release. *Atmospheric Environment* **32**:4367-4375

Syrakov, D., Yordanov, D., 1997, On the Surface Layer Parametrization in an Eulerian Multi-Level Dispersion Model, *Bulgarian Journal of Meteorology and Hydrology* **8**:74-81

Yordanov D, Syrakov, D., Djolov, G., 1983, A Barotropic Planetary Boundary Layer. *Boundary Layer Meteorology* **25**:363-373.

DISCUSSION

S. INCECIK — Could you consider the EMEP station in Turkey for your impact evaluation ?

E. BATCHVAROVA — Yes, I do. May be not in this particular study, because the station is out of the model area, but we plan to enlarge the domain as to include all Balkan countries and such an information will be very useful provided I have access to the data.

A. BAKLANOV — Your model uses the "open boundary" as the top boundary condition. As I understand it is a realisation of the PBL model with calculated flexible model top, suggested in the seventies by Yordanov, Penenko, Aloyan. Did you compare this approach with more common way of the fixed top of the model and calculated mixing height ? What are advantages and disadvantages of the used method ?

E. BATCHVAROVA — In fact, the top of the model domain is fixed to about 1500 m, no mixing layer is used.. The "open boundary" is realized as boundary condition to the vertical diffusion equation. Flux type boundary condition is set as proposed by Carmichael. Such a boundary condition is quite natural in this case where the model domain is only PBL. The gone out through the top boundary mass as well as masses going out through the lateral boundaries are controlled permanently. Comparisons with closed top boundary cases are performed giving very reasonable results.

This page intentionally left blank

REGIONAL AIR POLLUTION AND CLIMATE

Chairperson : S. Rafailidis

Rapporteur : A. Carvalho

This page intentionally left blank

$PM_{2.5}$ CONCENTRATIONS OVER EUROPE
Combining satellite data and modelling

Maarten van Loon, Peter Builtjes and Gerrit de Leeuw*

1. INTRODUCTION

Fine particles, aerosols have an adverse effect on human health at elevated levels. They also have an effect on radiative forcing and apart from black carbon will have a cooling effect. Currently the quantification of both the health and climate aspect of aerosols is hampered by the lack of adequate and sufficient observations. Concerning health effects one of the key components is the concentration of $PM_{2.5}$. At the moment $PM_{2.5}$ is the standard in the USA, in Europe it is still PM_{10}, which standard will be reviewed in 2003. In Europe very few $PM_{2.5}$ observations are performed at the moment, which makes an analysis of the present concentration levels, let alone the determination of adequate abatement strategies nearly impossible.
From satellite, the observation of the tropospheric integrated vertical aerosol content, the Aerosol Optical Depth-AOD, is possible. Modelling of the aerosol-concentrations using a 3D Eulerian grid model is also possible, with still some restrictions. The model results of the AOD have been integrated with the satellite observations by applying data-assimilation techniques. In this way a first attempt has been made to derive $PM_{2.5}$ concentrations over Europe for the month of august 1997.

2. SATELLITE OBSERVATIONS OF AOD

AOD-values have been derived using data from the Along Track Scanning Radiometer - ATSR 2-, on board the European Remote Sensing Satellite-ERS-2. The AOD over land was retrieved using the dual view algorithm developed by Veefkind et al. (1998), and the results over land were presented and discussed by Robles Gonzalez et al. (2000). Over

* Maarten van Loon (M.vanLoon@mep.tno.nl) and Peter Builtjes, TNO Energy, Environment and Process Innovation (TNO-MEP), P.O.box 342, 7300 AH Apeldoorn, The Netherlands. Gerrit de Leeuw, TNO Physics and Electronics Laboratory, P.O. Box 96864, 2509 JG The Hague, The Netherlands.

Air Pollution Modeling and Its Application XV, Edited by
Borrego and Schayes, Kluwer Academic/Plenum Publishers, New York, 2002

water the dual view algorithm may yield erroneous results (Veefkind et al., 1999b). It is based on the assumption that the ratio of the surface reflectance for the two views of the ATSR-2 is independent of the wavelength (Flowerdew and Haigh, 1995). Over land, the surface reflectance in both the forward and the nadir view is one order of magnitude higher than the aerosol reflectance and can be accurately deduced. However, over turbid coastal waters (usually referred to as case 2 waters) the surface reflectance in the nadir view is similar to the aerosol reflectance and thus the distinction between both effects becomes difficult. Therefore, over water the single view algorithm, which assumes a dark surface (Veefkind and de Leeuw, 1998), was applied to data from the forward view. Although over case 2 waters the assumption of a dark surface does not always apply, the results are more accurate than those from the dual view algorithm, and are usually within a factor of 2 of sunphotometer measurements. This may occasionally result in discontinuities in the retrieved AOD across the coast line. However, in general results from both algorithms are in good agreement with the AOD derived from ground-based sun-photometers (Veefkind et al., 1998; Veefkind et al., 1999a,1999b; Robles-Gonzalez et al., 2000).

3. MODELLING OF AOD

Modelling of aerosols have been performed by the LOTOS model. The CBM-IV gasphase chemistry has been extended with the aerosol module MADE/MARS (Ackermann et al., 1995). With this module the concentrations of the anorganic sulphate, nitrate and ammonium can be calculated. Comparison with observations from the EMEP network shows a reasonable agreement on a yearly average basis (Builtjes et al., 2001). Also the model is capable of reproducing daily averages. An example is given in Figure 1, where the modelled and observed daily average concentrations of aerosol nitrate are plotted at the location Kollumerwaard (NL) for the months June –August 1994.

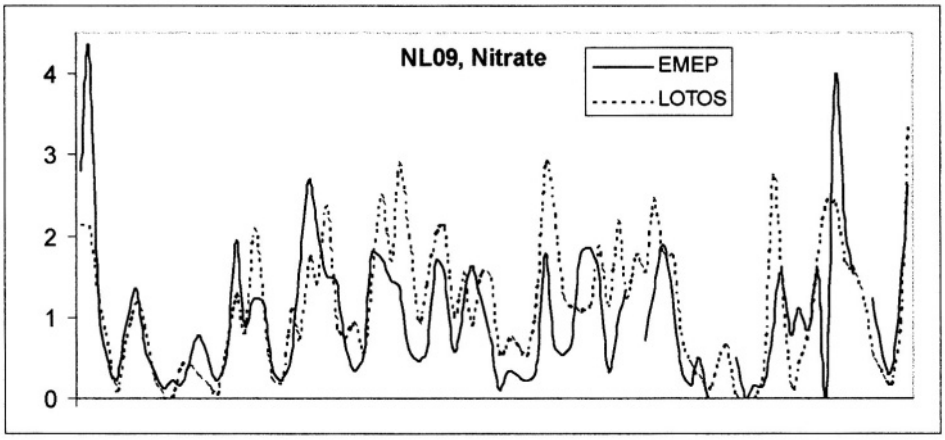

Figure 1 Modelled versus measured aerosol nitrate at the EMEP station NL09 (Kollumerwaard) in the period June – August 1994.

From Figure 1 it is seen that the model resolves the temporal fluctuations of the nitrate concentration quite reasonable. Before results of LOTOS can be compared and later assimilated with the AOD-values from ATSR, a conversion of aerosol mass concentration to aerosol optical depth has to be performed. This is done using the assumption of Ten Brink et al. (1996) that the sulphate and nitrate aerosols are in the form of their ammonium salts. Hence, the modeled AOD values are based only on the simulated concentrations of sulphate and nitrate: primary aerosol as well as organic and sea salt aerosols are missing. On the one hand this is due to the fact that the latter two are not modeled (yet) in LOTOS. On the other hand, the contribution of the primary aerosols to the total AOD could not be computed because no information is available on their extinction coefficients. Therefore we applied a factor of two to the modeled AOD in order to correct for the 'missing' aerosols. This is in agreement with ground level observations, which indicate that anorganic aerosols contribute for about 50% to the total mass of $PM_{2.5}$. We realize that this is rather crude, but doing so results into observed and modeled AOD values that are in the same range and enables the application of data assimilation. The assumption is also made that all aerosols are contained in the lower part of the troposphere (up to about 2 km). Recall that this study is only meant as a feasibility study, aimed at investigating the applicability of satellite retrieved aerosol information.

4. DATA ASSIMILATION OF AEROSOL SATELLITE DATA WITH LOTOS

Three data assimilation simulations for the month August 1997 have been carried out. Below the measurements that are used in the simulations are described, followed by a specification of the simulations and a presentation and discussion of their results. For details on the data assimilation technique used (a special version of the Kalman Filter), the interested reader is referred to Builtjes at al. (2001).

4.1 Measurements taken into account

Apart from AOD fields also ground level ozone measurements have been assimilated in two of the three simulations. The first reason to include ozone measurements is because a lot of experience with assimilation of ozone measurements into LOTOS has been obtained in a number of previous studies (see for example van Loon et al., 1999; van Loon et al., 2000). These studies showed the capability of the Kalman Filter technique to improve ozone simulations by LOTOS. The second, more important, reason is that secondary aerosol formation and ozone formation are coupled processes because both have in part the same precursors. Also, a number of overlapping (non-emitted) chemical compounds plays a role in both secondary aerosol formation and ozone production (for example HNO_3 and the OH radical). Therefore, the assimilation of ozone measurements will have a potential impact on the secondary aerosol concentrations and vice versa. Hence it is interesting to examine the behavior of the system when in addition to ozone measurements also AOD fields are assimilated.

AOD values from ATSR2 have been derived over Europe for August 1997 at the pixel size of ATSR, 1×1 km^2. The time of the overpass is at about 10:30 GMT, the frequency is once per three days. The observed AOD fields have been aggregated to averages over the

LOTOS grid cells. The LOTOS grid cells are 0.5*1.0 latlong. The standard deviation (to be used in the data assimilation) is set to 20% of the aggregated values. The number of grid cells for which an average could be determined varied from 255-700, with one exception: on August 22 only 78 grid cells were covered. Recall that only cloud-free pixels can be taken into account. This explains why the number of grid cells for which an average can be constructed is varying.

The ozone observations consisted of a selected set of measurement from the EMEP network (18) and the UBA network (9), as listed in Table 1.

EMEP code	location	EMEP code	location	UBA location
AT05	Vorhegg	GB43	Narberth	Angermuende
CH02	Payerne	GB44	Somerton	Helgoland
DK32	Frederiksborg	IE31	Mace Head	Hohenwestedt
ES03	Tortosa	NL09	Kollumerwaard	Kyritz
GB02	Eskdalemuir	NO45	Jeloya	Schwerin
GB14	High Muffles	NO52	Sandve	Teterow
GB15	Strath Vaich	PL04	Leba	Ueckermuende
GB38	Lullington Heath	SE02	Rorvik	Waldhof
GB39	Sibton	SE11	Vavihill	Westerland

Table 1 Ozone measurement locations taken into account in this study.

In principle, also aerosol sulphate and nitrate observations could have been used in the data assimilation procedure. However, the analysis has shown that the uncertainty in the nitrate observations is very large. Also, because of the fact that cloud chemistry is not included in LOTOS yet, a direct assimilation of sulphate observations and calculations might lead to dubious results. In forthcoming studies we hope to address this matter, as LOTOS is to be extended with cloud processes in the near future.

4.2 Description of the simulations

Three data assimilation simulations over the month August 1997 have been carried out. The measurements that have been assimilated in these simulations were:

- Simulation 1: retrieved AOD fields + a set of ground level ozone measurements from the EMEP and UBA network
- Simulation 2: only the retrieved AOD fields
- Simulation 3: only the ozone ground level measurements.

As is described earlier, the modeled fraction of the AOD values is estimated to be 50% of the measured values. Hence the observed values have been divided by two to account for the model fraction. In the remainder of this paper we will refer to a model simulation without data assimilation as 'model'.
In all three assimilation simulations the same noise specifications have been used. Colored noise with a correlation length of 12 hours has been added to the emission fields of NO_x, SO_x, NH_3 and VOC. The standard deviations have been set to 50%. This may seem rather

high, but one has to keep in mind that this percentage concerns the temporal (hourly) distribution of the emissions and not the yearly total. In fact the filter assumes the average emissions to be equal to the emissions prescribed by the model.

4.3 Results of the simulations

In the left panel of (Fig. 2) the simulated and observed daily averaged AOD values are plotted. Simulation 3 is omitted because it practically coincides with the model simulation (see also right panel) which does not come as a big surprise since in simulation 3 no AOD values have been assimilated. Apparently the impact of assimilation of ozone measurements on the AOD values is not large. The average for each day is computed by just averaging the observed values in all grid cells for which a value is available. In the right panel of the same figure the residue of the simulations are plotted. The residues are computed by taking the average of the cell-wise absolute difference between the simulated and the observed values.

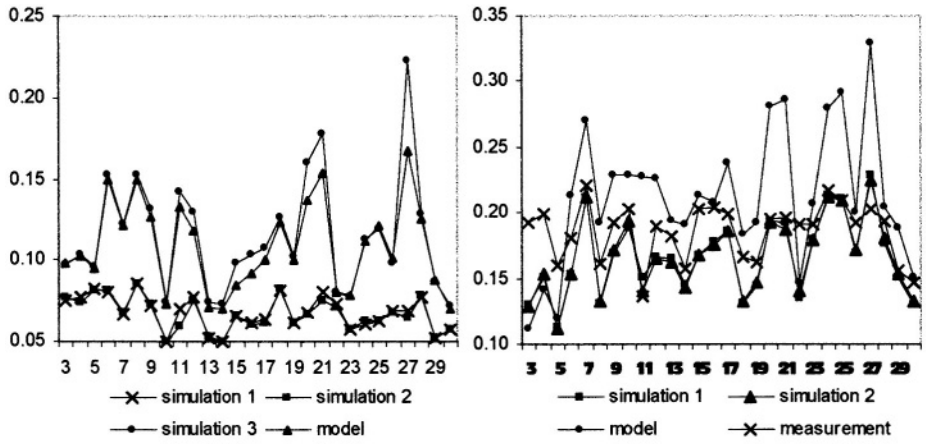

Figure 2 Modelled and measured daily averaged AOD values (left) and residues (right).

Figure 2 shows that the data assimilation system is capable of reducing the gap between the modelled and measured AOD values quite well. For the simulations in which the AOD values have been assimilated the plot in the left panel (Fig. 2) shows a decrease of the residue to about one third of the value obtained in case these values have not been assimilated. The typical behaviour in time of the AOD values is an artefact of the way of plotting: the daily averages are taken from different tracks. Recall that the frequency of the overpass of the satellite at a particular location is once per three days only.
A similar pattern is seen for the residues of the simulated ozone time series. The average residues are given in Table 2.

	Simulation 1	Simulation 2	Simulation 3	Model
Residue	8.9	11.8	8.8	11.5

Table 2 Residues of ozone (ppb) over averaged over all stations

Again we see that the residues from simulations in which ozone measurements are assimilated, are very close to each other. The same holds for the simulations in which they have not been assimilated.

5. CONCLUSIONS AND OUTLOOK

The final product of the preceding chapter is the total hour-by-hour AOD-field over Europe on grids of 0.5x1.0 lat-lon based on satellite observations and model results.
The aim of the project is to derive air quality relevant information from the satellite data. There is a clear relation of AOD with fine particles, as $PM_{2.5}$. The satellite sees in fact a large part of the $PM_{2.5}$.
Using data-assimilation, the original sulphate and nitrate AOD from LOTOS (already first multiplied with the described factor 2) have been corrected by the noise factors based on the satellite AOD. These corrected sulphate+nitrate values in the mixing layer can be seen as the best estimate of $PM_{2.5}$ concentrations which can be made using the satellite data as starting point. In Figure 3 the averaged concentrations of $PM_{2.5}$ for August 1997 are given that are determined in this way.

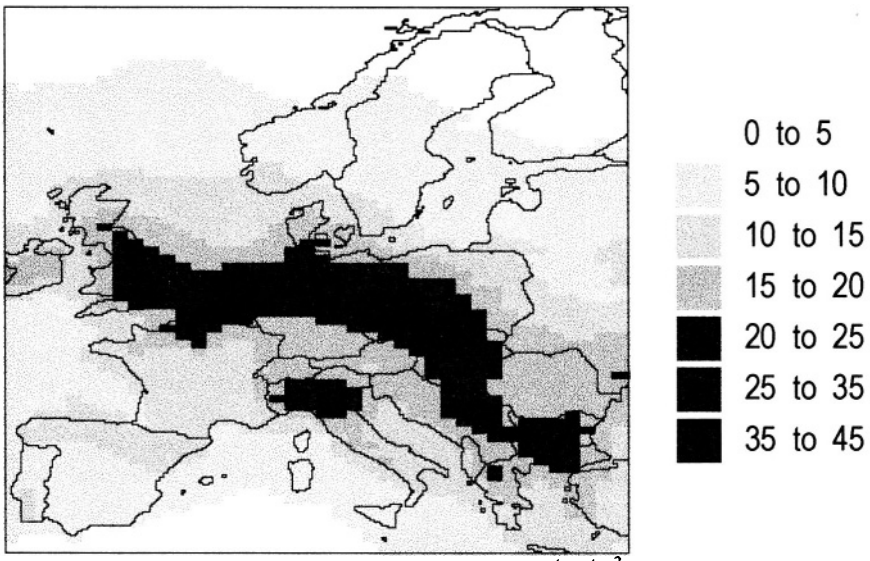

Figure 3 Preliminary estimate of the average $PM_{2.5}$ ($\mu g/m^3$) concentration for August 1997, based on ATSR-2 data.

The assessment of the overall quality and accuracy of this $PM_{2.5}$ result is difficult to give. This project has led to a method by which $PM_{2.5}$ can be determined from satellites in principle, however the current method contains many assumptions and weaknesses. They can be listed as follows:

1. The current version of the LOTOS-model contains only sulphate and nitrate aerosol,

which is only a part of the total $PM_{2.5}$. The model should be extended to include organic aerosols and anthropogenic and natural primary emissions, and the chemical composition of these to be able to determine extinction-coefficients. When the LOTOS-model is ' complete', the current factor 2 can be abandoned. Although this might not be so serious for the month of August 1997, the impact of cloud chemistry will be more important for other months.

2. The LOTOS model should be extended to incorporate cloud chemistry. Although the current underestimation of sulphate and nitrate will be compensated by applying data-assimilation, the resulting noise factors for emissions are unrealistic because the underestimation is due to the missing cloud chemistry
3. The assumption is that all aerosols contributing to the AOD-values are in the lower, say 3 km, of the atmosphere. When this is not the case, the current method will lead to an overestimation of $PM_{2.5}$
4. The current method uses only the AOD-values from ATSR-2 for inclusion in the data-assimilation procedure. Although very valuable, the amount of observations is relatively scarce, a maximum of 11 observations per month per pixel, which means on a total of 744 hours per month only in about 1.5 % of the cases (in fact the satellite observation is not an hourly averaged value, but much shorter). The use of a geo-stationary satellite would be a great improvement in this respect. In the data-assimilation also ground-level observations of sulphate could be included to improve the output of the system. The same holds for other observations, like nitrate, or $PM_{2.5}$, if they are of good quality.
5. The Angstrom coefficient which is also determined from ATSR gives an indication of the size distribution of the aerosols. This information could be used, in combination with the LOTOS-model, to improve the accuracy of the current $PM_{2.5}$ estimates
6. Calculations can be performed on fine scales by using UAM+aerosols (a nested version of LOTOS with grid sizes that can be as fine as 1×1 km^2). These results could also be assimilated with the fine-scale AOD-values from ATSR to obtain detailed information for selected areas, for example a specific city. This might improve the current $PM_{2.5}$ concentrations, and could help to determine whether the found large spatial gradients in observed AOD-values are a result of local primary emissions of $PM_{2.5}$.

In principle, all the above given 6 points can be improved upon.

The method described here is in principle working, taking all the uncertainties which could be improved upon, for granted. It should be noted that at the moment the retrieval of AOD is rather time consuming because there is no operational and automated method yet to determine whether a pixel is cloud free or not.
The method would gain in accuracy in case reliable ground level observations would be available. Lidar observations are useful to determine whether indeed all aerosols are below 3 km, but they seem not to be strictly needed for an operational method.
In conclusion, a method has been developed by which $PM_{2.5}$ concentrations can be determined at fine spatial scales, down to in principle 1x1 km2, using satellite observations. The current method might have an accuracy of only a factor 2-3. Most of the current weaknesses of the

method can be improved upon, as is indicated in the 6 points mentioned.
So, in conclusion, using satellite data in combination with a validated model with data assimilation, a method has been developed by which estimates of $PM_{2.5}$ at ground level can be determined.
The recommendation is that, referring to the points mentioned above, the method should be improved and applied to a finer grid scale. Also, a more automated method should be developed for the determination of a pixel being could-free or not.

6. ACKNOWLEDGEMENT

The project was funded by the Netherlands Remote Sensing Board (BCRS) and by the TNO internal project 'Dedicated Aerosol Retrievals using Earth Observation (DARE)'.

7. REFERENCES

Ackermann I. J., H. Hass, M. Memmesheimer, C. Ziegenbein, A. Ebel, 1995, The parametrization of the sulphate-nitrate-ammonia aerosol system in the long range transport model EURAD, Meteorol. Atmos. Phys., **57**: 101.

Brink, H.M. ten, J. P. Veefkind, A. Waijers-IJpelaan, and J. C. van der Hage, 1996, Aerosol light-scattering in The Netherlands, Atmospheric Environment, **30**:251.

Builtjes, P.J.H. et al., 2001 (in press), Aerosol Air Quality Satellite Data, Final Report of BCRS project 4.1/AP-06.

Flowerdew R. J., and J. D. Haigh, 1995, An approximation to improve accuracy in the derivation of surface reflectances from multi-look satellite radiometers, Geophysical research letters, **23**: 1693.

Loon, M. van, P.J.H. Builtjes, and M.G.M. Roemer, 1999, Reactive trace gas data assimilation – Final Report. BCRS publication USP-2 99-12.

Loon, M. van, I. J. Ackermann, M. Schaap, and P. J. H. Builtjes, 2000, Primary and secondary aerosol simulation using LOTOS, J. Aerosol Sci., **31**(Suppl. 1): S52.

Robles Gonzalez C., J. P. Veefkind, and G. de Leeuw, 2000, Aerosol optical depth over Europe in August 1997 derived from ATSR-2 data, Geophysical Research Letters, **27** (No 7):955.

Veefkind J. P., G. de Leeuw, P. A. Durkee, 1998, Retrieval of Aerosol Optical Depth over Land using two angle view Satellite Radiometry during TARFOX, Geophysical Research Letters, **25**: 3135.

Veefkind J. P., G. de Leeuw, P. A. Durkee, P. B. Russell, P. V. Hobbs, and J. M. Livingston, 1999a, Aerosol optical depth retrieval using ATSR-2 data and AVHRR data during TARFOX, J. Geophys. Res., **104** (D2):2253.

Veefkind J. P., G. de Leeuw, P. Stammes, R. B. A. Koelemeijer, 1999b, Regional Distribution of Aerosol over land derived from ATSR-2 and GOME, Accepted for publication in Rem. Sens. of the Env.

DISCUSSION

S. VARDOULAKIS — What is the reason for the large discrepancies you observed between modelling results and measurements ?

M. VAN LOON — The particular station shown in the presentation (Vredepeel, NL, EMEP station NL10) is known to be a difficult one. In general the agreement of LOTOS results with measurements is much better.
At the same time, it was shown that with small adaptations (on average) to the model input the (assimilated) concentrations as produced by LOTOS are in much better agreement with the measurements.

A. HANSEN — Have you considered varying other parameters than emissions plus PM and O_3 deposition as part of your assimilation and optimization scheme ?

M. VAN LOON — Yes. But we have not done this yet, because of the increasing computational burden. In principle, all uncertainties that are present in the model and are likely to have impacts on the quantities to be assimilated, should be taken into account. The present study therefore only shows that non-linear data assimilation of ozone and aerosols can be a powerful tool. The values of the "noise" factors should not be taken for "real" estimates of emissions and deposition velocities.

N. FOURNIER — Following the previous question concerning discrepancies between model and observation, which type of cloud chemistry description is used in the model ?

M. VAN LOON — A simple parameterisation considering mainly sulphate and ammonium chemistry, i.e. oxidation of SO_2 to SO_4 aerosols by H_2O_2 and/or ozone and NH_3 conversion into NH_4 aerosols.

A. EBEL — Is an improvement of simulated concentrations through the assimilation of observed ozone data also noticed for other chemical species, e.g. NO_x (or NO_2), which have not been assimilated ?

M. VAN LOON

In principle this should be the case. However, the model used (LOTOS) is not suited for modelling of primary species (e.g. NO_x, VOC) and is known to underestimate NO_x by a factor of 2 to 3. This is due to the mixing layer concept used in LOTOS.

SIMULATING SOIL-DUST, SEA-SALT AND SULFATE AEROSOLS IN EAST ASIA USING RAMS-ONLINE CHEMICAL TRANSPORT MODEL COUPLED WITH CAM (CANADIAN AEROSOL MODULE)

Zifa Wang, Itsushi Uno, Sunling Gong, Meigen Zhang, and Hajime Akimoto*

1. INTRODUCTION

Aerosols are currently the focus of many studies due to the large uncertainties in their indirect radiative forcing, particle pollution, and to the adverse health effects associated with them (Penner, 1993). Aerosol processes in the East Asia region are of particular interest because anthropogenic emissions in this region are increasing rapidly and supplement the natural production of mineral dust, which together play an important role in tropospheric chemistry and regional and global climate change. The particles in the continental flow over East Asia consist of a complex, partially externally mixed combination of sea-salt aerosol, combustion-derived particles, including organic and soot components, mineral dust, and biogenic non-sea-salt sulfate and organic particles (Song and Carmichael, 2001; Uno *et al.,* 2001a;b; Wang *et al.*, 1996; 2000). The outflow of Asian aerosols may affect the chemistry and radiation budgets over a large area of the North Pacific(Qian, *et al.,* 2001). However, tropospheric aerosols are poorly characterized in global and regional climate models, and thus introduce a substantial uncertainty into predictions of climate change.

To improve this situation, both intensive measurements and comprehensive physical and chemical modeling on global and regional scales are required. Since the radiative properties of an aerosol population depend on the chemical composition, size distribution, and mixing state, models that resolve these characteristics are required. In this paper, we apply an online chemistry transport model system (OCTMs) coupled with RAMS (Regional Atmospheric Modeling System) to study the evolution of aerosol particles and their physical and chemical properties in the Asian Pacific region. The model system,

* Zifa Wang, Itsushi Uno, Meigen Zhang, Hajime Akimoto, Frontier Research System for Global Change, IGCR-Yokohama, 3173-25 Showa-machi, Yokohama 236-0001, Japan. Sunling Gong, Atmospheric Environment Service, 4905 Dufferin Street, Downsview, Ontario M3H 5T4 Canada.

Air Pollution Modeling and Its Application XV, Edited by
Borrego and Schayes, Kluwer Academic/Plenum Publishers, New York, 2002

which has also been coupled with the Canadian Aerosol Module (CAM), is capable of resolving the size and composition of aerosols of multiple types and providing the regional distribution of size-segregated sulfate, black carbon, soil dust, and sea-salt aerosols over the East Asia. Simulated total aerosol concentrations were evaluated with observations from an aircraft campaign along the coast of China in May 1993. Details of the regional soil dust, sea-salt and sulfur distribution are also addressed from the simulation as a function of particle size.

2. MODEL DESCRIPTION

An on-line chemical transport model system has been developed and applied to simulate the trans-Pacific transport of yellow sand and sulfur (Uno *et al.* 2001a, 2001b). In the system, the parallel version (4.3) of RAMS is used to simulate the meteorological fields including boundary turbulence, clouds and precipitation. A general description of RAMS and its capabilities are given by Pielke *et al.* (1992). RAMS includes the Kuo-type cumulus parameterization to represent sub-grid convective cumulus and a Kessler-type microphysical model (Walko *et al.,* 1995). The surface flux calculation module in RAMS was improved on the basis of the results of Uno *et al. (*1995).

A tracer transport model and the Canadian Aerosol Module (CAM) are fully coupled with RAMS with various options for representing the physical and chemical processes describing regional- and urban-scale atmospheric pollution. This is a unique approach to provide on-line the regional meteorological conditions, such as precipitation, cloud microphysics, the turbulence in the boundary layer, and vertical diffusion, which play a significant role in the evolution of the tracers. The on-line tracer model runs with the same time step as RAMS, so all the meteorological information is directly used by the tracer transport model at every time step.

The gas-phase chemical reaction scheme used in the present work is a slightly modified version of the CBM-IV (Gery *et al.,* 1989). Values of the reaction rate coefficient are updated with recent kinetic data and a more detailed chemistry of SOx is incorporated (Wang *et al.,* 1996). The modified mechanism includes 34 species and 86 photochemical, inorganic and organic reactions. The removal term is usually separated into dry removal due to sedimentation and deposition at the surface and wet removal due to precipitation.

CAM is a size-segregated multi-component aerosol algorithm which includes major aerosol processes in the atmosphere: production, growth, coagulation, nucleation, condensation, dry deposition, below-cloud scavenging, and activation, and includes an explicit micro-physical cloud module to treat the aerosol-cloud interactions and chemical transformation of sulfur species in clear air and in clouds [*Gong et al.,* 2001]. In CAM, the mass conservation equations are written for dry aerosol mass mixing ratio while the removal rates such as dry deposition and coagulation are calculated based on wet aerosol size. At the beginning of each time step, the ambient radius of aerosols in each bin is computed according to the relative humidity and composition. Nine bins are selected for the simulation with mid-radius of 0.03, 0.06, 0.12, 0.24, 0.48, 0.96, 1.92, 3.84, and 7.68μm.

The sources include the surface emission rate of both natural and anthropogenic aerosols and production of secondary aerosols. The latter, together with particle nucleation, condensation and coagulation contribute to the clear-air process. A semi-empirical formulation (*Monahan et al*., 1986) is used to relate the size-segregated surface emission rates of sea-salt aerosols to the surface wind speed. This source function has proved reasonable in simulating sea-salt observations (*Gong et al*., 1997). The emission of other species are from GEIA and China EPA. The module treats all the atmospheric processes of five major aerosol types, i.e. sea-salt, sulfate, black carbon, organics and soil dust aerosols, as a function of particle size with a sectional representation of the size distribution. The soil dust production scheme works within CAM and includes dependencies on particle size distribution, soil moisture, vegetation, and friction velocity (Wang *et al.,* 2000). The aerosols are assumed to be internally-mixed. The hydroscopic growth of mixed aerosols is calculated with a mixing rule for soluble components and black carbon and soil dust are assumed to be hydrophobic. The dry deposition velocity of both particles and gases is averaged based on the fractional contributions from 15 land-use categories in a grid. The inclusion of an explicit cloud module in CAM establishes the linkage between the aerosol concentration and cloud/precipitation properties and enables an assessment of the indirect impact of aerosols on climate.

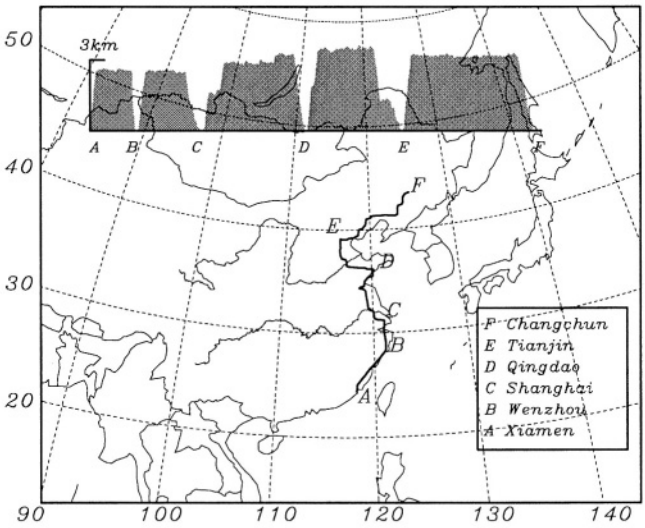

Figure 1. The model domain, flight tracks and height during the aerial survey of 25–27 May, 1993.

The simulation domain adopted is centered at 117°E, 38°N, and the horizontal grid consists of 71 by 56 grid box, with a resolution of 80 km. In the vertical it is divided into 23 layers and a terrain following coordinate has been used. An aircraft-based long-range measurement of air pollutants in the troposphere was conducted from the instrumented Yun-12 aircraft along the eastern coast of mainland China, from Changsha, Xiamen,

Wenzhou, Shanghai, Qingdao, and Tianjin to Changchun, during the time period of 25 May through 27 May 1993 (Xiao, *et al,* 1998). The tracks and flight heights during the survey are shown in Figure 1. The major items of the investigation were atmospheric SO_2, NO_X, O_3, aerosol number concentrations, airborne cloud-water collection, airborne aerosol filter sampling, and some meteorological components. The total flying time was 16hours with a travel distance of 4200 km and height between 2500-3500 m in the free troposphere (Figure 1). We perform a 3-D aerosol modeling study over East Asia utilizing the OCTMs introduced previously to investigate the distribution of aerosol particles including sulfate, black carbon, sea-salt and soil dust during the period from 22 May through 28 May. The meso-scale model has been initialized using NCEP-FNL data at 1 -degree resolution as well as sea surface temperatures.

3. SIMULATION RESULTS AND DISCUSSION

Quantitative verification of size-segregated aerosol distribution is somewhat problematic, due to lack of reliable, regional scale measurements, particularly for multiple compositions. Airborne measurement may give more detailed data and is suitable to use in process studies. The simulated aerosol concentrations along the flight track and the observed values are shown in Figure 2. Qualitatively, the model appears to represent the major peaks at Wenzhou (B), Shanghai(C), Qingdao(D), and Tianjin (E), though the values are underestimated. Relativly large concentrations of aerosols are distributed in the area between Shanghai and Qingdao. Both calculated and observed shows the same pattern. In northeast China, i.e., from Tianjin (E) to Changchun (F), the aerosols concentrations are relativly low, showing a clear sky in the late spring season.

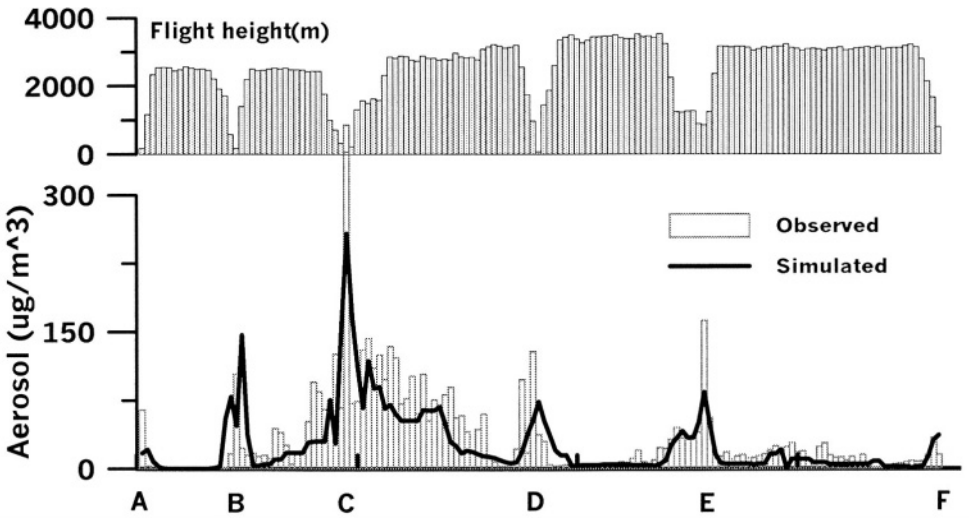

Figure 2. Comparison of simulated and observed aerosol concentrations along the flight track together with the flight height. The black line represents the simulated values. The names of city A-F are shown in Figure 1.

The evolution and fate of atmospheric aerosols are influenced by various dynamic aerosol processes, which cannot be constrained by measurements alone. Figure 3 shows the simulated and observed size distribution of aerosol particles over Shanghai at 100 meters above the surface. The two peaks are simulated well compared with the observations; one peak is mainly composed of sulfate and black carbon, and the other is mainly from sea-salt particles. The simulation results show that when the size is less than 0.12 μm, the main components of the particles are black carbon and sulfate, and for sizes larger than 1μm, nearly all the particles are sea-salt over Shanghai.

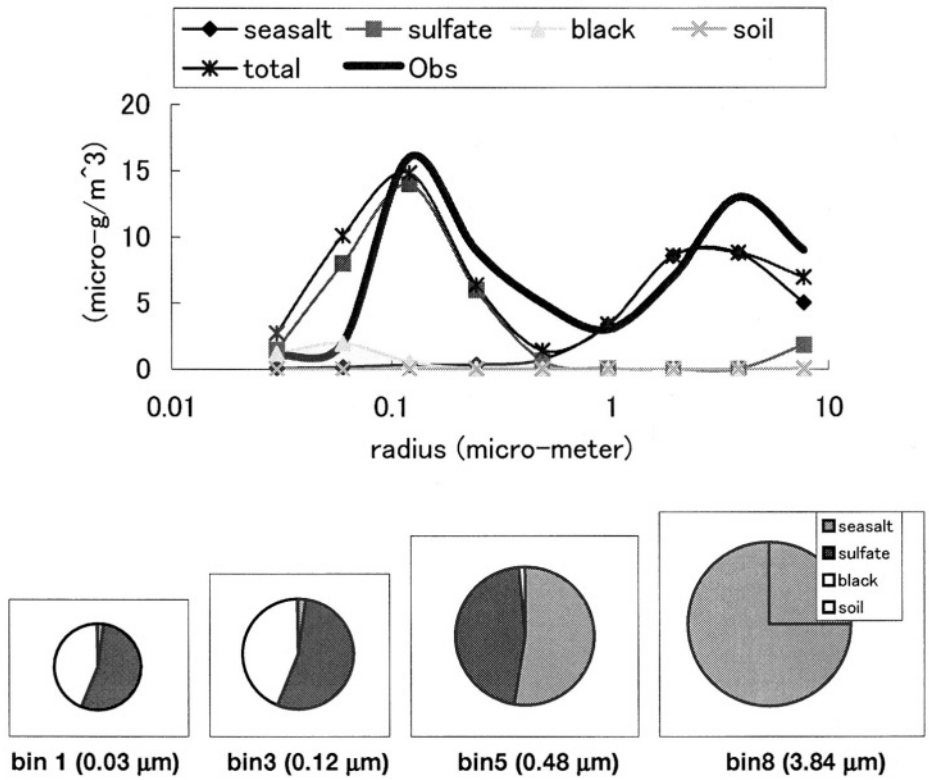

Figure 3. Simulated size distribution of the multiple-components of aerosols over Shanghai at a height of 100 meters. The thick line represents the observed size distribution. The ratio of each component in aerosol particles for bin 1, 3, 5, and 8 is also shown.

The distribution of sulfate, sea-salt, black carbon and soil dust particles in the boundary layer on May 22 are presented in Figure 4. The sulfate distribution shows clearly the high concentration regions in East China including Shanghai and the Qingdao area. The observations also show a similar pattern along the flight tracks. The sea-salt particles are mainly distributed in the Japan Sea and the area east towards Taiwan. There is also a small area with high sea-salt concentrations near Shanghai, which accounts for

the two peaks in the aerosol size distribution observed in the campaign. Soil dust aerosols are generated and distributed in northeast China with concentrations between 5-15$\mu g/m^3$. Also shown in Figure 5 is the fine and coarse mode sulfate and sea-salt. Sulfate is produced as a result of the nucleation, gas-phase oxidation, and heterogeneous oxidation of SO_2 on the surface of sea-salt particles. The distribution of size bin 5 follows SO_2 emissions closely while size bin 3 reflects to cloud patterns due to nucleation.

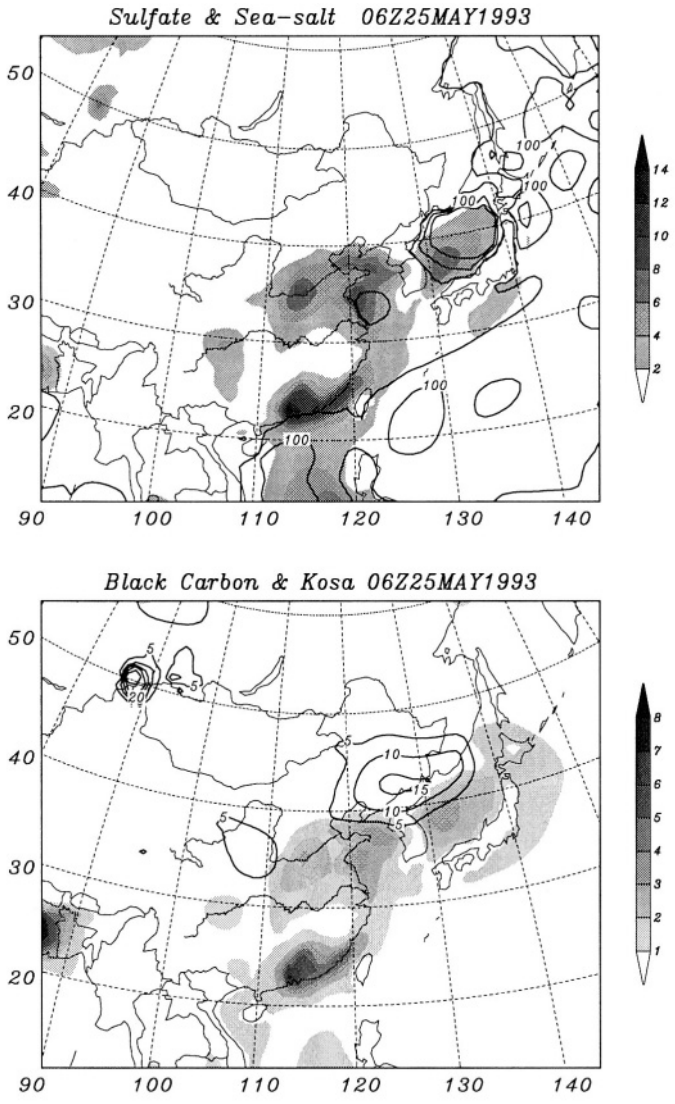

Figure 4. Calculated total sulfate (above, shaded), and sea-salt (above, line contours), black carbon (below, shaded), and yellow-sand (below, contour) distributions at 100 m at 06GMT on 25 May, 1993. The units are $\mu g/m^3$.

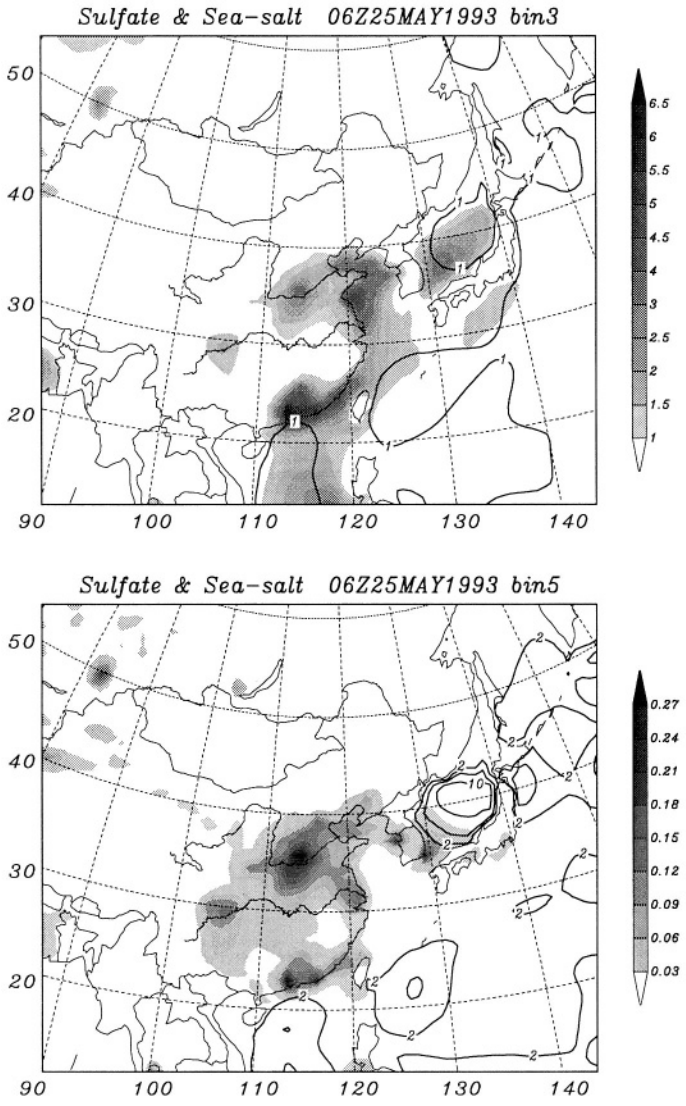

Figure 5. Calculated sulfate (shaded) and sea-salt (line contours) distributions at 100 m for size bin 3 (r=0.12 μm, above) and bin 5 (r=0.48 μm, below) at 06GMT on 25 May, 1993. The units are $\mu g/m^3$.

4. CONCLUSIONS

Soil dust, sea salt and sulfate of both anthropogenic and natural origin in East Asia are major aerosol sources that play an important role in tropospheric chemistry and regional and global climate change. A new on-line Chemistry Transport Model System

(OCTMs) is developed to simulate the regional distribution of size-segregated soil-dust, sea-salt, black carbon and sulfate aerosols in the atmosphere in East Asia. It considers advection, diffusion, chemistry, and deposition processes and is fully coupled with the Canadian Aerosol Module (CAM) and CSU-RAMS (Regional Atmospheric Modeling System. The CAM is a size-segregated multi-component aerosol algorithm which includes major aerosol processes such as production, coagulation, nucleation, condensation, dry deposition, below-cloud scavenging, and activation, and includes an explicit micro-physical cloud module to treat the aerosol-cloud interactions and chemical transformations. The soil dust production scheme works within the CAM and includes dependencies on particle size distribution, soil moisture, vegetation, and friction velocity. Simulated aerosol concentrations are evaluated against observations from an aircraft campaign along the coast of China in May 1993 and reasonable agreement is reached.

REFERENCES

Gery, M. W., Whitten, G.Z., Killus, J.P., and Dodge, M.C. 1989, A photochemical kinetics mechanism for urban and regional scale computer modeling. *J. Geophys. Res.* **94**: 12,925-12,956.

Gong, S.L., L.A., Barrie, and J.-P., Blanchet, 1997, Modeling sea-salt aerosols in the atmosphere, Part 1: Model development, *J. Geophys. Res.,* **102**: 3805-3818.

Gong, S.L., L.A., Barrie, *et. al,* 2001, CAM: Treatment of the size segregated atmospheric aerosols for climate and air quality models: 1. Module Development, *J. Geophys. Res.(submitted).*

Monahan, E.C., D.E., Spiel, and K.L., Davidson, 1986, A model of marine aerosol generation via whitecaps and wave disruption, in *Oceanic Whitecaps,* Monnhan, D., and G.M. Niocaill, ed., Redeil Publishing, Dordrecht, Holland, pp. 167-174.

Penner, J., 1993, Quantifying and minimizing uncertainty of climate forcing by anthropogenic aerosols, *technical report,* U.S. Dep. of Energy, Washington, D.C., pp.53.

Pielke, R.A., W.R. Cotton, R.L. Walko, C.J. Tremback, W.A. Lyons, L.D. Grasso, M.E. Nicholls, M.D. Moran, D.A. Wesly, T.J. Lee, and J.H. Copeland, 1992, A comprehensive meteorological modeling system-RAMS, *Meteorol. Almos. Phys.,* **49**:69-91.

Qian, Y., F. Giorgi, Y. Huang, W. Chameides and C. Luo, Regional simulation of anthropogenic sulfur over East Asia and its sensitivity to model parameters, *Tellus,* **53B**:171-191.

Song, C.-H., and G.R., Carmichael, 2001, A three-dimensional modeling investigation of the evolution processes of dust and sea-salt particles in east Asia, *J. Geophy. Res.,* **106**: 18,131-18,154.

Uno, I., S. Emori, and M. Baldi, 2001a, Chemical transport model on-line coupled with RAMS for regional chemical climate, in *Air Pollution Modeling and its Application XIV,* Grying and Schiermeier, Ed., Kluwer Academic/Plenum Publishers, New York, pp.75-85.

Uno, I., H., Amano, S., Emori, K., Kinoshita, I., Matsui, and N., Sugimoto, 2001b, Trans-Pacific yellow sand transport observed in April 1998: A numerical simulation, *J. Geophy. Res.,* **106**:18,331-18,344.

Walko, R.L., W.R. Cotton, M.P. Meyers, and J.Y. Harrington, 1995, New RAMS cloud microphysics parameterization, Part I, The single-moment scheme, *Atmos. Res.,* **38**:29-62.

Wang, Z., Huang, M., He, D., Xu, H., and Zhou, L., 1996, Sulfur distribution and transport studies in East Asia using Eulerian model, *Advances in Atmospheric Sciences* **13**:399-409.

Wang, Z., H. Ueda and M. Huang, 2000, A deflation module for use in modeling long-range transport of yellow sand over East Asia, *J. Geophy. Res.,* **105**:26,947 -26,960.

Xiao, H., Y. Wu, Z. Shen, Z. Wang, H. Lei, and L. Zhou, 1998, Aircraft-based measurements of atmospheric pollutants in the troposphere over the eastern coast of China, in *Air Quality and Atmospheric Science, Proceedings of the 6thinternational conference on atmospheric science and its applications to air quality,* Chen, Ed., China Ocean Press, pp. 398-406.

DISCUSSION

P. SUPPAN — How many size segments have you used ?

Z. WANG — Nine bins are used in the model, they are of mid-radius 0.03, 0.06, 0.12, 0.48, 0.96, 1.92, 3.84 and 7.68 μm

A. HANSEN — It appears that your model may be over-estimating nucleation in the nano-particle size range. It seems to me that in these areas of high particle loadings, you would not expect nucleation, but rather condensation on existing particles. Do you agree ?

Z. WANG — Thank you for your comments. Comparing with observations, it appears the model over-estimated nucleation in the particle size range. We need better quality observation data to evaluate the model results, especially for the size distribution and detailed checking of the micro-physical process in the CAM.

E. GENIKHOVICH — What were temporal and spatial averaging scales for measured and computed quantities ? How did you handle the fact that measurements were carried out from the moving platform and computations were not ?

Z. WANG — This is a good question. The temporal and spatial resolutions of measured data is about 5-minute and about 70 km. For the model computation, the temporal resolution is the same as in the observations, but for the spatial resolution (80 km), some interpolation errors can occur. We need to improve this as the future by using a higher resolution model or nested model.

This page intentionally left blank

NEW DEVELOPMENTS

Chairpersons :	E. Batchvarova C. Borrego S.E. Gryning R. San Jose
Rapporteurs :	K. De Ridder J. Ferreira C. Hogrefe A. Keiko

This page intentionally left blank

DATA ASSIMILATION FOR CT-MODELLING BASED ON OPTIMUM INTERPOLATION

Johannes Flemming, Eberhard Reimer, and Rainer Stern*

1 INTRODUCTION

Several studies to apply data assimilation to Chemical Transport Models (CTM) have been carried out in recent years (e.g. Elbern 1997, Loon 1997). There are comprehensive time dependent schemes such as 4D-VAR or Kalman-Bucy-Filters or more simpler 3/2D-schemes such as Optimum Interpolation and 3D-VAR. Providing initial fields for numerical weather forecasting which obey the physical laws and balance relationships has been the main motive for the development of data assimilation. The use of the techniques from numerical weather forecasting in chemistry transport modelling requires the adaptation to the special properties of the chemical concentration measurements and the CTMs.

The content of this paper is data assimilation for the Eulerian chemical transport model REM3 by means of Optimum Interpolation (OI). The focus is put on the implementation of OI for the inhomogeneous air quality data in section 4. Data assimilation with REM3 has been used for the diagnostic assessment of air quality standards according to the air quality framework directive (96/62/EC) of the European Council. An example of this work (NO2 concentrations in Germany) will be presented in section 5. Moreover, OI is employed for initialising the operational ozone forecasts carried out at the FU-Berlin.

The main result of data assimilation for Eulerian type models is an analysis of the concentrations field. The analysis is a representation of the concentration field in a certain resolution which is determined by the underlying model. It combines the fields of the model with observations. Both sources of information are blended according to their error statistics. This is a feature of all statistical based data assimilation techniques.

Optimum Interpolation (Gandin 1962) is an interpolation technique and can be compared to other spatial interpolation methods either based on statistics such as Kriging or on “purely mathematical” methods such as spline interpolation and distance density interpolation (Egmond Van 1981). The differences of the methods concern three

* Institut für Meteorologie, Freie Universität Berlin, 12165 Berlin, Germany

Air Pollution Modeling and Its Application XV, Edited by
Borrego and Schayes, Kluwer Academic/Plenum Publishers, New York, 2002

points: 1.) How are the measurement values weighted to form the value at analysis point. 2.) Whether and how the observation error is taken into account. 3.) Whether the impact of an inhomogeneous measurement network (declustering, Falke 1998) is compensated. A brief discussion of the properties and the equations of Optimum Interpolation is the content of section 3.

The performance of Optimum Interpolation depends on the efforts to determine error statistics. The proper determination of the error statistics, .i.e. the observation error variance and the background error covariance matrix, is essential for the success of the analysis scheme.

However, the application of those methods for ground based measurement of air quality data is not straight forward. One has to consider the inhomogeneous character of the concentration field due to the inhomogeneous emission patterns and the more dense net work in the urban environment. Section 4.2 deals with the determination of the error statistics for concentration data which discriminates different air pollution regimes in the measurements and in the calculated fields.

2 DESCRIPTION OF THE MODEL AND THE AIR QUALITY DATA BASE

REM3 (Stern 1994) is a transport model for the Planetary boundary layer that covers the area of Central Europe with a horizontal resolution of about 25x25 km. The vertical resolution of the model is based on three dynamically changing layers. CBM4 and SAPRC are the alternative chemistry schemes used in the model. Recently REM3 has been merged with the model CALGRID to form REM3/CALGRID - a model which offers a flexible way to treat different horizontal and vertical coordinate systems and includes aerosol modeling. Meteorological input is derived from synoptic meteorological surface data, upper air data and climatological information (Reimer and Scherer 1992). REM3 has been employed successfully for episodic applications (Hass 1997) and emission scenario calculations (http://www.umweltbundesamt.de/ozon-e). Current applications include the calculation of air quality standards for O3, NO2, SO2 and PM10 on a yearly basis according to the European Council Directive 96/62/EC. REM3 also runs operationally to forecast the ozone concentration in Central Europe since 1997 (Flemming 2001, http://trumf.fu-berlin.de/ozonprognose/).

The air quality data base has been obtained from the networks of the German states (Laender). It includes about 250 measurement sites for O3, NO2 and NO. Less measurement (about 150) are available for SO2 and TSP (total suspended matter). Additionally, measurements from other European countries have been acquired from the EMEP and the EEA data base. The data quality assurance (EU-directive) demands 90% completeness for the yearly time series. To meet this requirement about 15% (Ozone) to 50% (NO) of the data had to be rejected.

By means of a hierarchical clustering the measurement sites were classified in air quality regimes (Flemming 2001). The parameters for distinguishing the regimes are the median of the daily mean and the median of the daily variability of the time series for the years 1995-99. For each species separately regimes such as “mountain”, “rural”, “suburban”, “urban”, “urban-traffic” and “traffic” were identified.

The air quality regimes are a comprehensive climatological measure. It is fruitful to apply this concept also to modelled concentration time series. The centres of the clusters from the observed data in the parameter space were used to assign an air quality regime to every grid point of the REM3/CALGRID modelling area. The parameters for every model grid point were determined from a model run for the whole year 1999.

3 OPTIMUM INTERPOLATION

Optimum Interpolation (OI) was introduced in meteorology by Gandin (1962). It produces an analysis by correcting a first guess field that is called background. The background can be a calculated field, as in this application, a field derived from climatology or simply the mean of the measurements. An example of the application of OI for SO2 with the measured mean as background can be found in Egmond (1981).

In OI the value of the analysis x_{Ia} at grid point I is the sum of the background value x_{Ib} and the weighted mean of measurements increments from N nearby measurement sites (Eq. 1). The measurement increments at the measurement locations i=1...N are the differences between the measured value y_i and the respective background value x_{ib}.

$$x_{Ia} = x_{Ib} + \sum_{i=1}^{N} a_i \, (y_i - x_{ib}) \quad (1)$$

The vector of analysis weights a are found from minimising the variance of the analysis error with the additional constraint that the measurements and the background field have no mutual bias. This yields the following matrix equation:

$$(\mathbf{B} + \mathbf{R})\,\mathbf{a} = \mathbf{b} \quad (2)$$

B is the N x N covariance matrix of the background error at the measurement locations. **R** is a diagonal matrix containing the error variances for each observation in the diagonal line and zero elsewhere with the assumption that the observation error is not mutually correlated. **b** is a vector of the N covariance values of the background error between the measurement location and the analysis point I. Equation 2 leads to the following features of OI:

- The analysis weights a_i are mainly determined by the covariances (vector **b**) of the background error between the measurement sites and the interpolation point.
- A low error variance of an observation enhances its influences in the analysis (diagonal elements of matrix **R**).
- High covariances between the background errors at two measurements sites (off diagonal elements of **B**) reduces the individual weight of these observations.

The observation error includes the instrument error and errors due the fact that a measurement is not representative for the respective grid point value of the background (model field). The variance of the model error is a measure for the accuracy of model field at a certain point.

The covariance of the background describes the spatial relationship of the model error. Therefore it controls how far the influence of the measurement can be spread in the spatial domain.

4 EMPIRICAL MODELLING OF ERROR COVARIANCES

For the application of equation 1 the complete knowledge about the covariance of the background errors and the observation errors is needed. This is hardly feasible and therefore covariance models which describe the covariance structure under certain simplifications (homogeneity, isotropy) have to be formulated. The covariance model is formed by approximating an analytical function to empirically determined covariances. The value of the function *f(r)* at a certain separation r is used to obtain the covariance values in Equation 1. A discussion of the impact of the function type on the interpolation result is given in Daley (1991). In this work the following expression was used and the parameters C, β and ρ were obtained by a nonlinear approximation method (Marquard, 1963):

$$f(r) = C\left(\cos(\beta r) + \frac{\sin(\beta r)}{\beta \rho}\right) \exp\left(-\frac{r}{\rho}\right) \quad (3)$$

The typical simplification in almost all applications of OI is the homogeneity and isotropy of the background and observation errors statistics. This means that the background error variance is independent from the location, that its covariance is merely a function of the distance and that all observations have the same error variance. In this case the covariance model can be normalized by the error variance which yields equation 2 in terms of correlations.

The are well established methods to derive the background and observation error statistics for application in meteorology. The most common is based on the climatology of observation increments (Observational method, Hollingthworth 1986).

The common assumption homogeneity and isotropy is the main drawback for the application of OI for air quality data. Due to the irregular distributed emissions the fields of the ground level concentrations are very inhomogeneous. Moreover, the measurements sites are concentrated in the urban environments. This effects the validity of an homogeneous covariance model which will mainly reflect the situation in the urban concentration regime. The use of such a covariance model will cause the transfer of the urban air concentrations in the rural areas. Additionally, the estimation of the bias between model field and observation will be misleading when the measurements represent mainly the more polluted areas.

However, the spatial distribution of the emissions and therefore the location of the inhomogeneities is more or less fixed. It is known from emissions inventories and it is represented in the CTM fields. Compared to other inhomogeneous quantities (e.g. precipitation), this is an advantage of the air quality fields that is exploited in this work.

4.1 Observational method

In this work the observational method is used, which is based on empirical covariances of the observation increments, i.e. the differences between the observed value y_i and the modelled value x_i of the background. It assumes that the errors are Gaussian, the observation errors are uncorrelated and that there is no bias. Under these conditions the empirical covariance between two measurement locations i j equals the covariance of the background error b_{ij} and for the case i=j the observation error variance r_{ij} is added:

$$\left\langle (y_i - x_i)(y_j - x_j) \right\rangle = \begin{cases} b_{ii} + r_{ii} & i = j \\ b_{ij} & i \neq j \end{cases} \qquad (4)$$

The value of the observation error can be estimated by extrapolating a covariance model to zero separation which yields b_{ii}. The difference to the variance of the increments equals the variance of the observation error r_{ii}.

The ensemble to calculate the empirical expectation value (Eq. 4) has to be chosen according to the minimising condition of equation 1 (Egmond Van 1981). Two approaches have been used for the OI of air quality data. One relies on the instant set of measurements (α) and the other is based on time series of the observation increments (β). A comparison of the different approaches for NO2 is given in section 5.

(α): Under homogeneous and isotropic conditions a covariance model can be fitted by the data available at the time considered. The increments of the measurements within a an interval of separation are used to calculate the empirical spatial covariance directly. The covariance model is obtained from these covariance coefficients. The advantage of this approach is that no previous data are needed. The covariance model which is calculated for each analysis date reflects the change in the mean spatial variability due to temporal variations in the weather situations and the emissions. However, spatial patterns (inhomogeneity) can not be distinguished.

(β): The use of time series to calculate a empirical covariance of the background error is a common approach (Daley 1992). It leads to a large number of covariances for each pair of stations which are the base for the approximation of the spatial covariance model (Eq. 3). This type of covariance reflects more the climatological situation. The size of the ensemble allows the discrimination of different classes of covariance models (see section 4.2.)

However, the temporal covariance may lead to an overestimation of the spatial covariance due to temporal variations as the annual and diurnal cycle which have no equivalent in the spatial domain. If the increments show these variations they have to be removed by filtering.

4.2 Inhomogeneous covariance models for air quality data

The base for the development of an inhomogeneous covariance structure is the classification of the air quality regimes for both the measurements and the grid points of the model field which serves as the background for OI (see section 2). The knowledge of the air quality regime of the whole background (i.e. the modelled field) is an improvement for the interpolation performance because the covariance of the background error (**B** and **b** in Eq. 1) controls to a large extend the analysis weights. The observation error is mainly an error of representativity. In this context it quantifies how good the regime of the measurement coincides with that of corresponding background point.

The objective was to build a set of covariance models, one for each possible combination of air quality regimes in the background field. The covariance model for a given combination of regimes are supposed to have a simple distance dependency as in the homogeneous and isotropic case. The inhomogeneous character of the OI comes from the selection of the covariance model according to the combination of the regimes at the points I and i or i and j. For this reason, it reflects the inhomogeneous distribution of the air quality as it was derived from the model results.

The observational method based on times series covariances (approach β) is applied to obtain the covariance models. In order to avoid the influence of the diurnal cycle, the

covariance model is established separately for each hour of the day. The times series of the observation increments for each hour per day over the year 1999 was used to calculate an empirical covariance coefficient for each possible pair of stations (about 30000). They were used to obtain a distant dependent covariance model for every combination of air quality regimes of the background for every hour of the day.

In terms of the air quality regime each coefficient b_{IJ} is characterized by the two regimes of the background points I J and by the regimes of the two measurements. If the observation error was completely Gaussian and unbiased the observation error would cancel out according to equation 4. In this case a discrimination of the air quality regime of the observation sites for the determination of the background error covariance would not be necessary. However, a misfit in the air quality regime of the observation and the respective background point will affect the covariance of the observation increments. Therefore only increments from sites where the air quality regimes of the observation and the background is identical are used to fit the covariance model. Figure 1 shows an example of the background error covariance model for three combinations of background air quality regimes. The covariance among the urban regimes have high values for small distances and show a steep descent for larger distances. The covariance among the rural regimes indicates a relation over larger distances. The covariance function between the urban and rural regime is low and reflects the weak relationship between urban and rural regimes.

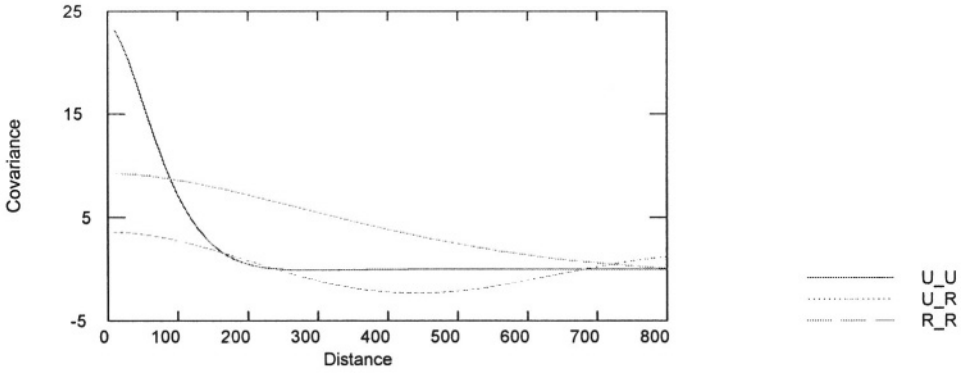

figure 1 Background error covariance models for NO2 at 7 UTC. U_U is covariance function for the combination among urban points, R_R is that among rural points and U_R that between urban and rural points.

The intersection at zero distance of the covariance model for identical regimes represent an estimate of the climatological background error variance for each regime. It is the basis to derive the observation error variance according to equation 4. The mean of the empirical variances of the observation increments for each combination of the air quality regime of the observation and the respective background is determined. By subtracting the variance of the background the observation error variance is obtained. The final result is not just one observation error variance as in the homogeneous and isotropic case but one value for each combination of the air quality regimes of the observation and the respective background point. It is a quantitative measure of the observation error due to the representativity of observation for the respective model grid point.

5 EXAMPLE: ANALYSIS OF NO2 CONCENTRATION IN GERMANY

In this section the analysis of NO2 concentrations in Germany is chosen as an example to demonstrate the application of data assimilation for the assessment of air quality. The analysis of the yearly mean concentration (1999) of NO2 in Germany was derived from hourly analyses of the NO2 field that were obtained from the modelled field (REM3) and the observations in Germany by OI. Due to the fact that the analysis represents a resolution similar to that of the model, subscale features (i.e. hot spots in street etc.) are not present in the analysis. However, this is not a real drawback because the objective is to present a nation wide overview about the air quality.

The measurements of 8 stations that are the nearest to the analysis grid point were selected for the analysis according to equation 1. The number of 8 stations was found by testing: more stations do not change the analysis result significantly – less stations would be in disagreement with the scale of the analysis.

The OI scheme was employed alternatively using the approach with homogeneous (α in section 4.1), respectively with inhomogeneous (β, described in section 4.2) covariance modelling. The resulting analysis of the yearly mean of the NO2 concentration is depicted in figure 2. The most obvious difference between the two pictures can be seen in the mean concentration in the more rural areas of Germany: The inhomogeneous approach avoids that the concentration measured mainly in cities is interpolated into the rural areas. However, in the large urban areas such as the Upper Rhine Valley or Berlin, the concentrations are the same or even higher then in the homogeneous approach.

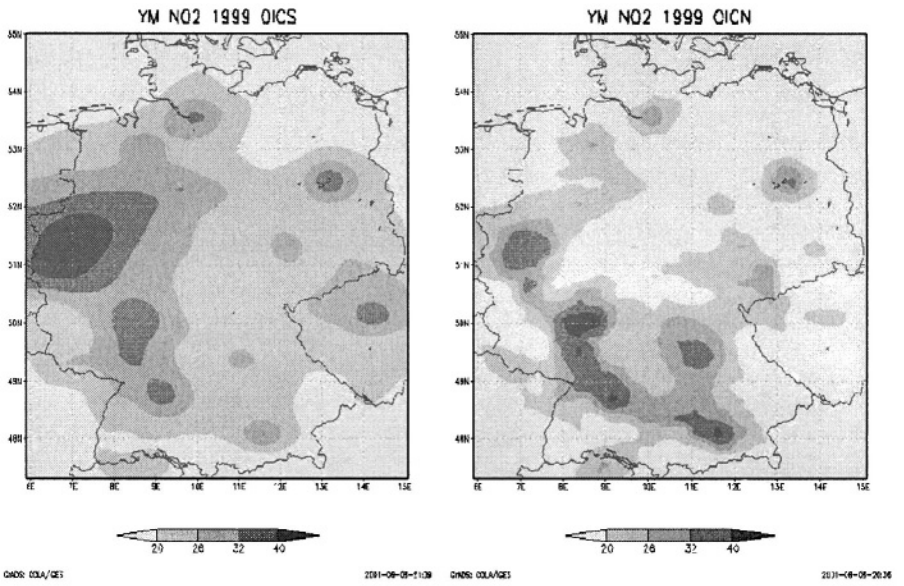

figure 2 Yearly mean of the NO2 concentration ($\mu g/m^3$) in Germany in 1999 obtained from measurements and modelled fields (REM3) by OI. For the left map OI was applied with homogeneous, for the right map with inhomogeneous error statistics models.

6 SUMMARY

In this work data assimilation of ground based concentration measurements into the fields of the Eulerian transport model REM3 was presented. The assimilation is based on the theoretical framework of Optimum Interpolation. Special emphasis was given to the modelling of the covariance of the background error and the variance of the observation error. An new scheme which accounts for the inhomogeneity of the concentration fields and their measurements was developed. It relies on the discrimination of air quality regimes in both the observations and the calculated fields of the model REM3. The performance of the new approach was compared with that of the "standard" homogeneous and isotropic covariance modelling. The new approach leads to more pronounced gradients in the NO2 concentrations, especially to lower concentration in rural areas, which seem to be more realistic.

The work should be considered as example to assess air quality by using all available information, i.e. observations, model results and climatological studies. The techniques of data assimilation are sophisticated tools to combine these information sources in an objective way. In order to apply these techniques, which were mainly developed for numerical weather forecasting, one has to adapt them to the specific problems of the air quality measurements as is was done in this work.

7 ACKNOWLEDGEMENTS

This work has been initiated and funded by the German Federal Environmental Agency (Umweltbundesamt) within the project "F+E-Vorhaben 299 43 246".

8 REFERENCES

Daley, R., 1991, *Atmospheric Data Analysis,* Cambridge University Press, Cambridge.

Egmond Van, N.D. and Onderdelinden, D., 1981, *Objective analysis of air pollution monitoring network data; spatial interpolation and network density,* Atmospheric Environment., 15, 1035-1046.

Elbern, H., Schmidt H., and A. Ebel, 1997, *Variational data assimilation for tropospheric chemisty modeling.* J. Geophys. Res., 102:15967–15985.

Falke, S.R. and Husar, R.B., 1998, *Declustering in the spatial interpolation of air quality data,* in: Preceedings of the Air & Waist Management Association Annual Meeting, San Diego.

Flemming, J., Reimer, E. and Stern, R, 2001, *Long Term Evaluation of the Ozone forecast by an Eulerian Model,* Physics and Chemistry of the Earth, to appear.

Flemming, J., 2001, *Charakterisierung der Messstationen nach dem Immissionsregime,* Zwischenbericht zum UBA FE-Vorhaben 299 43 246, Institut für Meteorologie, Freie Universität Berlin.

Gandin, J. L., 1963, *The Objective Analysis of Meteorological Fields,* Israel Program for Scientific Translations, Jerusalem.

Hass, H., Builtjes, P. J. H., Simpson, D., and Stern, R., 1997: *Comparison of model results obtained with several European regional air quality models,* Atmospheric Environment., 31, 3259-3279.

Hollingsworth, A. and Lönnberg, P., 1986, *The statistical structure of short-range forecast errors as determined from radiosonde data, Part I: The wind field,* Tellus, 38:A, 111-136.

Loon van, M. and Heemink, 1997, A.W., *Kalman Filtering for non linear atmopsheric chemistry models: First experiences,* Technical Report MAS-R9711, CWI, Amsterdam..

Marquardt, D.W. 1963, Journal of the Society for Industrial and Applied Mathematics, vol. 11,pp. 431–441

Reimer, E. and Scherer, B., 1992, *An operational meteorological diagnostic system for regional air pollution analysis and long-term modelling,* in: Air Pollution Modelling and its Applications IX., van Doop, H.., ed.., Plenum Press.

Stern R, 1994, *Entwicklung und Anwendung eines dreidimensionalen photochemischen Ausbreitungsmodells*, Meteorologische Abhandlungen Serie A, Band 8, Institut für Meteorologie der FU-Berlin.

DISCUSSION

A. HANSEN — In order to avoid imposition of assumptions of isotropy and homogeneity in your covariance models you might want to look into the methodology of Guttorp, Sampson, and Meiering in which pollutant fields are mapped into variance space, krigged and the unmapped back into geographic space. This interpolation is thus done on an isotropic field.

J. FLEMMING — Thank you for your comment.

E. GENIKHOVICH — Using the distance-dependent covariance function, one should assume that the field in question is isotropic. Did you test this hypothesis ?

J. FLEMMING — The covariance model presented here is not homogeneous and not isotropic.
In the case of the mixing of various covariance functions, the concepts of isotropy and homogeneity are linked together. This is due to the fact that the choice of the covariance function (CF) depends on the air quality regime of both grid points. The regimes are distributed according to a long term model calculation.
Each single CF represents the hypothetical situation, that one point has a certain AQ regime, say urban, and the rest of the field has a different one, say rural. In this sense the CF is isotropic.
I do not know how to test the hypothesis of isotropy in this case.

P. BUILTJES — You selected 5 air quality regimes. Are your results sensitive to your choice, especially for the rural regime ?

J. FLEMMING — We tried to make the classification of air quality parameters as objective as possible. The classification (hierarchical clustering) ensured stability and homogeneity of the obtained regimes.
Although we did not test it systematically – several classifications gave slightly different results but not in the conclusion that the inhomogeneous covariance model improves the performance of the scheme. The rural regime benifited the most. In the homogeneous case the urban stations “export” their properties into the rural areas.

This page intentionally left blank

INCLUSION OF AN IMPROVED PARAMETERISATION OF THE WET DEPOSITION PROCESS IN AN ATMOSPHERIC TRANSPORT MODEL

N. Fournier, K.J. Weston, M.A. Sutton, and A.J. Dore *

1. INTRODUCTION

Current pollution models describe the wet deposition of chemical species from the atmosphere using the concentration of the species, its scavenging coefficient and the rainfall rate. However, over the British Isles (BI), the spatial pattern of rainfall intensity often varies on a scale smaller than the spacing between rainfall stations, especially in mountainous areas. Indeed, it is well known that the rainfall rates occuring over mountainous and hilly regions are significantly greater than those over the surrounding low level ground. For the BI conditions, we must take into account the orographic enhancement of precipitation and hence wet deposition from the seeder-feeder effect, whereby orographically induced or enhanced clouds over high ground (feeder clouds) allow precipitation falling from higher-level clouds (seeder clouds) to grow rapidly, giving greater precipitation amounts than over neighbouring low ground (Bergeron, 1965). The quantitative effects of orographic enhancement over the BI are very dependent on flow direction.

A model of directional orographic enhancement of precipitation is developed which incorporates cloudwater generation by orographic and synoptic-scale lifting and the conversion of cloudwater to rainwater (Weston and Roy, 1994). The directional orographic precipitation given by this model is normalised to the BI orographic observed precipitation and incorporated in FRAME through a new parameterisation of the scavenging coefficients.

*N. Fournier, K.J. Weston, Department of Meteorology, University of Edinburgh, EH9 3JZ, UK. M.A. Sutton, A.J. Dore, Centre for Ecology and Hydrology, Edinburgh Research Station, EH26, UK.

Air Pollution Modeling and Its Application XV, Edited by
Borrego and Schayes, Kluwer Academic/Plenum Publishers, New York, 2002

Moreover, a more realistic description of the scavenging coefficients is undertaken. Instead of using a fixed value of the height of the atmospheric boundary layer, a calculated value is considered in the parameterisation. In this paper, we focus particularly on the United Kingdom (UK) wet reduced-N deposition as all the UK models underestimate it with respect to available measurements (RGAR, 1997).

2. WET DEPOSITION PARAMETERISATION

An atmospheric transport model, FRAME (Fine Resolution AMmonia Exchange), is used to assess the long-term annual mean NH_3 surface concentration and NH_x (NH_3 and NH_4^+) wet deposition over UK (Singles *et al.,* 1998). Further developments extended the domain of the model to the British Isles and improved its execution time to make more accurate and faster UK estimates (Fournier *et al.,* 2001). FRAME describes the main atmospheric processes (emission, diffusion, chemistry and deposition) taking place in a column of air moving along straight-line trajectories following specified wind directions.

Wet deposition is the removal of chemical species from the atmosphere through precipitation, and is dependent on scavenging, concentration and rainfall rate. The two major mechanisms are in-cloud and below-cloud scavenging. These processes can be modelled using scavenging coefficients, which describe the fraction of the airborne concentration removed per unit time. The amount of material c_i removed in a time period (Δt) is given by

$$\Delta c_i = c_i \left(1 - e^{-\lambda_i \Delta t}\right) \qquad (1)$$

where Δc_i is the decrease in concentration of species "i" due to removal by precipitation, and λ_i is its scavenging coefficient. Most models make no differentiation between in-cloud and below-cloud processes and use an averaged value of the washout coefficient Δ_i to represent the overall effect. Washout coefficients, consistent with those used in the EMEP model (Tarrason and Schaug, 1999), are combined with rainfall rate to produce appropriate scavenging coefficients. The rainfall data used are averages for the period 1989-1992 and are in the form of an annual rainfall field for British Isles on a 5km x 5km grid. These data are converted into constant drizzle values ($\mathrm{mm\ h^{-1}}$).

A parameterisation of the "seeder-feeder" effect had been previously included in the model by application of the method proposed by Dore *et al.* (1992). For locations with rainfall less than an assumed sea-level value of 700 $\mathrm{mm\ yr^{-1}}$ (P_{sl}; $\mathrm{mm\ h^{-1}}$), the scavenging coefficient for the species (λ_i) is $\Delta_i P$, where Δ_i is the washout coefficient for species "i", P is the precipitation rate ($\mathrm{mm\ h^{-1}}$). Over areas where rainfall exceeds 700 $\mathrm{mm\ yr^{-1}}$, it is assumed that this excess rainfall is due to altitudinal effects, and thus a fraction of the chemical species is removed by the seeder-feeder mechanism. In this case, λ_i is calculated by assuming that this excess rainfall will remove twice as much material as normal (enhancement of scavenging

coefficients by a factor 2 above the threshold rainfall amount of 700 mm yr^{-1}), and thus :

$$\lambda_i = \Delta_i P_{sl} + 2\Delta_i (P - P_{sl}) \quad (2)$$

Table 1 shows the United Kingdom 1996 reduced-N deposition budgets obtained with this version of FRAME (Run 1). The first column indicates the 1996 estimations derived from measurements (NEGTAP, 2001). The model underestimates wet reduced nitrogen deposition, but the dry deposition budget is broadly consistent with measurements (Fowler *et al.,* 1998). Moreover, the performance of the model predictions for NH_x wet deposition is illustrated for locations in UK included in the UK National Precipitation Composition Monitoring Network. The model shows a reasonable agreement with the 1995 – 97 measurements, but with the model giving smaller values (slope=0.69 and R^2=0.65). In this respect, the results of FRAME are similar to those of other models for the United Kingdom, which all underestimate total deposition (RGAR, 1997).

The constant drizzle approach, suitably weighted at each grid square by the frequency with which each wind direction occurs (British Isles wind rose), does not represent the directional-dependence of the enhancement of rainfall over complex orography. Although the seeder-feeder effect is not the only process to produce orographic precipitation in the British Isles (broad-scale up-slope rain, orographic convective showers and lee-waves (Lee *et al.,* 2000)), it is reasonnable to assume that the majority of annual rainfall falls as frontal precipitation, in conditions when the seeder-feeder effect occurs (Dore *et al.,* 1990; Dore *et al.,* 1992). Therefore, a more physical description of the precipitation over the British Isles is introduced with the development of a precipitation model.

Table 1 : UK 1996 reduced-N deposition budgets (ktonnes N yr^{-1})

UK reduced-N kt N yr^{-1}	Measurements 1996 estimations	FRAME Run 1	FRAME Run 2	FRAME Run 3
Dry deposition	99	99	100	98
Wet deposition	110	80	45	106
Total deposition	209	179	145	204

3. PRECIPITATION MODEL

A model is developed to represent the change of cloud water content in a column in response to both synoptically and orographically-induced vertical motion (Weston and Roy, 1994). The cloudwater is converted into rainwater by autoconversion. It can be summarised by the equations :

$$\Delta c = q_z \Delta z + (\Delta x / v)(P_0 - P) \quad (3)$$

$$P = k(c - c_0), \text{ for } c \geq c_0$$

$$P = 0, \text{ otherwise}$$

where c is the liquid water content of an air column, Δc its change in moving a horizontal distance Δx. c_0 is a threshold value below which no rain occurs, q_z the rate of increase of c with lifting of the cloud column. Δz is the ground altitude change over a distance Δx, v the horizontal speed, k the inverse of the time constant for conversion of cloudwater to rainwater. P is the precipitation rate and P_0 the non-orographic component of precipitation.

The first term, $q_z \Delta z$, represents the change in cloudwater due to orographic lifting of the cloud column. Any increase will lead to an increase in precipitation rate and a subsequent depletion of cloudwater content. Therefore, a range of hills will experience high precipitation, drying out the air stream, so that there is reduced orographic enhancement over succeeding high ground, or a rain shadow. The second term represents the increase in cloudwater due to large-scale vertical motion. This is related to the rainfall rate upwind of the high ground, P_0. The final term represents the decrease of cloudwater due to removal as rain. This is assumed to be proportional to the liquid water content of the cloud column above a threshold value, c_0, which converts to rainwater with a time constant of $1/k$. In the model, if c becomes zero, then any further drying of the air column leaves it under-saturated, so that some further ascent is required before condensation of cloudwater will again take place. The Weston and Roy (1994) model was applied along straight-line trajectories from 24 wind directions in a similar way to those used in FRAME. The results are combined statistically, depending on the frequency with which each wind direction occurs and on the percentage of rainfall from each wind direction in relation with the total mean annual rainfall. These latter weighting factors have been deduced from an analyse of 1985 wind data (K. Weston unpublished data) but are fairly representative of other years. To initialise the precipitation model, several parameters need to be assigned a value. The values are those used by Weston and Roy (1994) for q_z (5.0 kg m^{-2} km^{-1}), k (5.5×10^{-4} s^{-1}) and c_0 (1.0 kg m^{-2}). The trajectories are initialised with an uniform rainfall rate of 1 mm h^{-1}.

The modelled directional orographic precipitation is normalised to the observed orographic precipitation to preserve the total amount of the BI observed long-term average precipitation. The observed orographic component is the difference between the total precipitation and its non-orographic component. This non-orographic component is deduced from the observations and the application of a west to east gradient of 1000 to 400 mm yr^{-1}. This new normalised field of precipitation is used in FRAME where wet and dry periods are combined to quantify the wet reduced-N deposition over UK. According to the long-term (1961 – 1990) UK Meteorological Office's mapped averages, it is assumed that the wet periods represent one third of the time of the year.

4. SCAVENGING COEFFICIENTS PARAMETERISATION

Parameterisation of scavenging coefficients is the key to the description of the wet deposition process. As a result, particular attention is focused on this parameterisation. Firstly, the seeder-feeder effect previously developed, is uncorporated in the model (Run 2, section 4.1). Secondly, the basic parameterisation described in section 2 is improved (Run 3, section 4.2).

4.1 Seeder-Feeder Effect

The seeder-feeder process modifies the local concentrations of ions in precipitation because the feeder cloud water, scavenged by falling precipitation, contains larger average concentrations of the major pollutant ions than seeder rain. The larger concentrations in hill cloud result from the activation of aerosols containing the pollutants sulphate, nitrate and ammonium into cloud droplets as the air is cooled and force to rise. Thus, the seeder-feeder process leads to a larger increase in wet deposition of the major ions with altitude than that of precipitation (RGAR, 1997). A "seeder-feeder" enhancement factor must therefore be applied to the scavenging coefficients of these ions on the orographic component of precipitation. A factor of 2 is applied in FRAME following the studies of Fowler *et al.* (1988), Dore *et al.* (1992), Inglis *et al.* (1995) and Fowler *et al.* (1995). Hence, the parameterisation of the scavenging coefficients becomes :

$$\lambda_i = \Delta_i.P_{noc} + E_i.\Delta_i.P_{doc} \qquad (4)$$

where P_{noc} is the non-orographic component of the rainfall, P_{doc} is the directional orographic component of the rainfall (assessed in the previous section). E_i is the enhancement factor, equal to 2 for the ions sulphate, nitrate, ammonium and to 1 otherwise.

4.2 Mixing Layer Depth Effect

In the two previous parameterisations of the scavenging coefficients (Eq. (2) and (4)), a fixed depth of the mixing layer was considered. The washout coefficients in FRAME were consistent with those used in the EMEP model (see section 2) where an air column with a constant depth of 1000 m was assumed. In contrast, in FRAME, the diurnally varying mixing layers profile is calculted depending on insolation and cloud cover, wind speed and underlying surface. At nighttime, mixing layer depths are assigned according to Pasquill category and wind speed (Pasquill, 1961; ApSimon *et al.,* 1994). The vertical mixing in this mixing layer is then determined by the diffusion equation. To improve the physical description of the scavenging coefficients and to be consistent with the diffusion parameterisation, a

variable depth of the mixing layer is considered. Eq. (2) can be rewritten :

$$\lambda_i = \Delta_i(1000/H_{mix})P_{sl} + 2\Delta_i(1000/H_{mix})(P - P_{sl}) \quad (5)$$

where H_{mix} is the calculated depth of the mixing layer.

5. RESULTS AND DISCUSSION

The 1996 UK deposition budgets from the different runs with FRAME are given in Table 1. There is only a small difference for dry deposited reduced-N between the new parameterisation of the seeder-feeder process in FRAME (Run 2) and the constant drizzle approach (Run 1). In contrast, the different simulations indicate markedly different UK reduced-N wet deposition.

Run 2, with directional orographic precipitation and an enhancement factor of 2, underestimates the wet deposition from the measurements and from the basic model (Run 1) by 59 % and 44 %, respectively. However, with the exception of Scotland, the general pattern is respected with the highest wet deposition in hill areas of central northern England and Wales. The performance of the model predictions is illustrated for locations in United Kingdom and the comparison of the modelled NH_x wet deposition from Run 1 with the 1995-97 measurements (RGAR, 1997) shows a correct correlation coefficient (R^2=0.65), but the model is underestimating the measurements (slope=0.69). The main discrepancies between the measurements and Run 1 appear in Scotland; in Wales; in the Pennines; in Yorkshire Moors and in the East of Northern Ireland. The same scatter plot with the modelled NH_x wet deposition obtained from Run 2 gives a similar correlation coefficient (R^2=0.65) but with a smaller slope (0.30 against 0.69). It is mainly due to a drastic decrease of NH_4^+ wet deposition, in relation with Run 1, in the mountainous areas of the west coast of the Great Britain facing heavy orographic rainfalls but the air arriving from this direction is relatively clean, in contrast with the east polluted air which is washed out over England. This pattern of rainfall is more representative of the British Isles meteorological conditions than the constant drizzle approach but it suffers from a limitation of the model which uses straight-line trajectories. Indeed, this approach does not allow air from emission sources to be trapped in cyclonic conditions and so, to come back to a precipitating part of the depression. A better approach would be to consider curved trajectories by defining the intensity and the direction of the wind at each grid point.

Run 3 combines the constant drizzle approach and the use of a variable depth of the mixing layer in the parameterisation of the scavenging coefficients. This approach succeeds to simulate the UK reduced-N wet deposition budget with 106 kt N yr^{-1} (Table 1). This close agreement with the estimations derived from measurements (110 kt) is confirmed in the comparison of the modelled NH_x wet deposition with the 1995-97 measurements. A slope of 0.83 is obtained with a good correlation coefficient of 0.64. However, there is still some differences with measurements in Scotland, in Wales and in Northern Ireland. The increase of the reduced-N wet

deposition budget leads to a decrease of the UK NH_4^+ aerosol surface concentration improving the comparison with measurements. Whereas for Run 1 a slope of 1.19 (R^2=0.66) was obtained, in Run 3 an improvement is seen with a slope of 1.08 (R^2=0.63).

6. CONCLUSIONS

Most precipitation in the BI falls in westerly or southwesterly airflow, as frontal precipitation, in conditions when the seeder-feeder effect occurs. A model of orographic enhancement of rainfall over the British Isles has been presented. The precipitation model can reproduce the main features of the seeder-feeder process, allowing rain-shadows to occur downwind of mountainous areas. Directional orographic precipitation was obtained from this model on a finer spatial scale than observations. A seeder-feeder enhancement factor of 2 was applied on this directional orographic precipitation which was then combined with the non-orographic component of the precipitation in FRAME.

The results from FRAME with the new parameterisation were compared with 1995-97 measurements. The modelled UK wet deposition underestimates the UK reduced-N wet deposition budget and does not reproduce the peaks present in the mountainous regions of Scotland, Wales, Cornwall and the Pennines. These regions face heavy orographic rainfalls from the west but the air arriving from this direction is relatively clean, in contrast with the east polluted air which is washed out over England. Thus, although this parameterisation is more realistic than the previous constant drizzle approach, it suffers from the limitations of the FRAME model which considers straight-line trajectories. This weakness needs to be tackled before incorporating such detailed description of the seeder-feeder process.

Nevertheless, the FRAME UK reduced-N wet deposition budget had been improved by developing a more realistic description of the scavenging coefficients. The parameterisation combines now the constant drizzle approach with the use of a variable mixing layer depth leading to a better agreement with measurements.

7. Acknowledgments

Financial support for this work is gratefully acknowledged from the UK Natural Environment Research Council (NERC) and the Department of the Environment, Transport and the Regions, and the Ministry for Agriculture Fisheries and Food.

8. REFERENCES

ApSimon H.M., Barker B.M. and Kayin S. (1994) Modelling studies of the atmospheric release and transport of ammonia - applications of the TERN model to an EMEP site in eastern

England in anticyclonic episodes. *Atmos. Environ.* **28**, 665-678.

Bergeron T. (1965) On the low-level redistribution of atmospheric water caused by orography. In *Suppl. Proc. Int. Conf. Cloud Physics* Tokyo, May 1965, 96-100.

Dore A.J., Choularton T.W., Fowler D. and Storton-West R. (1990) Field measurements of wet deposition in an extended region of complex topography. *Q. J. R. Met. Soc.* **116**, 1193-1212.

Dore A.J., Choularton T.W. and Fowler D. (1992) An improved wet deposition map of the United Kingdom incorporating the seeder-feeder effect over mountainous terrain. *Atmos. Environ.* **26A**, 1375-1381.

Dore A.J., Choularton T.W., Fowler D. and Crossley A. (1992) Orographic enhancement of snow-fall. *Environmental Pollution* **75**, 175-179.

Fournier N., Pais V.A., Sutton M.A., Weston K.J., Dragosits U., Tang S.Y. and Aherne J. (2001) Parallelisation and application of an atmospheric transport model simulating dispersion and deposition of ammonia over the British Isles. *Environmental Pollution* (accepted the 12 April 2001).

Fowler D., Cape J.N., Leith I.D., Choularton T.W., Gay M.J. and Jones A. (1988) The influence of altitude on rainfall composition at Great Dun Fell. *Atmos. Environ.* **22**, 1355-1362.

Fowler D., Leith I.D., Binnie J., Crossley A., Inglis D.W.F., Choularton T.W., Gay M., Longhurst J.W.S. and Conland D.E. (1995) Orographic enhancement of wet deposition in the United Kingdom: continuous monitoring. *Water, Air and Soil Pollution* **85**, 2107-2112.

Fowler D., Sutton M.A., Smith R.I., Pitcairn C.E.R., Coyle M., (Campbell G. and Stedman J.) (1998) Regional mass budgets of oxidized and reduced nitrogen and their relative contribution to the N inputs of sensitive ecosystems. *Environ. Pollut. (Nitrogen Conference Special Issue)* **102**, S1, 337-342.

Inglis D.W.F., Choularton T.W. and Wicks A.J. (1995) The effect of orography on wet deposition in an industrial area. *Q. J. R. Met. Soc.* **121**, 1575-1588.

Lee D.S., Kingdon R.D., Garland J.A. and Jones M.R. (2000) Parameterisation of the Orographic enhancement of precipitation and deposition in a long-term, long range transport model. *Annales Geophysicae* **18**, 1447-1466.

NEGTAP (2001) Transboundary Air Pollution : Acidification, Eutrophication and Ground-level Ozone in the UK. *(First report of the National Expert Group on Transboundary Air Pollution),* Department of the Environment, Transport and the Regions (DETR), London.

Pasquill F. (1961) The estimation of the dispersion of windborne material. *Meteorological magazine* **90**, 33-49.

RGAR (1997) Acid deposition in the United Kingdom 1992-1994. *(Fourth report of the United Kingdom Review Group on Acid Rain),* Department of the Environment, London.

Singles R.J., Sutton M.A. and Weston K.J. (1998) A multi-layer model to describe the atmospheric transport and deposition of ammonia in Great Britain. *Atmos. Environ.* **32** (3) (Ammonia Special Issue), 393-399.

Tarrason L. and Schaug J. (1999) Transboundary acid deposition in Europe. *EMEP report* 1/99 (July 1999). EMEP- CCC/MSC-W. Norwegian Meteorological Institute, Blindern.

Weston K. J. and Roy M. G. (1994) The directionnal dependence of the enhancement of rainfall over complex orography. *Meteorol. Appl,* **1**, 267-275.

DISCUSSION

B. FISHER

The changes introduced improve agreement between the calculated and measured ammonia budget. Measurements of the wet deposition of ammonia tend to be in areas remote from S and NO_x sources but not necessarily ammonia sources. It would be useful to compare measurements and calculations for sites in different regimes e.g. rural sites (near ammonia sources), remote sites (distant from all sources) etc.

N. FOURNIER

Two points must be addressed. Firstly, concerning the improvement in the comparison with measurements, the results differ depending on the species you consider. NH_x and S perform well in contrast with NO_x. Secondly, following the distribution of the sources and measurement sites, the scatter plots between model and measurements should involve more specifically the difference between regions of UK.

This page intentionally left blank

MODELING OF URBAN AIR POLLUTION: PRINCIPLES AND PROBLEMS

Eugene Genikhovich, Irene Gracheva, and Elena Filatova

1. INTRODUCTION

Urban dispersion modeling (UDM) is usually based on applications of either numerical grid models or source-receptor type dispersion models. Numerical dispersion models are usually supplemented with numerical "sub-models" simulating the urban atmospheric boundary layer (UABL). Both types of the models are used to predict the fields of ground-level concentrations (GLC) inside the urban canopy. When analyzing numerous publications in UDM, one can notice that many of the models have similar deficiencies. In particular, numerical ones frequently do not account for the effect of blocking up by buildings the volume inside the canopy, which is available for dilution of pollutants. Corresponding UABL sub-models do not account for the fact that the wind speed, air temperature and other meteorological characteristics should be used only for the part of this volume, which is free of buildings.

Numerical models, used to simulate the urban air pollution, generate a set of values of concentrations averaged over the grid cells and attributed to some "receptor points" located inside these cells, *e.g.,* at their centers. Source-receptor type urban dispersion models also generate a set of concentrations attributed to the receptor point, but they usually do not include any spatial averaging. Actually, these concentrations also characterize a grid cell the size of which is defined by the spacing Δ of the receptor points. In both cases one should have certain information about characteristic features of the filed to be computed, in particular, the scale of its inhomogeneity, l_i, in order to understand whether the computed value of concentration can be considered as a good "representative" of all concentrations in the cell. For the most important urban air pollutants, like NOx, hydrocarbons and others, l_i is around 20 m, *i.e.,* a characteristic width of an urban street (it is known that concentrations at two sidewalks of the same street could differ as much as in three times). When mapping the air pollution in the big city with a source-receptor type dispersion model and using $\Delta >> l_i$, one can lose important features of concentration fields, which simply "fall through" the grid mesh. As a result, these fields could be grossly misrepresented. Corresponding problems are

Main Geophysical Observatory, 194021, St. Petersburg, Russia

Air Pollution Modeling and Its Application XV, Edited by
Borrego and Schayes, Kluwer Academic/Plenum Publishers, New York, 2002

discussed in this paper. In addition, some results of the urban field experiments are presented here.

2. GOVERNING EQUATIONS FOR THE URBAN AIR POLLUTION

Correct equations of UABL and the advection-diffusion equation, which could be applied to the urban environment including the urban canopy, were introduced by Popov (1975). A generalized version of these equations is derived in this section. For the sake of simplicity, let us consider the case of the passive conservative pollutant. Its dispersion is described by the standard advection-diffusion equation

$$\frac{\partial c}{\partial t} + \frac{\partial (u c_i)}{\partial x_i} = \frac{\partial (- < u_i' c' >)}{\partial x_i} + S, \qquad (1)$$

where summation over the repeated index is assumed. Here, c is the mean concentration of the pollutant considered as a function of coordinates in time (t) and space (x_i); u_i is the i-th component of the mean wind speed; c' and u_i' are fluctuations of c and u_i respectively; $<u_i'c'>$ is the turbulent flux along the i-th direction; S is the source/sink

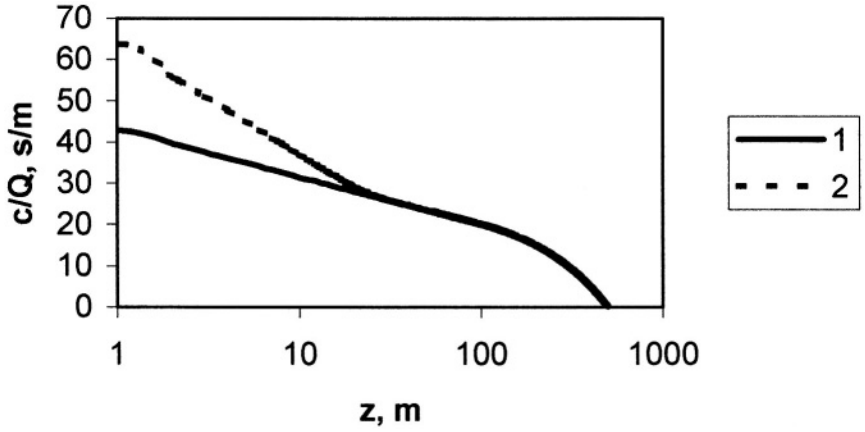

Figure 1. Vertical distribution of normalized concentrations from the ground-level area source in the absence (1) and presence (2) of porosity effects.

term. Eq. (1) is applicable, however, only outside buildings and structures, which can be considered as roughness elements of the urban canopy. In other words, Eq. (1) can be used only if the spacing Δ is small enough to resolve street canyons, buildings and so on. In order to obtain an equation which is applicable for the whole area of the city, one can multiply (1) by $I(x_i)$ where $I(x_i)$ is an indicator function of the ambient air:

$$I(x_i)=1 \quad \text{if } x_i \in \text{ambient air}; \tag{2a}$$

$$I(x_i)=0 \quad \text{if } x_i \notin \text{ambient air}. \tag{2b}$$

After averaging, it results in the following equation:

$$\frac{\partial Pc}{\partial t}+\frac{\partial Pu_i c}{\partial x_i}=\frac{\partial(-P<u_i' c>)}{\partial x_i}+S, \tag{3}$$

where P is the porosity of the urban canopy which could be defined as a depending on x_i probability for the receptor point to lie outside the buildings. Accordingly to Popov (1975), P is a result of the averaging $I(x_i)$ over the ensemble of similar cities with identical buildings stochastically re-distributed inside these cities. Therefore, P depends only on the vertical coordinate x_3. Such an approach, however, makes impossible any numerical simulations for a specific city. That is why we assume in this paper that P is determined as the moving average of $I(x_i)$ over the area determined by the spacing Δ. Thus, if $\Delta >> l_i$, P is a smooth function of coordinates. If $\Delta << l_i$, however, P coincides with $I(x_i)$ and Eq. (3) is transformed into (1). One should note that in this case P is a function of all three spatial coordinates and that S is not multiplied by P (because the sources, for example, are located at given point outside buildings).

Similar transformations could be applied, for example, to the first equations of motion in UABL:

$$\frac{\partial Pu_1}{\partial t}+u_i\frac{\partial Pu_1}{\partial x_i}=\frac{\partial(-P<u_1' u_i'>)}{\partial x_i}-PF_1-2\omega_z(G_y-u_2), \tag{4}$$

where F_1 is a horizontal component of the drag force due to the interaction of the wind flow with obstacles, and the last term in the right-hand side represents the Coriolis force. Other equations of motion are transformed in the same manner. The continuity equation is re-written in the following form:

$$\frac{\partial Pu_i}{\partial x_i}=0. \tag{5}$$

The same approach can be used to re-formulate the heat transfer-, TKE- and other equations. It should be stressed out, however, that Eq. (4) and (5) are different from those applied by Popov (he used $P \equiv 1$ here).

In the case of the spatially homogeneous city, P depends only on $x_3 = z$. An example of the vertical distribution of the normalized concentration, c/Q, from the infinite area source is given in Fig. 1. Here Q is the specific emission rate from one square meter of the source area. It is compared there with a similar distribution in the absence of porosity effects. The following approximation of function P(z) was used here:

$$P(z)=\frac{1}{\pi}a\tan\left(\gamma\frac{z-H_b}{H_b}\right)\cdot(1-P_0)+0.5\cdot(1+P_0), \tag{6}$$

where $P_0 = 0.4$; $H_b = 25$ m; $\gamma = 10$. It is seen on Fig. 1 that, due to porosity effects, ground-level concentrations from low sources can be higher than those in the absence of porosity.

3. MISREPRESENTATION, FILTERING AND REFINEMENT OF URBAN CONCENTRATION FIELDS CALCULATED WITH SOURCE-RECEPTOR DISPERSION MODELS

When using source-receptor dispersion models, the city area is usually covered with a regular grid mesh so that the concentration fields are "sampled" at regular receptor points. Such a sampling at the points that are arbitrarily located relative to the main roads and other sources resembles the sampling of stochastic time series. In particular, the effect of alaising (*i.e.,* confounding of frequencies), which is well known in the theory of time series, is responsible for significant fraction of the errors in computed fields. Here, the wave number k_Δ corresponding to the grid step Δ plays the role of the Nyquist frequency. Wave numbers larger than k_Δ cannot be correctly resolved on the grid. They, however, generate artificial oscillations on this grid with wave numbers less than k_Δ,

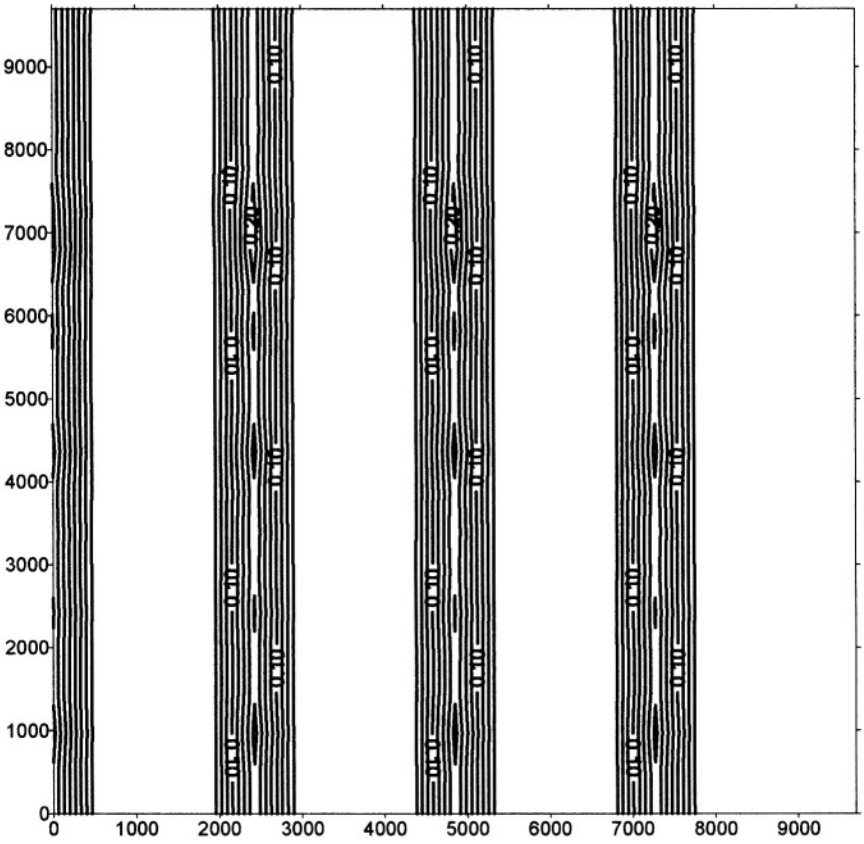

Figure 2. Local majorant concentration field calculated for four roads ($\alpha = 0$; $\Delta = 485$m).

which, actually, are nothing else but errors. The existing technologies of dispersion calculations in urban areas usually neglect these features of the concentration fields and, in particular, do not account for the "sampling effects". As a result, the concentrations computed at the regularly spaced grid points do not represent the air pollution in corresponding grid cells. Consequently, the errors in isolines drawn with the use of the computed values could be significant.

The effect of misrepresentation of the urban concentration fields with source-receptor type dispersion models could be understood better from calculations for a model city. These calculations were carried out with the Russian national regulatory model OND-86 (see Berlyand et al, 1987; Genikhovich, 1995), which directly generates upper-limit or majorant (actually, 98^{th} percentile) concentration fields. Similar results, however, could be obtained with any other source-receptor dispersion model.

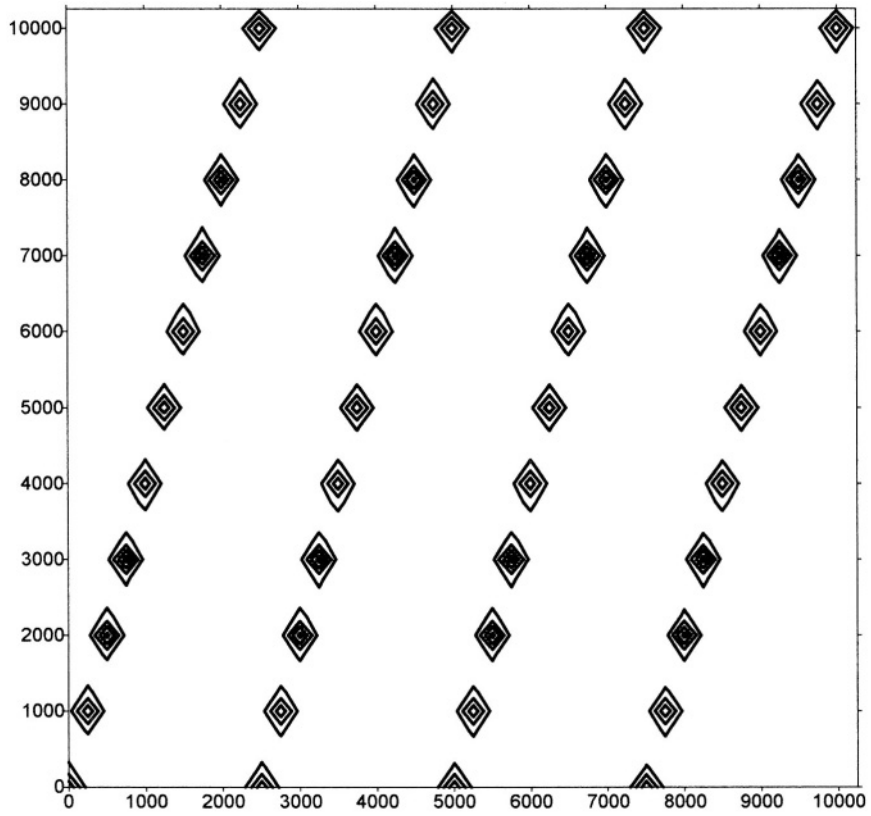

Figure 3. Local majorant concentration field ($\alpha = 14°$; $\Delta = 500$ m).

Let us consider four long evenly spaced identical parallel roads, the distance between the roads being 2910 m. The origin of the rectangular computational domain is located on the "left-hand" road, and α is the angle between the y-axis of the domain and the roads. For the sake of simplicity the roads are represented here as the line sources, and concentrations are calculated numerically as integrals along these straight lines from corresponding concentrations from the point sources. The majorant concentration field for such a layout calculated with $\alpha = 0$ and the grid step $\Delta = 485$ m along both, x- and y-

directions is shown on Fig. 2. Here, four "ridges" correspond to locations of the roads. Small fluctuations in the values of concentrations along these ridges can be attributed to errors in the numerical integration. Corresponding isolines are practically parallel to the roads. Numerical tests have confirmed that the same pattern of isolines is generated when doubling the resolution (i.e., when $\Delta = 242.5$ m; in this case the ridges have the same height but their width is decreased). It should be noted here that this and all other maps and graphs are mapped with the use of kriging; additional tests were used to prove that the results are not sensitive to interpolation techniques.

One could expect that the pattern of the majorant concentration field should not depend on orientation of the computational domain. These expectations are not supported by the results of computations with $\alpha = 14^{\circ}$ shown on Fig. 3 (the field there was computed with $\Delta = 500$ m). Instead of the ridges, one can see here a kind of a harrow turned upside down. The spikes are attributed to the receptor points located on the roads; they are separated one from another by the areas of low concentrations corresponding to receptor points off the roads. When doubling the resolution, the number of the spikes increases twofold but the pattern of the field does not improved but the number of the spikes increases.

The alaising effect is usually eliminated by filtering the oscillations with wave numbers larger than k_{Δ}. The simplest way to do it in our case is to average the initial

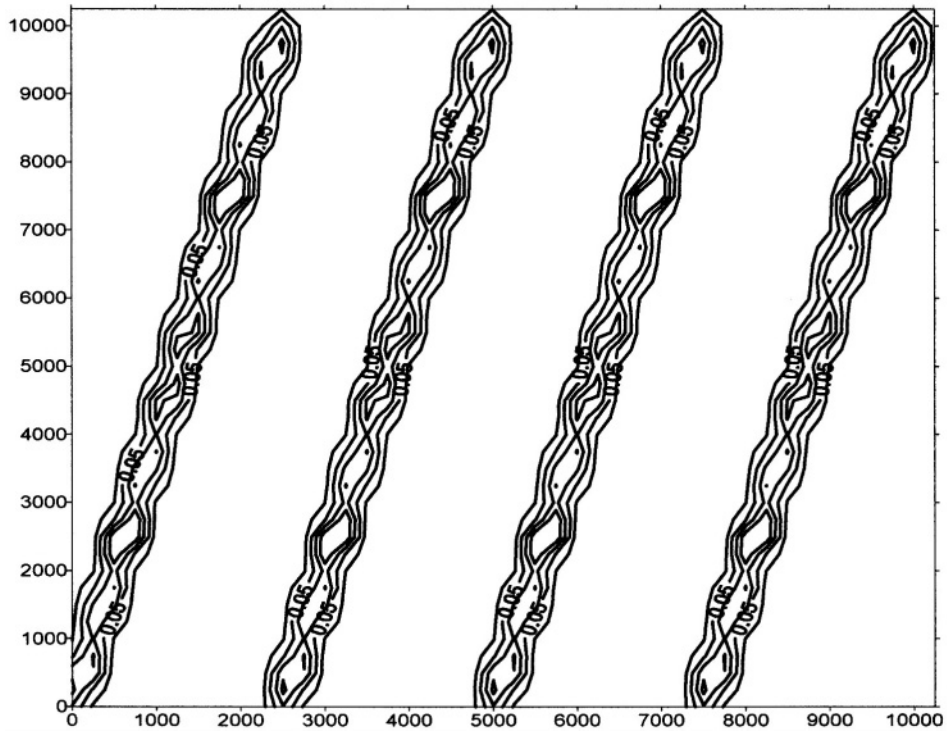

Figure 4. Filtered (averaged) majorant concentration field ($\alpha = 14^{\circ}$; $\Delta = 500$ m).

source-receptor relationships over the length scale Δ. In this work, crosswind and along-wind distributions from OND-86 were averaged separately over the same Δ (assuming, therefore, equal steps along x- and y-directions). To avoid writing corresponding bulky

formulae, one can illustrate this approach on Gaussian models. In this case the crosswind normal distribution $G_y[y;\sigma_y(x)] = \exp[-y^2/2\ \sigma_y^2(x)]/[\ \sigma_y(x)\sqrt{2\pi}]$ should be , for example, replaced with $G_{y,\Delta}$ which is defined as follows:

$$G_{y,\Delta}(y;\sigma_y(x))=\frac{1}{\Delta\sqrt{2\pi}}\int_{y-0.5\Delta}^{y+0.5\Delta}\frac{1}{\sigma_y(x)}\exp[-\frac{s^2}{2\sigma_y^2(x)}]ds.$$

A similar expression can be also introduced for $G_{z,\Delta}$.

In case of $\alpha = 0$, the pattern of the filtered (averaged over the cell) concentration field is essentially the same as those shown on Fig. 2 and 3 but maximum values of concentrations are about 50% less and the ridges are wider. More noticeable difference could be seen when comparing Fig. 3 and Fig. 4. When doubling the resolution, the pattern of the "averaged" concentration field resembles those on Fig. 2 even closer. Still, the magnitude of the concentrations is visible decreased there. Additional computations of NOx majorant concentration fields were carried out for a real Russian city of Pskov. The emission data in use reflected main sources of NOx including major roads. Resulting local (non-averaged) and filtered (averaged) fields are shown on Fig. 5. It is evident that the filtered field (b) reproduces the pattern of the roads better than the local one (a).

A standard way for testing sensitivity of the computed field to the spatial resolution is to compare the computed values of concentration at the same grid point using the steps Δ and $\Delta/2$. If the results do not differ significantly, they could be considered as a "final" estimate of the value of concentration at the given receptor point. If the difference is significant, the computed filtered field should be refined in the vicinity of this receptor point using the local-scale dispersion models. A corresponding algorithm will be discussed in this section. It should be noted first that, when calculating the filtered fields, there is no need to account for effects of buildings, structures and street canyons because they correspond to the scales smaller than the resolution of the model (they could be indirectly taken into account by the use of proper values of the roughness length and "porosity" of the area covered with roughness elements, displacement height and other input parameters). On the contrary, in the local-scale models these effects

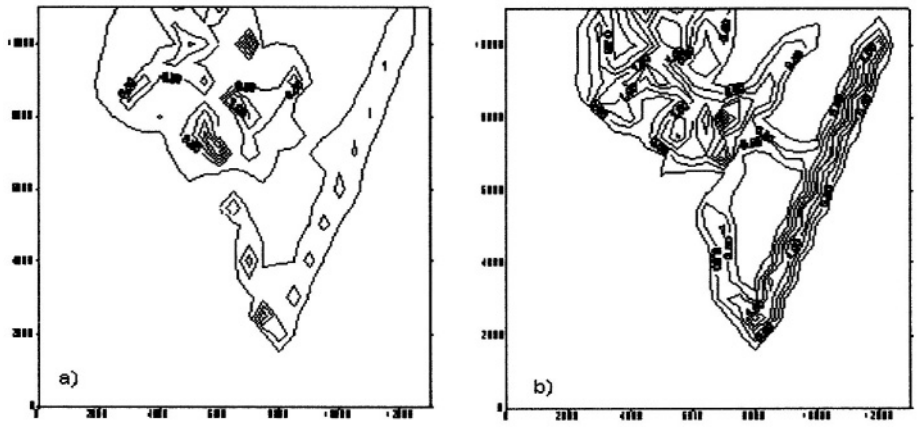

Figure 5. Non-filtered (a) and filtered (b) SO_2 concentration fields for the city of Pskov, Russia.

should be directly accounted for.

An algorithm of calculation of the refined concentration field could be described as follows:

1. Run calculations of the filtered concentration with grid steps Δ and $\Delta/2$.
2. Find the receptor points where concentrations are sensitive to variations of the grid step (*i.e.,* the differences are significant).
3. Find the sources that are responsible for major input into concentration at such a receptor point and sensitive to these variations ("sensitive sources").
4. Run the local-scale dispersion model for a cell surrounding the given receptor point, which is considered as a computation domain, with account for terrain and building effects on dispersion from the sensitive sources.
5. Repeat such a procedure for all receptor points where concentrations are sensitive to variations of the grid step

A computer program based on this algorithm is now under development.

4. CONCLUSION

Results presented in this paper indicate that the technology of urban dispersion modelling should be corrected in order to account for specific features of the urban air pollution. In particular, the effect of blocking up by buildings the volume inside the urban canopy should be explicitly included in the urban-scale numerical grid models. It is also important to remember that both numerical and source-receptor type dispersion models, when applied in the urban scale, generate values of concentrations which cannot be considered as "good representatives" of the concentrations in the computational cell. That is why the results of validation of those models upon data of monitoring in the cities should be taken with caution.

5. REFERENCES

Berlyand, M.E., Gasilina, N.K., Genikhovich, E.L., Onikul, R.I. and Glukharev V.A. (1987) Method for Calculation of Concentrations of Air Pollutants the Industrial Emissions Contain. National Regulatory Document OND- 86. Hydrometeorological Publishers, Leningrad. 92 p.(in Russian)

Genikhovich, E.L. (1995) Practical applications of regulatory diffusion models in Russia. I*nternational Journal of Environment and Pollution,* vol. 4-5, No 4-6, 530 – 537

Popov, A.M., 1975, On dispersion of pollutants in the urban atmosphere, *Meteorology and Hydrology,* No 11, p. 48 – 54 (in Russian)

DISCUSSION

D. STEYN — Can you relate "porosity" to the practical volume of air available for pollutant dilution ; and how does porosity depend on depth of the urban canopy layer ?

E. GENIKHOVICH — The "porosity" could be defined as a fraction of the volume of the grid cell which is available for dilution. It is, generally speaking, less than 1 inside the urban canopy and equal to 1 outside the canopy.

A. EBEL — The paper is focusing on grid point methods. Would finite element methods with better representation of city surface be able to circumvent the problems of grid point methods ?

E. GENIKHOVICH — The proposed approach is used to re-formulate the governing equations. Then they can be solved using different numerical techniques, finite elements included. I do not think, however, that finite elements alone (i.e. "without porosity") could "reflect" all the information about the structure and distribution of buildings inside the urban canopy.

This page intentionally left blank

MODELLING CLOUD CHEMISTRY IN A REGIONAL AEROSOL MODEL: BULK VS. SIZE RESOLVED REPRESENTATION

Wanmin Gong*

1. INTRODUCTION

Cloud and aqueous-phase chemistry plays an important role in the production and transformation of atmospheric aerosol. It is believed that a majority of sulphate aerosol production occurs in cloud via aqueous-phase reactions. Historically, cloud processing of aerosols is considered in the air quality models that deal with acid deposition issues, but is often represented in a highly simplified and parameterized fashion as most of the models only include gas and bulk aqueous phase and may have some representation of bulk aerosols. With atmospheric particulate matters emerging as a significant human health hazard in recent years, there is an increased interest to understand not only the bulk mass concentration but also chemical composition and size distribution of the atmospheric aerosols. Air quality models are also beginning to include size- and composition-resolved aerosols and the various processes affecting their formation and transformation in the atmosphere. However, most of the current regional PM models still adopt a bulk representation for the aqueous-phase chemistry, i.e., assuming that cloud droplets are monodisperse and homogeneous in chemical composition, for the sake of simplicity and the consideration of computational burden. On the other hand, there is observational evidence (e.g. Noone et al., 1988) that the solute concentration in cloud droplets is size dependent, and studies have shown (e.g. Hegg and Larson, 1990; Roelofs, 1993; Gong, 2000) that bulk aqueous-phase chemistry does not resolve the inhomogeneity in chemical composition and pH amongst cloud droplets, which impact on both mass and size distribution of cloud processing of aerosols.

A new multiple pollutants (unified) regional air quality modelling system, AURAMS, with size and chemical composition resolved aerosols is being developed (Moran et al., 1998). In the current version of AURAMS a bulk representation of the aqueous-phase chemistry is implemented, as a first step, and is coupled with the size resolved aerosol

* Wanmin Gong, Meteorological Service of Canada, 4905 Dufferin Street, Downsview, Ontario, M3H 5T4, Canada

Air Pollution Modeling and Its Application XV, Edited by
Borrego and Schayes, Kluwer Academic/Plenum Publishers, New York, 2002

dynamics. One of the objectives of the current study is to assess the impact of bulk versus size-resolved representation of aqueous-phase chemistry on modelled aerosols at a regional scale. In what follows, we will first briefly describe the aqueous-phase chemistry module and its implementation in AURAMS; we will present a preliminary examination of the impact of aqueous-phase chemistry on the modelled regional atmospheric aerosols, based on a simulation of the regional oxidants and aerosols in eastern Canada and the US north-east; we will then discuss some results from a test conducted with a stand-alone version of the aqueous-phase chemistry module to shed some light on the potential impact of size-resolved versus bulk representation of cloud/aqueous-phase chemistry on aerosol mass production and size distribution.

2. THE CLOUD CHEMISTRY MODULE AND ITS COUPLING WITH SIZE-RESOLVED AEROSOLS

Cloud/aqueous-phase chemistry usually refers to several processes including mass transfer between gas and aqueous-phase (cloud droplets), dissociation/ionisation of certain dissolved species and chemical reactions amongst various species in aqueous solution contained in cloud droplets. The aqueous-phase chemistry mechanism in the present study is adapted from ADOM (Acid Deposition and Oxidant Model, Venkatram et al., 1988; Fung et al., 1991). It includes mass transfer of SO_2, O_3, H_2O_2, ROOH, HNO_3, NH_3 and CO_2 and oxidation of S(IV) to S(VI) by dissolved ozone, hydrogen peroxide, organic peroxides and oxygen (in the presence of trace metals, e.g. iron and manganese). Mass transfer between gaseous and aqueous phases is treated as a diffusion process, and is written as a set of forward and backward reactions and integrated with the aqueous-phase oxidation reactions. The diffusion coefficients for the mass transfer process are determined from Fuchs and Sutugin (1971). The time integration of the chemistry system is done using a vectorized version of the Young and Boris predictor-corrector solver (Young and Boris, 1977).

The aqueous-phase chemistry is coupled with the explicit aerosol components in AURAMS, namely sulphate, nitrate and ammonium, which are represented by 12 size bins equally spaced on a logarithmic scale ranging from 0.01 to 40 μm. (Note that aerosol components in the current AURAMS also include organic aerosols and sea-salt aerosols, but they are not directly involved in aqueous-phase chemistry). The nucleation scavenging, which initialises the aqueous phase system, is done through aerosol activation in AURAMS. The aerosol activation is based on an empirical relationship between the aerosol number density $N_{aerosol}$ and the number density of cloud droplet $N_{droplet}$ formed on the activated aerosols (CCN) described in Jones et al. (1994):

$$N_{droplet} = 375(1\text{-}\exp(-2.5\text{x}10^{-3}N_{aerosol})) \ (\text{cm}^{-3})$$

The bulk cloud water content from the meteorological driver model is then distributed evenly amongst the activated aerosols, resulting in a relatively narrow cloud droplet spectrum. The ratios of liquid water content in each activated (or partially activated) size bins to the total (bulk) cloud water content are used to distribute the bulk mass increment of the various aerosol components, resulting from the aqueous-phase chemistry, into size

bins. While it is perhaps reasonable as far as particulate sulphate is concerned, this bulk-to-size conversion is less satisfactory when it comes to other inorganic aerosol components, such as particulate nitrate and ammonium (see discussion in section 4). For the bulk aqueous-phase chemistry integration, an average drop size is determined from the total number of activated aerosols (from the aerosol activation) and the bulk liquid water content from the meteorological driver model.

A fixed bin structure is used in AURAMS. This requires "rebinning" to be carried out to account for the growth of aerosols due to aqueous-phase production. This is done by ensuring conservation of both mass and number, (note that, while aqueous-phase chemistry will affect aerosol mass, it should not affect number concentration):

$$F_{i,j} = (m_{j,old}/m_{i,new})\,(m_{j+1,old} - m_{i,new})/(m_{j+1,old} - m_{j,old})$$
$$F_{i,j+1} = (m_{j+1,old}/m_{i,new})\,(m_{i,new} - m_{j,old})/(m_{j+1,old} - m_{j,old})$$

where $F_{i,j}$ and $F_{i,j+1}$ are partitioning factors for redistributing the "new" mass in bin i, $m_{i,new}$, after the aqueous-phase chemistry, into bin j and j+1. The sum of $F_{i,j}$ and $F_{i,j+1}$ should be unity.

3. PRELIMINARY RESULTS ON THE IMPACT OF CLOUD CHEMISTRY ON REGIONAL PM

Simulation of regional oxidants and PM over eastern Canada and north-eastern US, using AURAMS with the aqueous-phase chemistry module, is conducted for the period of August 1 - 6, 1988. This is compared to a previous AURAMS simulation of the same period without the aqueous-phase chemistry. While these simulations are conducted primarily for evaluating model against observations, here we will take a preliminary look

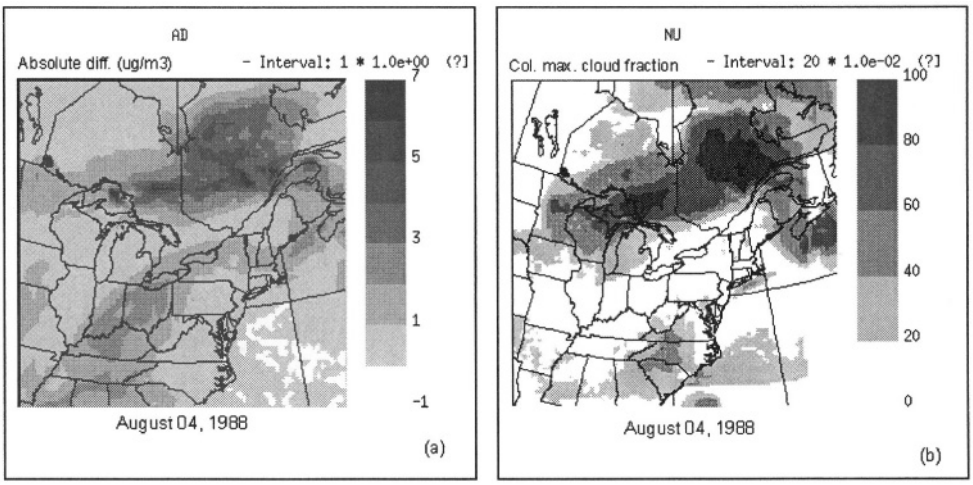

Figure 1. (a). Difference in 24-hour averaged total particulate sulphate concentration (μg m^{-3}) between the runs with and without the aqueous-phase chemistry, for August 4, 1988; (b) the 24-hour averaged 2-D cloud cover from the meteorological driver model for the same time period.

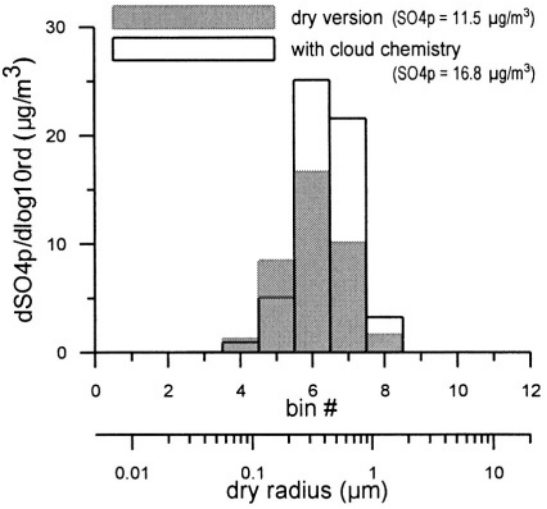

Figure 2. An example of modelled size distribution of sulphate aerosol with and without cloud chemistry.

at the impact of aqueous-phase chemistry on modelled regional aerosols (primarily sulphate aerosols). Note that wet removal processes, i.e. cloud-to-rain conversion and scavenging of aerosol particles and soluble gas by falling hydrometeors, are not included in either of the runs. Therefore this represents somewhat a upper bound as far as the cloud impact on modelled regional aerosols is concerned. Other processes involving aerosol included in the model are nucleation and condensation of sulphuric acid, condensation of secondary organic aerosols, coagulation, sedimentation and gravitational removal. (See Moran et al., 1998 for a detailed description on the conceptual design of AURAMS).

Figure 1 (a) shows the difference between the two runs in terms of 24-hour averaged total particulate sulphate concentration ($\mu g\ m^{-3}$), for August 4, 1988 at the ground level. To help with the understanding of the comparison, a 2-D cloud cover (fraction) field derived from the 3-D cloud fraction field from the meteorological driver model is shown in Figure 1 (b) for the same 24-hour period. It is seen that there is an increase in total sulphate aerosol mass concentration as a result of the inclusion of the aqueous-phase chemistry, and, as expected, that the areas with most significant increase in aerosol sulphate closely relate to the areas with most clouds. The enhancement in the modelled 24-hour averaged total sulphate aerosol is found up to $6\ \mu g/m^3$ for this particular day at this model level. Given that the averaged concentration of the total particulate sulphate from the dry run at this level is $\sim 5 \mu g/m^3$ with maximum concentration of $\sim 40\ \mu g/m^3$, the increase in sulphate aerosol mass owing to the inclusion of the cloud chemistry is significant. Overall, the modelled sulphate aerosol mass concentration averaged over the horizontal domain is increased by about 15% to 50% due to cloud chemistry below 2000 m for this one week period. However, the impact of aqueous-phase chemistry on the modelled aerosol will very much depend on the amount of cloud (liquid water) present and the location of the clouds as well as other atmospheric conditions.

For illustration purpose, Figure 2 shows an example of size distribution of modelled particulate sulphate from the two runs taken at one grid point at 20 Z August 4, 1988. It is seen that the main enhancement in particulate sulphate in the run with cloud chemistry

is in the 0.3 to 1 μm range (or bin # 6 - 8 in the model), and that there is a reduction in smaller size bins (bin # 4 and 5). This could be attributed to the growth of smaller aerosol particles into larger ones due to aqueous phase production. However one should bear in mind that this reflects not only the direct impact of aqueous-phase production but also the indirect interactions between aqueous-phase chemistry and other processes in the model, such as coagulation, sedimentation and gravitational removal.

4. STAND-ALONE TEST ON BULK VS. SIZE-RESOLVED REPRESENTATION

Although a final assessment of the impact of size-resolved vs. bulk representation of aqueous-phase chemistry on the modelled regional aerosols has to be carried out with a 3-D model, a great deal can be learned from a stand-alone test on the mechanisms responsible for such impact. In this section we will present some results from an aerosol parcel modelling study (Barth et al., 2001) where a stand-alone version of the current AURAMS aqueous-phase module was adapted to carry out both bulk and size-resolved aqueous-phase chemistry simulations.

The simulation is for sulphur oxidation (by dissolved H_2O_2 and O_3 only) in an air parcel containing initially pure ammonium bisulphate aerosols with a mass concentration of 2 $\mu g\ m^{-3}$ of SO_4^{2-} and 0.375 $\mu g\ m^{-3}$ of NH_4^+. A log-normal size distribution is specified for the initial aerosols. The parcel is lifted adiabatically with an updraft velocity of 50 cm s^{-1}. Cloud base temperature and pressure are 284.2 K and 939 mb, respectively, and the simulation is carried out for 40 min, or until the air parcel reaches 1200 m above cloud base. The initial gas-phase species concentrations are as follows: SO_2, 200 pptv; NH_3, 100pptv; H_2O_2, 500 pptv; HNO_3, 100 pptv, O_3, 50 ppbv; CO_2, 360 ppmv.

Two sets of results will be presented here: one from a size resolved simulation with 20 bins covering the range between 0.0014 and 4.61μm (diameter, dry), and the other from a bulk simulation. The time series of temperature, pressure and liquid water content are obtained from a bulk adiabatic calculation. The empirical aerosol activation formulation (Jones et al., 1994) as in the current AURAMS is used for both simulations, and the bulk simulation is coupled with the initial size distributed aerosols in the same manner as implemented in AURAMS described in section 2 above.

The final aerosol mass at the end of the 40 minute simulation is compared in Table 1 between the two runs. The major difference is in sulphate production - the binned run produces about 30% more sulphate mass over the 40 minute integration compared to the bulk run. There is no appreciable difference in the production of particulate nitrate and ammonium (due to mass transfer, or condensation of HNO_3 and NH_3) between the two runs. This is probably due to the way in which bulk water is distributed (equally) amongst

Table 1. Comparison of the final aerosol mass concentrations from the 40-minute simulations, bulk vs. binned.

	initial	final	
	(bulk and binned)	bulk	binned
SO4 ($\mu g\ m^{-3}$)	2.0	2.286	2.369
NH4 ($\mu g\ m^{-3}$)	0.375	0.3918	0.3921
NO3 ($\mu g\ m^{-3}$)	0.0	0.2186	0.2186

Table 2. Comparison of the net change in SO2, H2O2 and O3 concentration (due to aqueous-phase oxidation) between the two runs.

	$-\Delta SO_2$ (ppt)	$-\Delta H_2O_2$ (ppt)	$-\Delta O_3$ (ppt)	$\Delta H_2O_2/\Delta SO_2$	$\Delta O_3/\Delta SO_2$	final pH
bulk	155.42	122.44	32.36	0.79	0.21	4.85
binned	179.77	104.16	76.05	0.58	0.42	4.82

the activated aerosols in the binned case, which led to similar drop size and drop number, and therefore the total surface area in the two cases.

Table 2 shows the reduction in SO_2, H_2O_2 and O_3 as a direct result of S(IV)-to-S(VI) oxidation in aqueous phase, at the end of the 40-minute integration. The sum of the reductions in H_2O_2 and O_3 should, in theory, equal that in SO_2, while the relative size of the reductions in H_2O_2 vs. O_3 indicates the relative importance of the two oxidation pathways. The pH value at the end of the simulation is also shown in Table 2. In the "binned" case, this is an "overall" (or bulk-equivalent) pH weighted by the liquid water content in each of the bins. It is seen that, as well as more S(IV) is oxidized to S(VI) in the "binned" case, the O3 oxidation pathway plays a much more important role in this case than the bulk run (i.e. 42% in the binned run as opposed to 21% in the bulk run). Nonetheless the pH values from the two cases are quite similar! However, by looking at the results from the binned run a little more closely, we quickly realise that the "overall" pH does not represent well what happens in each individual bins. Figure 3 is a plot of a few pH time series for the 40-minute simulation. The pH from the bulk run, the overall pH, and the pH for bin #10 and #11 from the binned run are shown. These two bins are at the smaller end of the size spectrum which are activated. As seen, while the overall pH from the binned run compares closely with the one from the bulk run, the pH values for the activated bins that contain originally smaller particles are significantly higher, which would enable O_3 to play a much more important role in the aqueous-phase S(IV) oxidation. The lower acidity in these bins in the simulation is due to the fact that an equal amount of liquid water is distributed to all the activated aerosol particles in the model. However this may not be unexpected in the real world as it is known that the condensation of water vapour on smaller particles/drops is much faster than to the larger ones.

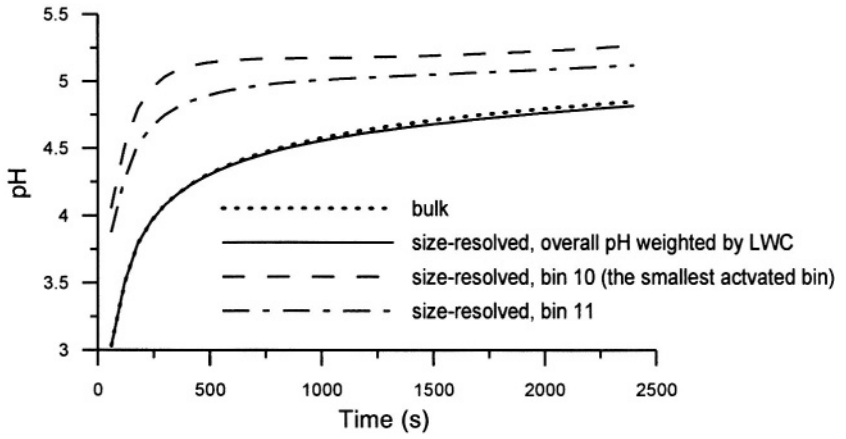

Figure 3. Comparison of the time series of pH during the 40 minute simulation.

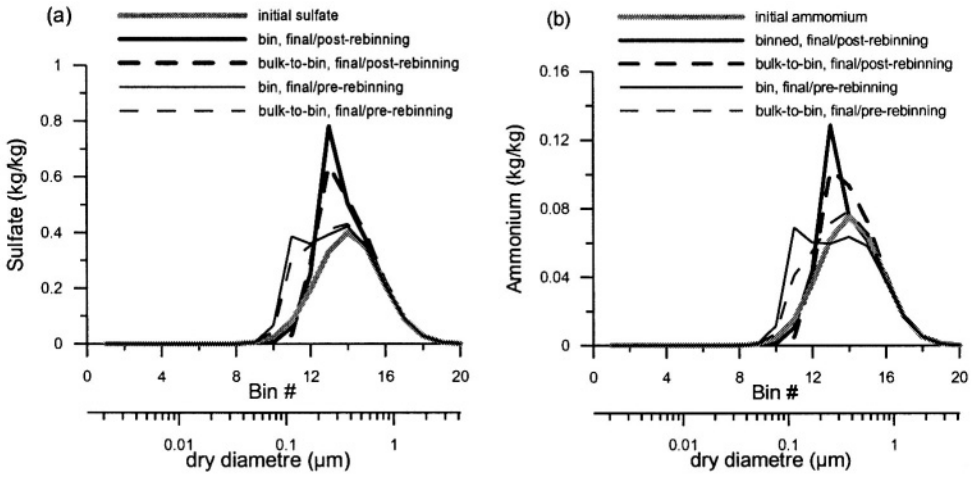

Figure 4. Comparison of the final sulphate (a) and ammonium (b) aerosol size distribution between the two runs (both before and after the "rebinning"). Note that the bulk-to-size conversion is done in the same way as implemented in the current version of AURAMS.

Therefore droplets grown from originally smaller particles can be much more dilute than those grown from the larger ones. However, this needs to be investigated further, ideally with a size-resolved aerosol model with fully coupled cloud microphysics and chemistry.

Another issue of interest is the impact of bulk vs. size resolved aqueous-phase representation on modelled aerosol size distribution. Figure 4 shows the size distribution of sulphate and ammonium aerosols at the end of the 40-minute integration from the two runs. In the case of the bulk run, the bulk-to-size conversion is done in the same way as in current AURAMS (see section 2). It is seen that for sulphate the distributions from the two runs are not too different particularly after rebinning. The binned run is seen to produce a double peak distribution (over bins) before rebinning, with a first peak centred at bin 11, while the bulk run does not show the same feature. This is a result of the enhanced sulphur oxidation in the smaller activated bins due to the enhanced role of O3 in the oxidation in the case of the binned run. The difference between the two runs is more significant in the distribution of ammonium aerosols. "Off-gassing" from larger size bins is clearly seen from the binned run, while it is not reflected in the bulk run since the bulk-to-size conversion is done using liquid water distribution. The difference is less significant after the rebinning.

5. CONCLUSIONS

A number of points can be made from the current study. Firstly, aqueous-phase chemistry is shown to have a significant impact on the modelled regional aerosols. It not only enhances aerosol production but also alters aerosol size distribution, which will further affect other aerosol processes (e.g. coagulation, sedimentation and gravitational removal etc.). The degree of this impact depends strongly on the presence of cloud, the amount of cloud water, its geophysical distribution and other atmospheric conditions.

It is seen, from the stand-alone test, that a size-resolved representation in aqueous phase oxidizes more sulphur than a bulk representation. This is in agreement with previous findings. The present study seems to indicate that the enhancement is a result of inhomogeneity in acidity (or solute concentration) amongst activated aerosols (drops). The drops originated/activated from the initially smaller aerosol particles are more dilute with lower acidity which are responsible for the enhanced S(IV) oxidation by aqueous-phase O_3. The bulk representation has another problem of regenerating the size distribution when coupled with size-resolved aerosols. Although it seems to work reasonably well for the sulphate aerosol component, the current scheme for bulk-to-size conversion does not work as well for other aerosol components, such as nitrate and ammonium, where "off-gassing" from larger size bins (or drops with higher solute concentration) will be difficult to represent with a bulk formulation.

Finally, a few things need to be pointed out as a caution. Particularly, the test on bulk vs. size-resolved chemistry presented here mainly addresses the issue of chemical inhomogenneity amongst cloud drops, and is influenced by the rather crude activation scheme and the distribution of bulk cloud water to activated aerosol particles used in the study. It would be more desirable to integrate the size-resolved chemistry with size-resolved cloud microphysics. However, this is still rather formidable to realise in 3-D regional scale models.

ACKNOWLEDGEMENT

Dr. V. Bouchet of MSC provided the results from the simulation with the "dry version" of AURAMS. Mr. S. Menard (now at CMC/MSC) provided programming support for the implementation of the cloud chemistry module in AURAMS.

REFERENCE

Barth, M.C., S.M. Keidenweis and R. Hudman, 2001. Comparison of cloud chemistry and aerosol parcel model simulations. To appear in WMO report on the 5th International Cloud Modelling Workshop, Aug 7 - 11, 2000, Glenwood Springs, Colorado.

Fuchs, N.A. and A.G. Sutugin, 1971. Highly dispersed aerosols. In *Topics in Current Aerosol Research, Vol. 2,* G.M. Hidy and J.R. Brock, Editors, Pergamon Press,, New York, 1-60.

Fung, C.S., P.K. Misra, R. Bloxam and S. Wong, 1991. A numerical experiment on the relative importance of H2O2 and O3 in aqueous conversion of SO2 to SO42-, *Atmos. Environ.,* Vol. 25A, No. 2, 411-423.

Gong, W., 2000. Bulk vs. size-resolved representations in modelling mass transfer and aqueous-phase chemistry in cloud droplets in regional models. *Preprint volume of the 11th Joint Conference on the Application of Air Pollution Meteorology with the A&WMA,* 376-378.

Hegg D. A. and T. V. Larsen, 1990. The effects of micro-physical parameterization on model predictions of sulphate production in cloud. *Tellus,* 42B, 272-284, 1990.

Jones, A., D.L. Roberts, and J. Slingo, 1994: A climate model study of indirect radiative forcing by anthropogenic sulphate aerosols, *Nature,* 370, 450-453.

Moran, M. D., A. P. Dastoor, S.-L. Gong, W. Gong and P. A. Makar, 1998. Conceptual design for the AES unified regional air quality modelling system. Air Quality Research Branch, Meteorological Service of Canada, Downsview, Ontario M3H 5T4, Canada.

Noone, K. J., R. J. Charlson, D. S. Covert, J. A. Ogren and J. Heintzenberg, 1988. Cloud droplets solute concentration is size dependent. *J. Geophys. Res.,* 93, 9477-9482.

Roelofs, G.J.H., 1993. A cloud chemistry sensitivity study and comparison of explicit and bulk cloud model performance. *Atmos. Environ.* 27A, 2255-2264.

Venkatram, A., P.K. Karamchandani and P.K. Misra, 1988. Testing a comprehensive acid deposition model. *Atmos. Environ.,* **22**, 737-747.

Young T.R. and Boris J. P., 1977. A numerical technique for solving stiff ordinary differential equations associated with the chemical kinetics of reactive-flow problems. *J. Phys. Chem.* 81, 2424-2427.

This page intentionally left blank

PARAMETERIZATION OF TURBULENCE–ENHANCED NUCLEATION IN LARGE SCALE MODELS: CONCEPTUAL STUDY

Olaf Hellmuth and Jürgen Helmert[1]

1. INTRODUCTION

Binary homogeneous nucleation of sulfuric acid and water vapor has long been suspected to be an important mechanism for new particle formation in the atmosphere (e. g., Stauffer, 1976). Nucleation is a highly nonlinear process, which is very sensitive to spatial and temporal variability. Owing to the coarse vertical and horizontal resolution, and rather long integration time steps in large scale models, unresolved subgrid-scale processes must be parameterized. Easter and Peters (1994) evaluated the effect of turbulent-scale variations on the binary nucleation rate. They found an enhancement factor, that is, the ratio of the nucleation rate in the presence of turbulence-scale fluctuations to that at mean-state conditions, of up to ≈ 70 for anticorrelated temperature and humidity fluctuations.

[1] Olaf Hellmuth and Jürgen Helmert, Institute for Tropospheric Research Leipzig, Permoserstr. 15, Leipzig, D–04303, Germany

Air Pollution Modeling and Its Application XV, Edited by
Borrego and Schayes, Kluwer Academic/Plenum Publishers, New York, 2002

Based on the approach of Easter and Peters (1994), here an extended diagnostic parameterization scheme to consider nonlinear effects of subgrid-scale turbulence on grid-scale binary nucleation rates in large scale models is presented.

2. MODEL DESCRIPTION

2.1 Filter approximation

Any grid-scale variable $\overline{\vec{\chi}}$ of an Eulerian model represents the spatio-temporal average of $\vec{\chi}$ over the model integration time step Δt and the grid cell volume $\Delta V = \Delta x\,\Delta y\,\Delta z$ with the location vector $\vec{r} = (x, y, z)^T$; analogeous, this is valid for any physical process function of $\vec{\chi}$, that is, $\Psi(\vec{\chi})$ (e. g., condensation). In the present approach, the grid-scale value $\overline{\Psi}$ is approximated by a weighted average over the parameter space $\langle\vec{\chi}\rangle$ with a suitable PDF $p_\chi(\vec{\chi})$:

$$\overline{\Psi} = \frac{1}{\Delta V \Delta t} \int_{\vec{r}}^{\vec{r}+\Delta\vec{r}} \Psi\{\vec{\chi}(\vec{r})\}\, d\vec{r}\, dt \approx \langle\Psi\rangle = \int_{-\infty}^{\infty} \Psi(\vec{\chi})\; p_\chi(\vec{\chi})\, d\vec{\chi} \qquad (1)$$

For the PDF, a multivariate Gaussian distribution is used. The elements of the covariance matrix are determined from diagnostic equations for first and second order moments. The infinite lower and upper limits of the PDF integral are truncated to $\vec{\chi}_1 = \langle\vec{\chi}\rangle - 3\vec{\sigma}$, $\vec{\chi}_2 = \langle\vec{\chi}\rangle + 3\vec{\sigma}$, using the standard deviations $\vec{\sigma} = (\sigma_1, \sigma_2, \ldots, \sigma_n)^T$, which ensures that 99.73 % of the realizations of the "Gaussian" distributed random variable $\vec{\chi}$ are located within the integral limits.

2.2 Nucleation rate (process function)

The binary nucleation rate $J_{nuc} \equiv \Psi(T, q_1, q_2)$ with temperature T, and the mixing ratio's of water vapor and sulfuric acid, q_1 and q_2, is determined from different approaches (J1–J4):

J1: "Exact" classical binary homogeneous nucleation theory with correction of the influence of hydration on the critical cluster composition and radius (e. g., Kulmala et al., 1998, Eqs. (1)–(16)).

J2: Parameterization of Kulmala et al. (1998, Eqs. (17)–(22)) for the binary homogeneous nucleation rate on the base of the hydrate-corrected classical binary nucleation theory.

J3: Parameterization of Liu et al. (2001, Eq. (3)) for the binary homogeneous nucleation rate.

J4: Parameterization of Liu et al. (2001, Eq. (21)) for ternary homogeneous nucleation rate at an implicit NH_3 concentration of 0.5 pptv.

2.3 First order moments

The grid-scale profiles of $\overline{T}$, $\overline{q_1}$, $\overline{q_2}$ are usually available from the large scale model. For the conceptual study presented here, these profiles are derived diagnostically from similarity theory of the convective boundary layer (CBL) (Stull 1997, p. 368–374).

Temperature: The vertical gradient of the temperature $\overline{T}$, and potential temperature $\overline{\theta} = \overline{T}(p_0/p)^{R/c_p}$, reads as:

$$\partial_z \overline{T} = \overline{T}\partial_z\overline{\theta}/\overline{\theta} - \gamma^\star \ , \ \partial_z\overline{\theta} = \begin{cases} \Phi_h \, \theta_\star^{SL}/(\kappa z) & \forall\, x \le 0.1 \\ F_\theta \, \theta_\star^{ML} w_\star^2/(z_i\sigma_w^2) & \forall\, 0.1 < x \le 0.9 \\ \hat{\gamma}_\theta & \forall\, x > 0.9 \end{cases} , \tag{2}$$
$$\Phi_h = 0.74(1 - 9z/L)^{-1/2} \ , \ F_\theta = 2.5x^{2/3}(1 - 0.8x)^2 \ .$$

In (2), Φ_h is the surface layer (SL) similarity function for nonzero surface stress, and F_θ the mixed layer profile function. The temperature gradient at the CBL top z_i is $\hat{\gamma}_\theta$, and $\theta_\star^{SL}$ and $\theta_\star^{ML}$ are the kinematic and convective temperature scale related to the SL heat flux $(\overline{w'\theta'})_s = -u_\star\theta_\star^{SL} = w_\star\theta_\star^{ML}$, with the kinematic and convective velocity scales $u_\star$, $w_\star = [(g/\overline{\theta})(\overline{w'\theta'})_s z_i]^{1/3}$. Furthermore, L is the Monin-Obukhov length, $x = z/z_i$ the dimensionless height, $\sigma_w = (\overline{w'^2})^{1/2}$ the standard deviation of the vertical velocity, and $\gamma^\star$ the dry adiabatic temperature lapse rate.

Humidity, acidity: The vertical gradient of the water vapor mixing ratio $\overline{q}_1$ reads as:

$$\partial_z\overline{q}_1 = \begin{cases} \Phi_h \, q_{1,\star}^{SL}/(\kappa z) & \forall\, x \le 0.1 \\ F_{q_1} \, q_{1,\star}^{ML} w_\star^2/(z_i\sigma_w^2) & \forall\, 0.1 < x \end{cases} , \ F_{q_1} = -9x^{2/3}(1 - 2x)^2 \ . \tag{3}$$

Here, $q_{1,\star}^{SL}$ and $q_{1,\star}^{ML}$ are the kinematic and convective water vapor mixing ratio scales, related to the SL humidity flux $(\overline{w'q_1'})_s = -u_\star q_{1,\star}^{SL} = w_\star q_{1,\star}^{ML}$. It is determined from the Bowen ratio for given SL heat flux. The water vapor partial pressure results from $\overline{p}_1 \approx p\overline{q}_1/0.622$. The sulfuric acid vapor pressure $\overline{p}_2$ is assumed to be in constant ratio to the water vapor pressure, preset in the surface layer, that is, $\overline{p}_2 \approx \overline{p}_1(z)(\overline{p}_2/\overline{p}_1)_s$ with $(\overline{p}_2/\overline{p}_1)_s$ = const..

Wind: Rotating the coordinate system to align the wind direction with the $x-$**axis,** the vertical gradient of wind velocity $\overline{u}$ is given as:

$$\partial_z\overline{u} = \begin{cases} \Phi_h u_\star^{SL}/(\kappa z) & \forall\, x \le 0.1 \\ 0 & \forall\, 0.1 < x \le 0.9 \\ \hat{\gamma}_u & \forall\, x > 0.9 \end{cases} \ . \tag{4}$$

Here, $\hat{\gamma}_u$ is the vertical wind gradient at the CBL top.

2.4 Second order moments

Heat flux: The heat flux results from the heat flux equation under horizontally homogeneous and quasi-steady state conditions with Boussinesq approximation (Holtslag and Moeng, 1991, Eqs. (1)–(8)):

$$\overline{w'\theta'} = -K_\theta(\partial_z\overline{\theta} - \gamma_{cg}) \ , \ \gamma_{cg} = bw_\star^2\theta_\star^{ML}/(\overline{w'^2}z_i) \ . \tag{5}$$

Here, K_θ is the eddy diffusivity for heat, $b \approx 2$ an empirical parameters for CBL turbulence.

Turbulent kinetic energy (TKE): The prognostic equation for the TKE $\overline{e}$ of a horizontally homogeneous Boussinesq fluid (Therry and Lacarrère, 1983) reads as:

$$\partial_t\overline{e} = -\partial_z(\overline{w'e} + \overline{p'w'}/\overline{\rho}_0) - \overline{u'w'}\partial_z\overline{u} + \beta\overline{w'\theta'} - \varepsilon \ . \tag{6}$$

Here, $\overline{\rho}_0$ and $\overline{\theta}_0$ are the density and potential temperature of air at the reference state, and $\beta = g/\overline{\theta}_0$ is the buoyancy parameter. The terms on the r.h.s. describe respectively vertical diffusion, shear production, buoyancy production and viscous dissipation. The vertical turbulent fluxes of momentum and heat and the TKE diffusivity term are parameterized as $\overline{u'w'} = -K_u\partial_z\overline{u}$, $\overline{w'\theta'} = -K_\theta(\partial_z\overline{\theta} - \gamma_{cg})$, $\overline{w'e} + \overline{p'w'}/\overline{\rho}_0 = -K_e\partial_z\overline{e}$, with the countergradient term γ_{cg}, and the eddy diffusivities for momentum, heat and TKE $K_u = c_k l_k\sqrt{\overline{e}}$, $K_\theta = \alpha_\theta K_u$, $K_e = \alpha_e K_u$. Here, $c_k = 0.5$, $\alpha_\theta = 1.35$ (reciprocal of the turbulent Prandtl number), and $\alpha_e = 1$. The dissipation rate is parameterized as $\varepsilon = c_\varepsilon\overline{e}^{3/2}/l_\varepsilon$, with the dissipation length scale l_ε and the dissipation parameter c_ε. Inserting the previous parameterizations into (6), we obtain for the quasi-steady state, $\partial_t\overline{e} \approx 0$, the following diagnostic equation:

$$\begin{aligned} &\partial_z^2\overline{e} = \mathcal{A}\,\partial_z\overline{e} + \mathcal{B}\,(\partial_z\overline{e})^2/\overline{e} + \mathcal{C}\,\overline{e} + \mathcal{D} \ , \\ &\mathcal{A} = -\partial_z l_k/l_k \ , \ \mathcal{B} = -0.5 \ , \ \mathcal{C} = c_\varepsilon/(\alpha_e c_k l_k l_\varepsilon) \ , \\ &\mathcal{D} = [\beta\alpha_\theta(\partial_z\overline{\theta} - \gamma_{cg}) - (\partial_z\overline{u})^2]/\alpha_e \ . \end{aligned} \tag{7}$$

Temperature and humidity variance: The variance equation for the temperature and water vapor mixing ratio $\sigma_\chi^2 = \overline{\chi'^2}$ with $\chi = (\theta, q_1)$ of a horizontally homogeneous Boussinesq fluid (André et al., 1978) reads as:

$$\partial_t\overline{\chi'^2} = -\partial_z\overline{w'\chi'^2} - 2\overline{w'\chi'}\partial_z\overline{\chi} - \varepsilon_{\chi\chi} \ . \tag{8}$$

Inserting the parameterizations of the turbulent fluxes $\overline{w'\chi'} = -K_\chi(\partial_z\overline{\chi} - \gamma_{cg})$ (γ_{cg} only for $\chi = \theta$), the turbulent transport terms $\overline{w'\chi'^2} \approx -K_\chi\partial_z\overline{\chi'^2}$, and the dissipation terms $\varepsilon_{\chi\chi} = c_{\chi\chi}\overline{\chi'^2}\varepsilon/\overline{e}$, with $c_{\chi\chi} = 2.5$, $\varepsilon = c_\varepsilon\overline{e}^{3/2}/l_\varepsilon$, $K_\chi = \alpha_\theta K_u$, and $K_u = c_k l_k\sqrt{\overline{e}}$ into (8), we obtain the following diagnostic equation for steady-state conditions, $\partial_t\overline{\chi'^2} \approx 0$:

$$\begin{aligned} &\partial_z^2\overline{\chi'^2} = \mathcal{E}_\chi\,\partial_z\overline{\chi'^2} + \mathcal{F}_\chi\,\partial_z\overline{e}\,\partial_z\overline{\theta'^2}/\overline{e} + \mathcal{G}_\chi\,\overline{\chi'^2} + \mathcal{H}_\chi\,, \\ &\mathcal{E}_\chi = -\partial_z l_k/l_k\,,\ \mathcal{F}_\chi = -0.5\,,\ \mathcal{G}_\chi = c_{\chi\chi}c_\varepsilon/(\alpha_\theta c_k l_k l_\varepsilon)\,, \\ &\mathcal{H}_\theta = -2\partial_z\overline{\theta}(\partial_z\overline{\theta} - \gamma_{cg})\,,\mathcal{H}_{q_1} = -2(\partial_z\overline{q}_1)^2\,. \end{aligned} \tag{9}$$

The standard deviation of the temperature and the sulfuric acid mixing ratio reads as $\sigma_T = (\overline{T'^2})^{1/2} = \sigma_\theta\,\overline{T}/\overline{\theta}$, and $\sigma_{q_2} = (\overline{q_2'^2})^{1/2} = \sigma_{q_1}\,\overline{p}_2/\overline{p}_1$.

2.5 Miscellaneous

Boundary conditions: At the *lower boundary* ($x_s = z_s/z_i = 0.01$ with SL height z_s), the TKE $\overline{e}|_{z_s} = 0.5(\overline{u'^2}|_{z_s} + \overline{v'^2}|_{z_s} + \overline{w'^2}|_{z_s})$ is determined using empirical variances of wind velocity. The temperature variance $\overline{\theta'^2}|_{z_s} \approx 0.4\ \mathrm{K}^2$ results from $\overline{\theta'^2} = 1.8\theta_\star^{ML\,2}x^{-2/3}$, $\theta_\star^{ML} \approx 0.1$ K, and the humidity variance $\overline{q_1'^2}|_{z_s} \approx 3.8\cdot10^{-7}$ from $\overline{q_1'^2} = 1.8q_{1,\star}^{ML\,2}x^{-2/3}$, $q_\star^{ML} \approx 0.1$ g/kg.

At the *upper boundary* (z_i), the TKE reads as

$$\overline{e}|_{z_i} = \{-R_E\,(\overline{w'\theta'})_s/[\alpha_\theta c_k l_k|_{z_i}(\partial_z\overline{\theta}|_{z_i} - \gamma_{cg}|_{z_i})]\}^2\,,$$

resulting from CBL top heat flux $(\overline{w'\theta'})_i = -K_\theta|_{z_i}(\partial_z\overline{\theta}|_{z_i} - \gamma_{cg}|_{z_i})$ with heat flux ratio $R_E = (\overline{w'\theta'})_s/(\overline{w'\theta'})_i$, and $K_\theta|_{z_i} = \alpha_\theta K_u|_{z_i}$, $K_u|_{z_i} = c_k l_k|_{z_i}\sqrt{\overline{e}|_{z_i}}$. The gradient of the temperature variance $(\Delta\overline{\theta'^2}/\Delta z)|_{z_i} \approx (1.98\ldots3.3)\cdot10^{-3}\ \mathrm{K}^2/\mathrm{m}$ is derived from CBL measurements, that is, $(\Delta\overline{\theta'^2}/\Delta z)|_{z_i} \approx (198\ldots330)\,\theta_\star^{ML\,2}/z_i$ (Caughey and Palmer, 1979, Fig. 5), $\theta_\star^{ML} \approx 0.1$ K, $z_i = 1000$ m, and that of the humidity variance $(\Delta\overline{q_1'^2}/\Delta z)|_{z_i} \approx (0.25\ldots4.5)\cdot10^{-8}\ \mathrm{m}^{-1}$ from humidity variances for Day 33, Wangara (Stull 1997, p. 129, Fig. 4.7) , that is, $(\Delta\overline{q_1'^2}/\Delta z)|_{z_i} \approx (250\ldots4500)\ q_{1,\star}^{ML\,2}/z_i$, $q_{1,\star}^{ML} = 10^{-4}$, $z_i = 1000$ m.

Length scales: The characteristic turbulence length scale is parameterized as $l_k = z_i[0.1 + 1.36(z/z_i)^{1.27}(1.02 - 0.96z/z_i)^{1.61}]$, derived from LES of a CBL (Hellmuth and Helmert, 2001, subm.). For l_ε, peak wavelength of the vertical velocity spectrum in the CBL is used, $l_\varepsilon \approx \lambda_{p,w} = 1.8z_i(1 - e^{-4z/z_i} - 0.0003e^{8z/z_i})$, which is related to the dissipation rate, $\varepsilon = \sigma_w^3/(a_\varepsilon\lambda_{p,w})$, with $a_\varepsilon \approx 0.26$ (Caughey and Palmer, 1979). With $\varepsilon = c_\varepsilon\overline{e}^{3/2}/l_\varepsilon = \sigma_w^3/(a_\varepsilon\lambda_{p,w})$, and $\overline{e} = 0.5(\sigma_u^2 + \sigma_v^2 + \sigma_w^2)$, we have $c_\varepsilon \approx \{a_\varepsilon[0.5(1 + (\sigma_u^2 + \sigma_v^2)/\sigma_w^2)]^{3/2}\}^{-1}$.

Velocity variances: In (2), (3), (5), and to determine c_ε and $\overline{e}|_{z_s}$, parameterized velocity variances are used (Kerschgens et al., 2000, Eq. (4.1)).

Correlation coefficients: For the correlation of the water vapor and sulfuric acid mixing ratio, $\rho_{q_1,q_2} = \rho_{q_2,q_1} \approx 0.9$ is assumed. The temperature-humidity correlation coefficient results from equation (9.6.4k), (9.6.3d), and (9.6.3e) of Stull (1997, p. 370–373), that is, $\rho_{q_1,T} = \rho_{T,q_1} \approx \rho_{q_2,T} = \rho_{T,q_2} \approx$ min [max (–0.95, $1 - 2z/z_i$), 0.95]. Here, the truncation is applied to avoid a degeneration of the PDF at the lower and upper model boundary.

3. RESULTS AND CONCLUSION

Interpretation: Fig. 1 shows the nucleation rate $J(\overline{T}, \overline{q_1}, \overline{q_2})$ at mean-state conditions $\overline{T} = 290$ K, $RH(\overline{T}, \overline{q_1}) = 60$ % (relative humidity), $RA(\overline{T}, \overline{q_2}) = 10^{-3}$ (relative acidity), $\rho_{T,q_1} = -0.8$, and the enhancement ratio

$$E = \log_{10} \frac{\overline{J(T, q_1, q_2)}}{J(\overline{T}, \overline{q_1}, \overline{q_2})} \approx \log_{10} \frac{\langle J(T, q_1, q_2) \rangle}{J(\langle T \rangle, \langle q_1 \rangle, \langle q_2 \rangle)}$$

as a function of the variation coefficients of temperature $\sigma_T/\overline{T}$, water vapor and sulfuric acid $\sigma_{q_1}/\overline{q_1} = \sigma_{q_2}/\overline{q_2}$ for the different nucleation models (J1–J4). The mean-state nucleation rates differ by several orders of magnitude between the different models, that is, $J_{1,nuc} = 1.12 \times 10^{-15}$ $cm^{-3}s^{-1}$, $J_{2,nuc} = 6.98 \times 10^{-10}$ $cm^{-3}s^{-1}$, $J_{3,nuc} = 1.13 \times 10^{1}$ $cm^{-3}s^{-1}$, $J_{4,nuc} = 2.22 \times 10^{5}$ $cm^{-3}s^{-1}$. Here, it should be considered that theoretical estimates of nucleation rates are very uncertain, primarily due to uncertainties in the requisite thermodynamic data (Liu et al. 2001). The enhancement ratio E strongly depends on the variation coefficients, and can exceed several orders of magnitude, that is, $E_{J1,max} \approx 10$, $E_{J2,max} \approx 6$, $E_{J3,max} \approx 5$, $E_{J4,max} \approx 7$. The shape of the isoline pattern is mainly affected by the correlation coefficient (not shown). In general, the enhancement ratio is by several orders of magnitude larger for anticorrelated than for correlated temperature-humidity fluctuations. In Fig. 2, the diagnostic profiles of first and second order moments and closure profiles for a typical CBL are presented. Fig. 3 shows the mean-state nucleation rate $\log_{10} J(\overline{T}, \overline{q_1}, \overline{q_2})$, the turbulence-enhanced nucleation rate $\log_{10} \overline{J(T, q_1, q_2)}$, and the enhancement ratio E for the different nucleation models (J1–J4). The mean-state nucleation rate increases by several orders of magnitude from the surface layer up to the CBL top in all cases. This is related to the decrease of the temperature and the increase of the relative humidity and acidity. The nucleation rate increases faster with height when considering subgrid-sale turbulence. The enhancement ratio is lowest in the surface layer, and assumes its maximum at the CBL top, that is, $E_{J1,z_i} \approx 5$, $E_{J2,z_i} \approx 3$, $E_{J3,z_i} \approx 3$, $E_{J4,z_i} \approx 5$.

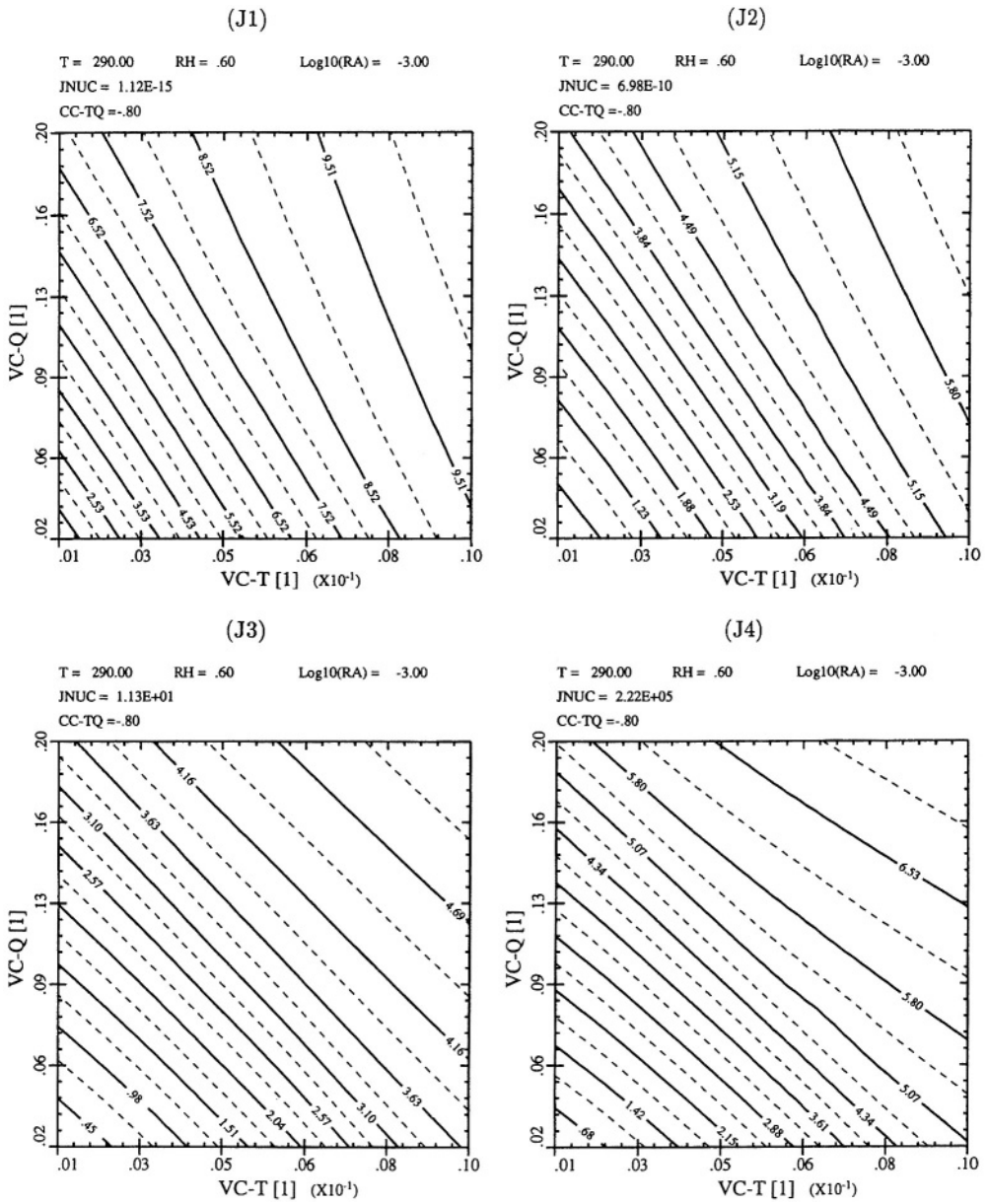

Figure 1: Nucleation rate $J(\overline{T}, \overline{q_1}, \overline{q_2})$ [$\mathrm{cm^{-3}s^{-1}}$] at mean-state conditions $\overline{T} = 290$ K, $RH = 60$ %, $RA = 10^{-3}$, $\rho_{T,q_1} = -0.8$, and enhancement ratio E (isolines) as a function of temperature variation coefficient $\sigma_T/\overline{T}$ (VC-T, abscissa: $0.1 - 1$ %), and mixing ratio variation coefficient of water vapor and sulfuric acid $\sigma_{q_1}/\overline{q_1} = \sigma_{q_2}/\overline{q_2}$ (VC-Q, ordinate: $2 - 20$ %) for different nucleation models (J1–J4).

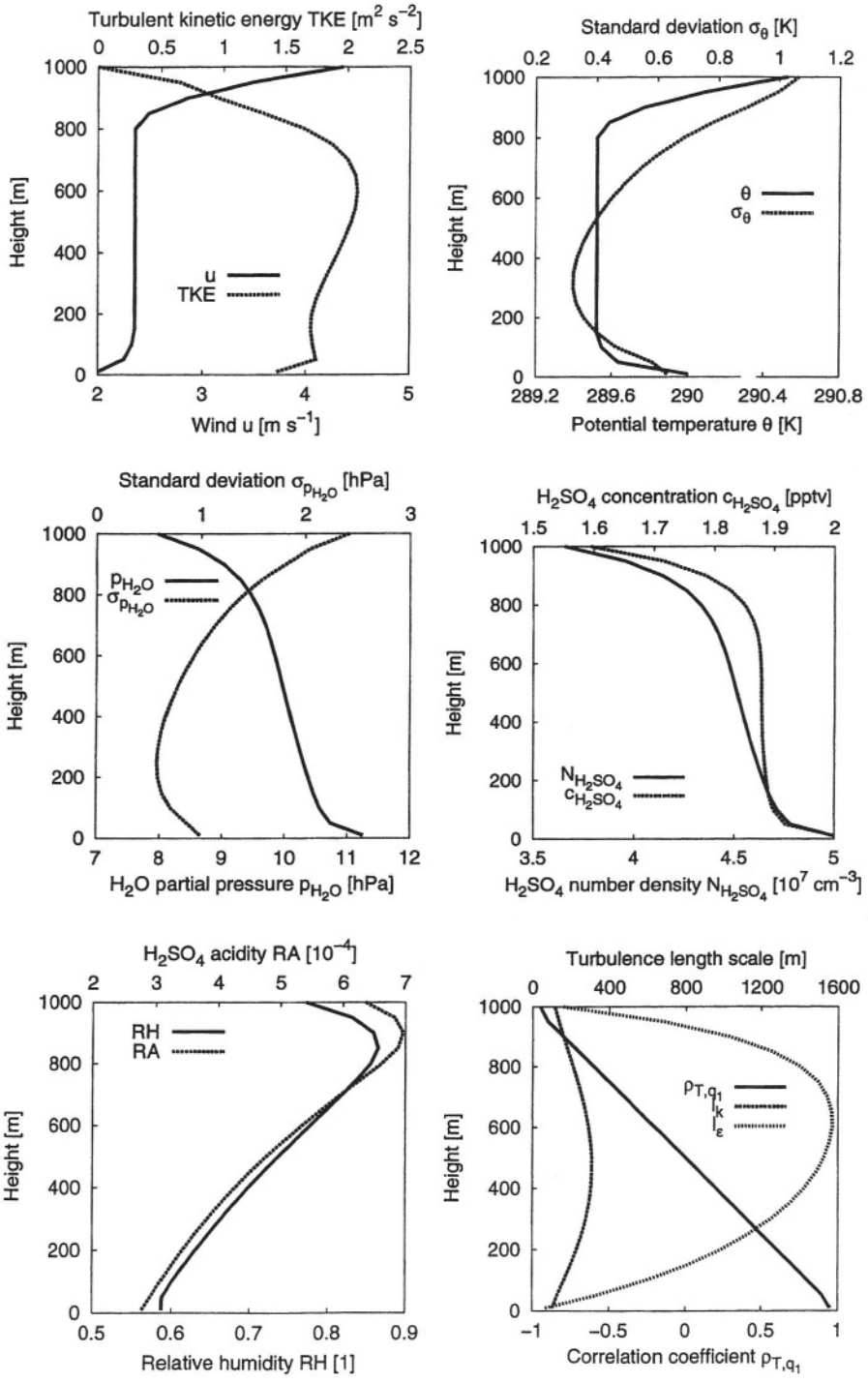

Figure 2: Diagnostic CBL profiles of first and second order moments and closure profiles.

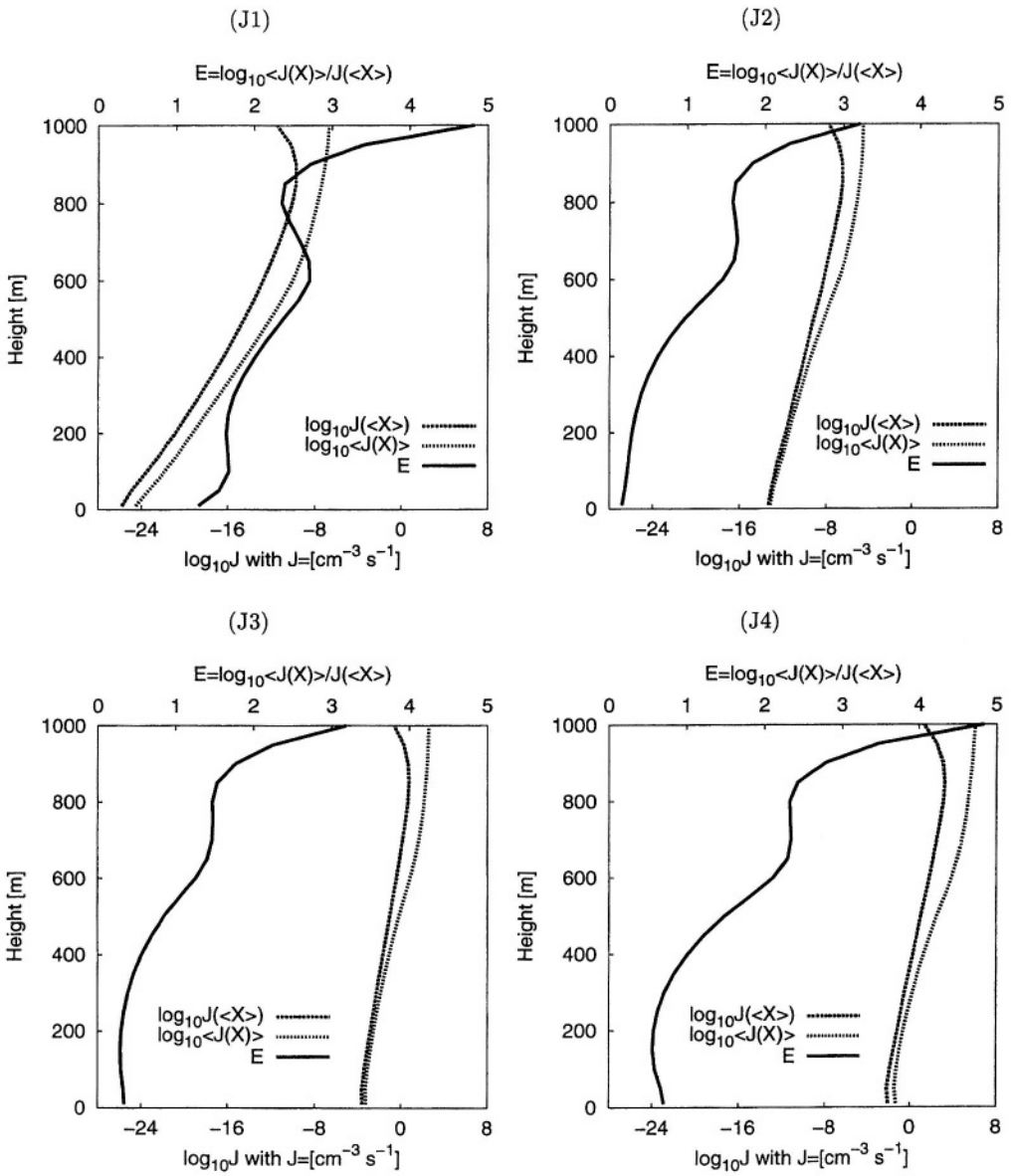

Figure 3: Mean-state nucleation rate $\log_{10} J(\overline{T}, \overline{q_1}, \overline{q_2})$, turbulence-enhanced nucleation rate $\log_{10} \overline{J(T, q_1, q_2)}$, and enhancement ratio E for different nucleation models (J1–J4).

Conclusion: Second order statistics provide useful information for the parameterization of the influence of subgrid-scale variations on the spatio-temporal average of the nucleation rate. In large scale models, the nucleation enhancement due to subgrid-scale turbulence can lead to nucleation events in grid cells with weak mean-state preconditioning for new particle formation. The effect is comparable to the effect of hydration of sulfuric acid as well as to the contribution of ammoniac in nucleation (Korhonen et al., 1999, Fig. 2). The results also show, that the upper part of the CBL is a favoured place of new particle formation. Considering the growth time of the critical nucleus to a detectable size, which is in the order of the large eddy turn over time, observed nucleation events in the surface layer are easily possible to result from top-down diffusion of faster formed new particles at the CBL top.

REFERENCES

André, J. C., G. De Moor, P. Lacarrère, G. Therry, and R. Du Vachat, 1978: Modeling the 24-hour evolution of the mean and turbulent structures of the planetary boundary layer. *J. Atmos. Sci*., **35**, 1861–1883.

Caughey, S. J., and S. G. Palmer, 1979: Some aspects of turbulence structure through the depth of the convective boundary layer. *Quart. J. Roy. Meteor. Soc.,* **105**, 811–827.

Easter, R. C., and L. K. Peters, 1994: Binary homogeneous nucleation: Temperature and relative humidity fluctuations, nonlinearity, and aspects of new particle production in the atmosphere. *J. Appl. Meteor*., **33**, 775–784.

Hellmuth, O., and J. Helmert, 2001: Length scale determination using large-eddy simulation of the convective boundary layer. *Meteorol. Z.*, **Subm.**

Holtslag, A. A. M., and C.-H. Moeng, 1991: Eddy diffusivity and countergradient transport in the convective atmospheric boundary layer. *J. Atmos. Sci*., **48**, 1690–1698.

Kerschgens, M., C. Nölle, and R. Martens, 2000: Comments on turbulence parameters for the calculation of dispersion in the atmospheric boundary layer. *Meteorol. Z.,* **9**, 155–163.

Korhonen, P., M. Kulmala, A. Laaksonen, Y. Viisanen, R. McGraw, and J. Seinfeld, 1999: Ternary nucleation of $H_2SO_4, NH_3,$ and H_2O in the atmosphere. *J. Geophys. Res.,* **104**, 26,349–26,353.

Kulmala, M., A. Laaksonen, and L. Pirjola, 1998: Parameterizations for sulfuric acid/ water nucleation rates. *J. Geophys. Res.,* **103**, 8301–8307.

Liu, X., D. A. Hegg, and M. T. Stoelinga, 2001: Numerical simulation of new particle formation over northwest Atlantic using MM5 mesoscale model coupled with sulfur chemistry. *J. Geophys. Res*., **106**, 9697–9715.

Stauffer, D., 1976: Kinetic theory of two-component ("heteromolecular") nucleation and condensation. *J. Aerosol Sci*., **7**, 319–333.

Stull, R. B., 1997: *An Introduction to Boundary Layer Meteorology.* Kluwer Academic Publishers, Dordrecht/ Boston/ London.

Therry, G., and P. Lacarrère, 1983: Improving the eddy kinetic energy model for planetary boundary layer description. *Boundary-Layer Meteor*., **25**, 63–88.

DISCUSSION

P. BUILTJES Many parameters and correlation coefficients are needed to perform your correlation. Is it possible to determine them experimentally, for example the correlation between water vapour and temperature ?

O. HELLEMUTH In principle, all elements of the PDF covariance matrix could be obtained by using additional forecast equations, i.e. for $\overline{q'_{H_20}T'}$, $\overline{q'_{H_2SO_4}T'}$ etc. For practical reasons, the present approach has been limited to the determination of the variances only, that is σ_T^2, $\sigma_{H_2O}^2$, $\sigma_{H_2SO_4}^2$. The cross-correlation coefficients of temperature and water vapor mixing ratio can be obtained from measurements, even they are scarce and highly uncertain. The most important problem is the determination of water vapor – sulfuric acid cross correlation due to the problem of getting highly time resolved sulfuric-acid measurements. The same is true for temperature – sulfuric acid cross correlation. A suitable way to overcome all sampling problems might be the use of LES to parameterize all cross-correlation terms as function of scaling properties (mixing layer height, Monin-Obukhov length and convective temperature, velocity, humidity, and concentration scales …).
Before such an approach is performed, the sensitivity of the aerosol evolution on the turbulence-enhanced nucleation rate should be investigated in a large and/or mesoscale model.

This page intentionally left blank

MODELS-3/COMMUNITY MULTISCALE AIR QUALITY (CMAQ) MODELING SYSTEM

2001 Java-based release

Sharon LeDuc and Steven Fine*

1. INTRODUCTION

The U.S.E.P.A. has developed the Models-3/CMAQ (Community Multiscale Air Quality) modeling system, with the initial release occurring during 1998. EPA/NOAA scientists and their colleagues are continuously striving to improve and to evaluate the scientific basis and the scientific algorithms in CMAQ. In addition, they are working to provide and improve the Models-3 framework to provide a user-friendly interface for air quality modeling. The application and functionality of an earlier version (version 3) of Models-3/CMAQ was presented at the Millennium **(24th)** NATO/CCMS International Technical Meeting on Air Pollution Modelling and Its Application (LeDuc *et al.,* 2000). This paper briefly describes Version 4.1, released during early 2001, and Version 5, scheduled for a November 2001 release. The November 2001 release will have an entirely new framework which has been designed to be extensible for cross-media modeling (air, water, soil, vegetation, exposure and risk) of pollutants. This is part of a new modeling effort is known as MIMS, Multimedia Integrated Modeling System, which is a multi-year effort by U.S.E.P.A. Air quality modeling is the first Amedium@ to be modeled in MIMS. The science used for that modeling has evolved from the Models-3/CMAQ modeling system. The November 2001 release will incorporate the Modified Euler Backward Iterative (MEBI) solver for selected gas-phase chemical mechanisms. The solver is considerably faster than the Quasi-Steady State Approximation Method and the Sparse-Matrix Vectorized Gear solver. Previous changes to Models-3/CMAQ will be presented along with the expected capability of the MIMS framework which will contain the latest version of Models-3/CMAQ modeling system.

* Atmospheric Sciences Modeling Division, Air Resources Laboratory, National Oceanic and Atmospheric Administration, on assignment to National Exposure Research Laboratory, U.S. Environmental Protection Agency, MD-80, Research Triangle Park, North Carolina 27711, U.S.A.

Air Pollution Modeling and Its Application XV, Edited by
Borrego and Schayes, Kluwer Academic/Plenum Publishers, New York, 2002

2. MODELS-3/CMAQ VERSION 4.1

The Models-3/CMAQ version 4.1 was released during the period February thru August 2001. A description of that system (Byun *et al.,* 2001) indicates the status of the science, including the emissions processor the Sparse Matrix Operator Kernel Emissions (SMOKE) modeling system from MCNC, North Carolina Supercomputing Center's Environmental Programs (MCNC, 2001). Both SMOKE and SMOKE Tool (Atmospheric Modeling Division *et al*., 2001) are integrated into version 4.1 of the framework. The latest version of SMOKE has new features for enhancing the quality assurance capability (Houyoux and Adelman, 2001). Science codes and scripts to execute all processing, referred to as a Astandalone@ version, are available for downloading from the Models-3 website (EPA, 2001b) for three computing platforms: Sun, SGI and Windows NT. Users have adapted these for other computing platforms, e.g. DEC Alpha and Linux. This standalone version is coded to execute a tutorial situation. Users will need to do additional processing for executing another geographic domain, using an alternate chemical mechanism, or simulating another time period. All components including SMOKE and SMOKE Tool will execute without the framework.

The framework assists users in setting up the domain and executables for simulating a case beyond the tutorial. The framework has been released for the Sun workstation and for the Windows NT computing platforms. The framework requires users to purchase several proprietary software packages (SAS and ARC/INFO) for the emissions processing, and a runtime license for the object-oriented communications software. For the Windows NT graphics, the user must also purchase and install software for PC X connectivity, e.g. Hummingbird Exceed, and the unix emulation software Interix. One graphic package that is in Version 4.1 and that will be integrated into the framework is PAVE (Thorpe *et al.,* 1996), which may be downloaded (MCNC, 2001).

3. PLANS FOR NOVEMBER 2001 RELEASE

The November 2001 release will include a new framework being developed for U.S.E.P.A.=s Multimedia Integrated Modeling System (MIMS). Design details of the framework are available at the MIMS website (EPA, 2001a). This release will replace the old Models-3 framework. The Amultimedia@ to be modeled in the MIMS system are the multiple physical media, such as air, water, and soil. The new MIMS framework will make it easier to configure and execute complex modeling studies. For instance, the new framework will provide facilities for easily re-executing model configurations with different data sets. This is a commonly needed capability, especially to simulate multiple episodes.

The MIMS framework has been designed to be portable across platforms and to require no software that will incur a cost for the end user. The model communication paradigm in MIMS is based on the Dynamic Information Architecture System (DIAS), a flexible object-based software framework that provides the structure and flexibility required to successfully interchange models of very diverse processes (Christiansen, 2000). The MIMS framework is being developed in Java, which provides portability across platforms. None of the third-

party libraries that are used have a distribution fee. Documentation for the MIMS framework will be in the form of both JavaHelp (a cross-platform hypertext help system) and hardcopy. As a result of all of these charateristics, the MIMS framework will be much easier for a user to obtain, install, and use than the Models-3 framework through Version 4.1.

The development and testing of the new framework has been accomplished with cooperation between the air quality modeling scientists and the software developers. The addition of features and functionality has been directed by a voting process following principles of Extreme Programming (Beck, 2000), which recommends a software development approach with a high degree of input and feedback from users. Additional features will be included in the November release, but because the last round of voting had not occurred at the time this paper was prepared, those high priority features were not known.

Major advancements in the models= functionality and capability in the November 2001 release are made possible by the use of Fortran 90 and dynamic allocation. This will enable users to change options, such as the geographic domain and the number of vertical layers, without recompiling. A windowing capability will allow extraction of subareas from larger domains. Users will have the ability to edit the chemical mechanism in the framework, although this should be used cautiously by knowledgeable users. SMOKE will be integrated into the framework which will be released in November, however, users will be expected to download it separately (MCNC, 2001).

Modular spatial allocation routines written in Fortran 90 will replace much, if not all, of the ARC/INFO functionality. It is questionable, however, whether or not the requirement for ARC/INFO can be dropped. As mentioned before, PAVE will be also included in the November release.

The November release will have new science features. The Biogenic Emissions Inventory System version 3 (BEIS3) will be included for simulating biogenic emissions in SMOKE. [It is unlikely that Mobile6 will be available in time to include in the November release.] The State Air Pollution Research Center (SAPRC) chemical mechanism will be included and the Modified Euler Backward Iterative (MEBI) solver will be expanded to process the Regional Acid Deposition Model version 2 (RADM2) chemical mechanism. Emissions will be processed in the vertical diffusion processing instead of in the chemistry processing as was done in earlier versions. The Plume-IN-Grid (PING) will be extended to include an aerosol processing capability. Atrazine emissions will be processed in CMAQ. MM5 version 3 output will be able to be processed by the meteorology chemistry interface processor (mcip). The emissions chemistry interface processor (ecip) is no longer needed with SMOKE.

The air quality modeling community recognizes the need to continue to improve the science and understanding used by models. The modeling results are used to make decisions that will influence future air quality. The science must be as correct and complete as possible. A modeling user-friendly modeling framework that will execute on a wide spectrum of computing platforms, and that does not require extensive, continuing software costs will make the air quality modeling available to a broad population of users. The Java-based release of Models-3/CMAQ intends to provide these capabilities in November 2001.

4. DISCLAIMER

This paper has been reviewed in accordance with the U.S. Environmental Protection Agency=s peer and administrative review policies and approved for presentation and publication. Mention of trade names or commercial products does not constitute endorsement or recommendation for use.

5. REFERENCES

Atmospheric Modeling Division, National Exposure Research Laboratory and EPA Systems Development Center, 2001, SMOKE Tool for Models-3 version 4.1: structure and operation documentation, EPA-600/R-01/04.

Beck, K., 2000, Extreme Programming Explained, Addison-Wesley, Reading, Massachusetts.

Byun, D., Benjey, W., Binkowski, F., Ching, J., Dennis, R., Eder, B., Gipson, G., Godowich, J., Lacser, A., LeDuc, S., Novak, J., Otte, T., Pierce, T., Pleim, J., Roselle, S., Schere, K., Young, J., Jang, C., Gillani, N., Biazar, A., Hanna, A., Coats, C., McHenry, J., Mathur, R., Shankar, U., Xiu, X., Odman, T., Tang, R., Wong, D. and Bourgeois, A., 2001, Description of Models-3/Community Multiscale Air Quality (CMAQ) model: system overview, governing equations, and science algorithms, EPA internal report.

Christiansen, J.H., 2000, A flexible object-based software framework for modeling complex systems with interacting natural and societal processes, in: 4th International Conference on Integrating GIS and Environmental Modeling (GIS/EM4): Problems, Prospects and Research Needs, Banff, Alberta, Canada, September 2-8, 2000.

EPA, 2001a, North Carolina,http://www.epa.gov/asmdnerl/mims/index.html.

EPA, 2001b,North Carolina, http://www.epa.gov/asmdnerl/models3/announce. html.

Houyoux, M. R. and Adelman, Z, 2001, Quality Assurance Enhancements to the SMOKE Modeling System, in: The Emission Inventory Conference: One Atmostphere, One Inventory, Many Challenges, 1-3 May, Denver, CO, U.S.Environmental Protection Agency.

LeDuc, S.K., Schere, K.L., Godowich, J.M. and Gipson G.L., 2001, Models-3/CMAQ Applications Which Illustrate Capability and Functionality, in: *Air Pollution Modeling and Its Application XIV*, S.-E. Gryning and F.A. Schiermeier., ed., Kulwer Academic/Plenum Publishers, New York, pp.737-738.

MCNC, 2001, North Carolina, http://envpro.ncsc.org/products/.

Thorpe, S., Ambrosiano, J., Coats, C., Eyth, A., Fine, S., Hils, D., Smith, T., Trayanov, A., Balay, R, Vouk, M., Turner, T., 1996, The Package for Analysis and Visualization of Environmental Data. Proc., Computing in Environmental Resource Management, 2-4 December, Research Triangle Park, NC, Air & Waste Management Assoc., 241-249.

FUZZY SETS APPLICATION FOR ESTIMATION OF AIR POLLUTED ZONE

Andry A. Dudatiev, Yuliya Y. Podobna, Pavlo A. Molchanov and Tatyana G. Holyeva*

1. INTRODUCTION

When the forecast of scales of pollution is realized directly after failure the concrete data about the amount of ejected SAPS (strongly affecting poisonous substances) and actual meteorological conditions are accepted (Ukraine Stuff of Civil Defense, 1999).

Generally, the area covered by a pollution zone consists of two parts:

- The equivalent amounts of poisonous substances in the primary and the secondary clouds are determined.
- The special table determines radiuses of pollution zones by the primary and the secondary clouds, accordingly G_1 and G_2. The full depth of a pollution zone, is stipulated by influence of the primary and the secondary SAPS clouds determined as follows:

$$G = G' + 0,5 \cdot G'' \quad (1)$$

where G is the full depth of a pollution zone, G " is the largest radius of pollution, G ' is the smallest radius of pollution.

In case of absence of accurate basic data about the influencing factors, the forecast of possible consequences is carried out using given parameters of meteorological data and the maximum possible SAPS ejection in a concrete situation. The given approach is not always optimum. It can be explained from the point of view both of the forecast accuracy, and the estimation of risk and unjustified costs for liquidation of consequences of an emergency.

The proposed technique allows to forecast a consequence of an emergency with a SAPS ejection when accurate basic data are absent. The purpose of the given technique is the minimization of the social and economic costs for liquidation of consequences of a failure on the basis of the Fuzzy Sets Theory (Zadeh, 1966).

---

*Andry A. Dudatiev, Yuliya Y. Podobna (envrisk@vstu.vinnica.ua), Pavlo A. Molchanov and Tatyana G. Holyeva, Department of Environmental/Industrial Safety, Vinnytsia State Technical University, 95 Khmelnytske Shosse, Vinnytsia 21010 Ukraine

Air Pollution Modeling and Its Application XV, Edited by
Borrego and Schayes, Kluwer Academic/Plenum Publishers, New York, 2002

2. DEVELOPMENT OF MATHEMATICAL MODEL FOR THE FUZZY INFERENCE OF FORECASTING CONSEQUENCES OF FAILURE WITH SAPS EJECTION

2.1. Representation of influencing factors in the form of linguistic variables

During the description of the influencing factors as linguistic variables the five-mark scale was offered and tested. The offered scale is intended for the estimation of consequences (losses) in case of a failure on the chemically dangerous object. The interrelation between the offered scale and determination of the influencing factors as linguistic variables is suggested to be estimated as a functional dependence:

$$Y_i = f(x_1, x_2, \dots, x_j) \tag{2}$$

where Yi is the possible consequences of failures; $X_1 - X_j$ are the appropriate set of the influencing factors.

The main parameter that characterizes the consequence of an emergency is the radius of a pollution zone. This distance, on which the dangerous for life concentration of poisonous substance is distributed during any period of time.

We shall introduce the following denotations: X_1 is the wind speed, X_2 is the SAPS volume of SAPS ejected into the atmosphere, X_3 is the environment temperature, Y is the depth of pollution zone. Thus, the solution of a problem of forecasting consequences of a failure on chemically dangerous object lies in the corresponding a possible combination of the factors $(X_1 - X_3)$ to the determined value Y:

$$\tilde{Y}_i = f(\tilde{X}_i) \tag{3}$$

where $\tilde{Y}_i$ is the radius of a pollution zone expressed as linguistic variable; $\tilde{X}_i$ is the influencing factors expressed as linguistic variables.

The base terms corresponding to linguistic variables describing the influencing factors $\tilde{X}_1 - \tilde{X}_3$ were determined by the experienced experts. We shall evaluate the lower and upper values of base terms corresponding to the values of linguistic variables $\tilde{X}_1 - \tilde{X}_3$ and $\tilde{Y}$ using the five-mark scale: low {small}, below the average, average, above the average, high {large} (Filinyuk *et al,* 1998). Each value of a linguistic variable represents fuzzy set which is defined with the help of the appropriate membership function (Rotshtayn, 1999). The following ranges of values with appropriate linguistic estimations represented in Table 1 were determined for the introduced linguistic variables $\tilde{X}_1 - \tilde{X}_3$ and $\tilde{Y}$.

The typical situations which take place when forecasting are offered to be classified on three groups. Each group describes typical situations which take place in case of certain possible state of atmosphere: isothermition, convection, and inversion. The structure of creation of the rules for the fuzzy inference is represented in Figure1.

In order to avoid difficulties in calculations of radius of pollution zones all possible situations, which can take place when forecasting, are offered to be reduced to a typical situation. And it is necessary to take into account linguistic terms and ranges, appropriate to them, which are represented in Table1.

Table1. Determination of influencing factors in the form of linguistic variables

Linguistic Variable	Linguistic Scale	Numerical Scale
Wind speed X_1	Low Below the average Average Above the average High	0-1 m/s 0-3 m/s 3-5 m/s 5-7 m/s > 7 m/s
Air temperature X_2	Low Below the average Average Above the average High	-20 ÷ (-10) °C -10 ÷ (- 0) °C 0 ÷ (-10) °C 10 ÷ (- 20) °C > 20
Waste volume X_3	Small Below the average Average Above the average Large	0-0,5 tonne 0,5-1 tonne 1 -3 tonne 3 -5 tonne > 5 tonne
Radius of pollution zone Y_i	Small Below the average Average Above the average Large	0 - 600 m 600 - 1500 m 1500 - 3000 m 3000 - 5000 m > 5000

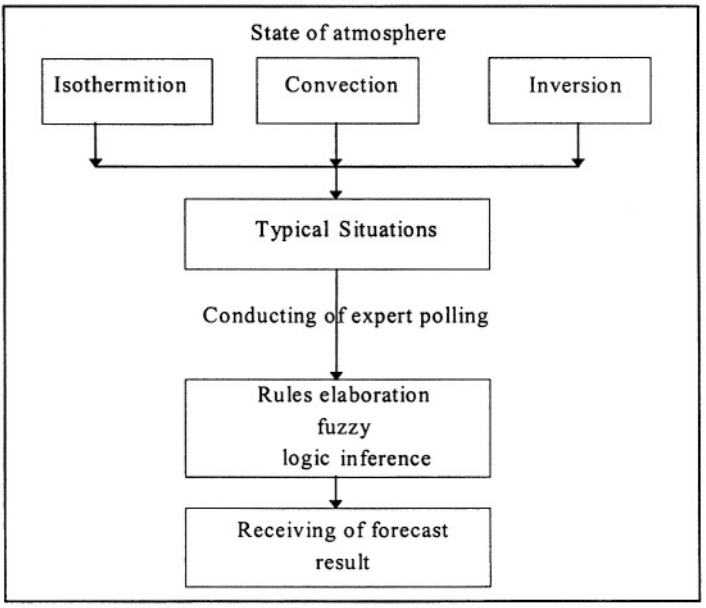

Figure 1. Structure of rules creation of fuzzy logic inference

2.2. Knowledge matrix and system of logical statements

A typical situation in this case is understood as value of the radius of pollution zone. This zone stands over the range at possible various values of the influencing factors.

The present technique shows, that the realization of forecasting at fuzzy basic data is conditionally carried out in five stages:

1. Determination of the equivalent SAPS contents in the primary and the secondary clouds expressed in terms by a linguistic variable (LV).
2. Determination of a correspondence between obtained values of equivalent values of SAPS in the primary and the secondary clouds and terms for LV " SAPS amount".
3. Determination of terms for LV " Wind speed " and other influencing factors.
4. Development of the fuzzy logical statements for realization of the forecast of the failure consequences in a case of SAPS ejection.
5. Realization of the forecast of the failure consequences on the basis of the obtained rules of the fuzzy inference.

The functional dependence between fuzzy value of the full depth of pollution zone and influencing factors is determined by the following equation:

$$\tilde{Y} = f(\tilde{Q}_{E1}, \tilde{Q}_{E2}, \tilde{X}_1, \tilde{X}_2, \tilde{X}_3) \tag{4}$$

where $\tilde{Q}_{E1}, \tilde{Q}_{E2}$ are the SAPS amounts are expressed as linguistic variables, $\tilde{X}_1 - \tilde{X}_3$ are the influencing factors.

The forecasting implements with the help of the developed rules of the fuzzy inference in the form: IF X = A THEN Y = B (Zadeh, 1966). Directly the development of the rules of the conditional inference has covered type of the following logical sentence:

$$\text{IF } x_1 \text{ is } a_1 \text{ and } x_2 \text{ is } a_2 \text{ and.... } x_n \text{ is } a_n \text{ THEN X is } d_1. \tag{5}$$

It is offered the given knowledge matrix that determines the system of the logical statements like « IF – THEN, ELSE », connecting value of input variables $x_1 \div x_n$ with one of possible values of an output variable d_j, $j = \overline{1, m}$:

IF $(x_1 = a_1^{l1})$ AND $(x_2 = a_2^{l1})$ AND ... AND $(x_n = a_n^{l1})$ OR
$(x_1 = a_1^{l2})$ AND $(x_2 = a_2^{l2})$ AND ... AND $(x_n = a_n^{l2})$ OR ...
$(x_1 = a_1^{lk_1})$ AND $(x_2 = a_2^{lk_1})$ AND ... AND $(x_n = a_n^{lk_1})$,
THAT $X = d_1$, ELSE

IF $(y_1 = a_1^{21})$ AND $(y_2 = a_2^{21})$ AND ... AND $(y_n = a_n^{21})$ OR
$(y_1 = a_1^{22})$ AND $(y_2 = a_2^{22})$ AND ... AND $(y_n = a_n^{22})$ OR ...
$(y_1 = a_1^{2k_2})$ AND $(y_2 = a_2^{2k_2})$ AND ... AND $(y_n = a_n^{2k_2})$,
THAT $Y = d_2$, ELSE ...

IF $(z_1 = a_1^{m1})$ AND $(z_2 = a_2^{m1})$ AND ... AND $(z_n = a_n^{m1})$ OR

$(z_1 = a_1^{m2})$ AND $(z_2 = a_2^{m2})$ AND ... AND $(z_n = a_n^{m2})$ OR ...

$(z_1 = a_1^{mk_m})$ AND $(z_2 = a_2^{mk_m})$ AND ... AND $(z_n = a_n^{mk_m})$,

THAT $Z = d_3$,

where a_i^{jp} is the linguistic estimation of input variables X, Y, Z, V in p^{th} row; j^{th} is the disjunction selected from an appropriate term set Ai, $i = \overline{1,n}$, $j = \overline{1,m}$, $p = \overline{1,k_j}$; k_j is the amount of the rules determining the value of the output variable $Q = d_j$.

In connection with this the knowledge matrix for input and output variables are developed and represented in Table 2.

Table 2. Knowledge matrix for input variables x_i and output variable X

Number of input combination of values	Input variables				Output variables
	x_1	x_2	...x_i...	x_n	X
$l1$ $l2$ ... lk_l	a_1^{l1} a_1^{l2} $a_1^{lk_l}$	a_2^{l1} a_2^{l2} $a_2^{lk_l}$	$\dots a_i^{l1} \dots$ $\dots a_i^{l2} \dots$ $\dots a_i^{lk_l} \dots$	a_n^{l1} a_n^{l2} $a_n^{lk_l}$	d_l
...					
$j1$ $j2$ ... jk_j	a_1^{j1} a_1^{j2} $a_1^{jk_j}$	a_2^{j1} a_2^{j2} $a_2^{jk_j}$	$\dots a_i^{j1} \dots$ $\dots a_i^{j2} \dots$ $\dots a_i^{jk_j} \dots$	a_n^{j1} a_n^{j2} $a_n^{jk_j}$	d_j
...					
$m1$ $m2$ ... mk_m	a_1^{m1} a_1^{m2} $a_1^{mk_m}$	a_1^{m1} a_1^{m1} $a_1^{mk_m}$	$\dots a_i^{m1} \dots$ $\dots a_i^{m2} \dots$ $\dots a_i^{mk_m} \dots$	a_n^{m1} a_n^{m2} $a_n^{mk_m}$	d_m

Using an operation $\bigcup$ (OR) and $\bigcap$ (AND) the system of the logical statements can be rewritten in a more compact notation:

$$\bigcup_{p=1}^{k_j}\left[\bigcap_{i=1}^{n}\left(x_i = a_i^{ip}\right)\right] \rightarrow X = d_j \quad \text{when} \quad j = \overline{1,m} \tag{6}$$

Thus we formalized target ratio (4) as the system of the fuzzy logical expressions which bases on the knowledge matrix.

3. RESEARCH RESULT

The research of possible depths of pollution zones allows making a conclusion, that it is necessary to accept inversion from the three possible states of the atmosphere during consequences of failure at fuzzy initial data. Inversion is considered as a state which lead to maximum depth of a pollution zone.

Therefore in case of equal conditions, the solution is accepted proceeding from a condition:

$$\tilde{Y} = \max(\tilde{Y}_{IS}, \tilde{Y}_{IN}, \tilde{Y}_{C}) \tag{7}$$

where $\tilde{Y}$ is the forecast depth or the radius of pollution zone; $\tilde{Y}_{IS}$ is the forecast depth of a pollution zone in case of isothermition; $\tilde{Y}_{C}$ is the forecast depth of a pollution zone in case of convection; $\tilde{Y}_{IN}$ is the forecast depth of a pollution zone in case of inversions.

Thus when forecasting consequences of failure with SAPS ejection, in case of absence of accurate initial data the rule of inference are applied to a state of atmosphere - inversion. It is proved from the point of view of minimization of the risk of the population losses in a pollution zone. Nevertheless, economic costs will be always maximum and not always justified. For example, in daytime the atmospheric state can be only isothermition or convection. Therefore in daytime the forecast of consequences is expedient to conduct taking into account isothermition, as states of atmosphere leading to the large radius of pollution. Proceeding from it, the determination of depth of a pollution zone at fuzzy initial data is offered to present as:

$$\tilde{Y} = \begin{cases} \tilde{Y}_{IN} = f(\tilde{Q}_{E1}, \tilde{Q}_{E2}, \tilde{X}_1, \tilde{X}_2, \tilde{X}_3) \\ \tilde{Y}_{IS} = f(\tilde{Q}_{E1}, \tilde{Q}_{E2}, \tilde{X}_1, \tilde{X}_2, \tilde{X}_3) \end{cases} \tag{8}$$

where ($\tilde{Y}_{IN}$ - for night, $\tilde{Y}_{IS}$ - for day)

As a result of researches the values of radius of pollution zone during isothermition are obtained and are represented in Table 3.

Table 3. Values of radius of pollution zone in case of isothermition

Ejection volume	Wind speed	Temperature	Radius of pollution zone	
			Linguistic estimation	Numerical range
L	H	*	L	≤ 600 m
L	AA	*	BA	600-1500 m
L	H	*	BA	
BA	AA	*	BA	
BA	AA	*	A	1500-3000 m
H	AA	*	A	
BA	BA	L	AA	3000-5000 m
A	AA	*	AA	
AA	H	AA	AA	
BA	L	A	H	>5000 m
A	AA	*	H	

4. CONCLUSION

Divergence of calculation results of radius and area of polluted zone during certain period of time do not exceed:

- On the accurate input data for radius of polluted zone - 3 %; for pollution area - 20 %.
- On the recommended traditional technique with use of maximum volume of an ejection, inversion and wind speed (1 m\s) for radius of polluted zone - to 10 %; for pollution area - 50-150%.
- On the model use on the expert evaluations basis for radius of polluted zone -4 %; for pollution area 0-30%.

The offered engineering approach allows effectively conducting the first forecast in case of absence of the initial data. The advantage of the given technique is that its use allows saving significant costs at the expense of more actual forecasting.

5. REFERENCES

Filinyuk N., Molchanov P., Dudatiev A., 1998, *A Comprehensive Evaluation of Industrial Vehicle* Safety , AVCS ' 98: International Conference on Advances in Vehicle Control and Safety to Publication Chair HEUDIASYC/UTS-Compiegne, France, pp.105-107.

Rotshtayn A.P., 1999, *Intellectual Technologies of Identification: Fuzzy Sets, Genetic Algorithm,* Universum-Vinnitsa, Vinnytsia, P 320.

Ukraine Stuff of Civil Defense, 1999, *Technique of forecasting of scopes of infection toxic substances for failures on chemical dangerous objects and transport,* Kiev, p. 42.

Zadeh L.A., 1966, Fuzzy Sets, *Inf.Control,* vol. 18, pp. 338-353.

DISCUSSION

M. KAASIK — Did you use the degrees centigrade (°C) to calibrate the linguistic temperature scale ? If yes, then the scale seems to fit to arctic regions.

Y. PODOBNA — Yes, we used the (°C) for the calculation and appropriate determination of this influencing factor (air temperature) as a linguistic variable and numerical scale.
This was shown for typical example (chemically dangerous object, Vinnytsia).

A. HANSEN — Do you plan to extend your estimation methodology to include pollutant concentrations as well as pollutant zone ?

Y. PODOBNA — We will plan to extend the evaluation of concentrations. (as soon as possible). But now we have a work about assessment of primary forecast, and primary calculation for cases when the exact initial data are absent.

INITIAL APPLICATION OF THE ADAPTIVE GRID AIR QUALITY MODEL

M. Talat Odman, Maudood Khan, Ravi Srivastava, and D. Scott McRae*

1. INTRODUCTION

Grid size (or resolution), when inadequate, can be an important source of uncertainty for air quality model (AQM) simulations. Coarse grids used because of computational limitations may artificially diffuse the emissions, leading to significant errors in the concentrations of pollutant species, especially those that are formed via non-linear chemical reactions. Further, coarse grids may result in large numerical errors. To address this issue, multi-scale modeling and grid nesting techniques have been developed (Odman and Russell, 1991; Odman et al., 1997). These techniques use finer grids in areas that are presumed to be of interest (e.g., cities) and coarser grids elsewhere (e.g., rural locations). Limitations include loss in accuracy due to grid interface problems and inability to adjust to dynamic changes in resolution requirements. Adaptive grids are not subject to such limitations and do not require *a priori* knowledge of where to place finer grids. Using grid clustering or grid enrichment techniques, they automatically allocate fine resolution to areas of interest. They are thus able to capture the physical and chemical processes that occur in the atmosphere much more efficiently than their fixed grid counterparts.

The adaptive grid methodology used here is based on the Dynamic Solution Adaptive Grid Algorithm (DSAGA) of Benson and McRae (1991). It employs a structured grid with a constant number of grid nodes. The modeling domain is partitioned into $N \times M$ quadrilateral grid cells. The grid nodes are re-positioned in a two dimensional space throughout the simulation according to a weight function which represents the resolution requirements. The area of the grid cells change due to grid node movements but the connectivity of the grid nodes remains the same. Further, since the number of grid nodes is fixed, refinement of grid scales in some regions is accompanied by coarsening in other regions where the weight function has smaller values. This results in optimal use of computational resources and yields a continuous multiscale grid where

* Talat Odman, Georgia Institute of Technology, Atlanta, Georgia, 30332-0512, talat.odman@ce.gatech.edu, Telephone: 770-754-4971, Fax: 770-754-8266. Maudood Khan, Georgia Institute of Technology, Atlanta, Georgia, 30332-0512. Ravi Srivastava, U.S. Environmental Protection Agency, Research Triangle Park, North Carolina, 27711. Scott McRae, North Carolina State University, Raleigh, North Carolina, 27695-7910.

Air Pollution Modeling and Its Application XV, Edited by
Borrego and Schayes, Kluwer Academic/Plenum Publishers, New York, 2002

the scales change gradually. Unlike nested grids there are no grid interfaces therefore, numerical problems related to the discontinuity of grid scales are avoided.

The adaptive grid algorithm was applied to problems with increasing complexity and relevance to air quality modeling. Starting with pure advection tests (Srivastava et al., 2000), it was applied to reactive flows (Srivastava et al., 2001 a) and to the simulation of a power-plant plume (Srivastava et al., 2001b). In all these applications, the adaptive grid solution was more accurate than a fixed, uniform grid solution obtained by using the same number of grid nodes. To achieve the same level of accuracy with the fixed uniform grid required significantly more computational resources than the adaptive grid solution. In this paper, we describe how the adaptive grid algorithm was implemented in an urban-to-regional scale AQM. After a brief discussion of model components, we report preliminary results from the first application of the adaptive grid AQM.

2. METHODOLOGY

An adaptive grid AQM simulation has two fundamental steps: a grid adaptation step, that is responsible for repositioning of grid nodes according to the grid resolution requirements, and a solution step, that simulates the physical and chemical processes that occur in the atmosphere. The solution (i.e., concentration fields) remains unchanged during the adaptation step and the weight function clusters the grid nodes in regions where finer resolution grids are required. In preparation for the solution step, the fields of meteorological inputs and emissions must be mapped onto the new grid locations. This task is also considered part of the adaptation step and is undertaken by efficient search and intersection algorithms. During the solution step, the grid nodes remain fixed while the solution is advanced in time. Ideally, the adaptation step should be repeated after each solution step owing to the change in resolution requirements. However, since the mapping of meteorological and emissions data is computationally expensive, we have chosen to apply the adaptation step less frequently. Whereas, the solution is advanced in time by one hour in several time steps, the adaptation step is performed once every hour. In order to ensure numerical stability, we require that the Courant number be smaller than unity as we determine the time step of the solution. The rest of this section consists of a more detailed description of the adaptation and solution steps.

2.1. Adaptation Step

The key to adaptation is a weight function that determines where grid nodes need to be clustered for a more accurate solution. Such a weight function, *w,* can be built from a linear combination of the errors in the concentrations of various chemical species:

$$w \propto \sum_n \alpha_n \nabla^2 c_n \qquad (1)$$

where ∇^2, the Laplacian, represents the error in c_n, the computed value of the concentration of species *n.* The chemical mechanisms used in AQMs usually have a large number of species. Due to non-homogeneous distribution of emissions and disparate residence times, each species may have very different resolution requirements.

Determining α_n such that pollutant concentrations (e.g., ozone) can be estimated most accurately is a current research topic. Here, all α_n are set to zero, except the one for NO. Further, the grid adaptation is restricted to the horizontal plane and the same grid structure, which is determined by the surface layer NO concentrations, is used for all vertical layers. This combined with the requirement that the Courant number should be less than unity may result in very small solution time steps because of high wind speeds aloft. Adaptation in the vertical direction is possible but significantly more complicated.

Repositioning of the grid nodes is accomplished by using the weight function. The new position of the grid node *i*, $\vec{P}_i^{new}$, is calculated as,

$$\vec{P}_i^{new} = \sum_{k=1}^{4} w_k \vec{P}_k \Big/ \sum_{k=1}^{4} w_k \tag{2}$$

where $\vec{P}_k$, $k = 1,\ldots,4$, are the original positions of the centroids of the four cells that share the grid node *i* and w_k are the associated weight function values.

Once the grid nodes are repositioned, cell-averaged species concentrations must be recomputed for the adapted grid cells. Holding the concentration field fixed and moving the grid is numerically equivalent to simulating the advection process on a fixed grid. Therefore, we use a high-order accurate and monotonic advection scheme known as the piecewise parabolic method (Collela and Woodward, 1984) to interpolate concentrations from the old to the new grid locations.

The calculation of the weight function, the movement of the grid nodes and the interpolation of species concentration from the old to the new grid locations are three distinct tasks of an iterative process. The process continues until the maximum grid node movement is less than a preset tolerance. A very small tolerance may lead to a large number of iterations. On the other hand, a large tolerance may not assure adequate resolution of the solution field. Currently, we stop iterating when, for any grid node, the movement is less than 5% of the minimum distance between the node in question and the four nodes that it is connected to.

After the grid nodes are repositioned, emissions and meteorological data must be processed to generate the necessary inputs for the solution step. Note that, unlike the practice with fixed grid AQMs, this processing could not be performed prior to the simulation because there is no *a priori* knowledge of where the nodes would be located at any given time. In case of meteorological data, an ideal solution would be to run a meteorological model (MM), which can operate on the same adaptive grid, in parallel, with the AQM. This would assure dynamic consistency of meteorological inputs but such a MM is currently nonexistent. Therefore, hourly meteorological data is obtained from a high-resolution, fixed grid MM simulation and interpolated onto the adaptive grid. For mass conservation, as a minimum requirement, the vertical wind components are readjusted later during the solution step as described in Odman and Russell (2000).

The processing of emission data is computationally an expensive task that requires identification of various emission sources falling into the adapted grid cells. Here, we treat all emissions in two categories: point and area source emissions. For simplicity, the mobile sources have been included in the area-source category, but treating them as line sources would yield better resolution. For the point sources, the grid cell containing the

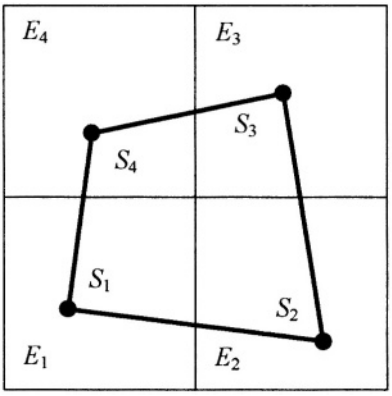

Figure 1. Intersection of an adapting grid cell with the area-source emissions grid.

location of each stack must be identified. The search may be quite expensive if there are thousands of stacks in the modeling domain. However, assuming that the cell containing the stack before adaptation would still be in close proximity of the stack after adaptation, the search can be localized. The localization of the search provides significant savings over more general, global searches. As for the area sources, they are first mapped onto a uniform high-resolution *emissions grid* using geographic information systems. This is done in order to avoid higher computational costs associated with processing of emissions from highly irregular geometric shapes presented by highways and counties. Around each adaptive grid cell there is a box of emissions grid cells $E_i, i = 1,\ldots,n$, as illustrated in Figure 1. Once E_i are identified, then their polygonal intersections with the adaptive grid cell are determined. Finally, the areas of these polygons, S_i, are multiplied by the emission fluxes of E_i and summed over n to yield the total mass emitted into the adaptive grid cell. This process is performed for all adaptive grid cells.

The final step in preparation for the solution step is reestablishing a uniform grid for easy computation of the solution. This requires computation of a transformation from the *(x, y)* space where the grid is non-uniform to the (ξ,η) space where the grid would be uniform. The calculation of the Jacobian of the transformation and other necessary metrics (i.e., $\partial\xi/\partial x, \partial\xi/\partial y, \partial\eta/\partial x, \partial\eta/\partial y$) concludes the adaptation step.

2.2. Solution Step

The atmospheric diffusion equation in the (ξ,η,σ) space can be written as

$$\frac{\partial(Jc_n)}{\partial t}+\frac{\partial\left(Jv^{\xi}c_n\right)}{\partial\xi}+\frac{\partial\left(Jv^{\eta}c_n\right)}{\partial\eta}+\frac{\partial\left(Jv^{\sigma}c_n\right)}{\partial\sigma}+\frac{\partial}{\partial\xi}\left(JK^{\xi\xi}\frac{\partial c_n}{\partial\xi}\right)$$
$$+\frac{\partial}{\partial\eta}\left(JK^{\eta\eta}\frac{\partial c_n}{\partial\eta}\right)+\frac{\partial}{\partial\sigma}\left(JK^{\sigma\sigma}\frac{\partial c_n}{\partial\sigma}\right)=JR_n+JS_n \tag{3}$$

where c_n, R_n and S_n are the concentration, chemical reaction and emission terms of species *n*, respectively, and σ is a terrain-following vertical coordinate. *J* is the Jacobian of the coordinate transformation:

$$J = \frac{1}{m^2}\frac{\partial z}{\partial \sigma}\left(\frac{\partial x}{\partial \xi}\frac{\partial y}{\partial \eta} - \frac{\partial y}{\partial \xi}\frac{\partial x}{\partial \eta}\right) \tag{4}$$

where *m* is the scale factor of a conformal map projection in the horizontal. The components of the wind vector in ξ and η directions are v^{ξ} and v^{η}:

$$\begin{aligned} v^{\xi} &= m\frac{\partial \xi}{\partial x}U + m\frac{\partial \xi}{\partial y}V \\ v^{\eta} &= m\frac{\partial \eta}{\partial x}U + m\frac{\partial \eta}{\partial y}V \end{aligned} \tag{5}$$

where *U* and *V* are real horizontal wind velocities rotated in the map's coordinate directions. The turbulent diffusivity tensor is assumed to be diagonal and its elements are $K^{\xi\xi}$, $K^{\eta\eta}$ and $K^{\sigma\sigma}$. The last element can be expressed in terms of the vertical diffusivity K^{zz} as

$$K^{\sigma\sigma} = \left(\frac{\partial \sigma}{\partial z}\right)^2 K^{zz}. \tag{6}$$

The expressions for v^{σ}, the wind component in the σ direction, as well as $K^{\xi\xi}$ and $K^{\eta\eta}$ are omitted here due to space limitations. Since the grid is uniform in the (ξ,η) space, solution algorithms can be taken directly from existing AQMs. We use those described by Odman and Ingram (1996).

3. MODEL VERIFICATION

The adaptive grid AQM is being verified by simulating ozone air quality in the Tennessee Valley region for the July 7-17, 1995 period. Meteorological data from a 4×4 km resolution simulation with the Regional Atmospheric Modeling System (RAMS) is being used. The emissions inputs for the region were developed from the Southern Appalachian Mountains Initiative (SAMI) inventory. There are over 9000 point sources in this domain including some of the largest power plants in the U.S.A. The area sources were mapped onto a 4×4 km emissions grid. The AQM grid consists of 112 by 64 cells, initially at 8×8 km resolution. In the vertical, there are 20 unequally spaced layers extending from the surface to 5340 m. Starting with 32 m, the thickness of each layer increases with altitude.

Figure 2 shows the grid at 7:00 EST on July 7. Since the adaptation step is performed once an hour, the grid shown will not change until 8:00 EST. Note that the grid size

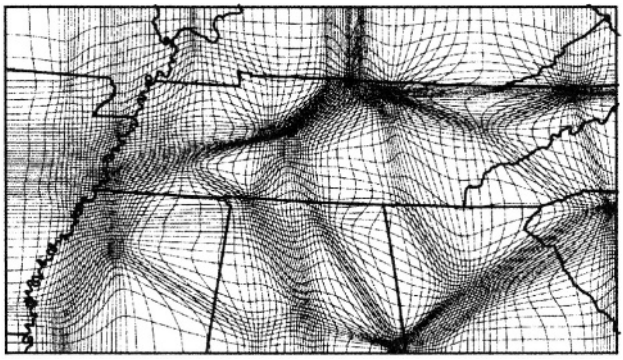

Figure 2. The grid used from 7:00 to 8:00 EST during the simulation of July 7, 1995.

reduced to few hundred meters around large point sources. With wind speeds larger than 10 m/s aloft, the solution time step can drop below one minute to keep the Courant number less than unity. Because of this the simulation is progressing at the speed of about

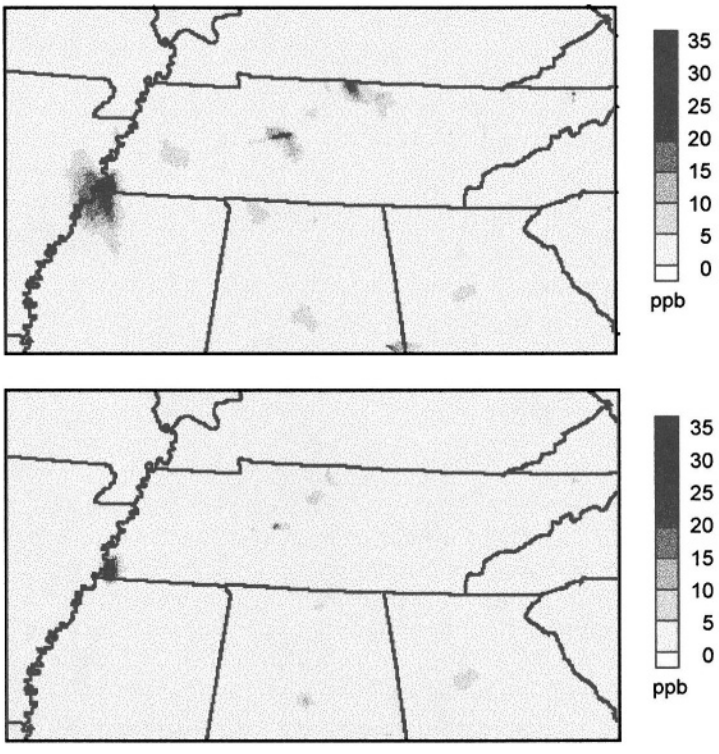

Figure 3. NO concentrations at 7:00 EST on July 7, 1995 from adaptive grid (top) and 4x4 km fixed grid (bottom) AQM simulations.

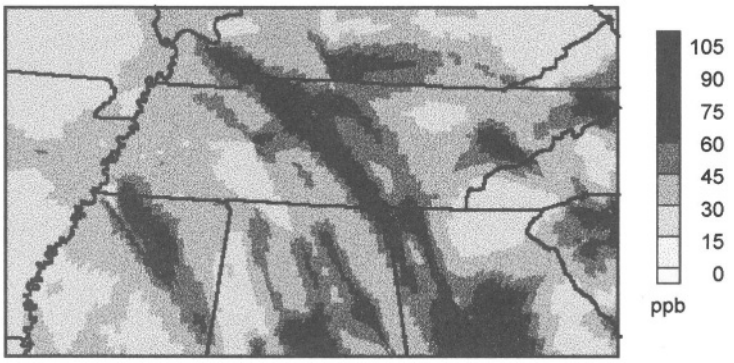

Figure 4. O_3 concentrations at 17:00 EST on July 7, 1995 from the adaptive grid AQM simulation.

2 hours of CPU time per simulation hour on a SUN Blade workstation (Model 1000) with a 750 MHz Ultra SPARC III processor.

The surface layer NO concentrations at 7:00 EST that were used in generating the grid in Figure 2 are shown in Figure 3 (top frame). Also shown are the NO concentrations at the same hour from a 4×4 km resolution fixed grid AQM simulation (bottom frame). The adaptive grid captures the NO gradients near source areas with a level of detail that is far superior to the fixed grid even though the latter used four times more grid nodes. It should be noted that some large power plant stacks, such as Cumberland, are emitting above the stable boundary layer at this hour. Since their plumes do not affect the surface layer NO concentrations, no grid clustering is observed in Figure 2 around such stacks. During daytime hours, as such plumes mix down and start affecting the surface layer NO concentrations grid nodes are clustered around them, along with other sources.

Figure 4 shows the ozone concentrations obtained from the adaptive grid AQM simulation at 17:00 EST on July 7, 1995. Since this is only the first day of the simulation, the ozone concentrations are probably still sensitive to the uniform initial conditions (35 ppb everywhere). However, the observed level of variability in the field and the captured detail in the gradients are encouraging. Once this simulation is finished, ozone fields will be compared to those obtained from fixed grid AQM simulation at 4×4 km and 8×8 km resolutions using the same inputs and solution algorithms. To complete the verification, all simulated ozone fields will be compared to observations from routine monitoring network as well as intensive field studies conducted in the region during this episode.

4. CONCLUSION

An adaptive grid, urban-to-regional scale AQM has been developed. A simulation with this model evolves as a sequence of adaptation and solution steps. During the adaptation step the solution (i.e., concentration fields) is frozen in time. A weight function that can detect the error in the solution is used to move the nodes of a structured grid. Iterative movement of the grid nodes continues until the solution error is reduced sufficiently. During the solution step, the grid is held fixed and the solution is advanced

in time. However, before this can be done, the meteorological and emissions inputs must be mapped onto the adapted grid. For meteorological inputs, data are interpolated from a very high-resolution mesoscale model simulation. For emissions, efficient search and intersection algorithms were developed to assure proper allocation of point and area sources to the cells of the adapted grid. Using coordinate transformations, the non-uniform grid can be mapped into a space where it becomes uniform. The atmospheric diffusion equation in this new space has been derived. Since the form of the equation is very similar to forms in existing AQMs and the grid is uniform, numerical algorithms developed for fixed uniform grid AQMs can be used to advance the solution.

To verify the model, the July 7-17, 1995 ozone episode in the Tennessee Valley is being simulated. So far, the grid is adapting to dynamic changes in the NO fields as expected. Nodes are clustered around major emission sources with grid resolutions around 200 m. The NO and O_3 fields show gradients with a level of detail that is likely unprecedented for a regional simulation of this scale. However, the simulation is progressing slowly due to very short solution time steps. This will probably necessitate changes in solution algorithms such as using an implicit advection scheme that is not subject to the Courant stability limit. Adaptation criteria are also being developed that would consider the errors not only in NO but in other species as well, especially those involved in important ozone formation reactions.

5. ACKNOWLEDGEMENTS

This research is supported by the U.S. Environmental Protection Agency under Grant Agreement No. R 827028-01-0. We thank Dr. Steve Mueller of the Tennessee Valley Authority for providing the meteorological data.

6. REFERENCES

Benson, R. A., and McRae, D. S., 1991, A Solution adaptive mesh algorithm for dynamic/static refinement of two and three-dimensional grids, in: *Proceedings of the Third International Conference on Numerical Grid Generation in Computational Field Simulations,* Barcelona, Spain, p. 185.

Collela, P., and Woodward, P. R., 1984, The piecewise parabolic method (PPM) for gas-dynamical simulations, *J. Comput. Phys.* **54**:174.

Odman, M. T., and Russell, A.G., 1991, A multiscale finite element pollutant transport scheme for urban and regional modeling, *Atmos. Environ.* **25A**: 2385.

Odman, M. T., and Ingram, C., 1996, *Multiscale Air Quality Simulation Platform (MAQSIP): Source Code Documentation and Validation,* MCNC Technical Report ENV-96TR002, Research Triangle Park, North Carolina, pp. 11-32.

Odman, M. T., Mathur, R., Alapaty, K., Srivastava, R. K., McRae, D. S., and Yamartino, R. J., 1997, Nested and adaptive grids for multiscale air quality modeling, in: *Next Generation Environmental Models and Computational Methods,* G. Delic, and M. F. Wheeler, eds., SIAM, Philadelphia, pp. 59-68.

Odman, M. T, Russell, A. G., 2000. Mass conservative coupling of non-hydrostatic meteorological models with air quality models, in: *Air Pollution Modeling and its Application XIII,* S.-E.Gryning, and E. Batchvarova, eds., Kluwer Academic/Plenum Publishers, New York, pp. 651-660.

Srivastava, R. K., McRae, D. S., and Odman, M. T., 2000, An adaptive grid algorithm for air quality modeling; *J. Comput. Phys.* **165**: 437.

Srivastava, R. K., McRae, D. S., and Odman, M. T., 2001(a), Simulation of a reacting pollutant puff using an adaptive grid algorithm, *J. Geophys. Res.,* in press.

Srivastava, R. K., McRae, D. S., Odman, M. T., 2001(b), Simulation of dispersion of a power plant plume using an adaptive grid algorithm, *Atmos. Environ.,* in press.

DISCUSSION

C. MENSINK — Your adaptive grid method is applied in two dimensions, using a Laplacian weighting function. Assuming that vertical diffusion processes are more important than horizontal diffusion processes it might be interesting to use grid refinement in the vertical direction. Do you think it is possible to extend the method to 3 dimensions ?

M. KHAN — Although it would be possible to perform grid adaptions in a 3-dimensional space, the additional computational costs are likely to be high and improvement in results might not to significant enough to justify these costs.

O. HELLMUTH — The scale dependency of the physical parameterizations becomes more important in adaptive grid air quality models compared to models using a static grid. This might be true especially for the design of the eddy diffusivity. How you are going to deal with that ? (maybe the concept of cut-off-wave length (grid size dependent) in connection with the evaluation of empirical or synthetical turbulence spectra to determine the eddy diffusivity might be worth to be considered). It would be nice to see, that your grid approach give arguments for turbulence modellers to deal further on with scale-dependent turbulence parameterizations.

M. KHAN — We are aware of these issues and plan to look at other parameterization techniques that might be more appropriate for adaptive grid air quality models.

A. HANSEN — Is your adaptive grid methodology mass conservative ?
What is the magnitude of numerical diffusion associated with your scheme ?

M. KHAN — We are conserving mass and using the same numerical algorithms as are used by the static grid to advance the solution in time.

C.FUNG It seems that the adaptive grid also balances the chemistry solver load. Has the run time increased or decreased ?

M. KHAN Run time has increased but the improvement in air quality modeling results more than justifies these additional computational costs.

APPLICATION OF INVERSE MODELING AND SENSITIVITY THEORY TO AIR POLLUTION STUDIES

Vladimir Penenko*

1. INTRODUCTION

A methodology of modeling for studies of atmospheric pollution of industrial regions is discussed. The methodology is based on variational principles. It includes the solutions of direct, adjoint and inverse problems for the model of transport and transformation of pollutants. The goal functionals and algorithmic constructions are designed in such a way that the model is used together with data of measurements. The algorithms are the combination of the direct and inverse procedures for the models of Lagrangean and Eulerian types. The variational principle provides the agreement of numerical schemes on all stages of computations. The links between the variations of functionals and input parameters of the model are established by means of sensitivity functions.

In the paper, a structure of numerical algorithms for transport and transformation of pollutants in the atmosphere of industrial regions is presented. The methodology develops the investigation on the atmospheric and environmental problems described by Marchuk (1982), Marchuk and Penenko (1979), Penenko (1981,1996), Penenko and Aloyan (1985), Penenko and Tsvetova (2000a).

The combined methods of the direct and inverse modeling are discussed. Such a combination is necessary for the solution of inverse problems, sensitivity studies and data assimilation. Their theoretical background leans upon variational principles which are specifically constructed. As a result, mathematical models turn out to be connected with observational data and some functionals defined on the space of the state functions.

In essence, variational principles are intended for estimation of the functionals and, as a consequence, for the solution of inverse problems. They generate the whole set of numerical algorithms and discrete analogs of the models. In their turn, mathematical models become both the constraints on the set of the state functions and the linkages between the state functions, parameters and external sources. Using the observations,

* Institute of Computational Mathematics and Mathematical Geophysics SD RAS 630090 Novosibirsk, Russia

Air Pollution Modeling and Its Application XV, Edited by
Borrego and Schayes, Kluwer Academic/Plenum Publishers, New York, 2002

mathematical models are applied for estimation of initial fields, for reconstruction of the time and space structure of the state functions and for more precise definition of model parameters. The proposed algorithms allow the estimation of model quality and data assimilation to be made simultaneously. To this purpose the optimization methods combined with the methods of model sensitivity evaluation are used. Adjoint problems play an essential role in the realization of this approach.

The basic elements of four types should be defined to represent the methodology (Penenko, 1996). They are:

- mathematical models of investigated processes,
- mathematical "models of observations" and the functions of environment quality,
- set of functionals on the space of the state functions,
- criteria for the model quality , design of observation and management planning.

The term " model of observations" describes the transformation of the state function to the observed process characteristics. Observations can be of contact, indirect and remote types. They determine the structure of the corresponding models.

2. MODELS OF THE PROCESSES

The advantage of operator notations is used to describe a general structure of algorithms . The model is written in the form

$$B\frac{\partial \vec{\varphi}}{\partial t} + G(\vec{\varphi}, \vec{Y}) - \vec{f} = \vec{r}(\vec{x}, t), \quad \vec{\varphi} \in Q(D_t), \quad \vec{Y} \in R(D_t). \tag{1}$$

The following notations are used here: $\vec{\varphi}$ is a state vector, $\vec{Y}$ is a parameter vector, B is a diagonal matrix, some diagonal elements of which can be zero, $G(\vec{\varphi}, \vec{Y})$ is a non-linear space operator , $\vec{f}$ is a function of sources, $D_t = D \times [0, \vec{t}]$, D is a domain of spatial variables $\vec{x}$, $[0, \vec{t}]$ is the time interval, $Q(D_t)$ is the space of state functions satisfying the boundary conditions, $R(D_t)$ is the range of admissible parameter values. For the considered class of problems the operator $G(\vec{\varphi}, \vec{Y})$ is defined by the hydrodynamic equations of the "atmosphere-water-earth" system, transport and transformation of pollutants, and by the relations at the interface boundaries. It includes all the terms of equations except the time derivatives.

The initial conditions at $t = 0$ and the model parameters can be written in the form

$$\vec{\varphi}^0 = \vec{\varphi}_a^0 + \vec{\xi}_0(\vec{x}), \quad \vec{Y} = \vec{Y}_a + \vec{\zeta}(\vec{x}, t). \tag{2}$$

Here, $\vec{\varphi}_a^0$ and $\vec{Y}_a$ are the given a priori estimates of the initial fields $\vec{\varphi}^0$ and the parameters' vector $\vec{Y}$. The boundary conditions for the closure of the model are the consequences of the physical content of the problem under investigation. To include observational data into the model processing, it is necessary to formulate the functional relationship between the measurements themselves and the state functions. Let this relation take the form

$$\vec{\Psi}_m = M(\vec{\varphi}) + \vec{\eta}(\vec{x},t)\,. \tag{3}$$

Here $\vec{\Psi}_m$ is the set of observed values; $M(\vec{\varphi})$ is the set of measurement models. The values of $\vec{\Psi}_m$ are defined on the set of points $D_t^m \in D_t$. The terms $\vec{r}(x,t)$, $\vec{\xi}(x)$, $\vec{\zeta}(x,t)$, and $\vec{\eta}(x,t)$ in (1)-(3) take into account the errors and uncertainties of the models, initial state, parameters and measurement models respectively. If the model and input data are exact, then the error terms should be omitted.

3. VARIATIONAL DESCRIPTION OF THE MODEL

To construct the direct and inverse modeling algorithms, it is necessary to have both the differential and variational formulations of the models. Let us give the variational form of the model (1)-(3) by means of the integral identity (Penenko, 1996)

$$I(\vec{\varphi},\vec{Y},\vec{\varphi}^*) = \left(B\frac{\partial\vec{\varphi}}{\partial t} + G(\vec{\varphi},\vec{Y}) - \vec{f} - \vec{r}\,,\ \vec{\varphi}^* \right) = 0, \tag{4}$$

$$\vec{\varphi} \in Q(D_t), \vec{\varphi}^* \in Q^*(D_t),\ \vec{Y} \in R(D_t)\,.$$

Here $\vec{\varphi}^*$ is an arbitrary sufficiently smooth co-state function, $Q^*(D_t)$ is the space of sufficiently smooth functions defined in D_t that is conjugated to $Q(D_t)$. The functional $I(\vec{\varphi},\vec{Y},\vec{\varphi}^*)$ in (4) is formed so that all the equations of model (1), initial and boundary conditions, conditions at the interface boundaries and external sources are included in it simultaneously. The form of the functional and inner scalar product in (4) are generated from the form of the total energy balance equation for model (1).

For example, the identity (4) for the model of transport and transformation of pollutants in the atmosphere has the form

$$\begin{aligned} I(\vec{\varphi},\vec{Y},\vec{\varphi}^*) \equiv \sum_{i=1}^{n} \Bigg\{ \int\!\!\int_{D_t} \Bigg[\left(\frac{\partial c_i}{\partial t} + \Lambda c_i, c_i^* \right) + \left((H\vec{\varphi})_i - f_i - r_i \right) c_i^* + \\ \mu_x \frac{\partial c_i}{\partial x}\frac{\partial c_i^*}{\partial x} + \mu_y \frac{\partial c_i}{\partial y}\frac{\partial c_i^*}{\partial y} + \mu_z \frac{\partial c_i}{\partial z}\frac{\partial c_i^*}{\partial z} \Bigg] dD\,dt + \\ \int_{\Omega_t} \left(\left((L\vec{\varphi}) - \vec{q} \right)_i - \mu_n \frac{\partial c_i}{\partial n} \right) c_i^*\, d\Omega dt \Bigg\} = 0\,, \end{aligned} \tag{5}$$

where $\vec{\varphi} = \{c_i\}, \vec{\varphi}^* = \{c_i^*\}$, $\vec{Y} = \{\mu_x, \mu_y, \mu_z, c_i^0, f_i, q_i, \ldots\}$ are the state function, adjoint or co-state function and parameter vector, c_i are the concentrations of pollutants, n is the number of substances, Λ is the transport operator, H is pollutants' transformation operator L is the boundary conditions operator, Ω and Ω_t are the boundaries of the domains D and D_t (Penenko and Aloyan, 1985, Penenko, Skubnevskaya et al., 1997 , Penenko and Tsvetova, 1999a).

4. FUNCTIONALS AS GENERALIZED CHARACTERISTICS OF THE PROCESSES

From the point of view of computational technology, the methods of inverse modeling are more suited to the work with global (integral) characteristics of the models and processes than to the work with the local ones. That is why we determine the set of such objects in the form

$$\Phi_k(\vec{\varphi}) = \int_{D_t} F_k(\vec{\varphi}(\vec{x},t))\chi_k(\vec{x},t)dDdt, \quad k = \overline{0,K},\ K \geq 1. \tag{6}$$

Here $F_k(\vec{\varphi})$ are some functions of $\vec{\varphi}$ of the given form and $\chi_k(\vec{x},t)$ are non-negative weight functions; $\chi_k(\vec{x},t)dDdt$ are the corresponding Radon's or Dirac's measures (Schwartz, 1967). In particular, the functions $\chi_k(\vec{x},t)$ can have a finite support in D_t. A low limit case occurs when one point acts as a support. Then the Dirac delta-function is the weight function $\chi_k(\vec{x},t)$ for this case. In the finite dimensional formulation, it is replaced by the Kronecker delta-function.

The functionals of five main types should be outlined: functionals of generalized description of the system behavior; quality functionals which evaluate deviations between measured and calculated values, measurement functional; restriction functionals, objective or cost functionals for control and design. The restriction functionals are introduced to take into account both the local and global constrains to the atmospheric quality in the problems of ecological management and design.

5. GENERAL FUNCTIONAL FOR INVERSE MODELING ALGORITHMS

Let us use the ideas of optimization theory and variational technique for the statement of inverse problems and for the construction of methods for their solution. In this case, all approximations are defined by the structure of the quality functional and by the way of its minimization on the set of values of the state functions, parameters and errors of the discrete formulation of the model. The basic functional is formulated so that all the available data, errors of the numerical model and input parameters are taken into account (Penenko, 1996):

$$\tilde{\Phi}^h(\vec{\varphi}) = \Phi_k^h(\vec{\varphi}) + 0.5\Big\{(\vec{r}^T W_0 \vec{r})_{D_t^h} + (\vec{\xi}^T W_1 \vec{\xi})_{D^h} + \tag{7}$$
$$+ (\vec{\zeta}^T W_2 \vec{\zeta})_{R^h(D_t^h)} + (\vec{\eta}^T W_3 \vec{\eta})_{D_t^m}\Big\}^h + \Big[\mathbf{I}^h(\vec{\varphi},\vec{Y},\vec{\varphi}^*)\Big]_{D_t^h},$$

where $W_i, i = \overline{0,3}$ are weight matrices. Here the first term is given by (6), the second term takes into account the model errors, the third term describes errors in the initial data, the fourth term is responsible for the errors of the parameters, the fifth term is evaluation of measured data errors , and the last one is a numerical model of the processes in a variational form, indexes h and T denote discrete analog and operation of transposition of corresponding objects .To continue, a minimization functional problems with respect to

the components of the vectors $\vec{r},\vec{\varphi}_0,\vec{Y}$ with the help of variational principles are formulated . Then, with the use of (2),(3), the set of computational algorithms is obtained from the stationary conditions for $\tilde{\Phi}^h(\vec{\varphi})$ to variations of the components of vectors $\vec{\varphi}^*,\vec{\varphi},\vec{\varphi}^0,\vec{Y},\vec{r}$ on D_t^h. As a result of the problem solution, functions $\vec{\varphi},\vec{\varphi}^0$ describe the space-time system behavior, function $\vec{r}$ shows the model errors estimated with respect to data Ψ_m. Simultaneously, the solutions of adjoint problems and the set of sensitivity functions for the quality functionals presented by the first term in (6) are obtained. They can be used for design of observational experiments and ecological planning.

The construction of discrete analogs of the models, adjoint problems and sensitivity functions is built with the help of a sum analog of identity (4), (5)

$$I^h(\vec{\varphi},\vec{Y},\vec{\varphi}^*)=0,\ \vec{\varphi}\in Q^h(D_t^h),\ \vec{\varphi}^*\in Q^{*h}(D_t^h),\ \vec{Y}\in R(D_t^h). \qquad (8)$$

The method of weak approximation with fractional steps (splitting technique) is applied for time discretization. Numerical schemes for model (1) are obtained from the stationary conditions of the functional $I^h(\vec{\varphi},\vec{Y},\vec{\varphi}^*)$ at arbitrary and independent variations of the grid functions $\vec{\varphi}\in Q^h(D_t^h)$ and $\vec{\varphi}^*\in Q^{*h}(D_t^h)$ at the grid nodes D_t^h. Constructively, these conditions are realized by the operations

$$\frac{\partial}{\partial\varphi^*}I^h(\vec{\varphi},\vec{Y},\vec{\varphi}^*)=0,\quad \vec{\varphi}^*\in Q^{*h}(D_t^h). \qquad (9)$$

The adjoint system is derived from the stationary conditions for the extended functionals $I^h(\vec{\varphi},\vec{Y},\vec{\varphi}^*)+\Phi_k^h(\varphi)$ with respect to the variations of the grid components of the state function $\vec{\varphi}$ on D_t^h:

$$\frac{\partial}{\partial\varphi}\left\{I^h(\vec{\varphi},\vec{Y},\vec{\varphi}^*)+\Phi_k^h(\varphi)\right\}=0,\quad \vec{\varphi}\in Q^h(D_t^h). \qquad (10)$$

The differentiation in (9)-(10) is realized with respect to the function grid components at every grid point. As a result, the systems of governing and adjoint equations are mutually coordinated via sum functional. For applications it is convenient to use direct and inverse problems (9) and (10) in combination, being in frames both the Lagrangean and Eulerian descriptions of the model (1) (Penenko and Tsvetova, 1999b).

The boundary conditions in (9)-(10) are taken into account by the coefficients and parameters of discrete equations. This is a consequence of the sum functional. If fractional time steps and decomposition into subdomains are used in the construction of identity (8) and functional (7), equations (9) and (10) are the numerical splitting schemes. The descriptions of specific approximations and methods for realization of splitting schemes for direct and adjoint problems are given by Marchuk (1982, 1995), Penenko (1981), Penenko and Aloyan (1985). It should be mentioned that approach proposed provides the stability of computational algorithms due to the energy balance that is inherent in the identity (4). The energy balance can be obtained from(4) if $\vec{\varphi}^*$ is replaced by $\vec{\varphi}$. The numerical model is constructed from (8) using this namely property. The set of adjoint equations is a consequence of approximations of the basic model.

6. ALGORITHMS FOR SENSITIVITY STUDIES

The analysis of the model sensitivity to the variations of input parameters is an essential step in the solution of the numerical simulation problems. Especially, this is necessary to be done when studying the real physical system behavior with the help of numerical models. In this case, sensitivity functions play a substantial role .If the model is considered together with observational data, the sensitivity functions make it possible to realize interrelations between observations and models. Algorithmically, the sensitivity analysis gives numerical values of the gradients of the functional (6) with respect to model parameters that are required for realizing optimization methods. By the way, we pose the problem of data assimilation in the models as a problem of optimization.

The construction of the main sensitivity relation is made according to algorithm

$$\delta\Phi_k^h(\vec{\varphi}) = \frac{\partial}{\partial\alpha} I^h(\vec{\varphi}, \vec{Y} + \alpha\,\delta\vec{Y}, \vec{\varphi}_k^*)\Big|_{\alpha=0} \equiv A^h(\vec{\varphi}, \delta\vec{Y}, \vec{\varphi}_k^*), \tag{11}$$

where $\delta\Phi_k^h(\vec{\varphi})$ is the variation of evaluated functional, $\vec{\varphi}, \vec{\varphi}_k^*$ are the solution of the (10) and (11) with the unperturbed values of $\vec{Y}$, α is real parameter, $\delta\vec{Y} = \{\delta Y_i, i = \overline{1,N}\}$ are the variations of $\vec{Y}$.

The calculation of the sensitivity function is made by the formula

$$\Gamma_{ki} \equiv \frac{\partial\Phi_k^h(\vec{\varphi})}{\partial Y_i} = \frac{\partial}{\partial\delta Y_i} A^h\left(\vec{\varphi}, \vec{\varphi}_k^*, \delta\vec{Y}\right), \; i = \overline{1,N}, \; k = \overline{1,K}. \tag{12}$$

The sensitivity relations for the model of transport and transformation of pollutants (5) have the form

$$\delta\Phi_k^h(\vec{\varphi}) \equiv \left(\mathrm{grad}_{\vec{Y}}\,\Phi_k^h(\vec{\varphi}), \delta\vec{Y}\right) \equiv \sum_{i=1}^{N}\left(\Gamma_{ki}\delta Y_i\right) = \frac{\partial}{\partial\alpha} I^h\left(\vec{\varphi}, \vec{Y} + \alpha\delta\vec{Y}, \vec{\varphi}_k^*\right)\Big|_{\alpha=0} =$$

$$= \sum_{i=1}^{n}\left\{\int_{D_t}\left[\left(\delta(\Lambda c_i), c_i^*\right) + \delta\mu_x\frac{\partial c_i}{\partial x}\frac{\partial c_i^*}{\partial x} + \delta\mu_y\frac{\partial c_i}{\partial y}\frac{\partial c_i^*}{\partial y} + \delta\mu_z\frac{\partial c_i}{\partial z}\frac{\partial c_i^*}{\partial z} + \right.\right.$$

$$\left.(\delta(H\vec{\varphi})_i - \delta f_i)c_i^*\right]dDdt - \int_D \delta c_i^0 c_{ik}^*\Big|_{t=0} dD +$$

$$\left.\int_{\Omega_t}\left((\delta L\vec{\varphi})_i - \delta q_i - \delta\mu_n\frac{\partial c_i}{\partial n}\right)c_i^*\,d\Omega dt\right\} = 0. \tag{13}$$

Here symbol δ denotes variations of corresponding elements. The variations of the operators in (13) are calculated with the use of the variation of their parameters.

Multipliers at variations are the sensitivity functions of $\Phi_k^h(\varphi)$ to the corresponding variations. The definition of sensitivity functions allows the equations of feedback between parameters and functionals (6) to be introduced into the model set:

$$\frac{dY_i}{dt} = \gamma_i \Gamma_{ki}, \quad i = \overline{1, N} \ , \tag{14}$$

where γ_i are the proportional coefficients that are calculated during the functional estimation procedure. The methods of direct modeling are based on the solution of the problem (9). The field of application of inverse modeling is wider than that of direct one. In our case the structure of inverse modeling algorithms are defined by the relations (10)-(14).

7. APPLIED PROBLEMS

Depending on the statements of the problems and the purposes of investigation, the different applications of the modeling technology can be realized. Here we list the most typical cases oriented to the problems of forecasting, monitoring and ecological design. In addition to the problems that are usually solved in the frameworks of direct modeling procedure, the following problems are connected with the combination of the direct and inverse modeling: calculation of sensitivity functions and variations of functionals; inverse problems for diagnosis and identification of parameters and sources of the model; data assimilation; comparison of the models and fitting the models of different scales; zoning the domains in accordance with the man-induced load levels; ecological design and risk evaluation; detection of the sources of pollution; atmospheric quality control; estimation of the informative content of monitoring systems; planning observations. Algorithms to the solution of the above listed problems are obtained as modifications of the general inverse modeling algorithm. The different aspects of methodology presented are described in the papers of the author and co-authors. The calculations are made on the base of the global model of pollutant transport. The atmospheric circulation for scenarios are reconstructed from Reanalysis data (Kalnay et al., 1996) in assimilation mode with the help of the system described by Penenko and Tsvetova (1999c). The "direct" problems of the "source-receptor" type and inverse problems of the "receptor-source" type are of great interest for the environmental quality studies. They allow ecologically dangerous regions for surroundings to be revealed and high risk vulnerability territories to be detected. Some examples of such problems are given by Penenko, Aloyan et al., (1989), Penenko and Tsvetova (1999b, 2000a, 2000b), Penenko (2001).

Penenko and Tsvetova (1999b) study the scales of interconnections in the climatic system. The two scenarios agreed with respect to the time interval are considered. The first one is the "direct" scenario on transport of pollutants while the Chernobyl accident. The second one is the inverse modeling scenario on estimation of danger for Lake Baikal to be polluted within the above mentioned time interval.

The inverse scenarios in Lagrangean and Eulerian statements are presented by Penenko and Tsvetova (2000a). The problem on identification of the sources that spread the bio-aerosols in the Western Siberian region is considered. Besides, estimation of the sources observability areas is made for the measuring site. The scenario on estimation of the domains in the Northern Hemisphere that could be polluted as the consequence of the release from aggregated sources in Central Europe is described by Penenko and Tsvetova (2000b). The technique for estimation of ecological risk is done by Penenko (2001). Japan, and the Russian Far East are revealed as examples of the domains of high ecological risk.

The problems under discussion are very complicated. In this connection some ways of increasing the efficiency of the algorithms should be mentioned. The general functional (7) is constructed so that all the models and functionals are additively included in it. As a consequence of the fact, we are able to generate multilevel parallel schemes by means of variational principles. This is one more evidence that the proposed approach appears to have considerable promise.

8. CONCLUSION

The proposed approach extends the capabilities of the models for diagnosing and predicting the processes in the climatic system and for planning and evaluating the information quality of observations.

ACKNOWLEDGEMENTS

The work is supported by the RFBR under the Grants 99-07-90422, 00-15-98543, 01-05-65313, the Russian Ministry of Industry and Science (0201.06.269/349), and European Commission (ICA2-CT-2000-10024).

REFERENCES

Kalnay, E., Kanamitsu, M., Kistler, R., et al.,1996, The NCEP/NCAR 40-year reanalysis project. *Bull. Amer. Meteorol. Soc.* **77**, 437-471.

Marchuk, G. I.,1982,*Mathematical Modeling in the Environmental Problem,* [in Russian], Nauka, Moscow, 320 p.

Marchuk, G. I. ,1995, *Adjoint Equations and Analysis of Complex Systems* Kluwer Academic Publication.

Marchuk, G. I., Penenko, V.V.,1979, Application of optimization methods to the problem of mathematical simulation of atmospheric processes and environment. Proc. IFIP-TC7 Conf., N.Y. Springer., 240-252.

Penenko, V.V.,1981, *Methods of Numerical Modeling of the Atmospheric Processes,* [in Russian], Leningrad, Gidrometeoizdat, p. 352.

Penenko, V.V., 1996, Some aspects of mathematical modeling using the models together with observational data. *Bull. Nov. Comp. Center, Num. model. in atmosph.,* N 4, 31-52.

Penenko, V.V., 2001, Revealing the areas of high ecological vulnerability: the concept and approach to realization. *Atmos. Oceanic. Opt.,* **14**, 596-601.

Penenko, V.V., Aloyan, A.E., 1985, *Models and Methods for Environment Protection Problems,* [in Russian], Nauka, Novosibirsk, 256 p.

Penenko, V.V., Aloyan, A.E., Tsvetova, E.A. et al.,1989, Numerical estimation of anthropogenic loads on Lake Baikal , *Soviet Meteor. and Hydrol.* No 7, 76-84.

Penenko, V.V., Skubnevskaya.G.I., Tsvetova, E.A. et at., 1997, Numerical simulation of chemical kinetics and transfer of pollutants in the atmosphere of industrial regions. *Chemistry for sustainable development,* 5, 505-510.

Penenko, V.V., Tsvetova, E.A., 1999a, Mathematical models for the study of interactions in the system Lake Baikal-atmosphere of the region. *J. of Applied Mechanics and Technical Physics,* **40**, 308-316.

Penenko, V.V., Tsvetova,E.A., 1999b, Modeling of pollutant transport in direct and inverse problems of climatic-ecological monitoring and prediction, *Atmos. Oceanic Opt.,* **12**, 462-467.

Penenko, V.V., Tsvetova, E.A., 2000a, Some aspects of solving interrelated problems of ecology and climate. *J. of Applied Mechanics and Technical Physics,* **41**, 907-914.

Penenko, V.V., Tsvetova, E.A., 1999c, Preparation of data for ecological studies with the use of Reanalysis. *Atmos. Oceanic Opt.,* **12**, 447-449.

Penenko, V.V., Tsvetova, E.A., 2000b, A scale analysis of anthropogenic impact in the atmosphere. *Atmos. Oceanic Opt.,* **13**, 392- 396.

Schwartz, L ., 1967 *Analise Matematique,* Hermann.

SENSITIVITY ANALYSIS OF NESTED PHOTOCHEMICAL SIMULATIONS

Ioannis A. Kioutsioukis and Andreas N. Skouloudis*

1 INTRODUCTION

Photochemical models predict species concentrations based on a series of physical processes and data describing the status of the domain like, the boundary conditions and the emissions. The outcome of recent studies, regarding photochemical formation in large urban environments demonstrated that among the subtle issues to be fully explored (Peters et al. 1995; Pielke, 1998) is an evaluation of the sensitivity of an atmospheric chemical model due to perturbations. The magnitude of the perturbations should reflect the inherent inaccuracies in the observed data.

One of the first studies that utilised photochemical models for examining the importance of boundary conditions in emission control strategies was that of Winner et al. (1995). Specifically, they used the 3D photochemical model CIT (Harley et al., 1993) for the Los Angeles area (250 km x 150 km) in order to construct the isopleths of O_3 for 64 different scenarios of NO_X and VOC emission reductions. The runs of the model were executed in a supercomputer with 64 processors, which allowed them to produce two isopleth diagrams. In the first, they used clean (future) boundary conditions while in the second observed (present) boundary concentrations. Their results indicate that only with clean boundary conditions, the emission reduction scenario can lead to a harmonisation of the maximum concentration of O_3 with the existing limits. In the other case, O_3 will never be in line with the desired limits, for all emission reduction scenarios.

In another study, Hanna et al. (1998) studied the sensitivity of UAM-IV for various uncertainty parameters including the boundary conditions of O_3, NO_X and VOC. The model was executed for the New York domain (230 km x 290 km) and the sensitivity method employed was Monte Carlo. Having 109 uncertain parameters, they performed only 50 runs, where the uncertain parameters were selected randomly. The result of this preliminary study is that the maximum concentration of O_3 is affected mainly by the VOC emissions followed by the O_3 boundary concentrations.

* Ioannis A. Kioutsioukis (TP.361) and Andreas N. Skouloudis (TP.280), European Commission, Joint Research Centre, Environment Institute, Ispra, 21020, Italy.

Air Pollution Modeling and Its Application XV, Edited by
Borrego and Schayes, Kluwer Academic/Plenum Publishers, New York, 2002

A study of the impact of boundary conditions in real time simulations was conducted by Vautard (2000). The author used the results of the simplified synoptic scale photochemical model CHIMERE (operationally executed for Paris domain: http://callas.ens.fr) for the summer of 1999 and checked diagnostically the effect of boundary conditions by comparing the forecasted and observed concentrations. A Lagrangian back-trajectory model calculates the boundary conditions in CHIMERE while the meteorological data used were from ECMWF forecasts (http://www.ecmwf.int). The result of the study is that about 50% of the prognostic error in the forecasted concentrations is due to bad prediction of the boundary conditions.

In another study, Ziomas et al. (1998) studied the effect of alternative emission scenarios for the Athens domain, using data from the MEDCAPHOT-TRACE (Ziomas, 1998) campaign. The UAM-IV model was utilised in this work and the results indicate that the strategies should be focusing on VOC emission reductions.

In this work, are presented an outline of the research funded by European Commission, Directorate General of Research under the grant ENV4-CT97-5080. In the following sections are examined the effects in the modelled concentrations through variations of the boundary conditions and of emissions. This study was carried out with the Tangent Linear Model (TLM) of the 3D Air Quality model CAMx (Comprehensive Air-Quality Model with eXtensions). The TLM of CAMx is obtained by utilising the automatic differentiation tool ADIFOR (Automatic Differentiation in FORtran). The TLM has been extensively used for sensitivity studies in Meteorology (Errico et al., 1993; Vukicevic 1991, 1993).

2 SENSITIVITY ANALYSIS USING COMPUTATIONAL DIFFERENTIATION

Whether presented as a table of results from a set of exploratory runs, or formally encapsulated as a sensitivity coefficient, most parametric sensitivity studies either are equivalent or can be embedded in a problem of estimating derivatives. By differentiating the output of a model with respect to its parameters, one can quantify how sensitive or robust are the predictions of a model, relative to variations of that parameter, as well as gain insight into how to adjust parameters that are poorly known.

Automatic differentiation techniques augment, in a completely mechanical fashion, an existing code such that it also simultaneously and efficiently computes derivatives. The technique (Rall, 1981; Griewank, 1989) rely on the fact that every function, no matter how complicated, is executed on a computer as a sequence of elementary operations, such as addition or multiplication, and elementary functions, such as square root or log. By applying the chain rule of differential calculus to each stage in this sequence, one can compute derivatives of a function exactly (Bischof et al., 1992, 1994, 1996, 1998), in a completely mechanical fashion and efficient time saving (Horwedel, 1992; Hwang et al., 1997; Carmichael et al., 1997).

A large number of packages for automatic differentiation of model codes written in various programming languages are currently available. These tools mechanically generate from an existing code an augmented code that in addition computes derivatives. For these sensitivity studies, we used the ADIFOR package. The principal merit of using ADIFOR is that, for just one model run, we can assess the sensitivities of all model outputs with respect to all input parameters. Other advantages of the method include the

superb computational precision, ease of creature, as well as the less computational demands.

2.1. Methodology

Consider for example the boundary concentration of the pollutant j. If we perturb it by a factor e_j (Park et al., 2000):

$$C_{BND}{}^{j}(x,y,z,t,e_j)=(1+e_j)\,C_{BND}{}^{j}(x,y,z,t) \quad (1)$$

Then, any concentration field C_i that is influenced by the boundary concentration of j implicitly depends upon e_j. Expanding $C_i(e_j)$ in a Taylor series about the reference solution $[C_i(e_j=0)]$ and retaining only the first-order term, we obtain an approximation of the sensitivity of C_i with respect to e_j.

The interpretation of sensitivity information will be performed in two different ways: (a) the effect in the system of perturbing a variable and (b) the effect in a variable of perturbing another variable. The linear estimation of the change in concentration C_i that originates from a unitary perturbation in variable e_j is evaluated by means of the local sensitivity coefficient (LSC) (Saltelli et al., 2000):

$$S_i^{ij} = \frac{\partial C_i}{\partial e_j} \quad (2)$$

S_i can be interpreted as the sensitivity of C_i to a uniform relative change in the boundary concentrations of specie j. On the other hand, the global effect of perturbing a variable is studied in terms of a control function of the form:

$$J = \sqrt{\sum_{i=1}^{n}(C_i - C_i^0)\bullet(C_i - C_i^0)} \quad (3)$$

where, C_i is the perturbed concentration and C_0 the unperturbed one. The symbol • denotes the inner product of matrices A and B. The sensitivity of the control function can be calculated by the LSC as (global sensitivities):

$$\frac{\partial J}{\partial e_j} = \sqrt{\sum_{i=1}^{n}\frac{\partial C_i}{\partial e_j}\bullet\frac{\partial C_i}{\partial e_j}}\,. \quad (4)$$

3 RESULTS AND DISCUSSION

The domains for this sensitivity analysis were three cities with fundamental differences in the topography and the emissions. Namely, Athens (Ziomas, 1998; Ziomas et al., 1998), Milan (Volta et al., 1997; Silibello, 1998) and London (Derwent, 1993). These cities represent a typical subset out of eleven cities studied in the Auto-Oil II program (Skouloudis et al., 2001). Also, the CAMx model (Environ, 1998), which is a

Eulerian photochemical grid model that allows for integrated assessment of gaseous and paniculate air-pollution over many scales, was selected for the air-quality simulations. This model was utilised in a two-way nested formation with an outer-grid resolution of 0.06 degrees and with an inner-grid resolution of 0.02 degrees. The exact position of these grids is given in Table 1. The simulation period was an ozone episode lasting for several days and included the 98%tile concentration for 1995 (base year for AutoOil-II).

Table 1. The southwest coordinates in decimal degrees of the inner and outer domains.

Domain of	SW Corner – Outer grid	SW Corner – Inner grid
Athens	21.9 E, 36.6 N	23.1E, 37.5 N
London	2.4 W, 50.1 N	0.9 W, 51.0 N
Milan	8.1 E, 43.8 N	8.7 E, 45.0 N

3.1. Sensitivity of the System

Figure 1a shows the time evolution of the control function J, which indicates the effect of each perturbation (boundary conditions) in the system. It is interesting to observe that the sensitivity of the system is formed into clusters. The highest sensitivity to the whole system arises from perturbations at the boundary conditions of O_3, followed by the perturbations at VOC and NO_X. This hierarchical sequence was reproduced for all the cities. This implies that these results have a general character. The relative importance of perturbations at the boundary conditions of O_3, VOC, NO_X and CO to the system is 1: 0.2: 0.09: 0.04 (at the time of observed maximum O_3).

The investigated species are shown in Table 1. Among the many available results (Kioutsioukis, 2001), we will concentrate in the effects to the system and to O3.

Table 2. Species used in boundary and emission sensitivity simulations [a].

Species for Boundary Simulations	Species for Area Emission Simulations
NO, NO2, O3, PAN, NXOY, OLE, PAR, TOL, XYL, FORM, ALD2, ETH, CRES, MGLY, OPEN, PNA, CO, HONO, H2O2, HNO3, ISOP, MEOH, ETOH, ISPD, NTR	NO, NO2, OLE, PAR, TOL, XYL, FORM, ALD2, ETH, CO

[a] Acronyms can be consulted at Environ, 1998.

Similarly, in Figure 1b is shown the effect of perturbations at "area emissions". In this case also, the results for each city are sorted, but not for pollutants. In other words, the highest overall sensitivities are found in Milan and the lowest in London. This follows in analogy with the ratio of VOC/NO_X among the cities (maximum in Milan, minimum in London). However, we should not forget that the high values of the control function for perturbations in O_3 and VOC are related to the sensitivity of O_3 and VOC to their own conditions (net transport of O_3 and VOC inside the domain).

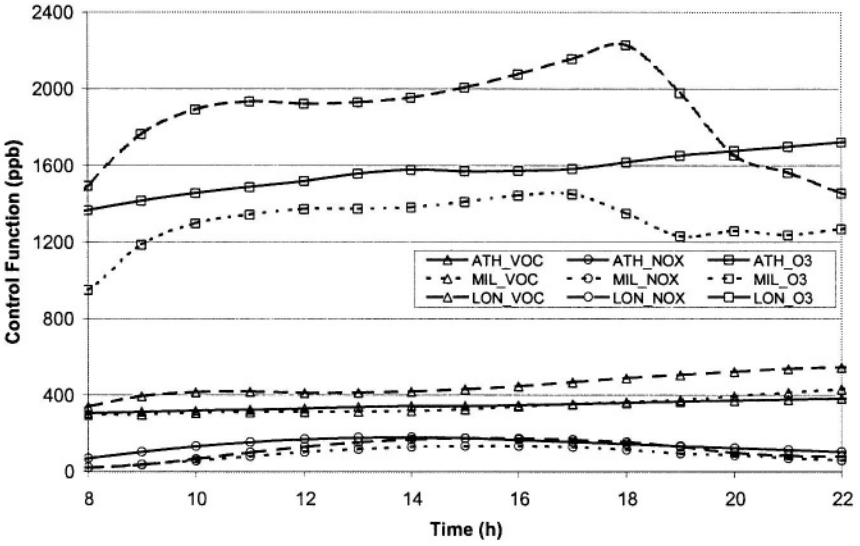

(a)

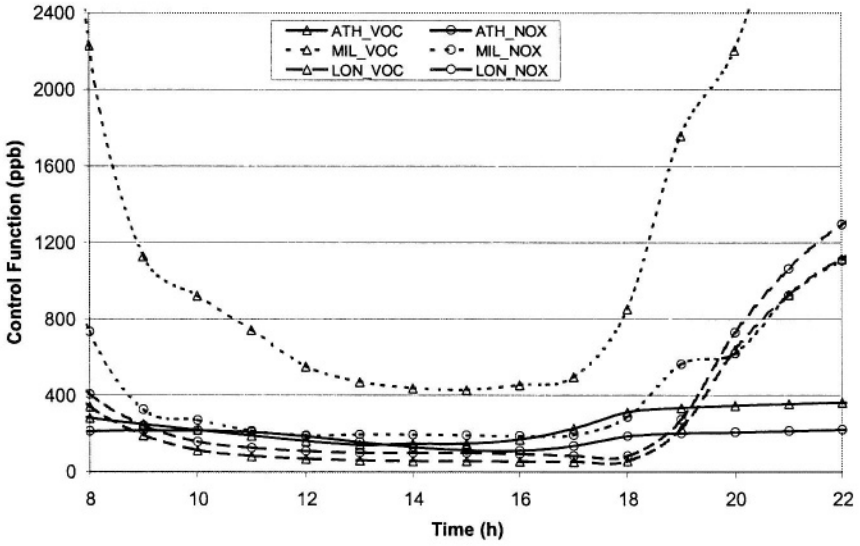

(b)

Figure 1. Sensitivity of the Control Function J for perturbations at (a) the boundary conditions and (b) the area emissions.

3.2. Sensitivity of O_3

Having examined the sensitivity of the system under various perturbations at the boundary conditions, we also demonstrate in this section the effect of the most significant overall perturbations (occurring at the highest sensitivity of the control function in Figures 1a and 1b) to O_3. Figure 2 shows the surface (a) non-linear and (b) tangent linear perturbation fields of O_3 at the time of the observed maximum O_3 concentration for 50% perturbation in the boundary conditions of O_3. The boundary conditions of O_3 in the unperturbed trajectory were 60 ppb.

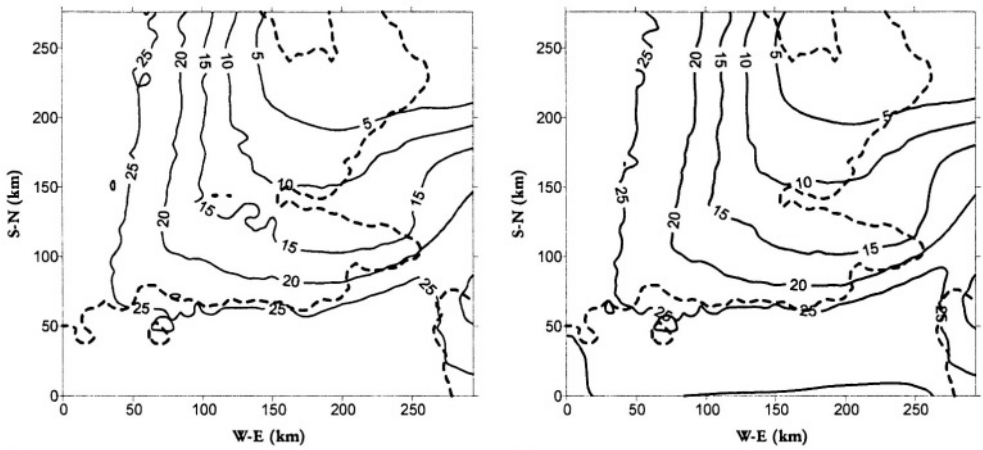

Figure 2. Surface O_3 sensitivities for 50% (a) non-linear perturbation and (b) linear perturbation at the boundary conditions of O_3.

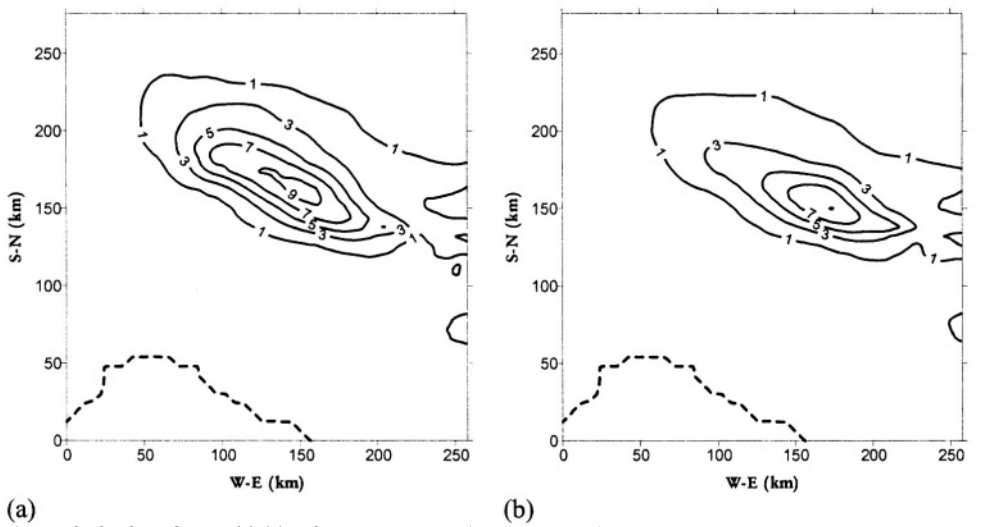

Figure 3. Surface O_3 sensitivities for 50% (a) non-linear perturbation and (b) linear perturbation at the area emissions of VOC.

The tangent linear perturbation fields predict the decay of the perturbation downwind from the boundaries and agree quite well with the non-linear sensitivities in both magnitude and location. This result was found in all three investigated cities. We also observe that S_1^{MAX} from O_3 equals always the boundary value of O_3 and its field decreases downwind from the boundaries. This is obvious since the boundary conditions of O_3 result in net transport of O_3 inside the domain. The percentage of the perturbation that reaches the nested inner area of interest is 30% for the city of Athens (150 km distance from the boundaries), 40% in London (125 km) and 50% in Milan (100 km).

The sensitivity of O_3 to the area emissions of VOC (Figure 3) indicates that O_3 is sensitive to the area emissions of VOC in downwind areas for large NO_X sources (hydrocarbon-limited areas). These areas of high sensitivity were reproduced well in the tangent linear solution. The maximum sensitivities calculated for each domain were a linear function of the VOC/NO_X ratio. The higher the ratio the higher the absolute change of O_3 that originates from perturbations at the VOC area emissions.

4 CONCLUSIONS

It is apparent that the evolution of the concentration fields, and thus, their predictability using a numerical model, is strongly influenced by the uncertainty in boundary concentration fields and the emission inventories. In this work, we applied an automatic differentiation tool (ADIFOR) to investigate the sensitivity of model outputs with respect to perturbations in the boundary conditions of 25 species and emission rates of 10 species. Then, we computed the relative importance of the most important perturbations in the system and in O_3 fields. *The inserted perturbations had a magnitude similar to observational uncertainties.*

The tangent linear model solutions, which describe the evolution of perturbations along trajectories of a time-dependent non-linear base state, represent well the corresponding non-linear perturbation fields accurately for the modelled period, which included the 98%tile O_3 concentration. This type of sensitivity analysis identifies, for the same change in each variable, which variable may include a larger forecast error at some specific time. Although this sensitivity information does not include non-linear effects, it does provide the fundamental characteristics of the changes in solution behaviour and forecast error. All simulations demonstrate that the highest sensitivity in an atmospheric system arises from perturbations at the boundary conditions of O_3.

5 ACKNOWLEDGEMENTS

The authors are grateful to Directorate General of Research of the European Commission for the grant ENV4-CT97-5080. Also, to Dr. P. Suppan from the Ludwig-Maximilians-Universitaet Muenchen, Germany for providing the emission files for the AutoOil-II cities and Mr Bruce Walker for all geographical data.

6 REFERENCES

Bischof C., P. Khademi, A. Mauer and A. Carle (1996): *ADIFOR 2.0 – automatic differentiation of Fortran 77 programs,* IEEE Computational Science & Engineering, 3, 18-32

Bischof C. (1994): *Automatic differentiation, tangent linear models and pseudo-adjoints,* High-Performance Computing in the Geosciences, Kluwer Academic Publishers, 462, 59-80.

Bischof C., A. Carle, G. Corliss, A. Griewank and P. Hovland (1992): *ADIFOR - Generating derivative codes from Fortran programs,* Scientific Programming, 1, 11-29.

Bischof C., A. Carle, P. Hovland, P. Khademi and A. Mauer (1998): *ADIFOR 2.0 User's Guide,* Mathematics and Computer Science Division, Argonne National Laboratory, Technical Memorandum 192.

Carmichael G.R., A. Sandu and F.A. Potra (1997): *Sensitivity analysis for atmospheric chemistry models via automatic differentiation,* Atmospheric Environment, 31, 475-489.

Derwent R.G. (1993): *United Kingdom Photochemical Oxidants Review Group, Ozone in the United Kingdom,* prepared at the request of the Air Quality Division, Department of the Environment, London.

Environ (1998): *User's Guide for Comprehensive Air Quality Model With Extensions (CAMx) 2.0,* 123p.

Errico R., T. Vukicevic and K. Raeder (1993): *Examination of the accuracy of a tangent linear model,* Tellus, 45A, 462-477 and , 45A, 539-557.

Griewank A. (1989): *On Automatic Differentiation,* Mathematical Programming: Recent Developments and Applications, Kluwer Academic Press, 83-108.

Hanna S., J. Chang and M. Fernau (1998): *Monte Carlo estimates of uncertainties in predictions by a photochemical grid model (UAM-IV) due to uncertainties in input variables,* Atmospheric Environment, 32, 21, 3619-3628.

Horwedel J., R. Raridon and R. Wright (1992): *Automated Sensitivity Analysis of an Atmospheric Dispersion Model,* Atmospheric Environment, 26A, 1643-1649.

Hwang D., D.W. Byun and M.T. Odman (1997): *An automatic differentiation technique for sensitivity analysis of numerical advection schemes in air quality models,* Atm. Envir., 31, 879-888.

Kioutsioukis I., A. (2001): Sensitivity Analysis of 3D Air Quality Models, PhD thesis, University of Thessaloniki, Greece.

Park S.K. and K.K. Droegemeier (1999): *Sensitivity analysis of a moist 1D Eulerian cloud model using automatic differentiation,* Monthly Weather Review, 127, 2180-2196.

Park S.K. and K.K. Droegemeier (2000): *Sensitivity analysis of a 3D convective storm - Implications for variational data assimilation and forecast error,* Monthy Weather Review, 128, 140-159.

Park S.K. and K.K. Droemegeier (1997): *Validity of the tangent linear approximation in a moist convective cloud model,* Monthly Weather Review, 125, 3320-3340.

Peters L., C. Berkowitz, G. Carmichael, R. Easter, G. Fairweather, S. Ghan, J. Hales, R. Leung, W. Pennell, F. Potra, R. Saylor and T. Tsang (1995): *The current state and future direction of direction models in simulating the tropospheric chemistry and transport of trace species – A review,* Atmospheric Environment, 29, 2, 189-222.

Pielke R. (1998): *The need to assess uncertainty in Air Quality Evaluations,* Atmospheric Environment, 32, 1467-1468.

Rall L. (1981): *Automatic Differentiation - Techniques and Applications,* Lectrure Notes in Computer Science, Vol. 120, Springer-Verlag, Berlin.

Saltelli A., K. Chan and E. Scott (2000): *Sensitivity Analysis,* John Wiley & Sons, 475p.

Silibello C., G. Calori, G. Brusasca, G. Catenacci and G. Finzi (1998): *Application of a photochemical grid model to Milan metropolitan area,* Atmospheric Environment, 32, 2025-2038.

Skouloudis A.N. (2001): *The Auto-Oil II Programme – Air Quality Report,* Version 7.2, 31 March, EUR Report 19725 EN.

Vautard R. (2000): *Real-Time validation of a forecasting chemistry transport model,* Proc. of the EUMENET Workshop on Ground-Level Ozone Forecasting, Langen, Germany.

Volta M. and G. Finzi (1997): *Photochemical pollution in Northern Italy. Emission inventory analysis and processing.* Environmental Research Forum, 7-8, 416-419.

Vukicevic T. (1991): *Nonlinear and linear evolution of initial forecast errors,* Monthly Weather Review, 119, 1602-1611.

Vukicevic T. and R.M. Errico (1993): *Linearization and adjoint of parameterized moist adiabatic processes,* Tellus, 45A, 493-510.

Winner D.M., G.R. Cass and R.A. Harley (1995): *Effect of alternative boundary conditions on predicted ozone control strategy performance: A case study in Los Angeles area,* Atmospheric Environment 29, 3451-3464.

Ziomas I. (1998): *The Mediterranean Campaign of Photochemical Tracers-Transport and Chemical Evolution (MEDCAPHOT-TRACE): An Outline,* Atmospheric Environment, 32, 2045-2053.

Ziomas I., P. Tzoumaka, D. Balis, D. Melas, C. Zerefos and O. Klemm (1998): Ozone episodes in Athens, Greece. A modelling approach using data from the MEDCAPHOT-TRACE, Atmospheric Environment, 32, 2313-2321.

DISCUSSION

A. HANSEN — Please clarify the objectives of your sensitivity analyses. Are the results intended to have policy relevance ?

I. KIOUTSIOUKIS — The main objective is to develop and validate a computationally efficient technique for the sensitivity analysis of complex 3D models. The technique can provide, in only one simulation, the sensitivities of all output variables with respect to all input parameters. However, since it is based on linear perturbation theory, it is valid for finite (realistic) perturbations in the input variables.

The relevance with policy is the following: We employ this technique first, to identify in one simulation, the influential and non-influential factors. After this screening, where we have reduced dramatically the uncertain parameters, we can employ a Monte Carlo analysis with e.g. FAST sampling (requires about 1000 simulations for 5 uncertain parameters) in order to explore the entire input phase space.

This page intentionally left blank

REVISITING OZONE-PRECURSOR RELATIONSHIPS

Bruce Ainslie and D.G. Steyn[1]

1. INTRODUCTION

The most widely accepted approach to investigating the sensitivity of ozone to precursor emissions is through the use of grid based Eulerian photochemical models. Unfortunately, these models are cumbersome; requiring immense input data (which may not always be available or of suspect quality) and involving considerable computing power all the while proving difficult to validate. The complexity of these models leads to them being treated as 'black boxes'. As a result, observation-driven methods (ODM) have been developed which provide a qualitative understanding of ozone sensitivity while corroborating the complex Eulerian models.

Observation-driven methods make use of ambient measurements and as such provide a more fundamental approach to assessing ozone sensitivities. One such model, the Integrated Empirical Rate (IER) model, derived from environmental chamber experiments (Johnson, 1984), consists of a simple set of functional relationships describing the formation of photochemical oxidant termed 'Smog Potential' (SP) defined as the concentration of NO consumed by photochemical reactions plus the amount of ozone produced. Observations show that SP evolves by a two stage process: 'light limited' and 'NOx limited'. Initially, photochemical oxidant production is linearly dependant on the cumulative light flux while in the 'NOx limited' stage, smog production ceases and maximum SP is proportional to initial NOx concentration only:

$$SP_{\max} = \beta [NOx]_o \qquad (1)$$

While the IER model provides an analytic form of ozone dependence to precursor concentrations, concerns have been raised about its validity. Equation (1) implies ozone production efficiency, defined as ozone produced for each NOx consumed, is independent of NOx, contrary to modeling studies (Liu et al., 1987). Blanchard et al. (1999), based on further chamber studies, showed that Eq. (1) should be replaced by:

[1] Atmospheric Science Programme, University of British Columbia, Vancouver, Canada.

Air Pollution Modeling and Its Application XV, Edited by
Borrego and Schayes, Kluwer Academic/Plenum Publishers, New York, 2002

$$SP_{\max} = \beta NOx^{\alpha} \tag{2}$$

calling their result the SP model with a equal to 2/3. Further analysis of outdoor chamber experiments by Chang and Rudy (1993) show that ozone concentrations, in the NOx-limited region, can be described by:

$$O_{3\max} = \gamma [NOx]^{1/2} \tag{3}$$

The purpose of this paper is to highlight a new approach for developing these models. This approach is based on the structure of a NOx/VOC ozone isopleth diagram and provides an analytic basis for Chang and Rudy (1993), encompasses Blanchard (2000) and Johnson (1984) while extending the models to analyze VOC reactivities.

2. DEVELOPMENT OF THE OZONE-PRECURSOR RELATIONSHIP

In order to develop a framework for the ozone-precursor relationship, consider an isopleth diagram with ozone concentration of zero at the origin. Consider any point A on the diagram with coordinates $([VOC]_A,[NOx]_A)$ and ozone concentration $[O_3]_A$ (see Figure 1 A). Let the ratio of VOC to NOx be given by R. The change in ozone, going from the origin to A, along the path R = constant, is given by the directional derivative:

$$DO_3 = \nabla O_3 \cdot \underline{u} = \left(\frac{\partial [O_3]}{\partial [VOC]}, \frac{\partial [O_3]}{\partial [NOx]} \right) \cdot (\cos\theta, \sin\theta) \tag{4}$$

where $\underline{u}$ is the unit normal along the path R = constant with slope θ (where $\tan\theta = 1/R$).

For [VOC] >> [NOx] (i.e. away from $[VOC] \approx 0$ region), $\theta \approx 1/R$ so $\cos\theta \approx 1$ and $\sin\theta \approx 1/R$. Substitution into Eq. (4) gives:

$$DO_3 \approx \left(\frac{\partial [O_3]}{\partial [VOC]} + \frac{\partial [O_3]}{\partial [NOx]} \cdot \frac{1}{R} \right) \tag{5}$$

Equation (5) can be further simplified by expressing the partial derivative, with respect to VOC, along the path R = constant, as a partial with respect to NOx. This then gives:

$$DO_3 \approx \frac{2}{R} \frac{\partial [O_3]}{\partial [NOx]} \tag{6}$$

Finally, the change in ozone concentration from the origin to point A can be expressed as:

$$DO_3 \approx \Delta O_3 / \| length \| \tag{7}$$

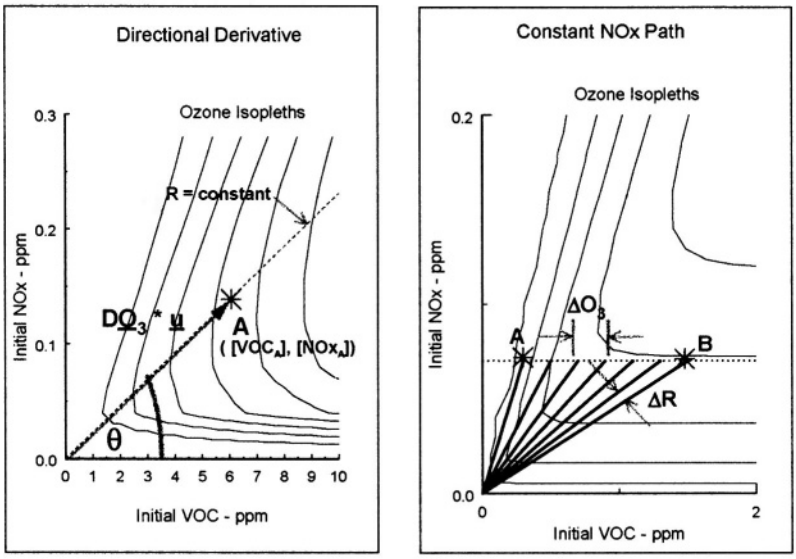

Figure 1. Schematics showing structure of NOx/VOC ozone isopleth diagram (symbols defined in text).

where the Cartesian length can be approximated by $\Delta[VOC]$ (for [VOC]>>[NOx]). Hence the change in ozone concentration is given by:

$$DO_3 \approx \frac{\Delta[O_3]}{\Delta[VOC]} = \frac{[O_3]_A - [O_3]_O}{[VOC]_A - [VOC]_O} = \frac{[O_3]_A}{[VOC]_A} \tag{8}$$

Equating Eq. (6) and Eq. (8) (and dropping the subscript A), we solve to find:

$$O_3 = g(R)[NOx]^{1/2} \tag{9}$$

which determines the general ozone-precursor relationship with $g(R)$ an unknown function of R only.

3. NORMALIZED OZONE FORMATION CURVE

In order to develop a model for $g(R)$, note that in the NOx-limited regime, Akimoto et al. (1979) and Blanchard (2000) have shown Eq. (3) is a good model for ozone concentration. Hence it is reasonable to expect $g(R) \to \gamma$ (a constant value) as $R \to \infty$. Also, the ozone concentration for a fixed amount of NOx is much smaller without hydrocarbons than in their presence, so expect $g(R) \to 0$ as $R \to 0$. In this way, $g(R)$ acts like a weighting function, reducing the maximum (NOx-limited) ozone concentration by the initial precursor ratio. Letting $g(R) = \gamma f(R)$ and following the ideas

of Sakamaki et al. (1982), we find $f(R)$ represents a normalized ozone formation curve, since it is expected that by Eq. (9), $[O_3]/\sqrt{[NOx]}$ will collapse ozone-precursor data to a single common curve characterizing the ozone formation of a NOx-VOC mixture.

To understand the shape of the normalized ozone formation curve, consider an isopleth diagram with two points A and B lying along a line of constant NOx (see Figure 1B). The ozone concentration at A can be expressed as the concentration at B less the difference in concentration between B and A. If we choose point B to have sufficiently large VOC concentration, so that it lies in the NOx limited region, its ozone concentration can be described by Eq. (3). Next, let the difference in ozone concentrations between A and B (called $\Delta(B-A)$) be broken it into a sum of small changes i.e.:

$$\Delta(B-A) = \sum_{[VOC]_A}^{[VOC]_B} \Delta[O_3] \tag{10}$$

where each $\Delta[O_3]$ is formed by the intersection of rays of constant R ranging from $R_A(=[VOC]_A/[NOx]_A)$ to $R_B(=[VOC]_B/[NOx]_B \approx \infty)$. Each small change of ozone can be expressed as:

$$\Delta O_3 = \gamma[NOx]^{1/2} f(R+\Delta R) - \gamma[NOx]^{1/2} f(R) \approx \gamma[NOx]^{1/2} f'(R)\Delta R \tag{11}$$

and in the limit as $\Delta R \to 0$ (with $f(R) \to 1$ as) $R \to \infty$ the concentration at A becomes:

$$[O_3]_A = \gamma[NOx]^{1/2} \int_0^R f'(R)dR \tag{12}$$

To understand the nature of $f'(R)$, consider that the highest ozone concentration, for a fixed amount of NOx, occurs in the NOx-limited region, so Eq. (11) can be rewritten as:

$$f'(R)\Delta R \approx \Delta O_3/[O_3]_{MAX} \tag{13}$$

The above can be given the following interpretation: $f'(R)$ describes the relationship between a small relative change in ozone stemming from a small change in the ratio of VOC to NOx. To further explore this, consider that when R is large (in the NOx-limited region), small changes in R (which along a path of constant NOx represent small changes in VOC), produce little relative change in ozone. Additionally, when R is zero (i.e. no VOCs), adding a small amount of VOC will produce a small amount of additional ozone resulting in only a small relative change. Hence, the bulk of the ozone change occurs between the very small and large values of R. Thus, $f'(R)$ describes a curve which is zero at the origin, rises to a maximum before tending back to zero for large R.

Two useful curves which satisfy above criteria are the lognormal and the Weibull distributions. Both of these curves have two parameters which can be adjusted to fit a range of shapes. Adopting the lognormal model for $f'(R)$, one finds the relation describing the concentration of ozone from initial precursor concentrations is:

$$O_3=\gamma NOx^{1/2}\int_0^R \frac{1}{\sqrt{2\pi}\sigma R}e^{-\frac{1}{2}\left(\frac{\log(R)-\mu}{\sigma}\right)^2}dR \qquad (14)$$

For the Weibull, one obtains.

$$O_3 = \gamma NOx^{1/2}\int_0^R \frac{\alpha}{\beta^{\alpha}}R^{\alpha-1}e^{-(R/\beta)^{\alpha}}dR \;=\; \gamma NOx^{1/2}(1-e^{-aR^b}) \qquad (15)$$

which is exactly the form suggested by Chang and Rudy (1993) (using the substitution $b=\alpha$ and $a=\beta^{-\alpha}$) developed through a semi-empirical analysis of smog chamber data. Both curves have 2 unknown parameters which are dependent on the VOC mixture.

4. AGREEMENT WITH MODEL OUTPUT

An example of the Weibull and Lognormal models are shown in Figure 2A. Model output was obtained from an OZIPR simulation using the CAL mechanism with VOC speciation given by Chang and Rudy (1990) and no dilution. The two parameters in each model were determined by a non-linear optimisation. Figure 2B shows how the lognormal model characterises ozone formation. The solid lines represent isopleths from the OZIPR simulation, the dashed lines are isopleths based on Eq. (14). The correlation coefficient between the two sets of isopleths is $r^2 = 0.995$.

5. HYDROCARBON REACTIVITIES

Another motivation for ozone-precursor research involves determining which compounds have a greater propensity for ozone formation. To measure the ozone forming capability of VOCs, numerous reactivity scales have been developed (Carter, 1994) and having an analytic model for ozone formation allows one to derive functional forms for these scales.

5.1 Maximum Ozone Reactivity (MOR)

The MOR refers to the situation where initial NO_x concentrations produce the maximum ozone levels for an initial VOC mixture. The resulting $[VOC]/[NO_x]$ ratio corresponds to the ridgeline (R_r) as defined by $\partial[O_3]/\partial[NOx]=0$. The lognormal model gives the following expression for this ridgeline (R_r):

$$f(R_r)-2R_r f'(R_r)=0 \qquad (16)$$

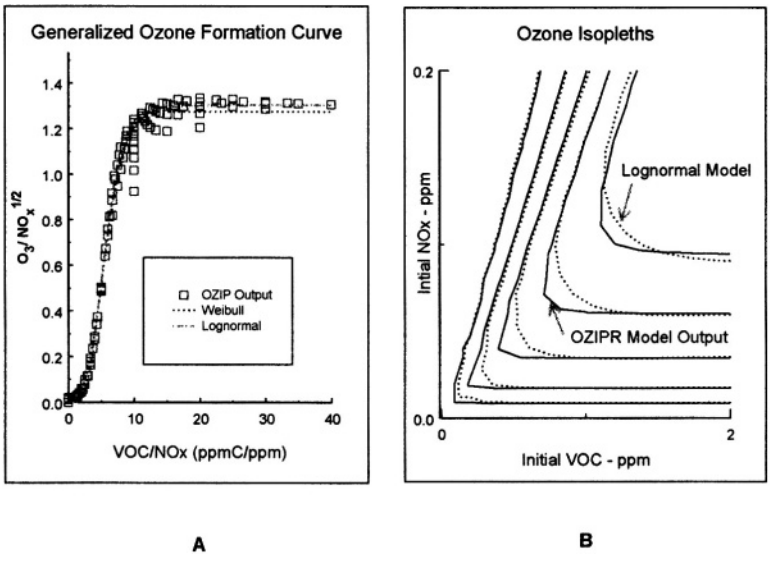

Figure 2. Comparison between model output and the lognormal and Weibull models.

which defines a straight line (R = constant). This line is determined by the VOC dependant parameters of $f(R)$ and divides the isopleth diagram into 2 regions: NOx sensitive and VOC sensitive.

5.2 Incremental Reactivity

The incremental reactivity (IR) of a hydrocarbon is defined as the change in peak ozone resulting from a small change in the VOC concentration (i.e. $IR=\partial[O_3]/\partial[VOC]$) which, for the lognormal model gives:

$$IR=\gamma\cdot\frac{1}{\sqrt{2\pi}\sigma}\cdot[NOx]^{-\frac{1}{2}}\cdot\frac{1}{R}\cdot e^{-\frac{1}{2}\left(\frac{\log R-\mu}{\sigma}\right)^2} \tag{17}$$

Equation (17) shows that IR is not a scalar but instead a complex function involving the initial NOx concentration and initial VOC to NOx ratio. From Eq. (17) one finds that for small R, IR is low but increases as R increases until it reaches a maximum. As R continues to increase, IR tapers off. This suggests there is a VOC/NOx ratio where IR is greatest (called Maximum Incremental Reactivity (MIR)). Taking the derivative of Eq. (17) with respect to R, setting it to zero allows one to solve for this ratio (R_c):

$$R_C = \exp\{\mu - 1/2\sigma^2\} \tag{18}$$

This shows the critical ratio is dependent, again, on only the two parameters of $f(R)$. Further analysis using the lognormal model, reveals that R_e must always be less than R_r (independent of VOC) consistent with modelling by Carter and Atkinson (1989).

5.3. Equal Benefit Incremental Reactivity (EBIR)

The EBIR refers to the condition where the initial NOx concentrations are adjusted so that the change in ozone due to a small change in VOC equals the change in ozone to a small change in NOx. Taking the derivative of Eq. (14) with respect to both NOx and VOC and equating the two gives the following expression:

$$2(1+R_e)f'(R_e)=f(R_e) \tag{19}$$

Which again defines a straight line determined by the ratio R_e and is uniquely determined by the two parameters. A sketch of changing reactivities against changing NOx concentrations was produced by Carter in his paper (1994) and is reproduced in Figure 3. A graph of the change in ozone with respect to VOC and NO_x, generated using the lognormal model is shown in Figure 4. The three ratios (MOR, MIR, EBIR) are marked on the graph. The data are not plotted against the initial ratio of $[VOC]/[NO_x]$, but against 'scaled' $[NO_x]$ - defined as the ratio of initial NO_x to the amount of NO_x required to produce the maximum ozone concentration (for a fixed amount of VOC). These curves clearly capture the ozone dependence sketched by Carter (1994) and have the advantage of being generated by an objective, theoretically developed model.

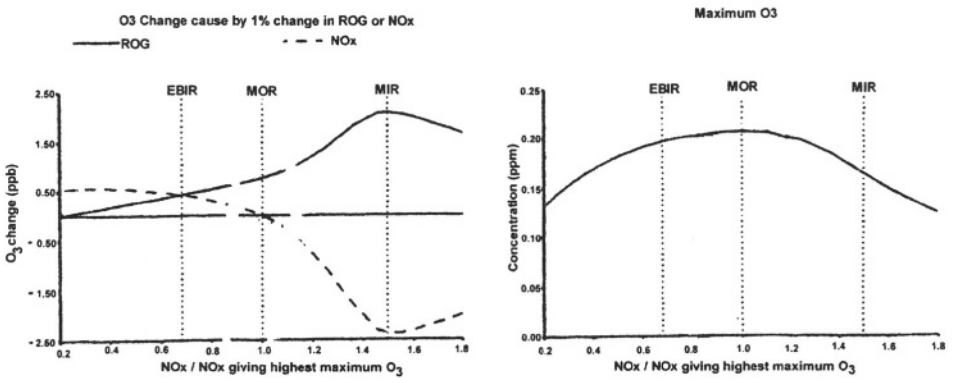

Figure 3. Qualitative sketch by Carter (1994) showing ozone behaviour versus scaled NOx.

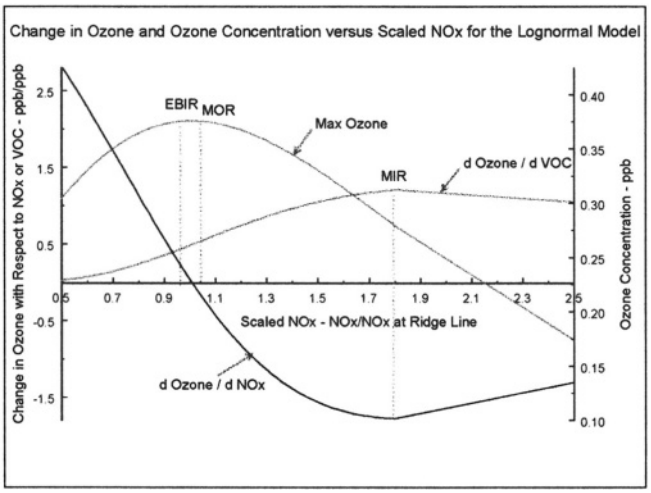

Figure 4. Reactivity scales as calculated by the lognormal model

6. CONCLUSIONS

An analytic model for ozone precursor relationships has been developed. It ties together the IER model (Johnson, 1984), SP model (Blanchard, 1999), work of Chang and Rudy (1993) and Carter (1994). Further research will add in effects of dilution, deposition and varying emission injection in order to use model in an urban environment.

7. REFERENCES

Akimoto, H., Sakamaki, F., Hoshino, M., Inoue, G. and Okuda, M., 1979. Photochemical Ozone Formation in Propylene-Nitrogen Oxide-Dry Air System. Environmental Science & Technology 13, 53-58.

Blanchard, C.L., 2000. Ozone Process Insights from Field Experiments – Part III: Extent of Reaction and Ozone Formation. Atmospheric Environment 34,2035-2043.

Blanchard, C.L., Lurman, F.W., Roth, P.M., Jefferies, H.E. and Korc, M., 1999. The Use of Ambient Data to Corroborate Analyses of Ozone Control Strategies. Atmospheric Environment 33, 369-381.

Carter, W.P.L., 1994. Development of Ozone Reactivity Scales for Volatile Organic Compounds. Journal of Air and Waste Management Association 44, 881-899.

Carter, W.P.L. and Atkinson, R., 1989. Computer Modeling Study of Incremental Hydrocarbon Reactivity. Environmental Science and Technology 23, 864-880.

Chang, T.Y. and Rudy, S.J., 1990. Ozone Forming Potential of Organic Emissions from Alternative-Fueled Vehicles. Atmospheric Environment 24A, 2241-2430.

Chang, T.Y. and Rudy, S.J., 1993. Ozone-Precursor Relationships: a Modelling Study of Semi-Empirical Relationships. Environmental Science and Technology 27, 2213-2219.

Johnson, G.M., 1984. A Simple Model for Predicting Ozone Concentration of Ambient Air. Proceedings of the Eighth International Clean Air Conference, Melbourne, Australia, pp.715-713.

Liu, S.C., Trainier, M., Fehsenfeld, F.C., Parrish, D.D., Williams, E.J., Fahey, D.W., Hubler,G. and Murphy, P.C., 1987. Ozone Production in the Rural Troposphere and the Implications for Regional and Global Ozone Distribution. Journal of Geophysical Research 92 (D4), 4191-4207.

Sakamaki, F., Okuda, M. and Akimoto, H., 1982. Computer Modeling Study of Photochemical Ozone Formation in the Propene-Nitrogen Oxides-Dry Air System. Generalized Maximum Ozone Isopleth. Environmental Science & Technology 16, 45-52.

DISCUSSION

A. HANSEN How do you derive the O_3 isopleths used in your simplified model ?

B. AINSLIE Isopleths are developed from plotting the ozone-precursor relationship. The unknown parameters in the model are found from regression to the model output. This then allows the ozone-precursor relationship to be fully defined and isopleths created.

This page intentionally left blank

ON THE RELATIONSHIP BETWEEN THE LAGRANGIAN AND EULERIAN TIME SCALE: A PRELIMINARY EVALUATION WITH LES DATA

U. Rizza[1], D. Anfossi[2], C.Mangia[1], G. A.Degrazia[3]

1.INTRODUCTION

In the Planetary Boundary Layer (PBL), Eulerian (i.e, fixed point) wind measurement is the only type of measurement which is generally feasible on a routinely way. However, when studying the atmospheric diffusion, interest focuses on the variation of velocity with time which would be observed following the air motion (Lagrangian description). Thus the basic problem of relating Eulerian and Lagrangian statistics (autocorrelation functions, structure functions, spectra and, in particular, time scales T_E, T_L) arises. Despite of substantial experimental and theoretical efforts (see, for instance: Gifford, 1955; Hay and Pasquill, 1959; Wandel and Kofoed, 1962; Corrsin, 1963; Saffman, 1963; Smith, 1967; Angell et[1] al., 1971; Hanna, 1981; Li and Meroney, 1985; Squires and Eaton, 1991; Wang et al., 1995; Querzoli, 1996; Koeltzsch, 1999; Phillips, 2000), a complete theoretical derivation of the T^L/T^E ratio in the PBL is not yet available. At present, most workers use the relationship

[1]Consiglio Nazionale delle Ricerche, Istituto ISIATA, Lecce, Italy, [2]Consiglio Nazionale delle Ricerche, Istituto di Cosmogeofisica, Turin, Italy, [3]Universidade Federal de Santa Maria, Departamento de Física, Santa Maria, RS, Brazil

Air Pollution Modeling and Its Application XV, Edited by
Borrego and Schayes, Kluwer Academic/Plenum Publishers, New York, 2002

$$T_i^L / T_i^E = \beta_i = \gamma \bar{u} / \sigma_i \qquad (1)$$

(where $i=u,v,w$, σ_i is the wind velocity standard deviation, γ is a numerical coefficient and $\bar{u}$ is the wind speed). This was suggested by Gifford (1955) and Hay and Pasquill (1959), on the basis of intuitive hypotheses and broad assumptions (i.e., at a first approximation Eulerian and Lagrangian correlograms are identical after appropriate rescaling of the time axis is done), to interpret their experimental results and approximately confirmed by other works (Wandel and Kofoed, 1962; Corrsin, 1963; Hinze, 1975; Hanna, 1981; Panofsky and Dutton, 1984; Degrazia and Anfossi, 1998, Anfossi et al., 2000).

The basic assumption (Gifford, 1955: Hay and Pasquill, 1959; Pasquill, 1974) of the above T_i^L / T_i^E ratio expression, is that

$$R_i^L(\xi) = R_i^E(t) \qquad \text{when} \qquad \xi = \beta t \qquad (2)$$

(R_i^L and R_i^E referring to the Lagrangian and Eulerian autocorrelation functions, respectively) which implies that the following relationship between Lagrangian (F_i^L) and Eulerian (F_i^E) spectrum function holds:

$$nF_i^L(n) = \beta n F_i^E(\beta n), \qquad (3)$$

where n is the frequency. The second assumption (Wandel and Kofoed, 1962; Corrsin, 1963) is that the T_i^L / T_i^E ratio is proportional to the turbulence intensity $\bar{u}/\sigma_i$. However the precise implications and limitations of equation (1) are not yet completely clear (Pasquill, 1974). Consequently it is the aim of this work to reconsider the problem. We will seek for an estimate of the T_i^L / T_i^E ratio by using a Large Eddy Simulation (LES) numerical technique, that has become an established tools to study turbulent flows at high Reynolds numbers. We performed the simulation of a typical flat terrain convective PBL (CBL) by means of the LES developed by Moeng (1984) and Sullivan et (1994).

Eulerian autocorrelation functions were directly estimated in the bulk of the CBL (a vertical layer around $0.5z_i$) from which the Eulerian time scales were estimated too. During such simulation, a large number of "particles" were released in the computation domain, spaced uniformly in the same region, and moved according to the LES turbulent field at each time step.

In the present analysis, following Squires and Eaton (1991), Wang et al. (1995) and Querzoli (1996), we did not account for the subgrid contribution to the particle displacement. According to Wang et al. (1995) LES is a viable technique for measurement of Lagrangian statistics, such as autocorrelation functions, because these quantities are strongly influenced by the large scales. Armenio et al. (1999) have

discussed the effects of the subgrid velocity fluctuations on particle motion finding that it can generally be disregarded. Nieuwstadt and Meeder (1997) included in their LES the subgrid contribution to the Lagrangian particle motion. This aspect will be closely considered in the future development of the present analysis. From the ensemble of computed trajectories the Lagrangian autocorrelation function and time scale were derived. In the present paper the first results of this work are presented.

2. AN OVERVIEW OF SIMULATION PERFORMED

2.1 Les Model

The LES model used in the present study was developed by C.H. Moeng at NCAR and described in detail by Moeng (1984) and Sullivan et al (1994). The numerical scheme is pseudo-spectral in the horizontal, and second-order centered finite difference in the vertical direction. The grid resolution is 128^3 in a (10x10x2) km domain. With such resolution the sub-grid eddies are of such small size that they receive their own energy from the energy cascade, thus being less sensitive to flow geometry. The eddy viscosity model is the new formulation proposed by Sullivan et al (1994). This in particular allows better matching with surface layer similarity theory as showed by the authors.
Turbulent regimes are generated by varying geostrophic wind and surface vertical heat flux. Moeng and Sullivan (1994) made a sensitivity analysis over such forcing parameters generating different turbulent regimes. We utilized data from their named experiment B to initialize our simulation. The initial and calculated CBL parameters are depicted in the following Table 1.:

Table 1. – LES parameters

Initial parameters				Simulated CBL parameters			
$(Z_i)_0$ (m)	(U_g,V_g) (m/s)	H_0 $ms^{-1}K$	u^* ms^{-1}	W^* ms^{-1}	(Z_i) m	$(Z_i)/L$	τ sec
1000	(10, 0)	0.24	0.56	2.02	1100	-18	540

Where $(z_i)_0$ is the initial inversion height, (U_g, V_g) are the components of geostrophic wind, H_0 is the surface temperature flux, u_* the friction velocity and finally $\tau = h/w_*$ is the large-eddy turnover time. Our simulation lasted around 15 turnover time to reach a nearly statistically stationary CBL. In such turbulent field the particles will be injected from uniformly distributed grid points in the mid-CBL.

2.2 Eulerian statistics

In order to calculate Eulerian auto-correlation and integral time scale forty fictitious Eulerian points have been distributed uniformly along the mid-CBL region $0.4 \le z/z_i \le 0.6$. This can be considered as a surrogate of anemometer wind velocity measurements. The corresponding auto-correlation function was determined as the average of each single one-point auto-correlation function.

$$R_i^E(\tau) = \frac{\overline{u_{Ei}(t_0)u_{Ei}(t_0+\tau)}}{\overline{u_{Ei}^2(t_0)}^{1/2}} \tag{4}$$

where u_{Ei} is the velocity in the x_i direction for the single Eulerian point.

2.3 Lagrangian statistics

After obtaining a statistically stationary Eulerian velocity field, 10.000 Particles were released in a range $0.4 \le z/z_i \le 0.6$ regularly distributed over the x-y plane.
The motion of particle trajectories is computed by solving the usual equation:

$$\frac{d\mathbf{x_p}(t)}{dt} = \overline{\mathbf{v}}_p(t) = \mathbf{u}_E\left[\mathbf{x_p}(t), t\right] \tag{5}$$

where $\mathbf{x_P}(t)$ is the particle-position vector and $\overline{\mathbf{v}}_p(t)$ is the resolved LES velocity field at the particle location. Each particle is transported in the fluid field and, in general, its position does not correspond with the grid points at which Eulerian field is defined. For this reason the velocity field needs to be interpolated onto the particle position. The evaluation of velocities at the particle position is carried out by a bilinear interpolation scheme among the closest grid points. This technique represents a good compromise between accuracy and computational efficiency. At the boundaries, in the x and y directions, a particle that moves out of the domain is re-introduced using the periodic boundary conditions, whereas a particle that reaches a wall is reflected.
Velocity of particles were used to compute the single-particle Lagrangian velocity autocorrelation. Assuming the flow stationary and homogeneous the Lagrangian velocity autocorrelation is defined:

$$R_i^L(\tau) = \frac{\left\langle v_{pi}(t_0)v_{pi}(t_0+\tau)\right\rangle}{\left\langle v_{pi}^2(t_0)\right\rangle^{1/2}} \tag{6}$$

where v_{pi} is the velocity of fluid particle in the x_i direction, and the angle brackets denote an average over the N particles released in the Mid CBL.
R_L is then a statistical measure of the coherent structures encountered by an ensemble of the particle during their motion through the fluid.

3. PRELIMINARY RESULTS

Figura 1 shows the Eulerian and Lagrangian autocorrelation functions for each component. It is evident that Eulerian velocity correlations are always smaller than the Lagrangian ones for small time separations. Concerning the estimation of time scales, both Eulerian and Lagrangian, three methods are generally used in the literature: best fit of autocorrelogram, integration of autocorrelogram and determination of the time at which the autocorrelogram decreases to 1/e. In the first and third method, an exponential decay for $R_i(\tau)$ is assumed. Hanna (1981) discussed the second and third method only. Since the second method was found to be less reliable, because the observed autocorrelogram does not generally approach zero at the largest time lags, Hanna chose the 1/e method. Moore et al. (1985) tested all the three methods and found that the first one (best fit) was the more accurate. Anfossi et al. (2000) choose the first one. Therefore, in the present analysis we evaluated T_i^E and T_i^L from the best fit of autocorrelation functions, assumed exponential (Figure 2).

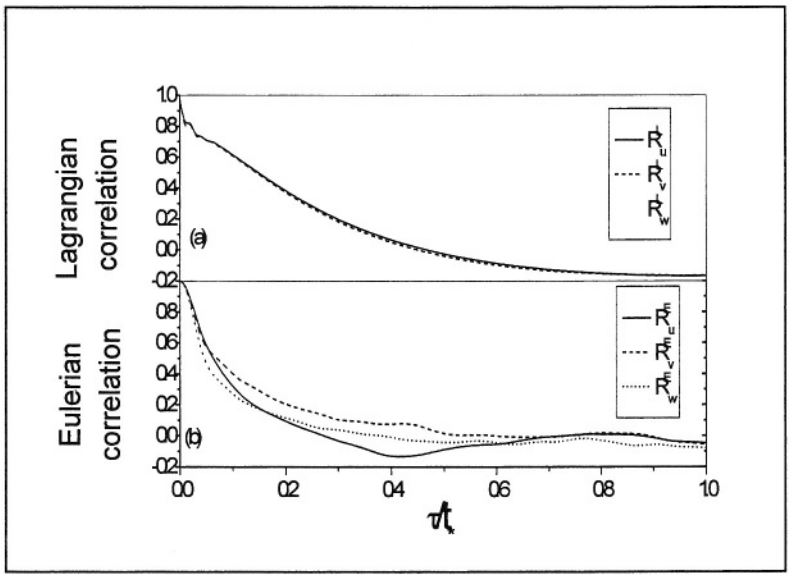

Figure 1 Velocity autocorrelation coeffiocients. (a) Lagrangian. (b) Eulerian

In Table 2 there are summarised the numerical values of Lagrangian/Eulerian time scale and the value of the ratio TL/TE. Results obtained are in the range of values found in literature. However they have to be considered preliminary. Further investigations and simulations have been planed in order to analyse the dependence on stability for the three components and the subgrid contributions.

Table 2 – Lagrangian and Eulerian time scale for each component

	TL	TE	TL/TE
U	98	41	2.4
V	96	64	1.5
W	96	39	2.4

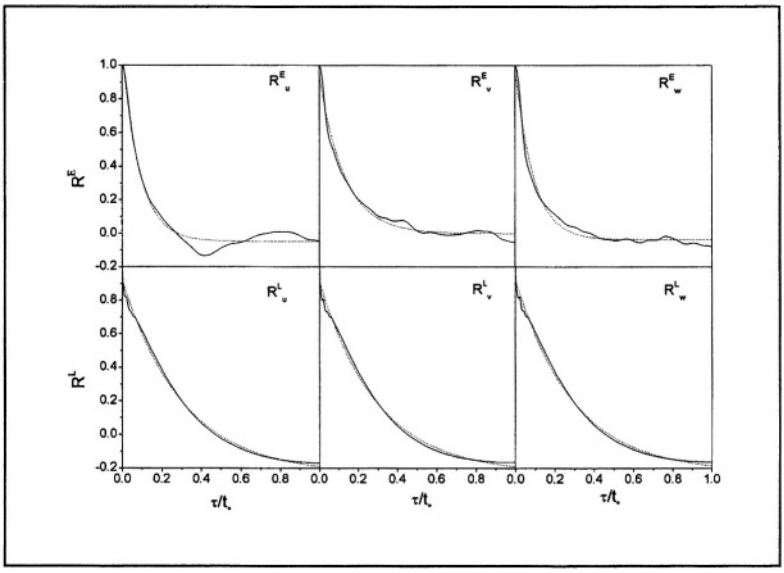

Figure 2 . Lagrangian and Eulerian velocity autocorrelation coefficients for each component. --- indicate exponential fit.

4. REFERENCES

Anfossi D., G. Degrazia, E. Ferrero, S.E. Gryning, M.G. Morselli, S. Trini Castelli, 2000, Estimation of the Lagrangian structure function constant C0 from surface layer wind data, *Bound.-Layer Meteor.* **95:** 249.

Angell J.K., Pack D.H., Hoecker W.H. and Delver N., 1971, Lagrangian-Eulerian time-scale estimated from constant volume balloon flights past a tall tower, *Quart. J. Roy. Meteorol. Soc.,* **97:** 87.

Armenio V., Piomelli U. and Fiorotto V., 1999, Effect of subgrid scales on particle motion, *Phys. Fluids,* **11:** 3030.

Corrsin S.,1963, Estimates of the relations between Eulerian and Lagrangian scales in large Reynolds Number turbulence, *J. Atmos. Sci.,* **20:** 115.

Deardorff J.W. and Peskin R.L.: 1970, 'Lagrangian statistics from numerically integrated turbulent shear flow', *Phys. Fluids,* **13**, 584-595

Degrazia G.A. and Anfossi D., 1998, Estimation of the Kolmogorov constant C_0 from classical statistical diffusion theory, *Atmos. Environ.,* **32:** 3611.

Gifford F.A., 1955, A simultaneous Lagrangian-Eulerian turbulence experiment, *Monthly Weather Rev.,* **83:** 293.

Hanna S.R.: 1981, Lagrangian and Eulerian time-scale in the daytime boundary layer. *J. Appl. Meteorol.,* **20:**242.

Hay J.S. and Pasquill F.:1959, 'Diffusion from a continuous source in relation to the spectrum and scale of turbulence'. *Atmospheric Diffusion and Air Pollution,* F.N. Frenkiel and P.A. Sheppard eds., *Advances in Geophysics,* **6**, 345, Academic Press

Hinze J.O., 1975, *Turbulence,* Mc Graw Hill, 790 pp

Koeltzsch K, 1999, On the relationship between the Lagrangian and Eulerian time scale, *Atmos. Environ.* **33:** 117.

Li W.W. and Meroney R.N., 1985, Re-examination of Eulerian-Lagrangian turbulence relationships, *Atmos. Environ.,* **19:** 853.

Moeng C.H., 1984, A Large Eddy Simulation Model for the Study of Planetary Boundary Layer Turbulence, *J. of Atmos. Sci.,* **41**, 13: 2052.

Moeng C.H. and Sullivan, P.P, 1994, A comparison of shear and buoyancy driven Planetary Boundary Layer flows, *J. of Atmos. Sci.* 51, **7**: 999.

Nieuwstadt F.T.M. and Meeder J.P., 1997, Large-Eddy simulation of air pollution dispersion: a review, in *New tools in turbulence modelling,* O. Metais and J. Ferziger editors, Lecture 13, 265-280

Panofsky H.A. and Dutton J.A., 1984, *Atmospheric Turbulence - Model and methods for Engineering applications,* John Wiley and Sons, New York, 397 pp

Pasquill F., 1974: '*Atmospheric diffusion*', Wiley & Sons, 429 pp

Phillips W.R.C., 2000, Eulerian space-time correlations in turbulent shear flows, *Phys. Fluids,* **12:** 205.

Querzoli G.: 1996, 'A Lagrangian study of particle dispersion in the unstable boundary layer', *Atmos. Environ.* **30:** 2821.

Saffman P.O.,: 1963, An approximate calculation of the Lagrangian autocorrelationcoefficient for stationary homogeneous turbulence, *Applied Science Res.,* **11**, 245

Smith F.B., 1967, Eulerian and Lagrangian time-scale relationship in one-dimensional turbulence, *USAEC Meteorological Information Meeting,* Chalk River, Canada (AECL-2787), 476-483

Squires K.D. and Eaton J.K., 1991, Lagrangian and Eulerian statitistics obtained from direct numerical simulations of homogeneous turbulence, *Phys. Fluids,* **A3:** 130.

Sullivan, P.P., Mc Williams, J.C., Moeng , C.H. 1994, A subgrid-scale model for large-eddy simulation of planetary boundary layer flows', *Bound.- Layer Meteor.,* **71**, 247.

Wandel C.F. and Kofoed-Hansen O.,1962, On the Eulerian-Lagrangian transform in the statistical theory of turbulence, *J. Geophys. Res.,* **76:** 3089.

Wang Q., Squires K.D. and Wu X., 1995, Lagrangian statistics in turbulent channel flow, *Atmos. Environ.* **29:** 2417.

DISCUSSION

O. HELLMUTH — As in the case of the autocorrelation length sales these should be a strong height dependency of the Eulerian time scale. Which results hereon you have found ? To which height your presented findings are related to ?

D. ANFOSSI — As I mentioned in my presentation, Eulerian measurements were carried out in the layer $0.4\ z_i - 0.6\ z_i$ and the Lagrangian trajectories started in the same layer.

A. BAKLANOV — Why did you study the CBL cases only ? I think, the SBL case is more interesting and important) for the relationship study (as 1 remember, the LES datasets of Mocny and Sullivan include some SBL cases as well). The most interesting case would be the SBL capped by free-flow stability with possible penetration of the internal gravity waves in the SBL.

D. ANFOSSI — We considered CBL cases only till now but we will consider stable cases also in the near future. We agree that stable cases are important for the reasons you mention.

NEW ALGORITHMS FOR THE DETERMINATION OF SOLAR RADIATION, SURFACE TEMPERATURE AND PBL HEIGHT IN CALMET

Maffeis G., Bellasio R., Scire J.S., Longoni M.G., Bianconi R., Quaranta N.*

1. INTRODUCTION

CALMET (Scire et al., 1999) is a diagnostic meteorological model that parametrises slope flows, kinematic terrain effects, terrain blocking effects, and includes a divergence minimisation procedure. CALMET contains also a micrometeorological model for the calculation of the planetary boundary layer parameters both overland and overwater. Since 1999 CALMET is the diagnostic meteorological model suggested by the US-EPA.

This work presents new algorithms thought to overcome some limitations currently present into the model. The modifications concern the energy balance equation, the temperature interpolation and the PBL height calculation. The original version of CALMET considers only the direct radiation impinging over the ground and does not include shadowing effects. New routines were added in order to take into account topography induced shadows and to calculate direct, diffuse and reflected radiation. Moreover CALMET determines ground temperature at grid points doing a pure spatial interpolation of measurements that does not consider the different heights above the sea level of the points themselves. New routines were added to take into account the vertical temperature gradient, topography properties such as slope and aspect and the vegetation cover. Finally the algorithm originally present in CALMET to calculate the planetary boundary layer height were substituted with those described by Batcharova and Gryning (1991) for daytime conditions and by Zilitinkevich (1989) for nighttime conditions. The algorithms for the calculation of the PBL parameters will be not described in the following of this paper. A comprehensive description of these algorithms can be found for example in Seibert et al. (2000).

* Maffeis G., TerrAria srl - via Zarotto 6 - 20124 Milano – Italy. Bellasio R. Enviroware srl - Centro Direzionale Colleoni, Andromeda 1 - 20041 Agrate Brianza (MI) – Italy. Scire J.S. Earth Tech, Inc. - 196 Baker Avenue – Concord, MA 01742 – USA. Longoni M.G. TerrAria srl - via Zarotto 6 - 20124 Milano – Italy. Bianconi R. Enviroware srl - Centro Direzionale Colleoni, Andromeda 1 - 20041 Agrate Brianza (MI) – Italy. Quaranta N. Office for Risk Prevention, Civil Protection, Lombardy Region - Via Fara, 26 - 20124 Milano – Italy.

Air Pollution Modeling and Its Application XV, Edited by
Borrego and Schayes, Kluwer Academic/Plenum Publishers, New York, 2002

The effect of the new algorithms introduced in CALMET is particularly significant for model applications over complex topography. The results of a simulation in the northern part of Italy, where the presence of the Alpes draws a very complex terrain, are presented.

2. BRIEF DESCRIPTION OF THE MODIFICATIONS

A schematic representation of the modifications introduced in CALMET is presented in Figure 1.

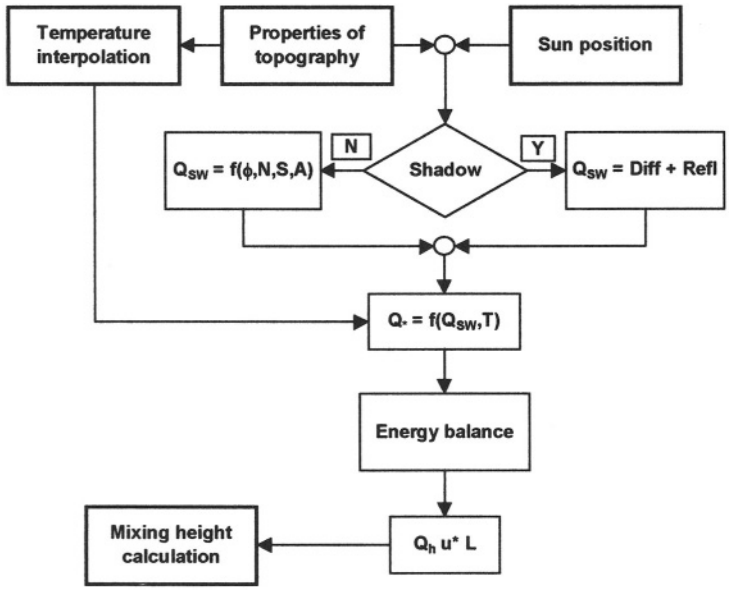

Figure 1. Schematic representation of the modifications introduced in CALMET.

During the setup process some properties of the topography, such as slope (S), aspect (A), horizon angle and view factor are calculated as explained for example in Dozier et al. (1981), Dozier and Frew (1990) and Gallant and Wilson (1996). For each hour of simulation and for each grid cell, the position of the sun is calculated. In order to determine if a given grid cell is shadowed by other topography, the horizon angle along the direction of the solar azimut is compared with the solar zenith. If the horizon angle exceeds the solar zenith, the cell is shadowed by the surrounding topography. In that case the direct component of the short wave radiation is null. The radiation balance is obtained considering both short wave and long wave ratiation. The latter is obtained using the atmospheric temperature calculated with the new interpolation algorithms that consider also terrain elevation and topography properties. Finally, solving the energy balance equation it is possible to obtain the scale parameters of the planetary boundary layer.

3. RADIATION BALANCE

The radiation balance over any surface, with arbitrary orientation in the space, can be written as (Moore et al., 1993):

$$Q_* = (1-\alpha)(R_{dir} + R_{dif} + R_{ref}) + \varepsilon_s L_{in} - L_{out}$$

Where Q_* is the net radiation (W/m^2), α is the albedo, R_{dir} is the direct short wave radiation (W/m^2), R_{dif} is the diffuse short wave radiation (W/m^2), R_{ref} is the reflected short wave radiation (W/m^2) ε_S is the emissivity of the ground, L_{in} is the long wave incoming radiation (W/m^2) and L_{out} is the long wave outcoming radiation (W/m^2).

The outcoming long wave radiation is given by the well known Stefan Boltzmann relation:

$$L_{out} = \varepsilon_s \sigma T_s^4$$

where σ is the stefan Boltzman constant ($5.67 * 10^{-8}$ $W/(m^2 K^4)$) and T_S is the ground temperature (K). The incoming long wave radiation is given by:

$$L_{in} = \varepsilon_a \sigma T_a^4 \upsilon + (1-\upsilon) L_{out}$$

where ε_a is the atmospheric emissivity, T_a is the atmospheric temperature and υ is the view factor. The atmospheric emissivity is a function of atmospheric temperature, vapour pressure of atmospheric water and cloud cover. The view factor indicates the fraction of sky visible from a specific point; it depends from surface slope, and topography around the point. A fast algorithm for the calculation of the view factor was presented by Dozier and Frew (1990).

Since ground temperature is not always available, and since it is not available in CALMET, the fourth power of that variable can be substituted by the fourth power of the atmospheric temperature plus the correction term $c_3 Q_*$, as done in Holtslag and van Ulden (1983). With this assumption the net radiation over a surface is written as:

$$Q_* = \frac{(1-\alpha)(R_{dir} + R_{dif} + R_{ref}) + \left[\varepsilon_s^2 (1-\upsilon) + \varepsilon_s (\varepsilon_a \upsilon - 1)\right] \sigma T_a^4}{1 - c_3 \left[\varepsilon_s^2 (1-\upsilon) - \varepsilon_s\right]}$$

In order to evaluate the net radiation, expressions for the short wave radiation components are needed. These expressions require the knowledge of properties of the actual topography such as slope and aspect that can be calculated as illustrated by Gallant and Wilson (1996).

Entering into the atmosphere the short wave radiation is attenuated along its optical path. An equation for the attenuation factor is (Thornton and Running, 1998):

$$\tau(\theta) = \tau_0^{m(\theta)\frac{p}{p_0}}$$

where τ_0 is the attenuation factor at nadir (typically 0.6), θ is the solar zenith, $m(\theta)$ is the non dimensional optical path and p and p_0 are the atmospheric pressures at current height and at sea level respectively. More complete formulation should consider also some pollutants (e.g. particulate matter) and water vapour.

The direct short wave radiation impinging on a sloping surface is written as:

$$R_{dir} = (\tau(\theta) + \gamma\,\chi) Z\, R_0\, \beta$$

where γ is the atmospheric transmission coefficient for the diffuse radiation (Liu and Jordan, 1960), χ is the circumsolar coefficient (typically 0.25), Z is the local zenith with respect to the sloping surface (Gallant and Wilson, 1996), R_0 is the solar constant corrected by the orbital vector (i.e. the ratio between the actual sun-earth distance and their average distance) and β is an attenuation factor due to cloud cover. This equation is valid if current topography is not shadowed by the surrounding topography, otherwise $R_{dir} = 0\ W/m^2$. Finally the diffuse and reflected components of the short wave radiation are respectively given by

$$R_{dif} = \gamma(1-\chi)\cos(\theta)\upsilon R_0$$

$$R_{ref} = (\tau(\theta) + \gamma)\cos(\theta)\alpha(1-\upsilon) R_0$$

4. TEMPERATURE INTERPOLATION

Present version of CALMET mainly calculates surface temperature field with a spatially weighted average of surface station temperature observations, where the dimensionless weighting factors are based on the distance r from the (i,j)th grid cell to the various surface meteorological stations (1/r or $1/r^2$ function could be used). This procedure is correct on an almost homogenous terrain, but begins to fail, for istance, in a complex terrain (close grid points along the horizontal direction could have different temperature if they have different altitudes).

The newly developed algorithms try to overcome these limitations taking into account the following parameters:

- different altitude respect to reference monitoring station;
- temperature vertical gradient;
- geometric characteristics (slope, aspect ..) of each grid cell;
- vegetation coverage.

Moore et al. (1993) present a specific algorithm to calculate temperature at a different altitude within a valley, where only one measure point is present. The following simple equation is proposed:

$$T_i = T_b - T_{lapse}\frac{z_i - z_b}{1000} + CS_i\left(1 - \frac{LAI_i}{LAI_{max}}\right) \quad S_i \geq 1$$

$$T_i = T_b - T_{lapse}\frac{z_i - z_b}{1000} - \frac{C}{S_i}\left(1 + \frac{LAI_i}{LAI_{max}}\right) \quad S_i < 1$$

where T_i is the unknown atmospheric temperature (K) at a z_i altitude (m), T_b is the measured atmospheric temperature (K) at a z_b altitude (m), T_{lapse} is the vertical temperature gradient (K/km), C is a constant usually equal to one, LAI_{max} and LAI_i are, respectively, maximum Leaf Area Index and its value at z_i, S_i is the ratio between net short radiation on the real surface (with its slope and aspect) and on an horizontal free surface. Temperature, following these two equations, increases for South oriented surfaces (S_i greater than one). Moreover the correction is a function of the leaf coverage (Running et al., 1987): surfaces poor of vegetation ($LAI_i \rightarrow 0$ respect to LAI_{max} used, equal to 10) obtain the maximum temperature increase or decrease. Net short radiation takes into account the surface albedo, the reflected and diffuse radiation term. The difference in altitude is transformed in difference in temperature through the vertical temperature gradient.

To eliminate the discontinuity between the two previous equations when $S_i = 1$, a new formulation has been introduced:

$$T_i = T_b - T_{lapse}\frac{(z_i - z_b)}{1000} + C\left(S_i - \frac{1}{S_i}\right)\left(1 - \frac{LAI_i}{LAI_{max}}\right).$$

It should be noted that all these formulations do not apply to night-time conditions, when S_i equal zero. During night a simplified formulation derived from the previous one is used: the second term of the sum is set equal to zero.

New CALMET temperature computation methodology includes the following steps:

1 all temperature measurements are carried back to a reference altitude (zero meters) and to a reference vegetation coverage (LAI_i equal to zero), through the last equation where the vertical temperature gradient used in the equation is calculated by CALMET for each hour from the measured vertical profiles;

2 the original CALMET interpolation scheme is now used for the "referenced" temperature (a virtual homogeneous terrain has been built);

3 at the end of the interpolation, temperatures are recomputed correcting for actual condition of altidude, slope, aspect and vegetation of the specific grid cell (inverse transformation of step 1).

5. FIRST APPLICATION TO A COMPLEX TERRAIN DOMAIN

Figure 2 represents topography of the domain used for the test of the new CALMET parametrization. The domain is positioned in the Northern part of Italy, centered on Lombardy Region. The 46x41 cells of $4x4\ km^2$ range from zero to more than 3000 meters of altitudes, passing through a plain rural landuse in the South -Pianura Padana, a very dense metropolitan area in the middle -Milan, ending with mountain and valleys in the

North -the Alps. Simulation day is the 20th of July 1994 during a photochemical smog episode studied by De Martini et al. (1998).

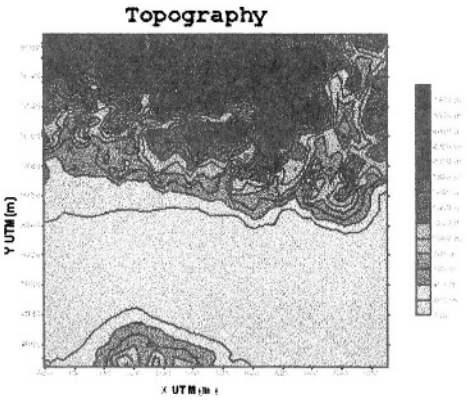

Figure 2. Topography used for the CALMET test (Northern part of Italy).

Figure 3 and Figure 4 show direct and diffuse radiation computed with the new algorithms during the 20th of July. Some interesting phenomena should be remarked:

- during the first hours of the day (6 a.m.) the diffuse radiation is an important part of the total short radiation (diffuse contribution is almost equal to direct one where the land is flat); the situation is very different in the afternoon (2 p.m.) when direct radiation prevails;
- diffuse radiation has a very different spatial pattern respect to the direct one: the first is almost spatially homogeneous with a longitudinal effect due to sun altitude; the second gives prominence to surfaces with favourable slope and aspect respect to the sun angle.

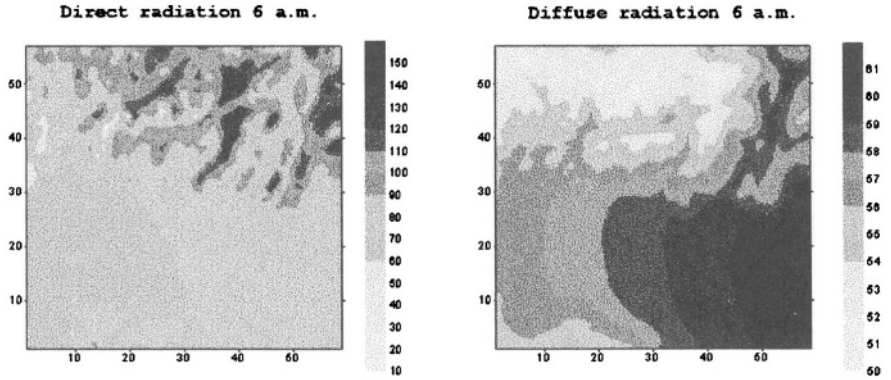

Figure 3. Direct and diffuse radiation (W/m^2) computed by CALMET over the test domain (morning).

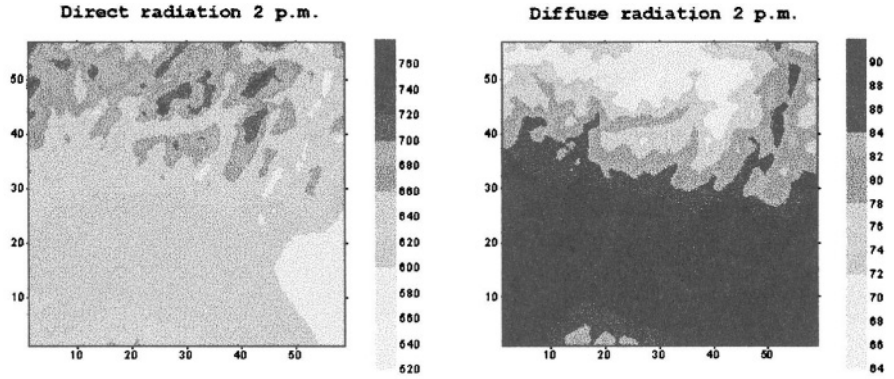

Figure 4. Direct and diffuse radiation (W/m^2) computed by CALMET over the test domain (afternoon).

Figure 5 shows the surface temperature computed by CALMET. The orographic effect is evident since mountains are the coldest part of the domain. A smoothing effect, respect to stations influence, is another point in favour of this new interpolation scheme.

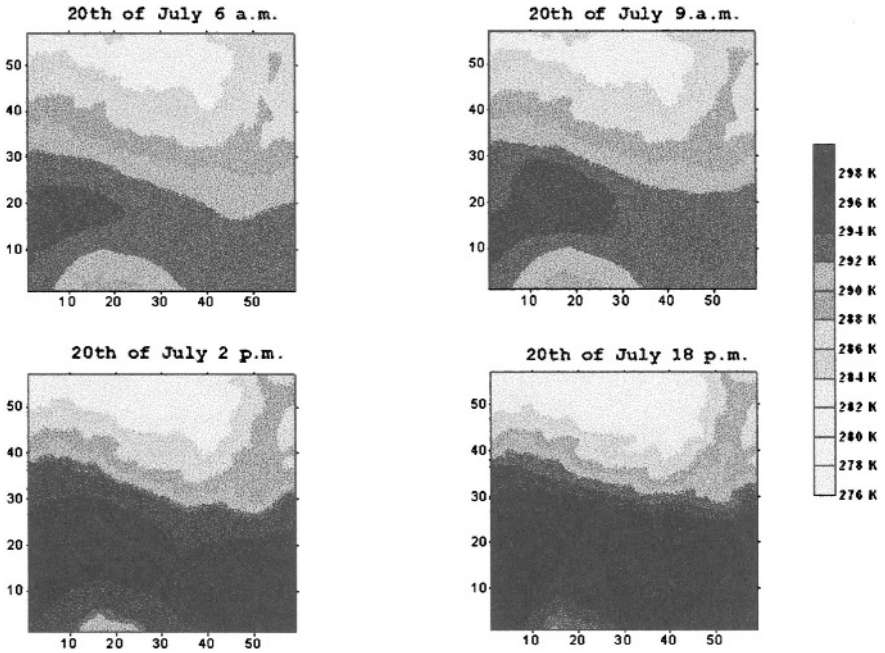

Figure 5. Surface temperature (K) computed by CALMET over the test domain.

6. ACKNOWLEDGMENTS

The authors wish to thank Dr. S. W. Running and Dr. J. Dozier for the useful material received.

5. REFERENCES

Batcharova E. and Gryning S.-E. (1991) *Applied model for the growth of the daytime mixed layer.* Boundary Layer Meteorology, 56, 261-274.

De Martini A., Pasi F., Maffeis G., Longoni M.G., Tamponi M., Graziani G., Lanzani G. (1998) *Modelling photochemical smog episodes in Lombardy Region.* 23rd NATO/CCMS International Technical Meeting on Air Pollution Modeling and Its Application Varna – Bulgaria.

Dozier J., Bruno J. and Downey P. (1981) *A faster solution of the horizon problem.* Comput. Geosci., 7, 145-151

Dozier J. and Frew J. (1990) *Rapid calculation of terrain parameters for radiation modeling from digital elevation model data.* IEEE Transactions on Geoscience and Remote Sensing, 28, 963-969.

Gallant, J.C. and Wilson, J.P. (1996) *TAPES-G: A grid-based terrain analysis program for the environmental sciences.* Computers and Geosciences vol. 22 no. 7 pp 713-722

Holtslag A.A.M. and van Ulden A.P. (1983) *A simple scheme for daytime estimates of the surface fluxes from routine weather data.* J. Of Climate and Applied Meteorology, Vol. 22, N. 4, 517-529.

Liu, B. Y. H. and Jordan, R. C. (1960) The interrelationship and characteristic distribution of direct, diffuse, and total solar radiation. Solar Energy 4:1-19.

Moore I.D., Norton T.W. and Williams J.E. (1993) Modeling environmental heterogeneity in forested landscapes. Journal of Hydrology, 150, 717-747

Running S.W., Nemani R.R. and Hungerford R.D. (1987) *Extrapolation of synoptic meteorological data in mountainous terrain and its use for simulating forest evapotranspiration and photosynthesis.* Can. J. For. Res., 17, 472-483.

Scire J.S., Robe F.R., Fernau M.E. and Yamartino R.J. (1999) *A user's guide for the CALMET meteorological model (Version 5.0).* Earth Tech Inc., September 1999.

Seibert P., Beyrich F., Gryning S.-E. Joffre S., Rasmussen A. and Tercier P. (2000) *Review and intercomparison of operational methods for the determination of the mixing height.* Atmospheric Environment, 34, 7, 1001-1027.

Zilitinkevich S.S. (1989) *Velocity profile, the resistance law and the dissipation rate of mean flow kinetic energy in a neutrally and stably stratified planetary boundary layer.* Boundary Layer Meteorology, 46, 367-387.

DISCUSSION

O. HELLMUTH To my understanding your refined radiation approach has been applied to the grid-resolved part of the model topography (azimuth, inclination, slope of terrain). What do you think about the importance to apply your approach also to the subgrid-scale topography in a sense comparable to the blending height concept for "flux averaging" ? (averaging of subgridscale, terrain corrected net radiation values in very complex regions ?)

J.S. SCIRE The approach in CALMET is applied to the grid resolved topography. However, with a diagnostic model it is possible to increase the grid resolution down to 50-100 m cells in order to explicitly evaluate small scale effects. This is usually not a practical way for prognostic models.
We apply a simple approach to determine mixing heights, which respond to the heat flux across many grid cells, if the grid spacing is small. The mixing heights is first computed at each grid cell using the local heat flux. An upwind-looking, spatially averaged mixing height is then computed to "blend" the effects of upwind grid cells with different heat flux characteristics.

This page intentionally left blank

USE OF NEURAL NETWORKS IN THE FIELD OF AIR POLLUTION MODELLING

Marija Zlata Boznar and Primoz Mlakar*

1. ABSTRACT

Different possibilities of using artificial neural networks are described. There are two different types of neural networks that are suitable for the use in the field of air pollution modelling. The first is the multi-layer Perceptron neural network and similar structures. The second is the Kohonen neural network. Both structures are briefly described. Several examples using both tools are demonstrated.

In the case of prediction of sulphur dioxide concentrations over complex terrain we developed a complete method of using a multi-layer Perceptron neural network including feature determination and pattern selection techniques that enhance the method's efficiency. In past years other research groups obtained good results in similar applications. Most of them dealt with ozone pollution over urban areas.

Multi-layer Perceptron neural networks can also be used in other applications. Two applications are explained: as a wind speed and direction forecasting tool in local scale applications over complex terrain, and as a SODAR measurements reconstruction tool. SODAR measurements on different layers above a basin were reconstructed from ground level wind measurements in the basin and on the hills.

The second tool described in this paper is the Kohonen neural network. This neural network is a self-organising classificator especially useful for cluster analysis.

Firstly it is explained how the Kohonen neural network was used to find significant wind fields over complex terrain on a small scale area. The wind field over the basin was represented by six ground level wind measurements on the plain of the basin and on the hills. A very large set of measurements was examined in the study. The Kohonen neural network classified the data set into around thirty groups. To judge the quality of the classification, wind roses were plotted for each measuring point using patterns from each group. The graphical representation of selected groups proved the extreme efficiency of the classification.

The second efficient use of the Kohonen neural network was in the preparation phase of multi-layer Perceptron neural network air pollution forecasting model construction. We developed a pattern selection technique based on the Kohonen neural network. In the paper main guidelines for its use are given.

* Jozef Stefan Institute, Jamova 39, SI-1000 Ljubljana, Slovenia

Air Pollution Modeling and Its Application XV, Edited by
Borrego and Schayes, Kluwer Academic/Plenum Publishers, New York, 2002

1. INTRODUCTION

Artificial neural networks are modern tools that can be widely use in the field of air pollution modelling. There are two different types of neural networks that are suitable for use in this field. The first type is a wide group of multilayer neural networks that is best represented by the multi-layer Perceptron neural network (Rumelhart[1] Lawrence[2],). The second type is the Kohonen neural network (Kohonen[3]). Their purposes are totally different. Their common feature is that both perform very well in highly non-linear systems such as cases of pollution of complex terrain.

2. MULTI-LAYER PERCEPTRON NEURAL NETWORK

The multi-layer Perceptron neural network with a non-linear sigmoid transfer function and two hidden layers is proven to be a universal approximator (with some minor exceptions regarding singularities, this also is true for the structure with one hidden layer) (Hornik[4]). This means that it may replace any non-linear function in multidimensional space. This important fact determines possible uses of the multi-layer Perceptron neural network. It can be used as a model in all cases where we want to teach the model to reproduce a non-linear function in multi-dimensional space for which we only have representative samples over the whole domain but do not know the exact mathematical relations between independent (the causes of the physical phenomenon that is being described) variables and dependent variable(s). This is possible due to the nature of neural networks. The process of constructing a neural network model is always a process where the neural network learns information from the group of training samples (Lawrence[2]). After the training is finished the model can also give the answers for new samples with unknown output values (the so-called generalising capability). The model can have one output (describing one physical value in time and space) or several outputs. Usually it is more efficient to build several models with one output instead of one model with several outputs.

The process of constructing the model consists of several stages that are well defined and ensure better model performance. Feature determination strategies (Mlakar[5,6], Boznar[7,8]) seek for the most important and significant independent variables that describe the studied process. Pattern selection strategies (Boznar[9,10,7,8]) construct the group of training samples in such a way that the model can learn the non-linear function behaviour over the whole domain. Both strategies in the ideal case should ensure that the whole domain of the studied function is uniformly and densely enough covered with the training samples. When these two stages are finished the modeller may begin to train the neural network using an appropriate algorithm. An example of such an algorithm is the Backpropagation algorithm. In the training stage the parameters of the learning process and the number of hidden neurones should be adjusted to suit the problem. When the training stage is finished, the model can be used on previously unknown test samples to determine its capabilities, or in the on-line mode where the model predicts output values for the new samples.

Implementation of multi-layer Perceptron neural network – based models provide the best illustration of their capabilities.

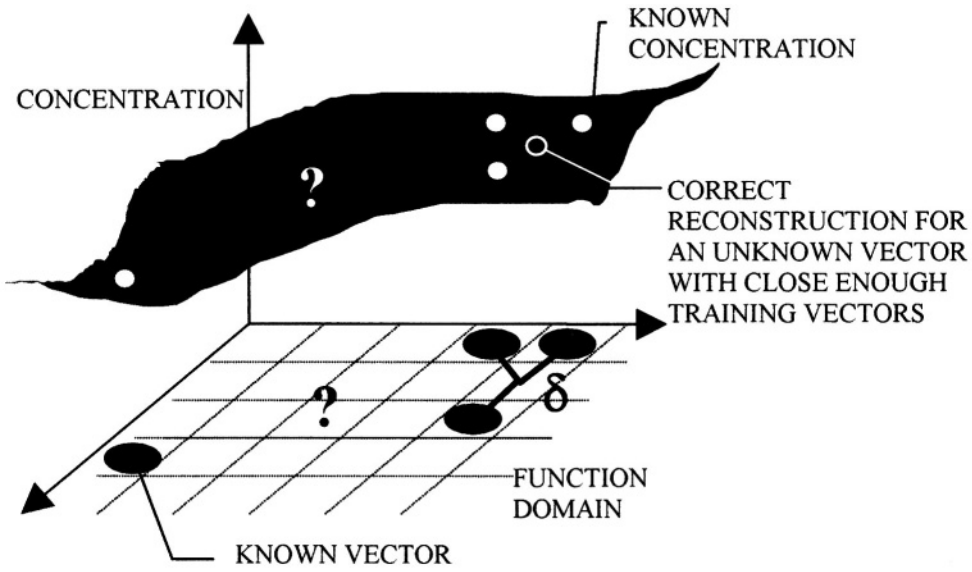

Figure 1. It should be ensured that the whole domain of the studied function is uniformly and densely enough covered with the training samples.

2.1. Forecasting Air Pollutant Concentrations

The first detailed development of methodology was done for prediction of sulphur dioxide concentrations using multi-layer Perceptron neural networks (Boznar[12]). It was applied on air pollution measuring sites around a thermal power plant in very complex terrain. In this application, which was studied further in detail, measurements of meteorological parameters and pollutant concentrations at several automatic stations were used to predict the pollutant concentration for one measuring interval in advance at one station. For different stations different models were built (Boznar[7,8] Mlakar[12-14]).

Similar applications are ones for prediction of ozone concentrations over urban areas (Yi[15]). Ozone seems to be a very good example, because its relations with other pollutants and with meteorological parameters are highly non-linear and not all the coefficients are well determined. A neural network-based model can overcome this problem by learning the necessary information directly from the training samples.

Multi-layer Perceptron neural network-based models can also be applied to test cases like Kincaid and others that are used for model verification. In such applications the model should be constructed to reproduce the concentration at one or several sampling points (always one output per one sampling point). The inputs may be any of the available meteorological measurements and emission rates. The available data set should be strictly divided into a training set (which also includes the optimising set) and a testing set. The results on the testing set given by the neural network-based model can be compared with the results of other models on the same data set. The problem is that neural network-based model constructed in this way is only useful for the particular application and "palette" of meteorological situations that it has been trained with. It

cannot simply be used on other data sets. But the methodology of model construction is transferable to other data sets.

2.2. Wind Speed And Direction Forecasting And SODAR Measurement Reconstruction

Air pollutant concentration forecasting and reconstruction are not the only possible applications of multi-layer Perceptron neural network-based models in the field of air pollution. The tool may be very efficient in any application where the exact mathematical function between the inputs and the output(s) is unknown, but a lot of historical data exist to show the relations.

One interesting application is wind speed and direction forecasting for the ground level wind (Boznar[16]) at an automatic measuring station at Graska gora in the above mentioned situation of air pollution over the complex terrain. For the prediction of wind at Graska gora for one averaging interval in the future, the present and one past interval in the ground level wind measurements at this station and the stations of Zavodnje and Veliki vrh were used.

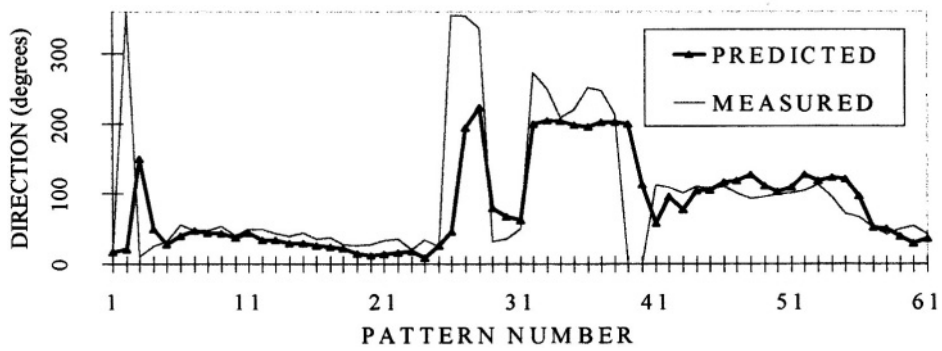

Figure 2. Ground level wind direction prediction at Graska gora station.

The other application was an attempt to reconstruct (without a time shift) missing SODAR wind measurements (Boznar[16]) in the basin from the ground level wind measurements from several measuring stations on near-by hills and in the basin. Such a model can help to reconstruct the missing data when SODAR does not perform well enough (due to disturbances from the environment) or it can even replace SODAR after a longer data collection period. The latter is only possible (with limitations) if there is a dense enough ground level wind measuring network over the whole of the studied domain.

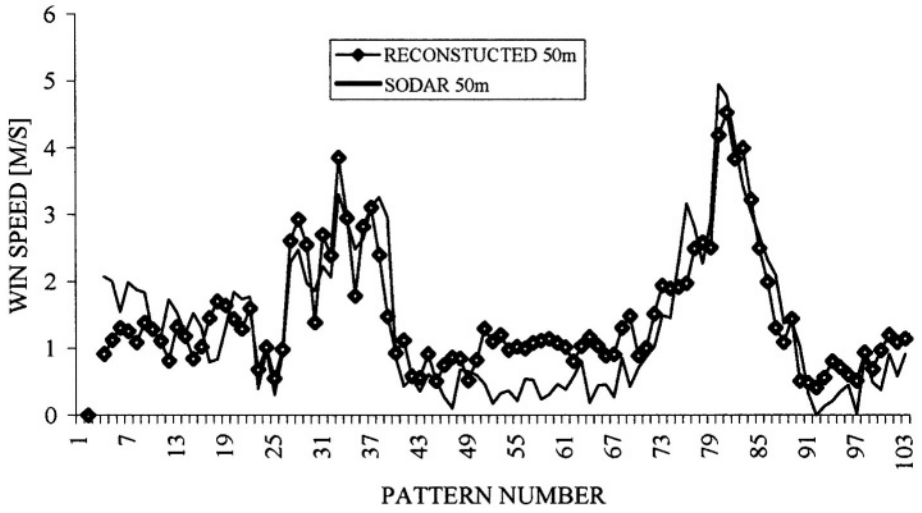

Figure 3. Reconstruction of SODAR data (wind speed; solid line - measured; line with dots - reconstructed) with four ground level stations on different atitudes.

3. KOHONEN NEURAL NETWORK

The second widely used tool, but one totally different from the multi-layer Perceptron neural network, is the Kohonen neural network (Kohonen[3]). This is a self – organising classificator. It is capable of finding groups of similar patterns (represented as multi-dimensional vectors) in huge data sets. It is very important that the most suitable number of groups need not be known in advance. Therefore the tool can also be used in the cases without a priori knowledge of the group distribution.

3.1. Classification Of The Wind Fields Over Complex Terrain

In many cases, especially for accident air pollution modelling, determination of the most similar "typical wind field" would enable the use of preprepared scenarios. But in cases of complex terrain the determination of typical wind fields is not a simple task at all.

We studied the problem in the case of the Sostanj basin where the wind field was represented by ground level measurements at five stations in the basin and on the surrounding hills (Mlakar[17]). Low winds are typical of the area. Thousands of half hour averaged wind measurements were examined in the study. One pattern was a vector of wind speed and direction measurements for one particular time interval. All the patterns from the training set of data were classified into several groups using the Kohonen neural network. The process was repeated for several numbers of groups from 10 to 60. For each classification the cost function – a weighted sum of the average standard deviation of wind speed and the average standard deviation of wind direction in the clusters - was

computed. The most suitable (natural) number of clusters is the number of clusters where the cost function value no longer decreases significantly if the number of clusters is increased. To understand the results and to judge the quality of the classification, wind roses were plotted for each measuring point using patterns from one cluster. The graphical representation in the form of wind roses that shows very little fluctuation in comparison with wind roses for the whole training data set proves the extreme efficiency of the classification. Once a model based on the Kohonen neural network is trained, it can be used on previously unknown data. A new pattern (the vector of wind measurements at a particular time for all five stations) is passed to the model that immediately returns the number of the cluster – the representative wind field.

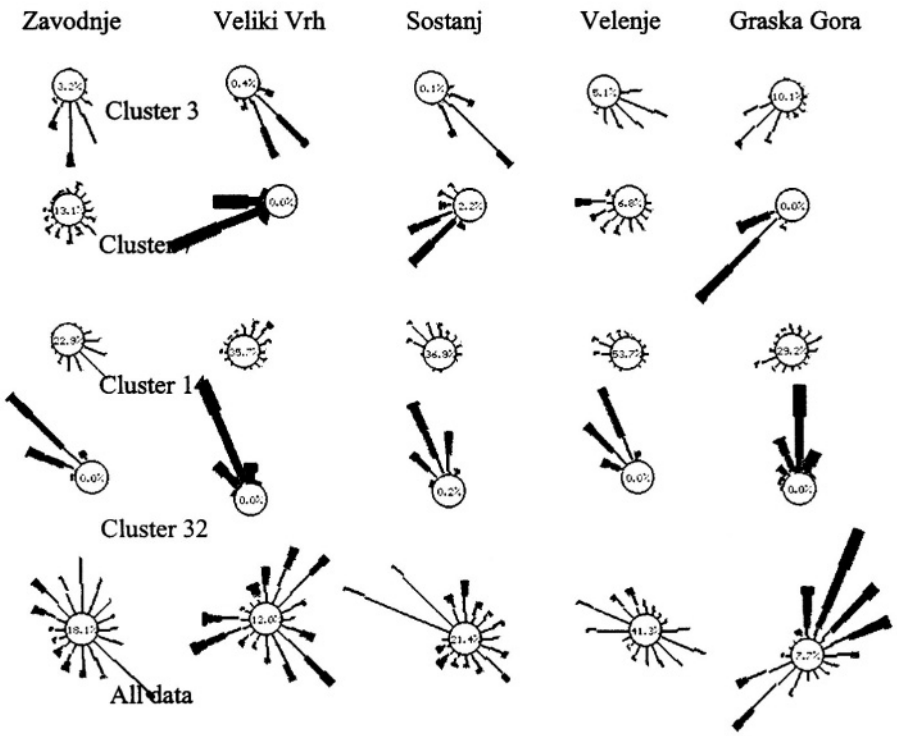

Figure 4. Wind roses for all data and 4 clusters organise by Kohonen neural network

The wind fields classification problem is a typical teaching example to show the principles and efficiency of classification using the Kohonen neural network. But a classification problems also arise in other fields of air pollution.

3.2. Pattern Selection Strategies Based On The Kohonen Neural Network

Our second application of the Kohonen neural network was classification of training patterns (Boznar[9,8,7,10]) in the process of constructing a sulphur dioxide air pollution forecasting model. The available data base for the Sostanj basin was huge and therefore the use of all training patterns would cause slow learning and poor results on the test data set. The idea of the Kohonen neural network-based pattern selection strategy is to find clusters of similar training patterns and to take only representative patterns from each cluster for the network training process. In this way the predicting neural network can learn rare pollution events as well as frequent cases. A similar selection of patterns can also be made manually on the basis of expert knowledge about air pollution in the studied domain. But this "manual" method requires enormously more time and effort in comparison to the method based on the Kohonen neural network.

When using the Kohonen neural network for classification of air pollution patterns it is no longer simple to judge the quality of the classification. When the pattern – vector consists of ten to twenty dimensions that vary from wind to vertical temperature difference and concentr, it is not possible to represent the clusters graphically. Cost functions based on standard deviations for each component can be useful. To avoid this problem, we simply construct the air pollution prediction model (based on the multi-layer Perceptron neural network) on the selected data from the clusters and compare this model's results to the results of a model constructed with unselected data. Both pattern selection strategies – the Kohonen neural network based one and the expert knowledge based one - show significant improvement in comparison to the model trained with unselected patterns. Pattern selection strategies are also important when only medium sized training sets (and not huge ones as in our case) are available because there is always the problem of frequent data prevailing over rare cases.

4. CONCLUSIONS

This paper is intended to show how to use efficient modern tools called artificial neural networks in the field of air pollution modelling. In our opinion these tools can be of great help in solving not only the tasks described in this paper, but also several others. We hope that the detailed explanation of cases given in the citied papers will inspire more ideas for using these tools.

5. REFERENCES

1. Rumelhart, D. E., McClelland, J. L., 1986, Parallel distributed processing 1,2, MIT Press, Cambridge, MA
2. Lawrence, J., 1991, Introduction to Neural Networks, California Scientific Software, Grass Valley
3. Kohonen, T., 1995, Self-organising maps, Springer - Verlag, Berlin
4. Hornik, K., 1991, Approximation capabilities of multilayer feedforward networks, Neural Networks, vol.4, 251-257
5. Mlakar, P., 1997, Determination of features for air pollution forecasting models, V: ADELI, H. , ed., Intelligent Information Systems IIS'97, Grand Bahama Island, Bahamas, December 8-10, *Proceedings.* Los Alamitos, California: IEEE Computer Society, 350-354.

6. Mlakar, P., Boznar, M., 1997, Feature determination for air pollution forecasting models. V: POWER, H. ed., Tirabassi, T. (Ur.), Brebbia, C. A. , ed., *Air pollution V: [modelling, monitoring and management].* Southampton; Boston: Computational Mechanics Publications, 577-586.
7. Boznar, M. Z., Mlakar, P., 2001, Artificial neural network-based environmental models, Air Pollution Modeling and its Application XIV, ed. by Gryning and Schiermeier, Kluwer Academic / Plenum Publishers, New York
8. Boznar, M., Mlakar, P., 1998, Improvement of air pollution forecasting models using feature determination and pattern selection strategies. V: Gryning, Sven-Erik ed., Chaumerliac, Nadine. *Air pollution modeling and its application XII,* (NATO challenges of modern society, vol. 22). New York; London: Plenum Press, 725-726.
9. Boznar, M., 1997, Pattern selection strategies for a neural network - based short term air pollution prediction model. V: ADELI, H. , ed., Intelligent Information Systems IIS'97, Grand Bahama Island, Bahamas, December 8-10, 1997. *Proceedings.* Los Alamitos, California: IEEE Computer Society, 340-344
10. Boznar, M., Mlakar, P., 1997, Pattern selection strategies for SO2 forecasting models. V: Power, H. (Ur.), Tirabassi, T. ed., Brebbia, C. A. , Ed., *Air pollution V : [modelling, monitoring and management].* Southampton; Boston: Computational Mechanics Publications, 547-556.
11. Boznar, M., Lesjak, M., Mlakar, P., 1993, A neural network-based method for short-term predictions of ambient SO2 concentrations in highly polluted industrial areas of complex terrain. *Atmos. environ., B Urban atmos., vol.* 27, 221-230.
12. Mlakar, P., Boznar, M., 1997, Perceptron neural network - based model predicts air pollution. V: ADELI, H. , ed., Intelligent Information Systems IIS'97, Grand Bahama Island, Bahamas, December 8-10, *Proceedings.* Los Alamitos, California: IEEE Computer Society, 345-349.
13. Mlakar, P., Boznar, M., Lesjak, M., 1994, Neural networks predict pollution. V: GRYNING, Swen-Erik ed., MILLÁN, Millán M. , ed., *Air pollution modeling and its applications* (NATO challenges of modern society, 18). New York; London: Plenum Press, 531-532
14. Mlakar, P., Boznar, M., 1994, Short-term air pollution prediction on the basis of artificial neural networks. V: Baldasano, J. M. , ed., *Air Pollution II. Volume 1, Computer simulation.* Southampton; Boston: Computational Mechanics Publications, 545-552.
15. Yi, J., Prybutok, R., 1996, A neural network model forecasting for prediction of daily maximum ozone concentration in an industrialised urban area, Environmental Pollution 92 (3), 349-357
16. Boznar, M., Mlakar, P., 1995, Neural networks - a new mathematical tool for air pollution modelling. V: Power, H. ed., Moussiopoulos, N. ed., Brebbia, C. A. , ed., *Air pollution III. Volume 1, Air pollution theory and simulation.* Southampton; Boston: Computational Publications, 259-266.
17. Mlakar, P., Boznar, M., 1996, Analysis of winds and SO2 concentrations in complex terrain. V: Caussade, B. ed., Power, H. ed., Brebbia, C. A. , ed., *Air pollution IV : monitoring, simulation and control.* Southampton; Boston: Computational Mechanics Publications, 455-464.

DISCUSSION

G. COSEMANS — You said it is difficult to predict the wind direction. Yet you are able to predict the time series of SO_2 at a monitoring site near the power plant, while this depends mainly on the wind direction. Can you explain this ?

M. BOZNAR — Wind direction certainly is important for SO_2 prediction model. We were not unsuccessful in wind direction forecasting, I just wanted to say, that we had more problems with wind direction. On the other hand the models for wind forecasting were only preliminary, but for SO_2 prediction we have done extended research. I am sure that further research should bring better results also for wind direction forecasting.

This page intentionally left blank

A POROSITY/DRAG APPROACH FOR THE MODELING OF FLOW AND DISPERSION IN THE URBAN CANOPY

B. Carissimo[12] and R. W. Macdonald[3]

1. INTRODUCTION

Numerical models of atmospheric flow and dispersion traditionally take into account the presence of buildings or urban area through an increased surface roughness and modifications in the parameterization of the heat and moisture exchanges with the ground. Here we will concentrate our discussion on the roughness aspect. The roughness increase is capable of reproducing the two basic urban effects, namely the increased friction on the flow and the increased dispersion above the canopy. Although this approach has proved very useful overall, it has some limitations, for example :

- it cannot represent the low level flow and dispersion that may exist below roof top level between the buildings,
- it is not able to distinguish between pollution sources located at the ground or at roof top level.

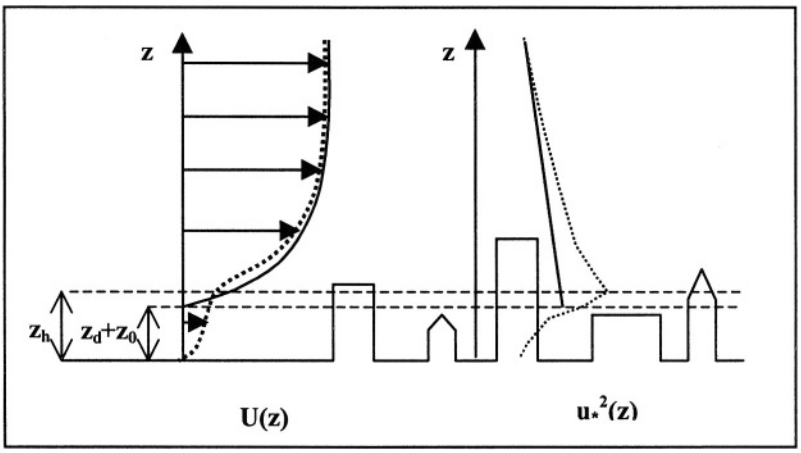

Figure 1: Vertical profiles of velocity (left) and Reynolds stress (right) in the urban canopy, as seen by a meso-sacle model (solid line) and obtained by averaging a detailed CFD simulation (dashed line)

1 George Mason University
2 on leave from : Electricité de France, Research and Development Division, email : bertrand@scs.gmu.edu
3 University of Waterloo

Air Pollution Modeling and Its Application XV, Edited by
Borrego and Schayes, Kluwer Academic/Plenum Publishers, New York, 2002

At the opposite scale, Computational Fluid Dynamics (CFD) models, have been used to simulate the flow and dispersion around a limited number of building. Due to computer limitations however, this simulations cannot be extended to a whole city in the near future.

We are therefore in need of an intermediate approach, that can take into account the entire urban canopy but without the computer requirements of the detailed CFD, while at the same time being compatible with the full physics of the mesoscale model.

The recent review by Brown (2000), describes the different attempts at developing such parameterization. The principle is to account for the area-average effect of the drag and turbulence production as additional terms in the equations of motion and the turbulence closure equations. Simpler parameterizations can be found in Hanna et al. (2001).

These new parameterizations however need to be calibrated and validated. So far, this has mainly been done crudely with available urban measurements.

In this paper we present an extended drag and porosity model, capable of representing the anisotropic effects of elongated buildings. In addition, we address the issue of calibration and validation by means of a series of high resolution, CFD, three dimensional (3D) simulations and also with physical modeling results obtained in the water flume. Both techniques have been used to study the same geometrical configurations of various idealized building setup.

2. DRAG AND POROSITY MODEL DESCRIPTION

The porosity/drag approach has been used more recently in several numerical models (Brown, 2000, Lacser, 2001) although often in incomplete form. In our approach, the building effects are taken into account by means of the following additional terms in the model (fig. 2):

- the drag force created by the buildings (modified momentum equations),
- the fraction of volume V occupied by solids within the flow (modified continuity equation),
- the increased turbulence level (modified turbulence equations).

Momentum equation : $\frac{\partial \vec{u}}{\partial t} + \vec{u}.\nabla\vec{u} = \frac{-1}{\rho}\nabla p + \vec{g} + \nu_t \Delta \vec{u} \boxed{-\overline{\overline{K}}.\vec{u}}$

Continuity equation : $\nabla.\left(\rho \boxed{V} \vec{u}\right) = 0$

Turbulence model : $\frac{\partial k}{\partial t} + \vec{u}.\nabla k = D_k + P + G - \varepsilon + \boxed{S_k}$ $(k-\varepsilon)$

similarly for ε

Figure 2

With this approach, the model ground remains at the level of the true ground and there is no need to take into account a displacement height due to the buildings.

Compared to earlier approaches, the drag term is formed by the product of a tensor and the velocity vector. This allows the possibility of an additional force (lift), perpendicular to the mean flow to act when the buildings are elongated (figure 3).

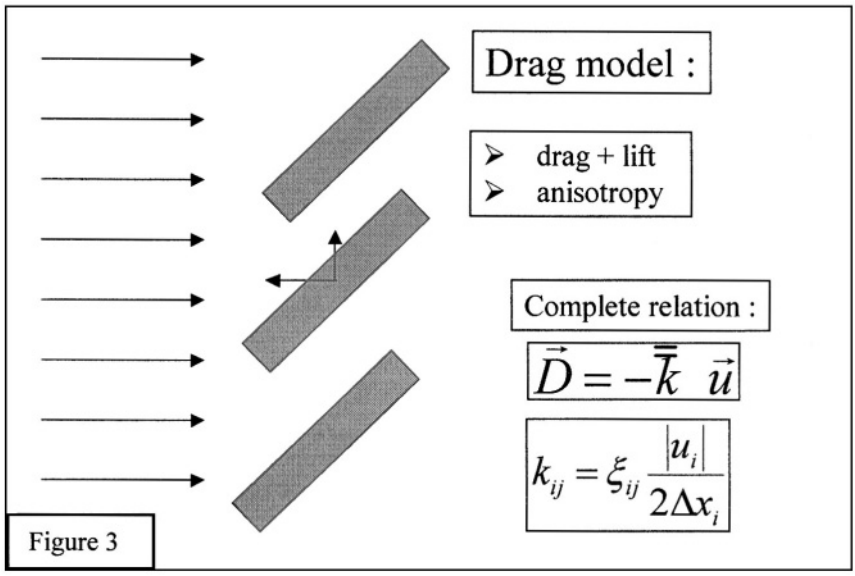

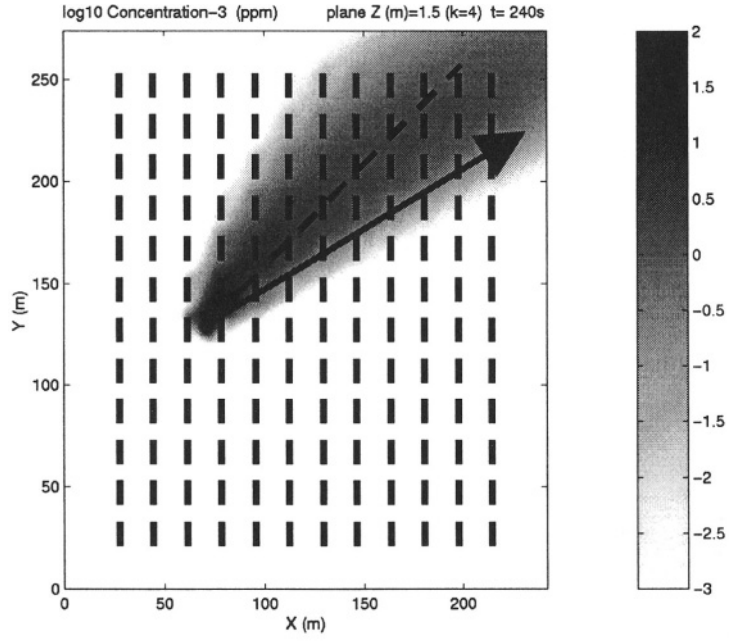

Figure 4 : Horizontal cross section of concentration within the canopy (z/h=0.5) for pre-simulations of the MUST experiment, obtained with high resolution numerical simulation. The solid arrow represents the wind direction (30° relative to x axis) and the dashed line is at 45°. In this type of canopy with elongated obstacles the dispersion is not isotropic and the plume does not follow the main wind direction.

In figure 4, we have an example of a plume dispersing inside an idealized canopy formed by elongated buildings. This figure is a result of a high resolution numerical simulation, performed with a k-ε turbulence closure, of the geometry that will be used for the Mock Urban Setting Test (MUST, Biltoft, 2001), that will be carried out in the field in September 2001. The obstacle are transport containers that will be laid out in the regular pattern shown in black in the figure. In this figure, the big arrow indicates the main wind direction outside the canopy, which is at 30° off the x axis. The dashed line indicates the 45° line and is much closer to the real plume axis in the canopy. In fact in this case the plume is entirely located to one side of the wind axis, a rather peculiar situation not taken into account by simpler "urban" models. This effect cannot be reproduced by a drag model, in which the drag force in only proportional to the velocity vector.

The additional term in the continuity equation (fig. 2) represents the volume fraction of the canopy that is occupied by the air and not the building. This term has been considered here but its relative importance on the resulting flow would require further study. Finally,, additional source terms have been implemented in the turbulence equations. As these are even more difficult to determine than the drag values, as a first approach, we have taken them as zero.

3. HIGH RESOLUTION SIMULATIONS AND WATER FLUME RESULTS

As mentioned in the introduction, our objective is to use an ensemble of high-resolution numerical simulations and additional experimental results, obtained in the water flume, to calibrate our parameterization. This section includes a description of both.

The water flume experiments are described in details in Macdonald et al. 2000 and 2001. Velocities were measured using an acoustic Doppler velocimeter (SonTek MicroADV™), providing high frequency measurements of all velocity components. The high frequency time series at different profile locations and different heights were then processed to extract the mean and turbulent values. Five vertical profiles were averaged to obtain the "canopy profile" (fig. 5).

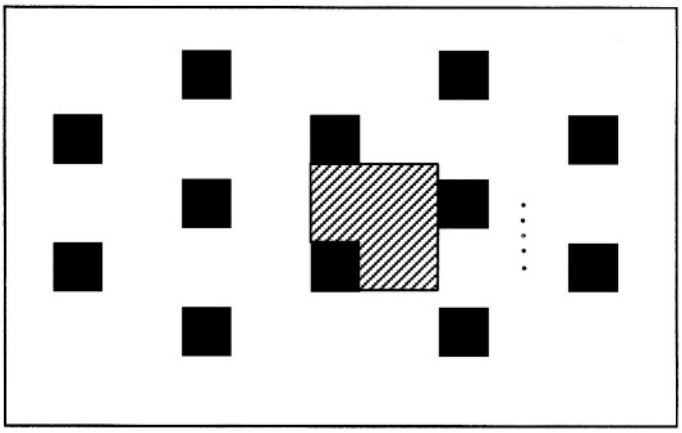

Figure 5 : sub-domain (hatched) used for averaging the 3D numerical results and the 5 positions (dots) used to average the water flume results.

The high-resolution numerical simulations are described in more details in Carissimo (2001) and Carissimo and Tehranian (2001). These simuations have been performed with the MERCURE atmospheric model, developed by Electricité de France for atmospheric dispersion studies. It is based on a CFD code (ESTET), used for other

applications, and capable of handling complex geometries. It solves the anelastic equations of motion on a variable structured mesh with different levels of turbulence closure. The model has been previously applied at different scales, ranging from an accidental release at an industrial site to dispersion on the urban scale (for the city of Paris for example). Here we have used the **k-ε** turbulence closure, which is well suited to the presence of obstacle in the flow (as opposed to a simpler closure such as k-1).

In the numerical simulations, the results are averaged over the fluid volume surrounding an obstacle, as illustrated in figure *5*.

A total of eight different geometries, consisting of regular arrays of cubes or billboard, were studied by both methods. One of them is illustrated in figure 6, together with an indication of the averaging procedure used in each case. This represents the middle packing density and other simulations were performed with lower and higher packing density, by replacing the staggered configuration by a regular array and by replacing cubes by billboard.

4. RESULTS AND DISCUSSION

The results of the high resolution 3D simulations are compared in more details in Carissimo (2001) with the water flume experiments (Macdonald et al. 2000, 2001) and with various turbulence city measurements reviewed by Roth (2000). Here, we only present a limited comparison with the 2D drag model simulations.

Figures 7 and 8 present a comparison of the vertical profiles of velocity and Reynolds stress. These represent mean profiles that are obtained by averaging all vertical profiles in the control sub-domain (cf. figure 6) for the high-resolution numerical simulations and over 5 representative profiles for the water flume. For the drag calculation, each profile is directly extracted from the 2D simulation.

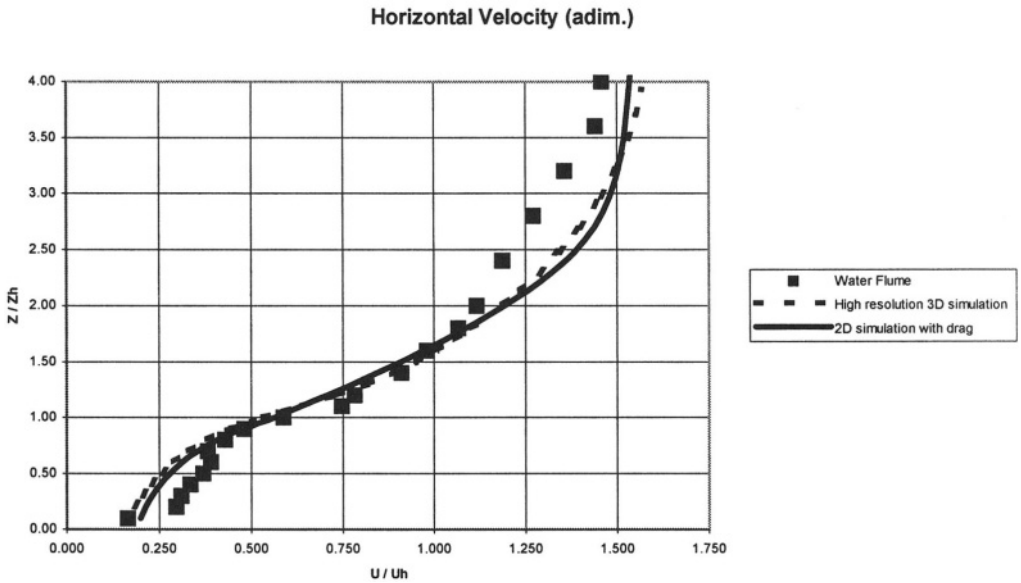

Figure 6 : Vertical profiles of horizontal velocity in the canopy for the water flume, the 3D simulation and the 2D simulation with drag.

The drag parameters have been optimized to obtain a velocity profile as close as possible to that of the 3D simulations, which are also close to the profile measured in the water flume. The value adopted for the drag coefficient is constant in height and confined to the region z < H. Other authors have adopted a value based on the obstacle area density A(z), which is observed to vary in height. However in our case with obstacle of the same height, this value is constant. This is a current limitation of our analysis that will be addressed in future work.

The Reynolds stress profiles, which also represent the square of the friction velocity u*, are presented in figure 8. In all cases a strong maximum is found about the canopy top, with rapidly decreasing values below and more slowly decreasing values above. In the water flume and in the 3D simulations, the maximum is slightly above the canopy top, while it is slightly below in the drag calculation. This is a small difference that might not be significant and the general shape of the three profiles is very similar.

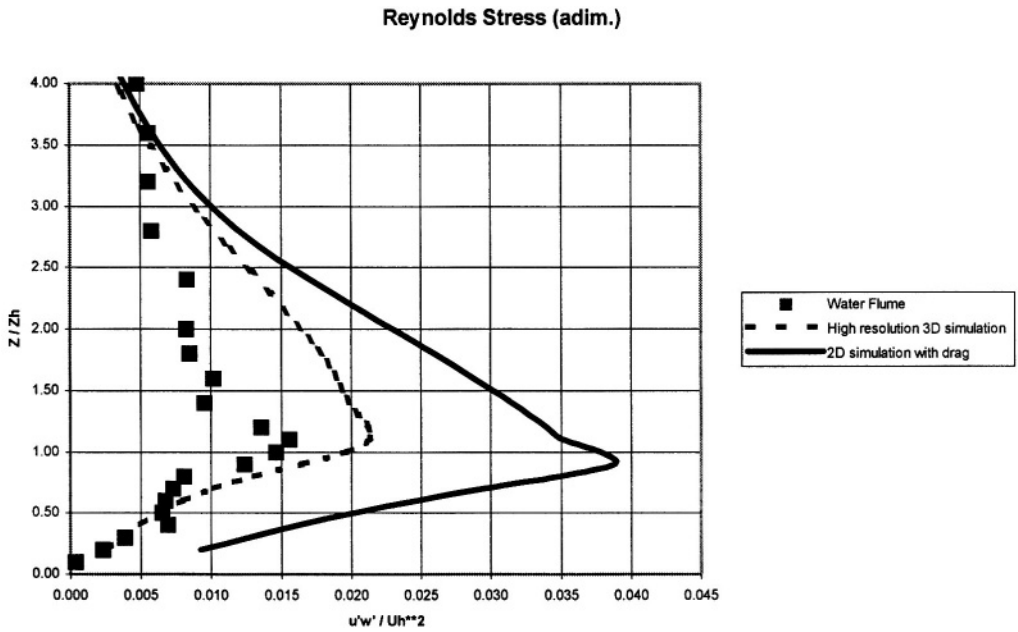

Figure 7 : Vertical profiles of Reynolds stress in the canopy for the water flume, the 3D simulation and the 2D simulation with drag.

The maximum value is lowest for the water flume and highest for the drag simulation. We have shown elsewhere (Carissimo, 2001) that the 3D, high resolution simulations give values of u* that are in line with the city observations reviewed by Roth (2000). This confirms a known tendency for the laboratory scale experiments to underestimate the full scale turbulence.

The higher values of Reynolds stress found for the drag calculation were somewhat unexpected, given that the source terms in the turbulence equations were taken as zero (cf. section 3). To explain this, we have to recall that the turbulence is produced by the velocity shear (and other buoyancy producing terms that do not play a role here). Our

result therefore indicates that the shear production is overestimated by using the averaged velocity profile, as compared to the real shear production that occurs in a fully 3D flow. We will therefore need to add "sink" terms in the turbulence equations to compensate for this increased production. This phenomenon clearly deserves further study with more varied geometrical configurations.

5. REFERENCES

Biltoft C., 2001 : Abbreviated test plan for Mock Urban Setting Test. DPG Document WDTC-TP-01-028. U.S. Army Dugway proving ground. Dugway, UT 84022-5000

Brown M.J., 2000 : Urban parameterizations for mesoscale meteorological models, in Mesoscale Atmospheric Dispersion (ed. Z. Boybeyi)

Carissimo B., 2001 : Numerical simulation of flow and turbulence in simple obstacle arrays. CHARM Report, George Mason University, July 2001

Carissimo B. and S. Tehranian, 2001 : Numerical Simulations of Flow and Turbulence in Simple Obstacle Arrays. 5th GMU Transport and dispersion modeling workshop, Fairfax VA, July 18-19, 2001

Hanna S.R., R.B. Britter, 2001 : Wind flow and vapour cloud dispersion at industrial and urban sites. to be published by AICHE,3 Park Ave, New York, NY 10016-5901

Lacser A. and T. L. Otte, 2001: Implementation of Urban Canopy Parameterization in a Mesoscale Model. 5th GMU Transport and dispersion modeling workshop, Fairfax VA, July 18-19, 2001

Macdonald R.W., S. Carter and P.R. Slawson, 2000 : Measurement of mean velocity and turbulence statistics in simple obstacle arrays at 1:200 scale. University of Waterloo. Thermal Fluids Report 2000-1, November 2000.

Macdonald R.W., S. Carter and P.R. Slawson, 2001 : Physical modeling of Urban Roughness using arrays of regular roughness elements. (Submitted to Water, Air and Soil Pollution Focus)

Roth M., 2000 : Review of atmospheric turbulence over cities. Q.J.R. Met. Soc., 126, 941-990

DISCUSSION

S. VARDOULAKIS — How the shape of the velocity and Reynold stress vertical profiles might influence the dispersion of pollutants within the Canopy (e.g. in a street canyon) ?

B. CARISSIMO — In our results we have considered spatially averaged profiles in the canopy which do not show the details within a street canyon. Nevertheless, the mean concentrations in the canopy are linked to the mean velocity profile (dilution) and to the Reynolds stress through the turbulent kinetic energy (diffusion).

D. STEYN — You identify the urban canopy layer height with the maximum in Reynolds stress. This is probably reasonable for a definition of the dynamical weight, but can you say something about the pollutant urban canopy layer height ?

B. CARISSIMO — First let me repeat that these simulations are performed in neutral conditions. Therefore we do not consider the case where unstable motions contribute to the additional mixing of pollutants.
My point here is that the maximum in Reynolds stress corresponds to the height of the canopy, which is well defined in this idealised case. This is found both in the laboratory and the numerical experiments. This is also in contrast with previous authors who found a maximum higher than the mean canopy height in more realistic situations.

S. RAFAILIDIS — As experiment shows in the urban setting the "vertical" main stress $\overline{u'w'}$ differs from the "horizontal" one $\overline{u'v'}$ (similar differences exist for the $\overline{u'w'}$ component). How can these effects be handled in a "wall function" 2-D numerical model which does not account for different parameterizations of these differences in the physical features of the flow ?

B. CARISSIMO — The fluxes $\overline{u'w'}$ we have presented are spatial averages. Both the numerical simulations and the laboratory experiments are bounded by vertical walls in the v direction and we have no mean motion in that direction. On average, we therefore also expect $\overline{u'v'}$ to be negligible although it could be locally significant.

H. APSIMON — You have illustrated the sensitivity of alignment of streets/blocks relative to the wind direction, and diversion non of the plume within the canopy. How important are other effects such as changing heights of alternate rows of blocks/buildings, inducing more vertical fluctuations and exchange ?

B. CARISSIMO — This is a first step to fully understand the mean and turbulent profiles in an idealised canopy. The next step could be, as you say, to include for example variability in obstacle height and geometry. We have already looked somewhat at this type of variability by comparing cubes and bilboard which have different effects on mixing in the canopy.

This page intentionally left blank

IMPROVED ALGORITHMS FOR ADVECTION AND VERTICAL DIFFUSION IN AURORA

Koen De Ridder and Clemens Mensink*

1. INTRODUCTION

AURORA is an urban- to regional-scale air quality model currently under development at Vito, containing terrain, emission, chemistry, and advection-diffusion modules. A first version, without chemistry and using simplified emissions, was briefly described and used in De Ridder (2000). A recent major overhaul of AURORA's computer code was seized to completely re-write the advection and diffusion routines, to optimise their functioning, and to carry out comparisons with analytical solutions. The description and testing of the new advection-diffusion module, which will further be referred to as the Eulerian Dispersion Model (EDM), constitute the focus of this paper.

The schemes dealt with here resolve (see, e.g., Jacobson, 1999)

$$\frac{\partial \rho Q}{\partial t} = -\vec{\nabla} \cdot \left(\rho \vec{v} Q\right) + \frac{\partial}{\partial z}\left(\rho K \frac{\partial Q}{\partial z}\right) + V(x, y, z). \tag{1}$$

The symbols are defined as follows: Q is the tracer mixing ratio (kg kg^{-1}), ρ is the air density (kg m^{-3}), $\vec{v}$ is the wind vector (m s^{-1}), K is the turbulent diffusion coefficient (m^2 s^{-1}), and V is a source term (kg m^{-3} s^{-1}) The first term at the right-hand side represents advection, and the second vertical diffusion. Horizontal diffusion is not accounted for, since it is generally small compared to artificial diffusion generated by the numerical advection scheme.

The model grid is staggered, with scalar quantities positioned at the cell centres, and vector components at the interfaces. This corresponds to the grid structure of the mesoscale model ARPS (Xue et al., 2000), which we use as meteorological driver for EDM. In the remainder of this paper, advection and diffusion are treated separately as they are implemented using operator splitting. Both schemes are briefly described, and results of comparisons with other schemes and with analytical solutions are shown.

* Koen De Ridder, Flemish Institute for Technological Research (Vito), Boeretang 200, B-2400 Mol, Belgium.

Air Pollution Modeling and Its Application XV, Edited by
Borrego and Schayes, Kluwer Academic/Plenum Publishers, New York, 2002

2. ADVECTION

Among the many existing advection algorithms we selected the recent scheme by Walcek (2000). This scheme guarantees mass-conservation and monotonicity (and hence positivity), and combines a relatively straightforward implementation with a very good performance, both in terms of accuracy and computational speed. In this section, Walcek's scheme is briefly described and compared with other schemes.

The advective part of Eq. (1), in one dimension (x-direction), is given by the following equation:

$$\frac{\partial \rho Q}{\partial t} = -\frac{\partial \rho u Q}{\partial x}, \tag{2}$$

where u is the wind component in the x-direction. Multi-dimensional advection is calculated by sequentially applying the one-dimensional algorithm.

Equation (2) is discretized as

$$Q_i^{t+\Delta t} = \frac{1}{D_d}\left[Q_i^t D_{d-1} - \frac{\left(\Delta t u \rho Q_f\right)_{i+1/2}}{\Delta x_i} + \frac{\left(\Delta t u \rho Q_f\right)_{i-1/2}}{\Delta x_i} \right], \tag{3}$$

where the superscript t denotes the time level, and the subscript i refers to grid position. Temporal and spatial increments are given by, respectively, Δt and Δx. The quantities D_d are used to correct density perturbations that follow from the sequential application of a one-dimensional advection algorithm in case the wind fields are not mono-dimensionally divergence free, which would otherwise lead to spurious gradients in initially uniform concentration fields (Clappier, 1998).

The advective fluxes at the cell interfaces are estimated using the second-order Van Leer (1977) scheme

$$\begin{aligned} Q_{f,i+1/2} &= Q_i + \frac{(Q_{i+1} - Q_{i-1})(1-c)}{4}\alpha \qquad && u_{i+1/2} \geq 0 \\ Q_{f,i-1/2} &= Q_i + \frac{(Q_{i-1} - Q_{i+1})(1-c)}{4}\alpha \qquad && u_{i-1/2} < 0. \end{aligned} \tag{4}$$

The variable c $(=u\Delta t/\Delta x)$ is the Courant number (which is kept below unity to maintain stability), and α is a so-called 'sharpening factor', which is used to maintain concentration gradients to the best possible extent during advection. In order to guarantee monotonicity, Q_f is put through a number of tests and, if required, adapted. It is also tested whether the algorithm produces new extrema in Q at $t+\Delta t$, in which case corrective measures are equally taken. For more details regarding this algorithm, including an extensive set of testing exercises, the reader is referred to the paper by Walcek (2000).

Walcek's scheme was subjected to a one-dimensional comparative test with the following advection schemes:

1. First-order upwind scheme (see, e.g., Jacobson, 1999). Owing to the low-order discretisation this algorithm generates excessive numerical diffusion, making it unsuitable for pollutant transport calculations. It has been included here solely as a reference.
2. Kappa=1/3 scheme (Hundsdorfer et al., 1995), which is composed of a third-order upwind-biased scheme with second-order Runge-Kutta time integration. Positivity is achieved using a flux limiter.
3. Flux-Corrected Transport scheme (Zalesak, 1979). This scheme combines low- and high-order advective fluxes so as to maximally preserve concentration gradients while preventing under- or overshooting. The high-order scheme used here is based on fourth-order spatial and centred time discretisation (leapfrog), and the low-order scheme is the first-order upwind scheme. Zalesak's scheme was used in the first version of EDM (De Ridder, 2000).

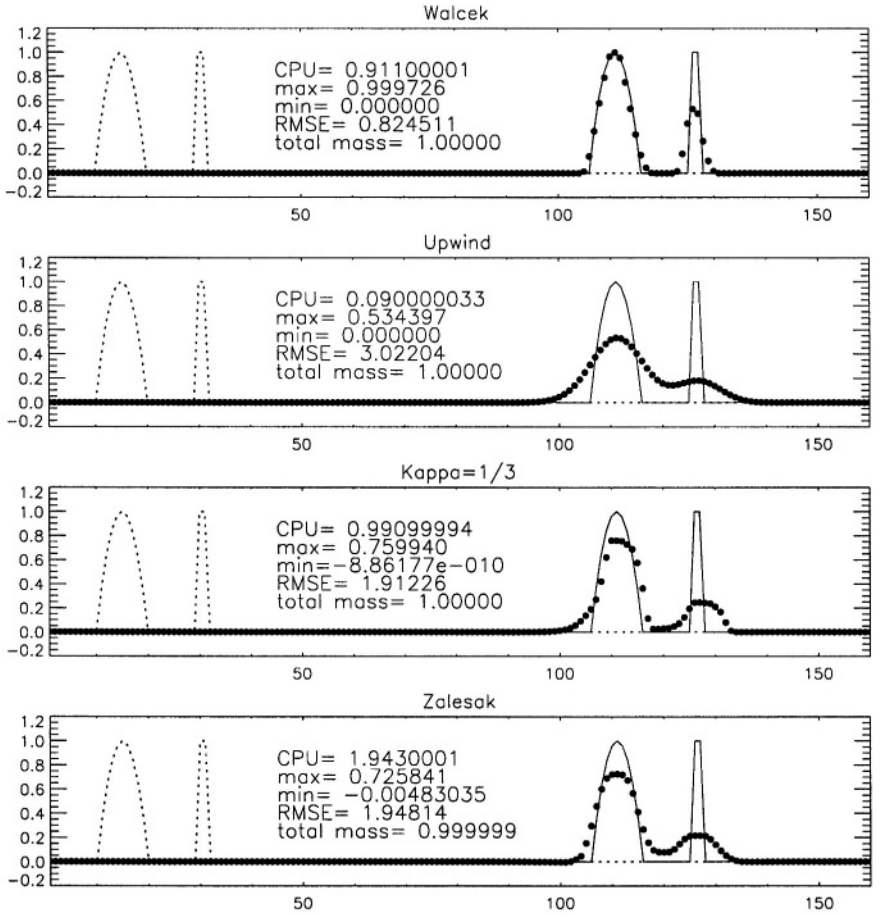

Figure 1. One-dimensional advection test. Initial concentrations are represented by the dashed line. The solid circles correspond to the advected profiles using the numerical schemes defined in the text, and the solid line shows the analytical solution.

The comparative test consisted of the one-dimensional advection of a parabolic initial concentration profile with a 10 grid point-wide base, combined with a 2 point-wide hat function (Fig. 1). Advection occurs over 120 time steps with a Courant number of c=0.8. The results, shown in Fig. 2, clearly demonstrate the excellent performance of the Walcek scheme. The parabolic shape is very well preserved during transport, and the small peak is distorted less than in the other schemes. Total mass and positivity are fully respected. CPU time is the lower of the schemes with exception of the first-order upwind scheme, which is no real competitor, though. Furthermore, it should be noted that the Walcek scheme requires storage of mixing ratios at one time level (at time t) only, as opposed to the Zalesak scheme using a leapfrog discretisation, which relies on two time levels (t and t-Δt), meaning that the Walcek algorithm has a favourable influence on computer memory resources.

3. VERTICAL DIFFUSION

The diffusive part of Eq. (1) is written as

$$\frac{\partial \rho Q}{\partial t} = \frac{\partial}{\partial z}\left(\rho K \frac{\partial Q}{\partial z} \right) + V(x, y, z), \tag{5}$$

where V represents a volume source term (units of $\mathrm{kg\ m^{-3}}$). Surface and point sources can be dealt with simply by dividing the corresponding emissions by, respectively, the vertical grid increment and the grid volume of the cell where the emission occurs. Line sources (e.g., from road traffic) are not mentioned as AURORA's emission module transforms these to surface sources.

For the discretisation of Eq. (5) we partly follow Jacobson (1999), the only difference being that emissions are dealt with by a source term rather than by specifying them in the boundary conditions, yielding

$$\frac{Q_k^{t+\Delta t} - Q_k^t}{\Delta t} = -\frac{1}{\rho_k}\frac{F_{k+1} - F_k}{z_{k+1} - z_k} + \frac{1}{\rho_k} V_k, \tag{6}$$

z_k indicating vertical level positions. Fluxes at the vertical cell interfaces are defined by

$$F_k = -(\rho K)_k \frac{Q_k - Q_{k-1}}{0.5(z_{k+1} - z_{k-1})}, \tag{7}$$

with the interface diffusivity taken as the average of the adjoining cells.

Mixing ratios at the right-hand side of Eq. (7) are specified as a weighted average of the mixing ratios at time levels t and t+Δt, using weighting factors μ_c and 1-μ_c, respectively. In practice we use μ_c=1/2, which results in the unconditionally stable Crank-Nicholson scheme. Regrouping terms results in a tridiagonal system of linear equations, which is resolved for $Q(t+\Delta t)$ using decomposition and forward substitution, followed by a backward substitution step (Press et al., 1992).

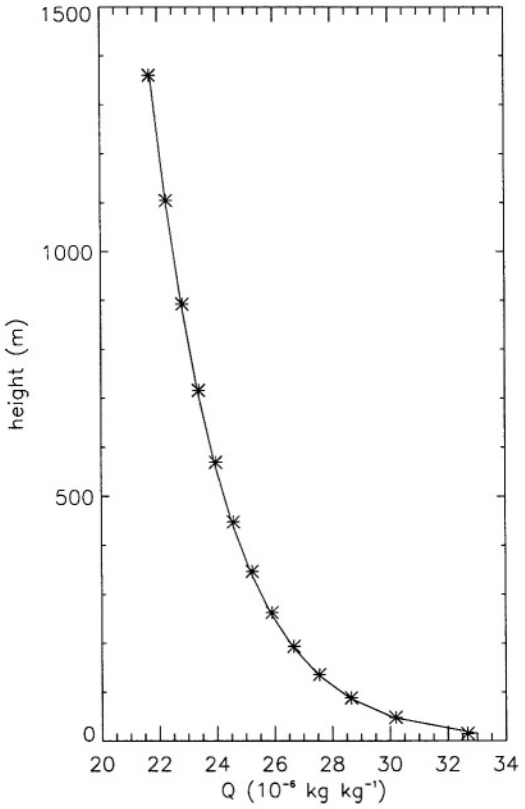

Figure 2. Comparison of analytical (solid line) and numerical (asterisks) solutions of the vertical diffusion equation.

In order to test the numerical diffusion scheme, a comparison was made with an analytical solution of Eq. (5). This was done for a one-dimensional vertical domain extending from the ground up to a mixing level height of z_i=1500 m. The initial concentration was zero everywhere, and the vertical turbulent diffusivity profile was taken as a parabolic shape defined by

$$K(z) = ku_* z\left(1 - \frac{z}{z_i}\right), \tag{8}$$

with k=0.4 von Kármán's constant and u_* the friction velocity, fixed at 1 m s^{-1}. At time t=0, a surface source is activated with a strength of 10^{-6} kg m^{-2} s^{-1}. The numerical simulation was performed using a time increment of 1800 s, during 20 subsequent steps. Use was made of 15 vertical levels, with depths varying from 30 m near the ground and increasing to approximately 300 m near the domain top at 1500 m.

The analytical solution is given by

$$Q(z,t) = \frac{S}{z_i}\left\{ t + \frac{z_i}{ku_*}\sum_{n=1}^{\infty}(-1)^n \frac{2n+1}{n(n+1)} P_n\left(2\frac{z}{z_i}-1\right)\left[1-\mathrm{e}^{n(n+1)\frac{ku_*}{z_i}t}\right]\right\} \qquad (9)$$

with t=36,000 s. The functions P_n are Legendre polynomials, which were obtained by means of a recurrence relation. Equation (9) was obtained by integration of Arya's (1999) Eq. (6.122) over the interval [0,t] and replacing the instantaneous surface source by a continuous one (S, units of $\mathrm{kg\ m^{-2}\ s^{-1}}$).

The result of the comparison between numerical and analytical solutions are displayed in Fig. 2, showing an excellent agreement. Note that the value of this exercise is limited, since the parameterisation of turbulent transport as a diffusion process is only a poor approximation of reality. Nonetheless, it has the merit of being a thorough check of the validity of the numerical implementation of Eq. (5).

4. CONCLUSIONS

Modules for advection and diffusion in AURORA were re-designed, resulting in a more accurate and faster version of the Eulerian Dispersion Model (EDM). In this new version, advection is treated by means of the recently developed algorithm by Walcek (2000), which is positive definite, mass conservative, accurate, and fast. The superior capacity of this scheme to preserve sharp concentration gradients was demonstrated. Vertical diffusion is treated with the well-established Crank-Nicholson scheme. The comparison of simulated concentration profiles with an analytical solution demonstrated the correct functioning of those schemes.

5. REFERENCES

Arya, S.P. (1999), *Air Pollution Meteorology and Dispersion.* Oxford University Press, Oxford.

Clappier, A. (1998), A correction method for use in multidimensional time-splitting advection algorithms: application to two- and three-dimensional transport, *Monthly Weather Review,* **126**, 232-242.

De Ridder, K., 2000, Modelling the impact of urban/regional scale land-use patterns on atmospheric flow and pollutant dispersion, Proceedings of the SIMPAQ-2000 Symposium, eds. Mensink et al., Vito report 2000/TAP/55 (available from the author).

Hundsdorfer, W., B. Koren, M. van Loon, and J.G. Verwer (1995), A positive finite-difference advection scheme, *Journal of Computational Physics,* **117**, 35-46.

Jacobson, M.Z. (1999), *Fundamentals of Atmospheric Modeling.* Cambridge University Press, Cambridge.

Press, W.H., S.A.Teukolsky, W.T. Vetterling, and B.P. Flannery (1992), *Numerical Recipes in Fortran 77,* Cambridge University Press, Cambridge.

Van Leer, B. (1977), Towards the ultimate conservative difference scheme. IV: a new approach to numerical convection, *Journal of Computational Physics,* **23**, 276-299.

Walcek, C.J. (2000), Minor flux adjustment near mixing ratio extremes for simplified yet highly accurate monotonic calculation of tracer advection, *Journal of Geophysical Research,* **105**, 9335-9348.

Xue, M., K. K. Droegemeier, and V. Wong, 2000, The Advanced Regional Prediction System (ARPS) - A multi-scale nonhydrostatic atmospheric simulation and prediction model. Part I: Model dynamics and verification, *Meteorology and Atmospheric Physics,* **75**, 161.

Zalesak, S.T. (1979), Fully multidimensional flux-corrected transport algorithms for fluids, *Journal of Computational Physics,* **31**, 335-362.

DISCUSSION

J. CHENEVEZ — You have compared four different advection schemes outcomes, but the Bott advection scheme, which is one of the most used scheme in air-pollution modelling, was not included. Have you considered to compare your results with the use of the Bott advection scheme ?

K. DE RIDDER — We did not ourselves include the Bott scheme in the comparison exercise, as Walcek (2000) already describes tests comparing his algorithm to Bott's and others.

A. BAKLANOV — You do not include the horizontal turbulent diffusion term in your model and mention that it is small compared to artificial numerical diffusion. However, for the urban scale and high-resolution simulations it can be not so. In this case it is necessary to control the level of the numerical diffusion (e.g. by horizontal grid size) to produce realistic fields of concentrations. Did you do it ?

K. DE RIDDER — With the increasing accuracy of numerical advection algorithms, there is indeed concern regarding whether horizontal diffusion may be ignored. We are currently analysing levels of physical and artificially generated diffusivities, and depending on the outcome the inclusion of horizontal diffusion in the transport equations will be considered.

A. HANSEN — Based on the 1-D test of the advection schemes the Walcek scheme appeared to have essentially no numerical diffusion, so that if you want to include horizontal diffusion you must explicitly add it since the numerical diffusion is negligible with the Walcek-scheme.

K. DE RIDDER — I refer to the previous answer.

This page intentionally left blank

MODEL ASSESSMENT AND VERIFICATION

Chairpersons :	H. Apsimon A. Ebel S. Incecik
Rapporteurs :	G. Cosemans Ph. Thunis

This page intentionally left blank

COMPARISON OF RESULTS FROM A HIGHER ORDER CLOSURE DISPERSION MODEL WITH MEASUREMENTS IN A COMPLEX TERRAIN

Babatunde J. Abiodunand Leif Enger*

1. INTRODUCTION

Air quality models are used as the most powerful and the only scientifically relevant tools for identifying effective strategies to improving air quality. They are very useful in getting air-quality data, particularly in the areas lacking observational data. Higher order closure dispersion models have been successfully used to simulate pollutant dynamics over many urban area and complex terrain (e.g. Enger and Koracin,1995 Abiodun et.al., 2001).

This paper presents a higher-order closure dispersion (HOCD) model, suitable for dispersion in urban area and complex terrain. The model is used to reproduced a tracer dispersion experiment in a complex terrain that was performed during an extensive field program, MOHAVE (Measurements Of Haze And Visibility Experiment) (see Green, 1999; Pitchford et al., 1999). A brief description of the model is presented in the next section. Section 3 discusses the project MOHAVE and the model initialization. Model results, in comparison to measurement, are discussed in section 4.

2. MODEL DESCRIPTION

The present model is an Eulerian diffusion model, which starts from the mass continuity equation

* Babatunde J. Abiodun, Department of Meteorology, Federal University of Technology, P.M.B. 704, Akure, Nigeria. Leif Enger, Department of Earth Sciences, Uppsala University, Villavägen 16, 752 36 Uppsala, Sweden

Air Pollution Modeling and Its Application XV, Edited by
Borrego and Schayes, Kluwer Academic/Plenum Publishers, New York, 2002

$$\frac{\partial C}{\partial t} = -U_j \frac{\partial C}{\partial x_j} - \frac{\partial \overline{u'_j c'}}{\partial x_j} + S \qquad (1)$$

The corresponding equations for the turbulence fluxes, if we neglect molecular terms and the effect of Coriolis force on the covariance, are

$$\frac{\partial \overline{u'_i c'}}{\partial t} = -U_j \frac{\partial \overline{u'_i c'}}{\partial x_j} - \overline{u'_i u'_j} \frac{\partial C}{\partial x_j} - \overline{u'_j c'} \frac{\partial U_j}{\partial x_j} - \frac{\partial \overline{u'_i u'_j c'}}{\partial x_j} - \frac{1}{\rho_0} \overline{c' \frac{\partial p'}{\partial x_i}} - \frac{g_i}{\Theta_0} \overline{\theta' c'} \qquad (2)$$

The equation for the covariance, $\overline{c'\theta'}$, is

$$\frac{\partial \overline{c'\theta'}}{\partial t} = -U_j \frac{\partial \overline{c'\theta'}}{\partial x_j} - \overline{u'_j \theta'} \frac{\partial C}{\partial x_j} - \overline{u'_j c'} \frac{\partial \Theta}{\partial x_j} - \frac{\partial \overline{u'_j c'\theta'}}{\partial x_j} - D \qquad (3)$$

The pressure covariance terms in equation (2) are parameterised according to Enger (1986) as

$$\frac{1}{\rho} \overline{c' \frac{\partial p'}{\partial x_i}} = \alpha_1 \frac{q}{\lambda} \overline{u'_i c'} - \frac{1}{3} \frac{g_i}{\theta_0} \overline{c'\theta'} \qquad (4)$$

where α_1 is a constant, and λ is a master turbulent length scale.

The vertical transport term is parameterized using a gradient diffusion approximation according to Donalson (1973) and Mellor (1973). The molecular destruction term D is parameterized according to Lumely (1975) as

$$D = \alpha_2 \frac{q}{\lambda} \overline{c'\theta'} \qquad (5)$$

The values for the constants, α_1, and α_2, are 0.3465 and 0.144 respectively. The formulations of the master length scale, λ, can be obtained in Enger (1990). A finite-difference numerical method is used to solve the set of the model equations. The model uses an expanding telescoping grid mesh with its origin at the source. This means that we get more dense grid mesh near the source where the plume is narrower than further downstream. The prognostic equations in the dispersion model are solved by using a third order advection scheme described in Enger and Grisogono (1997). The diffusion is solved with a semi-implicit scheme with weight 0.75 on the future time step. The Arakawa staggered C-grid is used for the model structure. The following boundary conditions are applied at the top of the model

$$\frac{\partial C}{\partial z} = \frac{\partial \overline{w'c'}}{\partial z} = \overline{u'c'} = \overline{v'c'} = \overline{c'\theta'} = 0 \qquad (6)$$

and the following at the surface

$$\frac{\partial C}{\partial z} = \overline{w'c'} = \frac{\partial \overline{u'c'}}{\partial z} = \frac{\partial \overline{v'c'}}{\partial z} = \frac{\partial \overline{c'\theta'}}{\partial z} = 0 \qquad (7)$$

3. MOHAVE PROJECT AND MODEL INITIALIZATION

MOHAVE project was conducted in the southwestern United States (see Figure 1) and included meteorological, chemical and visibility measurements at several stations. Upper-air observations were made at several sites using radiosondes, wind profilers and a radio acoustic sounding system (RASS). The main goal of the project was to assess the effects of the Mohave Power Plant (MOPP), a large coal-fired power plant in Colorado River Valley in southern Nevada, circa 120 km to the south-southeast of Las Vegas, upon visibility in the southwestern United States, in particular at Grand Canyon national park (Green, 1999). During the experiment, PTF ortho-perfluodimethylcyclohexane (oPDCH) was released continuously for 50 days in summer from the MPP. Forty-five percent of the oPDCH consists of the isomer ortho-cis (oc)PDCH, which was measured at the receptor sites. The tracers are inert, non-depositing, and non-toxic chemicals. The stack height of the power plant is 150m. The effective source height is calculated to be about 300m, and for the present study we use 300m in dispersion model. The average release rate of oPDCH for the period is about 0.042g/s. Details of the experiment and measurement can be obtained in Green (1999) and Isakov (1998). The measurement used for model comparison in the present study is obtained from Isakov (1998), but converted from femtoliters per liter (fl/L) to microgram per unit volume ($\mu g/m^3$).

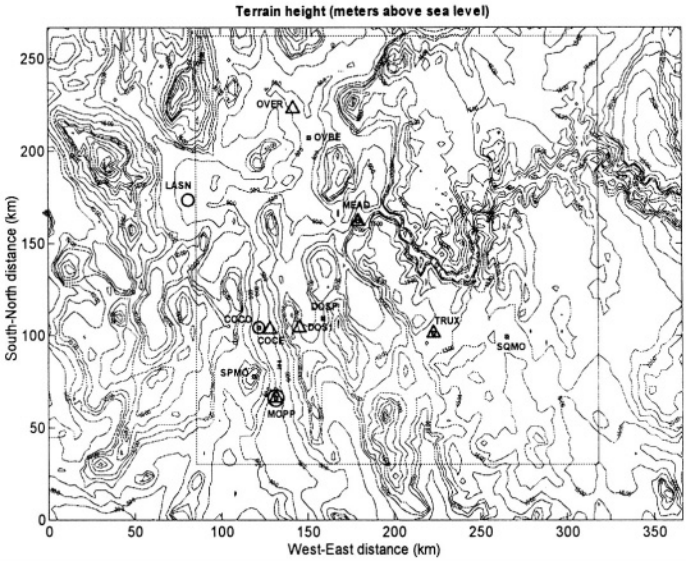

Figure 1. Domain and terrain of the study area, Colorado River valley. The total domain is used for the atmospheric model (MIUU) simulations while the inner square is used for the dispersion model (HOCD) simulations. Stations where observations were made are shown. Circles indicate meteorological surface observations, triangles meteorological upper-air observations and squares tracer measurements. For details and coordinates see Pitchford et al. (1999).

Dynamic flow fields and the turbulence over the study area for the period (5/8/92 – 14/8/92) have been simulated with the MIUU (Meteorological Institute Uppsala University) mesoscale model and reported in Morh. et.al 2001. The study shows that the simulated fields compare fairly well with the observations. For the present study, the simulated results for the first four days, which are stored at 1-hour interval, were interpolated to five minutes interval and used in the dispersion model. Figure 2(a) and 2(b) show the interpolated horizontal wind vector at 100m AGL from MIUU model domain to the dispersion model grid point at 1200 MST (5/8/92) and 1700 MST (6/8/92). Note that the wind vectors at every fifth grid point are plotted. The domain terrain and the receptor sites are shown in the background. The results generally show southerly and southwesterly flows over the area. The southerly flow is stronger along the Colorado valley and follows the bending shape of the valley. Effects of the anabatic and katabatic winds along the mountain slope, due to horizontal pressure gradient created by the temperature differences, are visible on the simulated flow at 1200 and 7000 MST respectively, especially around SPMO and the adjacent mountains.

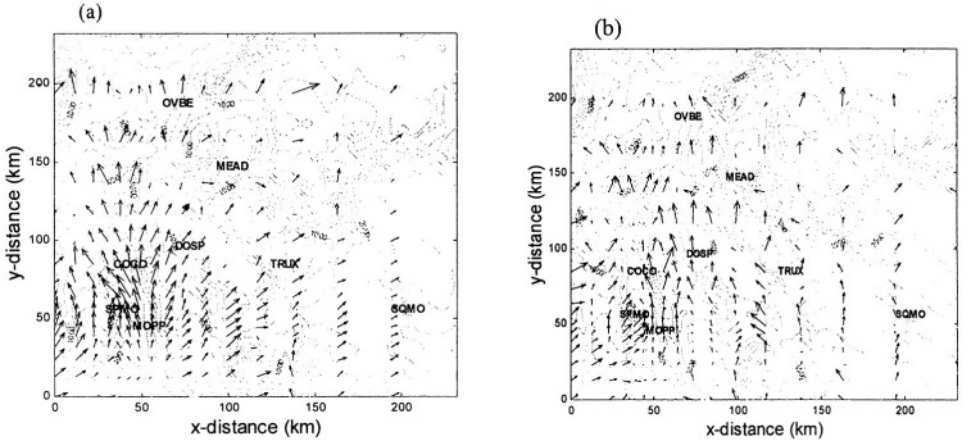

Figure 2. Simulated horizontal wind vectors at 100 m in study area. Panel (a) and (b) show typical flows during convective condition (1200 MST on 5/8/92) and stable condition (0700 MST on 6/8/92), respectively. Maximum vector lengths are 13 m/s and 19 m/s, respectively.

The tracer released at MOPP was represented in the dispersion model by a uniformly distributed area source over the nearest four horizontal grid points to the source location and three in the vertical grip points. The horizontal grid domain used is 81x81 km with 1km resolution close to the source. In the vertical we use 31 grid points with 50m resolution close to release height. The release started on the first day and continued until the fourth day.

4. MODEL EVALUATION AGAINST EXPERIMENTAL DATA

We first evaluate the performance of the HOCD model by comparing the spatial distribution of the 3-day mean of the simulated surface concentrations with the measurements in figure 3. From the figure we can see that the simulated concentrations are in the same order of magnitude as the measured ones, though there are differences in the actual values. The agreement between the simulated and measured concentration is quite good in that the model was able to reproduce the spatial pattern of the concentration over the domain. Moreover the model simulation shows that the main plume of tracer, released at MOPP, is transported northward along the valley, but part of the tracer is transported north-easterly to Grand Canyon and its vicinity. This is in agreement with the measurements.

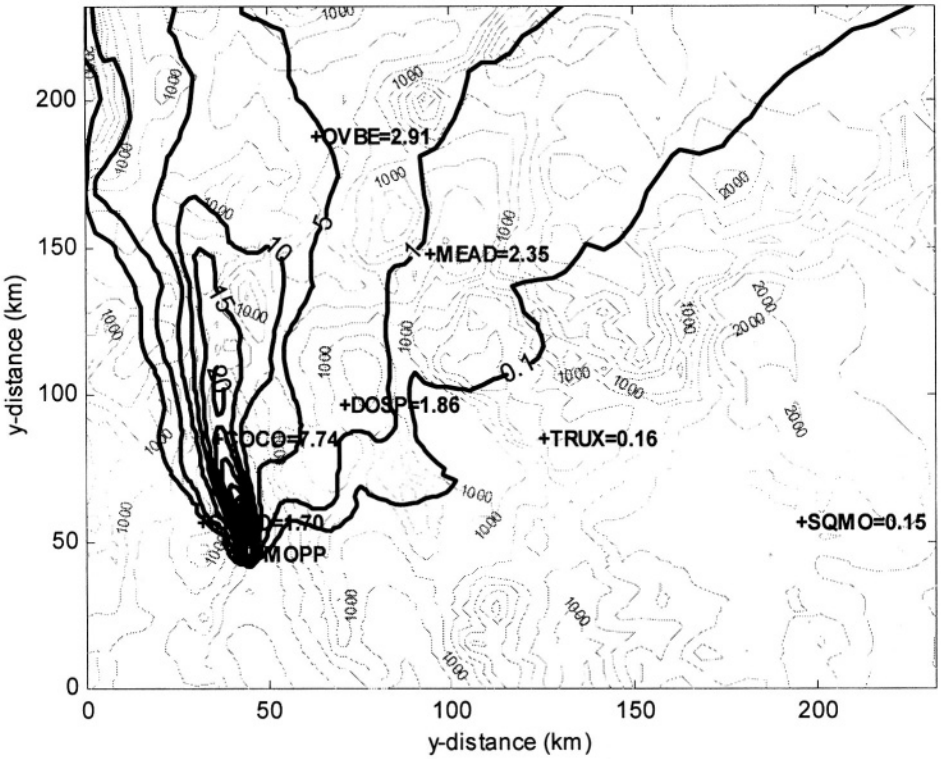

Figure 3. The contours of 3-day mean of the simulated surface concentration. Terrain, receptor locations, and the measured values are shown in the background. Both the simulated and measured concentrations are in 10^{-5} $\mu g/m^3$

The model performance is also evaluated through scatter-plot between observations ranked from high to low and similarly ranked models estimates. Such a plot is referred to as Quantile-Quantile (Q-Q) plot because each point corresponds to a specific quantile of the data set (Venkatram, 2001). Figure 4 shows the Q-Q plot for daily mean concentration. The figure shows that there is a good correlation between the model estimates and the observed. The squared correlation coefficients (R^2) is about 0.96. We can also observe from the figure that the model under predicts the concentrations at the lower end of the distribution and over predicts concentrations at the upper part of the distribution.

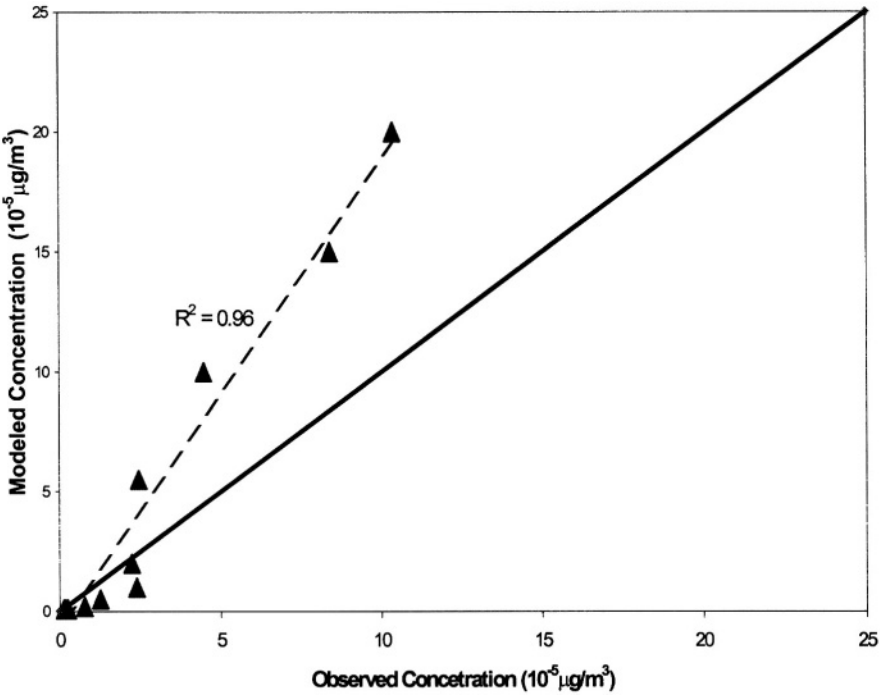

Figure 4. Quantile-Quantile (Q-Q) plot for daily mean concentration (at 7 receptor sites the sites for 3 days). The dashed line is the line of best fit, while the solid line is the line of accurate predictions.

The observed discrepancies between the model results and measurement in the present study could be attributed to (1) the inaccurate simulation of the wind flow and turbulence field by the MIUU model [see Morh et. al, 2001]. (2) the release of pollutants in the model did not start at same time as in the field experiment. (3) the insufficiently high grid resolutions used in both mesocale and dispersion models for the present study.

5. CONCLUSION

A higher-order closure model suitable for dispersion in complex terrain is developed. The model is applied over the US South West Coast complex terrain to study transport and diffusion of tracers released at MOPP during the MOHAVE 1992 field experiment. The stimulated pattern and order of magnitude are in good agreement with measurements made during the experiment. The model results also show that part of the pollutants released at MOPP is transported to Grand Canyon and its vicinity. The model simulations will be refined in the future with higher grid resolution to obtain better results. Also the dispersion model simulations would be extended to cover the entire period for the field experiment.

6. ACKNOWLEDGEMENTS

This study was sponsored by the Office of Naval Research (contract N00014-98-1-0557), by the Swedish National Research Council (contract G-AA/GU 12471-300), and by the International Science Program, Uppsala University (project NIG02).

7. REFERENCES

Abiodun B.J., L. Enger and M. Morh (2001) 'Modelling of atmospheric pollutants dispersion in complex terrain – part II: Development and validation of a Higher-Order Closure Dispersion model', Proceedings of 7th Int. Conference on Hamonisation within Atmospheric Dispersion Modelling for Regulatory Purposes, Belgirate, Italy. 355-359.

Donaldson, C. du P. (1973), 'Construction of a dynamic model of the production of atmosphere turbulence and the dispersal of atmospheric pollutants', In *Workshop on Micrometeorology* (edited by Haugen D.A.), American Meteorological Society publication, pp. 392.

Enger, L. (1986), 'A higher order closure model applied to dispersion in a convective PBL', *Atmos. Environ.,* Vol. 20, pp. 879-894.

Enger, L. (1990), 'Simulation of dispersion in moderately complex terrain-Part B. The higher order closure dispersion model', *Atmos. Environ*., Vol. 24, pp. 2447-2455.

Enger, L. and B. Grisogono (1997), 'The response of bora-type flow to sea surface temperature', *Q. J. R. Meteorol. Soc.,* Vol. 124, pp. 1227-1244.

Enger, L. and D. Koracin (1995), 'Simulations of dispersion in complex terrain using a Higher-Order Closure Model', *Atmos. Environ*., Vol. 29, No. 18, pp. 2449-2465.

Green, M.C., (1999), 'The Project MOHAVE tracer study: Study design, data quality, and overview of results', *Atmos. Environ.,* Vol. 33, pp. 1955-1968.

Isakov, V. (1998), 'Evaluation of Atmospheric and Dispersion models in complex terrain by using tracer measurements', *Ph.D. Thesis,* 119 pp. [Available from Division of Atmospheric Sciences, Desert Research Institute, 2215 Raggio Parkway , Reno, NV 89512]

Lumley, J.L. (1975), *Prediction methods for turbulent flows,* VKI-LS 76, Rhode-St-Genese, Belgium.

Mellor, G. (1973), 'Analytical prediction of the properties of stratified planetary surface layers', *J. Atmos. Sci*., Vol. 30, pp. 1061-1069.

Morh M, L. Enger and B.J. Abiodun (2001): 'Modelling of atmospheric pollutant dispersion in complex terrain – Part I: Development validation and comparison of Higher Order Closure Mesoscale models', Proceedings of 7th Int. Conference on Hamonisation within Atmospheric Dispersion Modelling for Regulatory Purposes, Belgirate, Italy. 350-354.

Venkatram, A. (2001) 'An Approach to developing air quality models for regulatory applications', Proceedings of 7th Int. Conference on Hamonisation within Atmospheric Dispersion Modelling for Regulatory Purposes, Belgirate, Italy. 37-41

Yamada, T. (1985), 'Numerical simulations of valley ventilation and pollutant transport. Proc. 7th Symposium on Turbulence and Diffusion with Boulder, Colorado. Amer. Meteor. Soc. 312-314.

DISCUSSION

A. HANSEN — Because of the overprediction of tracer concentrations in the far field, it appears that your model is creating mass. Is this possible ?

B.J. ABIODUN — A closer look at figure 4 actually suggests that the model overpredicts trace concentration close to the source, rather than in the far field as you said. The reason for this is that the MOHAVE point source is introduced in the model as an area source, due to the nature of the model.
Moreover we cannot also conclude that the model underpredicts tracer concentration in the far field, because a look at figure 3 reveals that downwind, the model underpredicts to the eastern side and overpredicts to the western side. This suggests a drift of the model plume more to the west than the measurements.
Lastly the mass conservation of the model had been tested in the previous experiments. We found that the model neither create nor destroy mass.

H. APSIMON — How sensitive are your model estimates in the MOHAVE experiment to the initial dispersion ? If this was slightly enhanced it would probably extend the spread of the plume and improve agreement with observations ?

B.J. ABIODUN — We did not investigate the sensitivity of the model estimates in the MOHAVE experiment to the initial dispersion. We will do this in our next validation experiment.

This page intentionally left blank

PARAMETERISATION OF SBL HEIGHT IN ATMOSPHERIC POLLUTION MODELS

Alexander Baklanov*

1. INTRODUCTION

Models of atmospheric transport of pollutants demand knowledge of the structure of the atmospheric boundary layer (ABL). A very important characteristic for such models, especially for stably stratified boundary layers (SBL), is the height of the atmospheric boundary layer, *h*. The upper boundary of the SBL often plays a role of a lid preventing pollutants to escape the SBL, so it is commonly called a mixing height (MH). The mixing height in the dispersion models can practically be determined by two basic ways. It can be obtained from profile measurements, either *in-situ* or by remote sounding. The other possibility is to use parameterisations with only a few measured parameters as input or to substitute output from numerical weather prediction models for observed parameters.

The working group 2 'Mixing Height Determination for Dispersion Modelling' of the EU COST Action 710 in the final project report (Seibert et al., 1998) has presented a very detailed analysis of the existing methods and approaches for the MH determination and, as a recommendation for future research, has stated that there is a general need for more research on SBL. Formulae for the mechanical mixing height, especially those based on Richardson numbers, should be tested on a number of data sets. The validity of the MH concepts originating from boundary layer studies to describe the pollutant dispersion should be studied, especially with respect to the effects of intermittent turbulence and of waves in outer SBL. Especially critical are the cases with long lived and very shallow SBLs of northern or coastal regions (Zilitinkevich et al., 2001a). In the thoroughly stable stratification (without the residual layer), typical for high latitudes and also for coastal zones, the vertical wave propagation is not blocked. As a result, the stable-boundary-layer turbulence becomes essentially non-local, and the traditional local theory predicts an insufficient turbulence mixing.

* Alexander Baklanov, Danish Meteorological Institute (DMI), Lyngbyvej 100 DK-2100 Copenhagen Denmark

Air Pollution Modeling and Its Application XV, Edited by
Borrego and Schayes, Kluwer Academic/Plenum Publishers, New York, 2002

In this paper determination of the stably stratified ABL height by ten different methods is analysed and verified versus the Cabauw experimental data set (Vogelezang & Holtslag, 1996). They include methods commonly used in atmospheric pollution transport models, e.g. the bulk Richardson number, turbulent energy and eddy viscosity depletion approaches, prognostic and diagnostic multy-limit formulations; and some newly proposed methods (Zilitinkevich et al., 200la; Zilitinkevich & Baklanov, 2001).

2. METHODS BASED ON THE BULK RICHARDSON NUMBER APPROACH

The bulk Richardson number approach, commonly proposed in scientific publications for the MH estimation, differs in choice of the levels over which the gradients are determined and in the value of the critical Richardson number, Ri_{bc}, and it can underestimate the SBL height (Seibert et al., 1998). E.g. this method of the SBL height parameterisation is used in the DMI-HIRLAM model and pollution dispersion models employed at DMI (Sørensen et al, 1996), namely, the Danish Emergency Response Model of the Atmosphere (DERMA) and the Danish Atmospheric Chemistry Forecasting System (DACFOS). Comparison of DERMA simulations for the ETEX experiment with the neutral and convective ABL showed a very good correspondence (Graziani et al, 1998). However, for the stably stratified ABL the model can underestimate the SBL height, so a limitation of a minimum value of the SBL height equal to 200 meters is incorporated into the model for practical reasons. The new version of the DMI-HIRLAM model (Saas et al., 1999) with the CBR turbulence scheme (Cuxard et al., 2000) uses a direct calculation of the ABL height from the turbulent energy depletion approach. However this method gives a considerable underestimation of the height of the nocturnal ABL as well (Baklanov, 2001).

Analysis of different estimations of Ri_{bc} for calculation of h shows a broad variation of Ri_{bc} values from 0.11 to 1.7. Zilitinkevich & Baklanov (2001) showed that the critical bulk Richardson number depends on the free flow stability parameter. They suggested a new formulation for the critical bulk Richardson number and a modification of the bulk Ri-number approach for the SBL height estimation. In comparison with the known method, it was suggested to simulate the SBL height proceeding from different values of the critical Richardson number (actually a function) for the free flow stability effects in the thoroughly stable stratification.

Figure 1 shows variations of the standard critical bulk Richardson number, Ri_{bc}, estimated at the measured SBL height, versus the external inverse Froude number, $\mathrm{Fr}_{10} = Nz/u$ (N is the Brunt-Väisälä frequency in the adjacent layer of the free atmosphere), for the Cabauw measurement data. Based on this and other experimental data sets Zilitinkevich & Baklanov (2001) suggested an empirical formulation for the critical bulk *Ri*-number. Here, following the new extension of the surface-layer similarity theory of Zilitinkevich and Calanka (2000) and Zilitinkevich et al. (2001b), another formulation of Ri_{bc} for the long lived SBLs (see details in Zilitinkevich et al. (2001b) and Baklanov (2001)) will be tested as a function of the external inverse Froude number, Fr_{10}:

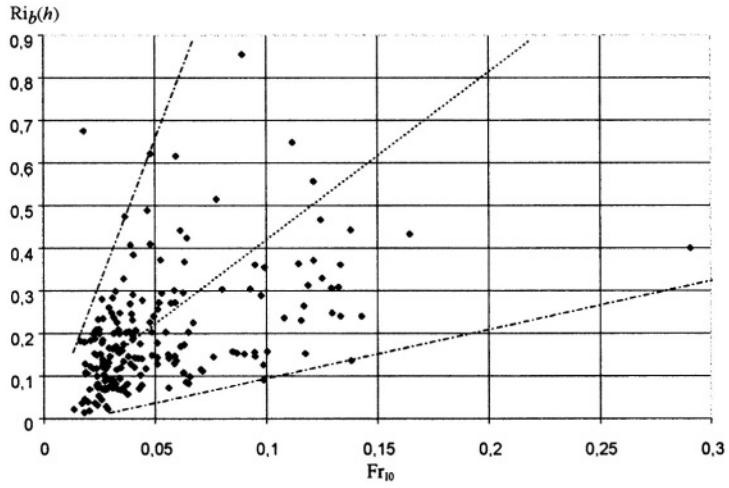

Figure 1. The standard critical bulk Richardson number, Ri_{bc}, estimated at the measured SBL height versus the external inverse Froude number, Fr_{10}, for the Cabauw measurement data.

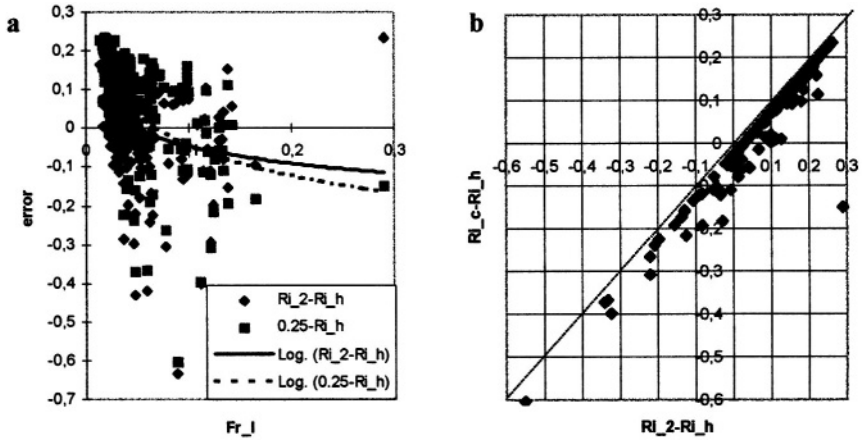

Figure 2. Comparisons of the two Ri_{bc}-based methods for SBL height estimation: the common method with Ri_{bc} = const and the suggested method with Ri_{bc}, calculated according to Eq. (1).
Errors of estimation of Ri_{bc} on the measured SBL height: Ri_{bc} - $Ri_b(h_{SBL})$, where Ri_{bc} = 0.25, and Ri_2 - $Ri_b(h_{SBL})$:
a) the errors versus external inverse Froude number, Fr_{10};
b) the scatter diagram for the errors of Ri_c - $Ri_b(h_{SBL})$ by the common Ri-method (vertical axe) and by the suggested method (horizontal axe).

$$\mathrm{Ri}_2 \approx \frac{k^2 C_\theta}{2k_T C_u^2}\left(1+\sqrt{1+\frac{4k_T C_u^4 a_\theta \lambda_T \mathrm{Fr}_{I0}^3}{k^3 C_\theta^2 \lambda_u}}\right), \qquad (1)$$

where: $k = 0.4$, $k_T = 0.42$ are the von Karman constants for momentum and heat, correspondingly; $\lambda_u \equiv \ln(z/z_{0u})$ and $\lambda_T \equiv \ln(z/z_{0T})$ are two parameters dependent on the height and roughness lengths; a_θ, C_θ, C_u, are empirical constants (according to Zilitinkevich et al. (2001a) $a_\theta \sim 1.6$, $C_\theta = 3.2$, $C_u = 2.1$).

Let's compare two Ri_{bc} -based methods for the SBL height estimation: the common method (e.g., Mahrt, 1981) with $\mathrm{Ri}_{bc} = \mathrm{const}$, and the suggested method with Ri_{bc}, calculated according to Eq. (1). Figure 2 shows errors of Ri_{bc} estimation on the measured SBL height: $\mathrm{Ri}_{bc} - \mathrm{Ri}_b(h_{SBL})$, where $\mathrm{Ri}_{bc} = 0.25$, and $\mathrm{Ri}_2 - \mathrm{Ri}_b(h_{SBL})$. In Figure 2a, the errors are presented vs. external inverse Froude number, Fr_{I0}, for the Cabauw data. Figure 2b presents a scatter diagram for the errors of $\mathrm{Ri}_{bc} - \mathrm{Ri}_b(h_{SBL})$ by the common Ri-method (vertical axis) and errors by the suggested method (horizontal axis). As seen, both graphs in Figure 2 show that the proposed approach, Eq. (1), considerably improves the method of the SBL height estimation. The bias of the estimated critical value of Ri_b on the top of the SBL height is 0.054 and 0.006 for the standard Ri_{bc} approach ($\mathrm{Ri}_{bc} = \mathrm{const}$) and the suggested modified method, Eq. (1), respectively.

However, it is necessary to note, that the discussed approach needs an additional improvement and verification vs. measurement data and testing with different models.

3. FORMULATIONS BASED ON EQUATION OF TKE BUDGET

Many different methods, commonly used in dispersion models for the MH estimation, are based on analysis of the turbulent kinetic energy budget and different length scales (e.g., Rossby & Montgomery, 1935; Zilitinkevich, 1972; Pollard et al., 1973; Arya, 1981; Mahrt et al., 1982; Nieuwstadt, 1984). Zilitinkevich and Mironov (1996) (henceforth ZM) summarised the SBL height parameterisation results from a number of earlier studies. The multi-limit diagnostic formulation of ZM became widespread among air pollution modellers (see e.g. Robertson et al., 1996; Brandt, 1998; Linqvist, 1998; Anquetin et al., 1999; Baklanov, 1999; Langer et al. 1999) during the last years. However, some authors (e.g. Zilitinkevich & Baklanov, 2001) pointed out an underestimation of SBL height by the formulation and, the constants had to be verified vs. experimental data. It was shown there that re-estimation of the constants and modification by incorporating the mean vertical velocity w_h at the SBL top gave a better correlation with the measurements. However, further analysis given by Zilitinkevich et al. (2001a) shows that two limits in the ZM formulation: $h \propto L$, for the SBL dominantly affected by the surface buoyancy flux (Kitaigorodskii, 1960), and $h \propto u_* / N$, for the SBL dominantly affected by the free-flow static stability (Kitaigorodskii and Joffre, 1988), are inappropriate for the Ekman layer.
Recent theoretical studies of non-local turbulence in the thoroughly stable stratification (Zilitinkevich & Calanca, 2000; Zilitinkevich, 2001; Zilitinkevich et al., 2001a) deepen understanding of its nature and provide an improved parameterisation of turbulence fluxes and PBL structure, which will be useful for parameterisation of the long-lived SBL height.

So, an alternative for ZM formulation for SBL height of the Ekman layer, h_E, including the effects of the free flow stability was proposed in Zilitinkevich et al. (2001a). According to that, extended surface-layer similarity theory taking into account possible distant interactions in the thoroughly stable stratification and interpolating with the known formulation of the neutrally stratified ABL yields new diagnostic (see below Eq. [8]) and prognostic formulations. The proposed method covers a broad spectrum of cases: both the nocturnal SBLs, typical for the middle latitudes, and the strongly stratified long-lived SBLs.

4. COMPARATIVE ANALYSIS OF DIFFERENT FORMULATIONS FOR SBL HEIGHT

Zilitinkevich et al. (2001a) and Zilitinkevich & Baklanov (2001) showed that the new modified formulation, Eq. [8], is in a reasonably good agreement with the experimental data and is better than the ZM multi-limit formulation, Eq. [7]. However, it is also necessary to give a comparative analysis of the discussed formulations with other different formulations for SBL height. Let's consider the comparative analysis with the Cabauw data set. The following eight formulations, commonly cited in the scientific literature (see e.g. Lena & Desiato (1999); Zilitinkevich & Baklanov (2001)), were used for the verification:

[1] after Zilitinkevich (1972) [1]: $$h = 0.42\left(\frac{u_* L}{f}\right)^{1/2} + 29.3;$$

[2] Nieuwstadt (1984): $$h = 0.4\left(\frac{u_* L}{f}\right)^{1/2}$$

[3] Arya (1981): $$h = 0.089\frac{u_*}{f} + 85.1$$

[4] Mahrt et al. (1982): $$h = 0.06\frac{u_*}{f}$$

[5] Benkley & Schulman (1979): $$h = 125u_{10}$$

[6] Nieuwstadt (1984): $$h = 28\left(u_{10}\right)^{3/2}$$

[7] Zilitinkevich and Mironov (1996): $$\left(\frac{fh}{0.5u_*}\right)^2 + \frac{h}{10L} + \frac{Nh}{20u_*} + \frac{h|f|^{1/2}}{(u_* L)^{1/2}} + \frac{h|Nf|^{1/2}}{1.7u_*} = 1$$

[8] Zilitinkevich et al. (2001a): $$h = \frac{0.4u_*}{|f|}\left[\left(1+0.3\frac{w_h}{u_*}\right)\Big/\left(1+\frac{0.16u_*(1+0.25NL/u_*)}{0.55L|f|}\right)\right]^{1/2}.$$

[1] Version modified by Aria (1981) with re-estimated constants.

The bulk Richardson number approach was not used in the simulations, because it was already analysed for different variants of the approach (Vogelezang & Holtslag, 1996) for the same data set. However, as it was shown in Chapt. 2, the modified bulk Richardson number method, Eq. (1), gives better results than the common bulk Richardson number approach.

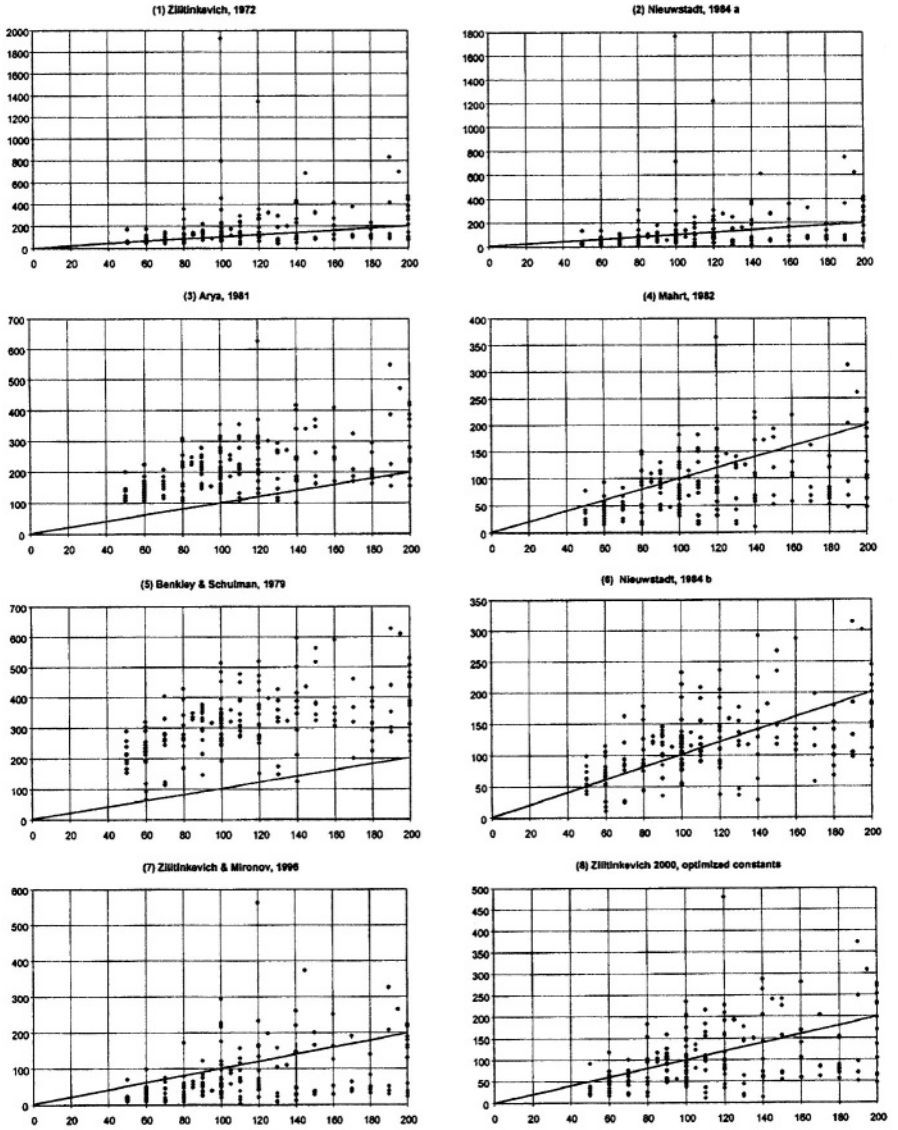

Figure 3. Simulation of SBL height by eight different parameterisations (see Eqs. [1]-[8]) for the Cabauw data: the vertical axis - the simulated SBL heights, h (in meters), the horizontal axis - the measured SBL height, h_{SBL} (in meters).

Results of the simulations and verification of the SBL height parameterisations [1] - [8] versus the Cabauw data are presented in Figure 3 and analysed in Zilitinkevich & Baklanov (2001). As it is seen, the new formulation of Zilitinkevich et al. (2001a), Eq. [8], is best supported by measurement data compared to the other seven formulations.

5. DISCUSSION AND CONCLUSION

Determination of the stably stratified ABL height by ten different methods is analysed and verified versus the Cabauw experimental data set (Vogelezang & Holtslag, 1996). The verified metods include methods commonly used in atmospheric pollution transport models, e.g. the bulk Richardson number, turbulent energy and eddy viscosity depletion approaches, the multy-limit formulations; and some newly proposed methods (Zilitinkevich et al., 2001a; Zilitinkevich & Baklanov, 2001).

It was shown that the critical bulk Richardson number, Ri_{bc}, is not a constant and depends on the free flow stability, including the external inverse Froude number, $\mathrm{Fr}_{I0} = Nz/u$. Following Zilitinkevich et al. (2001b) and Zilitinkevich & Baklanov (2001) the new formulation (1) for the critical bulk Richardson number, Ri_{bc}, and a modification of the bulk Ri-number approach for the SBL height estimation are discussed and verified. In comparison with the known method, it is suggested to simulate the SBL height proceeding from different values of the critical Richardson number (actually a function (1)) for the free flow stability effects in the thoroughly stable stratification. Comparison with measurement data showed that the proposed approach, Eq. (1), considerably improves the Ri-method of the SBL height estimation. However, it is necessary to note, that the discussed approach needs an additional improvement, verification and testing with different models.

It is shown that the last formulation for the SBL height, Eq. [8] (Zilitinkevich et al. (2001a), gives a better correspondence with the experimental data. The suggested parameterisations the SBL height will be tested in the DMI-HIRLAM model and pollution dispersion models employed at DMI, namely, the DERMA and DACFOS.

ACKNOWLEDGEMENTS

The author is extremely grateful to Sergej Zilitinkevich (Uppsala University) who have initiated this study and suggested many perfect ideas. Thanks to Bert Holtslag and Daan Vogelezang (KNMI) for providing the Cabauw data, Alix Rasmussen, Jens Havskov Sørensen and Niels Woetmann Nielsen (DMI) for their helpful advices and Alexander Mahura for comments on the manuscript. This work was partly supported by the Danish Forskningsstyrelsen – START-project No. 44.2207.4422.

REFERENCES

Anquetin, S., Chollet, J. P., Coppalle, A., Mestayer, P. G., Sini, J. F., 1999, The Urban Atmosphere Model: SUBMESO, *Proceedings of EUROTRAC Symposium '98,* P.M Sorrel & P. Borrel, Edits., WITpress.

Arya, S.P.S., 1981, Parameterizing the height of the stable atmospheric boundary layer, *J. Appl. Meteorol.* **20**, 1192-1202.

Baklanov, A., 1999, Modelling of episodes of atmospheric transport and deposition: Hypothetical nuclear accidents in North-West Russia, in: *Nuclear Risks, Environmental and Development Cooperation in the North of Europe.* CERUM, University of Umea, Sweden, pp. 65-80.

Baklanov, A., 2001, Parameterisation of the SBL height in atmospheric models. Presentation on the *Workshop on Stable Boundary Layers,* Uppsala University, Sweden, 12-14 September 2000 (as DMI Report).

Benkley, C.W. and Schulman, L.L., 1979, Estimating mixing depths from historical meteorological data, *J. Appl. Meteorol.* **18**, 772-780.

Brant, J., 1998, Modelling transport, dispersion and deposition of passive tracers from accidental releases. *PhD thesis.* RISO-NERI, Denmark, August 1998.

Cuxard, J., Bougeault, P. and Redelsperger, J.-R., 2000, A turbulence scheme allowing for mesoscale and large-eddy simulations. *Quart. J. Roy. Meteor. Soc.,* **126**, 1-30.

Graziani, G., Klug, W., and Mosca, S., 1998, Real-Time Long-Range Dispersion Model Evaluation of the ETEX first Release, *Office for Official Pub. of the European Communities,* Luxembourg, EUR 17754 EN.

Kitaigorodskii, S. A., 1960, On the computation of the thickness of the wind-mixing layer in the ocean, *Izvestiya, Ser. Geophys.*, **3**, 425-431.

Kitaigorodskii, S. A., and Joffre, S. M., 1988, In search of simple scaling for the heights of the stratified atmospheric boundary layer, *Tellus,* **40A**, 419-43.

Lena, F. and Desiato, F., 1999, Intercomparison of nocturnal mixing height estimate methods for urban air pollution modelling. *Atmospheric Environment,* **33**(15): 2385-2393.

Linqvist, J., 1999, *En stokastik partikelmodell i ett icke-metriskt koordinatsystem.* FOA report. FOA NBC-defence, Umeå, Sweden. 46 p. (in Swedish).

Mahrt, L., 1981, Modelling the depth of the stable boundary layer, *Boundary-Layer Meteoriol.,* **21**, 3-19.

Mahrt, L., Andre, J.C., Heald, R.C., 1982, On the depth of the nocturnal boundary layer. *J. Appl. Meteorol.* **21**, 90-92.

Nieuwstadt, F.T.M., 1984, The turbulent structure of the stable, nocturnal boundary layer, *J. Atmos. Sci.* **41**, 2202-2216.

Pollard, R. T., Rhines, P. B., and Thompson, R. O. R. Y., 1973, The deepening of the wind-mixed layer, *Geophys. Fluid Dyn.,* **3**, 381-404

Robertson, L., Langner, J. and Engardt, M., 1996, *MATCH - Meso-scale Atmospheric Transport and Chemistry modelling system. Basic transport model description and control experiments with* ^{222}Rn. SMHI RMK No 70, Norrkoping, Sweden

Rossby, C. G., and Montgomery, R. B., 1935, The layer of frictional influence in wind and ocean currents, *Pap. Phys. Oceanogr. Meteorol.,* **3**, No.3, 1-101

Saas, B.H., Nielsen, N.W., Jørgensen, J.U. and Amstrup, B., 1999, *The operational DMI-HIRLAM system.* DMI technical report #99-21.

Seibert, P., Beyrich, F., Gryning, S.-E., Joffre, S., Rasmussen, A. and Tercier, Ph., 1998, Mixing Height Determination for Dispersion Modelling. Report of Working group 2, in: *COST Action 710. Preprocessing of Meteorological Data for Dispersion Modelling.* May 1997.

Sørensen, J.H., Rasmussen, A. and Svensmark, H., 1996, Forecast of Atmospheric Boundary-Layer Height for ETEX Real-time Dispersion Modelling, *Phys. Chem. Earth,* **21**, No. 5-6, pp. 435-439.

Vogelezang, D.H.P. and Holtslag, A.A.M., 1996, Evolution and model impacts of the alternative boundary layer formulations. *Boundary-Layer Meteor.*, **81**, 245-269.

Zilitinkevich, S. S., 1972, On the determination of the height of the Ekman boundary layer, *Boundary-Layer Meteorol.*, **3**, 141-145.

Zilitinkevich, S. S., 2001, Third-order transport due to internal waves and non-local turbulence in the stably stratified surface layer. Submitted to *Quart. J. Roy. Meteorol. Soc.*

Zilitinkevich, S. and Baklanov, A., 2001, Calculation of the height of stable boundary layers in operational models. Submitted to *Boundary-Layer Meteorology.*

Zilitinkevich, S., Baklanov, A., Rost, J., Smedman, A.-S., Lykosov, V. and Calanca, P., 2001a, Diagnostic and prognostic equations for the depth of the stably stratified Ekman boundary layer. Accepted to *Quart. J. Roy. Meteorol. Soc.*

Zilitinkevich, S., and Calanca, P., 2000, An extended similarity-theory formulation for the stably stratified atmospheric surface layer. *Quart. J. Roy. Meteorol. Soc.,* **126**, no. 566, pp. 1970-85.

Zilitinkevich, S., and Mironov, D. V., 1996, A multi-limit formulation for the equilibrium depth of a stably stratified boundary layer, *Boundary-Layer Meteorol.*, **81**, 325-351.

Zilitinkevich, S. S., Perov, V. and King, J., 2001b, Near-surface turbulent fluxes in stable stratification: calculation techniques for use in general circulation models, Submitted to *Quart. J. Roy. Meteorol. Soc.*

DISCUSSION

S.E. GRYNING

Over the last 20 years, more than 15 parameterizations of the height of the SBL has been suggested, all based on the four parameters U_*, $\left(\overline{u'\theta'}\right)_s$ N and f. Comparison with data is generally poor. Do you consider that a general parameterization of the height of the SBL is possible ? I suggest to consider for future parameterization of the SBL height, a partitioning of the SBL into a weakly stable part (where $\left(\overline{u'\theta'}\right)_s$ increases with stability, and M-O theory is applicable), and a very stable part (where $\left(\overline{u'\theta'}\right)_s$ decreases with stability) where new scaling parameters has to be used likely including the effect of breaking waves.

A. BAKLANOV

Actually, most of the parameterisations used only three of the parameters mentioned above. The first attempt to include all four parameters was done by Zilitinkevich and Mironov (1996). However, it was done by asymptotic incorporation of all known limits, and two of them were not valid for the Ekman layer.

Your suggestion is correct. Actually, this principle to distinguish into two regimes of SBL was realised in the newest parameterisations of the height of the SBL, suggested by Zilitinkevich, Baklanov, Rost, Smedman, Lykosov and Calanca, (*Quarterly Journal of the Royal Meteorological Society,* 2001, Vol. 127, No. 578) and by Zilitinkevich and Baklanov (2001, *Boundary-Layer Meteorology,* accepted). The formula [8], which shows the relatively best correspondence with the measurements, includes the non-local effect of breaking waves for the very stable (long-lived) SBL and reduces to the well known formulation of Zilitinkevich (1972) for the weakly stable (flux-dominated) SBL, when M-O theory is valid.

EVALUATION OF MIXING HEIGHT PARAMETERIZATIONS FOR AIR POLLUTION MODELS

Laurent Delobbe, Olivier Brasseur, Jan Matthijsen, Clemens Mensink, Ferd J. Sauter, Guy Schayes, and Daan P.J. Swart*

1. INTRODUCTION

The mixing height (MH) is a fundamental parameter in many air pollution models. Its practical determination is often based on simple parameterizations, which only need a few input meteorological parameters. For validation purpose, it is useful to compare the results of these parameterizations with more sophisticated methods and with measurements

In this study, we evaluate the mixing height parameterization used in the photochemical transport model EUROS, developed at RIVM (van Loon, 1996). The MH evolution at Bilthoven (The Netherlands) for August 1997 calculated by EUROS has been compared with three other estimates: (1) from the ECMWF vertical profiles using a Richardson number method, (2) from the LIDAR measurements at RIVM (Bilthoven), (3) from a more sophisticated MH parameterization implemented in the EUROS model.

2. MIXING HEIGHT DETERMINATION

2.1 Standard Euros Formulation

In EUROS, the MH (H) is calculated from the friction velocity (u*), the Monin-Obukhov length (L) and the surface sensible heat flux (h_s), using simple parameterizations found in the literature (Nieuwstadt, 1981; Holtslag and Westrhenen,1989; Tennekes, 1973). Three stability cases are considered. In stable,

* Laurent Delobbe and Clemens Mensink, Flemish Institute for Technological Research (Vito), Boeretang 200, B-2400 Mol, Belgium. Olivier Brasseur and Guy Schayes, UCL, Institut d'Astronomie et de Géophysique G. Lemaître, Chemin du Cyclotron 2, B-1348 Louvain-la-Neuve, Belgium. Jan Matthijsen, Ferd Sauter, and Daan Swart, RIVM, Air Research Laboratory, PB1, 3720 BA Bilthoven, The Netherlands.

Air Pollution Modeling and Its Application XV, Edited by
Borrego and Schayes, Kluwer Academic/Plenum Publishers, New York, 2002

neutral and unstable conditions, the MH is formulated following (1), (2) and (3), respectively.

$$\frac{H}{L} = \frac{c_1 u_* / fL}{1 + c_2 H/L} \tag{1}$$

$$H = c_1 u^* / f \tag{2}$$

$$\frac{\partial H}{\partial t} = \frac{h_s}{\gamma H} \tag{3}$$

In these expressions γ is the potential temperature gradient above the convective boundary layer and f is the coriolis parameter. The surface meteorological parameters u^*, L, and h_s are calculated using a software library developed at KNMI (Beljaars and Holtslag, 1990). Input parameters are wind velocity (at 10 m for example), surface air temperature (at 2 m), aerodynamic roughness length and cloud cover from synoptical observations. These data are taken from the gridded NCAR synop observations.

The expression (3) used in convective case describes the growth of the convective mixing layer through a prognostic equation. The parameter γ expresses the stability of the layer above the convective layer. Its value is fixed to 0.005 K/m. This formulation considers the surface heating flux as the only relevant driving force, neglecting other contributions like the mechanical turbulence production due to surface friction.

2.2. New Formulation in Euros

The MH formulation in convective cases can be improved by taking into account the additional turbulence production due to surface friction as well as the entrainment heat flux at the top of the boundary layer. The entrainment flux can be parameterized in term of the surface heat flux. For example, the following expression proposed by Batchvarova and Gryning (1991) can be used:

$$\frac{dh}{dt} = (1 + 2a)\frac{hs}{\gamma h} + 2b\frac{u_*^3}{\gamma \beta h^2} \tag{4}$$

where β is the buoyancy parameter (β=g/T). The parameters a and b given in the literature differ considerably ranging between 0 and 1 for a (a = 0 correspond to no entrainment flux) and between 0 and > 10 for b (b = 0 corresponds to no mechanical production of turbulence). A discussion about these parameters can be found in Seibert et al. (2000). The parameters a and b have been first set to 0.2 and 2.5, respectively. Following Seibert et al. (2000), two other sets of parameters have been also tested: (1) a=0.4, b=5 and (2) a=0.4, b=2.5.

2.3. Richardson Number method applied on ECMWF vertical profiles

This method allows estimating the mixing height from the vertical profiles of temperature, moisture and wind. It has been used by numerous authors (e.g., Troen and Mahrt, 1986; Vogelezang and Holtslag, 1996; Sorensen et al.,1996). The top of the mixing height is given by the top of the layer defined by:

$$Ri_B = \frac{g\, z \left(\theta_v - \theta_{vs}\right)}{\theta_{vs}\left(U^2 + V^2\right)} \leq Ri_{critical} \qquad (5)$$

with g the gravity constant, z the height above the surface, U and V the horizontal wind components, θ_v the virtual potential temperatures at the height z, and θ_{vs} the surface value of θ_v . In convective conditions, several authors recommend to include in θ_{vs} a surface excess temperature, which is dependent on the surface sensible heat flux. Since the heat flux was not available in our data set, the excess temperature has not been applied.

As described in Delobbe et al. (2000), this Richardson method fails when the meteo data exhibit a thin and slightly stable layer near the ground under an unstable layer. To remedy this shortcoming, a modified method has been used, which combines the standard Richardson method with a criterion based on the vertically integrated buoyant energy.

2.4. LIDAR measurements

The third estimate of the MH is based on the LIDAR measurements carried out at the RIVM (Bilthoven, The Netherlands). The LIDAR determination of the MH is based on the backscatter of a laser beam by aerosol particles present in boundary layer (van Pul et al., 1994). The top of the MH is marked by a discontinuity in the backscatter profile.

3. COMPARISON AND DISCUSSION

The comparison has been carried out for August 1997. The results are illustrated in Figure 1 and 2 for a specific week. The comparison between the MH obtained from the standard formulation of EUROS and the estimates from LIDAR and ECMWF is shown in Figure 1. Significant discrepancies are found. For most days, the EUROS MH is 100 m during the night and grows in a motonic way up to a value around 1000 m in the late afternoon. The LIDAR and ECMWF estimates exhibit a much larger day to day variability. In the night, ECMWF values are comparable with the EUROS estimate while the LIDAR values significantly differ. It must be noted that the lowest MH that can be detected by the LIDAR is about 200 m. If the actual ML top is lower than 200 m, the LIDAR may consider the top of a residual layer as the ML top leading to unrealistically high MH values.

During daytime, the EUROS MH is usually small in comparison with the ECMWF and LIDAR values. The ECMWF estimates are only available at 00, 06, 12, and 18 UT but the MH value at 12 UT is systematically higher than the EUROS estimate. The

LIDAR provides hourly estimates of the MH. Large variations between two successive hours are regularly found.

Several causes of discrepancies between the three MH estimates can be mentioned. First of all, the method used in EUROS for the calculation of the MH has its own limitations. Errors may arise from the calculation of the surface meteorological parameters (Obukhov length, friction velocity and heat flux) but also from the determination of the MH from these parameters using expressions (1), (2) or (3). The meteo input used for the calculation of the surface meteo variables, for example the 2m-temperature and the 10-m wind, also induce some errors. The meteo input used in EUROS results from a spatial interpolation from synoptic observations and a time interpolation from the 4 input times of these synoptical observations (00, 06, 12, 18 UT). This interpolation partly explains the fact that the MH diurnal cycles simulated by EUROS are much smoother than the observed diurnal cycles from the LIDAR. Another possible cause of discrepancies arises from the fact that the LIDAR observations are local while, for ECMWF and EUROS, the estimate is an average over a grid cell, whose size is about $60 \times 60\ km^2$ (for both models). The LIDAR measurements are much more sensitive to local conditions such as updraft or downdraft in convective conditions.

Concerning the estimates from ECMWF using a Richardson number method, a first source of error results from the relatively coarse vertical resolution of the ECMWF data: around 400m in the boundary layer. The Richardson method exhibits also some shortcomings (e.g., Seibert et al., 2000). In this study, the surface excess temperature has not been applied which may induce significant underestimation of the MH in convective situations. A previous study has shown the high sensitivity of the MH estimate to the surface temperature used in Eq. (5) (Delobbe et al., 2000).

The determination of the MH from LIDAR measurements has also its limitations. We have already mentioned the minimal detectable value of 200 m, which may results in large errors for the night estimates. Another shortcoming is the large inaccuracies in case of rain or if the amount of aerosol or trace gas in the boundary layer is too low.

Even if large discrepancies are found between LIDAR and ECMWF estimates, both MH estimates are significantly higher than the results obtained with the standard formulation of EUROS. This formulation tends to underestimate the growth of the mixing layer during the convective hours of the day. The new formulation (Eq. 4) takes into account turbulence production due to surface friction and the entrainment heat flux at the top of the convective layer as well. As shown in Fig. 2, this formulation results in a deeper growth of the mixing layer. Using the first set of parameters (a=0.2, b=2.5), the MH maximum at the end of the afternoon is about 200 m higher. As mentioned earlier, the values of the parameters a and b found in the literature vary within a large range. In order the get a first idea of the sensitivity to these parameters, two others parameter sets have been tested (a=0.4, b=5 and a=0.4, b=2.5). These values are recommended by some authors as discussed in Seibert et al. (2000). The results are shown in Fig. 2. The MH maximum at the end of the afternoon is now about 400 m higher than with the standard formulation. For the two parameter sets, the results are almost identical. It means that the value of the parameter a is more critical than the value of the parameter b. The parameter a represents the ratio between the entrainment-layer and the surface-layer heat fluxes.

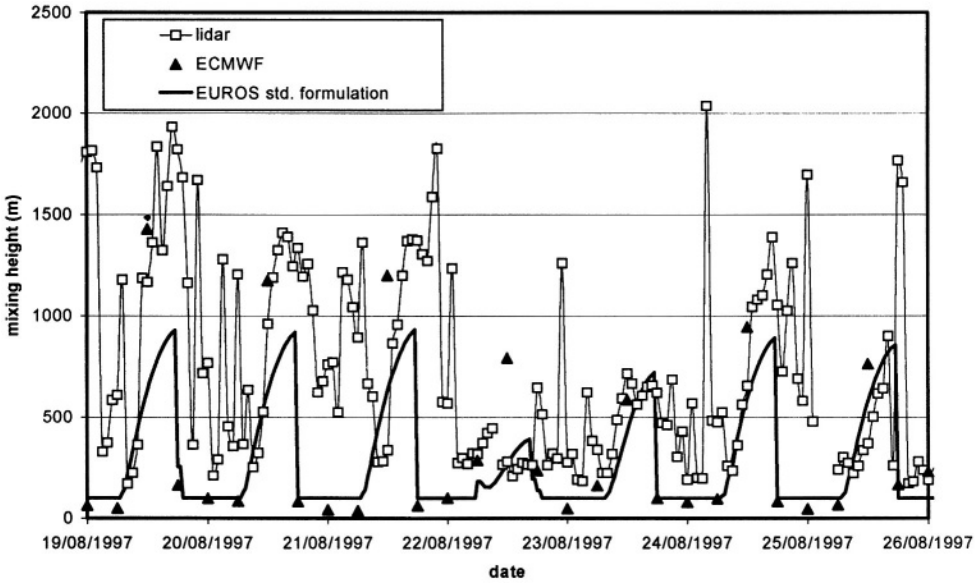

Figure 1. Mixing height evolution at Bilthoven (The Netherlands): (1) as derived from the LIDAR measurements at RIVM, (2) as estimated from the ECMWF data using a Bulk Richardson method, (3) as calculated by the EUROS model using the standard MH formulation.

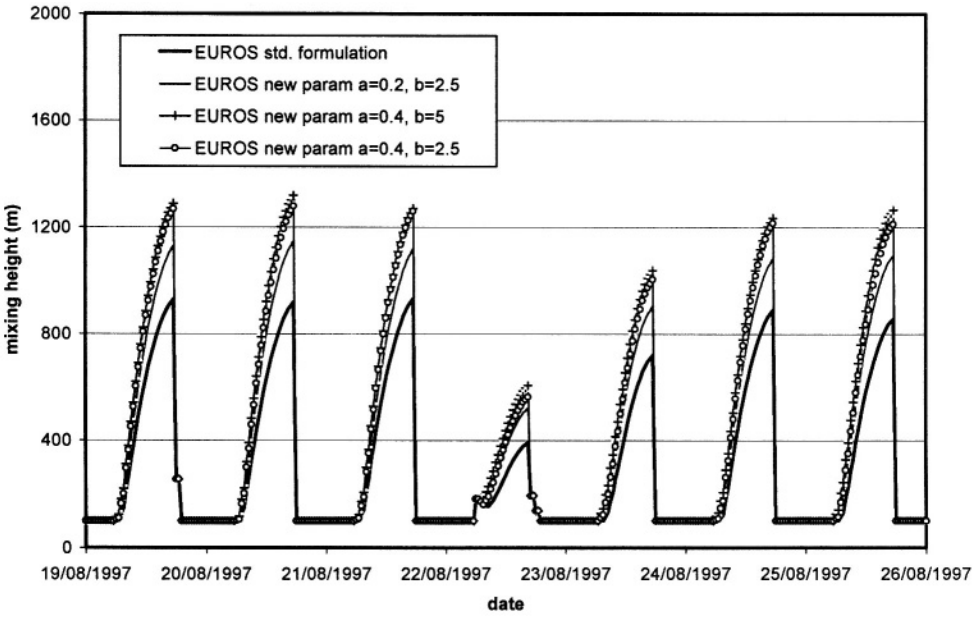

Figure 2. Mixing height evolution at Bilthoven (The Netherlands) calculated by the EUROS model (1) using the standard MH formulation, (2) using the alternative formulation (Eq. 4) taking into account surface friction and entrainment heat flux. For the alternative formulation, three parameter sets have been tested.

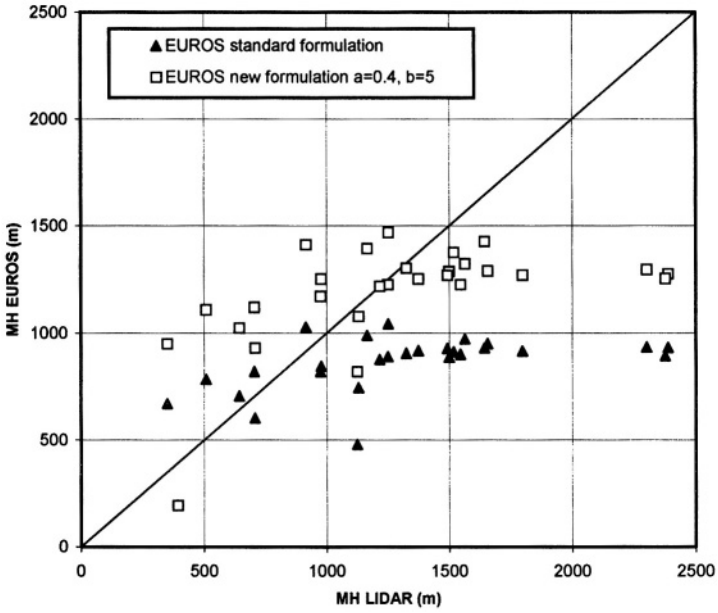

Figure 3. Comparison between the mixing height at 17 UT during the month August 1997 as estimated from the LIDAR measurements and as calculated by the EUROS model. The triangles correspond to the standard formulation of EUROS. The squares correspond to the new formulation (Eq. 4). The LIDAR estimate is the average over the period 16 to 18 UT.

The entrainment effect appears to be predominant with respect to the surface friction effect. The highest MH values are obtained with a=0.4 and b=5. For this set of parameters, Fig. 3 shows the comparison between the MH obtained at 17 UT with the new formulation of EUROS and the LIDAR values averaged over two hours from 16 to 18 UT. All the days of August 1997 for which LIDAR measurements are available are considered. The same Figure shows the results obtained with the standard formulation of EUROS. The agreement between the EUROS results and the LIDAR measurements is better using the new formulation. However, the variation range of the EUROS MH values remains quite small compared with MH values derived from the LIDAR measurements.

In this study, the sensitivity to the parameter γ has not been investigated. A fixed value has been used. This stability parameter plays however a key role in the description of the mixing layer growth. It is related to the vertical gradient of potential temperature just above the mixing layer and could be in principle be determined from meteorological vertical profiles. However, this would require a significant extension of the amount of meteorological input data.

The intercomparison of MH estimates presented here concerns the month August 1997. A deeper investigation would require to compare longer time series and on different locations where observational data are available. Besides, the comparison was limited here to the MH values. It would be useful to extend this comparison to some crucial input variables used in the MH formulations, e.g. the surface sensible heat flux

and the friction velocity. This would allow to distinguish between the errors related the deficiencies of the formulation itself and the errors due the inaccuracies in the input meteorological variables.

4. CONCLUSION

This study brings a contribution to the validation of MH parameterizations used in air quality models. The MH at Bilthoven (NL) simulated by EUROS has been compared with MH estimates from ECMWF meteorological vertical profiles and LIDAR measurements for the month August 1997. It has been found that the EUROS standard formulation tends to underestimate the MH values and the day to day variability. Besides, the estimate based on a Richardson number method applied on ECMWF vertical profiles is generally lower than the LIDAR estimate. A new MH formulation taking into account the turbulence production due to surface friction and the entrainment heat flux at the top of the convective layer has been implemented in EUROS. Our results show that this formulation allows a better representation of the mixing layer growth during daytime. However a deeper evaluation would require the intercomparison of various MH estimates on longer time periods and on different locations.

5. ACKNOWLEDGMENTS

This work is a contribution to EUROTRAC-2 subproject GLOREAM. It has been carried out in the framework of the BelEUROS project (Implementation and extension of the EUROS model for policy support in Belgium) funded by the Belgian Federal Office for Scientific Technical and Cultural Affairs.

6. REFERENCES

Batchvarova, E., and Gryning, S.E., 1991, Applied model for the growth of the daytime mixed layer, *Boundary-Layer Meteorology,* **56**: 261-274.

Beljaars, A.C.M., and Holtslag, A.A.M., 1990, A software library for the calculation of surface fluxes over land sea, *Environmental software,* **5**: 60-68.

Delobbe, L., O. Brasseur, and Mensink, C, 2000. Determination of the Mixing Height from ECMWF Data for Use in the Regional Photo-chemical Smog Model EUROS. To appear in Proceedings of EUROTRAC Symposium, 2000.

Holtslag, A.A.M., and van Westrhenen, R.M., 1989. Diagnostic derivation of boundary layer parameters from the outputs of atmospheric models. Sci. Rep. KNMI WR 89-04.

Loon, M. van, 1996, Numerical methods in smog prediction, *PhD thesis.* University of Amsterdam, 148 pp.

Nieuwstadt, F.T.M., 1981, The steady-state height and resistance laws of the nocturnal boundary-layer: Theory compared with Cabauw observations, *Boundary-Layer Meteorology,* **20**: 3-17.

Seibert P., Beyrich, F., Gryning, S.-E., Joffre, S., Ramussen, A., and Tercier, P., 2000, Review and intercomparison of operational methods for the determination of the mixing height, *Atmos. Environment,* **34**: 1001-1027.

Sorensen, J.H., Rasmussen, A., and Svensmark, H., 1996, Forecast of atmospheric boundary layer height utilised for ETEX real-time dispersion modelling, *Physics and Chemistry of the Earth,* **21**: 435-439.

Tennekes, H., 1973, A Model for the Dynamics of the Inversion Above a Convective Boundary layer, *J. Atmos. Science,* **30**: 558-567.

Troen, I. and Mahrt; L., 1986. A simple model of the planetary boundary layer. Sensitivity to surface evaporation. *Boundary-Layer Meteorology,* **37**, 129-148.

van Pul, W.A.J., and Holtslag, A.A.M., and Swart, D.P.J.,1996, A comparison of ABL-heights inferred routinely from lidar and radiosonde at noontime, *Boundary-Layer Meteorology,* **68**, 173-191.

Vogelezang, D.H.P., and Holtslag, A.A.M., 1996, Evolution and model impacts of alternative boundary layer formulations. *Boundary-Layer Meteorology,* **81**, 245-269.

DISCUSSION

A. BAKLANOV Your improvements and conclusions cover the Mixing height (MH) for unstable conditions only. For the nocturnal MH I do not see any improvement. Following your figures 1 and 2, it looks as if your model puts a constant value of MH for night time (~ 100m), probably due to the fact that the usual parameterization does not work satisfactory. Do you think it is a suitable method for calculation of the nocturnal MH ?

F. LEFEBRE The EUROS parameterisation for the MH takes a minimum MH of 100 m. If during the night, the formulations give a MH below 100 m, it is corrected to 100m.
In this presentation we have mainly been focusing on the mixing height formulations during unstable and neutral conditions. We did not analyze in detail the performance of the nocturnal MH parameterizations.

This page intentionally left blank

USING FUZZY NUMBERS TO TREAT PREDICTIONS FROM MORE THAN ONE MODEL

Bernard Fisher and Matt Ireland*

1. INTRODUCTION

The usual approach to the comparison of models is to compare the models' performance against some data sets and then to choose the model, which performs best according to some criteria. In practice insufficient data usually exists to make a clear preferred selection but for operational reasons one model is adopted. The selected model is then used to make decisions about the appropriate regulation of new and existing sources. In this paper an alternative approach is proposed for situations when results from several models are available assuming that each model has an acceptable level of performance. The basic assumption is that accepting the inevitable inaccuracies in each model it is better to try to obtain a combined estimate based on all the information available.

This may seem sensible qualitatively, but a decision maker has to make use of the extra information in a quantitative way. This can be illustrated by an example. Supposing that one has the results of two models. If the results are presented as just two numbers, one does not have much extra information on which to base a decision. The two predictions could be regarded as the either end of a range, so that the predictions provide an indication, perhaps, of the likely range of predictions. The air quality objective might lie above, below or within the range. Only in the case of the objective lying above the range would one be able to feel that there was no need for further investigation. A simple case is one in which one has predictions from one or more dispersion models.

---

*Bernard Fisher, Environment Agency, National Centre for Risk Assessment and Options Appraisal, Steel House 11 Tothill Street London SW1H 9NF U.K. Matt Ireland, Mott MacDonald, Victory House, Trafalgar Place, Brighton BN1 4FY U.K.

Air Pollution Modeling and Its Application XV, Edited by
Borrego and Schayes, Kluwer Academic/Plenum Publishers, New York, 2002

It is much more useful if predictions were always associated with some kind of uncertainty. There are various ways of expressing the uncertainty but it would need to be derived from validation exercises e.g. comparisons of dispersion model predictions with measurements reviewed in Hall et al (2000a). One could consider the situation shown in Fig 1 in which the predictions of two models are shown as fuzzy numbers. This means that there is a wide range of just possible values (with a low possibility). It is the most conservative estimate of the uncertainty about a quantity. At the other end of possibilities there is a best estimate, equal to the prediction, representing the most optimistic view of the degree of uncertainty. The wide range of uncertainty could be selected on the basis of the factor of two often assumed in dispersion models. There are other ways of representing the uncertainty, all of which depend on some subjective judgement, but the application of fuzzy numbers will suffice for an example.

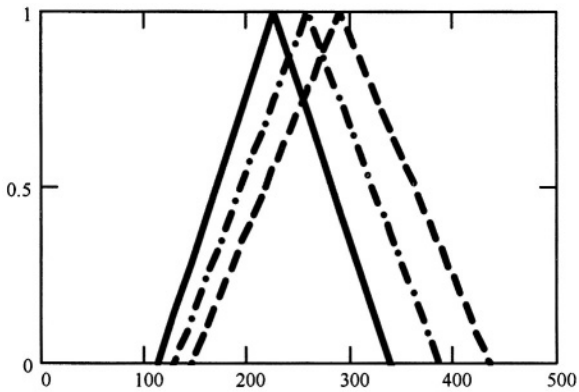

Figure 1. Comparison of two models predictions using fuzzy numbers. Model A (——) and model B (--------) are the models, the x-axis is the range of concentrations and the y-axis is the possibility or weighting on the predictions. The combined model (·-·-·-·) is an estimate taking the average of the two model predictions. These numbers are based on a real case of predictions from the AERMOD and ADMS dispersion models for a tall stack with buoyant plume in unstable conditions (Hall et al, 2000b) assuming a factor of two uncertainty to define upper and lower bounds.

2. WAYS OF COMBINING FUZZY NUMBERS

For the example considered above one sees that there is fair degree of overlap between the estimates and therefore a reasonable way to proceed is to combine the two fuzzy numbers. If one sets 0.05 as the possibility level (the qualitative description of the scale on the y-axis) one considers acceptable i.e. one is rather conservative about the range of possible values that could arise, one would estimate that the prediction lies between 135 and 381.

One may then compare the two fuzzy number representing predictions. The shape of the fuzzy number is a matter of opinion. However it depends on some estimate of the uncertainty in prediction so that some kind of bound, together with a best estimate, is needed from every model prediction. This is not routinely available from dispersion models, but it could be made available or could be requested from model users. This is

the situation assuming that the model is being applied in the usual way, in order to obtain the best estimate of the maximum ground-level concentration.

In contrast a screening model would be used in another way. A screening model would have a much wider range of possible predictions, without necessarily weighting the maximum possibility (best estimate) towards the upper bound of the range. The screening model is used to incorporate all, or as many results, as possible. It is anticipated that normally the predictions of a screening model would have to be refined using a more accurate model, in order to reduce the range of possible predictions.

Fuzzy numbers can be manipulated in a consistent manner. They arise as a refinement of intervals which are rather crude encapsulations of uncertainty (Ferson, Root and Kuhn, 1999). For instance, intervals imply that although we cannot give a quantity's value exactly, we can give exact bounds on the quantity. Fuzzy numbers generalise intervals. A fuzzy number can be thought of as a nested stack of intervals containing many levels of confidence about uncertainty. These levels of confidence range between 0 (corresponding to the most conservative, widest interval) and 1 (the narrowest interval, which assumes we are really good at making predictions). By definition, all fuzzy numbers must reach one and must be convex (single humped). The scale between 0 and 1 is said to measure the possibility that a number is within the interval at a particular level. This introduces the notion that possibilities can be graded. Fuzzy numbers and their arithmetic provide a simple and workable methodology that is valid for handling non-statistical uncertainty in calculations.

In the application under consideration one might wish to take the average of the two estimates and this leads to the combined estimate shown in the figure. As long as two fuzzy predictions contain a significant amount of overlap this seems a sensible way to proceed. However in situations where the fuzzy numbers are in ranges which do not overlap one would conclude that the predictions are significantly different. Model A is predicting values definitely lower than model B and taking some average would not be appropriate.

The reasons for a significant difference between model predictions are varied. They could arise because of an input error in one of the models. The models may be using different algorithms. For example the models may differ in the way they treat a plume near the top of the boundary layer or what happens to a plume near the top of the hill. One model may predict zero concentration at the ground, while the other model may predict substantial ground-level concentrations. The only way to deal with this situation is to consider the full specification of the model. This is the reason for the need for transparency in the descriptions of models. Of particular interest are the algorithms for which a small variation in parameter values leads to a large change in concentration.

An alternative approach is combining two estimates is to consider that predictions are uniformly distributed between the upper and lower bounds with equal probabilities. One can then obtain an average estimate by sampling each distribution at random. This assumes that one chooses values from the two distributions in an independent way to

obtain a combined distribution. If one chooses the 5 and 95 percentile points in the combined distribution as bounds on the estimate, one obtains the range 167 to 344.

The conventional, simple approach is just to quote a range with the upper and lower bounds chosen from the results from the best estimates of the two models e.g. between 226 and 290. This is a start to defining uncertainty, but the measure of uncertainty is arbitrary depending on predictions of models in specific situations without regard to model performance. The range can appear unrealistically small. An alternative, simple approach is to take the range from the higher of the upper bound of the two predictions and the lesser of the lower bounds of the two predictions, namely a range 113 to 425 in this case. The fuzzy number approach gives a more bounded range, 135 to 381, while the assumption that there are random independent errors associated with each model gives the smaller range, 167 to 344.

Thus taking ranges directly from models' best predictions does not appear to give a realistic estimate of uncertainty. Taking the maximum range has the advantage of simplicity but may be regarded as encompassing too broad a range of possibilities. The other two approaches are to some extent qualitative. Taking the mean of fuzzy numbers is related to taking the mean end points of intervals.

3. COMBINING TWO DIFFERENT MODELS

A similar idea can be adopted when one has separate models describing different parts of an overall system. An example described previously is of the NO_2 within an urban area, such as London. Fig 2 shows the NO_2 from all road transport sources. This does not show the impact from the roads. One needs different models to treat pollution dispersion on the local and regional scales. If one treats the urban area in an ideal way the local impact of emissions from major roads is not apparent. In an earlier paper methods for estimating roadside and background concentrations were described (Fisher and Sokhi, 2000). These have been applied to an idealised, version of London in which three major circular roads are imagined to surround areas of the city: an inner ring road, an outer ring road and an orbital road on the outskirts of the city. A cross-section of the annual average NO_2 concentration across the city is shown in Figure 3. The NO_2 air quality standard of 21ppb is exceeded within a central zone by the background concentration. However the exceedence around the outer ring road arises from the combined contributions of the background and the roadside concentrations. One precautionary way of estimating areas of exceedence taking account of uncertainty would be adopt an air quality standard of 19ppb. This would have the effect of greatly enlarging the size of the central air quality management area. The gradient in the background concentration as a function of distance is small so that small changes in the air quality standard produce large changes in the size of the air quality management area. In contrast the gradient in concentration close to the road is large, so that small changes in the air quality standard applied have a smaller effect on the size of the air quality management area. Thus applying a discrete criterion to define an air quality management area might be regarded as a far from ideal way of taking account of uncertainty. The estimates of the air quality management area are not robust and are very sensitive to qualitative estimates of the uncertainty.

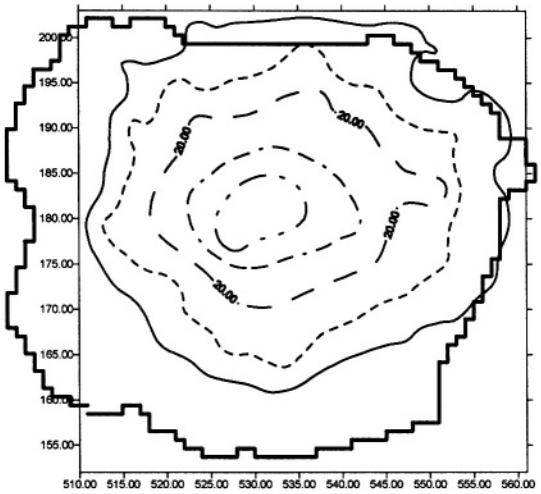

Figure 2. Background annual average NO_2 concentration in ppb over London from road transport emissions

An alternative approach is to assume that all estimates have some fuzziness or uncertainty associated with them, which will tend to smooth out the boundaries of any area to which a discrete, crisp criterion is applied. This approach can be applied to the example of a road within a city using the measure of fuzziness applied in an earlier paper (Fisher and Newlands, 2000). In this paper a simple form for the multiplicative error associated with estimates of concentration C(x) at a point x of the form $1/(1+C_0/C(x))^2$ was adopted where C_0 is the air quality standard. This had the advantage that functions could be easily manipulated. The membership function of an air quality management takes the simple form $1/(1+C_0/C(x))$, where higher values of the membership function denote greater certainty that the point x lies within the air quality management area and vice versa. (This choice is preferable to a step function for which $C>C_0$ implies exceedence and $C>C_0$ implies no exceedence.) It was possible to obtain an analytical formula for the membership of an air quality management area based on the aggregate of the membership functions of background and roadside air quality management areas considered separately.

If this approach is applied to the air quality management area around the outer ring road about 10km from the city centre, one obtains a membership function which looks like that in Fig 4. The membership function or weighting is shown on the y-axis and the distance from the city centre is shown on the x-axis in kilometres. Hence only distances of a few hundred metres from the road are being considered. High values represent more certainty that the point lies within an air quality management area and low values or weightings represent less certainty that the point lies within an air quality management area.

The result is dependent on choosing a form for the membership function and that the errors in the roadside concentration are independent of the errors in the background concentration. The result also depends on the assumption that an aggregation function

can be conveniently defined involving a convolution integral over the weighting of errors in the roadside and background concentrations. The basic conclusion is that the choice of an air quality management area is not a discrete step function but should rather be a smooth weighting function as shown in Fig 4. This is much more intuitively appealing since the profile of the annual average NO_2 concentration is itself a smooth function, albeit with a steep gradient near a road. In conclusion, estimates of harm or damage based on concentration values are to be preferred to estimates that artificially distinguish areas of exceedence (harm) from areas of no exceedence (no harm). The latter approach does have the advantage of simplicity, highlighting possible areas of concern in scoping or screening studies.

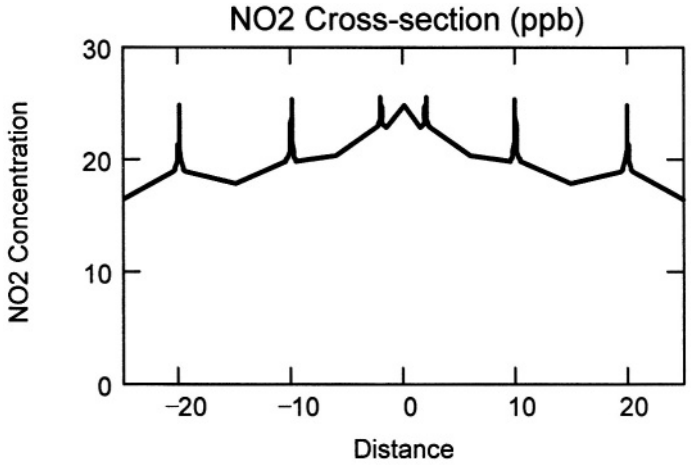

Figure 3. Idealised profile of the annual average NO_2 concentration in ppb in London along a cross-section through the centre of the city. The spikes denote high concentrations in the vicinity of major roads.

The approach illustrated here for combining the uncertainty results from two models is analogous to the problem of combining two concentration frequency distributions. This question arises when, for example, one has two different contributions, such as the urban background concentration and the concentration from a major stationary source. Similar aggregation methods based on the assumption of independent fluctuations may be applied.

The above example illustrates a situation when one is comparing the sum of two models against an air quality standard. Another way of illustrating how sharp boundaries or demarcations result in conclusions which are very sensitive to the initial assumptions would be to consider the number of people, who are exposed to exceedences of the annual average NO_2 standard. For this case it should be noted that the area, where there is a high weighting near to the road, is also an area where people may not be exposed. Houses are usually set back some way from the road carriageway so that the area of very high weighting does not necessarily correspond to a high number of people exposed. It is also not clear whether a street canyon would mean an increase or a decrease in the population exposed.

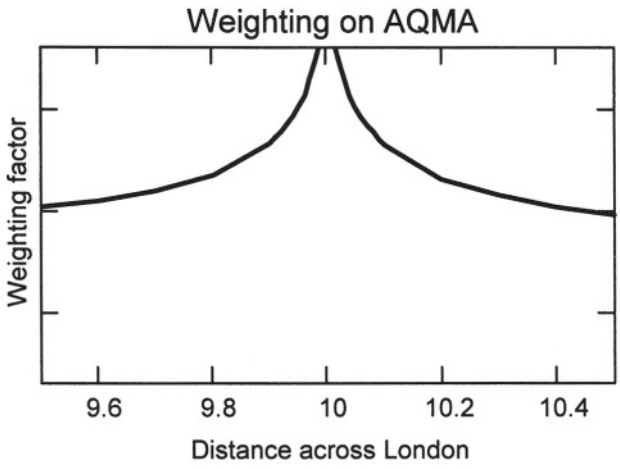

Figure 4. Weighting function representing the likelihood of exceeding the air quality standard for the annual average NO_2 concentration in the vicinity of an idealised major road 10km from the centre of London. High values of the weighting represent a high likelihood of an exceedence and vice versa.

For this idealised example the running of a single dispersion model with no account for uncertainty would suggest that all persons with in 240m of the road would be within an area where the annual average NO_2 standard was exceeded. If the air quality standard is assumed to be 20.5 ppb, then all persons within 540m of the road would live in a area of exceedence. The number of people exposed to an exceedence is very sensitive to uncertainty, suggesting that these results correspond to that part of the curve in Fig 4 where the gradient is shallow. This result is expressed by the curve in Fig 4 than by a single estimate of the number of persons exposed.

A third example considers two models compared with an air quality standard, a generalisation of the first case. For illustrative purposes the weighting on the uncertainty in each of two estimates of concentration C is taken to be $1/(1+C_0/C)^2$, where C_0 is the air quality standard. Then the similar analysis leads to an aggregate weighting shown in Fig 5, expressed as the weighting relative to the weighting, if both estimates had given concentrations exactly equal to the air quality standard.

4. CONCLUSIONS

The treatment of uncertainty is inevitably associated with some subjective judgements. This paper serves to illustrate that there are different approaches, which would deserve investigation. Using results from more than one model has distinct advantages in decision making if used with care.

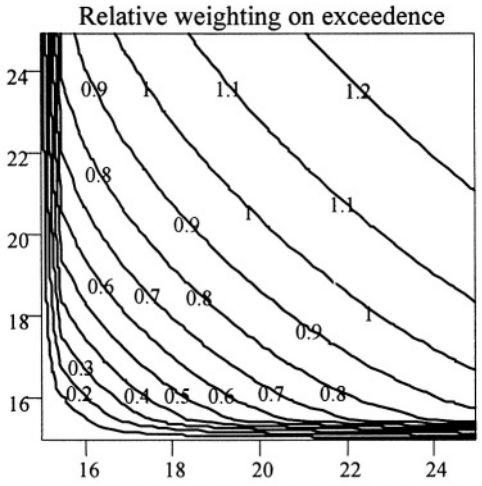

Figure 5. Relative weighting of an exceedence of the long-term air quality standard for NO_2 as a function of two estimates of the concentration. The x-axis is the best estimate from one model and the y-axis is the best estimate from another model. If both models give a high estimate then the standard is likely to be exceeded, while if both give low estimates then it is unlikely that the standard will be exceeded.

5. REFERENCES

Ferson S, Root W and Kuhn R, 1999, RAMAS RiskCalc: Risk assessment with uncertain numbers. Applied Biomathematics, Setauket, New York, http://www.ramas.com

Fisher B E A and Newlands A G, 2000, The designation of fuzzy air quality management areas, in: *Air Pollution Modeling and its Application,* S-E Gryning and F A Schiermeier, ed, Kluwer, New York, pp 97-105.

Fisher B and Sokhi R S, 2000, Investigation of roadside concentrations in busy streets using the model GRAM - Conditions leading to high short-term concentrations, *Int J of Env Technology and Management,* **14**, 488-495.

Hall D J, Spanton A M, Dunkerley F, Bennett M and Griffiths R F, 2000a, A review of dispersion model inter-comparisons studies using ISC, R91, AERMOD and ADMS, Environment Agency Technical Report P353, Bristol.

Hall D J, Spanton A M, Dunkerley F, Bennett M and Griffiths R F, 2000b, An inter-comparison of the AERMOD, ADMS and ISC dispersion models for regulatory applications, Environment Agency Technical Report P362, Bristol.

DISCUSSION

S. RAFAILIDIS In the presentation you tackle with the uncertainty in the concentrations. If on top of this you add the uncertainty in the health effects of the concentrations, does your final result become more "focused" or widens out ?

B. FISHER Taking into account the uncertainty in the health effect would not widen the overall uncertainty, as the health effect is usually interpreted as a threshold air quality standard. In reality the epidemiological data which is used to derive the air quality standard is uncertain. Hence if our assessment includes there, then the overall uncertainty is increased.

This page intentionally left blank

NARSTO MODEL COMPARISON AND EVALUATION STUDY (NMCES)

D. Alan Hansen*

1. INTRODUCTION

A major study comparing regional air quality modeling systems used for regulatory purposes in the USA and Canada is being conducted under the auspices of NARSTO. Groups from the Meteorological Service of Canada, US Environmental Protection Agency, New York State Department of Environmental Conservation, North Carolina Supercomputing Center, Environ International, and ICF Consulting are participating. These groups, their sponsors, the models they used and the gridding schemes employed are shown in Table 1.

Table 1. NMCES participants and their models

Participant/Sponsor	Met. Model	Air Quality Model	Grid-cell Size, km	Period Simulated
Meteorological Service of Canada	MC2	CHRONOS	10	5-18 July 1995
US EPA	MM5	CMAQ	36, 12, 4	5-18 July 1995
Environ/Coordinating Research Council	RAMS3b	UAM-V	36, 12	5-18 July 1995
North Carolina Supercomputing Center/Southeast States Air Resource Mgrs.	MM5	MAQSIP	36	5-18 July 1995
Environ, Coordinating Research Council	MM5	CAMx	36, 12	7-15 July 1995
ICF Consulting/Southern Co.	MM5	UAM-V	36, 12	7-15 July 1995

*D. Alan Hansen, EPRI, P.O. Box 10412, Palo Alto, CA 94303, USA

Air Pollution Modeling and Its Application XV, Edited by
Borrego and Schayes, Kluwer Academic/Plenum Publishers, New York, 2002

The opportunity for such a study presented itself when, stimulated by the need to meet regulatory milestones for attainment of national standards and objectives for ozone in the two countries, many public and private groups modeled time periods in July 1995 in overlapping domains covering most of eastern North America. By taking advantage of this rare opportunity, the comparability of modeling results between Canadian and American environmental agencies and among public and private groups could be established without undertaking an effort of much larger proportions.

To guide the study, a Working Group was organized and comparison protocols were developed by sub-working groups for emissions, meteorological and air quality modeling. EPRI was selected to coordinate the study and produce the comparison tables and graphics. Each of the protocols has been implemented to a greater or lesser degree, depending on resources and priorities, with the higher priority given to the air quality model comparison.

The study was conceived to take place in two phases. In the first phase the models were to be compared in their "native" mode, i.e., using the same input files and model configurations that each group used in their individual assessments, based on modeling a 9 to 14-day period in July 1995. The planners believed that, with a minimal amount of extra effort, existing model output files could readily be used for the comparison and valuable information would be gained on the relative performance of these disparate models, each of which has been used in exercises having significant policy implications. As the study has unfolded, the first phase has not been as straightforward as initially anticipated. Firstly, modeling errors were discovered that motivated some participants to withdraw their modeling files for replacement with new corrected files. Secondly, the Working Group asked two participants that had used two-way nested grids to run additional simulations with the entire domain coarsely gridded so that coarse and fine results over the same geographical areas could be compared. Thirdly, one participant decided to rerun its models at a finer grid over the entire domain. And finally all participants were asked to rerun their models with separate across-the-board 50% reductions in anthropogenic NOx and volatile organic compound emissions. As a result, completion of Phase 1 has been delayed by at least two years from the originally planned date, with an expected completion in late 2001.

The idea of a second phase was based on the realization that comparing models run in their native mode would provide insufficient information to diagnose why models might yield different results. A more comprehensive approach would need to be taken. Further, it would recognize the anticipated widespread desire to compare models with an aerosol simulation capability. Thus, in Phase 2 regional tropospheric aerosol models would be compared using harmonized model inputs. "Harmonization" means that models would be exercised, for example, on identical domains, employing the same horizontal gridding, topography, land use, vegetation distributions and emissions inputs. Meteorological inputs would be as similar as possible, consistent with maintaining mass conservation. Additionally, participating models would be expected to have a process analysis capability to facilitate diagnostic analyses. Whether or not there will be a send phase remains to be determined.

This paper describes Phase 1. The next section enumerates the modeling domains and sub-domains selected for comparison to determine if model performance varied geographically. That is followed by descriptions first of how the emissions files used as inputs to the air quality models and then how the meteorological files used to drive the air quality models were compared. Then the approach to comparing the air quality models is

described. Since this manuscript was prepared several months in advance of the NATO International Technical Meeting for which it serves as the basis for an oral presentation at the meeting, the results of the comparisons were not yet available and could not be included here. Therefore, the final section provides instructions on how to access the results of the study.

2. MODELING AND COMPARISON DOMAINS

Comparisons among models and between models and observations were made over the entire overlapping portions of domains, in subregional domains, and in urban and rural sub-domains of just a few gridcells each. The primary and larger regional sub-domains are shown in Figure 1.

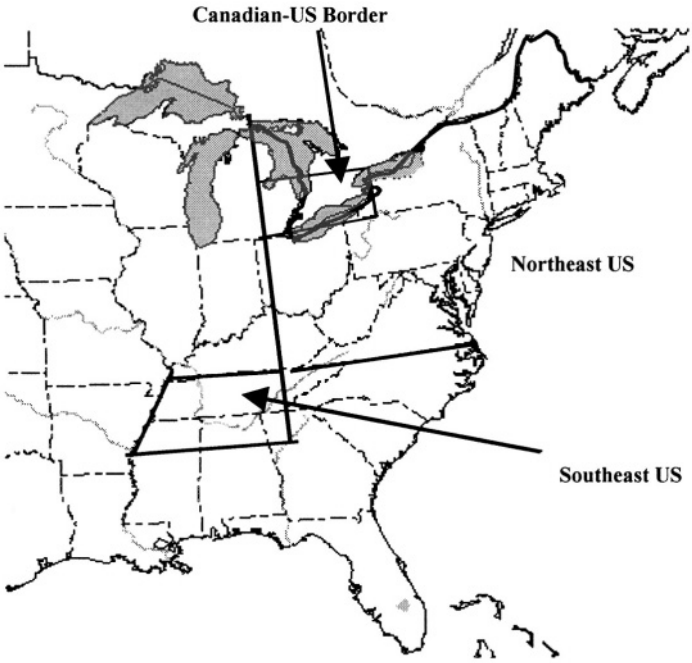

Figure1. Approximate modeling domain used by all participants except ICF Consulting, who used a more southerly portion of the largest domain. Three sub-domains (Canadian-US Border, Northeast US, and Southeast US) in which simulations and observations were compared are also shown. Not shown are three sub-domains along the northeastern US coast (New England Seaboard, Ozone Transport Region North and Ozone Transport Region South), the Northeast Regional-Rural sub-domain, that includes all rural stations not in the coastal sub-domains, and twelve urban sub-domains (Atlanta, Baltimore, Birmingham, Boston, Chicago, Detroit, Memphis, Nashville, New York, Philadelphia, Pittsburgh and Toronto). Meteorological parameters were also compared in these urban sub-domains and in twelve rural sub-domains (not shown).

3. EMISSIONS COMPARISON

Resource constraints forced an abbreviated version of the emissions comparison protocol to be conducted. It was comprised of each participant responding to the questionnaire shown in Table 2 and providing aggregated emissions totals for NOx and selected VOCs for the period 7-15 July 1995 for the states of MI, TN, MA, MD and NJ. This information would at least document details of how the emissions files were generated and allow a spot check for comparability among emissions files to be performed.

Table 2. Questionnaire completed by study participants to document how emissions files were generated

1. Which version of which emissions processor was used to prepare input emissions files?
2. Which version of which mobile-emissions-factor model was used to estimate mobile emissions factors?
3. Were mobile emissions factors dependent upon day-specific meteorology?
4. Which version of which biogenics emissions model was used to estimate biogenic emissions?
5. Were biogenic emissions dependent upon day-specific meteorology?
6. What was the base year of the U.S. emissions inventory (EI) used?
7. Which agency supplied the U.S. EI used?
8. What was the version and/or creation date of the U.S. emissions inventory used?
9. Were U.S. seasonal emission files or annual emission files used?
10. Were projection factors used to "grow" the U.S. emissions to 1995 values?
11. What was the base year of the Canadian EI used?
12. Which agency supplied the Canadian emissions inventory used?
13. What was the version and/or creation date of the Canadian emissions inventory used?
14. Were Canadian seasonal emission files or annual emission files used?
15. Were projection factors used to "grow" the Canadian emissions to 1995 values?
16. How many different spatial surrogate factors were used to spatially disaggregate U.S. emissions?
17. How many different spatial surrogate factors were used to spatially disaggregate Canadian emissions?
18. Were point sources partitioned into major and minor point sources (or elevated and surface point sources)?
19. Was plume rise calculated for major point sources?

Initial comparisons found large apparent differences between NOx and some VOC emissions totals reported by three participants. After diagnosing the factors contributing to these differences, corrections were made and the models rerun. It is the corrected files that are included in the study archives.

4. METEOROLOGICAL COMPARISON

Meteorological Service of Canada provided synoptic analyses for each day modeled to set the meteorological context for the simulated periods. Analogous to the situation regarding an abbreviated emissions comparison, a few spot checks were performed among modeling files. The layer-1 temperature, vertical diffusivity, wind speed, wind direction and ozone deposition velocity, the estimated mixing height, and the cloud fraction in the column at 12 urban and 12 non-urban grid cells provided the basis for these comparisons.

5. AIR QUALITY MODEL COMPARISON

Absolute model performance was assessed by comparing model outputs with observational data from AIRS, NARSTO-Northeast, the Southern Oxidants Study's Nashville/Middle Tennessee Ozone Study, and Canadian monitoring stations. To illustrate their locations, peak hourly ozone values from these sites for 13 July 1995 are plotted on a map in Figure 2.

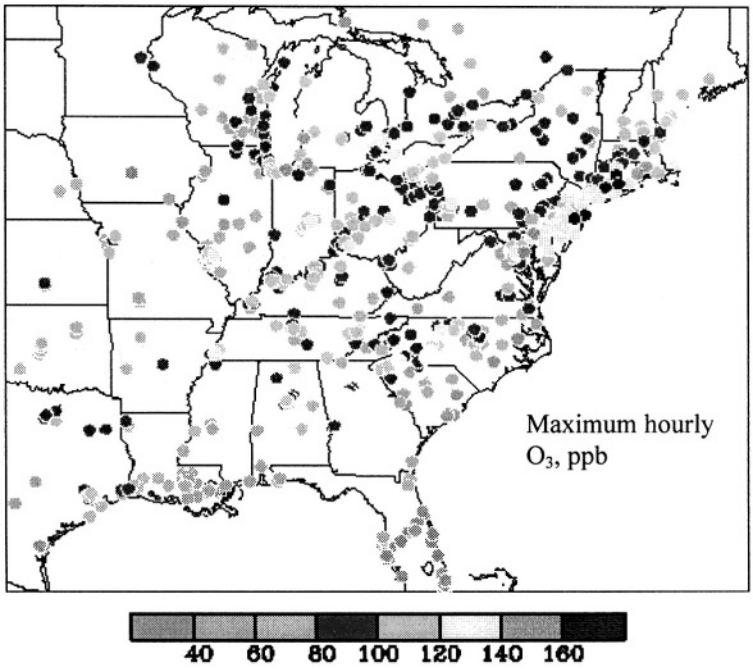

Figure 2. Locations of monitoring stations providing ozone observations for comparisons

In Section 2, the modeling sub-domains selected for comparing the models' performance were described. The basis for these selections was the desire to explore the possibility that, as configured, model performance might differ as a function of averaging time or time of day, between urban and rural areas, between coastal and inland areas and in widely separated geographic areas having distinct emissions distributions, topography or meteorological regimes. A number of metrics were selected as indicators of model performance. These are listed for ozone comparisons in Table 3.

Table 3. Air Quality Model Ozone Comparison Materials

Name	Metrics
Observations Plot (map)	Hourly and 8-hourly max O_3 over entire modeling domain
Contour Plot (map)	Isopleths of simulated daily 1-hour or 8-hour max O_3 over entire modeling domain
Scatter Plot (graph)	Simulated vs. observed hourly or 8-hourly max O_3 for the entire modeling domain and each sub-domain
Bias Plot (map)	Simulated minus observed hourly or 8-hourly max O_3 for each modeling sub-domain
Time-series plots	Simulated and observed hourly O_3 averaged over modeling sub-domains
Statistical Tables	Statistics for scientific analyses
	Number of stations, raw bias, normalized bias, gross error and normalized gross error for peak 1- and 8-hour ozone averages for each day in each sub-domain
	Number of stations, raw bias and raw gross error for ozone averaged over 0600-0900 and 0200-0500 periods for each day in each sub-domain
	Regulatory Statistics
	Number of stations, raw bias, normalized bias, raw gross error and normalized gross error of 1-hour average ozone exceeding 20, 40 and 60 ppp for each day for each sub-domain
Bar charts	Graphical renditions of information in statistical tables
Other plots and charts	Model-to-model comparison results

Two types of statistical tables are planned. The regulatory statistics are those recommended as performance measures for hourly peak O_3 predictions by the US EPA (1991), with the addition of 8-hour averages and of concentrations thresholds of 20, 40, and 60 ppb O_3. The statistics for scientific analyses, will be calculated without applying thresholds, over different time windows to investigate the models' ability to simulate not only peak O_3 concentrations but also those at night and in the early morning before the boundary layer is well mixed. Graphics will include contour map plots of observed and simulated concentrations, color-coded map plots of biases, time series plots of simulated and observed values averaged over the various sub-domains for ozone and representing the grid

cells having observations for NOx and selected VOCs., and scatter plots of simulated versus observed air quality variables and of one model's simulated values versus those of other models.

6. DATA AVAILABLE

By the time this paper is presented at the NATO International Technical Meeting, comparison results should be available and included in the presentation. Ultimately the comparison data and other documentation of methods and models will be archived in the NARSTO data archive (http://eosweb.larc.nasa.gov/project/narsto/table_narsto.html). Data used for air quality comparisons and the comparison products expected to be available are listed in Tables 4 and 5. In the interim, information can be obtained from the author (See section 9.)

Table 4. NMCES data files to be archived by NARSTO

Air Quality	Hourly average observational data and sites for 5-18 July 1995
	Hourly average or instantaneous hourly value in grid cells having observational stations
	Tables of bias and error statistics of simulated versus observed O_3 values
	Time series of observed and simulated hourly O_3, NOx, and selected VOC species' values
	Isopleth maps of hourly and 8-hourly maximum simulated O_3
	Color coded maps of bias in hourly and 8-hourly maximum O_3 in grid cells having observational stations

Table 5. Documentation and synthesis information available in NARSTO data archive.

Emissions	Documentation from Emissions Questionnaire
	Emissions totals for selected states
Meteorology	Description of meteorological modeling system
	Description of daily synoptic situation for period 5-18 July 1995
	Layer-1 T, k_z,, WS, WS, $V_d(O_3)$, estimated mixing height, and the cloud fraction in the column at 12 urban and 12 non-urban grid cells
Air Quality	Air quality modeling system attributes and parameter settings

7. REFERENCES

US EPA, 1991. Guidance for Regulatory Application of the Urban Airshed Model. Office of Air Quality Planning and Standards, Research Triangle Park, NC 27711. July 1991.

8. ACKNOWLEDGEMENTS

The author expresses his appreciation to EPRI, Meteorological Service of Canada, Tennessee Valley Authority, Texas Natural Resources Conservation Commission, and Ontario Ministry of the Environment for direct financial support of the project and to the Coordinating Research Council, the Southeast States Air Resource Managers, Meteorological Service of Canada, the US Environmental Protection Agency, the New York State Department of Environmental Conservation, and Southern Company for sponsoring initial modeling from which model comparison files were derived. In addition, the participating organizations provided substantial in-kind support in staff and resources. The assistance of Naresh Kumar of EPRI in co-managing the project is gratefully acknowledged, as is the processing of modeling data files into statistical tables and graphics provided by Sonoma Technology, Inc., led by Neil Wheeler. Other EPRI staff who contributed substantially to the effort include Mohan Gupta, George Bonne, and Randall Takemoto-Hambleton. Special recognition is given to Maris Lusis and S. Venkatesh of MSC for suggesting the study and to their colleagues, Mike Moran and Janusz Pudykiewicz for managing the emissions comparisons and CHRONOS modeling, respectively; and to Jeff Arnold and Robin Dennis of NOAA/USEPA, Rohit Mathur of NCSC, Gopal Sistla of NYDEC, Ralph Morris of Environ and Sharon Douglas of ICF Consulting for managing their organization's participation in the study.

9. FURTHER DETAILS

Contact Alan Hansen, EPRI, P.O. Box 10412, Palo Alto CA, 94303, USA. Telephone: 650.855.2738, fax: 650.855.2950, email: ahansen@epri.com.

DISCUSSION

P. BUILTJES Was an attempt made to make an evaluation of the observations before they were used in the model evaluation ?

A. HANSEN Not explicitly. However, we understand that the observations themselves have uncertainties associated with measurement error and variability within grid cells. Therefore we are generally using statistics based on averaging over many grid cell-site combinations and interpreting the results in a relative rather than absolute sense.

This page intentionally left blank

INFLUENCE OF UNDERLYING SURFACE ROUGHNESS TO THE DEPOSITION OF AIRBORNE PARTICLES IN NORTHERN WINTER CONDITIONS

Marko Kaasik*

1. INTRODUCTION

The surface roughness length is one of a few most important parameters determining the deposition velocity of airborne particles. In this context the mid-latitude flat rural areas could be divided into two substantially different categories: (1) forest and (2) open areas. The roughness difference is most dramatic, if the snow cover is thick enough to cover the grass and other small roughness elements at open sites. The typical roughness length of boreal and sub-boreal forest is 0.5 – 1 m, whereas the roughness length of snow surface does not usually exceed 0.001 m (except due to snow blown up by the strong wind). Consequently, the atmospheric resistance to the deposition is much larger over the open areas and therefore lower dry deposition velocities are expected.

The early experimental studies (see McMahon and Denison, 1979) support the above considerations despite the large scatter of results. Several model runs (Ruijgrok et al., 1995) show, that the deposition velocity of particles over the forested land can be tens of times higher than over the open one. The difference depends on particle size, being clearly larger for particles sized several micrometers than for the sub-micron ones. Donat and Ruck (1999) provided the wind tunnel simulations of deposition of sub-micron particles onto the ground below the trees and found the deposition fluxes 20 – 60 % (depending on tree crown shape) larger than onto the open surface in similar conditions. Although several field and wind tunnel experiments have been carried out recently, the main attention is paid to the deposition of small particles in the nearly neutral stratification.

The present study is focused to the deposition of mineral particles sized about 10 μm as average. Such particles occur typically in the fly ashes of thermal power plants and can contain remarkable amounts of sulphates, alkaline oxides and radionucleides. A natural

* Marko Kaasik, Tartu Observatory, Tõravere, Tartumaa, 61602 Estonia.

Air Pollution Modeling and Its Application XV, Edited by
Borrego and Schayes, Kluwer Academic/Plenum Publishers, New York, 2002

medium-term collector – snow cover – is used to trace the deposition fluxes. The role of dry and wet deposition is discussed.

2. METHODS

A case study was carried out in 1996 to clarify the effect of forest-induced roughness to the deposition flux of airborne fly ash particles (Kaasik et al, 2000). The research sites were chosen in the north-eastern part of Estonia, at distances of 1 – 130 km from two large thermal power plants (total maximum capacity 3 GW), consuming *Kukersite* oil shale. The *Kukersite* oil shale fly ash has rather specific elemental composition (Häsänen et al. 1995): 15 – 22% Ca, 6 – 10 % K, several trace metals, 5 – 6% S. As most of metals in the fly ash are in carbonaceous form, the reaction of fly ash solution is strongly alkaline.

The measurement was based on snow samples taken from 15 sites (6 from forested, 7 from open and 2 from mixed landscape) and representing 3 snow accumulation episodes (72 days in total) during one winter and analysed for main anions, cations and trace metals. The most remote sites (one forested and one open) were considered as background ones. Knowing the chemical composition of oil-shale fly ash, the deposition fluxes of fly ash particles were reconstructed.

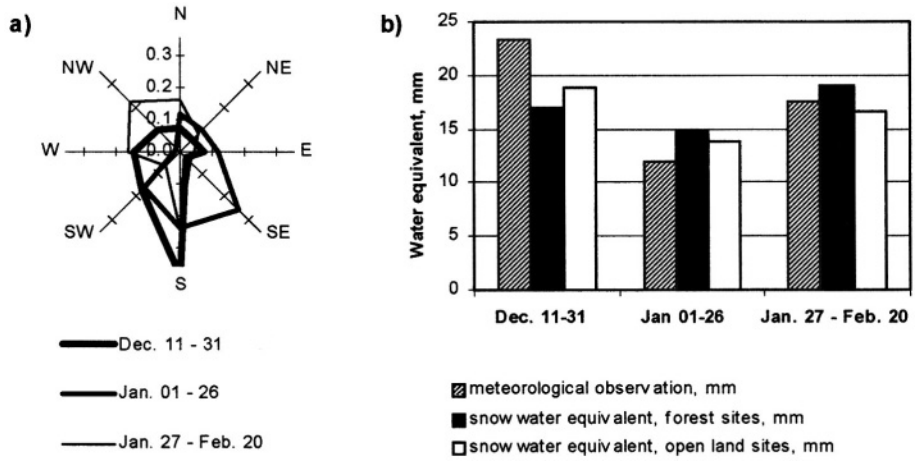

Figure 1. Distribution of wind directions (a) and average precipitation amounts (b) during the snow accumulation in 1995/96.

The wind during the snow accumulation was blowing predominantly from southern directions, which is typical for the research area and season. The average water equivalents of all three snow layers matched well with meteorological observations of precipitation amounts (Figure 1), which indicates, that no snow was lost due to melting. The average temperatures of the snow accumulation episodes were –8.9, –8.0 and

–11.8 °C, no substantial thawing was registered. No systematic or considerable discrepancies between snow accumulation at forested and open sites was found.

The deposition measurements were accompanied by the runs of air pollution dispersion and deposition model AEROPOL for the same episodes. The AEROPOL model (Kaasik, 1996) is a Gaussian plume model developed at Tartu Observatory, Estonia. The simple bulk deposition scheme includes only gravitational settling and precipitation scavenging for large particles, no landscape-dependent effects are included. The boundary-layer parameterisation is based on the Pasquill stability classes, which, although coarse, enables us to manage with routine (ground-based) meteorological observations only. A highly uncertain initial parameter for model calculation was the aerodynamic diameter of a ash particle. Earlier measurements (Aunela et al., 1995) suggest the particle sizes in the order of 10 μm, but due to high humidity of the flue gases considerably larger particles are expected after condensation and subsequent freezing of water. The effective particle size 30 μm is applied in this study, the sensitivity analysis is performed.

3. RESULTS

3.1. Deposition measurements

The results of the case study show that the deposition fluxes of fly ash particles over the forested areas are systematically higher than over nearby open (bog) areas (Figure 2), although the precipitation amounts were found nearly equal for both landscape types (see Section 2).

Considerable differences appear during each of three time episodes. Most likely the differences appear due to different dry deposition velocities. In the beginning of winter, when the nearly neutral thermal stratification prevailed due to mainly cyclonal weather, the deposition difference between the open and forest sites is small. During the midwinter the cyclonal weather gradually changed to more anticyclonal, with multiple rapid changes of air temperature and stratification. The corresponding deposition curve for forest is well above the one for open landscape. The total deposition is larger than for first episode due to larger share of northern and northeastern winds. During the late winter the weather was the most anticyclonal of these three episodes. Moderate snowfalls occurred between cold and calm days. The wind was blowing quite frequently from the direction of power plant, but less than 4 mm of precipitations occurred during such events. The deposition at forest sites is 1.5 – 2 times larger than in the open ones.

3.2. Model estimations

The modelled and measured deposition fluxes at the measurement sites are compared in Figure 3. For comparison the mixed sites (complicated pattern of woodland and open land) near power plants are added. The north-eastern direction should be understood under the negative distance. Another (called Baltic) power plant is located nearly at 17 km northeast (i.e. near the leftmost snow site) from the Estonian one.

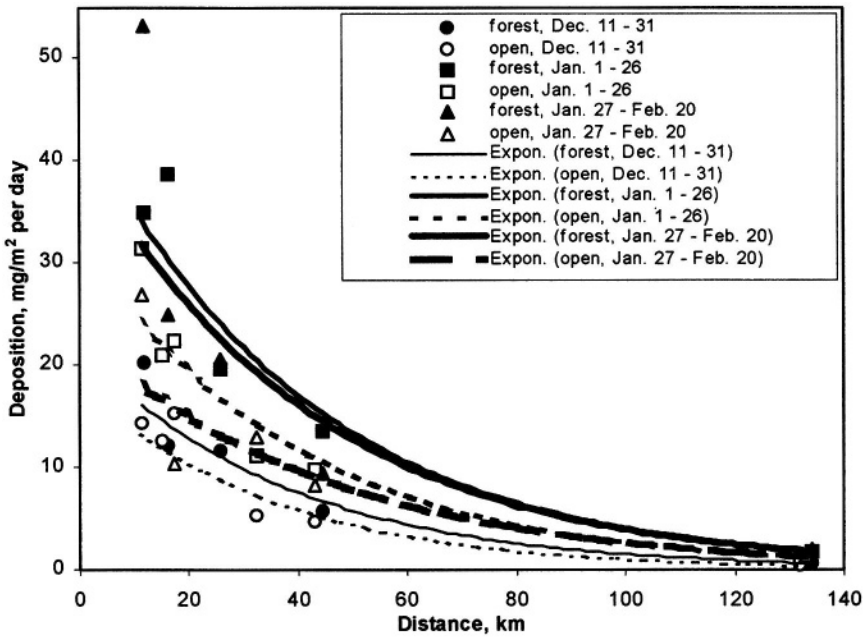

Figure 2. Deposition fluxes (experimental data and exponentially fitted curves) in open and forested sites to the southwest from the Estonian power plant.

The model predicts dominating wet deposition during the early winter, both dry and wet deposition in midwinter and highly dominating dry deposition during late winter. These results match well with the interpretation given in previous subsection. The total deposition near the sources is more or less matched despite large scatter of both modelling and measurement results. Away from the sources, the model tends to underestimate the deposition. A part of this underestimation could be explained with the nearly similar emissions from local sources. The measured deposition fluxes in background sites (far right in Figure 3), however, are less than the typical difference between measured and modelled deposition at moderate distances.

The mismatch of modelled and measured fluxes was exceptionally high during the second episode, for which the model failed to reproduce the main direction of fly ash transport. The probable reason is the overestimation of boundary-layer wind shear by 10 – 20 degrees for certain dispersion events.

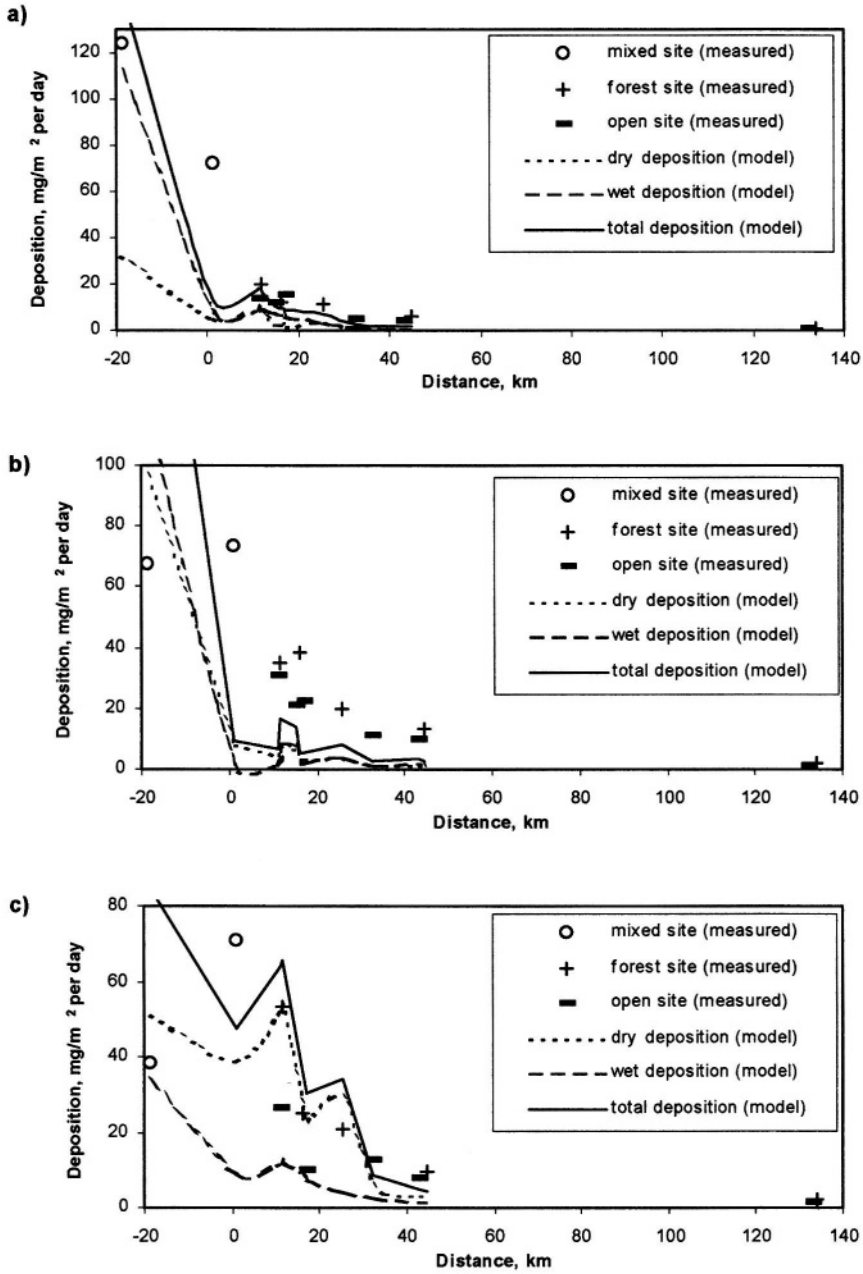

Figure 3. Measured and modelled deposition fluxes southeast from the Estonian power plant during: a) December 11 – 31, b) January 01 – 26 and c) January 27 – February 20, 1996.

3.3. Sensitivity studies

Applying for model runs the 10 μm particle diameter instead of 30 μm leads to the considerably lower deposition fluxes and large underestimation of measurement results. Although the scavenging efficiency depends on particle diameter and this is included into the model code, the considerable effect (up o 1.5 times) to the wet deposition appears only near the sources. Most probably the effect of particle size is compensated by the different plume depletion far from the sources.

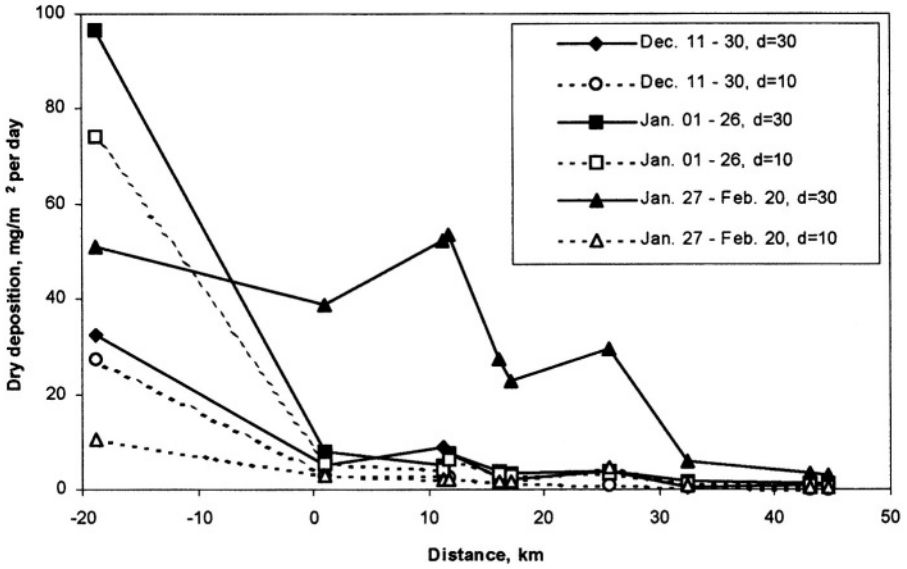

Figure 4. The modelled dry deposition fluxes for snow sampling sites to southwest from the Estonian power plant: comparative computations with different particle diameters: d = 30 μm and d = 10 μm.

In dry deposition process the particle diameter is more important (Figure 4). The difference is extremely large (5 – 15 times) for the last episode. In stable boundary-layer stratification, when the vertical dispersion is very slow, the gravitational fall of particles becomes especially important. It seems, that the possible condensation of emitted water vapour can play an important role in the deposition of fly ash particles.

4. DISCUSSION AND CONCLUSIONS

The results above show, that the forest at underlying surface affects the medium-term averaged deposition of solid particles by quite straightforward way, increasing the deposition flux presumably due to more intense inflow to the rougher surface. The deposition velocity of large particles consists of (1) gravitational settling velocity and (2)

turbulent part. For smooth surfaces (like open snow surface) the deposition velocities close to the settling velocity are suggested for particles considerably larger than 10 μm (see e.g. McMahon and Denison, 1979), i.e. the turbulent part is small compared to the gravitational one. The detail deposition models give controversy results for deposition of large particles to the forest: from nearly settling velocity to 10 – 20 times larger values by different models for 30 μm particles (overview by Ruijgrok et al., 1995). The deposition velocity is positively related to the friction velocity.

The results above (Figure 2) enable us to estimate approximately the turbulent part of deposition flux, leaving the share of gravitational settling and wet deposition quite uncertain. For the late winter episode the turbulence-dependent deposition flux at 10 – 12 km from the Estonian power plant was about 15 mg/m^2 per day or about a half of total deposition flux (assuming it negligible for the open snow surface, but not for forest). Consequently, the deposition velocity is at least twice larger than the settling velocity, but can be much larger, if the share of wet deposition is considerable. The model run suggests, that wet deposition consists 20 – 35 % of total one. Therefore the ratio of deposition velocity to the settling velocity can be in the range of 2.5 – 4. For other two episodes the turbulence-dependent part of dry flux is less, but the model-suggested share of dry deposition is considerably less as well. Therefore, the above ratio can be in the same range. This result is in agreement with Bache's one (Bache, 1979, referred by Ruijgrok et al., 1995).

The forest and open land pattern can affect the meso-scale and large-scale admixture transport processes through the friction at the underlying surface. It was shown (Kaasik, 2001), that large uncertainties of the underlying surface forest fraction affect seriously the turbulent dispersion calculation results through entire boundary layer and even in the lower troposphere above it. The effects of (1) deposition efficiency and (2) wind drag at higher altitudes are summarised in large scale. Therefore the land use data sets for regularly used atmospheric models, however, have to be critically reviewed and improved (Kaasik and Roosaare, 2000).

ACKNOWLEDGEMENTS

The results are based to the field work and theoretical studies granted by the Estonian Science Foundation (research grant No. 186). Author is grateful to the Norwegian Institute for Air Research for chemical analyses.

REFERENCES

L. Aunela, E. Häsänen, V. Kinnunen, K. Larjava, A. Mehtonen, T. Salmikangas. Emissions from Estonian oil shale power plant. *Oil Shale,* **12,** 2, pp. 165 – 177 (1995).

D. H. Bache, Particulate transport within plant canopies (II). Prediction of deposition velocities. *Atm. Environ.,* **13,** pp. 1681 – 1687(1979).

J. Donat, B. Ruck. Simulated ground deposition of fine airborne particles in an array of idealized tree crowns. *Water, Air and Soil Pollution* **93,** pp. 469 – 492 (1999).

E. Häsänen, L. Aunela., V. Kinnunen, K. Larjava, A. Mehtonen, T. Salmikangas, J. Leskelä and J. Loosaar. In: *10th World Clean Air Congress. Vol. 1,* edited by M. Tolvanen, P. Anttila and J. Kämäri (The Finnish Air Pollution Prevention Society, Espoo, 1995), pp. 057– 060.

M. Kaasik. Influence of underlying surface forest fraction to the meso-scale wind fields and dispersion conditions. In: *Air Pollution Modelling and Simulation,* edited by B. Sportisse, Springer (2001, in print).

M. Kaasik. Atmospheric dispersion and deposition of technogenic calcium: model estimation and field measurement, *Proc. Estonian Acad. Sci. Ecol.,* 1/2, 41 – 51 (1996).

M. Kaasik, J. Roosaare. New Estonian and Eastern Baltic region land use database for HIRLAM. *HIRLAM Newsletter* **35,** pp. 157-162 (2000).

M. Kaasik, R. Rõõm, O. Røyset, M. Vadset, Ü. Sõukand, K. Tõugu and H. Kaasik. Elemental and base anions deposition in the snow cover of north-eastern Estonia. The impact of industrial emissions, *Water, Air, and Soil Pollution* **121,** 324-366 (2000).

T. A. McMahon, P. J. Denison. Empirical atmospheric deposition parameters – a survey. *Atm. Environ.,* **13,** pp. 571–585 (1979).

W. Ruijgrok, C. I. Davidson, K. W. Nicholson. Dry deposition of particles. Implications and recommendations for mapping of deposition over Europe. *Tellus* **47B,** pp. 587 – 601 (1995).

DISCUSSION

D. HANSEN Can you explain the increased modeled oscillations and stnadard deviation with distance of the deposition when you increased the particle size from 10 μm to 30 μm ?

M. KAASIK Modelling results are oscillating due to interference of another power plant: a transect from one power plant crosses the plumes of the other (there were not many plumes modelled).
The 10 μm deposition fluxes were unrealistically low, but the relative oscillations were in the same range than for 30 μm case.

This page intentionally left blank

A STUDY OF SO2 DISPERSION AROUND A THERMOELECTRIC POWER PLANT IN THE SOUTH OF BRAZIL

Osvaldo L. L. Moraes, Rita C. M. Alves, Rodrigo Silva, Adriano C. Siqueira, Patrícia D. Borges, Tiziano Tirabassi, Umberto Rizza[1]

1. INTRODUCTION

As part of the Presidente Medici Thermoelectric Power Plant plume model validation study, a major field measurements program was carried out at Candiota town, south of Brazil. Project Candiota was a cooperative field study leaded by the Micrometeorological Laboratory from the Physics Department of the Federal University of Santa Maria (UFSM - Brazil) with groups of scientists from Universidade de São Paulo (Brazil), Instituto di Scienze dell´Atmosfera e dell´Oceano and Instituto per lo Studio dell' Inquinamento Atmosferico e l'Agrometeorologia both from Italy. The project had support of the Companhia Estadual de Energia Elétrica (CEEE) and Companhia de Geração Térmica de Energia Elétrica (CGTEE), owners of the thermoelectric, and from three differentes research foundations of Brazil (FAPERGS, FAPESP and CNPq) and from the Consiglio Nazionale delle Ricerche (Itália). The objective was to collect a comprehensive, meteorological diffusion and dispersion database to be used to evaluate and improve selected diffusion, and dispersion models. Candiota consists of an ideal laboratory to test and to validate dispersion models for a series of reasons, among which we can point: the thermoelectric is the only source of some pollutants in the whole area, e.g. SO2; the source is punctual and emits continually with a very known rate; the topography of the area is essentially homogeneous. The pollutant is emitted with buoyancy from a tower at a height of 150 m.

Over 1,000 hr of intensive observations were made during five field campaigns (winter 1994, summer 1995, autumn 1995, spring 1995 and winter 1999). Each field experiment was made during two weeks. Meteorological data was collected over a 2-

[1] Osvaldo L. L. Moraes, Rodrigo Silva, Adriano C. Siqueira, Patrícia D. Borges, Universidade Federal de Santa Maria. Departamento de Física, 97119.900 Santa Maria, Brazil, Rita C. M. Alves, Universidade Federal do Rio Grande do Sul, CEPSRM, Porto Alegre, BrazilTiziano Tirabassi, ISAO, Bologna, Italy, Umberto Rizza, ISIATA, Lecce, Italy.

Air Pollution Modeling and Its Application XV, Edited by
Borrego and Schayes, Kluwer Academic/Plenum Publishers, New York, 2002

week time resulting in a full set of daytime period and the database comprises measurements of wind speed, wind direction, turbulence, temperature, humidity, pressure, solar radiation, the boundary layer structure and upper-air-soundings. The campaign site (31.40S, 53.70W, 250 m above sea level) has previously been used for a number of experiments related to research on atmospheric boundary layer (Moraes et al 1998, Moraes 2000a). The base is located in a region known as the South America Pampa. The Pampa is the part of SA that covers all Uruguay territory, the south of Brazil and northwest of Argentina. The area around the experimental site is flat for over 10 Km in every direction.

In this paper we study the environmental impact in the region due to the thermoelectric emissions with a numerical 3D model and with a non-gaussian puff model. The performances of the models are evaluated with boundary layer parameterization derived from the fields campaigns.

2. THE MODELS

2.1 The Puff Model

The puff model is described in a series of papers (Tirabassi and Rizza, 1997a, Tirabassi and Rizza 1997b) and here we only outline its principal characteristics.

The advection diffusion equation describing the time evolution of the crosswind-integrated concentration χ due to an instantaneous release at time $t = 0$ by an elevated source placed at (0,0,1), in a horizontally homogeneous atmospheric boundary layer is

$$\frac{\partial \chi}{\partial t} + u\frac{\partial \chi}{\partial x} + = \frac{\partial}{\partial z}\left(K_z \frac{\partial \chi}{\partial z}\right) + K_h\left(\frac{1}{d^2}\frac{\partial^2 \chi}{\partial x^2}\right) + \delta(t)\delta(x)\delta(z-1) \qquad (1)$$

Considering that C is exponentially small at asymptotic distances from the source the moments of its distribution on any horizontal plane may be defined as

$$C_m(z,t) = \int_{-\infty}^{+\infty} x^m \chi(x,z,t)dx$$

where m is a non-negative integer. Multiplying equation (1) by x^m and integrating it in x we obtain the following set of equations for the time evolution of the moments

$$\frac{\partial C_0}{\partial t} = \frac{\partial}{\partial z}\left(K_z \frac{\partial C_0}{\partial z}\right) + \delta(t)\delta(z-1) \qquad (2.a)$$

$$\frac{\partial C_m}{\partial t} = \frac{\partial}{\partial z}\left(K_z \frac{\partial C_m}{\partial z}\right) + muC_{m-1} + \frac{K_h}{d^2}m(m-1)C_{m-2} \qquad (2.b)$$

with the following initial and boundary conditions

$$\lim_{t\to 0} C_m(z,t) = 0\,; \qquad K_z \frac{\partial C_m}{\partial z} = 0 \qquad \text{for} \quad z = 0 \quad \text{and} \quad z = z_i\,.$$

Tirabassi and Rizza (1997) solved this set of equations using the Gram-Charlier expansion of type A truncated to the fourth order and recovered the concentration field. They obtained

$$\chi(x,z,t) \cong C_0 \frac{e^{-\xi^2/2}}{\sigma\sqrt{2\pi}}\left[1 + \left(\frac{k_u - 3}{24}\right)\left(\xi^4 - 6\xi^2 + 3\right) + \frac{S_k}{6}\xi(\xi^2 - 3)\right] \tag{3}$$

where $\xi = (x-b)/\sigma$, $b = C_1/C_0$, $\sigma^2 = (C_2/C_0) - b^2$ and K_u and S_u are the skewness and kurtosis defined as

$$K_u = \frac{1}{\sigma^4}\left[\frac{C_4}{C_0} - 6b^2\sigma^2 - 4b\sigma^3 S_k - b^4\right] \qquad S_k = \frac{1}{\sigma^3}\left[\frac{C_3}{C_0} - 3b\sigma^2 - b^3\right]$$

In this paper the lateral diffusion was parameterized by means of a Gaussian-type factor and the concentration at any point was calculated as

$$C(x,y,z,t) = \frac{1}{(2\pi\sigma_y)^2} e^{\left(\frac{y^2}{2\sigma_y^2}\right)} \chi(x,z,t) \tag{4}$$

where σ_y represents the mean square particle displacement along the y – axis with the condition

$$\frac{1}{2}\frac{d\sigma_y^2}{dx} = \frac{K_y}{u} \tag{5}$$

2.2 The Numerical Model

The numerical model use a solution of the advection diffusion equation of air pollution in the atmosphere, that is essentially a statement of conservation of the suspended material and can be written:

$$\frac{\partial C}{\partial t} + u\frac{\partial C}{\partial x} + v\frac{\partial C}{\partial y} = \frac{\partial}{\partial z}\left(K_z \frac{\partial \chi}{\partial z}\right) + \frac{\partial}{\partial y}\left(K_y \frac{\partial C}{\partial y}\right) + Q \tag{6}$$

The equation is solved using a finite-difference scheme. A forward-in-time, upstream-in-space scheme is used for the advection terms. For diffusion terms, a semi-implicit centered scheme with weight 0.75 on a future time step is used. The lower and

top boundary conditions was the same as used in the first model. For the results presented in this paper the vertical resolution of the grid was defined as $\Delta z = H / N$ where H is the boundary layer height and $N = 30$ for all simulations. The horizontal grid has 100 x 100 points linearly spaced with 100 m of distance between them. The time step is 3 s.

3. THE BOUNDARY LAYER PARAMETERIZATIONS

In order to evaluate the diffusion coefficients that are in eqs (4) and (6), we have used the boundary layer parameterization proposed by Moraes (2000b). This parameterization is based on Hanna (1968) assumption that the mixing efficiency of the air is completely determined by the properties of the vertical velocity spectrum, and that the parameters σ_w and $\mathrm{k_m}$ are sufficient to describe the vertical velocity spectrum. Then it follows from dimensional reasoning that the vertical eddy diffusivity coefficient K_z may be written as

$$K_z = c_1 \sigma_w \mathrm{k_m^{-1}} \tag{7}$$

where c_1 is a constant equal to 0.09.

From the measurements done in the surface layer and using local scalings assumptions we obtained for the vertical turbulent diffusion coefficient in the whole boundary layer the following expressions for stable and convective regimes

$$K_z = c_1 z u_* (1 - z/h)^{\alpha_1/2} \frac{1 + (z/L)(1 - z/h)^{\alpha_2 - 1.5\alpha_1}}{0.27 + 0.50(z/L)(1 - z/h)^{\alpha_2 - 1.5\alpha_1}} \tag{8}$$

$$K_z = 0.5 w_* z (1 - z/z_i) \tag{9}$$

The lateral diffusion, for the puff model, is obtained through σ_y values proposed by Briggs (1973) for open country and given by

$$\sigma_y = C\, x (1 + 10^{-4} x)^{-1/2} \tag{10}$$

where C is a constante equal to (0.22, 0.16, 0.11, 0.08, 0.06, 0.04) if the Pasquill stability is (A, B, C, D, E, F) respectively. For the numerical simulations the lateral eddy diffusion coefficient is estimated as $0.1 w_* z_i$ in unstable conditions and as $2K_{Mz}$ in neutral-stable conditions, where K_{Mz} is the maximum of K_z.

4. RESULTS

We have evaluated the performances of the puff model using the Candiota data set. The concentration data set is composed of daily average of ground level concentration of SO_2. This pollutant is emitted with buoyancy from a tower at a height of 150 m, and collected at two points known as Três Lagoas and Candiotão. Três Lagoas is located 5 km to the southwest of the source. Candiotão is located 5.8 km to the west of the source. The velocity of the gas is about $20 m/s$ and the temperature of exhaustation of the gases is approximately 420K. For this period the rate of SO_2 emission, estimated from the coal burning and the sulfur content in the coal, is presented in table 1. The meteorological parameters monitored were the same for all set of observations. However only in the last experiment concentration data set was collected simultaneously and only for this field campaign the models was tested.

Table 1. Rate emission of SO2, by the power plant, during 10 days of 1999 field campaign.

Day	23/08	24/08	25/08	26/08	27/08	28/08	29/08	30/08	31/08	01/09
Kg/sec	1.68	1.57	0.75	0.44	0.39	0.42	0.92	1.15	0.47	0.82

Meteorological data was collected over a 2-week time resulting in a full set of daytime period and the database comprises measurements of wind speed, wind direction, turbulence, temperature, humidity, pressure, solar radiation, the boundary layer structure and upper-air-soundings. The data records were broken into 1-hr segments and those collected at 10 Hz were used to compute micrometeorological parameters (u_*, w_*, L) and data collected at 1 Hz were used to estimate wind speed, wind direction and air temperature. Before the analyse the time series were examined to detect any spikes, kings or missing portions in the data. Such problems were corrected suitable (Yadav et al 1996).

In figure 1, the observed daily average ground-level concentration at Três Lagoas receptor are compared with the estimated concentration calculculated by the Puff and by the numerical model. Figure 2 presents the same results for the Candiotão receptor.

Table 2 presents some statistical indices, defined as the normalized mean square error (nmse), correlation coefficient (r), factor of 2 (fa2), fractional bias (fb). and fractional standard deviation (fd). It should be stressed that from the observed concentration values no background value has been subtracted.

Table 2. Statistical evaluation of model results.

Receptor		nmse	r	fa2	fb	fs
Três Lagoas	Puff Model	0.172	0.580	1.0	0,087	-0,238
	Numerical Model	0,077	0.740	1.0	-0,057	-0,226
Candiotão	Puff Model	0.210	0.680	0.85	-0.139	-0.328
	Numerical Model	0.161	0.730	1.0	-0.107	-0.381

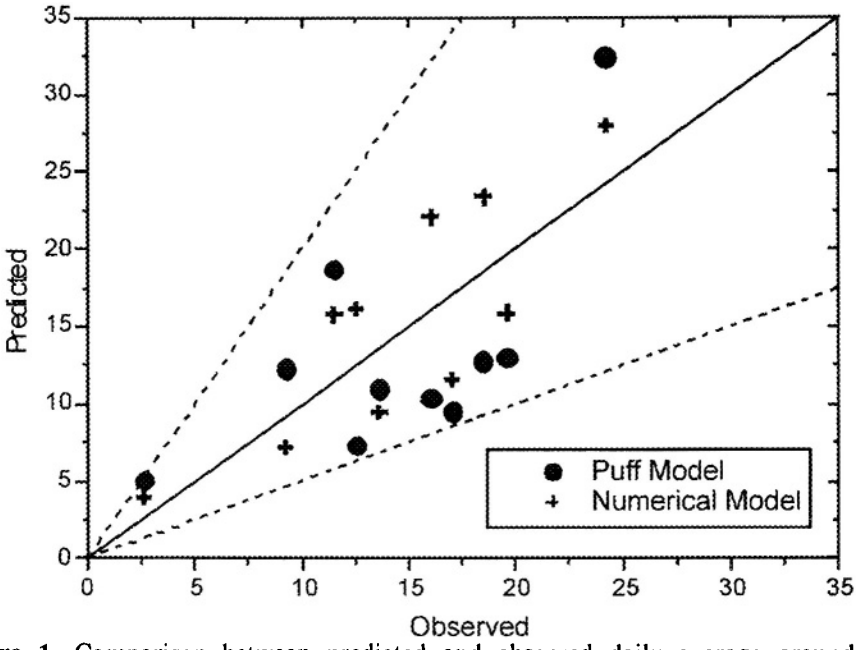

Figure 1. Comparison between predicted and observed daily average ground-level concentration at Três Lagoas receptor for ten day of 1999 Winter experiment. Points between dashed line have a factor of 2

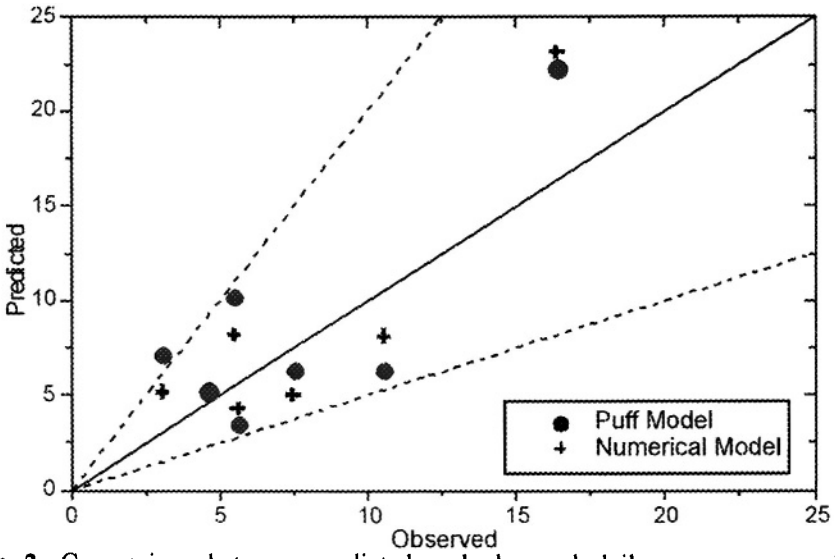

Figure 2. Comparison between predicted and observed daily average ground-level concentration at Candiotão receptor for ten day of 1999 Winter experiment. Points between dashed line have a factor of 2

5. CONCLUSIONS

This paper is a summary of the experimental design, observational domain, sampling strategy of the Candiota field experiments. A suite of five meteorological experiments of increasing complexity and realism was conducted during different seasons The philosophy followed in these experiments was to describe the structure of the Planetary Boundary Layer in the south of Brazil and its implication to study the dispersion of pollutants emitted by the Thermoelectric Power Plant located in the region. For the purpose of models evaluation it was presented and compared results obtained with an analytical and with a numerical dispersion models. The disagreement between experimental and modeled results is due to models assumptions and simplifications. However, for best evaluations it is necessary to have more comprehensive data sets and longer time series of pollutant concentrations with higher time and space resolution. Finally it should be stressed that the Candiota site consists of an ideal local to validate models through simultaneously meteorological and concentrations measurements.

Acknowledgements

This work was supported by the Brazilian agencies CNPq, FAPERGS, FAPESP, the Italian agency CNR and by the Brazilian Electric Companies CEEE and CGTEE.

REFERENCES

Hanna, S.R., 1968. A method of estimating vertical eddy transport in the planetary boundary layer using characteristics of the vertical velocity spectrum, J. Atmos. Sci. **25,** 1026.

Moraes, O. L. L, Alves, R. C. M., Tirabassi, T., and Ferro, M., 1998, Estimating eddy diffusivities coefficients from spectra of turbulence, Air Pollution Theory and Simulation, **6,** 57-65.

Moraes, O. L. L., 2000a, Turbulence characteristics in the surface boundary layer over the South America Pampa, Bound.-Layer Meteorol. **96,** 317-335.

Moraes, O.L.L., 2000b, A model for the turbulent coefficient exchange from experimental spectra, Hybrids Met. Engin., **3,** 345-357.

Tirabassi, T. and Rizza, U., 1997a, A non-Gaussian puff model, Nuovo Cimento, **20C**, 453-460.

Tirabassi, T. and Rizza, U., 1997b, Boundary layer parameterization for a non-gaussian puff model, **36,** 1031-1037.

Yadav, A.K., Raman, S., and Sarna, M., 1996, Surface layer turbulence spectra and dissipation rates during low winds in tropics, Bound.-Layer Meteorol., **79,** 205-223.

DISCUSSION

S.E. GRYNING The simulated plumes with the puff-model looks to be straight. Was the wind direction constant ?

O. MORAES The simulations showed in the presentation are with the numerical model. They show hourly average of ground level concentration. In each hour we consider the wind direction as a constant.

D. ANFOSSI Did you consider the plume rize in your simulations ?

O. MORAES We compare two models with no plume rise. As the puff model has no plume rise in the original version, we chose not to include plume rise in the numerical model in order to compare them.

B.J. ABIODUN Can you explain how you treat the boundary conditions in your model, because the results from the model simulations show a wall ? at the boundary ?

O. MORAES The lateral boundary condition is open.

A GLOBAL-THROUGH URBAN SCALE NESTED AIR POLLUTION MODELLING SYSTEM (MM5-CMAQ): APPLICATION TO MADRID AREA

R. San José, J. L. Pérez, J.I. Peña, I. Salas* and R.M. González**

1. INTRODUCTION

The research in the last decades on air pollution modelling systems has grown extraordinary in parallel with the important advances on computer power capabilities and INTERNET development. During 90's the mesoscale meteorological modules and the air quality transport models developed over limited domains and with simulations of the basic chemical reactions in the atmosphere. During the second generations of atmospheric air pollution models (Venkatram et al. (1989); Carmichael et al. (1991); McRae and Seinfeld (1983); San José et al. (1994)) a considerable attention was given to the 3d Eulerian simulations and the operational basis. A clear limitation of these models was found in several areas: the limited information provided by the boundary conditions so that long range transport was almost not present. Simplified aqueous and cloud processes were present and poor attention was given to biogenic emissions and the impact on the chemical reactions and subsequent products. This contribution focuses on results from simulations over short – medium range by covering al, the spatial domains affected by the temporal simulation. The so-called Third Generation of Air Pollution Models (Peters L.K. et al. (1995)) is present by using the MM5-CMAQ modelling system and comparing the results at high resolution level (almost street level) with the OPANA model (San José et al. 1999) – representative of the Second Generation of Air Pollution Models but with full on-line linkage between meteorology and chemistry -. The results show an important variability which represent the air pollution concentrations from the

* Environmental Software and modelling Group, Computer Science School, Technical University of Madrid (UPM) (Spain), Campus de Montegancedo, Boadilla del Monte 28660 Madrid (Spain) http://artico.lma.fi.upm.es.
** Department of Geophysics and Meteorology, Faculty of Physics, Universidad Complutense de Madrid (Spain).

Air Pollution Modeling and Its Application XV, Edited by
Borrego and Schayes, Kluwer Academic/Plenum Publishers, New York, 2002

air pollution monitoring stations in a much more realistic way. The preliminary results – due to the limited period of time of study – illustrate the importance of nesting the adequate number of levels to catch all the necessary information coming from the surrounding areas which will affect the local environment in an important manner.

2. THE MM5-CMAQ MODELLING SYSTEM

In this contribution we have used the MM5 model and the Community Muiltiscale Air Quality Modelling System (CMAQ) as representative of the third generation of Air Quality Modelling Tools to simulate the air quality concentrations over a selected period in April, 2001 over the Iberian Peninsula to understand the impact of traffic emissions over the ozone concentrations.

A scheme of the MM5 model can be seen in Figure 1. The PSU/NCAR mesoscale model is a limited-area, nonhydrostatic or hydrostatic (Version 2 only), terrain-following sigma-coordinate model designed to simulate or predict mesoscale and regional-scale atmospheric circulation (Chen F. and J. Dudhia (2001); Warner T.T. and H.M. Hsu (2000); Stensrud D. J. et al. (2000); Ge et al. (1997)). It has been developed at Penn State and NCAR as a community mesoscale model and is continuously being improved by contributions from users at several universities and government laboratories.

The Community Multiscale Air Quality Modelling System (CMAQ) and the peripheral modules are illustrated in Figure 2. We have selected for this simulation the piece parabolic method (PPM) Colella and Woodward (1984). The updated version of the CBM-IV mechanism (36 species, 94 reactions including 11 photolytic reactions) with the isoprene chemistry mechanism and the Arrhenius type rate constant expressions. We have also used aerosol formation processes and aqueous chemistry. Finally we have used the Modified Euler Backward Iterative (MEBI) Solver which is mechanism dependent but it is at least as precise as the QSSA but the computing time required is much lower.

3. THE OPANA MODELLING SYSTEM

The OPANA modelling system stands for Operational ANA model which means Atmospheric mesoscale Numerical pollution model for regional and urban Areas. The system is composed by a REgional MESoscale Transport model (REMEST) based on the MEMO model (Flassak and Moussiopoulos (1989)) and a CHEmical Model for Atmospheric processes (CHEMA) based on the SMVGEAR numerical technique (Jacobson M.Z. and Turco R.P. (1994)). The model essentially solves the chemistry every grid cell every 30 minutes and the advection and diffusion is solved by the meteorological model so that the chemistry is a subroutine of the meteorological module. This approach guarantees an excellent consistency for transporting the atmospheric constituents. The system includes a model called EMIMA (EMIssion model for Madrid Area) for anthropogenic and biogenic (BIOEMI model) emissions over the Madrid domain. Figure 3 shows the different modules of OPANA Modelling Systems and the linkage between them. OPANA model is currently used as operational tool for air pollution forecasts over the cities of Madrid (Spain), Bilbao (Spain) and Leicester (United Kingdom) (http://artico.lma.fi.upm.es).

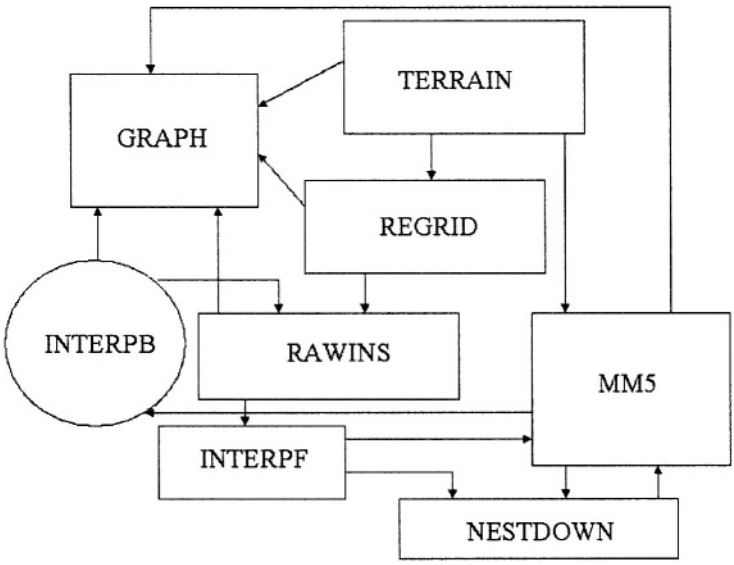

Figure 1.- MM5 mesoscale meteorological modelling system scheme.

EMISSIONS, METEOROLOGICAL MODELLING AND CMAQ SYSTEMS

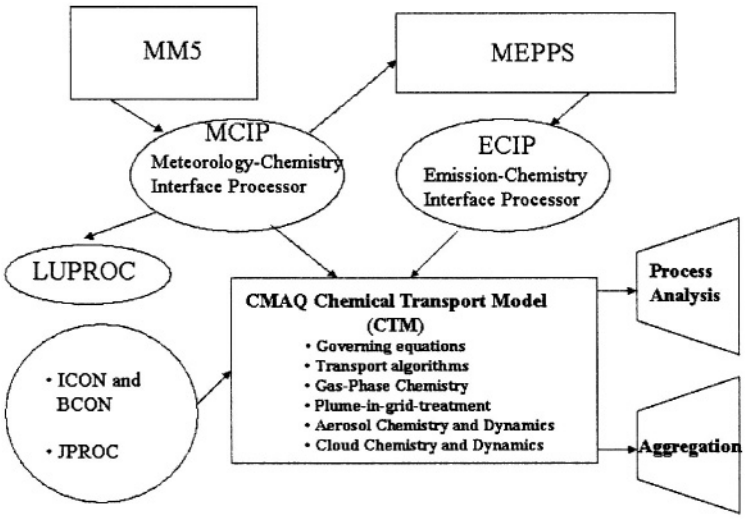

Figure 2.- CMAQ and peripheral modules.

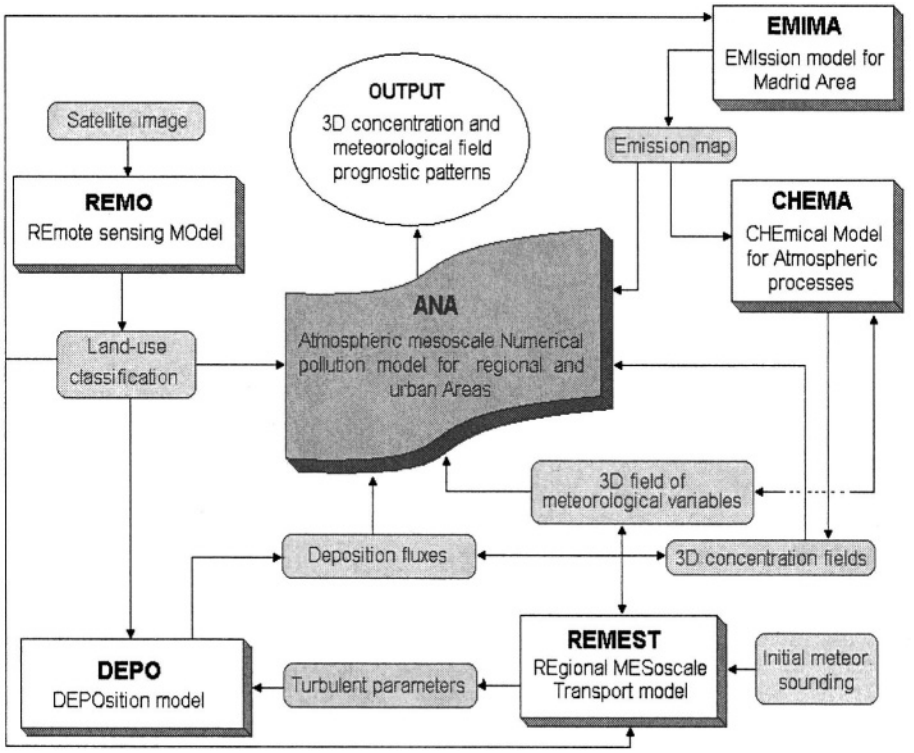

Figure 3.- Scheme of the different modules of OPANA.

4. MODELLING DOMAIN DESIGN

Consequently of providing full boundary conditions in a consistent manner for the length of the simulation and the spatial scales we have defined an experiment as follows. A mother domain centered in 40.00°N and 3.5°W (approximately Madrid City) and 108 km grid cell resolution with 75 columns and 60 rows. This domain covers an important part of North of Africa reaching the North of Scandinavian Peninsula. Figure 4 shows the mother and nesting domains in Lambert Conformal projection. This domain is used for MM5. The land use file is dimensioned as follows: 72 columns and 57 rows. The land use data set is obtained from the USGS EROS Data Center from Eurasia and Africa datasets Lambert Azimuthal Equal Area Projection (optimised for Europe) with 1 km spatial resolution. This information is extracted separately and the unified file is obtained by using ARC/INFO Geographic Information System. The resulted land use file is averaged for 4 km spatial resolution which is the highest resolution used in nesting level 3 in this specific application with CMAQ. This data set is having 2000 x 1600 4 km grid cells. The final CMAQ moth domain is 68 columns and 53 rows.

The nesting level 1 for CMAQ is 42 columns and 39 rows with 36 km grid cell spatial resolution, nesting level 2 is 30 columns and 36 rows with 12 km spatial resolution and final nesting level 3 is located over the Madrid Community and is having 21 columns and

27 rows with 4 km spatial resolution. For MM5 and CMAQ we have 23 vertical layers with top level with 10 Hpa.

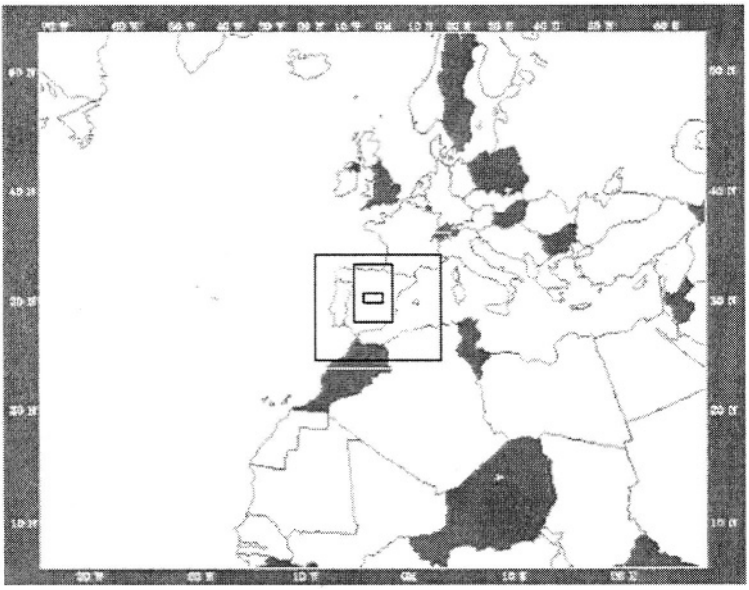

Figure 4.- Mother and nesting domains for our experiment.

The emission inventory is obtained by using the Emission Database for Global Atmospheric Research – EDGAR from RIVM and TNO. This emission inventory is for 1° x 1° spatial resolution and for annual dataset. The emission inventory is used as it is for mother domain and for nesting domains we use information from Digital Chart of the World and USGS ERIOS Data Center for refining the spatial resolution up to 4 km. The time profiles for hourly emission data sets for all domains are obtained from examples in Europe from IER emission dataset (University of Stuttgart, Germany) at different European regions. These calculations are made with our emission module called EMIMO 2.0 Figure 5 shows the NOx total annual emissions for the mother domain. The biogenic emissions are obtained by using our module called BIOEMI 2.0 which calculates the isoprene, monoterpene and natural NOx emissions for our experiment.

The experiment is carried out over the April, 17-23, 2001 period of time with the first 2 days for spin-off and 5 days for analysis of results. The initial and boundary conditions are determined by using the scheme presented in Figure 5.

5. RESULTS

The results show a high realistic patterns for ozone and other pollutants. The non-linearity associated to the observed ozone concentrations in monitoring stations is much more represented when using MM5-CMAQ system than when we use a limited area modelling system such as OPANA. Figures 6 and 7 shows the simulated and observed

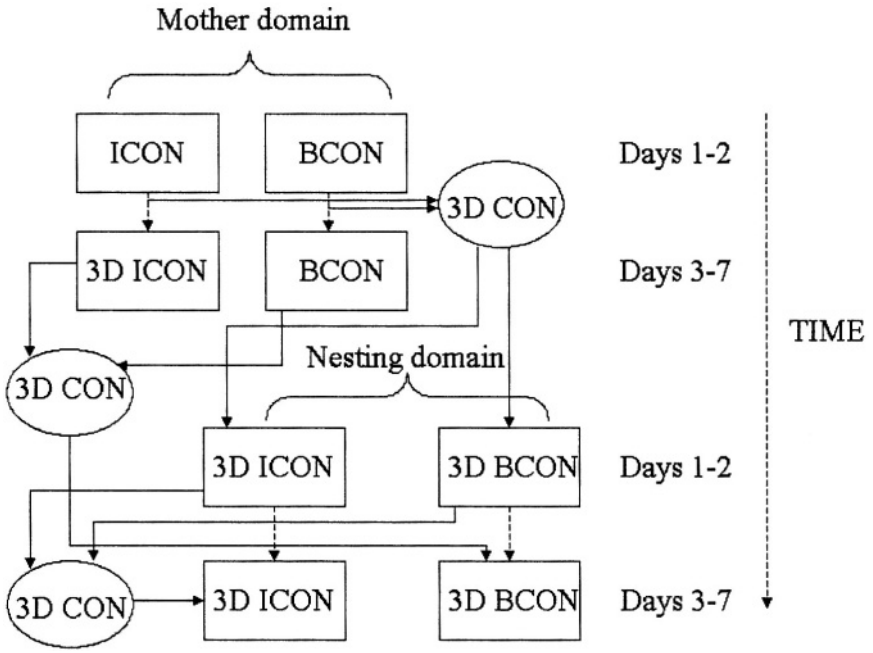

Figure 5.- Initial and boundary condition architecture for CMAQ nesting application in this experiment

patterns in two monitoring stations in Madrid model domain: Alcala de Henares and Coslada. Both stations are located to East of the Municipality of Madrid and both are located in centers of metropolitan areas.

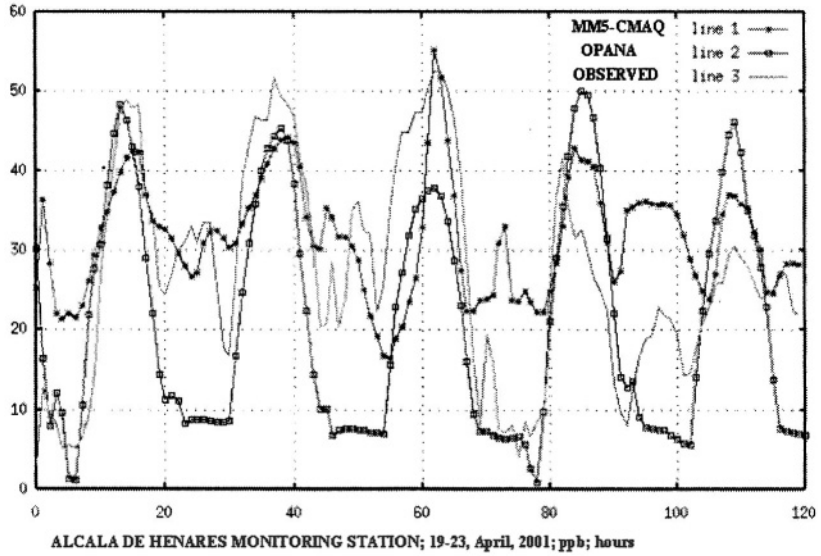

Figure 6.- Comparison between MM5-CMAQ and OPANA simulations with observed monitoring data in Alcalá de Henares monitoring station in Madrid model domain (nesting level 3).

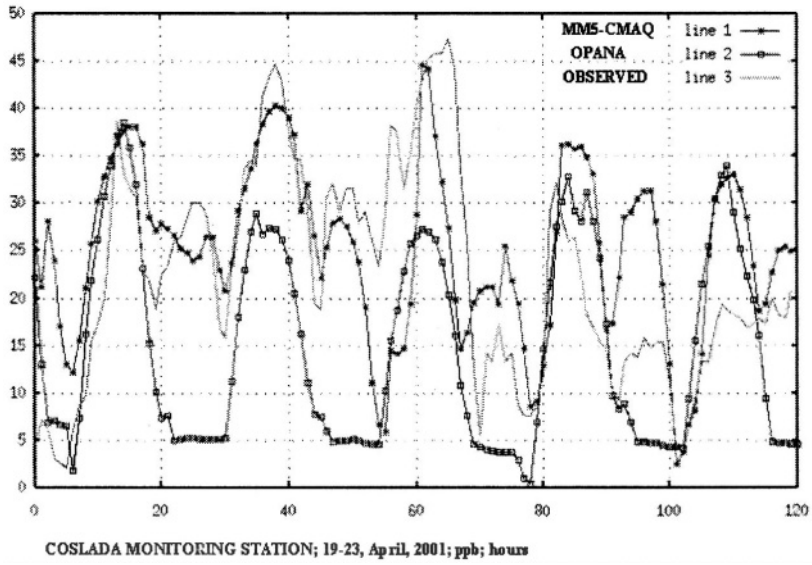

Figure 7.- Comparison between MM5-CMAQ and OPANA simulations with observed monitoring data in Coslada monitoring station in Madrid model domain (nesting level 3).

6. SUMMARY

We have implemented the standalone version of the Community Multiscale Air Quality Modelling System in a DIGITAL COMPAQ XP 1000 / 1GB RAM platform and the MM5 mesoscale meteorological model over a LINUX PC AMD 1 Ghz / 128 Mb RAM. We have run a mother domain and three nesting levels up to 4 km grid cell spatial resolution over the Madrid domain. We have simulated 17-18, April, 2001 as spin-off period and 19-23, April, 2001 as experimental period and we have run OPANA model over de same period of time. We have compared both results with some monitoring stations. Results with MM5-.CMAQ seems to be much more realistic which is associated to the proper boundary conditions obtained from nesting levels 2-1 and mother domain concentrations. Further experiments are necessary over different periods of the year and operational version under automatic mode over web will be deployed in the next months to assure the operational mode of the system.

6. REFERENCES

Carmichael G.R., Peters L.K. and Saylor R.D. (1991). The STEM-II regional scale acid deposition and photochemical oxidant model –1. An overview of model development and applications. *Atmospheric Environment* **25A,** 2077-2090.

Chen, F., and J. Dudhia, 2001: Coupling an advanced land-surface/hydrology model with the Penn State/NCAR MM5 modeling system. Part I: Model implementation and sensitivity. Mon. Wea. Rev., 129, 569-585.

Colella P. and P.R. Woodward (1984): The piecewise parabolic method (PPM) for gas-dynamical simulations. *J. Comp. Phys* **54,** 174-201.

Flassak T. and Moussiopoulos N. (1989) Simulation of the sea breeze in Athens with an efficient non-hydrostatic mesoscale model. In: Man and his ecosystem., **Vol. 3,** Eds. L.J. Brasser and W.C. Mulder. Elsevier. Amsterdam. 189-195.

Ge, Xiaozhen, Li, Feng, and Ge, Ming, 1997: Numerical analysis and case experiment for forecasting capability by using high accuracy moisture advectional algorithm. Meteorology and Atmospheric Physics, Vienna, Austria, 63(3-4), 131-148.

Jacobson M.Z. and Turco R.P. (1994) SMVGEAR: A sparse-matrix vectorized gear code for atmospheric models. *Atmospheric Environment,* **28,** 273-284.

McRae G. J. And Seinfeld J.H. (1983) Development of a second generation mathematical model for urban air pollution. II. Evaluation of model performance. *Atmospheric Environment,* **17,** 501-522.

Peters L.K., Berkowitz C.M., Carmichael G.R., Easter R.C., Fairweather G., Ghan S.J., Hales J.M., Leung L.R., Pennell W.R., Potra F.A., Saylor R.D. and Tsang T.T. (1995) The current state and future direction of Eulerian models in simulating the tropospheric chemistry and transport of chemical species: A review. *Atmospheric Environment,* **29, 2,** 189-222.

San José R., Rodríguez L. And Moreno J. (1994). An application of the "Big Leaf" deposition approach to the mesoscale meteorological transport and chemical modelling in a three dimensional context. Proceedings of the EUROTRAC Symposium. Eds. Borrel P.M., Borrell P., Cvitas T. and Seiler W. 620.

San José R., Rodríguez M.A., Pelechano A. And González R.M. (1999) Sensitivity studies of dry deposition fluxes. In Measuring and Modelling Investigation of Environmental Proceses. WITpress *Computational Mechanics Publications.* ISBN: 1-853125660. Ed. R. San José. 205-246.

Stensrud, D. J., J. -W. Bao, and T. T. Warner, 2000: Using initial condition and model physics perturbations in short-range ensemble simulations of mesoscale convective systems. Mon. Wea. Rev., 128, 2077-2107.

Venkatram A. and Karamachandani P. K. (1989). The ADOM II scavenging module: incorporation of improved cumulus cloud module. ENSR Doc. No. 0780-004-205.

Warner, T. T. and H. M. Hsu, 2000: Nested-model simulation of moist convection: The impact of coarse-grid parameterized convection on fine-grid resolved convection through lateral-boundary-condition effects. Mon. Wea. Rev., 128, 2211-2231.

DISCUSSION

M. ZHANG

1) Do you use the same emissions inventory for different model domains ? If so, how do you keep emission flux conservative for each domain ?
2) How did you specify emission rate for the lowest model layer, as the height of the layer in your model system changes with time ?

R. SAN JOSE

1) We use EDGAR emission inventory with 1x1 degree resolution annual total data set. We use USG5 1 x 1 km land use files (AVHRR/NOAA), DCW information and world population data base to assure inhomogeneity distribution of emissions by using our EMIMO model.
2) In this version, emissions are located at the surface since no information has been found related to the height of industrial chimmeneys in the original and other data bases.

D. STEYN

Does your modelling system incorporate stratospheric intrusions of ozone ?

R. SAN JOSE

No. It is planned to do it in the future because of the considerable importance that that process is having in predicting ozone concentrations.

This page intentionally left blank

ESTIMATES OF UNCERTAINTY IN URBAN AIR QUALITY MODEL PREDICTIONS

Sotiris Vardoulakis, Bernard Fisher, Norbert Gonzalez-Flesca, and Koulis Pericleous*

1. INTRODUCTION

The deterministic approach of running a single dispersion model using a specific input data set of fixed values has been traditionally adopted in air quality management. In some cases more than one model has been involved in inter-comparison studies and different emissions scenarios have been taken into account in order to assess future air quality trends. However, most of the modelling work has been so far oriented towards deterministic simulations of ambient air pollution. This approach does not reflect the uncertainties attached to the input data, model formulation and stochastic variability of the atmosphere. Given the complexities of urban environments and the inherent limitations of mathematical modelling, it is unlikely that a single model based on routinely available meteorological and emission data will give satisfactory short-term predictions. Moreover, deterministic air quality modelling might lead in same cases to erroneous decisions with serious financial and social implications when used for regulatory and planning purposes.

In this study, a method involving the use of more than one urban dispersion models, in association with different emission simulation methodologies and meteorological input data from different sources, is proposed for predicting best CO and benzene estimates, and related confidence bounds. This method was tested using experimental data obtained during intensive monitoring campaigns in busy street canyons in Paris, France. Three relatively simple dispersion models (OSPM, AEOLIUS and STREET) which are likely to be used for regulatory purposes were selected for this application. The comparison between simulated and observed concentrations demonstrated the advantages and limitations of this approach. Without resorting to sophisticated statistical techniques, this

* Sotiris Vardoulakis, Institut National de l'Environnement Industriel et des Risques (INERIS), and School of Computing and Mathematical Science, University of Greenwich. Bernard Fisher, National Centre for Risk Analysis & Options Appraisal, Environment Agency, 11 Tothill Street, London SW1H 9NF, UK. Norbert Gonzalez-Flesca, INERIS, Parc Technologique ALATA, B.P. 2, 60550 Verneuil-en-Halatte, France. Koulis Pericleous, School of Computing and Mathematical Science, University of Greenwich, Maritime Greenwich University Campus, 30 Park Row, London SE10 9LS, UK.

Air Pollution Modeling and Its Application XV, Edited by
Borrego and Schayes, Kluwer Academic/Plenum Publishers, New York, 2002

study explores practical methods for quantifying and presenting model uncertainties in a way that can be easily understood by local authority officers and general public.

2. INPUT DATA

Two comprehensive data sets were created from field experiments conducted at representative street canyon sites in Paris during winter (Bd. Voltaire, December 1998) and summer (Rue de Rennes, July 1999). The two sites are busy four lane streets with large pavements and uniform buildings lining up continuously on both sides. The height-to-width (H/W) ratios for Bd. Voltaire and Rue de Rennes were approximately equal to 0.8 and 1.1, respectively.

Traffic-related atmospheric pollutants were sampled during five and eight days in Bd. Voltaire and Rue de Rennes, respectively. Continuous CO monitoring and diffusive benzene sampling was carried out in both the canyons throughout the respective campaigns. The relative street and background contributions to the pollution levels observed on the roadside were derived from benzene measurements. The experimental lay out and monitoring results from these campaigns were presented elsewhere (Vardoulakis et al., 2001)

Synoptic wind data and other meteorological information were obtained from three permanent monitoring stations operated by Meteo France. Two of them were located in urban settings within Paris: (a) park Montsouris, and (b) St. Jacques tower. The third station was located at (c) Orly airport, in approximately 12 km distance from central Paris.

The average traffic volumes in Bd. Voltaire and Rue de Rennes during measurements were 30,000 and 23,000 veh/day, respectively. Hourly traffic data were obtained from automatic counters permanently operating in both the streets. The vehicle fleet composition was estimated from on site spot measurements during the campaigns.

The rate of release of emissions in the street was derived from traffic volumes and composite emission factors. Two different methods were applied for calculating CO emission factors: (a) The protocol used by Buckland and Middleton (1999), and (b) the IMPACT road traffic emission model commercialised by ADEME (1998). This model uses COPERT II methodology (Ntziachristos and Samaras, 1997) to quantify fuel consumption and atmospheric releases of a specified vehicle fleet in a given year in France. The required input information includes traffic volume and composition, average vehicle speed, and length and slope of the road segment of interest. In addition, the month of the year is used to estimate average ambient temperatures, which are further used for calculating evaporative and cold running emissions. The model provides default values for the average travelling distance and the fraction of this distance run with a cold engine in France.

The estimated values from both the methods, were compared for consistency with CO emission factors specific to the French vehicle fleet reported in other recent studies (Touaty and Bonsang, 2000; Jones et al., 2000). All values are summarised in Table 1.

Table 1: CO emission factors from road transport in the region of Paris

Author	CO emission factors (g/km veh)		
	Bd. Voltaire	Rue de Rennes	Paris
IMPACT (ADEME, 1998)	20.29	10.91	
Buckland and Midletton (1999)	7.23	8.73	
Touaty and Bonsang (2000)			8.11
Jones et al. (2000)			8.82

3. STREET CANYON MODELS

In this study, three parameterised dispersion models (STREET, OSPM, and AEOLIUS) were used to simulate pollutant dispersion within canyons. These relatively simple codes (or variations of them) have been widely used by local authorities and air quality networks in Europe. They are likely to be involved in a variety of applications including air quality and traffic management, urban planning, population exposure studies, etc.

Like most empirical street canyons models, they are based on the assumption that a wind recirculation zone is formed within the canyon when the roof-top wind blows perpendicularly or near-perpendicularly to the street axis (Berkowicz et al., 1997). This air vortex causes a downward flow of relatively clean air on the windward side of the canyon and an upward flow of air mixed with exhaust gases on the leeward side. This flow gives rise to high cross-road and vertical pollution gradients in the street.

Empirical models have been proved to describe quite efficiently concentration gradients in regular canyons, especially for the perpendicular wind situation. Nevertheless, more sophisticated modelling techniques might be needed to simulate dispersion under low wind conditions or in more complex urban environments (e.g. asymmetric and deep canyons, intersections, etc.). In these cases, the single vortex assumption does not appear realistic.

STREET and OSPM have been parameterised according to different field experiments and used successfully in many scientific and engineering applications (Johnson et al., 1973; Qin and Kot, 1993; Kukkonen et al., 2001). AEOLIUS is a more recent model based on the same formulation as OSPM and mainly used in the U.K. (Buckland, 1998).

4. QUANTIFYING UNCERTAINTY

The total uncertainty involved in modelling simulations can be considered as the sum of three components(Hanna, 1988): (a) The uncertainty due to errors in the model physics, (b) the uncertainty due to input data errors, (c) the uncertainty due to stochastic processes (e.g. turbulence) in the atmosphere.

STREET, OSPM and AEOLIUS were initially used in a traditional manner to produce estimates of roadside CO concentrations in Bd. Voltaire and Rue de Rennes. Three independent meteorological data sets and three different emission factors (as described in paragraphs 2) were used for each canyon, so as to create an ensemble set of

27 simulations for each case. It was considered that the use of different models enabled us to account, to a certain extent, for the uncertainty in model formulation. Furthermore, the use of independent wind and emission data sets was thought to represent the uncertainties due to errors in model inputs. This approach might be more realistic than defining a priori uncertainty ranges in different input variables.

The same methodology was followed for creating ensemble sets of weekly benzene averages corresponding to different receptor locations in both the canyons.

For quantifying the total uncertainty in model predictions, medians together with maximum and minimum concentrations were calculated for each set of 27 model outputs corresponding to a specific receptor location and time. The extreme concentrations were thought to bound the likely ranges of total uncertainty in the predictions. As it can be seen in Fig. 1 and 2, approximately 95% and 92% of CO observations in Rue de Rennes and Bd. Voltaire, respectively, fell within the predicted concentration ranges. In the case of benzene, all predicted values were within the estimated error bounds (Fig. 3 and 4).

5. DISCUSSION

In the previous examples, the observed concentrations fell in most cases within the estimated error (or "confidence") bounds. Nevertheless, it might be argued that these error limits were so large that they did not really provide any useful information. The fact is that, although large uncertainties do exist, dispersion models are still used in a traditional "deterministic" way, often returning results with several significant digits. It is, therefore, preferable to include error bounds (however large they may be) in the predictions in order avoid inappropriate reliance on modelling results.

A more rigorous approach would require that probability functions be developed for input and internal model parameter, and these be randomly sampled to obtain improved ensemble sets (Dabberdt and Miller, 2000). This, however, would risk to geometrically increase the time and consequently the cost of the simulations. It is believed that ensembles of less than 30 simulations, as shown in this study, can provide satisfactory air quality predictions and error bounds.

Model users some times assume that the total uncertainty in predictions decreases as the complexity of the model increases. This is true only for the uncertainty attributed to errors in the physical description of the model domain (e.g. incorrect assumptions, oversimplifications, etc.). On the other hand, sophisticated models require a larger amount of input information, which inevitably introduce a larger data uncertainty component in their calculations. It is, therefore, very important to define the appropriate degree of sophistication for a specific application, so as to achieve the lowest possible level of uncertainty in modelling results.

5.1. Uncertainty in emissions

It has been suggested by other authors (Kühlwein and Friedrich, 2000) that emission factors represent one of the most important source of uncertainty in modelling traffic pollution. That was confirmed in the present study. CO emission factors calculated with IMPACT were 25% and 180% higher than those calculated following Buckland and Middleton's methodology for Rue de Rennes and Bd. Voltaire, respectively (Table 1).

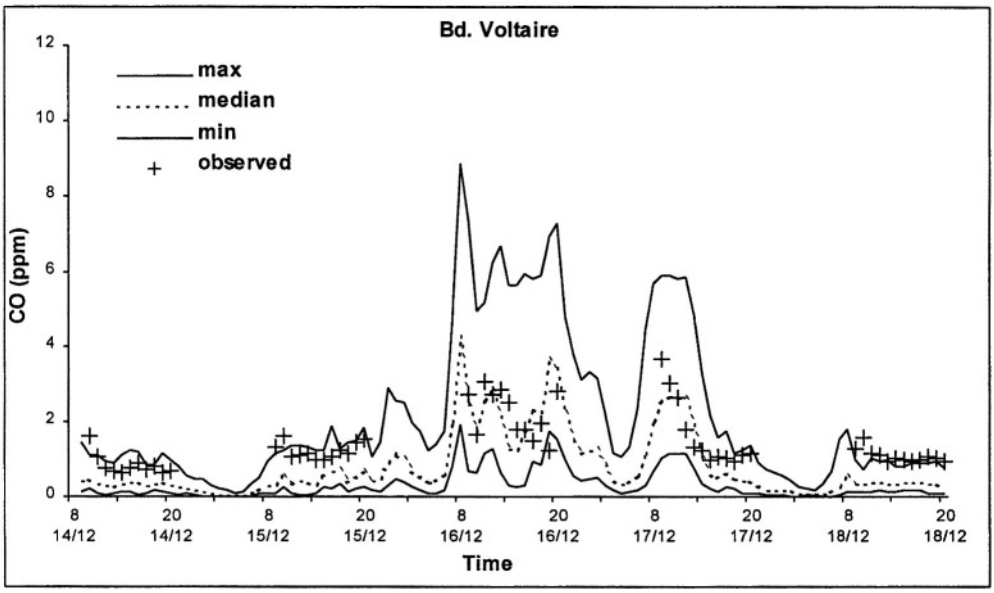

Fig. 1: Time series of CO best estimates (median), error bounds (max, min), and observed concentrations in Bd. Voltaire, Paris.

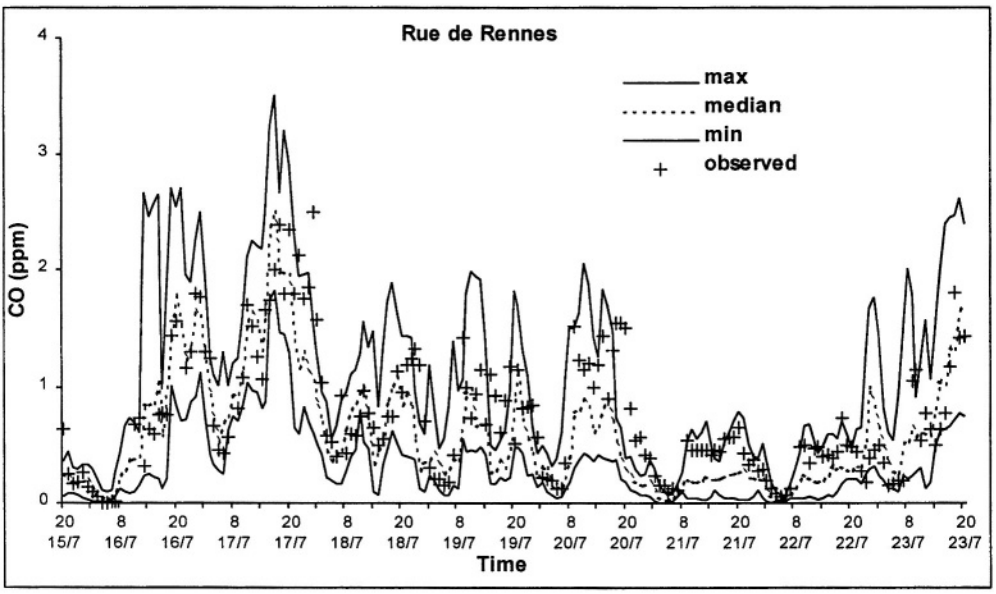

Fig. 2: Time series of CO best estimates (median), error bounds (max, min), and observed concentrations in Rue de Rennes, Paris.

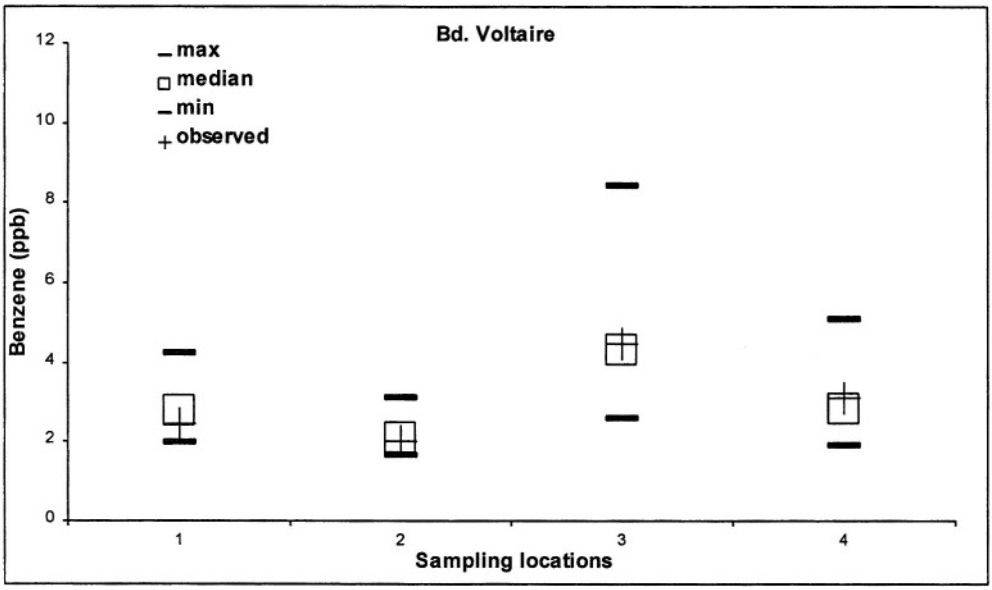

Fig. 3: Benzene best estimates (median), error bounds (max, min), and observed concentrations at different receptor locations in Bd. Voltaire, Paris.

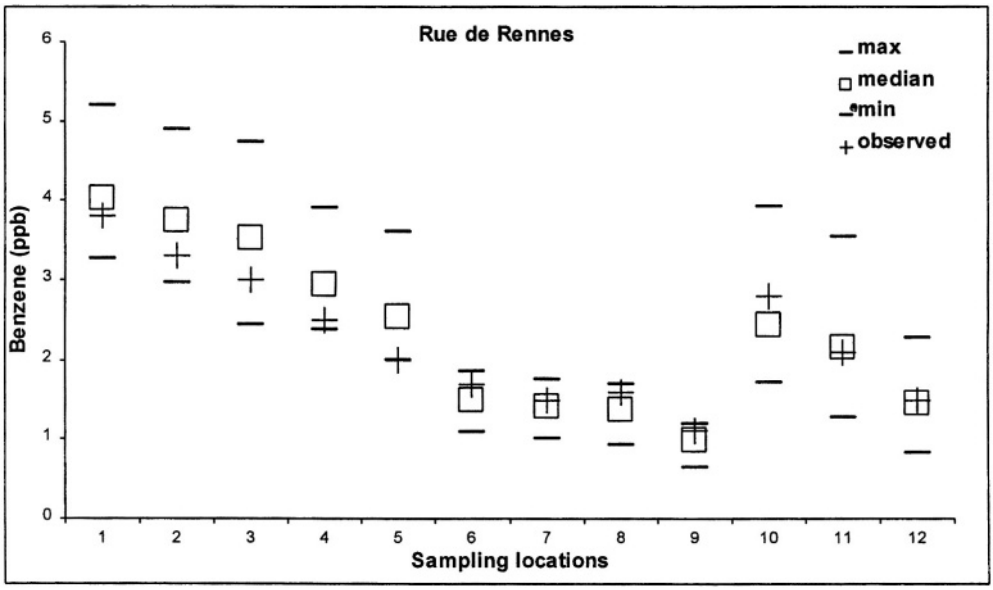

Fig. 4: Benzene best estimates (median), error bounds (max, min), and observed concentrations at different receptor locations in Rue de Rennes, Paris.

The large discrepancies, especially in the case of Bd. Voltaire, were probably due to the very significant cold start/running emissions calculated by IMPACT and added to the hot running values.

Cold start emissions are indeed expected to be important for urban driving conditions, because of the relative large number of short trips carried out with cold engines, especially in winter. In an on-road experiment in Belgium (De Vlieger, 1997), it was found that the average CO vehicle emissions measured during the cold phase were 4 to 40 times higher than emissions with a hot start (i.e. a hot engine + a warmed-up three way catalyst). Other experimental results showed significant seasonal differences in cold starts due to ambient temperature variations (Mensink et al., 2000).

Further uncertainties in vehicle emissions may be related to the driving behaviour. It has been reported that emissions obtained from aggressive driving can be up to four times higher than those obtained from normal driving (De Vlieger, 1997). In addition to this, emission factors typically increase by a factor up to ten during congestion compared to smooth driving conditions (Sjodin et al., 1998). Finally, it should be remembered that the vast majority of fleet emissions come from a small number of poorly maintained vehicles (Singh and Huber, 2000). For all these reasons, it is practically impossible to determine vehicle emission factors with great accuracy.

5.2. Uncertainty in meteorology

Although meteorological data from different urban monitoring stations might differ significantly for short time periods (i.e. few hours), it is mainly between urban and airport wind data where larger discrepancies are usually encounter.

When the first street canyon models were developed few decades ago, it was assumed that the local roof-top wind information needed as an input would not be generally available, and that airport wind data would have to be used. For this reason, empirical expressions relating airport and roof-top winds were derived (Johnson et al., 1973).

Exploring the sensitivity of AEOLIUS to wind data from different sources, Manning et al. (2000) observed that model concentrations were significantly lower when airport wind speeds were used rather than local roof-top winds. That was in agreement with findings of the present study, which showed that simulations carried out using airport winds produced lower concentrations than those produced using wind data from the other two urban sites. For this reason, predictions made using Orly airport data were eventually excluded from the calculation of the error bounds in Fig. 1, 2, 3, and 4.

Nowadays, there is usually at least one weather station permanently operating in big European cities like Paris. It is, therefore, suggested that only wind information from urban monitoring sites be used, when available, for street canyon simulations. The use of airport wind data is expected to increase uncertainty in predictions.

6. CONCLUSIONS

A practical methodology for quantifying uncertainties in air quality model predictions was developed and tested on experimental data obtained in two street canyons in Paris.

This method was based on the use of three different models, independent meteorological data sets and different emission factors, for creating ensemble sets of street canyon simulations. That enabled us to calculate best estimates of CO and benzene concentrations, and related error bounds.

It was not the intention of the authors to simulate all possible sources of uncertainty in urban dispersion modelling. Uncertainties due to stochastic atmospheric processes or due to errors in some of the input parameters (e.g. dimensions of the street, traffic volumes, etc.) were not here taken into consideration. However, it is believed that the above presented methodology strikes a reasonable balance between simplicity and reliability on urban dispersion models.

ACKNOWLEDGEMENTS

The authors would like to thank J-C. Pinard and A. Frezier (INERIS) for their technical assistance, and Dr. R. Berkowicz (NERI) for providing and discussing OSPM.

REFERENCES

ADEME, 1998, Emissions de polluants et consommations liées à la circulacion routière, ADEME, Paris.

Berkowicz R., Hertel O., Larsen S.E., Sorensen N.N., Nielsen M., 1997, Modelling traffic pollution in streets, NERI, Roskilde, Denmark.

Buckland A. T., 1998, Validation of a street canyon model in two cities, *Env. Monitor. & Assess.* **52**: 255-267.

Buckland A. T., Middleton D. R., 1999, Nomograms for calculating pollution within street canyons, *Atmospheric Environment* **33:** 1017-1036.

Dabberdt W. F., Miller E., 2000, Uncertainty, ensembles and air quality dispersion modeling: applications and challenges, *Atmospheric Environment* **34:** 4667-4673.

De Vlieger I., 1997, On-board emission and fuel consumption measurement campaign on petrol-driven passenger cars, *Atmospheric Environment* **31:** 3753-3761.

Hanna S. R., 1988, Air Quality Model Evaluation and Uncertainty, *J. Air Pollution Control Assoc.* **38:** 406-412.

Johnson W. B., Ludwig F. L., Dabberdt W. F., Allen R. J., 1973, An urban diffusion simulation model for carbon monoxide, *J. Air Pollution Control Association* **23:** 490-498.

Jones S. G., Fisher B. E. A., Gonzalez-Flesca N., Sokhi R., 2000, The use of measurement programmes and models to assess concentrations next to major roads in urban areas, *Env. Monitor. & Assess.* **64:** 531-547.

Kühlwein J., Friedrich R., 2000, Uncertainties of modelling emissions from road transport, *Atmospheric Environment* **34:** 4603-4610.

Kukkonen J., Valkonen E., Walden J., Koskentalo T., Aarnio P., Karppinen A., Berkowicz R., Kartastenpää R., 2001, A measurement campaign in a street canyon in Helsinki and comparison of results with predictions of the OSPM model, *Atmospheric Environment* **35:** 231-243.

Manning A. J., Nicholson K. J., Middleton D. R., Rafferty S. C., 2000, Field study of wind and traffic to test a street canyon pollution model, *Env. Monitor. & Assess.* **60:** 283-313.

Mensink C., De Vlieger I., Nys J., 2000, An urban transport emission model for the Antwerp area, *Atmospheric Environment* **34:** 4595-4602.

Ntziachristos L., Samaras Z., 1997, COPERT II: Computer programme to calculate emissions from road transport - User's manual, European Environment Agency, Copenhagen.

Qin Y., Kot S. C., 1993, Dispersion of vehicular emission in street canyons, Guangzhou city, South China (P.R.C.), *Atmospheric Environment* **27B:** 283-291.

Singh R. B., Huber A. H., 2000, Development of a microscale emission factor model for CO for predicting real-time motor vehicle emissions, *J. Air Waste Manage. Assoc.* **50:** 1980-1991.

Sjodin A., Person K., Andreasson K., Arlander B., Galle B., 1998, On-road emission factors derived from measurements in a traffic tunnel, *Int. J. Vehicle Design* **20:** 147-158.

Touaty M., Bonsang B., 2000, Hydrocarbon emissions in a highway tunnel in the Paris area, *Atmospheric Environment* **34:** 985-996.

Vardoulakis S., Gonzalez-Flesca N., Fisher B. E. A., 2001, Assessment of traffic-related air pollution in two street canyons in Paris: implications for exposure studies, *Atmospheric Environment* (in the press).

DISCUSSION

S. RAFAILIDIS — In comparing the sensitivity of the different models against observations you do not include the experimental error bands. How would the conclusions have changed (e.g. ranges of variability in the input parameters) if you had included also this experimental variability in the comparison ?

S. VARDOULAKIS — I agree that uncertainties in measurements should be eventually taken into account. Nevertheless, measurement uncertainties are generally expected to be smaller than modelling uncertainties and for this reason we believe that our preliminary conclusions are valid.

This page intentionally left blank

EFFECTS OF INPUT DATA ERRORS ON SOME INDICES FOR STATISTICAL MODEL EVALUATION

Ann Wellens*

1. INTRODUCTION

Nowadays, air quality modeling has become an essential tool for determining compliance with regulations. Predictions made by any air quality model used in scientific studies or in regulatory applications should be sufficiently reliable, and quality assurance of a specific model is a pre-requisite to be able to use it with sufficient confidence.

The past ten years, model formulation has improved significantly, diminishing in this way the influence of inherent model formulation errors (Venkatram, 1999). However, differences between model predictions and observations have not disappeared with the diminishing of inherent model errors, which makes clear that also attention should be paid to the existence of data errors and their propagation through the model. Data errors often seem to be forgotten in the common belief that monitoring data are "the real world". As models rely upon emissions and meteorological inputs, an important feature for any model is accessibility to reliable input data. Often the error in the determination of these inputs fully justify the disagreements between predictions and observations (Irwin, *et al.,* 1987).

To quantify differences between model output and observations, different standard evaluation techniques have being developed the past years, as for example the Model Validation Kit (Olesen, 1995) or the ASTM procedure (Cooper, 1999); being the first of these still the most widely used evaluation technique. The Model Validation Kit (MVK) is a collection of three experimental data sets accompanied by software for model evaluation. It is a practical tool, meant to serve as a common frame of reference for modelers, although it does have well recognized limitations. In this study, the statistical indices included in the model validation kit were analyzed in terms of error propagation.

* Ann Wellens, DEPFI-UNAM, P.O. Box 70-256, Mexico, D.F., 04510, wann@servidor.unam.mx

Air Pollution Modeling and Its Application XV, Edited by
Borrego and Schayes, Kluwer Academic/Plenum Publishers, New York, 2002

2. ERROR PROPAGATION

Defining the *absolute error* as the difference between the exact value and its approximation and the *relative error* as the quotient of the absolute error and the true value, the global data error due to propagation of the individual data errors can be calculated.

Consider two numbers $a^* = a + \Delta a$ and $b^* = b + \Delta b$, where Δa and Δb represent the absolute errors of numbers a and b respectively. The asterisk in a^* and b^* indicate that both numbers include an exact part *(a* or *b)* and an inherent data error (Δa and Δb). Their relative errors ε_a and ε_b can be found dividing the respective absolute error by the real quantity *a* or *b,* where absolute errors have the same dimension as their corresponding variables and relative errors are expressed in percent.

$$\varepsilon_a = \Delta a / a \tag{1}$$

$$\varepsilon_b = \Delta b / b \tag{2}$$

The propagation of the relative numerical errors in arithmetic operations as sums, multiplications and divisions, due to errors on the operands, are found in table 1:

Table 1: Propagation of relative errors in arithmetic operations.

	Relative error ε
Addition $(a + b)$	$\varepsilon_{a+b} = (a\varepsilon_a + b\varepsilon_b)/(a + b)$
Subtraction $(a - b)$	$\varepsilon_{a-b} = (a\varepsilon_a - b\varepsilon_b)/(a - b)$
Multiplication (ab)	$\varepsilon_{ab} = (\varepsilon_a + 1)(\varepsilon_b + 1) - 1$
Division (a/b)	$\varepsilon_{a/b} = \left[(\varepsilon_a + 1)/(\varepsilon_b + 1)\right] - 1$

Relative errors are calculated in an exact way, without ignoring second order error terms, as these can become significant when individual relative data errors are important.

Note that:

- Propagated relative errors in addition and subtraction operations are a weighted average of the individual relative errors in *a* and *b.*
- Propagated relative errors in multiplications and divisions do not depend on the values of *a* and *b*, only on their individual relative errors.

3. STATISTICAL INDICES

The model validation kit (MVK) uses a basic set of statistical indices that can be used to evaluate air pollution dispersion models. The included indices are the mean and standard deviation of observed and simulated concentration values, bias and fractional bias of the simulated concentrations, fractional standard deviation, normalized mean square error, correlation coefficient and proportion of values that lies between a factor of 2 (see for example Canepa and Builtjes, 1999).

These indices are resumed in table 2, where n is the total number of the receptors and O_i and P_i are respectively the observed and predicted concentration at the i-th receptor. Their significance is explained in numerous papers and will not be repeated here.

Table 2: Statistical indices used in the Model Validation Kit.

Name	Formula
Average value of observed and predicted concentrations, $\overline{O}$ and $\overline{P}$	$\overline{O} = \frac{1}{n}\sum_{i=1}^{n} O_i$ and $\overline{P} = \frac{1}{n}\sum_{i=1}^{n_P} P_i$
Standard deviation of observed and predicted concentrations, S_O and S_P	$S_O = \sqrt{\frac{1}{n}\sum_{i=1}^{n}(O_i - \overline{O})^2}$ and $S_P = \sqrt{\frac{1}{n}\sum_{i=1}^{n}(P_i - \overline{P})^2}$
Bias or mean error, B	$B = \frac{1}{n}\sum_{i=1}^{n}(P_i - O_i)$
Fractional bias, FB	$FB = 2[(\overline{O} - \overline{P})/(\overline{O} + \overline{P})]$
Fractional standard deviation, FS	$FS = 2[(S_O - S_p)/(S_O + S_p)]$
Normalized mean squared error, $NMSE$	$NMSE = (P - O)^2/(\overline{P}\,\overline{O})$
Linear correlation coefficient, r	$r = \sum_{i=1}^{n}(O_i - \overline{O})(P_i - \overline{P}) \Big/ \sigma_O \sigma_P$
Fraction of two, $FA2$	$0.5 \le (P_i/O_i) \le 2$

4. ERROR PROPAGATION THROUGH STATISTICAL INDICES

The previously presented error propagation formulas were applied to find the relative error made in each of the presented statistical indices, when model results and observations present data errors. In the following formulas, ε_{Oi} corresponds to the data error of observation i, while ε_{Pi} corresponds to the data error of the predicted value i.

4.1. Average Value of Observed and Predicted Concentrations, $\overline{O}$ and $\overline{P}$

The error propagated when calculating the average value of the observed and predicted values equals a weighted average of the relative errors associated to the observed or predicted concentrations at the i-th receptor.

$$\varepsilon_{\overline{O}} = \sum_{i=1}^{n} O_i \varepsilon_{O_i} \Big/ \sum_{i=1}^{n} O_i \qquad \text{and} \qquad \varepsilon_{\overline{P}} = \sum_{i=1}^{n} P_i \varepsilon_{P_i} \Big/ \sum_{i=1}^{n} P_i \tag{3}$$

Note that if all observations or all predicted values have respectively the same data error in each data point ($\varepsilon_{O_i} = \varepsilon_O$ or $\varepsilon_{P_i} = \varepsilon_P$, $\forall_i$) the error propagated in the average value would be constant and equal:

$$\varepsilon_{\overline{O}} = \varepsilon_{O_i} = \varepsilon_O \quad \text{or} \quad \varepsilon_{\overline{P}} = \varepsilon_{P_i} = \varepsilon_P \tag{4}$$

4.2. Standard Deviation of Observed and Predicted Concentrations, S_O and S_P

The errors propagated when calculating the standard deviation of the observed and predicted values equal:

$$\varepsilon_{S_O} = \sqrt{\sum_{i=1}^{n}\left[O_i(1+\varepsilon_{O_i}) - \overline{O}(1+\varepsilon_{\overline{O}})\right]^2 \Big/ \sum_{i=1}^{n}(O_i - \overline{O})^2} - 1 \tag{5}$$

and

$$\varepsilon_{S_P} = \sqrt{\sum_{i=1}^{n}\left[P_i(1+\varepsilon_{P_i}) - \overline{P}(1+\varepsilon_{\overline{P}})\right]^2 \Big/ \sum_{i=1}^{n}(P_i - \overline{P})^2} - 1 \tag{6}$$

Note that when all observed or predicted values have the same error in each data point, Eqs. (5) and (6) reduce to:

$$\varepsilon_{S_O} = \sqrt{(1+\varepsilon_O)^2} - 1 = \varepsilon_O \qquad \text{or} \qquad \varepsilon_{S_P} = \sqrt{(1+\varepsilon_P)^2} - 1 = \varepsilon_P \tag{7}$$

4.3. Bias, *B*

Propagated error when calculating the bias, ε_{bias}, equals $(\overline{O}\varepsilon_{\overline{O}} - \overline{P}\varepsilon_{\overline{P}})/(\overline{O} - \overline{P})$. The error propagated when calculating the bias, is the weighted average of the propagated errors in the mean value of observed and predicted values. Note that when the propagated error in the mean of the observed and predicted values equal each other, the bias would propagate this same error. When this is not so, and the difference between $\varepsilon_{\overline{O}}$ and $\varepsilon_{\overline{P}}$ is small, the error propagated in the bias can become quite high.

4.4. Fractional Bias, *FB*

When calculating fractional bias, data errors propagate in the following way:

$$\varepsilon_{FB} = \frac{\left[\overline{O}(1+\varepsilon_{\overline{O}}) - \overline{P}(1+\varepsilon_{\overline{P}})\right]\left(\overline{O} + \overline{P}\right)}{\left[\overline{O}(1+\varepsilon_{\overline{O}}) + \overline{P}(1+\varepsilon_{\overline{P}})\right]\left(\overline{O} - \overline{P}\right)} - 1 \tag{8}$$

When the propagated errors in the mean of the observed and predicted values are the same ($\varepsilon_{\overline{O}} = \varepsilon_{\overline{P}}$), the propagated error for the fractional bias would be zero.

4.5. Fractional Standard Deviation, *FS*

For the fractional standard deviation, data errors propagate in the following way:

$$\varepsilon_{FS} = \frac{\left[S_o(1+\varepsilon_{S_o}) - S_P(1+\varepsilon_{S_P})\right]\left(S_o + S_P\right)}{\left[S_o(1+\varepsilon_{S_o}) + S_P(1+\varepsilon_{S_P})\right]\left(S_o - S_P\right)} - 1 \tag{9}$$

When all observed and predicted values have the same error in each data point, and at the same time $\varepsilon_O = \varepsilon_P$, it would follow that $\varepsilon_{S_o} = \varepsilon_{S_p} = \varepsilon_O$, and Eq. (9) reduces to zero.

4.6. Normalized Mean Squared Error, *NMSE*

Error propagation in the normalized mean square error equals:

$$\varepsilon_{NMSE} = \left[\sum_{i=1}^{n} [O_i(1+\varepsilon_{O_i}) - P_i(1+\varepsilon_{P_i})]^2 \Big/ (1+\varepsilon_{\overline{O}})(1+\varepsilon_{\overline{P}}) \sum_{i=1}^{n} [O_i - P_i]^2 \right] - 1 \qquad (10)$$

When all observed and predicted values have the same error in each data point, but not necessarily $\varepsilon_O = \varepsilon_P$, Eq. (10) reduces to zero.

4.7. Linear Correlation Coefficient, *r*

The error propagated when calculating the linear correlation coefficient is:

$$\varepsilon_r = \frac{\sum_{i=1}^{n} [O_i(1+\varepsilon_{O_i}) - \overline{O}(1+\varepsilon_{\overline{O}})][P_i(1+\varepsilon_{P_i}) - \overline{P}(1+\varepsilon_{\overline{P}})]}{(1+\varepsilon_{S_O})(1+\varepsilon_{S_P}) \sum_{i=1}^{n} [O_i - \overline{O}][P_i - \overline{P}]} - 1 \qquad (11)$$

Again, when all observed and predicted values have the same error, the previous equation would reduce to 0% and the correlation coefficient would not propagate any data error. In case ε_{O_i} = constant, the error propagated in the correlation coefficient does only depend on the error of $\overline{O}$, $\varepsilon_{\overline{O}}$, and something similar would happen for propagated errors in predicted values.

4.8. Fraction of Two, *FA2*

When data errors exist in observed and predicted values, factor of two will consider the fraction of observations for which

$$0.5\left[\frac{(\varepsilon_{P_i}+1)}{(\varepsilon_{O_i}+1)} - 1\right] \le \frac{P_i}{O_i} \le 2\left[\frac{(\varepsilon_{P_i}+1)}{(\varepsilon_{O_i}+1)} - 1\right] \qquad (11)$$

and not the fraction for which the relationship P_i/O_i has a value between 0.5 and 2.

5. APPLICATION OF ERROR PROPAGATION THROUGH STATISTICAL INDICES

The formulas presented in the previous section are useful in sensitivity analysis, where the influence of input data errors on model evaluation results is studied. When errors are propagated through statistical indices, the calculated quantity for each of them

can vary significantly. This will be demonstrated by calculating the presented statistical indices for the modeling results from the Belgian IFDM and the Rumanian Inpuff models, for the Copenhagen data set available through the Model Validation Kit (Olesen, 1995).

Different error scenarios were studied, taking into account over- and/or underestimation of the variable in study. For the *observed* values, a constant data error of 10% was considered, which is consistent with data presented for concentration measurements (see for example Moussiopoulos, 1999). For the *predicted* values, a hypothetical propagated data error of 35% was considered.

Determination of the way in which data errors propagate through mathematical models was not the goal of this investigation, however, it can be stated that the relative propagated error changes with the position vector *(X, Y, Z)* and depends on the model formulation, including for example for Gaussian models (Wellens, 1999) the used stability scheme and plume rise formulas, consideration of reflection at ground level or mixing height, wind speed determination at emission height and so on.

In this study the hypothetical value of 35% was used, although real propagated data error can become a lot bigger if adverse conditions are present. This error cannot be considered constant, exactly because it depends even on the distance from the source; for simplification, the same quantity of 35% for all predicted values is used, but some values are overestimated while others are underestimated.

The used error scenarios are:

	Data error in observed value	Data error in predicted value
Scenario 1	10%	-35% [a, b]
Scenario 2	-10% [a]	35% [a]

[a] Negative values correspond to underestimations; positive values correspond to overestimations.

[b] To avoid a constant error in the predicted values, arbitrarily the first 11 data points were considered to have the specified error, while the last 12 data points had the the same error but opposite in sign.

For both scenarios, all described indices were calculated; results were compared with the indices calculated in absence of data errors. Tables 3 and 4 resume the results of these calculations, indicating also the relative error made for each statistical index and error scenario, for the·IFDM and Inpuff models respectively.

Tables 3 and 4 prove numerically that data errors can propagate through statistical indices, presenting higher or lower values than the "correct" ones, depending on the used data set.

The following results are notorious:

- For scenario 1, the "correct" negative biases of –80.8 (IFDM model) and –72.10 (Inpuff model) convert into positive biases of 35.88 and 29.39 respectively, which corresponds to respective errors of –144.4% and –140.8% with respect to the "correct" values. As negative values correspond to underestimation and positive values to overestimation, this result indicates that presence of input data errors can change the judgment according to over- or underestimation of the model.

Table 3: Calculations of different indices for both error scenarios, IFDM.

IFDM	without error	ε_{O_i} = -10%, ε_{P_i} = 35%		ε_{O_i} = 10%, ε_{P_i} = -35%	
		value	error	value	error
$\overline{O}$ =	632.7	569.4	-10.0%	695.9	10.0%
$\overline{P}$ =	551.9	605.3	9.7%	498.5	-9.7%
S_O =	450.26	405.23	-10.0%	495.29	10.0%
S_P =	345.27	513.74	48.8%	269.48	-22.0%
r =	0.84	0.78	-8.0%	0.68	-19.2%
B =	-80.78	35.88	-144.4%	-197.45	144.4%
FB =	-0.07	0.03	-144.8%	-0.17	142.4%
FS =	0.13	-0.12	-189.5%	0.30	123.7%
$NMSE$ =	0.19	0.31	62.6%	0.50	165.5%
Inferior limit $FA2$ =	0.50	0.41	-17.9%	0.61	21.8%
Superior limit $FA2$ =	2.00	1.64	-17.9%	2.44	21.8%

Table 4: Calculations of different indices for both error scenarios, Inpuff

Inpuff	without error	ε_{O_i} = -10%, ε_{P_i} = 35%		ε_{O_i} = 10%, ε_{P_i} = -35%	
		value	error	value	error
$\overline{O}$ =	632.7	569.4	-10.0%	695.9	10.0%
$\overline{P}$ =	560.6	598.8	6.8%	522.3	-6.8%
S_O =	450.26	405.23	-10.0%	495.29	10.0%
S_P =	352.65	505.41	43.3%	312.74	-11.3%
r =	0.49	0.48	-2.1%	0.33	-32.7%
B =	-72.10	29.39	-140.8%	-173.59	140.8%
FB =	-0.06	0.03	-141.6%	-0.14	135.8%
FS =	0.12	-0.11	-190.5%	0.23	85.8%
$NMSE$ =	0.50	0.66	31.9%	0.75	49.7%
Inferior limit $FA2$ =	0.50	0.42	-15.7%	0.59	18.0%
Superior limit $FA2$ =	2.00	1.69	-15.7%	2.36	18.0%

- For scenario 2, the negative bias values increment in respectively 144.4 and 140.8 percent to –197.45 (IFDM model) and –173.59 (Inpuff model). In other words, considering the error propagated in this scenario, the underestimation would be judged to me more than 2 times the "correct" value.
- No other scenarios are presented, but some error combinations can provide an erroneous bias value very close to zero, although the model indicates a clear under- or overestimation when no data errors are present.
- In general, overestimation of the model output and/or observations does not have the same effect on the final value of the statistical indices as underestimation. This would only be so for so called linear indices as average values and bias. In tables 3 and 4 it can be seen that the error propagated in bias and mean values is exactly the same in magnitude for both scenarios, but opposite in sign. For all other presented indices, the effect can be a lot bigger in case of overestimation that in case of underestimation, or vice versa. For

example, in scenario 2 the correlation coefficient was underestimated in 19.2% (IFDM) and 35.4% (Inpuff) respectively, while for scenario 1 the error propagated in the correlation coefficient was only 8% (IFDM) and 2.1% (Inpuff) respectively.

6. CONCLUSIONS

This paper studies the propagation of data errors in observations and model results, through statistical indices used to evaluate air dispersion models. Presented results for two models evaluated previously with the model evaluation kit, the Belgian IFDM model and the Rumanian Inpuff model, indicate that statistical indices are influenced by existing data errors. This has been corroborated for the indices proposed in the Model Validation Kit, but in fact it is valid for whatever index that can be used for the statistical evaluation for dispersion models.

A constant error of 10% for observations was considered; for predictions, a conservative value of 35% was used, although model propagation through the different models was not studied. If data errors in each of the input variables are considered, propagation through different models can also be found.

Overestimation does generally not have the same effect as underestimation. Generally one of them produces much worse results than the other one. Although sometimes errors are cancelled, generally the propagation is worse when individual data errors in observations and predicted values increase. In occasions, propagation of data errors can change the judgment about the performance of the model of interest. As different models propagate data errors in a different way, a model can be classified as the "worst performing" without deserving it, or the other way around.

In this paper only some results were presented, and some may seem to be only slightly significant. However, different data sets, models and statistical indices should be studied to understand to which extend data errors can influence model results and even performance evaluation judgments.

7. REFERENCES

Canepa, E. and Builtjes, P. J. H., 1999, Methodology of model testing and application to dispersion simulation above complex terrain, *6th International Conference on Harmonisation within Atmospheric Dispersion Modelling for Regulatory Purposes,* Rouen, France.

Irwin, J. S., Rao, S. T., Peterson, W. B. and Turner, D. B., 1987, Relating error bounds for maximum concentration estimates to diffusion meteorology uncertainty, *Atmos. Environment,* 21 (9): 1927-1937

Moussiopoulos, N., Sahm, P., Münchow, S., Tonnesen, D. F., de Leeuw, F. and Tarrasón L., 1999, Uncertainty analysis of modeling studies included in air quality assessments. *6th International Conference on Harmonisation within Atmospheric Dispersion Modelling for Regulatory Purposes,* Rouen, France.

Olesen, H. R., 1995, Datasets and protocol for model validation kit for the workshop on operational short range atmospheric dispersion models for environmental impact assessments in Europe'. *J. of Environment and Pollution,* **5**(4-6): 693-701.

Venkatram, A., 1999, Applying a framework for evaluating the performance of air quality models, *6th International Conference on Harmonisation within Atmospheric Dispersion Modelling for Regulatory Purposes,* Rouen, France.

Wellens, A., 2001, Comparison of the inherent data error in plume rise models, *Int. J. Environment and Pollution,* in Press.

DISCUSSION

D. HANSEN

1) Perhaps assuming constant relative error in observations is an inappropriate model since relative error normally increases rapidly as one approaches the limit of detection.
2) How can you identify the most sensitive variables (input) by examining the statistically indices you displayed ?

A. WELLENS

1) In effect, relative errors in observations are not necessarily constant. Analysis of the measurement errors (for example increase close to the detection limit) was not the aim of this paper. However, it should definitely be studied, as relative errors in measurements can provoke a in some cases quite important differences between predictions and observations.

2) Some variables or approximations (for example: plume rise, whether or not reflection is included, etc.), may not cause big differences in the predicted concentration values, and will consequently not have a big influence on a specific statistical index used to evaluate a certain model. On the contrary, this specific index could be affected very much by the existence of a relative error in some other variable (for example the gas exit temperature), which would produce a concentration result differing very much from the "real" estimated value that would have been calculated if the error in this input variable would have been absent.
In this case, the value of the statistical index is not reflecting differences between models, but sensitivity of the model and/or statistical index to errors in the input data. As analytical propagation formulas are available, the proposed procedure can be used to learn which variables provoke the biggest differences in the statistical indices used.

This page intentionally left blank

POSTER SESSION

This page intentionally left blank

ASSESSMENT OF POLLUTION IMPACT OVER TURIN SUBURBAN AREA USING INTEGRATED METHODS

G. Tinarelli, S. Alessandrini, D. Anfossi, F. Pavone, S. Cuffini*

1. INTRODUCTION

Urban and suburban areas are often characterized by the presence of industrial facilities, goods distribution systems and major roads networks. In this respect, the air pollution control over these areas is an important activity for the protection of both the environment and the population health. Control strategies involve the integration among different methodologies, the management and use of air quality networks, the construction of emission inventories, and the use of atmospheric dispersion modeling techniques. The last two items allow to extend the information available from a local network to areas not covered by the stations and to build possible future impact scenarios caused by new installations or by alternative pollution reduction strategies

2. GENERAL DESCRIPTION OF THE ACTIVITIES

Close to the southern boundary of the city of Turin, in Northern Italy, the Province of Turin, one of the local authorities involved in the air pollution management, has started activities including the development of emission inventories and the use of dispersion models. The overall scope of this project is to cross check the emission inventory and dispersion model reliability, comparing model simulation results with available measurements. The work described here involves the verification of a modeling system in managing both severe pollution episodes and future emission scenarios. In this respect, two preliminary test cases have been carried out over a target area of $10 \times 10\ km^2$ south of the city of Turin. The first one is centered on the impact verification of a single industrial source present in that area, considering in particular its odorous emissions. The second and more complex one, is the simulation of the possible impact generated by the new wholesale agricultural market (CAAT), starting to operate on that site. This second task involves the reconstruction of both the road traffic modifications and the impact of these

* G. Tinarelli, ARIANET S.r.l., viale Elvezia 42, 20052 Monza (Milano), Italy. S. Alessandrini, CESI S.p.a., Via Reggio Emilia 39, 20039 Segrate (Milano), Italy. D. Anfossi, CNR, Istituto di Cosmogeofisica, Corso Fiume 4, 10133 Torino, Italy. F. Pavone and S. Cuffini, Provincia di Torino, Area Ambiente, Via Valeggio 5, 10128 Torino, Italy

Air Pollution Modeling and Its Application XV, Edited by
Borrego and Schayes, Kluwer Academic/Plenum Publishers, New York, 2002

modifications on the pollution levels over the whole area. The entire set of simulations have been made by using a three dimensional modeling approach over complex terrain, that uses a diagnostic mass-consistent wind reconstruction model MINERVE coupled with the Lagrangian particle dispersion model SPRAY version 2 (Tinarelli et al. 2000). To estimate the emission factors from road sources for the dispersion model, a program implementing the COPERT methodology over a complex grafo has been used.

3. SUMMARY OF MAIN RESULTS

Two simulation periods, each lasting two complete days, have been chosen as representative of typical meteorological conditions, potentially critical for pollutant dispersion. The first one is a summer period representing convective conditions with light winds blowing in a breeze regime, the second one is a winter period characterized by a low windspeed, stable condition. This choice has been made analyzing the time series available from the local anemometers of the monitoring network. Simulations of the odorous emission from the industrial source have shown a satisfactory spatial correspondence with the available data representing the area of the impact episodes. Dilution factors at different distances from the source have been estimated from concentration levels, allowing the definition of the area of potential impact around the emission point and the amount of population involved. Results from the simulation of the road traffic impact involved the reconstruction of hourly and daily averaged CO and NO_x concentration fields, generated by the normal traffic levels before the installation of CAAT. These results represent the background concentration levels. A future scenario providing new emission factors, obtained taking into account the road traffic due to the CAAT only, has been simulated and systematic comparison with the background levels performed. As regards CO, the new emissions due to the presence of CAAT do not determine a significant impact both for hourly peak and daily average concentration levels. This is due to the kind of vehicles involved by CAAT, typically having Diesel engines. Concerning NO_x, hourly concentration levels due to CAAT are instead comparable with those of the background traffic, whereas, on the contrary, NO_x daily averages are still substantially lower of background levels, due to the limited number of hours involved by the traffic related to the market.

4. REFERENCES

Tinarelli G., D.Anfossi, M. Bider, E.Ferrero, S. Trini Castelli, A new high performance version of the Lagrangian particle dispersion model SPRAY, some case studies, *Air Pollution Modelling and its Applications XIII,* S.E. Gryning and E. Batchvarova eds., pp 499-507 (Kluwer Academic / Plenum Press, New York, 2000).

ASSESSING UNCONTROLLED EMISSIONS NEAR A LEAD WORKS

Guido Cosemans and Edward Roekens*

1. INTRODUCTION

The directive 96/62/EC allows, under certain conditions, for the use of air quality models for the assessment of ambient air quality. In eight monitoring sites located near a lead works (Figure 1) near Antwerp, Belgium, daily mean concentrations of airborne lead are measured. This modelling study was set up in order to investigate whether this monitoring network can be replaced in all or in part by air quality modelling.

2. THE MODELLING

Modelling is done for the two year period 1996-1997. During this period, 12 metric tons of lead per year are emitted through 29 stacks of the lead works. These emissions, together with the heat content of the stack gasses and the stack height, are used to calculate the concentrations of lead in ambient air near the factory, using the IFDM-model[1]. According to these calculations, the emissions through the stacks contribute for only 6 % to the concentrations measured near the fence of the lead works yard and for about 20 % to the concentrations measured at 4 km from the plant. The fact that emissions through the stacks contribute little to the concentrations of heavy metals in airborne dust in the neighbourhood of a non-ferrous industry, was known from an in-depth investigation near an antimony plant, conducted in 1978-1991.

It is very difficult to measure the diffuse emissions of a non-ferrous metal plant. In order to proceed with the study, reverse modelling was used to estimate the diffuse lead emissions. The diffuse emissions were found to be 6 tons of lead per year. Taking into account these diffuse emissions, the agreement between measured and IFDM-calculated two year average concentrations is good. For monitoring sites under the dominating wind direction, we find at 10 m from the fence 1286 ng Pb /m³ measured and 1210 ng/m³ modelled; at 250 m 772 ng/m³ measured and 770 ng/m³ calculated; at 600 m: 399 ng/m³ measured and 346 ng/m³ modelled; at 4 km: 78 ng/m³ measured and 35 ng/m³

* Guido Cosemans, Flemish institute for technological research Vito, Remote Sensing and Atmospheric Processes, Boeretang 200, B 2400 Mol, Belgium.
Edward Roekens, Flemish Environmental Agency (VMM), Department Networks and Research, A. Van de Maelestraat 96, B 9320 Aalst, Belgium.

Air Pollution Modeling and Its Application XV, Edited by
Borrego and Schayes, Kluwer Academic/Plenum Publishers, New York, 2002

modelled. At the latter site, lead emissions by traffic (not included in the calculations) were still important in 1996-1997.

A further analysis of measured and calculated daily mean concentrations (Figure 2) revealed that about 50% of the diffuse emissions are varying in time proportional to the third power of the wind speed.

3. CONCLUSIONS

The study revealed the impact of the fugitive emissions at the lead works. The existing monitoring network can not be replaced by modelling only. Some monitoring sites will be needed to assess the evolution in time and space of the diffuse emissions of airborne lead in the vicinity of the lead works.

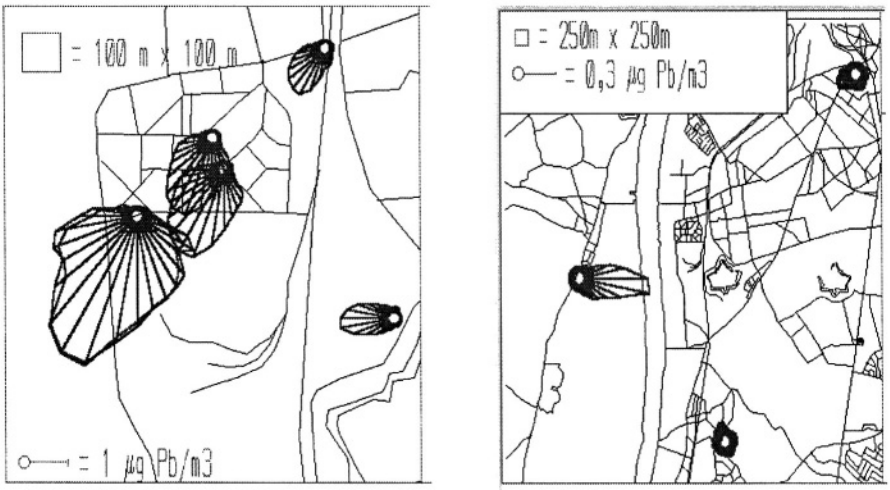

Figure 1. Pollution roses of Pb in monitoring sites near the lead works.

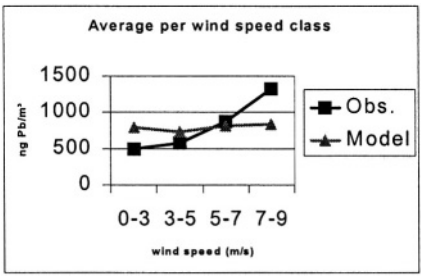

Figure 2. Observed daily Pb-concentrations increase with wind speed, while calculated Pb concentrations using constant fugitive emissions do not.

REFERENCES

1. H. Bultynck and L. Malet, Evaluation of atmospheric dilution factors for effluents diffused from an elevated continuous point source', Tellus, No. 24, pp. 445-472 (1972).
2. Air pollution near a non-ferrous metal industry, a comprehensive study, Volume 20 of the Final Scientific Report, National R&D Program on Environment-Air, Services of the Prime Minister, Brussels, /1982/1191/5/20 , 376 pages.

DESIGN FOR METEOROLOGICAL MONITORING FOR AIR POLLUTION MODELING IN INDUSTRIAL ZONE OF PANCEVO, BASED ON EXPERIENCES DURING BOMBING

Zoran Grsic, Predrag Milutinovic, Milena Jovasevic-Stojanovic, Marko Popovic*

1. INTRODUCTION

Before conflict, no one environmental black spot in FRY had any appropriate air pollution monitoring system, not any local meteorological measurements. A consequence was that local media informations about degree of dangers were confused at the beginning of the bombing. The same situation was in Pancevo, a large industrial center of oil, chemical and petrochemical industry. It is only 20 km away from the center of Belgrade, the capital of FR Yugoslavia. In the industrial zone of Pancevo, only 3.5 km from the center of the city, about 7000 workers are employed.

When appearing of tremendous clouds over sky began every day event, municipal Pancevo three weeks after starting of bombing moved action of a meteorological measured system establishing.

With very limited funds, this system was realized. System was semi-automated, so presence of an operator was necessary. This concept was effective in calm situations, but during air-raid alarm this was not effective because everybody had to be in shelters, meteorological operator too.

On the opposite side of Danube, about ten kilometers away, institute of nuclear sciences "Vinca " is located. At the 23rd NATO/CCMS meeting in Varna, automated meteorological station stationed in the institute was presented. This station was a constitutive part of defense of the institute if it would be bombed. All measured data were on-line delivered to the civil information center of Belgrade, where set of atmospheric

*Zoran Grsic, Milena Jovasevic-Stojanovic, Institute of the Nuclear Sciences Vinca, POB 522, YU-11001 Belgrade. Predrag Milutinovic, Marko Popovic, Institute of Physics, Pregrevica 118, YU-11000 Belgrade.

Air Pollution Modeling and Its Application XV, Edited by
Borrego and Schayes, Kluwer Academic/Plenum Publishers, New York, 2002

dispersion codes was installed. Fortunately, institute was not bombed. Due to the vicinity of the institute to the industrial zone 'Pancevo', we were in opportunity to model air pollution distribution from the bombed industrial zone 'Pancevo'.

2. BIG CHEMICAL ACCIDENTS IN INDUSTRIAL ZONE OF PANCEVO ON APRIL 18^{th} 1999

On April 18^{th}, 1999 at $1^{h}10^{min}$ GET, Pancevos industrial zone was hardly bombed. That wasn't the first bombing of the industrial area of Pancevo, but it was the most severe air strike. That night factories in Pancevos industrial zone were hit by six missiles, which destroyed The Oil Refinery (petrol and diesel), The Petrochemical Complex (chlorine, vinyl-chloride-monomer, ethylene and HIP Azotara Fertilizer Co., (ammonia, NPK, fertilizer tanks). The bombing caused explosions and fires, as well as a release of huge quantities of hazardous substances in the surrounding area and emissions of toxic gases in the air.

It was reported that during bombing of the petrochemical complex in Pancevo about 20 tones of chlorine was released from damaged tank (250 tons capacity) and 440 tons of vinyl chloride monomer (VCM) burned out from spherical VCM tanks (1500 tons capacity) and rail loading ramp of VCM with six train-cisterns. At the same time storage tanks were damaged in neighbor fertilizer factory and in oil refinery.

A direct hit on the ethylene dichloride (EDC) storage's of 1800 tons and a loss of 1400 tons of liquid. Damage of the ammonia storage of the capacity of 15000 tons. Damage of the tank of hydrochloric acid (33%) and the loss of 800 tons of liquid. The storage of natrium-hidroxide, of the capacity of 12000 tons was hit. About 3000 tons of liquid poured out into the Danube, A direct shot on the factory of chloralcalic electrolysis, with about 100 tons of mercury, which contaminated the soil.

Detailed meteorological situation, recorded with automated meteorological station in the institute "Vinca", shaw that, from the point of view of air pollution transport, situation was very complicated in the first 30 minutes after industrial zone Pancevo was bombed on that April 18, i.e. average 10 minutes wind direction three times was dramatically changed. In the moment of attack wind direction was **WNW**, after 10 minutes **WSW** and than **ENE**. For the local conditions it was of the mostly importance, especially because only few minutes after bombing fire companies and engines and the other persons were in the middle of the tremendous air pollution plumes. It was very important for the modeling of transboundary transport of air pollution too, because input parameters, which relate to the source characteristics, are strongly determined with local meteorological conditions.

The movement of polluted air in the area between Pancevo and Belgrade threatened to provoke the poisoning of inhabitants of Pancevo, Belgrade, and particularly it's northeast suburbs, and villages. About 40000 inhabitants of Pancevo were evacuated from city.

3. AD HOC METEOROLOGICAL STATION

Solitaire of the municipal Pancevo, in the center of the city Pancevo, was promoted in meteorological tower! Wind speed and direction sensors were mounted on tenth floor. Air temperature and humidity sensors were mounted on some the other floors. And that

was all of local meteorology during these the biggest chemical accidents. Relation between dimension of the accident and meteorological measurement obviously was deeply unequal.

4. EXPERIENCES AFTER BOMBING

Our assessments were that any war activities in the vicinity of the institute could cause panic if there would be lack of information. So one of the first thing we had to do was to supply civil information center of Belgrade with prompt information about level of contamination and moving of the radioactive clouds if they would be formed.
Meteorological monitoring based on the concept presented at the 23rd NATO/CCMS meeting in Varna, could solve some possible problems about air pollution transport and diffusion if the institute would be hit, but war conditions with electric power plants temporary disabled, forced additional requirements special about continuous power supply and on-line transfer data to the civil information center of Belgrade.
In peaceful times all levels of thinking are at least one order lower than in war times, so some solutions we had make in the past, before bombing, we had to adapt to the war demands. To illustrate this, during bombing appeared problem what will we do if our meteorological tower or meteorological room would be hit. We had to make reserve solution, and it was classical meteorological station with appropriate crew, dislocated from the institute location, but relatively close to the institute location.
After 77 days bombing, resume is that automated station had only several interruptions, when interruption of the power supply was 30 hours longer, and once during thunderstorm. Institute was not bombed, but the nearest distance where dropped bomb was 200-300m far from the fence of the institute, i.e. about one kilometer far from the reactor.

5. CONCLUSION

All characteristics of Vincas meteorological monitoring concept we checked in the worst possible situations while bombs dropped, and tremendous polluted clouds covered the whole sky, but it is an extraordinary experience.
On these experiences we proposed project of automated meteorological station located at the representative location in industrial zone Pancevo, similar to the automated meteorological station of the nuclear institute “Vinca”. The project is in progress.

Reference

Grsic Z., Milutinovic P.: Automated meteorological station and appropriate software for air pollution distribution assessment, *Air pollution Modeling and Its Application XIII,* edited by S.-E. Gryning and E.Batchvarova, Kluwer Academic/Plenum Publishers, 2000, pp.781-782.
Grsic Z., Milutinovic P., Jovasevic-Stojanovic M.: Some results of the meteorological monitoring and modeling activities, in the nuclear institute “Vinca”, during the recent NATO bombing. V Intern. Symp. and Exib. on Environm. Contam. in Central and Eastern Europe. Prague 2000. In press.

This page intentionally left blank

THE OPTIMAL CHOICE OF AERMOD INPUT DATA IN COMPLEX AREAS

G. Latini, R. Cocci Grifoni, G. Passerini*

1. INTRODUCTION

AERMOD is a steady-state plume dispersion model for the assessment of pollutant concentrations from point, volume, and area source. The model is based on the principles of the 'new generation' meteorology: it employs continuous variables to characterise atmospheric conditions, rather than a fixed number of categories used by traditional Gaussian models. We present tests showing that the model is very sensitive to different land use parameters and variants of complex coastal terrain. An exact information about the sensitivity of the model in these different scenarios is a fundamental step to evaluate the accuracy required for input values of AERMOD.

2. SENSITIVITY TESTS

The AERMOD modelling system is composed of a main model (AERMOD) and two preprocessors: a meteorological preprocessor (AERMET)[1] and a terrain preprocessor (AERMAP)[2]. Terrain data supplied by the U.S. Geological Survey were considered while fictitious source information for the modelling analysis was used for facility. Thus, the considered meteorological and terrain figures are real while source data and its location were shaped to simplify the analysis. A special effort was made to keep the modelling runs consistent to better understand the potential differences amongst different scenarios.

3. RESULTS AND CONCLUSIONS

AERMOD's performance was evaluated against observed SO_2 concentrations for impacts emitted from North Dakota refinery and Esino Valley[3] refinery in the middle of

* Dipartimento di Energetica, Università di Ancona, 60131 Ancona, Italy

Air Pollution Modeling and Its Application XV, Edited by
Borrego and Schayes, Kluwer Academic/Plenum Publishers, New York, 2002

Italy. Observed concentrations were obtained from monitoring stations located in the above mentioned complex areas. Consequently, sensitivity of the design concentration predictions was evaluated by selecting land use parameters and different source positions. The sets of field observations used in this study represent a cross-section of typical scenarios. Due to the lack of input data sets, the most significant results have been obtained for North Dakota region. Figure 1 identifies some of investigated scenarios.

In the first part of this study we altered all three land use parameters, namely Albedo, Bowen Ratio and roughness length (left side in Figure 1). In the second part, only Base Case, that represents approximate mid-range values of each parameters, was considered. In this typical situation shrewd locations for the refinery and surrounding sources were selected (right side in Figure 1).

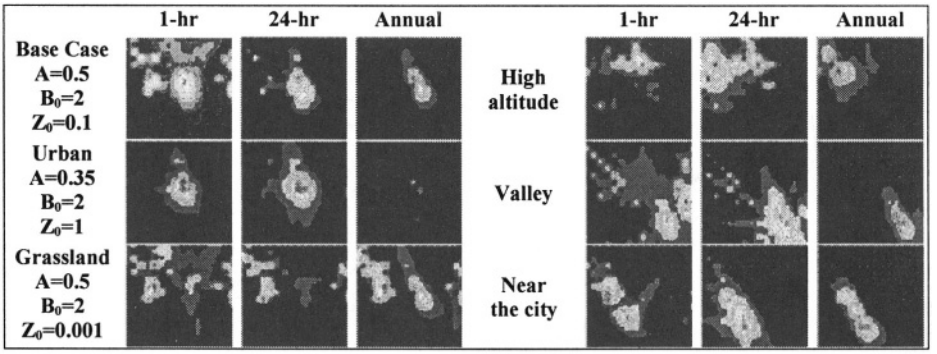

Figure 1. Effects of land use parameters and plant positions on design concentrations.

It is well known that AERMAP uses regular grids and discrete receptors to identify maximum impacts in complex terrain. DEM data are utilized to establish receptor elevations using coarse or fine receptors spacing. This study suggests the use of USGS 7.5-minute DEM instead of 1 degree DEM data. In fact the 1-degree DEM data often lose details available in the finer 7.5-minute resolution data. In addition, it is necessary to use caution close to source elevation because of the extreme dependency on complex terrain. The effects of changes in land use parameters and variants of orography on the modelled design concentrations in AERMOD are extremely complex. A reasonably accurate estimates of these characteristics are necessary for AERMOD to provide correct results. Choosing the right AERMOD input data is an all important first step in a successful assessment of pollutant concentrations.

4. REFERENCES

1. U.S. EPA, 1998. User's Guide for the AERMOD Meteorological Preprocessor (AERMET). Office of Air Quality Planning and Standards, Research Triangle Park, NC.
2. U.S. EPA, 1998. User's Guide for the AERMOD Terrain Preprocessor (AERMAP). Office of Air Quality Planning and Standards, Research Triangle Park, NC.
3. G. Latini., R. Cocci Grifoni, G. Passerini, and G. Fava, 1999, Applicability of a Photochemical Box Model over complex coastal areas, in: *Air Pollution 99,* C.A. Brebbia, M. Jacobson, H. Power, ed., Wit Press, Southampton and Boston, pp.697-706.

THE BLACK TRIANGLE AREA – FIT FOR EUROPE?
Numerical Air Quality Studies for the Black Triangle Area

Eberhard Renner, Wolfgang Schröder, Detlef Theiss and Ralf Wolke
Institute for Tropospheric Research, Leipzig, Germany

1. INTRODUCTION

The „Black Triangle" area (covering Northern Bohemia, Southern Saxony and part of Lower Silesia) has been one of the most polluted areas in Central Europe. The main sources of air pollution in the Black Triangle region were the emissions of sulfur and dust by power plants, industrial facilities, residential houses heating units, which were using lignite as fuel, and road traffic. After the political changes at the end of the eighties the region was financially supported by the European Commission to reduce the amount of air pollution. Owing to a substantial effort of the governments of Czech Republic, Germany and Poland as well as of industry a significant improvement of air quality has been achieved up to day. This has resulted mainly in a dramatic reduction of sulfur and dust emissions in this region. Unfortunately, this declining trend can not be seen concerning the nitrogen emissions. The nitrogen emissions are increasing mainly as a result of increasing traffic. Nitrogen oxide (NO_x) plays an important role in atmospheric chemistry. It produces tropospheric ozone by photochemical reactions in the presence of volatile organic compounds (VOC).

As a consequence, most likely we will not have a „sulfur problem" in the future, but we will have to demand our attention to the photooxidants, especially ozone. These changes in air pollution have been investigated. With special focus on the situation in Saxony, the species sulfur dioxide, ozone, and aerosol particles have been studied. The model results have been evaluated for the general pollutant situation for past (1996; The winter 95/96 was the last „London smog" episode in this region.), present (1998) and future (2005) emission scenarios. Relevant limit values for protection of human health defined or suggested in directives by the European Commission were checked in worst case scenarios for the year 2005. A summary of the results of the modelling work within the research program OMKAS (Optimization of Emission Reduction and Control of Air Pollution for the Border-Region of Saxony), funded by the Ministry of Environment of Saxony and the European Commission, is given.

Air Pollution Modeling and Its Application XV, Edited by
Borrego and Schayes, Kluwer Academic/Plenum Publishers, New York, 2002

2. MODEL SYSTEM AND SIMULATION SETUP

The studies are performed by utilizing the coupled mesoscale model system METRAS-MUSCAT. METRAS is a three-dimensional nonhydrostatic meteorological model. MUSCAT is a multiscale three-dimensional chemistry transport model, which was developed by Knoth and Wolke. It has an online coupling to METRAS. For the estimation of ozone concentrations the gas phase mechanism Euro-RADM is used. For simulation of aerosol dynamical processes the modal model MADMAcS I has been included in MUSCAT. For the application presented on the poster two modes of particles with mean radii of $0.3\ \mu m$ for the PM 2.5 fraction and $7.0\ \mu m$ for the PM 10 fraction are considered. Only transport of primary emitted „inert" particulate matter has been simulated as well as coagulation, deposition and sedimentation of these particles. Formation of secondary particles are not considered.

High values of SO_2 and particle concentrations typically occur in the model domain by winter high pressure conditions with a strong inversion and moderate winds from the east. Summer smog with high ozone concentrations can be expected during high pressure conditions on hot summer days. Typical realistic meteorological conditions for such cases were introduced in a conceptual way, to simulate „worst case scenarios" for summer and winter. In this manner the results of the second day of two days simulations can be checked against short-time (8-hour resp. 24-hour mean) limit values for the protection of human health given by relevant EU-guidelines. The simulations are not qualified to estimated annual limit values for the protection of ecosystems.

3. RESULTS

One can sum up the results as follows:

- The reduction of sulfur dioxide emissions was up to now and will be most effective on the improvement of air quality. The concentrations of sulfur dioxide will not exceed the relevant EU-limit values for human health.
- From predictions of the concentration of aerosol particles for 2005 it can be concluded that the relevant EU-limit value for PM 10 mass concentrations will be fulfilled at this time. However, these results are a preliminary estimate. There are still a lot of subjects to be discussed in the future, like the uncertainties of particle emissions (amount and size distribution), the influence of the chemical composition of the particles and the formation of secondary organic and inorganic aerosol particles by nucleation and condensation.
- The present and future reduction of local emissions in the modelling area itself has only a small effect on lowering ozone concentrations. Assuming the background concentrations of ozone are on the present european level furthermore, the simulations for the emission scenario 2005 in the model domain show nearly the same exceedances of the suggested EU-limit values for ozone as present. The EU-guideline will probably be met only for lower background values. This leads to the - well known - conclusion that emission reduction strategies have to be performed on a larger, at least the European scale.
- The answer on the question „The Black Triangle Area – Fit for Europe?" is YES! The remaining air pollution problems are more or less the same like in the other EU-countries and can be solved only by their joint efforts!

SURFACE LAYER TURBULENCE DURING THE TOTAL SOLAR ECLIPSE OF 11 AUGUST 1999

Guy Schayes[+], Jean-Luc Mélice[*] and Valérie Dulière[+]

1. INTRODUCTION

Total solar eclipses are not frequent events although they are not rare. Clearly no effect on air pollution is expected but we expect that the sudden reduction of solar radiation will influence on the atmospheric boundary layer. The decay of radiative forcing during the occulting phase of an eclipse is about 4 to 5 times more rapid than during a normal sunset. It is thus interesting to look at the atmospheric reactions in this unusual circumstance.

Frequently, standard meteorological observations are made during these events like air temperature, humidity or wind speed. However to our knowledge, an experiment measuring the air turbulence was never conducted during a total eclipse, maybe for the simple reason that such an event rarely traverses a region where these measurements are easily available without moving adequate equipment for long distances.

2. THE DATA

The total eclipse of 11 August 1999 traversed a line through Northern France and Southern Belgium. Unfortunately the weather was not optimum for this observation but the effects are still clearly visible. About five hours of measurements (resolved at one second) are available for the 3 wind components, the temperature and a few other additional measurements.

The effect of the eclipse is clearly visible on* the temperature record. Despite the fact of the variable cloudiness, the first temperature maximum (before totality) of 16.6°C falls to 13.8 some 20 minutes after totality, and a second maximum of 17.3 around the time of the last contact (a thick cloud cover came then and the temperature started to drop again

+Institut d'Astronomie et de Géophysique G. Lemaître, UCL, B-1348 Louvain-la-Neuve, Belgium
*IRD, Laboratoire d'Océanographie Dynamique et de Climatologie, UPMC, F-75005 Paris, France

Air Pollution Modeling and Its Application XV, Edited by
Borrego and Schayes, Kluwer Academic/Plenum Publishers, New York, 2002

after the eclipse). Obviously the temperature behaviour would have been much different with a clear sky, but even so the effect is clearly visible. The mean wind speed dropped from 3.4 to 2.0 m/s during the eclipse.

3. RESULTS

The change in the turbulent regime due to the rapid change of stratification is obvious. The figure 1 shows the evolution of the u,w and T variances. First contact is at point 4700 s, totality around 9350 s and last contact is at 14000 s. The temperature variance drops first with a time constant estimated to 50 min, then the vertical component of the wind (time constant of 30 min) and finally the horizontal components decrease more slowly (time constant of about 2 hours).

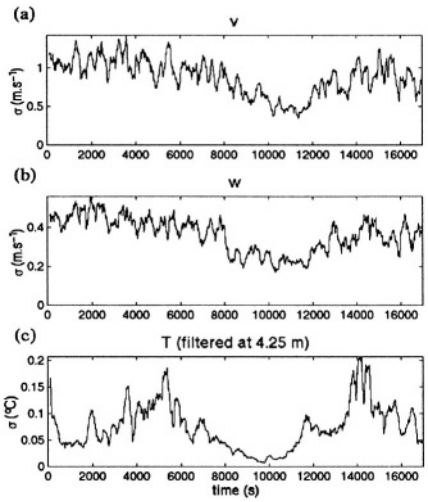

Figure 1. Time evolution of the observed variances of u,w and T.

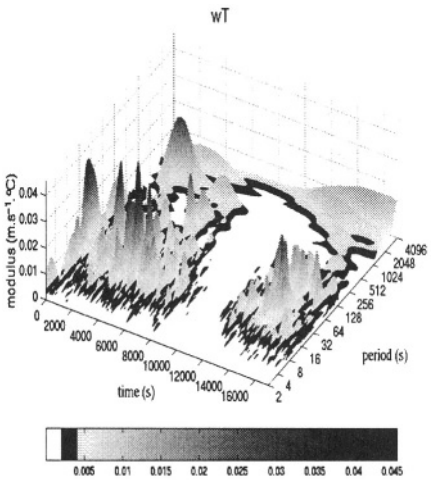

Fig 2. Wavelet transform of the heat flux showing the relevant frequencies.

The figure 2 shows the modulus of the cross-wavelet spectrum of the w and T signals. This spectrum decomposes the sensible heat flux w'T' intensity in the time-frequency space. The vertical axis is proportional to the intensity of the signal at a given frequency. The valley around 9000 s (totality) indicates that the flux had dropped to zero. A clear separation between the high frequencies (front) attributed to ordinary turbulence and the low frequencies (back) attributed to effect of passing clouds is clearly visible.

Reference

Schayes G., Mélice J.L. and Dulière V., 2001. Atmospheric turbulence during the solar total eclipse of 11 august 1999. (in preparation).

SEASONAL SIMULATION OF THE AIR QUALITY IN EAST ASIA USING CMAQ

Seiji Sugata*

1. INTRODUCTION

Importance of long-term air quality simulation has grown to understand long-term change of the air quality, such as, the impact of climate change. This study attempts to address a challenge for improvement of capability of an air quality modeling system, CMAQ (Community Multiscale Air Quality) modeling system with RAMS (Regional Atmospheric Modeling system) to achieve long-term simulation. Results will be evaluated by comparing with observations.

2. CONFIGURATION

A modeling system used in this study is the CMAQ modeling system modified for linkage with RAMS meteorological data (Sugata et al., 2001, hereafter SBU2001, Byun and Ching, 1999). Except for a minor change in the CTM code to update SO_2 gas-phase reaction, same options and configurations as SBU2001 were used for running RAMS and CMAQ. The modeling system was run for half year from 27 December 1996 to 31 June 1997. RAMS was run by continuous six times one month run with historical restart and CMAQ was run by continuous twelve times half month run with historical restart. ECMWF data was used for RAMS assimilation.

Emission data for the simulation has been updated from the one in SBU2001 with Zhang (2001), which archives sophisticatedly emission data from some projects, such as GEIA, EDGAR, and ACE-Asia/TRACE-P.

3. RESULTS

Time series of meteorological fields simulated by RAMS are compared with observational ones at two site in Japan, where RAMS data is at the first layer of the model, about 50m, and observational data are hourly ones at the surface. One site is Osaka, which is the second largest city in Japan, and the other is Matsue, which is along the coast to

* Seiji Sugata, National Institute for Environmental Studies, Tsukuba, Ibaraki 305-0053, Japan

Air Pollution Modeling and Its Application XV, Edited by
Borrego and Schayes, Kluwer Academic/Plenum Publishers, New York, 2002

Japan Sea and is supposed as an semi-urban-rural area. Long-term variations (week-to-week, seasonal) of temperature are essentially well reproduced at both sites (Figure 1., Osaka), while shorter-term variations show some small differences. Variations of wind speed are also compared with observations and they are generally well simulated although the speed is underestimated at Osaka. With considering RAMS data are come from 80km mesh data and observational data are come from hourly surface observations independent from the ECMWF data used for assimilation, we can say meteorological fields are well reproduced for long period by RAMS.
CMAQ results are also compared with observational ones at the two sites. Most species have tendency to be underestimated compared to observation. One possible reason is emission problem.

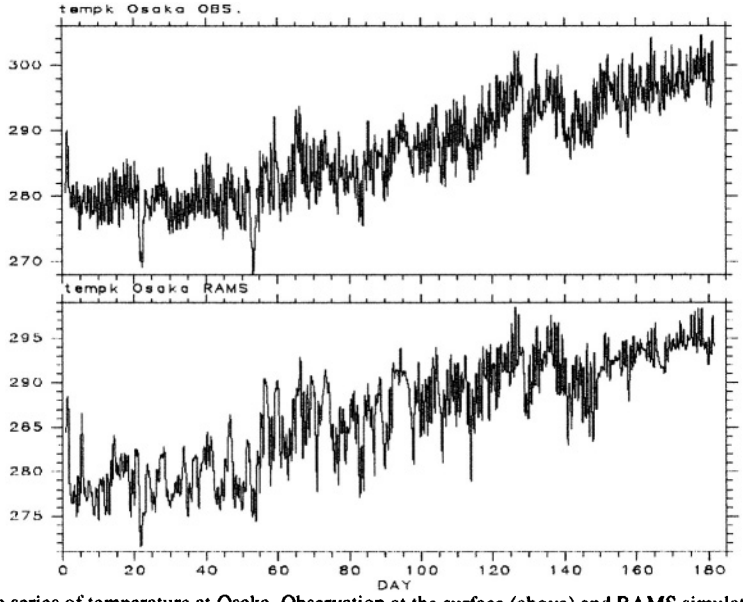

Figure1. Time series of temperature at Osaka. Observation at the surface (above) and RAMS simulation at the first layer about 50m (below).

4. SUMMARY

We have presented simulation results of RAMS/CMAQ system applied to East Asia for half year. The meteorological results were reasonable for whole the period compared with observations. Further evaluation is needed for air quality modeling results.

REFERENCE

Byun, D.W. and J.K.S. Ching, ed., 1999, *Science Algorithms of the EPA Models-3 Community Multi-scale Air Quality (CMAQ) Modeling System,* NERL, Research Triangle Park, NC. [Available from National Exposure Research Laboratory, U.S. Environmental Protection Agency, Research Triangle park, NC 27711]

Sugata, S., D. Byun, I. Uno, Simulation of sulfate aerosol in East Asia using Models-3/CMAQ with RAMS meteorological data, *Air Pollution Modeling and its Application XIV,* Gryning and Schiermeier eds., 267-275,. 2001

Zhang, M, 2001, (private communication)

THE ROLE OF ENERGY SOURCES OF DIFFERENT TYPES IN ATMOSPHERIC POLLUTION AND HEAT SUPPLY OPTIONS IN IRKUTSK CITY

Sergei P. Filippov and Alexandra V. Keiko*

The structure of energy (heat) sources making up the heating system of Irkutsk city is typical of old Siberian cities, which became industrial centres in the XX century. The high fraction of small-capacity sources, including large number of household stoves is peculiar for such cities. The installed capacity of stoves is 30% of the overall, while their fuel consumption is 8.5% only. 76% of boiler houses have unit capacity less than 5 MW; they use mostly fixed-bed combustion. One more feature of Irkutsk heating system is the large fraction of coal in the fuel balance: in Irkutsk it comprises 80%, while in the European Russia natural gas constitutes the major fraction.

According to the existing practice the emission factors of heat sources are determined mostly using computational technique and for the small sources they are often considerably underestimated. In order to reveal the actual emission factors of small heat sources we performed a series of measurements at operated boilers and stoves (Table 1). In order to disclose the most important factors causing the deviation of actual emission factors from the designed values we carried out a series of comparative combustion of a number of Siberian coals under a wide range of combustion conditions (Filippov S.P. *et al,* 1999). It was shown that the proper operation of boilers and stoves can result in an appreciable decrease in emissions of products of incomplete burning like CO, soot, and PAH. The study of sulphurous substances emission is complicated by high variability of their composition. The fraction of initial coal sulphur emitted in the form of SO_2 varies from 30 to 85% depending on the quality of burning operation.

The atmospheric dispersion of emissions over the city has been studied using the standard model ISC3 developed by US EPA. The requirements to a model for analysis of heating systems and the applicability of ISC3 for such studies in Siberia are discussed by Keiko *et al* (1999) and Keiko *et al* (2000). The considered emission sources include Novo-Irkutsk CHP plant (2 point sources), organic fuel-fired boiler houses (250 point sources), areas of residential combustion (11 area sources), and 5 CHP-plants outside Irkutsk (12 point sources). These sources are broken into five groups according to the combustion technology and capacity (Table 2). Some results of model study are

*Energy Systems Institute, Russian Academy of Sciences. 130, Lermontov Rd., Irkutsk 664033 Russia

Air Pollution Modeling and Its Application XV, Edited by
Borrego and Schayes, Kluwer Academic/Plenum Publishers, New York, 2002

summarised in the Table 2. Small heat sources are shown to provide the largest contribution to the air pollution in Irkutsk. The zones of the most pollution from domestic stoves coincide the contours of quarters of few-storied houses. The Russian air quality standards for CO, Nox, SO_2, particulate matter and PAH may be breached during the heating season over the whole territory of the city.

Table 1. Emission factors, average values[1], kg/TJ (fuel)

Heat source	SO_2		NO_2		CO		Particulates	
	1	2	1	2	1	2	1	2
1. Coal-fired heat sources								
1.1 Fixed-bed combustion (Azey lignite)								
- manual feed (< 0,7 MW)	320	480	240	150	3000	2000	2700	2000
- periodic mech. feed (0,7–2 MW)	330	480	250	180	1800	690	2500	2000
- continuous feed (2–10 MW)	360	480	310	180	1500	690	1900	460
1.2 Pulverised combustion								
- boiler houses (Azey lignite)	420	480	330	190	50	58	...	400
- NICHP (Borodinsky lignite)	410	350	500	190	8	5	170	270
2. Mazut boiler houses								
- small (< 5 MW)	1000	770	300	300	2000	1900	550	100
- large (5 MW and more)	...	770	...	600	...	20	...	10
3. Household stoves								
- hard coal (Cheremkhovsky)	220	–	230	–	4500	–	500	–
- fire wood	0	–	140	–	5000	–	60	–

Note: 1 – measured values, 2 – reported values (computational).

Table 2. Specific concentrations of pollutants in the atmosphere of Irkutsk and relative contributions of different groups into winter average concentration

Source group	SO_2	NO_2	CO	Particulates[1]
Maximum daily average concentrations, ($\mu g/m^3$)/GW (fuel)				
1. NI CHP plant	5,4	6,0	0,15	16
2. large boiler houses	87	40	302	51
3. small boiler houses	284	208	3765	2016
4. residential stoves	66	95	4324	494
5. External CHP plants[2]	2,3	3,0	0,09	5,6
Relative contribution into winter average concentration, %				
NI CHP plant	0,1-2	0,1-4	0,001-0,01	1-4
external CHP plants	1-15	5-14	0,01-0,1	1-14
residential stoves	7-25	10-50	50-85	10-40
large boiler houses	62-80	35-75	3-15	8-30
small boiler houses	12-30	10-30	12-30	50-80

Note: 1. Including fly ash and soot.

The obtained results allowed for the option of the most efficient ways to lessen air pollution in Irkutsk: (1) substitution of small heat sources with larger ones; (2) substitution of small boiler houses in local heating systems with electric boiles; (3) the

change of individual houses from residential burning to electric heating; and (4) bettering the structure of fuel consumption.

On the base of the above analyses there have been formulated and studied fifteen scenarios of the development of heating system in Irkutsk. They represent hypothetical marginal variants and allow the limits of air quality control to be revealed. Beside the environmental consideration the actual scenario of the heating system development will account for economical and resource factors and will be an intermediate scenario with respect to those considered. It is shown that a change in the fuel consumption structure may result in two-fold decrease in concentrations of sulphur dioxide and particulate matter compared with the modern case. The priority is to be given to Tugnuy and Borodinsky coals while the use of Mugun and Cheremkhovsky coals causes a rise of SO_2 concentrations. The change of large heat sources from coal to gas does not lead to a considerable improvement in air quality because the largest contribution into atmospheric pollution is made by those of small capacity.

REFERENCES

Filippov S.P., Pavlov P.P., Keiko A.V., 1999, Environmental characteristics of small-capacity heat sources. Energy Systems Institute, RAS, Irkutsk. 46 p. (In Russian)

Keiko A.V., Kuchmenko E.V., Filippov S.P., Pavlov P.P., 1999, Modelling the air quality impact of energy production. Energy Systems Institute, RAS, Irkutsk. 44 p. (In Russian)

Keiko A.V., Filippov S.P., Pavlov P.P., 2000, On the methods of the evaluation of air quality impact of energy production. *Geogr. Naural. Resources,* **1,** pp.127-132. (In Russian)

This page intentionally left blank

TRANSPORT SENSITIVITY ANALYSIS ON OZONE CONCENTRATIONS IN IBERIAN PENINSULA BY USING MM5-CMAQ MODELLING SYSTEM

R. San José, J. L. Pérez, I. Salas[*] and R.M. González[**]

1. INTRODUCTION

In the last decades the interest for investigating the ozone concentrations in the atmosphere in the tropospheric layer has increased extraordinary. The ozone species is recognized as one of the most important oxidants in the atmosphere and also as a toxic pollutant since the health consequences in human beings when high concentrations are present are important. It is also a greenhouse gas so that important climatic consequences are also derived from those high concentrations. Tropospheric ozone is formed by the chemical reactions in the atmosphere when NOx and VOC's are present and activated depending the pressure, temperature and solar radiation. Vehicle traffic in urban and rural areas is important. In Spain more than 25000000 and in the Iberian Peninsula is more than 32000000. The local impact of the NOx and VOC's emissions on ozone production are being investigated intensively in the last decades. Little attention has been put on larger domains and the possible impact of the total ozone tropospheric budget. This contribution shows the impact on ozone total budgets of traffic emissions over the Iberian Peninsula. Results show that for the first day of simulation an increase up to 25% of ozone is found and for the rest of the days of simulation increase values ranging between 2 – 5 % are found. Although the 25 % increase cannot be neglected as a whole the impact over the total tropospheric ozone budget is limited. Additional experiments over several more different periods over the year are necessary for more conclusive results.

[*] Environmental Software and modelling Group, Computer Science School, Technical University of Madrid (UPM) (Spain), Campus de Montegancedo, Boadilla del Monte 28660 Madrid (Spain) http://artico.lma.fi.upm.es.
[**] Department of Geophysics and Meteorology, Faculty of Physics, Universidad Complutense de Madrid (Spain).

Air Pollution Modeling and Its Application XV, Edited by
Borrego and Schayes, Kluwer Academic/Plenum Publishers, New York, 2002

2. THE MM5-CMAQ SYSTEM

In this contribution we have used the MM5 model and the Community Muiltiscale Air Quality Modelling System (CMAQ) as representative of the third generation of Air Quality Modelling Tools to simulate the air quality concentrations over a selected period in April, 2001 over the Iberian Peninsula to understand the impact of traffic emissions over the ozone concentrations.

The PSU/NCAR mesoscale model is a limited-area, nonhydrostatic or hydrostatic (Version 2 only),terrain-following sigma-coordinate model designed to simulate or predict mesoscale and regional-scale atmospheric circulation. It has been developed at Penn State and NCAR as a community mesoscale model and is continuously being improved by contributions from users at several universities and government laboratories.

The Community Multiscale Air Quality Modelling System (CMAQ) and the peripheral modules are illustrated in Figure 2. We have selected for this simulation the piece parabolic method (PPM) Colella and Woodward (1984). The updated version of the CBM-IV mechanism (36 species, 94 reactions including 11 photolytic reactions) with the isoprene chemistry mechanism and the Arrhenius type rate constant expressions. We have also used aerosol formation processes and aqueous chemistry. Finally we have used the Modified Euler Backward Iterative (MEBI) Solver which is mechanism dependent but it isat least as precise as the QSSA but the computing time required is much lower.

3. APPROACH AND RESULTS

We have used a mother domain of about 8100 km x 6480 km with 108 km grid cell resolution centered over the Iberian Peninsula and three different nesting levels up to 4 km grid cell resolution with a domain of 108 km x 84 km over the Madrid City. Nesting level 2 is the Iberian Peninsula domain with 32 km grid cell resolution. For nesting levels 1 and 2 the impact on the first day is about 25 % on the maximum levels and this impact is increased for nesting level 3 (since the urban emission becomes more important in relation to the total of the model domain). The consequence of these results is that the biogenic emissions (NOx from agricultural areas and VOC's from forest areas) play a crucial role on the total budget of tropospheric ozone formation particularly when large areas are considered.

DEVELOPMENT OF THE EMISSION INVENTORY SYSTEM FOR SUPPORTING TRACE-P AND ACE-ASIA FIELD EXPERIMENTS

Jung-Hun Woo, David G. Streets, Gregory R. Carmichael, James Dorwart, Narisara Thongboonchoo, Sarath Guttikunda, Youhua Tang*

New emission inventories were developed in support of the Aerosol Characterization Experiments(ACE)-Asia and Transport and Chemical Evolution over the Pacific (TRACE-P) experiments work on. We combine our inventories into the ACCESS(Ace-Asia and Trace-P Modeling and Emission Support System) for more integrated support for these two field studies. To support field experiments and complex atmospheric models such as STEM-II, highly resolved level of spatial, temporal, and species-component detail are needed in emission inventories.

To satisfy these requirements we include not only the gaseous pollutants SO_2, NO_x, CO, and NMVOC, but particulate pollutants such as Black Carbon, Organic Carbon, PM_{10}, and $PM_{2.5}$ for the study domain of Asia. Our domain was designed to cover –13°~53° in latitude and 60°~157° in longitude. It includes 22 Asian countries, 60 sub-regions. 115 active LPSs and 22 volcanos are also included as point sources.

The data system includes information on various emission sources, compiled by fuels and by economic sector activities, and natural emission sources such as volcano and forest fires. So, the methodologies for estimating emission are different between anthropogenic and biomass burning from fires.

For anthropogenic emission, we use year 2000 emission database from Argonne National Laboratory. The data themselves are administrative–level estimates recently compiled from official national statistics and projections. For spatial allocation of regional emission, we use geographical data from The International Institute for Applied Systems Analysis (IIASA), Global Emissions Inventory Activity (GEIA), Central

* Jung-Hun Woo, Center for Global and Regional Environmental Research(CGRER), University of Iowa, Iowa City, IA52242, USA. David G. Streets, Argonne National Laboratory, 9700 South Cass Avenue Argonne, IL 60439, USA. Gregory R. Carmichael, James Dorwart, Narisara Thongboonchoo, Sarath Guttikunda, and YouHua Tang, CGRER, University of Iowa, Iowa City, IA52242, USA.

Air Pollution Modeling and Its Application XV, Edited by
Borrego and Schayes, Kluwer Academic/Plenum Publishers, New York, 2002

Research Institute of the Electric Power Industry (CRIEPI), Digital Chart of the World(DCW.), and LandScan Global Population database from Oak Ridge National Laboratory(ORNL). The combined use of RS and GIS data enhances the spatial allocation capability. The system produces gridded emission datasets from 1 degree by 1 degree down to 30second by 30second.

For biomass burning emission from fires, we use different approach of what we did on anthropogenic emission. Total emission from fire was estimated from previous research. For more realistic temporal variability, we spatially allocate fire emission using on-line information, i.e., we use Advanced Very High Resolution Radiometer (AVHRR) data to "spot" fires and then distribute the emissions from that. We also included Total Ozone Mapping Spectrometer (TOMS) aerosol index (AI), satellite coverage, cloud coverage, and precipitation data to reduce noise of AVHRR data.

For anthropogenic SO_2, more than 60% of total anthropogenic emission comes from China. But, for NO_x, CO, and VOC, emission contribution from China is decreased to 48~ 34%. For these species, portion of India, Japan, South Korea, Indonesia, and Thailand are increased. Power generation and Industrial sector are dominant for SO_2 and transportation sector is dominant for NO_x emission. For CO emission, domestic biofuel is greatest contributor. For VOC, transport and domestic sectors are the significant contributors. For SO_2 emission distribution, Sichuan, Yunnan, Jiangsu, Shandong, Hebei, Shanxi and Henan are large in China. Emission from Thailand and Indonesia are also large. Emission with finer grid may useful for more detail analysis for smaller domain. We selected 4° × 4° domain near Shanghai to see how emission distributions are different along to the spatial resolution. From this test, we found effect of certain emission area is strongly depends on it's geographical feature – e.g. shape, length, and area etc. For example, Lake Tai (about 20% of a 1 deg by 1 deg grid cell)'s effect can be seen at 30' × 30' resolution, but Yangtze River's effect cannot clearly seen even in 5' × 5' resolution. So, we must use more than 5' × 5' grid resolution when we want to see the effect of Yangtze River in Nanjing area, otherwise it should be neglected.

For biomass burning emission from fires, high emission grid cells are located mainly in the part of Indian sub-continent and west part of Southeast Asia, during experiment period. After applying our noise reduction procedure, south and southeast part of China also have high emission grids. We hope, therefore, it may help to explain high CO concentration in southern China. Temporal variation of fire emission is usually large day by day, not only due to the variation of fire event but noise of AVHRR data. This variability also reduced by noise reduction procedure.

At present we are working on the evaluation procedure of out emission inventory through flight operation data from these two field campaigns. Amount and distribution of concentration field calculated from our chemical model are fairly well matched with observation data, at large. In the presentation more evaluation features can be included according to the new findings.

PARTICIPANTS

The 25th NATO/CMS International Technical Meeting on Air Pollution Modelling and Its Application, Louvain-la-Neuve, Belgium, October 15-19, 2001

AUSTRALIA

Lee S.	Commonwealth Scientific and Industrial Research Organisation, Atmospheric Research 107-121 Station Street, Aspendale 3195 Melbourne E-mail: sunhee.lee@dar.csiro.au

BELGIUM

Berger A.	Université catholique de Louvain Institut d'Astronomie et de Géophysique G. Lemaître 2, Chemin du Cyclotron 1348 Louvain-la-Neuve E-mail: berger@astr.ucl.ac.be
Beten D.	NATO - CCMS CCMS Progr. NATO 1110 Bruxelles E-mail:ccms@hq.nato.int
Cosemans G.	Vlaamse Instelling voor Technologisch Onderzoek Boeretang 200 B-2400 MOL E-mail: guido.cosemans@vito.be

De Ridder K.
Vlaamse Instelling voor Technologisch Onderzoek
Vito-TAP
Boeretang 200
B-2400 Mol
E-mail: koen.deridder@vito.be

Fettweis X.
Université catholique de Louvain
Institut d'Astronomie et de Géophysique G. Lemaître
2, Chemin du Cyclotron
1348 Louvain-La-Neuve
E-mail: fettweis@astr.ucl.ac.be

Hamdi R.
Université catholique de Louvain
Institut d'Astronomie et de Géophysique G. Lemaître
2, Chemin du Cyclotron
1348 Louvain-La-Neuve
E-mail: hamdi@astr.ucl.ac.be

Lefebre F.
VITO-TAP
Centre for Remote Sensing and Atmospheric Processes
Boeretang 200
2400 Mol
E-mail: filip.lefebre@vito.be

Mensink C.
Vito
Boeretang 200
2400 Mol
E-mail: clemens.mensink@vito.be

Nihoul J.
Université catholique de Louvain
Institut d'Astronomie et de Géophysique G. Lemaître
2, Chemin du Cyclotron
1348 Louvain-la-Neuve
E-mail: j.nihoul@ulg.ac.be

Person A.
Université catholique de Louvain
Institut d'Astronomie et de Géophysique G. Lemaître
2, Chemin du Cyclotron
1348 Louvain-La-Neuve
E-mail: porson@astr.ucl.ac.be

Schayes G.
Université catholique de Louvain
Institut d'Astronomie et de Géophysique G. Lemaître
2, Chemin du Cyclotron
1348 Louvain-La-Neuve
E-mail: schayes@astr.ucl.ac.be

BRAZIL

Moraes Osvaldo L.L
UFSM
Campus Universitario
E-mail: moraes@oslo.ccne.ufsm.br

BULGARIA

Batchvarova E.
National Institute of Meteorology
And Hydrology
66 Tzarigradsko chaussee
1784 Sofia
E-mail: Ekaterina.Batchvarova@meteo.bg

CANADA

Ainslie B.
Atmospheric Sciences Programme
University of Bristish Columbia
Department of Earth and Ocean Sciences
6339 Stores Road
V6T 1Z4 Vancouver, B.C.
E-mail: bainslie@eos.ubc.ca

Gong W.
Meteorological Service of Canada
4905 Dufferin Street, Downsview.Ontario
M3H 5T4 Toronto
E-mail: wanmin.gong@ec.gc.ca

Steyn D.
The University of British Columbia
Room 464, 6356 Agriculture Road
V6T 1Z2 Vancouver
E-mail: dsteyn@eos.ubc.ca

Tang A.
Ministry of Environment, Ontario, Canada
125 Resources Road
M9P 3V6 Etobicoke
E-mail: al.tang@ene.gov.on.ca

CHINA

Fung C.
Hong Kong Environmental Protection Department
33/f, Revenue Tower
5 Gloucester Road, WanChai
Hong Kong Special Administrative Region
E-mail: cfung@epd.gov.hk

CZECH REPUBLIC

Brechler J.
Charles University in Prague, Fac. of Mathem. and Physics
Dept. of Meteorology and Environment Protection
V Holesovickach 2
180 00 Prague
E-mail: josef.brechler@mff.cuni.cz

Halenka T.
Charles University in Prague, Fac. of Mathem. and Physics
Dept. of Meteorology and Environment Protection
V Holesovickach 2
180 00 Prague 8
E-mail: tomas.halenka@mff.cuni.cz

DENMARK

Baklanov A.
Danish Meteorological Institute
Lyngbyvej 100
DK-2100 Copenhagen
E-mail: alb@dmi.dk

Chenevez J.
Danish Meteorological Institute
Lyngbyvej 100
DK-2100 Copenhagen
E-mail: jerome@dmi.dk

Gryning S.- E.
Riso National Laboratory
Wind Energy Department
Riso National Laboratory
DK-4000 Roskilde
E-mail: sven-erik.gryning@risoe.dk

ESTONIA

Kaasik M.
Tartu Observatory
Toravere
61602 Tartumaa
E-mail:marko@apollo.aai.ee

FRANCE

Brasseur O.
Laboratoire d'étude des Transferts en Hydrologie et Environnement
Institut National Polytechnique de Grenoble
Domaine Universitaire
Rue de la piscine, 1023-1025 BP 53
38041 Grenoble
E-mail: olivier.brasseur@hmg.inpg.fr

Carissimo B.
Electricité de France
Recherche et Developpement
6 Quai Watier
78400 Chatou
E-mail: bertrand.carissimo@edf.fr

Poisson N.
Agence de l'environnement et de la maîtrise de l'énergie
27 rue Louis Vicat
F-75015 Paris
E-mail: nathalie.poisson@ademe.fr

Vardoulakis S.
Institut National de l'Environnement industriel et des risques
Parc Technologique ALATA, B.P.2
60550 Vernieul-en-Halatte
E-mail: sotiris.vardoulakis@ineris.fr

Wroblewski A.
Ecole des Mines de Douai
941 rue Charles Bourseul
59508 Douai
E-mail: wroblewski@ensm-douai.fr

GERMANY

Ebel A.
University of Cologne, Institute for Geophysics and Meteorology, EURAD Project
Aachener Str. 201 - 209
50931 Cologne
E-mail: eb@eurad.uni-koeln.de

Flemming J.
Freie Universität Berlin
Institut für Meteorologie
Carl-Heinrich-Becker Weg 6-10
12165 Berlin
E-mail: flemming@zedat.fu-berlin.de

Hellmuth O.
Institute for Tropospheric Research
Permoser Strasse 15
04318 Leipzig
E-mail: olaf@tropos.de

Reimer E.
Institute for Meteorology
Freie Universität Berlin
Carl-Heinrich-Becker-Weg 6-10
D-12165 Berlin
E-mail: reimer@zedat.fu-berlin.de

Renner E.
Institute for Tropospheric Research
Permoser Strasse 15
04318 Leipzig
E-mail: renner@tropos.de

Suppan P.
Fraunhofer Institute for Environmental Atmospheric Research
Kreuzeckbahnstrasse 19
82467 Garmisch-Partenkirchen
E-mail: suppan@ifu.fhg.de

GREECE

Rafailidis S.
EREL – NRCPS "Demokritos"
GR-15031 Aghia Peraskevi Athikis
E-mail: rafailidis@hotmail.com

Varinou M.
University of Athens
Panepistimioupolis, Phys. Bld V
157 84 Athens
E-mail: varinou@mg.uoa.gr

Voudouri A.
University of Athens
Panepistimioupolis, Phys. Bld V
157 84 Athens
E-mail: voudouri@mg.uoa.gr

ITALY

Alessandrini S.
CESI S.p.A
Via Rubattino, 54
20100 Milano
E-mail: alessandrini@cesi.it

Anfossi D.
Istituto di Cosmogeofisica del CNR
Corso Fiume 4
10133 Torino
E-mail: anfossi@to.infn.it

Cocci Grifoni R..
Roberta Dipartimento di Energetica
Università di Ancona
Brecce Bianche
60100 Ancona
E-mail: rcg@popcsi.unian.it

Kioutsioukis I.
Joint Research Center
Via Fermi 1
21020 Ispra
E-mail: ioannis.kioutsioukis@jrc.it

Skouloudis A. N.
European Commission
Joint Research Centre Ispra
Institute for Environment and Sustainability, TP. 280
I-21020 Ispra
E-mail: andreas.skouloudis@jrc.it

Thunis P.
Joint Research Centre
Via Fermi
21020 Ispra
E-mail: philippe.thunis@jrc.it

Tinarelli G.
Arianet srl
Viale Elvezia 42
20052 Monza
E-mail: g.tinarelli@aria-net.it

JAPAN

Sugata S.
National Institute for Environmental Studies
16-2 Onogawa
305-8506 Tsukuba, Ibaraki
E-mail: sugatas@nies.go.jp

Wang Z.
Frontier Research System for Global Change
IGCR Yokohama
3173-25 Showa-machi, Kanazawa-ku
236-0001 Yokohama
E-mail: zifawang@jamstec.go.jp

Zhang M. Frontier Research System for Global Change
IGCR Yokohama
3173-25 Showa-machi, Kanazawa-ku
236-0001 Yokohama
E-mail: mgzhang@jamstec.go.jp

MEXICO

Wellens A. National Autonomous University of Mexico
DEPFI-UNAM, Sección Ingeniería Ambiental
Apdo. Postal 70-256, Cd. Universitaria
4510 Mexico DF
E-mail: wann@servidor.unam.mx

NETHERLANDS

Builtjes P. P.O Box 342
7300 AH Apeldoorn
E-mail: p.j.h.builtjes@mep.tno.nl

Van Loon M. TNO Energy,Environment and Process Innovation
P.O. BOX 342
7300 AH Apeldoorn
E-mail: loon@mep.tno.nl

NIGERIA

Abiodun B. J. Federal University of Technology
Department of Meteorology,
P.M.B. 704 Akure
E-mail: bjabiodun@yahoo.com

PORTUGAL

Borrego C. Departement of Environment and Planning
University of Aveiro
Campus Universitario de Santiago, 3810-193 Aveiro
Aveiro
E-mail: borrego@dao.ua.pt

Carvalho A. — Departement of Environment and Planning
University of Aveiro
Campus Universitario de Santiago, 3810-193 Aveiro
Aveiro
E-mail: avc@dao.ua.pt

Ferreira J. — Departement of Environment and Planning
University of Aveiro
Campus Universitario de Santiago, 3810-193 Aveiro
Aveiro
E-mail: ferreira@dao.ua.pt

Martins H. — Departement of Environement and Planning
Univesity of Aveiro
Campus Universitario de Santiago 3810-193
Aveiro
E-mail: hmartins@dao.ua.pt

Miranda A. I.l — Departement of Environement and Planning
Univesity of Aveiro
Campus Universitario de Santiago 3810-193
Aveiro
E-mail: aicm@dao.ua.pt

Monteiro A. — Departement of Environement and Planning
Univesity of Aveiro
Campus Universitario de Santiago 3810-193
Aveiro
E-mail: alexandra@dao.ua.pt

RUSSIA

Genikhovitch E. — Main Geophysical Observatory
194021 St. Petersburg
E-mail: ego@mailbox.alkor.ru

Keiko A. — Energy Systems Institute
130, Lermontov Rd.
664033 Irkutsk
E-mail: keiko@isem.sei.irk.ru

Penenko V. — Institute of Computational Mathematics and Mathematical Geophysics SD RAS
pr. acad. Lavrent'eva,6
630090 Novosibirsk
E-mail: penenko@sscc.ru

SLOVENIA

Boznar M. Z.
Jozef Stefan Institute
Jamova 39
SI-1000 Ljubljana
E-mail: marija.boznar@ijs.si

SPAIN

Baldasano J. M..
Universidad Politecnica de Catalunya
Avda. Diagonal 647, planta 10
08028 Barcelona
E-mail: baldasano@pe.upc.es

Gelpi I.
Group of nonlinear physics
University of Santiago de Compostela
Faculty of Physics. Campus Sur
15706 Santiago de Compostela
E-mail: ivan@fmmeteo.usc.es

Lumbreras J.
Univeridad Politénica de Madrid
José Gutiérrez Abascal, 2
28006 Madrid
E-mail: jlumbreras@etsii.upm.es

San Jose R.
Technical University of Madrid
Campus de Montegancedo Boadilla
Madrid
E-mail: roberto@fi.upm.es

TURKEY

Incecik S.
Istanbul Technical University, Departement of Meteorology
Maslak
80626 Istanbul
E-mail: incecik@itu.edu.tr

UKRAINE

Podobna Y.
Vinnytsia State Technical University
Departmental Chair for Environmental/Industrial Safety
39 Keletskaya st,apt 178
21036 Vinny163.68 pttsia
E-mail: envrisk@vstu.vinnica.ua

UNITED KINGDOM

Apsimon H.
Imperia College of Science, Technologgy + Medecine
Dept of Environmental Science + Technology
RSM 4.28,Prince Consort Road
SW7 2BP London
E-mail: h.apsimon@ic.ac.uk

Fisher B.
Environment Agency
Steel House, 11 Tothill Street
SW1H 9NF London
E-mail: bernard.fisher@environment-agency.gov.uk

Fournier N.
University of Edinburgh, Department of meteorology
Centre for Ecology and Hydrology, Edinburgh, Scotland
University of Edinburgh, JCMB - KB, Mayfield Road
EH9 3JZ Edinburgh
E-mail: nicolas@met.ed.ac.uk

UNITED STATES

Khan M.
Georgia Institute of Technology
330537 Georgia Tech Station
30332 Atlanta
E-mail: maudood@themis.ce.gatech.edu

Guttikunda S.
The University of Iowa
Center for Global and Regional Environmental Research
204 IATL The University of Iowa
52242 Iowa City
E-mail: sguttiku@cgrer.uiowa.edu

Hansen A. D.
EPRI
P.O. Box 10412
CA 94303-0813 Palo Alto
E-mail: ahansen@epri.com

Hogrefe C.
Department of Earth and Atmospheric Sciences
State University of New York at Albany
1400 Washington Av
NY-12222 Albany
E-mail: chogrefe@air.dec.state.ny.us

Scire J.
Earth Tech, Inc.
196 Baker Avenue
01742 Concord, MA
E-mail: jss@src.com

YUGOSLAVIA

Grsic Z. Institute of Nuclear Sciences-“Vinca”
P.O.Box 522
11001 Belgrade
E-mail: grsa@rt270.vin.bg.ac.yu

AUTHOR INDEX

SUBJECT INDEX